

NISTIR 8271 DRAFT SUPPLEMENT

Face Recognition Vendor Test (FRVT) Part 2: Identification

Patrick Grother
Mei Ngan
Kayee Hanaoka
*Information Access Division
Information Technology Laboratory*

This document is a draft supplement of [NIST Interagency Report 8271](#)

2022/03/30



NISTIR 8271 DRAFT SUPPLEMENT

Face Recognition Vendor Test (FRVT) Part 2: Identification

Patrick Grother
Mei Ngan
Kayee Hanaoka
*Information Access Division
Information Technology Laboratory*

This document is a draft supplement of [NIST Interagency Report 8271](#)

February 2022



U.S. Department of Commerce
Gina M. Raimondo, Secretary

National Institute of Standards and Technology
James K. Olthoff, Performing the Non-Exclusive Functions and Duties of the Under Secretary of Commerce for Standards and Technology & Director, National Institute of Standards and Technology

RELEASE NOTES

2022-03-30: The 1:N track of the FRVT remains open.

- ▷ This document is the sixteenth draft update to [NIST Interagency Report 8271](#). It includes results for algorithms submitted by three first-time participants: Digidata, Intellivision, and Pangiam.
- ▷ The document also includes results for algorithms from three returning developers: Fujitsu Research and Development Center, Idemia, and Gorilla Technology.
- ▷ The [1:N results page](#) has been updated.

2022-02-23: The 1:N track of the FRVT remains open.

- ▷ This document is the fifteenth draft update to [NIST Interagency Report 8271](#). It includes results for algorithms submitted by four first-time participants: Cloudwalk - Moontime Smart Technology, Decatur Industries Inc, NotionTag Technologies Private Limited, and Reveal Media Ltd.
- ▷ The document also includes results for algorithms from three returning developers: Cognitec Systems GmbH, Sensetime Group, and Viettel Group
- ▷ The [1:N results page](#) has been updated.

2022-01-20: The 1:N track of the FRVT remains open.

- ▷ This document is the fourteenth draft update to [NIST Interagency Report 8271](#). It includes results for algorithms recently submitted by two first-time participants: Daon and SQIsoft.
- ▷ The document also includes results for algorithms from five returning developers: Cyberlink Corp, NEC, Neurotechnology, Paravision, and Rank One Computing.
- ▷ The [1:N results page](#) has been updated.

2021-12-16: The 1:N track of the FRVT remains open.

- ▷ This document is the thirteenth draft update to [NIST Interagency Report 8271](#). It includes results for algorithms from six returning developers: Dahua Technology, Imagus Technology, Line Corporation, N-Tech Lab, Qnap Security, and Realnetworks Inc.
- ▷ The [1:N results page](#) has been updated.

2021-11-22: The 1:N track of the FRVT remains open.

- ▷ This document is the twelfth draft update to [NIST Interagency Report 8271](#). It includes results for algorithms recently submitted by three first-time participants Clearview AI, Griaule, and Mantra Softech India.
- ▷ This document and the [1:N results page](#) also include results for algorithms from six returning developers: Acer Incorporated, Canon, Dermalog, Samsung S1, VisionLabs, and Veridas Digital Authentication.

2021-10-28: The 1:N track of the FRVT remains open.

- ▷ This document is the eleventh draft update to [NIST Interagency Report 8271](#). It includes results for algorithms recently submitted by three first-time participants (20Face, Fujitsu Research and Development Center, and Vision-Box), and five returning participants (Alchera, Gorilla Technology, Tevian, Thales-Cogent, and Visidon). Visidon
- ▷ Both the main [1:N results page](#) and the small-gallery [paperless travel page](#) have been updated.

2021-09-21: The 1:N track of the FRVT remains open. Three news items:

- ▷ This document is the tenth draft update to [NIST Interagency Report 8271](#). It includes results for algorithms recently submitted by six first-time developers: Cubox, Fincore, HyperVerge, Qnap Security, Staqu Technologies, and Tripleize (Aize, 3-ize).
- ▷ It includes results also for four returning developers: Cognitec Systems, Incode Technologies, Innovatrics, Neurotechnology, and Rank One Computing.

2021-08-02: The 1:N track of the FRVT remains open. Three news items:

- ▷ This document is the ninth draft update to [NIST Interagency Report 8271](#). It includes results for algorithms recently submitted by eight participants: Cyberlink Corp, NEC Corp, N-Tech Lab, Realnetworks Inc., Sensetime Group, Veridas Digital, Viettel Group, and Vigilant Solutions.
- ▷ Algorithms submitted since July 24 will be included in the next update scheduled for September 9, 2021.
- ▷ A new report, NIST Interagency Report 8381 - FRVT Part 7: Identification for Paperless Travel and Immigration, has been released [[PDF](#), [webpage](#)]. It documents the use of FRVT 1:N algorithms in positive access control and immigration status update travel applications where the enrolled population size is as low as 420 people for aircraft boarding, and 42 000 for an airport security line. These population sizes are much smaller than those used in the main [1:N evaluation](#). Going forward, we will update the report and webpage with results for new algorithms.

2021-07-07: The 1:N track of the FRVT remains open. One update:

- ▷ This document is the eighth draft update to [NIST Interagency Report 8271](#). It include results for an algorithm from one participant: Kakao Enterprises.

2021-06-22: The 1:N track of the FRVT remains open. Three updates:

- ▷ This is the seventh draft of the update to [NIST Interagency Report 8271](#). It includes results for algorithms from three new participants: Line Corporation, Rendip, and Samsung S1 Corp.
- ▷ We have also added results for algorithms from five returning developers: Imagus Technology, Kneron, Tevian, Visidon, and Xforward AI Technology.
- ▷ The algorithm-specific report cards (examples: [1](#), [2](#), and [3](#)) now include figures showing how low threshold values can be used to reduce candidate list lengths for human review, while (usually) elevating miss rates (FNIR) only modestly. The reports also feature some minor additions and clarifications.

2021-03-26: The 1:N track of the FRVT remains open. Three updates:

- ▷ This is the sixth draft of the update to [NIST Interagency Report 8271](#). It includes results for algorithms from three returning developers: Neurotechnology, Guangzhou Pixel Solutions, and Tech5 SA.
- ▷ We have added results on the webpage and in the report for a new ageing dataset in which border crossing photos are searched against a gallery of border crossing photos collected between 10 and 15 years prior to the mated search photos. See section [2](#) for a description of the images. Table [1](#) has a new entry describing the experiment.
- ▷ We will mostly discontinue running the mugshot ageing test, reserving it for algorithms that show high accuracy on the new border-crossing set.

2021-03-26: Regarding the fifth draft of the update to [NIST Interagency Report 8271](#):

- ▷ In addition have added results for first algorithms from two new participants: Viettel Group and Veridas Digital Authentication Solutions.
- ▷ We have added results for algorithms from two returning developers: Idemia and Cognitec Systems.
- ▷ In addition to the report, the [results page](#) and its hyperlinked [report cards](#) have been updated.

2021-02-08: Regarding the fourth draft of the update to [NIST Interagency Report 8271](#):

- ▷ We have added results for eight algorithms submitted by eight developers: Cyberlink, Dermalog, Imagus, Paravision, Sensetime, Trueface, Vigilant Solutions, and X-Forward AI. With the exception of Trueface, all of these developers have participated previously.
- ▷ We anticipate updating this report again in the first week of March 2021.
- ▷ The main [results page](#) has been revised with tabs for the investigative and lights-out identification tables, and a new tab dedicated to speed and resource consumption.
- ▷ The report cards (example [here](#)) hyperlinked from the [results page](#) have been revised to improve content and format.

2020-12-14: Regarding third draft of the update to [NIST Interagency Report 8271](#):

- ▷ We have added results for fifteen algorithms submitted by thirteen developers. The four first-time participants are: Acer, Akurat Satu Indonesia, Canon, and Xforward AI Technology. The ten returning developers are: AllGoVision, Cyberlink Corp, Dahua Technology, Deepglint, Guangzhou Pixel Solutions, IIT Vision, Innovatrics, Rank One Computing, Scanovate, Sensetime Group, Synesis, and VisionLabs.
- ▷ We have added two new datasets to the evaluation: First a set of “visa-border” photos, representing search of an airport immigration lane photo against a database of closely ISO standard portraits; second a “visa-kiosk” set representing search of a photo collected in a registered traveller kiosk against the same ISO portrait gallery. The images are described in section 2.1.
- ▷ As in previous reports, we include results for searching mugshots against a mugshot gallery containing a single image of each of 12 million people. However we have suspending running searches against a gallery in which multiple lifetime photos per person are present, because this is computationally expensive. We retain a N = 3 million search test dedicated to ageing in which mugshots taken up to 18 years after the first photograph are searched - see Table 7.
- ▷ Tables containing computational resource information, Table 2..., now include duration of the finalization step, in which search algorithms can, at their option, build fast-search data structures.
- ▷ We have linked revised per-algorithm PDF report cards from the main [results page](#).
- ▷ We have regenerated all figures and tables to drop algorithms submitted before June 2018. Results for prior algorithms appear in [archived editions](#) of this report.
- ▷ Going forward, we anticipate producing more frequent updates to this report. Developers may submit one algorithm to this evaluation every four calendar months.

2020-03-24: Regarding the second draft of the update to [NIST Interagency Report 8271](#):

- ▷ Adds results for three algorithms from three developers, Dermalog, Innovatrics, and Synesis.
- ▷ Adds Table 7 on ageing showing the increase in false negative rates with time elapsed between two photos. Some of the results were contained in graphs in prior editions of this report, but the table adds results for some newly submitted algorithms.
- ▷ Adjusts frontal mugshot results (for recent and lifetime consolidated galleries) to include the effect of removing some images that should not have been included in image test sets. These images were mostly profile views, images of tattoos containing faces, images of faces on tee shirts, and images of photographs on walls behind the intended subject. This affects many tables and reduces false negative identification rates for all algorithms. The reduction is larger for “recent” enrollments than for “lifetime consolidated” ones with the consequence that accuracy on recent images is now superior.

2020-02-26: Regarding the first draft of the update to [NIST Interagency Report 8271](#):

- ▷ Adds results for 38 algorithms from 31 different developers, eleven of whom are entirely new to the 1:N track of FRVT. These are Allgovision, Cyberlink, Deepsea Tencent, Farbar F8, Imperial College London, Intsys MSU, Kedacom, Kneron, Pixelall, and Scanovate.

DISCLAIMER

Specific hardware and software products identified in this report were used in order to perform the evaluations described in this document. In no case does identification of any commercial product, trade name, or vendor, imply recommendation or endorsement by the National Institute of Standards and Technology, nor does it imply that the products and equipment identified are necessarily the best available for the purpose.

INSTITUTIONAL REVIEW BOARD

The National Institute of Standards and Technology's Research Protections Office reviewed the protocol for this project and determined it is not human subjects research as defined in Department of Commerce Regulations, 15 CFR 27, also known as the Common Rule for the Protection of Human Subjects (45 CFR 46, Subpart A).

ACKNOWLEDGMENTS

The authors are grateful for the support and collaboration of the the Department of Homeland Security's Science & Technology Directorate (S&T), Office of Biometric Identity Management (OBIM), and Customs and Border Protection (CBP).

Additionally, the authors are grateful to staff in the NIST Biometrics Research Laboratory for infrastructure supporting rapid evaluation of algorithms.

Executive Summary

This document is a draft revision of the September 2019 report [NIST Interagency Report 8271](#). That report gave extensive documentation of face recognition applied to mugshots. This report extends that by adding more two more challenging datasets containing images with serious departures from canonical frontal image standards. The report also adds results for algorithms submitted to NIST since in 2019 and 2020. The algorithms, which implement one-to-many identification of faces appearing in two-dimensional images, are prototypes from the research and development laboratories of mostly commercial suppliers, and are submitted to NIST as compiled black-box libraries implementing a NIST-specified C++ test interface. The report therefore does not describe how algorithms operate. The report lists accuracy results alongside developer names and will therefore be useful for comparison of face recognition algorithms and assessment of absolute capability. The report is accompanied by a [webpage](#) with sortable results.

The evaluation uses six datasets: frontal mugshots, profile view mugshots, desktop webcam photos, visa-like immigration application photos, immigration lane photos, and registered traveler kiosk photos. These datasets are sequestered at NIST, meaning that developers do not have access to them for training or testing. This aspect is important because face recognition algorithms are very often deployed without the developer having access to the customers image data. A possible exception to this would be in a cloud-based application where the operational image data is uploaded to a cloud operated by a face recognition developer.

The major result in NIST IR 8271 was that massive gains in accuracy have been achieved in the years 2013 to 2018 and these far exceed improvements made in the prior period, 2010 to 2013. While the industry gains were broad - at least 30 developers' algorithms outperformed the most accurate algorithm from late 2013, there remains a wide range of capability. While this report shows accuracy gains only over the period 2018-2020, the most accurate algorithm reported here is substantially more accurate than anything reported in NIST IR 8271. This is evidence that face recognition development continues apace, and that FRVT reports are but a snapshot of contemporary capability.

From discussion with developers, the accuracy gains stem from the adoption of deep convolutional neural networks. As such, face recognition has undergone an industrial revolution, with algorithms increasingly tolerant of poorly illuminated and other low quality images, and poorly posed subjects. One related result is that a few algorithms correctly match side-view photographs to galleries of frontal photos, with search accuracy approaching that of the best c. 2010 algorithms operating on purely frontal images. The capability to recognize under a 90-degree change in viewpoint - pose invariance - has been a long-sought milestone in face recognition research.

With good quality portrait photos, the most accurate algorithms will find matching entries, when present, in galleries containing 12 million individuals, with rank one miss rates of approaching 0.1%. The remaining errors are in large part attributable to long-run ageing, facial injury and poor image quality. Given this impressive achievement - close to perfect recognition - an advocate might claim that cooperative face recognition is a solved problem, a statement that can be refuted with the following context and caveats:

- ▷ **Mugshots vs. less constrained captures:** The low error rates reported here are attained using mostly excellent cooperative live-capture mugshot images collected with an attendant present. Recognition in other circumstances, particularly those without a dedicated photographic environment and human or automated quality control checks, will lead to declines in accuracy. This is documented here for side-view images, poorer quality webcam images, and, particularly, for newly introduced ATM-style kiosk photos that were not originally intended for automated face recognition. In this case, recognition error rates are much higher, often in excess of 20% even with the more accurate algorithms which variously remain intolerant of face cropping (at image edge) and of large downward head pitch.
- ▷ **Algorithm accuracy spectrum:** Recognition accuracy is very strongly dependent on the algorithm and, more

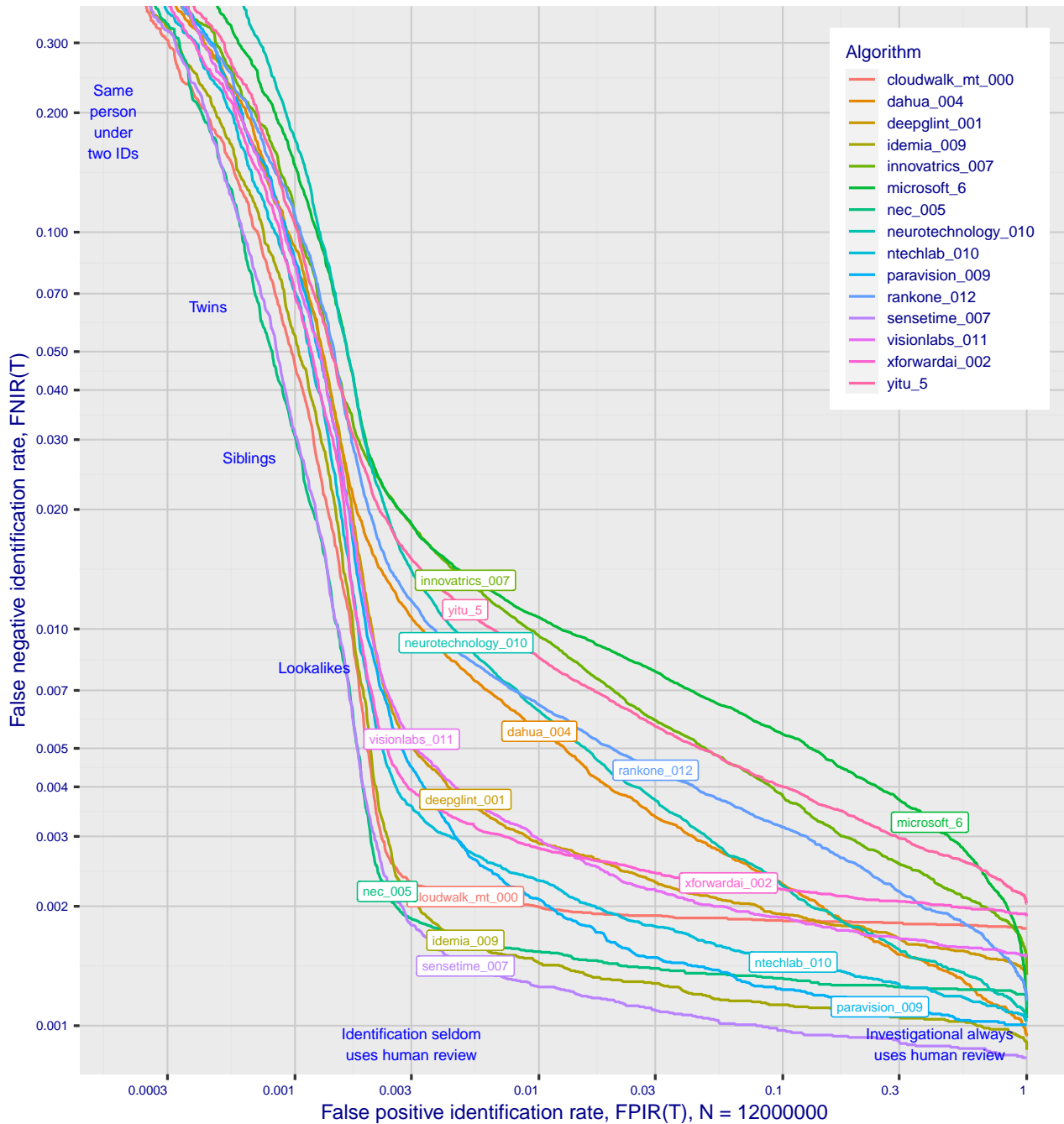


Figure 1: Identification miss rates across the false positive range. $N = 12$ million individuals are enrolled with one recent image.

generally, on the developer of the algorithm. False negative error rates in a particular scenario range from a few tenths of one percent to beyond fifty percent. This is tabulated exhaustively later: For example Table 10 shows accuracy across datasets. Figure 1 here compares algorithms on mugshot searches in a consolidated gallery of 12 million subjects and 12 million photos. Many algorithms do not achieve the low error rates noted above, and while many of those may still be useful and valuable to end-users, only the most accurate excel on poor quality images and those collected long after the initial enrollment sample.

▷ **Versioning:** While results for up to ten algorithms from each developer are reported here, the intra-provider

accuracy variations are usually smaller than the inter-provider variations. That said different versions give an order of magnitude fewer misses. Some developers demonstrate speed-accuracy tradeoffs¹. See Figs. 18, 19.

- ▷ **Low similarity scores:** In thousands of mugshot cases the correct gallery image is returned at rank 1 but its similarity score is nevertheless low, below some operationally required score threshold. This is not so important when face recognition is used for “lead generation” in investigational applications because human reviewers are specifically required to review potentially long candidate lists and the threshold is effectively 0. In applications where search volumes are higher and labor is not available to review the results from searches, a higher threshold must be applied. This reduces the length of candidate lists and false positive identification rates at the expense of increased false negative miss rates. The tradeoff between the two error rates is reported extensively later.
- ▷ **Population size:** As the number of enrolled subjects grows, some mates are displaced from rank one, decreasing accuracy. As tabulated later for N up to 12 million, false negative rates generally rise slowly with population size. This enables use of face recognition in very large populations. However in most positive and negative identification applications², a score threshold is set to limit the rate at which non-mate searches produce false positives. This has the consequence that some mated searches will report the mate below threshold, i.e. a miss, even if it is at rank 1. The utility of this is that many non-mated searches will return no candidate identities at all. As the error-tradeoff characteristic shows, investigational miss rates on the right side are very low but then rise steadily (in the center region) as threshold is increased to support “lights-out” applications, and ultimately rise quickly (left side) as discussed below. Thus, if we demand that just one in one thousand non-mate searches produce any false positives, the most accurate algorithms there (Sensetime-004 and NEC-3) would fail on between 3 and 5% of mated searches. Even though the graph shows results for the most accurate algorithms, all but two would fail to find the mate in more than 8% of mated searches. While the two most accurate algorithms produce a relatively flat error tradeoff until the threshold is raised to limit false positives to about 1 in 400 non-mated searches³.

Thereafter, as the threshold is raised to further reduce false positives, miss rates rise rapidly. This means that low false positive identification rates are inaccessible with these algorithms, a result that does not apply for ten-finger identification algorithms. The rapid rise occurs because the lower mate scores are mixed with very high non-mate scores, the low scores from poor image quality and ageing, the high non-mates from the presence of lookalikes persons (doppelgangers), twins (discussed next) and, ultimately, the presence of a few unconsolidated subjects i.e. persons present under multiple IDs.

- ▷ **False negatives from ageing:** A large source of error in long-run applications where subjects are not re-enrolled on a set schedule is ageing. Changes in facial appearance increase with the time elapsed between photographs. These will depress similarity scores and eventually cause false negatives. All faces age and while this usually proceeds in a graceful and progressive manner, drug use can accelerate this [28]. Elective surgery may be effective in delaying it although this has not been formally quantified with face recognition. As ageing is essentially unavoidable, it can only be mitigated by scheduled re-capture, as in passport re-issuance. To quantify ageing effects, we used the more accurate algorithms to enroll the earliest image of 3.1 million adults and then search

¹For example, NEC-0 prepares templates much faster than NEC-2 but gives twenty times more misses. Dermalog-5 executes a template search much more quickly than Dermalog-6 but is also much less accurate.

²In a positive identification application such as a registered traveler system, a user is making an implicit claim to be enrolled in the system - most users will be. In a negative application, such as with deportees, the implicit claim is that the subject is not enrolled - most will not be.

³The gallery size here is 12 million people, one image per person. Given 331 201 non-mated searches, an exhaustive implementation of one-too-many search would execute almost 4 trillion comparisons. At a false positive identification rate of 0.0025 the number of false positives is, to first order, 828 corresponding to single-comparison false match rate of $828 / 4 \text{ trillion} = 2.1 \times 10^{-10}$ i.e. about 1 in 5 billion. Strictly this FMR computation is meaningful only for algorithms that implement 1:N search using N 1:1 comparisons, which is not always the case.

with 10.3 million newer photos taken up to 18 years after the initial enrollment photo. Figure 2 puts ageing into context by contrasting it with the increase in false negatives that occurs when the number of individuals in an enrollment database becomes larger and the chance of a false positive increases such that higher thresholds may become necessary⁴.

The Figure shows, from top to bottom, increases in false negative identification rates (FNIR) with the algorithm being tested. This applies to increases due to N on the left side, and increases due to ageing on the right side. The relative spacing of the dots shows that for all algorithms the dependency of FNIR on N (up to 12 million) is considerably less than on ΔT (up to 18 years).

In the inset table, accuracy is seen to degrade progressively with time, as mate scores decline and non-mates displace mates from rank 1 position. More accurate algorithms tend to be less sensitive to ageing. The more accurate algorithms give fewer errors after 18 years of ageing than middle tier algorithms give after four. Note also we do not quantify an ageing rate - more formal methods [2] borrowed from the longitudinal analysis literature have been published for doing so (given suitable repeated measures data). See Figures 60, 83 and 95.

⁴Some algorithms implement strategies to automatically adjust scores to account for increased population size. This relieves the system owner of having to increase thresholds as N increases.

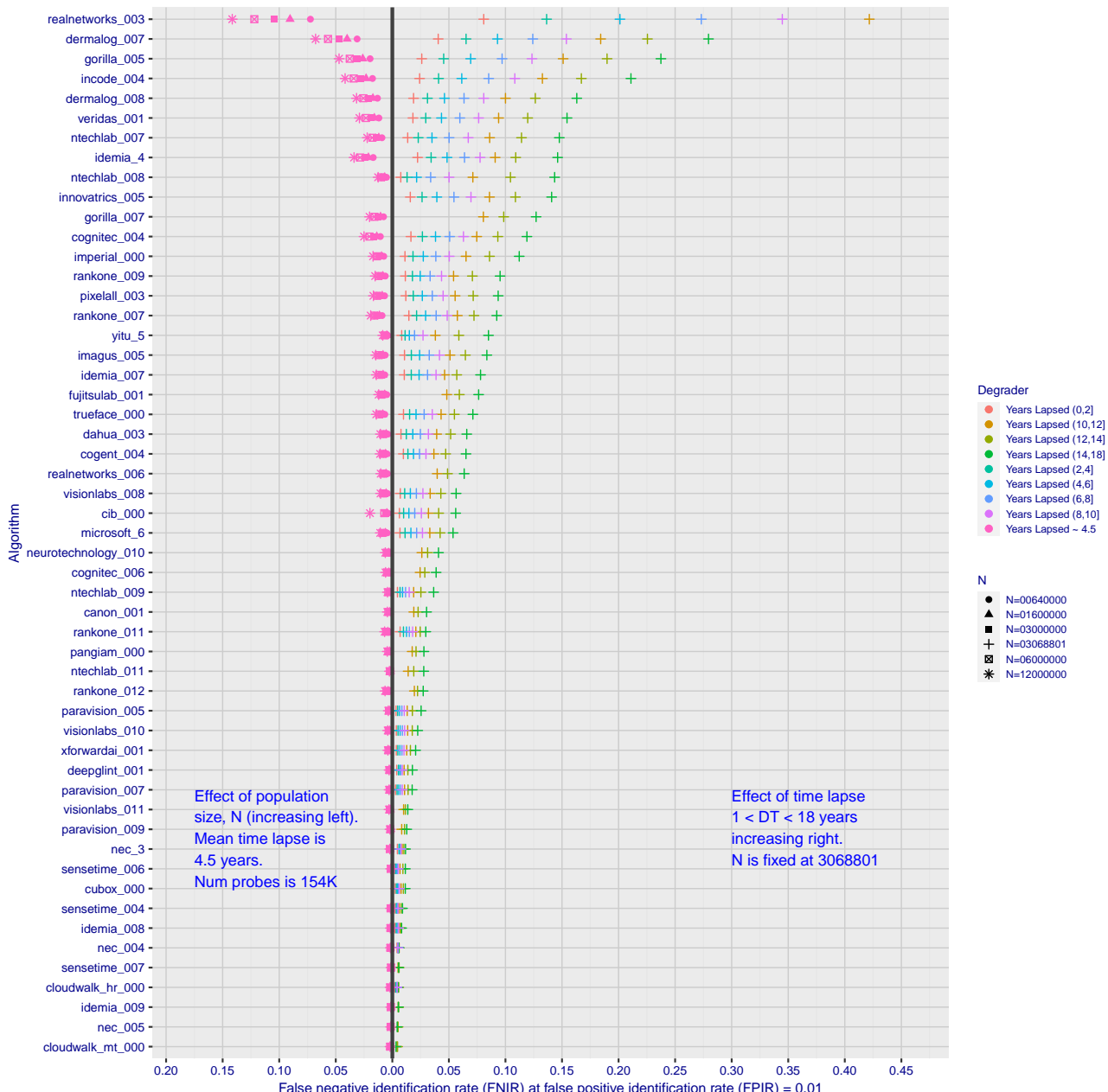


Figure 2: Identification miss rates as a function of enrolled population size, N , and time-lapse, ΔT .

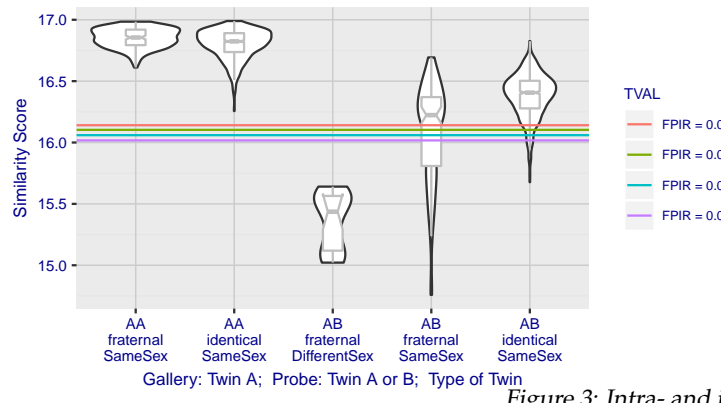


Figure 3: Intra- and inter-twin scores

▷ **False positives from twins:** By enrolling 640 000 mugshots, adding photos of one twin, and then searching photos of those subjects and their twin the inset figure shows, for one typical algorithm, the similarity is generally greater when searching twins against themselves (A) than when searching twins against their sibling (B) but very often still above even stringent thresholds i.e. those corresponding to one in one thousand searches producing a false positive. Thus twins will very often produce a high-scoring non-match on a candidate list and a false alarm in an online identification system. The plot of Fig. 3 shows that fraternal twins are sometimes correctly rejected at those thresholds - including most different sex twins (at center). Figure ?? shows substantially similar behavior for all algorithms tested. In an investigative search, a twin would typically appear at rank 1, or rank 2 if their sibling happened to also be the gallery. Twins (and triplets etc.) constituted 3.3% of all live births [17] in recent years⁵, and because that number is higher today than when the individuals in current adult databases were born, the false positives that arise from twins are now, and will increasingly be, an operational problem. Relative to the United States, twins are born with considerable regional variation. For example they are much less common in East Asia, and much more common in Sub-Saharan Africa [21].

The presence of twins in the mugshot database is inevitable given its size, around 12.3 million people. As this is not an insignificant sample of the domestic United States population, people with other familial ties will be present also. The data was collected over an extended period and because location information is not available, we are unable to estimate the proportion of the domestic population that is present in the dataset. However, if we assume twins are neither more or less disposed to arrest than the general population, we can estimate that hundreds of thousands of individuals in the dataset are twins. This will affect false positive rates because we randomly set aside 331 201 individuals for nonmate searches, and some proportion of those will be twins with siblings in the gallery.

▷ **Database integrity:** An operational error rate should be added to all false negative rates in this report reflecting the proportion of images in a real database that are un-matchable. Such anomalies arise from images that: do not contain a face; include multiple persons; cannot be decoded; are rotated by 90° or 180°; depict a face on clothing; and others introduced by a long tail of various clerical errors. While the mugshot trials in this report have been constructed to minimize such effects, they are a real problem in actual operations.

This report is being updated continuously as new algorithms are submitted to FRVT, and run on new datasets. Participation in the [one-to-many identification track](#) is independent of participation in the [one-to-one verification track](#) of FRVT.

⁵See the CDC's National Vital Statistics Report for 2017: https://www.cdc.gov/nchs/data/nvsr/nvsr67/nvsr67_08-508.pdf

Scope and Context

Audience: This report is intended for developers, integrators, end users, policy makers and others who have some familiarity with biometrics applications. The methods and metrics documented here will be of interest to organizations engaged in tests of face recognition algorithms. Some of these have been incorporated in the ISO/IEC 19795 Part 1 Biometric Testing and Reporting Framework standard, now nearing publication.

Prior benchmarks: Automated face recognition accuracy has improved massively in the two decades since initial commercialization of the various technologies. NIST has tracked that improvement through its conduct of regular independent, free, open, and public evaluations. These have fostered improvements in the state of the art. This report serves as an update to the [NIST Interagency Report 8271](#) on performance of face identification algorithms, published in September 2019.

Demographics: In December 2019, NIST published a first report on demographic dependencies in face recognition, [NIST Interagency Report 8280](#) that documented age, sex and race differentials in one-to-one and one-to-many false positive and false negative rates.

Scope: NIST IR 8271 documented recognition results for four databases containing in excess of 30.2 million still photographs of 14.4 million individuals. That constituted the largest public and independent evaluation of face recognition ever conducted. It includes results for accuracy, speed, investigative vs. identification applications, scalability to large populations, use of multiple images per person, images of cooperative and non-cooperative subjects.

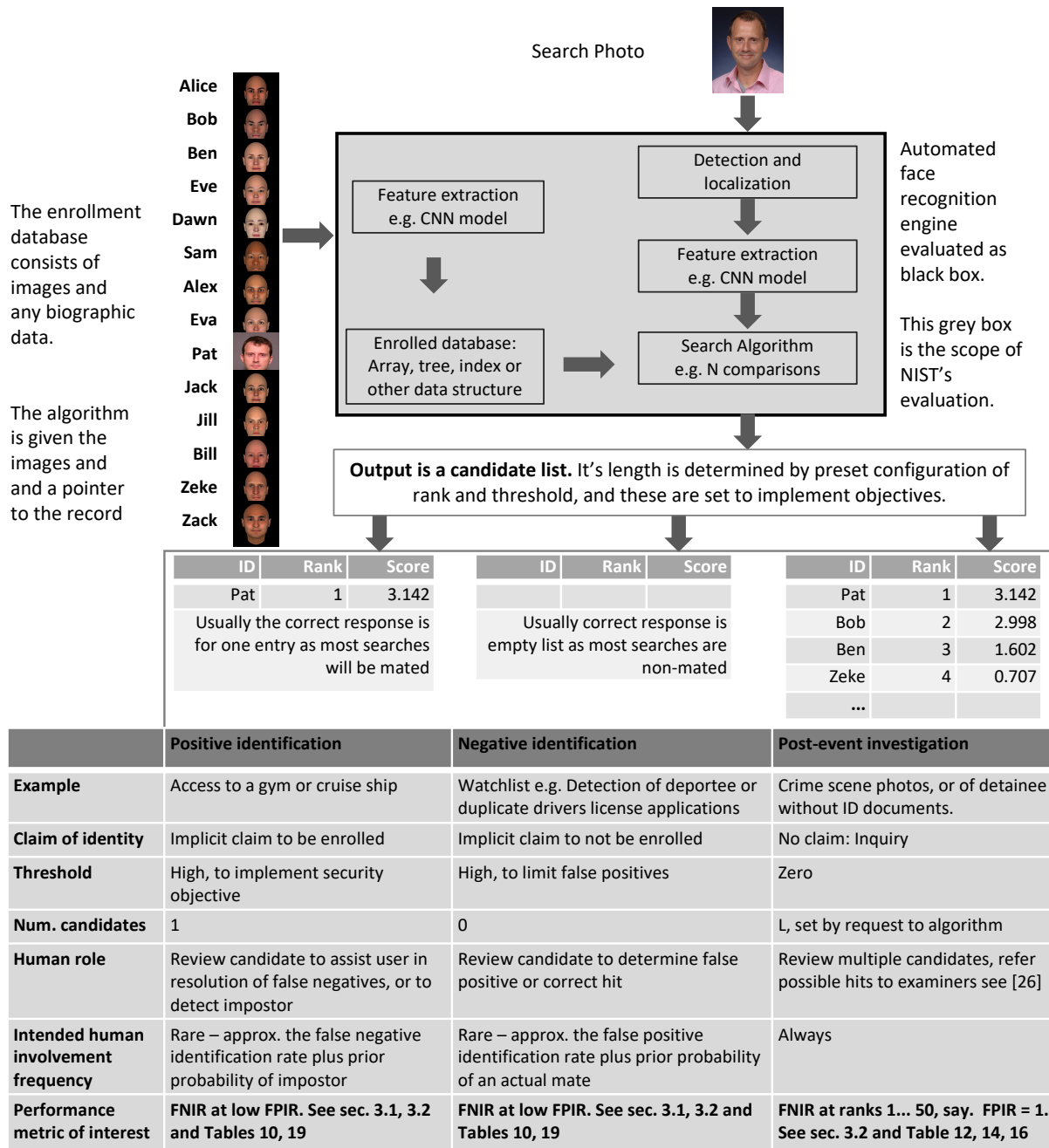
The report also includes results for ageing, recognition of twins, and recognition of profile-view images against frontal galleries. It otherwise does not address causes of recognition failure, neither image-specific problems nor subject-specific factors including demographics. Separate reports on demographic dependencies in face recognition will be published in the future. Additionally out of scope are: performance of live [human-in-the-loop transactional systems](#) like automated border control gates; human recognition accuracy as used in forensic applications; and recognition of persons in video sequences (which NIST evaluated separately [9]). Some of those applications share core matching technologies that *are* tested in this report.

Images: Five kinds of images are employed; these are either compared with images of the same kind, or against others from different capture environments as follows. The primary dataset is a set of law enforcement mugshot images (Fig. 5) which are enrolled and then searched with three kinds of images: other mugshots (i.e. within-domain); profile-view photographs (90 degree cross-view); and lower quality webcam images (Fig. 6) collected in similar detention operations (cross-domain). Additionally we compare high quality visa-like photos collected in immigration offices, with: medium quality border crossing images collected in primary immigration lanes; poor quality images collected in ATM-like registered traveller kiosks.

Participation and industry coverage: The report includes performance figures for prototype algorithms from the research laboratories of commercial developers and a few universities. This represents a substantial majority of the face recognition industry, but only a tiny minority of the academic community. Participation was open worldwide. While there is no charge for participation, developers incur some software engineering expense in implementing their algorithms behind the NIST application programming interface (API). The test is a black-box test where the function of the algorithm, and the intellectual property associated with it, is hidden inside pre-compiled libraries.

Recent technology development: Most face recognition research with deep convolutional neural networks (CNNs) has been aimed at achieving invariance to pose, illumination and expression variations that characterize photojournalism and social media images. The initial research [18, 22] employed large numbers of images of relatively few ($\sim 10^4$) individuals to learn invariance. Inevitably much larger populations ($\sim 10^7$) were employed for training [11, 20] but the benchmark, Labeled Faces in the Wild with (essentially) an equal error rate metric [12], represents an easy task,

one-to-one verification at very high false match rates. While a larger scale identification benchmark duly followed, Megaface [15], its primary metric, rank one hit rate, contrasts with the high threshold discrimination task required in most large-population applications of face recognition, namely credential de-duplication, and background checks. There, identification in galleries containing up to 10^8 individuals must be performed using a) very few images per individual and b) stringent thresholds to afford very low false positive identification rates. This track of FRVT was launched to measure the capability of the new technologies, including in these two cases. FRVT has included open-set identification tests since 2002, reporting both false negative and positive identification rates [7].



Performance metrics for applications: This report documents the performance of one-to-many face recognition algorithms. The word "performance" here refers to recognition accuracy and computational resource usage, as measured

by executing those algorithms on massive sequestered datasets.

This report includes extensive tabulation of recognition error rates germane to the main use-cases for face search technology. The Figure below, inspired by the Figure 1 in [23] differentiates different applications of the technolgy. The last row directs readers to the main tables relevant to those applications, respectively threshold-based and rank-based metrics that are special cases of the metrics given in section 3. The terms negative identification and positive identification are taken from the ISO/IEC 2382-37:2017 standardized biometrics vocabulary.

The algorithms are specifically configured for these applications by setting thresholds and candidate list lengths. Both rank-based metrics and threshold-based metrics include tradeoffs. In investigation, overall accuracy will be reduced if labor is only available to review a few candidates from the automated system. Note that when a fixed number of candidates are returned, the false positive identification rate of the automated face recognition engine will be 100%, because a probe image of anyone not enrolled will still return candidates. In identification applications where false positives must be limited to satisfy reviewer labor availability or a security objective, higher false negative rates are implied. This report includes extensive quantification of this threshold-based tradeoff.

See Sec. 3

Template diversity: The FRVT is designed to evaluate black-box technologies with the consequence that the templates that hold features extracted from face images are entirely proprietary opaque binary data that embed considerable intellectual property of the developer. Despite migration to CNN-based technologies there is no consensus on the optimal feature vector dimension. This is evidenced by template sizes ranging from below 100 bytes to more than four kilobytes. This diversity of approaches, suggests there is no prospect of a standard template something that would require a common feature set to be extracted from faces. Interoperability in automated face recognition remains solidly based on images and documentary standards for those, in particular the ICAO portrait [27] specification deriving from the ISO/IEC 19794-5 Token frontal [24] standard, which are similar to certain ANSI/NIST Type 10 [26] formats.

Training: The algorithms submitted to NIST have been developed using image datasets that developers do not disclose. The development will often include application of machine learning techniques and will additionally involve iterative training and testing cycles. NIST itself does not perform any training and does not refine or alter the algorithm in any way. Thus the model, data files, and libraries that define an algorithm are fixed for the duration of the tests. This reflects typical operational reality where recognition software, once installed, is fixed and constant until upgraded. This situation persists because on-site training of algorithms on customer data is atypical essentially because training is not a turnkey process.

Automated search and human review: Virtually all applications using automated face search require human review of the outputs at some frequency: Always for investigational applications; rarely in positive identification applications, after rejection (false or otherwise); and rarely in negative identification applications, after an alarm (false or otherwise). The human role is usually to compare a reference image with the query image or the live-subject if present, to render either a definitive decision on “exclusion” (different subjects), or “identification” (same subject), or a declaration that one or both images have “no value” and that no decision can be made. Note that automated face recognition algorithms are not built to do exclusion - low scores from a face comparison arise from different faces *and* poor quality images of the same face.

Human reviewers make recognition errors [5, 19, 25] and are sensitive to image acquisition and quality. Accurate human review is supported by high resolution - as specified in the Type 50, 51 acquisition profiles of the ANSI/NIST Type 10 record [26], and by multiple non-frontal views as specified in the same standard. These often afford views of the ear. Organizations involved in image collection should consider supporting human adjudication by collecting high-resolution frontal and non-frontal views, preparing low resolution versions for automated face recognition [24], and retaining both for any subsequent resolution of candidate matches. Along these lines, the ISO/IEC Joint Technical

Committee 1 subcommittee 37 on biometrics has just initiated projects on image quality assessment and face-aware capture.

Release Notes

FRVT Activities: Since February 2017, NIST has been evaluating one-to-one verification algorithms on an ongoing basis. NIST then restarted FRVT's one-to-many track in February 2018, inviting participants to send up to prototype algorithms. Both tracks allows developers to submit updated algorithms to NIST at any time but no more frequently than four calendar months. This more closely aligns development and evaluation schedules. Results are posted to the web within a few weeks of submission. Details and full report are linked from the [Ongoing FRVT site](#).

FRVT Reports: The results of the FRVT appear in the series NIST Interagency Reports tabulated below. The reports were developed separately and released on different schedules. In prior years NIST has mostly reported FRVT results as a single report; this had the disadvantage that results from completed sub-studies were not published until all other studies were complete.

Date	Link	Title	No.
2014-03-20	PDF	FRVT Performance of Automated Age Estimation Algorithms	7995
2015-04-20	PDF	Face Recognition Vendor Test (FRVT) Performance of Automated Gender Classification Algorithms	8052
2014-05-21	PDF	FRVT Performance of face identification algorithms	8009
2017-03-07	PDF	Face In Video Evaluation (FIVE) Face Recognition of Non-Cooperative Subjects	8173
2017-11-23	PDF	The 2017 IARPA Face Recognition Prize Challenge (FRPC)	8197
2018-11-27	PDF	Face Recognition Vendor Test - Part 2: Identification	8271
2019-09-11	PDF	Face Recognition Vendor Test - Part 2: Identification	8271
2019-12-11	PDF	Face Recognition Vendor Test - Part 3: Demographic Effects	8280
2020-01-03	WWW	Face Recognition Vendor Test (FRVT) - Part 1 Verification	Draft

Details appear on pages linked from <https://www.nist.gov/programs-projects/face-projects>.

Appendices: This report is accompanied by appendices which present exhaustive results on a per-algorithm basis. These are machine-generated and are included because the authors believe that visualization of such data is broadly informative and vital to understanding the context of the report.

Typesetting: Virtually all of the tabulated content in this report was produced automatically. This involved the use of scripting tools to generate directly type-settable L^AT_EX content. This improves timeliness, flexibility, maintainability, and reduces transcription errors.

Graphics: Many of the Figures in this report were produced using the **ggplot2** package running under **R**, the capabilities of which extend beyond those evident in this document.

Contents

Release Notes	1
Disclaimer	5
Institutional Review Board	5
Acknowledgments	5
Executive Summary	6
Scope and Context	12
Release Notes	16
1 Introduction	18
2 Evaluation datasets	19
3 Performance metrics	25
4 Results	41
Appendices	78
A Accuracy on large-population FRVT 2018 mugshots	78
B Effect of time-lapse: Accuracy after face ageing	123
C Effect of enrolling multiple images	184
D Accuracy with poor quality webcam images	191
E Accuracy for profile-view to frontal recognition	201
F Search duration	205
G Gallery Insertion Timing	212

1 Introduction

One-to-many identification represents the largest market for face recognition technology. Algorithms are used across the world in a diverse range of biometric applications: detection of duplicates in databases, detection of fraudulent applications for credentials such as passports and driving licenses, token-less access control, surveillance, social media tagging, lookalike discovery, criminal investigation, and forensic clustering.

This report contains a breadth of performance measurements relevant to many applications. Performance here refers to accuracy and resource consumption. In most applications, the core accuracy of a facial recognition algorithm is the most important performance variable. Resource consumption will be important also as it drives the amount of hardware, power, and cooling necessary to accommodate high volume workflows. Algorithms consume processing time, they require computer memory, and their static template data requires storage space. This report documents these variables.

1.1 Open-set searches

FRVT tested open-set identification algorithms. Real-world applications are almost always “open-set”, meaning that some searches have an enrolled mate, but some do not. For example, some subjects have truly not been issued a visa or drivers license before; some law enforcement searches are from first-time arrestees⁶. In an “open-set” application, algorithms make no prior assumption about whether or not to return a high-scoring result, and for a mated search, the ideal behaviour is that the search produces the correct mate at high score and first rank. For a non-mate search, the ideal behavior is that the search produces zero high-scoring candidates.

Many academic benchmarks execute only closed-set searches. The proportion of mates found in the rank one position is the default accuracy metric. This hit rate metric ignores the score with which a mate is found; weak hits count as much as strong hits. This ignores the real-world imperative that in many applications it is necessary to elevate a threshold to reduce the number of false positives.

⁶Operationally closed-set applications are rare because it is usually not the case that all searches have an enrolled mate. One counter-example, however, is a cruise ship in which all passengers are enrolled and all searches should produce exactly one identity. Another example is forensic identification of dental records from an aircraft crash.

2 Evaluation datasets

This report documents accuracy for four kinds of images - mugshots, webcam, profiles and wild - as described in the following sections.

2.1 Immigration-related images

This report includes benchmark tests sharing a common enrollment of high quality frontal portrait images collected while subject make applications for various immigration benefits. We then search that with two kinds of images, webcam images collected during in-bound immigration and also images collected from registered travelers using a ATM-style kiosk. These are described below and depicted in Figure 4.



Figure 4: Example photos.

- ▷ **Application reference photos:** The images are collected in an attended interview setting using dedicated capture equipment and lighting. The images, at size 300x300 pixels, are smaller than normally indicated by ISO. The images are all high-quality frontal portraits collected in immigration offices and with a white background. As such, potential quality related drivers of high false match rates (such as blur) can be expected to be absent. The images are encoded as ISO/IEC 10918-1 i.e. JPEG. Older images had a compression ration of about 16:1, while newer images, since 2010, are more lightly compressed at 4:1. When these images are provided as input into the algorithm, they are labeled with the type "iso". This report enrols 1 600 000 application images, one per person.
- ▷ **Border crossing photos:** Most images are have width 320 and height 240 pixels. They are JPEG compressed at 16:1 i.e. filesize just below 15KB. The images present challenges for face recognition in that subjects often exhibit non-zero yaw and pitch (associated with the rotational degrees of freedom of the camera mount), low contrast (due to varying and intense background lights), and poor spatial resolution (due to inexpensive cameras). There are often subjects standing in the background, usually at very low resolution (see Figure 4b). In such cases, algorithms should detect all faces and determine which is the largest and most centered. When these images are provided as input into the algorithm, they are labeled with the type "wild".
- ▷ **Kiosk photos:** These photos were collected from subjects whose attention was focused on interaction with an immigration kiosk. They images were not intended for use with automated face recognition. The camera is situated above a display which the user touches, and is triggered either without directing the subject to look at it, or without waiting for the subject to comply. The images are therefore characterized by pitch-down pose, sometimes exceeding 45 degrees, as in Figure 4c. Yaw-angle variation is mild, with most images close to frontal. The images

have width 320 pixels and height 240 pixels and therefore tall individuals are sometimes cropped. This is often just above the eyes and can occur at the nose or mouth. Conversely, short individuals are sometimes cropped such that only the top part of the face is visible. In a quite small number of cases, there other subjects standing just behind the primary subject such that algorithms should detect all faces and determine which is the largest and most centered. Background ceiling lighting is often visible and this sometimes leads to under-exposure of the face. When these images are provided as input into the algorithm, they are labeled with the type "wild".

2.2 Law enforcement images

The main mugshot dataset used is referred to as the FRVT 2018 set. This set was collected over the period 2002 to 2017 in routine United States law enforcement operations. This set yields three subsets

- ▷ **Mugshots:** Mugshots comprise about 86% of the database. They have reasonable compliance with the ANSI/NIST ITL1-2011 Type 10 standard's subject acquisition profiles levels 10-20 for frontal images [26]. The most common departure from the standard's requirements is the presence of mild pose variations around frontal - the images of Figure 5 are typical. The images vary in size, with many being 480x600 pixels with JPEG compression applied to produce filesizes of between 18 and 36KB with many images outside this range, implying that about 0.5 bits are being encoded per pixel. When these images are provided as input into the algorithm, they are labeled with the type "mugshot".

Example images appear in Fig. 5

[NIST Interagency Report 8238](#) includes a comparison of this set of mugshots with the smaller and easier sets of mugshots used in tests run in 2010 and 2014.

- ▷ **Profile images:** Profile-view images have been collected in law enforcement for more than 100 years, as human capability is improved with orthogonal information. The profile images used in this report were collected during the same session as the frontal mugshot photograph, in the same standardized photographic setup. These would not therefore be used with automated face recognition. A small subset, 200 000 images, were set aside for testing. When these images are provided as input into the algorithm, they are labeled with the type "wild".

Example images appear in Fig. 7

- ▷ **Webcam images:** The remaining 14% of the images were collected using an inexpensive webcam attached to a flexible operator-directed mount. These images are all of size 240x240 pixels, that are in considerable violation of most quality-related clauses of all face recognition standards. As evident in the figure, the most common defects are non-frontal pose (associated with the rotational degrees of freedom of the camera mount), low contrast (due to varying and intense background lights), and poor spatial resolution (due to inexpensive camera optics) - see examples in Fig 6. The images are overly JPEG compressed, to between 4 and 7KB, implying that only 0.5 to 1 bits are being encoded per color pixel. When these images are provided as input into the algorithm, they are labeled with the type "wild".

Example images appear in Fig. 6

These are drawn from NIST Special Database 32 which may be downloaded [here](#).

These images were partitioned in galleries and probesets for the various experiment listed in Table 1.

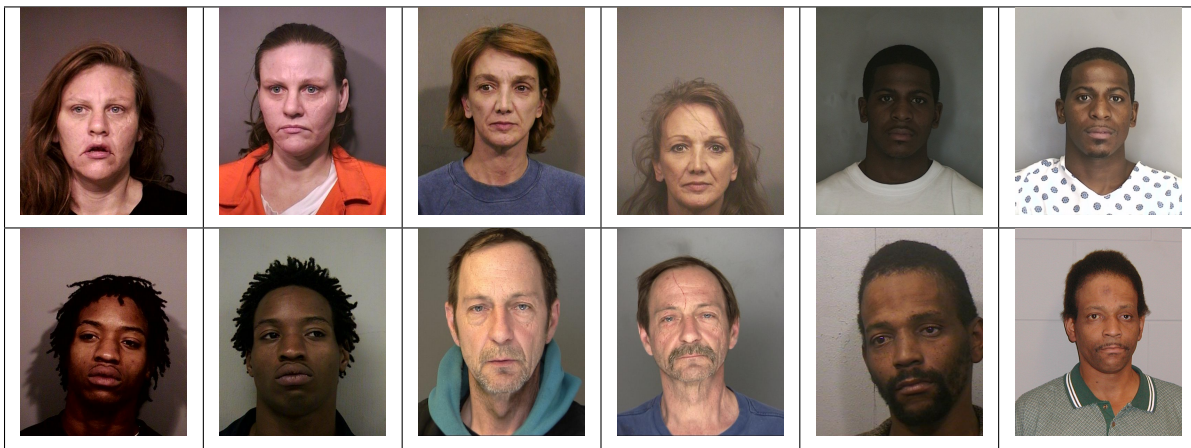


Figure 5: Six mated mugshot pairs representative of the FRVT-2014 (LEO) and FRVT-2018 datasets. The images are collected live, i.e. not scanned from paper. Image source: NIST Special Database 32 the Multiple Encounter Deceased Subjects dataset.



Figure 6: Twelve webcam images representative of probes against the FRVT-2018 mugshot gallery. The first eight images are four mated pairs. Such images present challenges to recognition including pose, non-uniform illumination, low contrast, compression, cropping, and low spatial sampling rate. Image source: NIST Special Database 32 the Multiple Encounter Deceased Subjects dataset.



Figure 7: **[Profile views]** The three images are a frontal enrollment, subsequent frontal probe, and same-session ninety degree profile view. While collection of both frontal and profile views has been typical in law enforcement for more than a century, the recognition of profile to frontal views has essentially been impossible. However, reasonably high accuracy results is now possible - see section E.

Image				
Encounter	1	...	$K_i - 1$	K_i
Capture Time	T_1	...	T_{K_i-1}	T_{K_i}
Role RECENT	Not used	Not used	Enrolled	Search
Role LIFETIME	Enrolled	Enrolled	Enrolled	Search

Figure 8: Depiction of the “recent” and “lifetime” enrollment types. Image source: NIST Special Database 32

2.3 Enrollment strategies

Many operational applications include collection and enrollment of biometric data from subjects on more than one occasion. This might be done on a regular basis, as might occur in credential (re-)issuance, or irregularly, as might happen in a criminal recidivist situation [4]. The number of images per person will depend on the application area. In civil identity credentialing (e.g. passports, driver’s licenses), the images will be acquired approximately uniformly over time (e.g. ten years for a passport). While the distribution of dates for such images of a person might be assumed uniform, a number of factors might undermine this assumption⁷. In criminal applications, the number of images would depend on the number of arrests. The distribution of dates for arrest records for a person (i.e. the recidivism distribution) has been modeled using the exponential distribution but is recognized to be more complicated⁸.

In any case, the 2010 NIST evaluation of face recognition showed that considerable accuracy benefits accrue with retention and use of *all* historical images [6].

To this end, the FRVT API document provides $K \geq 1$ images of an individual to the enrollment software. The software is tasked with producing a single proprietary undocumented “black-box” template⁹ from the K images. This affords the algorithm an ability to generate a *model* of the individual, rather than to simply extract features from each image on a sequential basis.

As depicted in Figure 8, the i -th individual in the FRVT 2018 dataset has K_i images. These are labelled as x_k for $k = 1 \dots K_i$ in chronological order of capture date. To measure the utility of having multiple enrollment images, this report evaluates three kinds of enrollment:

- ▷ **Recent:** Only the second most recent image, x_{K_i-1} is enrolled. This strategy of enrollment mimics the operational policy of retaining the imagery from the most recent encounter. This might be done operationally to ameliorate the effects of face ageing. Obviously retaining only the most recent image should only be done if the identity of the person is trusted to be correct. For example, in an access control situation retention of the most recent successful *authentication* image would be hazardous if it could be a false positive.
- ▷ **Lifetime-consolidated:** All but the most recent image are enrolled, $x_1 \dots x_{K_i-1}$. This subject-centric strategy might be adopted if quality variations exist where an older image might be more suitable for matching, despite the ageing effect.

⁷For example, a person might skip applying for a passport for one cycle, letting it expire. In addition, a person might submit identical images (from the same photography session) to consecutive passport applications at five year intervals.

⁸A number of distributions have been considered to model recidivism, see for example [3].

⁹There are no formal face template standards. Template standards only exist for fingerprint minutiae - see ISO/IEC 19794-2:2011.

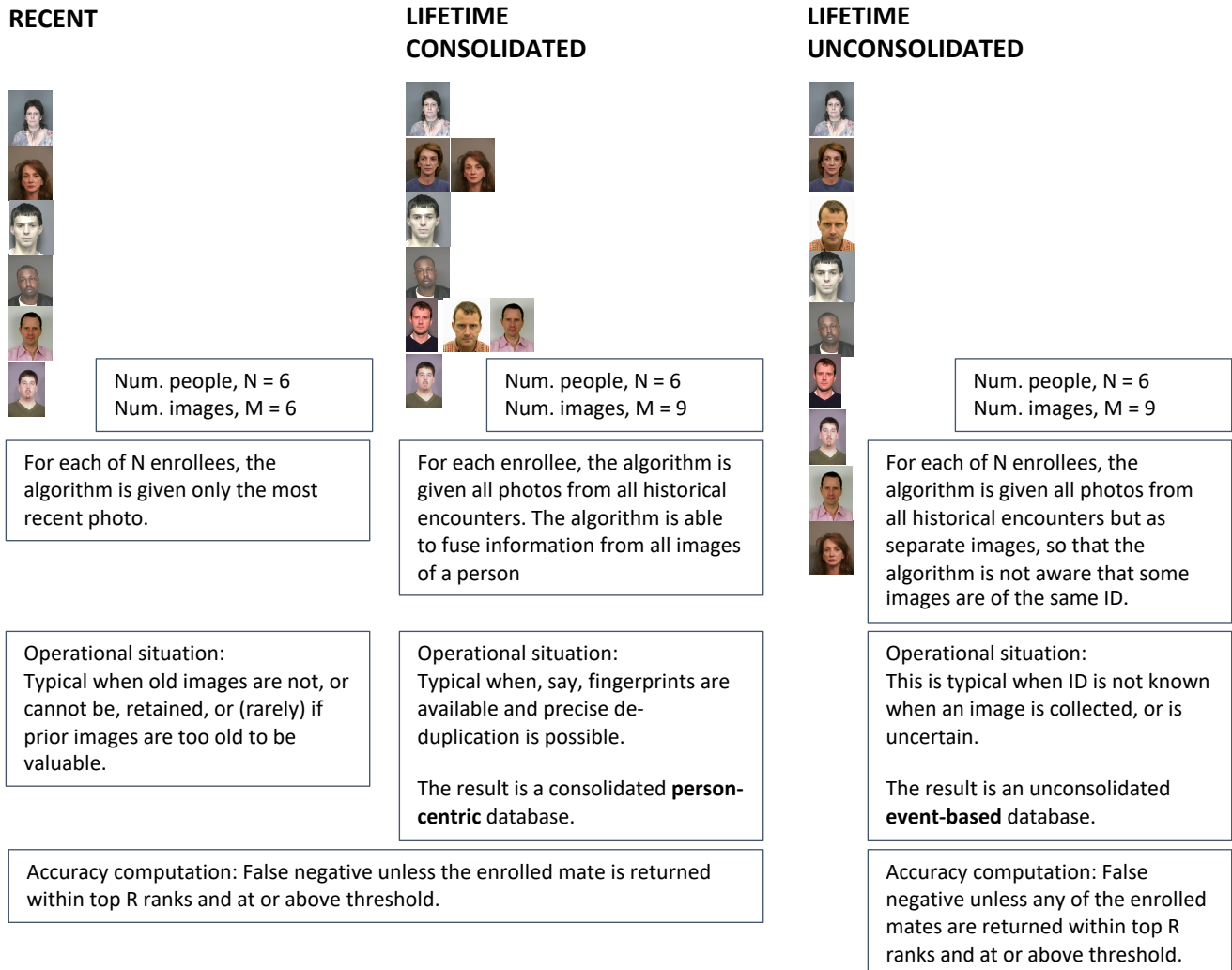


Figure 9: Enrollment strategies. The figure shows the three kinds of enrollment databases examined in this report. Image source: NIST Special Database 32

	ENROLLMENT				SEARCH			
	TYPE SEE SECTION 2.3	POPULATION FILTER	N-SUBJECTS	N-IMAGES	MATE N-SUBJECTS	NON-MATE N-IMAGES	N-SUBJECTS	N-IMAGES
Mugshot trials from enrollment of single images								
1	RECENT	NATURAL	640 000	640 000	154 549	154 549	331 254	331 254
2	RECENT	NATURAL	1 600 000	1 600 000				
3	RECENT	NATURAL	3 000 000	3 000 000				
4	RECENT	NATURAL	6 000 000	6 000 000				
5	RECENT	NATURAL	12 000 000	12 000 000				
Cross-domain								
13	MUGSHOTS AS ON ROW 2				82 106 WEBCAM	82 106 WEBCAM	331 254 WEBCAM	331 254 WEBCAM
Cross-view								
14	MUGSHOTS AS ON ROW 2				100 000 PROFILE	100 000 PROFILE	100 000 PROFILE	100 000 PROFILE
Mugshot ageing								
17	OLDEST	NATURAL	3 068 801	3 068 801	2 853 221	10 951 064	0	0
Border crossing ageing								
17	OLDEST	NATURAL	1 600 000	1 600 000	903 655	1 922 393	1 393 076	1 680 000
Visa-border								
19	PRIOR	NATURAL	1 600 000 VISA	1 600 000 VISA	80 000 BORDER	80 000 BORDER	80 000 BORDER	80 000 BORDER
20	VISA AS ON ROW 18				21 016 BORDER	21 016 BORDER	21 016 BORDER	21 016 BORDER

Table 1: Enrollment and search sets. Each row summarizes one identification trial. Unless stated otherwise, all entries refer to mugshot images. The term “natural” means that subjects were selected without heed to demographics, i.e. in the distribution native to this dataset. The probe images were collected in a different calendar year to the enrollment image. Missing values in rows 2-12 are the same as in row 1.

▷ **Lifetime-unconsolidated:** Again all but the most recent image are enrolled $x_1 \dots x_{K_i-1}$ but now separately, with different identifiers, such that the algorithm is not aware that the images are from the same face. This kind of event- or encounter-centric enrollment is very common when operational constraints preclude reliable consolidation of the historical encounters into a single identity. This aspect also prevents the recognition algorithm from a) building a holistic model of identity (as is common in speaker recognition systems) and b) implementing fusion, for example template-level fusion of feature vectors, or post-search score-level fusion. The result is that searches will typically yield more than one image of a person in the top ranks. This has consequences for appropriate metrics, as detailed in section 3.2.1

NIST first evaluated this kind of enrollment in mid 2018, and the results tables include some comparison of accuracy available from all three enrollment styles.

In all cases, the most recent image, x_{K_i} , is reserved as the search image. For the 1.6 million subject enrollment partition of the FRVT 2018 data, $1 \leq K_i \leq 33$ with $K_i = 1$ in 80.1% of the individuals, $K_i = 2$ in 13.4%, $K_i = 3$ in 3.7%, $K_i = 4$ in 1.4%, $K_i = 5$ in 0.6%, $K_i = 6$ in 0.3%, and $K_i > 6$ is 0.2% for everyone else. This distribution is substantially dependent on United States recidivism rates.

We did not evaluate the case of retaining only the highest quality image, since automated quality assessment is out of scope for this report. We do not anticipate that such strategies will prove beneficial when the quality assessment apparatus is imperfect and unvalidated.

3 Performance metrics

This section gives specific definitions for accuracy and timing metrics. Tests of open-set biometric algorithms must quantify frequency of two error conditions:

- ▷ **False positives:** Type I errors occur when search data from a person who has never been seen before is incorrectly associated with one or more enrollees' data.
- ▷ **Misses:** Type II errors arise when a search of an enrolled person's biometric does not return the correct identity.

Many practitioners prefer to talk about "hit rates" instead of "miss rates" - the first is simply one minus the other as detailed below. Sections 3.1 and 3.2 define metrics for the Type I and Type II performance variables.

Additionally, because recognition algorithms sometimes fail to produce a template from an image, or fail to execute a one-to-many search, the occurrence of such events must be recorded. Further because algorithms might elect to not produce a template from, for example, a poor quality image, these failure rates must be combined with the recognition error rates to support algorithm comparison. This is addressed in section 3.5.

Finally, section 3.7 discusses measurement of computation duration, and section 3.8 addresses the uncertainty associated with various measurements. Template size measurement is included with the results.

3.1 Quantifying false positives

It is typical for a search to be conducted into an enrolled population of N identities, and for the algorithm to be configured to return the closest L candidate identities. These candidates are ranked by their score, in descending order, with all scores required to be greater than or equal to zero. A human analyst might examine either all L candidates, or just the top $R \leq L$ identities, or only those with score greater than threshold, T . The workload associated with such examination is discussed later, in 3.6.

False alarm performance is quantified in two related ways. These express how many searches produces false positives, and then, how many false positives are produced in a search.

False positive identification rate: The first quantity, FPIR, is the proportion of non-mate searches that produce an adverse outcome:

$$\text{FPIR}(N, T) = \frac{\text{Num. non-mate searches where one or more enrolled candidates are returned with score at or above threshold}}{\text{Num. non-mate searches attempted.}} \quad (1)$$

Under this definition, FPIR can be computed from the highest non-mate candidate produced in a search - it is not necessary to consider candidates at rank 2 and above. FPIR is the primary measure of Type I errors in this report.

Selectivity: However, note that in any given search, several non-mate may be returned above threshold. In order to quantify such events, a second quantity, selectivity (SEL), is defined as the *number* of non-mates returned on a candidate list, averaged over all searches.

$$\text{SEL}(N, T) = \frac{\text{Num. non-mate enrolled candidates returned with score at or above threshold}}{\text{Num. non-mate searches attempted.}} \quad (2)$$

where $0 \leq \text{SEL}(N, T) \leq L$. Both of these metrics are useful operationally. FPIR is useful for targeting how often an

adverse false positive outcome can occur, while SEL as a number is related to workload associated with adjudicating candidate lists. The relationship between the two quantities is complicated - it depends on whether an algorithm concentrates the false alarms in the results of a few searches or whether it disburses them across many. This was detailed in FRVT 2014, NISTIR 8009. It has not yet been detailed in FRVT 2018.

3.2 Quantifying hits and misses

If L candidates are returned in a search, a shorter candidate list can be prepared by taking the top $R \leq L$ candidates for which the score is above some threshold, $T \geq 0$. This reduction of the candidate list is done because thresholds may be applied, and only short lists might be reviewed (according to policy or labor availability, for example). It is useful then to state accuracy in terms of R and T , so we define a “miss rate” with the general name **false negative identification rate** (FNIR), as follows:

$$\text{FNIR}(N, R, T) = \frac{\text{Num. mate searches with enrolled mate found outside top } R \text{ ranks or score below threshold}}{\text{Num. mate searches attempted.}} \quad (3)$$

This formulation is simple for evaluation in that it does not distinguish between causes of misses. Thus a mate that is not reported on a candidate list is treated the same as a miss arising from face finding failure, algorithm intolerance of poor quality, or software crashes. Thus if the algorithm fails to produce a candidate list, either because the search failed, or because a search template was not made, the result is regarded as a miss, adding to FNIR.

Hit rates, and true positive identification rates: While FNIR states the “miss rate” as how often the correct candidate is either not above threshold or not at good rank, many communities prefer to talk of “hit rates”. This is simply the **true positive identification rate**(TPIR) which is the complement of FNIR giving a positive statement of how often mated searches are successful:

$$\text{TPIR}(N, R, T) = 1 - \text{FNIR}(N, R, T) \quad (4)$$

This report does not report true positive “hit” rates, preferring false negative miss rates for two reasons. First, costs rise linearly with error rates. For example, if we double FNIR in an access control system, then we double user inconvenience and delay. If we express that as decrease of TPIR from, say 98.5% to 97%, then we mentally have to invert the scale to see a doubling in costs. More subtly, readers don’t perceive differences in numbers near 100% well, becoming inured to the “high nineties” effect where numbers close to 100 are perceived indifferently.

Reliability is a corresponding term, typically being identical to TPIR, and often cited in automated (fingerprint) identification system (AFIS) evaluations.

An important special case is the **cumulative match characteristic**(CMC) which summarizes accuracy of mated-searches only. It ignores similarity scores by relaxing the threshold requirement, and just reports the fraction of mated searches returning the mate at rank R or better.

$$\text{CMC}(N, R) = 1 - \text{FNIR}(N, R, 0) \quad (5)$$

We primarily cite the complement of this quantity, $\text{FNIR}(N, R, 0)$, the fraction of mates *not* in the top R ranks.

The **rank one hit rate** is the fraction of mated searches yielding the correct candidate at best rank, i.e. $\text{CMC}(N, 1)$. While this quantity is the most common summary indicator of an algorithm’s efficacy, it is not dependent on similarity scores, so it does not distinguish between strong (high scoring) and weak hits. It also ignores that an adjudicating reviewer is often willing to look at many candidates.

3.2.1 False negative rates for unconsolidated galleries

As detailed in section 2.3 a common type of gallery, here referred to as the lifetime unconsolidate type, is populated with all images of an individual without any association between them. That is, the gallery construction algorithm is not provided with any ID labels that would support processing of a person's images jointly. This contrasts with the lifetime consolidate type where an algorithm may explicitly fuse features from multiple images of a person, or select a best image. In such cases, where the number of enrolled images is a random variable, we define two false negative rates as follows.

The first demands that the algorithm place any of the K_i mates in the top $R \geq 1$ ranks. The proportion of searches for which this does not occur forms a false negative identification rate:

$$\text{FNIR}_{\text{any}}(N, R, T) = 1 - \frac{\text{Num. mate searches where any enrolled mate is found in the top } R \text{ ranks and at-or-above threshold}}{\text{Num. mate searches attempted.}} \quad (6)$$

The second demands that the algorithm place all K_i mates in the top $R \geq K_i$ ranks. The proportion of searches for which this does not occur forms a false negative identification rate:

$$\text{FNIR}_{\text{all}}(N, R, T) = 1 - \frac{\text{Num. mate searches where all enrolled mates are found in the top } R \text{ ranks and at-or-above threshold}}{\text{Num. mate searches attempted.}} \quad (7)$$

Placing all mates in the top ranks is a more difficult task than correctly retrieving any image, so it holds that: $\text{FNIR}_{\text{all}} \geq \text{FNIR}_{\text{any}}$. This is evident in the results presented for November 2018 algorithms in Tables starting at ??.

The information retrieval community might prefer to compute and plot *precision* and *recall*; this is a valid approach, but we advance the two metrics above because they relate to our normal definition of consolidated FNIR, and they cover the two extreme use-cases of wanting any hit vs. all hits.

3.3 DET interpretation

In biometrics, a false negative occurs when an algorithm fails to match two samples of one person – a Type II error. Correspondingly, a false positive occurs when samples from two persons are improperly associated – a Type I error.

Matches are declared by a biometric system when the native comparison score from the recognition algorithm meets some threshold. Comparison scores can be either similarity scores, in which case higher values indicate that the samples are more likely to come from the same person, or dissimilarity scores, in which case higher values indicate different people. Similarity scores are traditionally computed by fingerprint and face recognition algorithms, while dissimilarities are used in iris recognition. In some cases, the dissimilarity score is a distance possessing metric properties. In any case, scores can be either mate scores, coming from a comparison of one person's samples, or nonmate scores, coming from comparison of different persons' samples.

The words "genuine" or "authentic" are synonyms for mate, and the word "impostor" is used as a synonym for non-mate. The words "mate" and "nonmate" are traditionally used in identification applications (such as law enforcement search, or background checks) while genuine and impostor are used in verification applications (such as access control).

An error tradeoff characteristic represents the tradeoff between Type II and Type I classification errors. For identification this plots false negative vs. false positive identification rates i.e. FNIR vs. FPIR parametrically with T. Such plots

are often called detection error tradeoff (DET) characteristics or receiver operating characteristic (ROC). These serve the same function – to show error tradeoff – but differ, for example, in plotting the complement of an error rate (e.g. $TPIR = 1 - FNIR$) and in transforming the axes, most commonly using logarithms, to show multiple decades of FPIR. More rarely, the function might be the inverse of the Gaussian cumulative distribution function.

The slides of Figures 10 through 15 discuss presentation and interpretation of DETs used in this document for reporting face identification accuracy. Further detail is provided in formal biometrics testing standards, see the various parts of ISO/IEC 19795 Biometrics Testing and Reporting. More terms, including and beyond those to do with accuracy, appear in ISO/IEC 2382-37 Information technology – Vocabulary – Part 37: Harmonized biometric vocabulary.

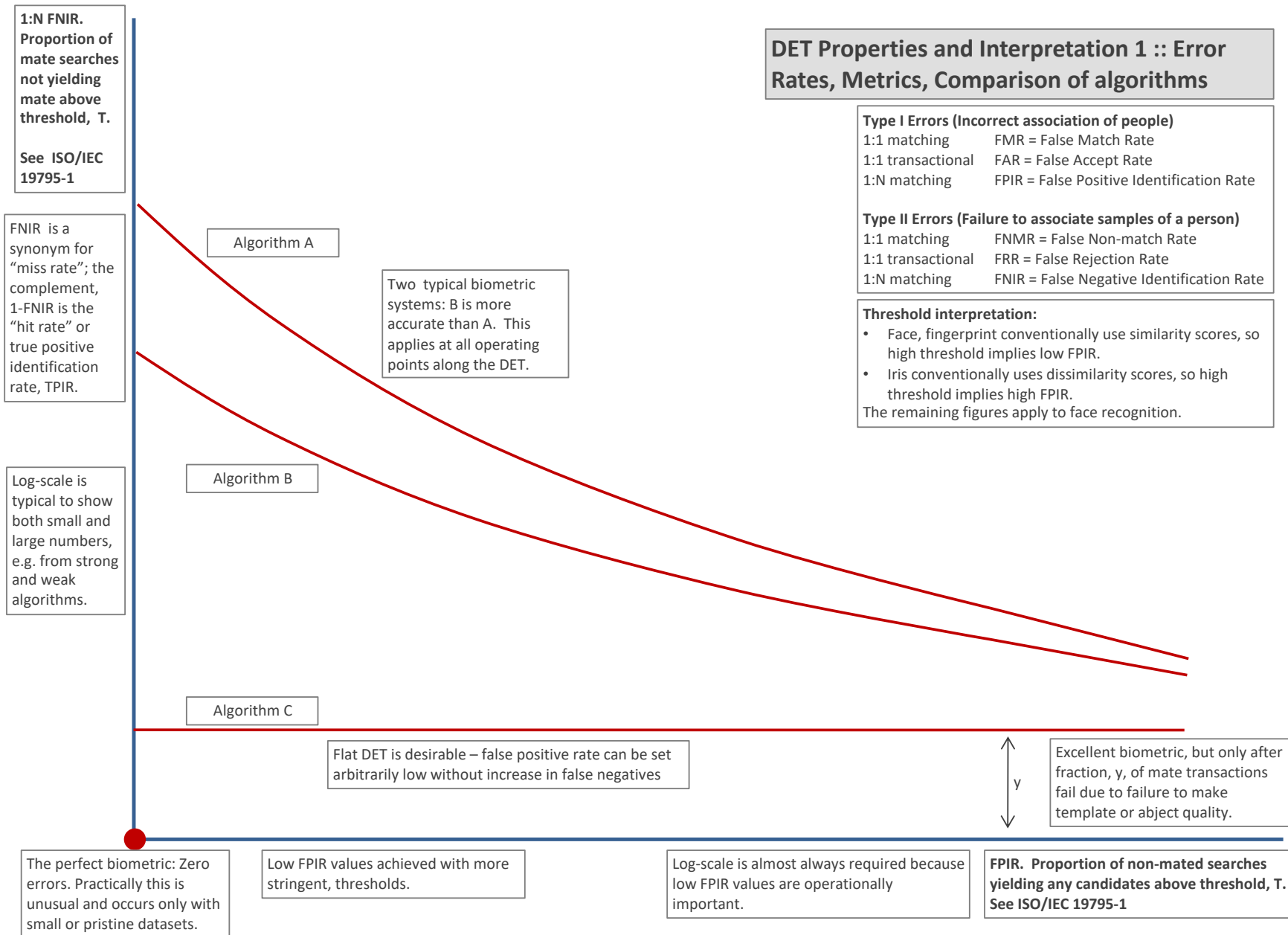


Figure 10: DET as the primary performance reporting mechanism.

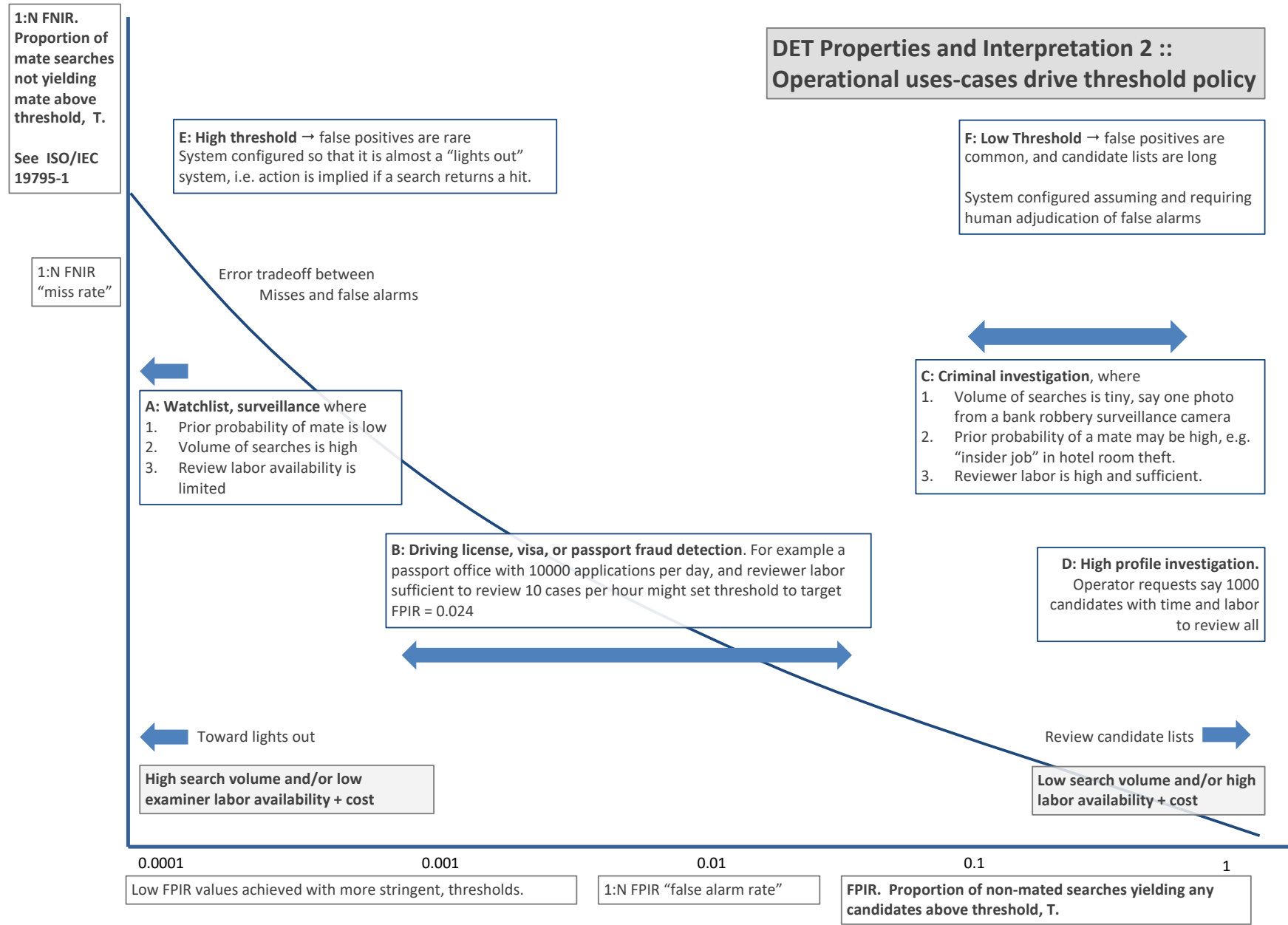
2022/03/30
17:50:48FNIR(N, R, T) = False neg. identification rate
FPIR(N, T) = False pos. identification rate
N = Num. enrolled subjects
R = Num. candidates examined
T = ThresholdT = 0 → Investigation
T > 0 → Identification

Figure 11: DET as the primary performance reporting mechanism.

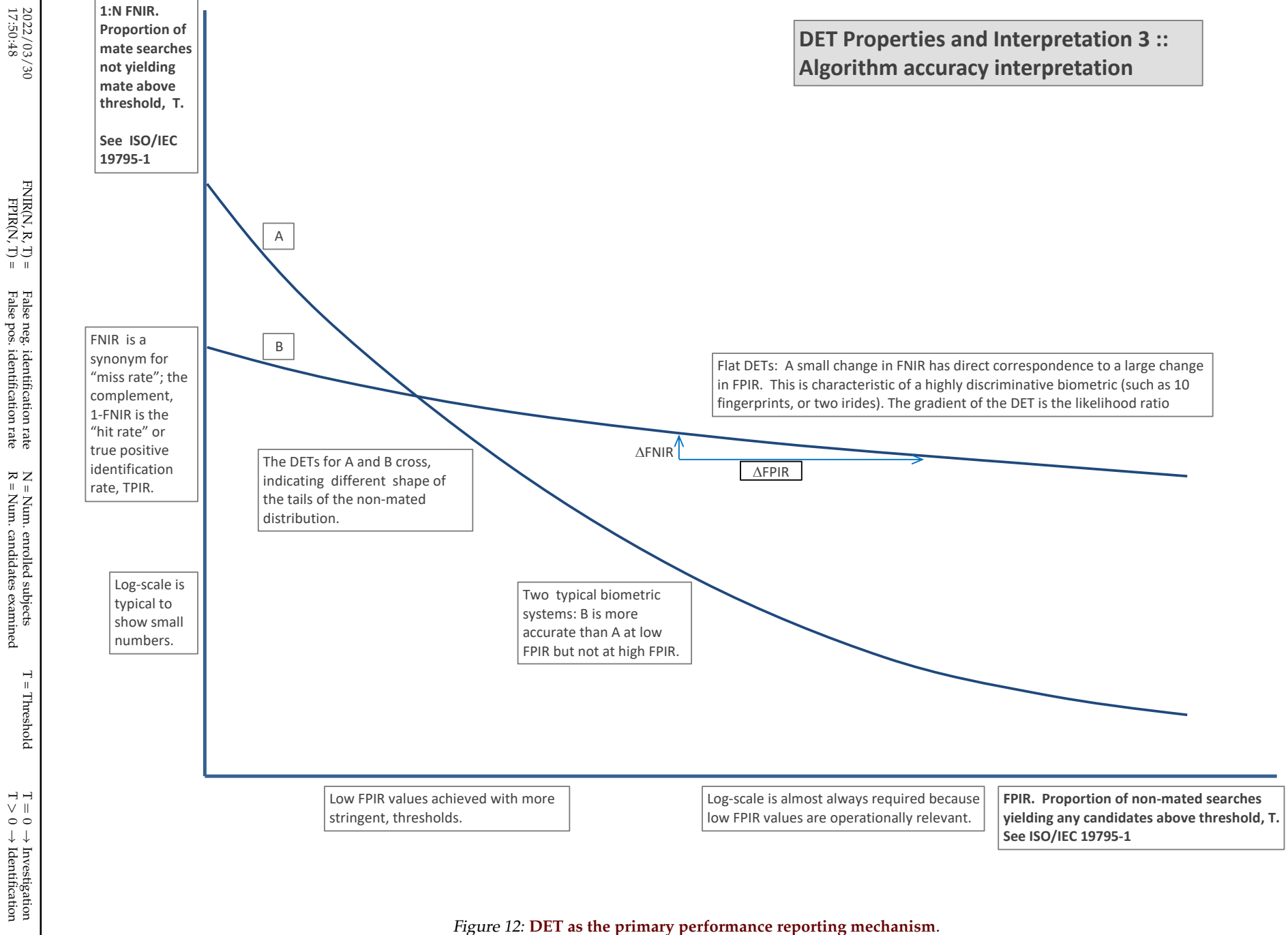


Figure 12: DET as the primary performance reporting mechanism.

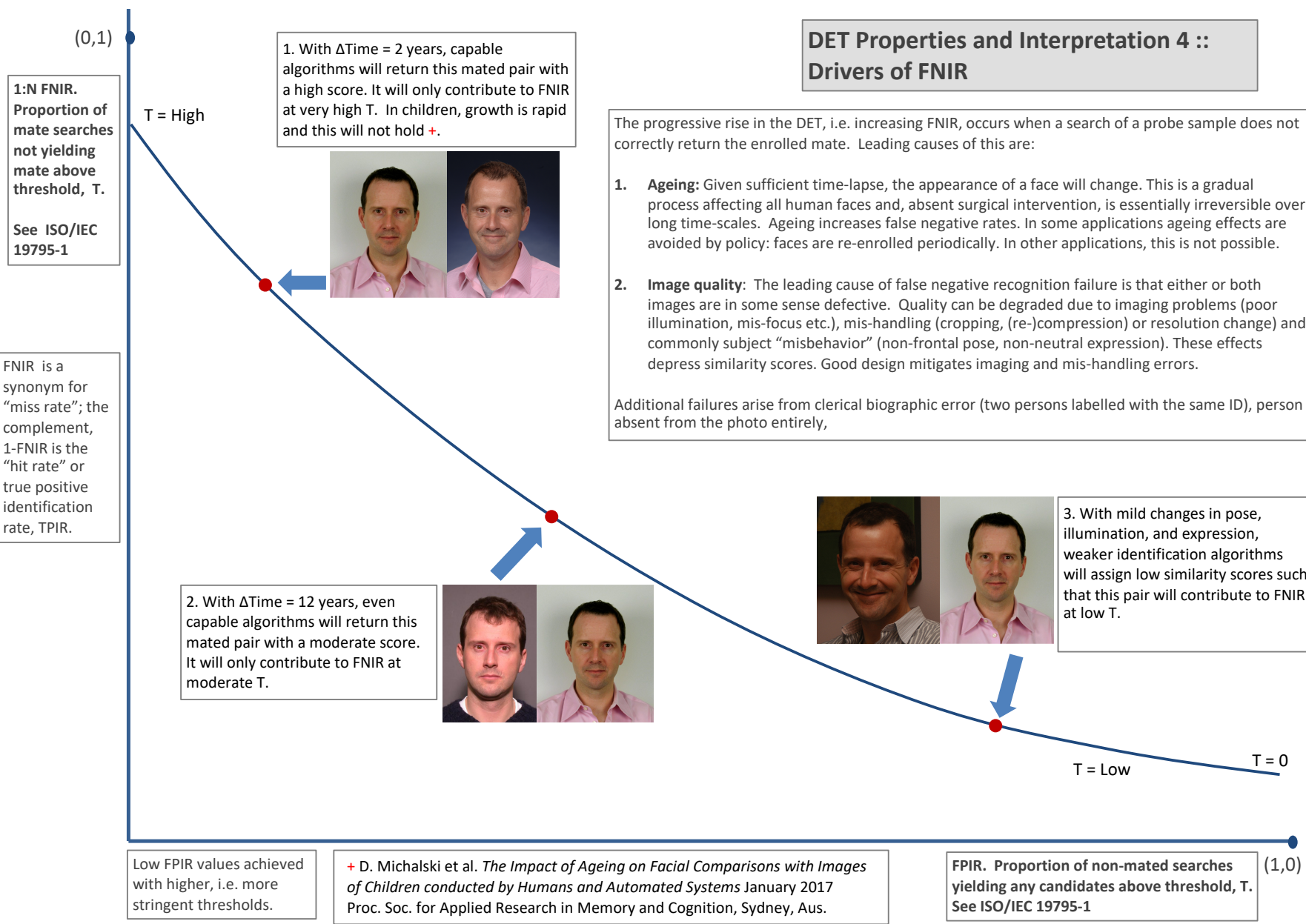
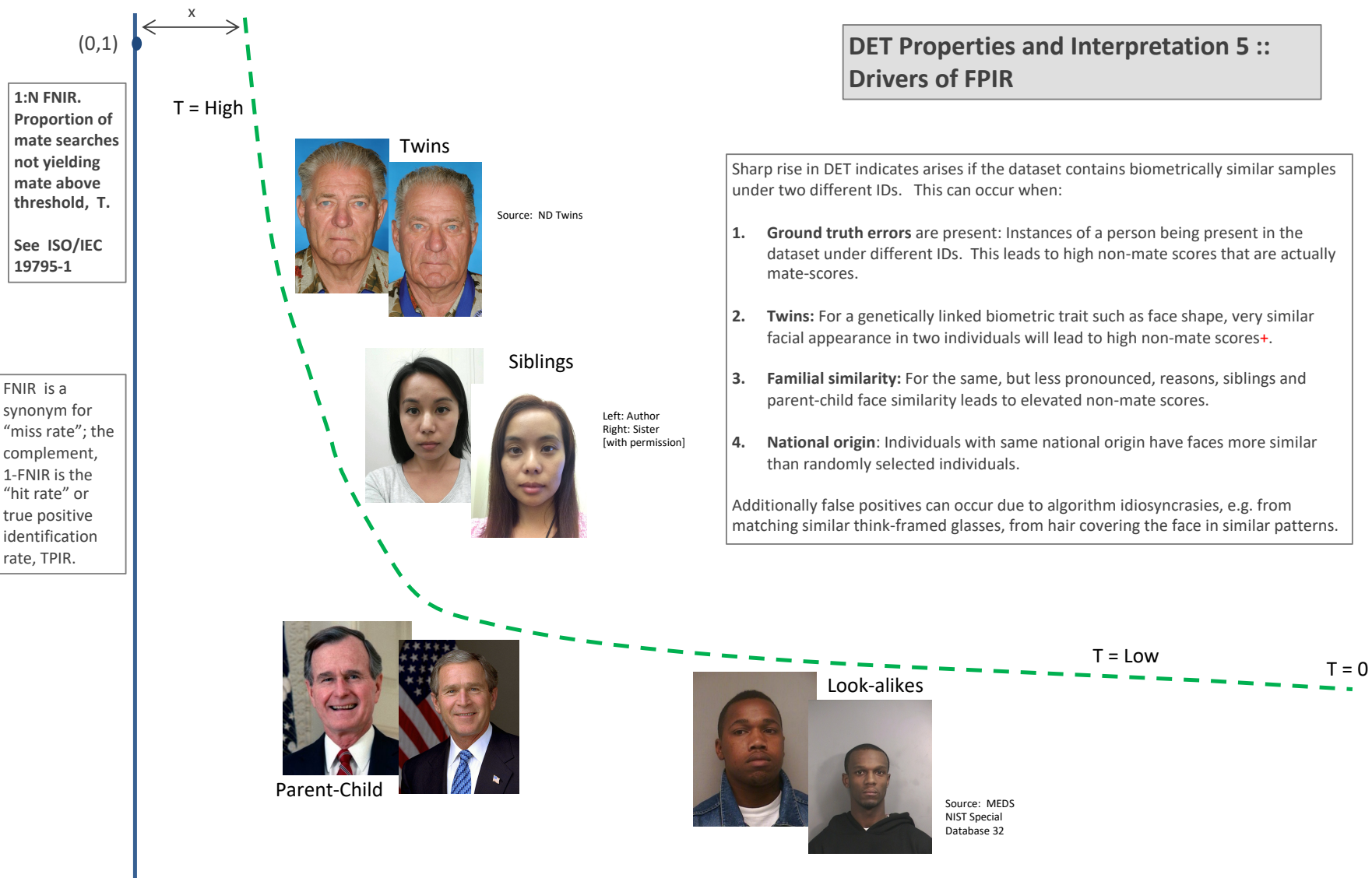


Figure 13: DET as the primary performance reporting mechanism.



Low FPIR values achieved with higher, i.e. more stringent thresholds.

+ NOTE: While most algorithms will not recognize twins correctly, there is at least one face recognition algorithm that can correctly distinguish twins [US Patent: [US7369685B2](#)].

FPIR. Proportion of non-mated searches yielding any candidates above threshold, T.
See ISO/IEC 19795-1

Figure 14: DET as the primary performance reporting mechanism.

2022/03/30
17:50:48

$\text{FNIR}(N, R, T) =$
False neg. identification rate
 $\text{FPIR}(N, T) =$
False pos. identification rate

$N = \text{Num. enrolled subjects}$
 $R = \text{Num. candidates examined}$

$T = \text{Threshold}$

$T = 0 \rightarrow \text{Investigation}$
 $T > 0 \rightarrow \text{Identification}$

1:N FNIR.
Proportion of mate searches not yielding mate above threshold, T .
See ISO/IEC 19795-1

Algorithm X,
Condition 1

Algorithm X,
Condition 2

FNIR is a synonym for "miss rate"; the complement, 1-FNIR is the "hit rate" or true positive identification rate, TPIR.

Log-scale is typical to show small numbers.

If system X is used with images of different properties, say from different imaging systems, or from different populations, generally both FNIR and FPIR will change. The dotted line joins points of the same threshold. Horizontal (vertical) lines indicate change in FPIR (FNIR) only. Two cases concerning population size are shown below (A and B), for the blue curves.

Algorithm Y,
Condition 1

Algorithm Y,
Condition 2

If DETs are computed for two categories (men and women) or (cameras A and B) or (indoor vs. outdoor), generally the Type I and Type II errors will differ and the line of constant threshold will be neither horizontal nor vertical.

The ideal situation in most applications is that a fixed threshold yields a fixed FPIR so that system owners see no change in false alarms across populations or conditions.

Low FPIR values achieved with higher, i.e. more stringent, thresholds.

Log-scale is often required because low FPIR values are operationally relevant.

FPIR. Proportion of non-mated searches yielding any candidates above threshold, T . See ISO/IEC 19795-1

Figure 15: DET as the primary performance reporting mechanism.

DET Properties and Interpretation 6 :: Fixed thresholds, change in image properties or demographics

1:N FNIR.
Proportion of mate searches not yielding mate above threshold, T.
See ISO/IEC 19795-1

FNIR is a synonym for "miss rate"; the complement, 1-FNIR is the "hit rate" or true positive identification rate, TPIR.

Log-scale is typical to show small numbers.

A: Typical case: In theory, and often in practice, a 1:N search is implemented by executing N 1:1 comparisons independently and then sorting by similarity score:

Mate scores: A mate comparison score is independent of the rest of enrollment data, and so independent of N. This implies the horizontal line above $\text{FNIR}(T, N) = \text{FNMR}(T, 1)$.

Non-mate scores: FPIR increases linearly with N from binomial theory: $\text{FPIR}(N, T) = 1 - (1 - \text{FMR}(T))^N \rightarrow N \text{ FMR}(T)$ for small FPIR.

Pop. N1

Pop. N2 > N1

B: Special case: An enrollment database is not just a linear data structure, it could be an index, or tree, then search is not simply N 1:1 comparisons and a sort. In that case:

Mate scores become dependent on the enrollment data, either its size or actual content, then generally $\text{FNIR}(T, N) \neq \text{FNIR}(T, 1)$.

Non-mate scores are normally no longer just the highest 1:1 comparison score. Instead, for example, scores may be normalized as the implementation attempts to make FPIR independent of N will yield the vertical line linking points of equal threshold.

Low FPIR values achieved with higher, i.e. more stringent, thresholds.

Log-scale is often required because low FPIR values are operationally important.

DET Properties and Interpretation 7 :: Effect of enrolled population size.

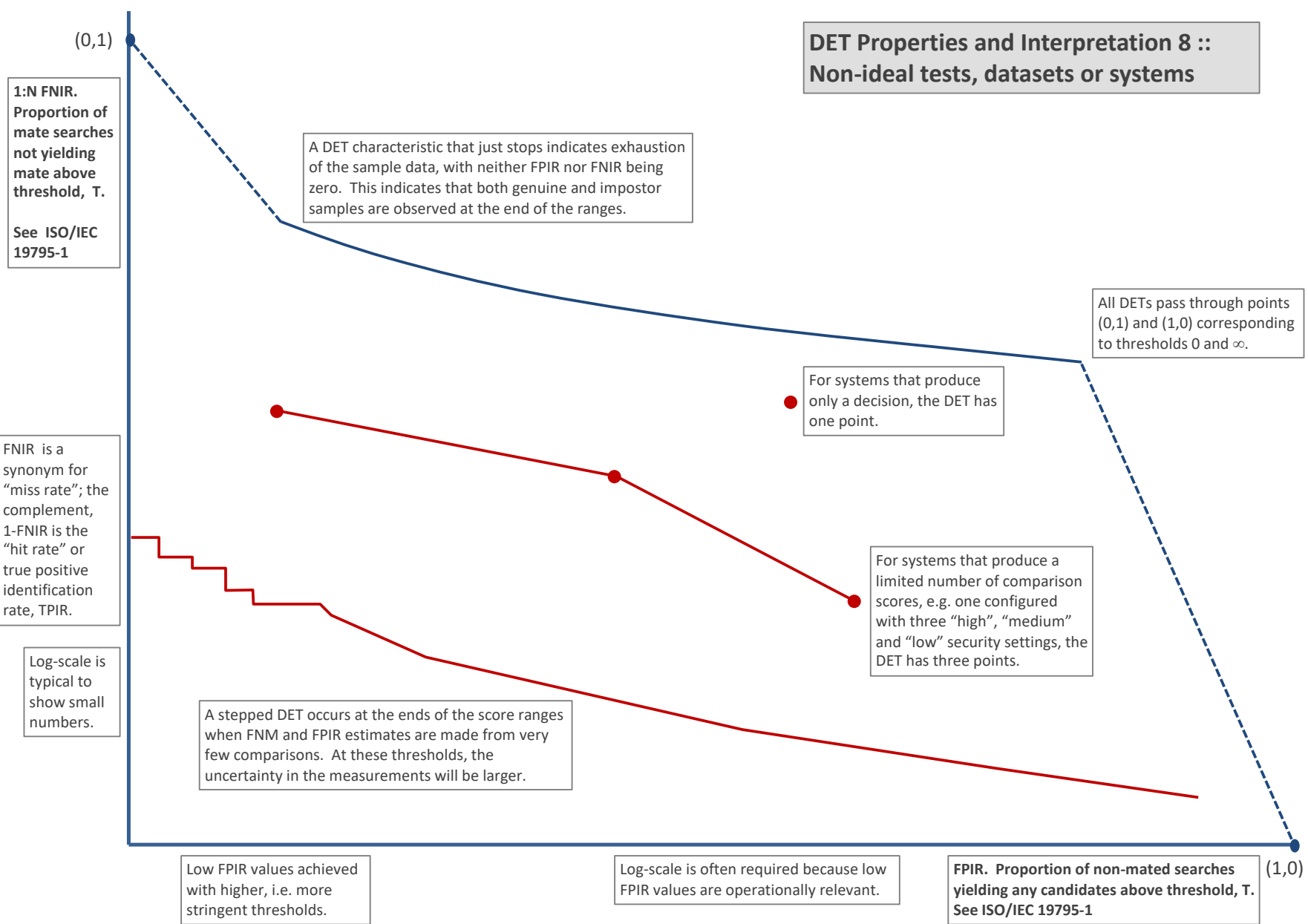


Figure 17: DET as the primary performance reporting mechanism.

3.4 Best practice testing requires execution of searches with and without mates

FRVT embeds 1:N searches of two kinds: Those for which there is an enrolled mate, and those for which there is not. The respective numbers for these types of searches appear in Table 1. However, it is common to conduct only mated searches¹⁰. The cumulative match characteristic is computed from candidate lists produced in mated searches. Even if the CMC is the only metric of interest, the actual trials executed in a test should nevertheless include searches for which no mate exists. As detailed in Table 1 the FRVT reserved disjoint populations of subjects for executing true non-mate searches.

3.5 Failure to extract features

During enrollment some algorithms fail to convert a face image to a template. The proportion of failures is the failure-to-enroll rate, denoted by FTE. Similarly, some search images are not converted to templates. The corresponding proportion is termed failure-to-extract, denoted by FTX.

We do not report FTX because we assume that the same underlying algorithm is used for template generation for enrollment and search.

Failure to extract rates are incorporated into FNIR and FPIR measurements as follows.

- ▷ **Enrollment templates:** Any failed enrollment is regarded as producing a zero length template. Algorithms are required by the API [10] to transparently process zero length templates. The effect of template generation failure on search accuracy depends on whether subsequent searches are mated, or non-mated: Mated searches will fail giving elevated FNIR; non-mated searches will not produce false positives so, to first order, FPIR will be reduced by a factor of $1 - \text{FTE}$.
- ▷ **Search templates and 1:N search:** In cases where the algorithm fails to produce a search template from input imagery, the result is taken to be a candidate list whose entries have no hypothesized identities and zero score. The effect of template generation failure on search accuracy depends on whether searches are mated, or non-mated: Mated searches will fail giving elevated FNIR; Non-mated searches will not produce false positives, so FPIR will be reduced. Thus given a measurement of false negative and positive rates made over only those where failures-to-extract did not occur, those rates - call them FNIR^\dagger and FPIR^\dagger - could be adjusted by an explicit measurement of FTX as follows

$$\text{FNIR} = \text{FTX} + (1 - \text{FTX})\text{FNIR}^\dagger \quad (8)$$

$$\text{FPIR} = (1 - \text{FTX})\text{FPIR}^\dagger \quad (9)$$

This approach is the correct treatment for positive-identification applications such as access control where cooperative users are enrolled and make attempts at recognition. This approach is not appropriate to negative identification applications, such as visa fraud detection, in which hostile individuals may attempt to evade detection by submitting poor quality samples. In those cases, template generation failures should be investigated as though a false alarm had occurred.

¹⁰For example, the [Megaface benchmark](#). This is bad practice for several reasons: First, if a developer knows, or can reasonably assume, that a mate always exists, then unrealistic gaming of the test is possible. A second reason is that it does not put FPIR on equal footing with FNIR and that matters because in most applications, not all searches have mates - not everyone has been previously enrolled in a driving license issuance or a criminal justice system - so addressing between-class separation becomes necessary.

3.6 Fixed length candidate lists, threshold independent workload

Suppose an automated face identification algorithm returns L candidates, and a human reviewer is retained to examine up to R candidates, where $R \leq L$ might be set by policy, preference or labor availability. For now, assume also that the reviewer is not provided with, or ignores, similarity scores, and thresholds are not applied. Given the algorithm typically places mates at low (good) ranks, the number of candidates a reviewer can be expected to review can be derived as follows. Note that the reviewer will:

- ▷ Always inspect the first ranked image Frac. reviewed = 1
- ▷ Then inspect those candidates where mate not confirmed at rank 1 Frac. reviewed = 1-CMC(1)
- ▷ Then inspect those candidates where mate not confirmed at rank 1 or 2 Frac. reviewed = 1-CMC(2)

etc. Thus if the reviewer will stop after a maximum of R candidates, the expected number of candidate reviews is

$$M(R) = 1 + (1 - CMC(1)) + (1 - CMC(2)) + \dots + (1 - CMC(R - 1)) \quad (10)$$

$$= R - \sum_{r=1}^{R-1} CMC(r) \quad (11)$$

A recognition algorithm that front-loads the cumulative match characteristic will offer reduced workload for the reviewer. This workload is defined only over the searches for which a mate exists. In the cases where there truly is no mate, the reviewer would review all R candidates. Thus, if the proportion of searches for which a mate does exist is β , which in the law enforcement context would be the recidivism rate [3], the full expression for workload becomes:

$$M(R) = \beta \left(R - \sum_{r=1}^{R-1} CMC(r) \right) + (1 - \beta)R \quad (12)$$

$$= R - \beta \sum_{r=1}^{R-1} CMC(r) \quad (13)$$

3.7 Timing measurement

Algorithms were submitted to NIST as implementations of the application programming interface(API) specified by NIST in the Evaluation Plan [10]. The API includes functions for initialization, template generation, finalization, search, gallery insert, and gallery delete. Two template generation functions are required, one for the preparation of an enrollment template, and one for a search template.

In NIST's test harness, all functions were wrapped by calls to the C++ std::chrono::high_resolution_clock which on the dedicated timing machine counts 1ns clock ticks. Precision is somewhat worse than that however.

3.8 Uncertainty estimation

3.8.1 Random error

This study leverages operational datasets for measurement of recognition error rates. This affords several advantages. First, large numbers of searches are conducted (see Table 1) giving precision to the measurements. Moreover, for the two mugshot datasets, these do not involve reuse of individuals so binomial statistics can be expected to apply to recognition error counts. In that case, an observed count of a particular recognition outcome (i.e. a false negative or false positive) in M trials will sustain 95% confidence that the actual error rate is no larger than some value.

As an example, the minimum number of mugshot searches conducted in this report is $M = 154\,549$, and for an observed FNIR around 0.002, the measurement supports a conclusion that the actual FNIR is no higher than 0.00228 at 99% confidence level. On the false positive side, we tabulate FNIR at FPIR values as low as 0.001. Given estimates based on 331 254 non-mate trials, the actual FPIR values will be below 0.00115 at 99% confidence. In conclusion, large scale evaluation, without reuse of subjects, supports tight uncertainty bounds on the measured error rates.

3.8.2 Systematic error

The FRVT 2018 dataset includes anomalies discovered as a result of inspecting images involved in recognition failures from the most accurate algorithms. Two kinds of failure occur: False negatives (which, for the purpose here, include failures to make templates) and false positives.

False negative errors: We reviewed 600 false negative pairs for which either or both of the leading two algorithms did not put the correct mate in the top 50 candidates. Given 154 549 searches, this number represents 0.39% of the total, resulting in $\text{FNIR} \sim 0.0039$. Of the 600 pairs:

- ▷ **A: Poor quality:** About 20% of the pairs included images of very low quality, often greyscale, low resolution, blurred, low contrast, partially cropped, interlaced, or noisy scans of paper images. Additionally, in a few cases, the face is injured or occluded by bandages or heavy cosmetics.
- ▷ **B: Ground truth identity label bugs:** About 15% of the pairs are not actually mated. We only assigned this outcome when a pair is clearly not mated.
- ▷ **C: Profile views:** About 35% included an image of a profile (side) view of the face, or, more rarely, an image that was rotated 90 degrees in-plane (roll).
- ▷ **D: Tattoos:** About 30% included an image of a tattoo that contained a face image. These arise from mis-labelling in the parent dataset metadata.
- ▷ **E: Ageing:** There is considerable time-lapse between the two captures.

All these estimates are approximate. Of these, the tattoo and mislabelled images can never be matched. These constitute an accuracy floor in the sample implying that FNIR cannot be below 0.0018¹¹. The profile-views, low-quality images, and images with considerable ageing can, in principle, be successfully matched - indeed some algorithms do so - so are not part of the accuracy floor.

¹¹This value is the sum of two partial false negative rates: $\text{FNIR}_B = 0.15 * 0.0039$ plus $\text{FNIR}_D = 0.3 * 0.0039$

For the microsoft-4 algorithm the lowest miss rate from (recent entry in Table 23) is $\text{FNIR}(640\,000, 50, 0) = 0.0018$. This is close to the value estimated from the inspection of misses. It is below the 0.0039 figure because the algorithm does match some profile and poor quality images, that the yitu-2 algorithm does not.

For many tables (e.g. Table 23), the FNIR values obtained for the FRVT-2018 mugshots could be corrected by reducing them by 0.0018. The best values would then be indistinct from zero. The results in this report *were not* adjusted to account for this systematic error.

False positive errors: As shown in Figure 1 and discussed in Figure 14 many of the DET characteristics in this report exhibit a pronounced turn upward at low false positive rates. The shape can be caused by identity labelling errors in the ground truth of a dataset, specifically persons present in the database under two IDs such that some proportion of non-mate pairs are actually mated. To look for such possibilities, we merged the highest 1000 non-mate pairs produced by three different algorithms which resulted in 1839 unique pairs. This constitutes 0.56% of all non-mate searches. We assert that it is *very* difficult for human reviewers to assign the pairs into the following three categories: twins; doppelgangers; or ground-truth errors (instances of the same person under two IDs). Given this difficulty we made no attempt to correct any possible ground truth errors except by removing 57 pairs in the following categories:

- ▷ **A: Profile views:** Thirteen pairs included one or two profile-view images. As described in Figure 133, these can cause false positives.
- ▷ **B: Same-session photographs:** For twelve pairs, the images were identical or trivially altered (e.g. cropped) versions of the same photo. These were present under a different ID likely due to some clerical or procedural mistake.
- ▷ **C: Tattoos of faces:** There were fourteen instances of tattoo photographs that contained faces causing false matches.
- ▷ **D: T-shirt faces:** There were six instances of T-shirt photographs (of Bob Marley and Che Guevara) being detected instead of the face and causing false positives.
- ▷ **E: Background faces:** There were twelve instances of one subject appearing in the background of two otherwise correct portrait photos.

Note we did not remove any images where there was a chance that the pair was actually a different person.

In any case, the results in this report have not been adjusted for this systematic error.

4 Results

This section gives extensive results for algorithms submitted to FRVT 2018. Three page “report cards” for each algorithm are contained in a [separate supplement](#). Performance metrics were described in section 3. The main results are summarized in tabular form with more exhaustive data included as DET, CMC and related graphs in appendices as follows:

- ▷ The three tables 2-4 list algorithms alongside full developer names, acceptance date, size of the provided configuration data, template size and generation time, and search duration data.
 - The **template generation duration** is most important to applications that require fast response. For example, an eGate taking more than two seconds to produce a template might be unacceptable. Note that GPUs may be of utility in expediting this operation for some algorithms, though at additional expense. Two additional factors should be considered¹²¹³.
 - The **search duration** is the time taken for a search of a search template into a gallery of N enrollment templates. This performance variable, together with the volume of searches, is influential on the amount of hardware needed to sustain an operational deployment. This is measured here with the algorithm running on a single core of a contemporary CPU. Search is most simply implemented as N computations of a distance metric followed by a sort operation to find the closest enrollments. However, considerable optimization of this process is possible, up to and including fast-search algorithms that, by various means, avoid computation of all N distances.
 - The **template size** is the size of the extracted feature vector (or vectors) and any needed header information. Large template sizes may be influential on bus or network bandwidth, storage requirements, and on search duration. While the template itself is an opaque data blob, the feature dimensionality might be estimated by assuming a four-bytes-per-float encoding. There is a wide range of encodings. For the more accurate algorithm, sizes range from 256 bytes to about 2KB bytes, indicating essentially no consensus on face modeling and template design.
 - The **template size multiplier** column shows how, given k input images, the size of the template grows. Most implementations internally extract features from each image and concatenate them, and implement some score-level fusion logic during search. Other implementations, including many of the most accurate algorithms, produce templates whose size does not grow with k . This could be achieved via selection of the best quality image - but this is not optimal in handling ageing where the oldest image could be the best quality. Another mechanism would be feature-level fusion where information is fused from all k inputs. In any case, as a black-box test, the fusion scheme is proprietary and unknown.
 - The size of the **configuration data** is the total size of all files resident in a vendor-provided directory that contains arbitrary read-only files such as parameters, recognition models (e.g caffe). Generally a large value for this quantity may prohibit the use of the algorithm on a resource-constrained device.

¹²The FRVT 2018 API prohibited threading, so some gains from parallelism may be available on multiple-cores or multiple processors, if the feature extraction code could be distributed across them.

¹³Note also that factors of two or more may be realizable by exploiting modern vector processing instructions on CPUs. It is not clear in our measurements whether all developers exploited Intel’s AVX2 instructions, for example. Our machine was so equipped, but we insisted that the same compiled library should also run on older machines lacking that instruction. The more sophisticated implementations may have detected AVX2 presence and branched accordingly. The less sophisticated may be defaulted to the reduced instruction set. Readers should see the FRVT 2018 API document for the specific chip details.

▷ Tables 23-24 report core rank-based accuracy for mugshot images. The population size is limited to $N = 1.6$ million identities because this is the largest gallery size on which all algorithms were executed. Notable observations from these tables are as follows:

- **Accuracy gains since 2018:** NIST Interagency Report 8238 documented massive gains over those reported in the FRVT 2014 report, NIST Interagency Report 8009. Further gains are documented in this report. Comparing the most accurate algorithm in November 2018, NEC-3, the value of $\text{FNIR}(N, L, T)$ reduced from 0.0031 to 0.0024 for the Sensetime-004 algorithm with $N = 12$ million recent images. The tables show broader gains: many developers have made advances since 2018 with between two and five-fold reduction in errors.
- **Wide range in accuracy:** The rank-1 miss rates vary from $\text{FNIR}(N, 1, 0) = 0.0012$ for sensetime-004 up to about 0.5 for the very fast but inaccurate microfocus-x algorithms. Among the developers who are superior to NEC in 2013, the range is from 0.002 to 0.035 for camvi-3. This large accuracy range is consistent with the buyer-beware maxim, and indicates that face recognition software is far from being commoditized.

▷ Tables 27-28 report threshold-based error rates, $\text{FNIR}(N, L, T)$, for $N = 1.6$ million for mugshot-mugshot accuracy on FRVT 2014, FRVT 2018, and also (in pink) mugshot-webcam accuracy using FRVT 2018 enrollments. Notable observations from these tables are as follows:

- **Order of magnitude accuracy gains since 2014:** As with rank-based results, the gains in accuracy are substantial, though somewhat reduced. At $\text{FPIR} = 0.01$, the best improvement over NEC in 2014 is a 27 fold reduction in FNIR using the NEC_2 algorithm. At $\text{FPIR} = 0.001$, the largest gain is a six-fold reduction in FNIR via the NEC_3 algorithm.
- **Broad gains across the industry:** About 19 companies realize accuracy better than the NEC benchmark from 2014. This is somewhat lower than the 28 developers who succeeded on the rank-1 metric. This may be due to the ubiquity of, and emphasis on, the rank-1 metric in many published algorithm development papers.
- **Webcam images:** Searches of webcam images give $\text{FNIR}(N, T)$ values around 2 to 3 times higher than mugshot searches. Notably the leading developers with mugshots are approximately the same with poorer quality webcams. But some developers e.g. Camvi, Megvii, TongYi, and Neurotechnology do improve their relative rankings on webcams, perhaps indicating their algorithms were tailored to less constrained images.

▷ Tables 17, 20, 21 and show, respectively, high-threshold, rank 1, and rank 50 FNIR values for all algorithms performing searches into five different gallery sizes, $N = 640\,000$, $N = 1\,600\,000$, $N = 3\,000\,000$, $N = 6\,000\,000$ and $12\,000\,000$. The $\text{FPIR} = 0.001$ table is included to inform high-volume duplicate detection applications. The Rank-1 table is included as a primary accuracy indicator. The Rank-50 table is included to inform agencies who routinely produce 50 candidates for human-review. The notable results are:

- **Slow growth in rank-based miss rates:** $\text{FNIR}(N, R)$ generally grows as a power law, aN^b . From the straight lines of many graphs of Figure 20 this is clearly a reasonable model for most, but not all, algorithms. The coefficient a can be interpreted as FNIR in a gallery of size 1. The more important coefficient b indicates scalability, and often, $b \ll 1$, implies very benign growth in FNIR. The coefficients of the models appear in the Tables 20 and 21.
- **Slow growth in threshold-based miss rates:** $\text{FNIR}(N, T)$ also generally grows as a power law, aN^b except at the high threshold values corresponding to low FPIR values. This is visible in the plots of Figure 36 which

show straight lines except for $FPIR = 0.001$, which increase more rapidly with N above 3 000 000. Each trace in those figures shows $FNIR(N, T)$ at fixed $FPIR$ with both N and T varying. Thus at large N , it is usually necessary to elevate T to maintain fixed $FPIR$. This causes increased $FNIR$. Why that would no-longer obey a power-law is not known. However, if we expect large galleries to contain individuals with familial relations to the non-mate search images - in the most extreme case, twins - then suppression of false positives becomes more difficult. This is discussed in the Figures starting at Fig. 10

▷ Figure ?? shows false positives from twins against their enrolled siblings, broken out by type of twin: fraternal or identical. The Figure is based on the enrollment of 104 single images on one of a pair of twins, and then the search of 2354 second images. Note that the dataset is heavily skewed towards identical twins which is not representative of the true population. There is also a skew towards same sex fraternal twin pairs compared to different sex fraternal twin pairs again not representative of the true population.

The notable results are:

- For all algorithms tested, the 1087 mated searches (Twin A vs. Twin A) produce scores almost always above typical operational thresholds, with (not shown) matches at rank 1. The images are of good quality, so this is the result expected from the rest of this report.
- For the 1066 identical twin searches (AB), almost all produce the twin at rank 1, with a few producing the mate at further down the candidate lists rank and low score.
- For the 169 fraternal searches (AB) from same sex pairs, most algorithms give a large number of very high scores, implying false positives at all thresholds. However, there are long tails containing lower scores that are correctly below threshold. In general, scores that are higher in this distribution are all rank 1 whereas the lower scores have much higher ranks.
- (Not shown) Of the 169, there are 24 fraternal searches (AB) involving different sex twins. Here most algorithms correctly report scores well below the lowest threshold, and usually not on the candidate list at all.

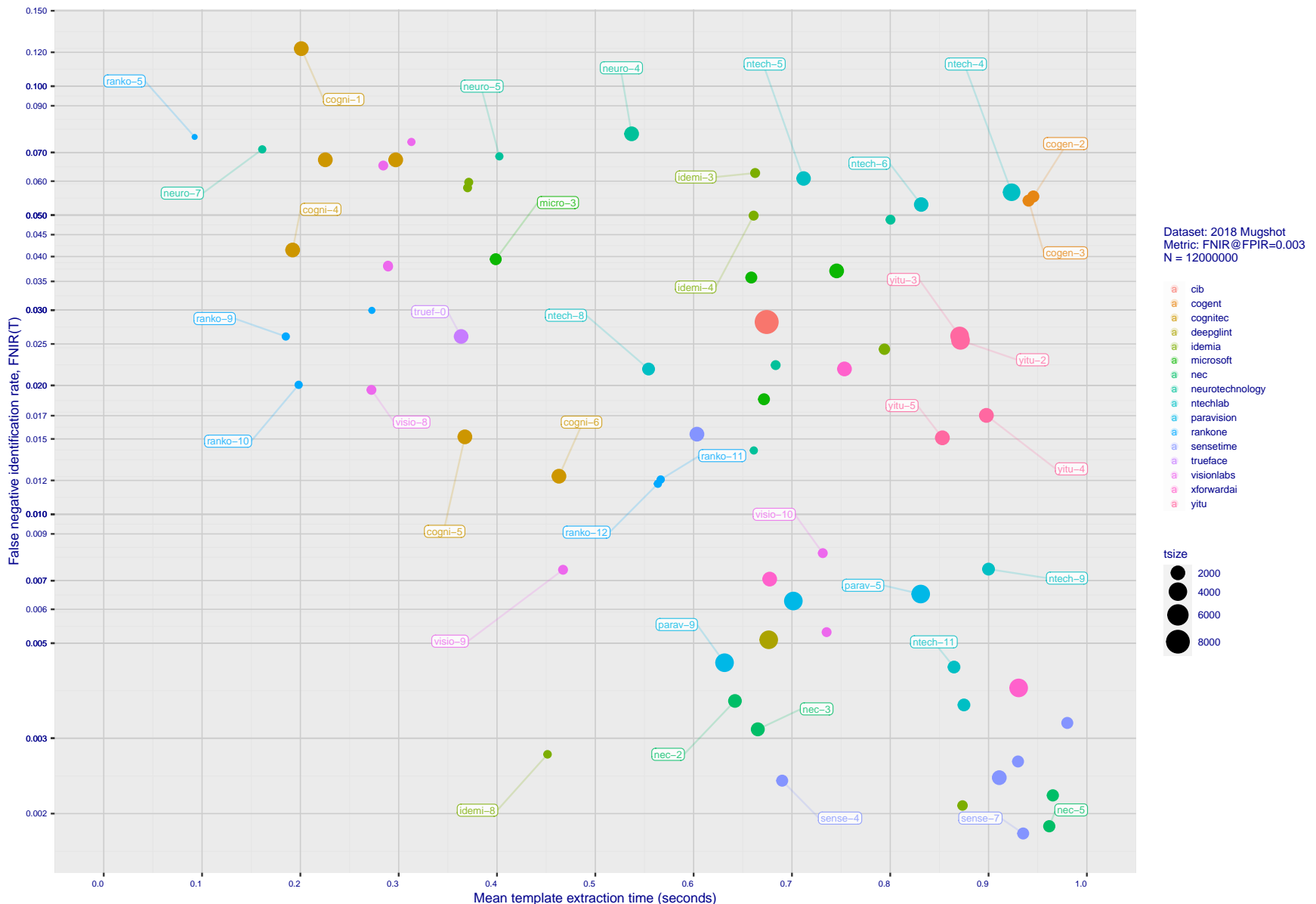
2022/03/30
17:50:48

Figure 18: [Mugshot Dataset] Speed-accuracy tradeoff. For developers of the more accurate algorithms the plot shows the tradeoff of high-threshold recognition miss-rates, $\text{FNIR}(N, N, T)$ for $\text{FPIR}(N, T) = 0.003$, and template generation time. Developers are coded by color. Template size is encoded by the size of the circle. Some labels are quite distant from the respective point, to avoid superposing text. Without any other influences, the assumption would be that taking time to localize the face, and extract features, would lead to better accuracy. The most notable result, for NEC, is that their slower algorithms are much more accurate than the version that extract features in fewer than 90 milliseconds.

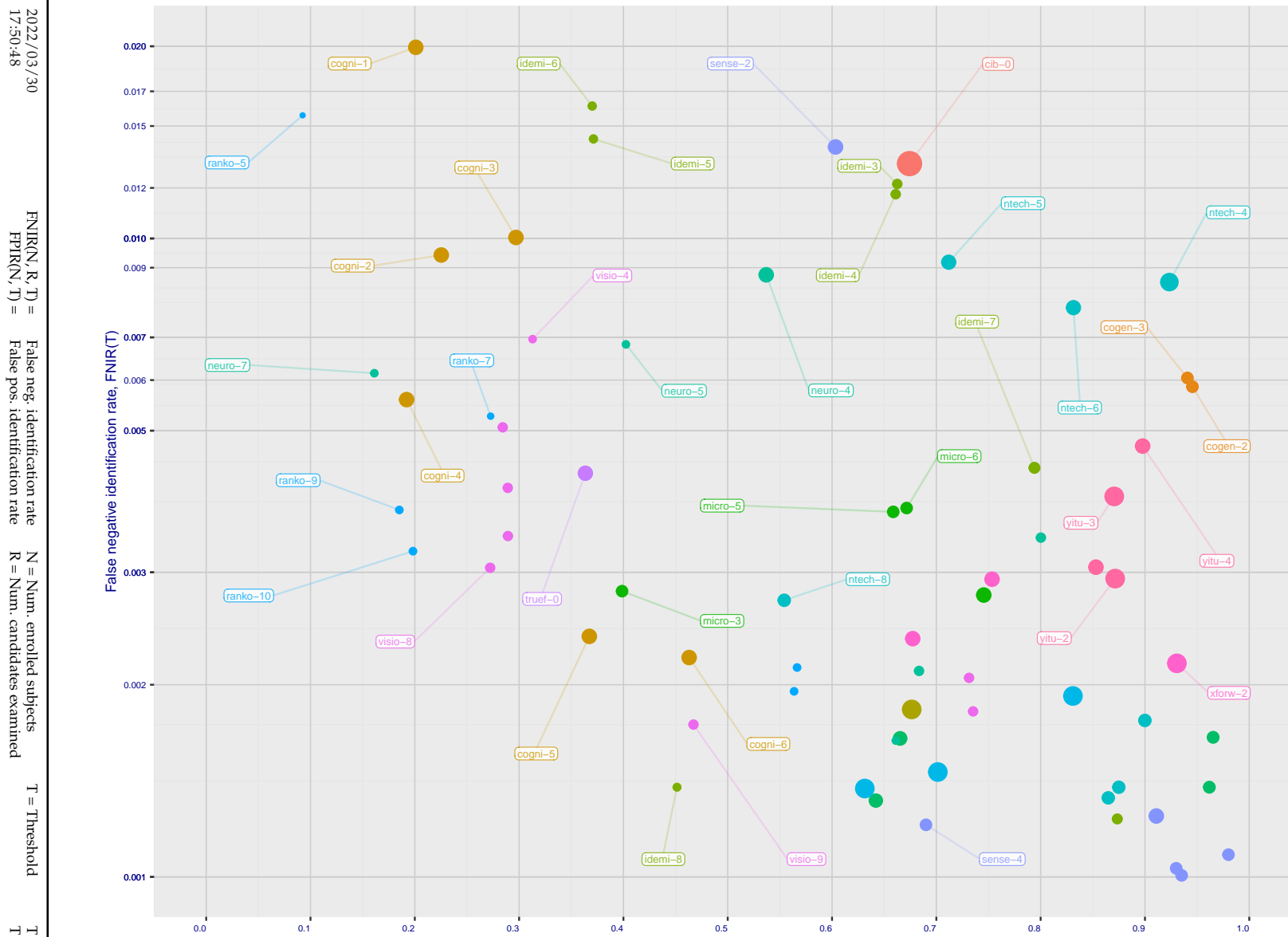


Figure 19: [Mugshot Dataset] Speed-accuracy tradeoff. For developers of the more accurate algorithms the plot shows the tradeoff of rank-one recognition miss-rates, FNIR($N, 1, 0$), and template generation time. Developers are coded by color. Template size is encoded by the size of the circle. Some labels are quite distant from the respective point, to avoid superposing text. Without any other influences, the assumption would be that taking time to localize the face, and extract features, would lead to better accuracy. This occurs for NEC with their slower algorithm being much accurate than the version that extract features in fewer than 90 milliseconds.

	DEVELOPER	SHORT	SEQ.	VALIDATION	CONFIG ¹	LIB ¹	TEMPLATE GENERATION			FINALIZE ²	SEARCH DURATION ⁵ MILLISEC						
							DATA (MB)	DATA (MB)	SIZE (B)		N=1.6M	N=1.6M	N=3M	N=6M	N=12M	(μ s)	
	FULL NAME	NAME	NUM.	DATE													
1	20Face	20face	000	2021-10-01	112	319	111	2048	-	20	236	64	9	(201)	6355	(203) 6341	
2	3Divi	3divi	5	2018-10-26	186	51	197	4096	k	109	638	163	28	(92)	538	(91) 537	
3	3Divi	3divi	6	2018-10-26	187	51	35	528	k	110	640	26	5	(12)	33	(13) 33	
4	Acer Incorporated	acer	000	2020-08-12	35	67	31	512	-	16	198	16	4	(58)	295	(56) 295	
5	Acer Incorporated	acer	001	2021-11-08	42	610	133	2048	-	11	184	61	9	(103)	619	(99) 575	
6	Akurat Satu Indonesia	ptakuratsatu	000	2020-10-23	0	572	40	538	-	203	905	214	28633	(6)	15	(6) 16	
7	Alchera Inc	alchera	2	2018-10-30	7	14	131	2048	k	6	114	194	63	(179)	2923	(182) 2929	
8	Alchera Inc	alchera	3	2018-10-30	251	14	121	2048	k	87	531	195	63	(180)	2955	(158) 6546	
9	Alchera Inc	alchera	004	2021-09-17	476	24	98	2048	-	179	853	175	35	(202)	6657	(209) 6851	
10	Alivia / Innovation Sys	isystems	3	2018-10-30	350	784	110	2048	1	170	825	135	16	(70)	385	(74) 389	
11	AllGoVision	allgogvision	000	2019-07-30	168	150	96	2048	k	52	404	91	12	(183)	3226	(186) 3193	
12	AllGoVision	allgogvision	001	2020-07-14	283	126	144	2048	-	156	777	97	13	(182)	3174	(185) 3183	
13	Anke Investments	anke	0	2018-10-30	779	27	179	2072	k	60	429	135	16	(105)	675	(112) 748	
14	Anke Investments	anke	1	2018-10-30	779	27	178	2072	k	61	430	125	15	(110)	707	(115) 769	
15	Anke Investments	anke	002	2019-06-27	341	401	169	2056	k	103	623	106	13	(104)	624	(106) 682	
16	Aware	aware	5	2018-10-30	368	27	188	3100	k	163	792	177	34	(16)	95	(21) 98	
17	Aware	aware	6	2018-10-30	368	27	2	124	k	162	789	32	2	(32)	158	(32) 162	
18	Ayonix	ayonix	1	2018-10-29	74	2	60	1036	k	12	86	86	11	(54)	279	(54) 279	
19	Ayonix	ayonix	2	2018-10-30	74	2	59	1036	1	11	11	112	14	(53)	279	(53) 276	
20	Camvi Technologies	camvitech	4	2018-10-30	233	220	49	1024	1	126	686	175	31	(13)	33	(12) 32	
21	Camvi Technologies	camvitech	5	2018-10-30	257	220	47	1024	1	148	751	175	31	(11)	31	(10) 30	
22	Canon Inc	cib	000	2020-10-19	426	127	215	8196	-	120	674	201	113	(184)	3589	(188) 3604	
23	Canon Inc	canon	001	2021-10-27	1139	91	199	4096	-	194	885	152	21	(204)	6804	(207) 6789	
24	Clearview AI Inc	clearviewai	000	2021-11-12	358	316	200	4096	-	153	765	170	30	(116)	802	(104) 657	
25	Cloudwalk - Hengrui AI Technology	hr	000	2021-02-10	501	392	120	2048	-	202	905	120	15	(55)	282	(52) 276	
26	Cloudwalk - Moontime Smart Technology	cloudwalk	000	2022-01-31	716	573	130	2048	-	186	869	79	10	(81)	440	(70) 371	
27	Cognitec Systems GmbH	cognitec	2	2018-10-30	463	26	148	2052	k	19	225	167	20	(158)	1733	(160) 1763	
28	Cognitec Systems GmbH	cognitec	3	2018-10-30	465	26	156	2052	k	297	30	157	16	(157)	1719	(161) 1791	
29	Cognitec Systems GmbH	cognitec	004	2021-03-08	384	60	155	2052	-	14	192	104	13	(156)	1673	(158) 1727	
30	Cognitec Systems GmbH	cognitec	005	2021-07-30	460	61	153	2052	-	39	367	66	9	(148)	1556	(150) 1551	
31	Cognitec Systems GmbH	cognitec	006	2022-02-10	689	61	162	2052	-	70	463	76	10	(127)	1006	(127) 1002	
32	Cubox	cubox	000	2021-08-24	529	298	141	2048	-	206	917	75	10	(185)	3646	(190) 4076	
33	Cyberlink Corp	cyberlink	000	2019-06-12	217	93	158	2052	1	113	654	169	30	(107)	696	(108) 701	
34	Cyberlink Corp	cyberlink	001	2019-10-07	459	102	154	2052	1	58	423	166	28	(108)	698	(107) 700	
35	Cyberlink Corp	cyberlink	002	2020-07-31	333	109	208	4140	-	141	724	205	6875	(145)	1353	(187) 3198	
36	Cyberlink Corp	cyberlink	003	2021-01-05	333	100	210	6212	-	129	691	181	35	(84)	488	(107) 723	
37	Cyberlink Corp	cyberlink	004	2021-07-16	371	100	211	6212	-	143	728	156	23	(86)	492	(89) 504	
38	Cyberlink Corp	cyberlink	005	2022-01-07	371	100	212	6212	-	145	733	175	30	(86)	501	(85) 498	
39	DAON	daon	000	2021-12-23	274	2	175	2069	-	93	583	47	8	(91)	524	(103) 625	
40	Dahua Technology Co Ltd	dahua	0	2018-10-29	276	167	97	2048	k	44	374	154	22	(50)	258	-	
41	Dahua Technology Co Ltd	dahua	1	2018-10-29	276	167	115	2048	k	40	369	162	28	(49)	257	(49) 602	
42	Dahua Technology Co Ltd	dahua	002	2019-12-02	607	137	138	2048	k	125	685	147	19	(44)	243	(51) 269	
43	Dahua Technology Co Ltd	dahua	003	2020-11-18	889	154	137	2048	-	140	723	140	18	(56)	283	(46) 249	
44	Dahua Technology Co Ltd	dahua	004	2021-11-18	812	116	109	2048	-	151	758	81	11	(78)	423	(76) 411	
45	Decatur Industries Inc	decatur	000	2022-02-09	411	383	159	2052	-	182	863	68	9	(159)	1761	(167) 2023	
46	Deepglint	deepglint	001	2019-11-15	448	265	195	4096	-	122	676	178	35	(106)	677	(148) 1495	
47	Dermalog	dermalog	5	2018-10-26	0	440	4	128	1	86	528	204	3155	(1)	0	(1)	0
48	Dermalog	dermalog	6	2018-10-26	0	453	9	256	1	82	507	4	2	(29)	142	(29) 144	
49	Dermalog	dermalog	007	2020-02-12	0	424	3	128	1	55	410	1	(22)	98	(19)	96	
50	Dermalog	dermalog	008	2021-01-25	0	531	29	512	-	41	370	18	4	(64)	335	(44) 246	
51	Dermalog	dermalog	009	2021-11-09	0	318	24	512	-	35	347	13	3	(48)	253	(45) 246	
52	FarBar Inc	f8	001	2019-10-03	266	19	93	2048	k	167	810	109	14	-	-	-	

Notes																
1 Configuration size does not capture static data present in libraries. Libraries are included but the size also includes any ancillary libraries for image processing (e.g. openCV) or numerical computation (e.g. blas).																
2 Finalization is the processing of converting $N = 1600000$ templates into a searchable data structure an operation which can be a simple copy, or the building of an index or tree, for example. The duration of the operation may be data dependent, and may not be linear in the number of input templates.																
3 This multiplier expresses the increase in template size when k images are passed to the template generation function.																
4 All durations are measured on Intel® Xeon®@CPU E5-2630 v4 @ 2.20GHz processors. Estimates are made by wrapping the API function call in calls to std::chrono::high_resolution_clock which on the machine in (3) counts 1ns clock ticks. Precision is somewhat worse than that however.																
5 Search durations are measured as in the prior note. The power-law model in the final column mostly fits the empirical results in Figure 134. However in certain cases the model is not correct and should not be used numerically.																

Table 2: Summary of algorithms and properties included in this report. The blue superscripts give ranking for the quantity in that column. Missing search durations, denoted by "-", are absent because those runs were not executed, usually because we did not run on the larger galleries. Caution: The power-law model is sometimes an incorrect model. It is included here only to show broad sublinear behavior, which is flagged in green. The models should not be used for prediction.

DEVELOPER	FULL NAME	SHORT	SEQ.	VALIDATION	CONFIG ¹	LIB ¹	TEMPLATE GENERATION			FINALIZE ²	SEARCH DURATION ⁵ MILLISEC						POWER LAW		
							DATA (MB)	DATA (MB)	SIZE (B)		TIME (S)	L=1	L=50	L=50	L=50	N=1.6M	N=1.6M		
53	Fincore Ltd	fincore	000	2021-08-18	250	224	146	2048	-	73	475	57	9	(98)	562	(96)	560	-	-
54	Fujitsu Research and Development Center	fujitsulab	000	2021-10-12	497	337	54	1032	-	213	945	28	5	(155)	1668	(154)	1657	(133)	3140
55	Fujitsu Research and Development Center	fujitsulab	001	2022-03-15	675	386	57	1032	-	193	882	58	9	(161)	1854	(162)	1817	(136)	3451
56	Gorilla Technology	gorilla	2	2018-10-29	91	1252	67	1132	k	34	338	158	24	(30)	145	(30)	146	(26)	293
57	Gorilla Technology	gorilla	3	2018-10-26	94	1252	181	2156	k	89	559	209	12020	-	(168)	2047	-	-	-
58	Gorilla Technology	gorilla	004	2020-01-06	182	1244	182	2192	k	47	388	181	41	(57)	286	(79)	1191	(79)	2416
59	Gorilla Technology	gorilla	005	2021-02-22	306	1420	213	6288	-	77	483	197	78	(115)	802	(116)	799	(94)	1514
60	Gorilla Technology	gorilla	006	2021-09-30	377	691	216	8336	-	154	767	209	99	(151)	1626	(151)	1612	(113)	2422
61	Gorilla Technology	gorilla	007	2022-02-16	392	322	214	6290	-	85	526	199	89	(113)	765	(111)	745	(89)	1408
62	Griaule	griaule	000	2021-11-01	0	584	164	2052	-	57	417	41	8	(97)	5827	(201)	6150	(167)	11473
63	Guangzhou Pixel Solutions Co Ltd	pixelall	002	2019-07-01	0	165	185	2560	k	13	190	124	15	(142)	1296	(144)	1334	(120)	2526
64	Guangzhou Pixel Solutions Co Ltd	pixelall	003	2019-11-05	0	690	184	2560	k	134	703	153	22	(139)	1273	(140)	1307	(117)	2474
65	Guangzhou Pixel Solutions Co Ltd	pixelall	004	2020-07-02	0	538	186	2560	k	62	449	139	17	(138)	1259	(139)	1300	(116)	2465
66	Guangzhou Pixel Solutions Co Ltd	pixelall	005	2021-03-23	0	717	183	2560	-	176	840	88	11	(150)	1606	(149)	1528	(123)	2609
67	Hikvision Research Institute	hikvision	5	2018-10-29	593	9	73	1408	1	98	607	130	16	(121)	883	(122)	895	(102)	1908
68	Hikvision Research Institute	hikvision	6	2018-10-29	593	9	72	1408	1	96	598	132	16	(119)	871	(121)	877	-	-
69	HyperVerge Inc	hyperverge	001	2021-08-11	1791	212	48	1024	-	178	845	24	5	(109)	705	(105)	681	(84)	1346
70	Idemia	idemia	5	2018-10-29	417	48	23	352	1	43	371	25	5	(26)	137	(27)	138	(32)	437
71	Idemia	idemia	6	2018-10-29	417	48	25	352	1	42	370	22	4	(27)	137	(26)	138	(33)	442
72	Idemia	idemia	007	2020-01-17	738	113	45	860	1	164	794	110	14	(31)	151	(31)	152	(54)	683
73	Idemia	idemia	008	2021-03-15	378	65	21	300	-	64	451	14	3	(25)	132	(25)	131	(23)	247
74	Idemia	idemia	009	2022-03-01	735	68	43	636	-	188	873	36	7	(40)	211	(39)	205	(31)	389
75	Imagus Technology Pty Ltd	imagus	005	2021-01-15	222	311	140	2048	-	161	786	108	14	(43)	236	(61)	313	(52)	651
76	Imagus Technology Pty Ltd	imagus	006	2021-05-27	248	369	126	2048	-	201	904	69	9	(62)	317	(42)	234	(38)	499
77	Imagus Technology Pty Ltd	imagus	007	2021-11-16	248	366	104	2048	-	99	609	53	9	(42)	234	(43)	238	(44)	442
78	Imperial College London	imperial	000	2019-08-28	461	15	139	2048	1	92	577	96	13	(67)	360	(73)	379	(95)	1626
79	Incode Technologies Inc	incode	2	2018-10-29	71	31	125	2048	1	28	289	129	15	(76)	411	(75)	404	-	-
80	Incode Technologies Inc	incode	3	2018-10-29	133	31	101	2048	1	132	697	115	15	(75)	408	(70)	412	(60)	847
81	Incode Technologies Inc	incode	004	2019-06-24	254	50	106	2048	1	74	475	89	12	(68)	365	(72)	378	(92)	1482
82	Incode Technologies Inc	incode	005	2021-07-29	259	21	129	2048	-	79	500	71	10	(61)	316	(83)	454	(65)	890
83	Innovatrics	innovatrics	4	2018-10-30	0	400	64	1076	k	48	399	206	10902	(5)	8	(4)	11	(2)	9
84	Innovatrics	innovatrics	005	2019-09-30	0	455	39	538	1	172	827	208	11897	(4)	8	(5)	8	(3)	9
85	Innovatrics	innovatrics	007	2021-08-16	175	58	38	538	-	158	777	111	14	(21)	97	(22)	100	(18)	188
86	Intellivision	intellivision	001	2022-03-08	62	130	168	2056	-	54	406	149	20	(71)	388	(71)	377	-	-
87	IrexAI	irex	000	2021-02-09	724	46	187	3080	-	177	844	149	19	(102)	616	(100)	600	(74)	1120
88	Kakao Enterprise	kakao	000	2021-06-23	404	124	149	2052	-	175	835	43	8	(41)	213	(40)	215	(39)	510
89	Kedacom International Pte	kedacom	001	2019-09-16	239	36	29	292	1	81	507	112	6	(74)	764	(113)	760	(103)	1940
90	Kneron	kneron	000	2020-03-03	366	13	112	2048	k	84	523	103	13	(37)	2535	(179)	2506	(153)	4752
91	Kneron	kneron	001	2021-06-10	270	69	102	2048	-	72	472	59	9	(177)	2690	(181)	2642	-	-
92	Line Corporation	line	000	2021-06-02	138	397	128	2048	-	75	481	48	8	(192)	5433	(196)	5418	(165)	10144
93	Line Corporation	line	001	2021-11-21	471	396	147	2048	-	204	907	49	8	(162)	1872	(165)	1934	(140)	3647
94	Lomonosov Moscow State University	instsysmu	000	2019-08-19	375	168	124	2048	1	101	614	102	13	(79)	430	(81)	431	(63)	860
95	Lookman Electroplast Industries	lookman	3	2018-10-28	203	24	19	292	1	33	336	12	3	(111)	739	(110)	745	(88)	1394
96	Lookman Electroplast Industries	lookman	4	2018-10-28	184	24	42	548	1	31	320	21	4	(124)	981	(126)	998	-	-
97	Lookman Electroplast Industries	lookman	005	2019-09-16	239	36	41	548	1	80	506	17	4	(126)	1005	(128)	1008	(121)	2597
98	Mantra Softtech India	mantra	000	2021-10-28	460	61	150	2052	-	56	412	75	10	(123)	916	(123)	910	(97)	1714
99	Megvii/Face++	megvii	1	2018-10-28	1703	41	201	4096	1	105	631	176	32	(94)	552	(97)	561	(82)	1221
100	Megvii/Face++	megvii	2	2018-10-28	1735	42	20	4096	1	107	635	171	31	(95)	553	(94)	558	-	-
101	MicroFocus	microfocus	5	2018-10-29	94	26	11	256	k	23	262	82	1	(37)	182	(36)	186	(29)	354
102	MicroFocus	microfocus	6	2018-10-29	94	26	12	256	k	24	262	102	1	(38)	183	(35)	186	-	-
103	Microsoft	microsoft	5	2018-10-29	381	155	46	1024	1	114	658	87	11	(149)	1606	(155)	1673	(132)	3076
104	Microsoft	microsoft	6	2018-10-29	478	155	50	1024	1	118	671	123	15	(152)	1642	(153)	1618	(142)	3710

Notes

- Configuration size does not capture static data present in libraries. Libraries are included but the size also includes any ancillary libraries for image processing (e.g. openCV) or numerical computation (e.g. blas).
- Finalization is the processing of converting $N = 1600000$ templates into a searchable data structure an operation which can be a simple copy, or the building of an index or tree, for example. The duration of the operation may be data dependent, and may not be linear in the number of input templates.
- This multiplier expresses the increase in template size when k images are passed to the template generation function.
- All durations are measured on Intel®Xeon®@CPU E5-2630 v4 @ 2.20GHz processors. Estimates are made by wrapping the API function call in calls to std::chrono::high_resolution_clock which on the machine in (3) counts 1ns clock ticks. Precision is somewhat worse than that however.
- Search durations are measured as in the prior note. The power-law model in the final column mostly fits the empirical results in Figure 134. However in certain cases the model is not correct and should not be used numerically.

Table 3: Summary of algorithms and properties included in this report. The blue superscripts give ranking for the quantity in that column. Missing search durations, denoted by “-”, are absent because those runs were not executed, usually because we did not run on the larger galleries. Caution: The power-law model is sometimes an incorrect model. It is included here only to show broad sublinear behavior, which is flagged in green. The models should not be used for prediction.

	DEVELOPER	SHORT	SEQ.	VALIDATION	CONFIG ¹	LIB ¹	TEMPLATE GENERATION	FINALIZE ²	SEARCH DURATION ⁵ MILLISEC						
									L=1	L=50	L=50	L=50	L=50	POWER LAW	
									N=1.6M	N=1.6M	N=1.6M	N=3M	N=6M	N=12M	
105	N-Tech Lab	ntech	5	2018-10-30	1685	113	84 1940 k	138 711	192 55	(46) 243	(47) 246	(41) 538	(41) 1100	(48) 2867	146 0.02N ^{1.1}
106	N-Tech Lab	ntech	6	2018-10-30	1686	117	85 1940 k	174 831	193 63	(45) 243	(46) 246	(43) 546	(42) 1104	(49) 2873	148 0.02N ^{1.1}
107	N-Tech Lab	ntechlab	007	2019-06-25	2450	51	189 3348 k	165 795	196 73	(72) 393	(80) 427	(58) 780	(65) 1768	(60) 3499	94 0.16N ^{1.0}
108	N-Tech Lab	ntechlab	008	2020-01-06	1111	51	70 1300 k	88 554	182 36	(36) 179	(33) 184	(28) 341	(28) 683	(24) 1395	46 0.11N ^{1.0}
109	N-Tech Lab	ntechlab	009	2021-03-01	1208	42	71 1300 -	199 899	180 35	(35) 178	(34) 184	(27) 336	(27) 676	(31) 1704	113 0.05N ^{1.1}
110	N-Tech Lab	ntechlab	010	2021-06-24	351	213	68 1280 -	189 874	29 6	(80) 440	(82) 435	(59) 821	(60) 1645	(57) 3337	62 0.22N ^{1.0}
111	N-Tech Lab	ntechlab	011	2021-12-07	679	208	69 1280 -	183 864	31 6	(85) 488	(84) 483	(66) 912	(68) 1869	(72) 5003	130 0.07N ^{1.1}
112	NEC	nec	2	2018-10-30	705	35	80 1616 k	111 642	143 18	(73) 405	(77) 409	(72) 1072	(63) 1755	(67) 4255	137 0.06N ^{1.1}
113	NEC	nec	3	2018-10-30	774	110	81 1712 k	116 665	150 21	(3) 7	(3) 7	(5) 14	(9) 40	(10) 82	156 0.00N ^{1.2}
114	NEC	nec	004	2021-07-19	971	63	66 1104 -	216 965	32 7	(65) 349	(66) 351	(53) 662	(51) 1330	(44) 2685	51 0.20N ^{1.0}
115	NEC	nec	005	2021-12-13	922	88	65 1104 -	215 961	33 7	(83) 473	(92) 551	(70) 1017	(71) 2091	(65) 4242	59 0.28N ^{1.0}
116	Neurotechnology	neurotech	5	2018-10-30	266	53	12 256 k	49 402	9 2	(117) 835	(118) 839	(96) 1690	(94) 3219	(101) 8955	119 0.19N ^{1.1}
117	Neurotechnology	neurotech	6	2018-10-30	564	53	8 256 k	142 726	7 2	(118) 839	(119) 842	-	-	-	-
118	Neurotechnology	neurotech	007	2019-10-03	57	51	10 256 k	7 161	6 2	(131) 1118	(132) 1110	(108) 2143	(103) 4397	(102) 9045	66 0.55N ^{1.0}
119	Neurotechnology	neurotechnology	008	2021-03-22	355	49	36 514 -	166 800	20 4	(134) 1167	(135) 1149	(110) 2266	(108) 4573	(109) 9586	73 0.55N ^{1.0}
120	Neurotechnology	neurotechnology	009	2021-09-01	246	82	31 513 -	124 683	11 3	(129) 1035	(130) 1049	(105) 1977	(101) 4270	(97) 8756	106 0.32N ^{1.1}
121	Neurotechnology	neurotechnology	010	2022-01-07	247	83	14 256 -	115 661	2 2	(125) 988	(124) 984	(100) 1897	(99) 3977	(93) 8048	98 0.36N ^{1.0}
122	Newland Computer Co Ltd	newland	2	2018-10-30	96	27	99 2048 -	181 855	125 15	(207) 8741	(212) 8854	(179) 17892	(176) 39356	-	132 1.32N ^{1.1}
123	Nobilis	noblis	1	2018-10-30	114	176	134 2048 1	17 206	124 15	(140) 1273	(138) 1272	-	-	-	-
124	Nobilis	noblis	2	2018-10-30	153	176	209 6144 1	83 517	185 43	(175) 2513	(180) 2522	(154) 5649	(155) 12432	(161) 44262	168 0.04N ^{1.3}
125	NotionTag Technologies Private Limited	notiontag	000	2022-01-14	265	945	180 2120 -	65 453	7 10	(206) 8619	(211) 8705	(166) 2052	(175) 38794	(172) 90607	136 1.15N ^{1.1}
126	Pangiam	pangiam	000	2022-02-22	453	23	127 2048 -	108 636	138 17	(50) 276	(62) 319	(48) 601	(47) 1210	(41) 2443	50 0.18N ^{1.0}
127	Paravision (EverAI)	everai	2	2018-10-30	224	304	105 2048 1	38 366	17 30	(52) 278	(56) 283	-	-	-	-
128	Paravision (EverAI)	everai	3	2018-10-30	438	304	116 2048 1	139 717	164 28	(51) 278	(55) 281	(45) 572	(43) 1146	(38) 2278	87 0.12N ^{1.0}
129	Paravision (EverAI)	everai-paravision	004	2019-06-19	527	128	194 4096 1	119 672	188 45	(96) 559	(95) 559	(123) 2611	(132) 6445	(136) 14519	176 0.00N ^{1.5}
130	Paravision (EverAI)	paravision	005	2019-12-11	543	154	193 4096 1	173 830	190 48	(97) 561	(98) 564	(71) 1056	(74) 2298	(71) 4966	110 0.16N ^{1.1}
131	Paravision (EverAI)	paravision	007	2021-02-01	529	235	190 4096 -	133 701	191 48	(99) 569	(93) 558	(73) 1086	(72) 2111	(66) 4254	20 1.11N ^{0.9}
132	Paravision	paravision	009	2021-12-14	672	300	203 4100 -	106 631	198 82	(186) 3690	(191) 4230	(162) 8037	(161) 16532	(157) 31422	89 1.62N ^{1.0}
133	Qnap Security	qnap	000	2021-07-28	182	15	100 2048 -	66 457	62 9	(136) 1231	(139) 1763	-	-	-	-
134	Qnap Security	qnap	001	2021-12-09	191	13	91 2048 -	100 613	44 8	(154) 1666	(147) 1429	(137) 3472	(138) 7375	(141) 15159	153 0.11N ^{1.2}
135	Quantasoft	quantasoft	1	2018-10-30	276	452	117 2048 k	46 385	30 6	(208) 15422	(213) 14858	(176) 14717	-	(145) 18323	-
136	Rank One Computing	rankone	4	2018-10-09	0	101	185 k	3 36	34 7	(23) 101	(23) 101	(19) 190	-	-	27 0.07N ^{1.0}
137	Rank One Computing	rankone	5	2018-10-24	0	101	5 133 k	4 92	35 7	(28) 140	(28) 144	(24) 266	(23) 525	(22) 1049	24 0.11N ^{1.0}
138	Rank One Computing	rankone	006	2019-06-03	0	133	7 165 k	22 245	42 8	-	-	-	-	-	-
139	Rank One Computing	rankone	007	2019-11-12	0	137	6 165 k	26 272	38 7	(24) 116	(24) 115	(21) 215	(21) 439	(19) 877	48 0.07N ^{1.0}
140	Rank One Computing	rankone	009	2020-06-26	0	105	12 260 k	128 185	84 11	(17) 95	(20) 96	(16) 181	(16) 362	(17) 727	37 0.06N ^{1.0}
141	Rank One Computing	rankone	010	2020-10-05	0	135	16 261 -	15 198	78 10	(18) 95	(16) 95	(14) 178	(15) 357	(14) 714	33 0.06N ^{1.0}
142	Rank One Computing	rankone	011	2021-08-27	0	175	12 261 -	91 566	50 8	(20) 96	(17) 95	(17) 183	(17) 370	(14) 714	44 0.06N ^{1.0}
143	Rank One Computing	rankone	012	2021-12-27	0	257	17 261 -	90 563	40 8	(19) 95	(18) 95	(15) 179	(15) 361	(16) 718	36 0.06N ^{1.0}
144	Realnetworks Inc	realnetworks	2	2018-10-30	105	104	205 4104 k	21 241	163 28	(163) 2008	(169) 2048	(145) 4194	(144) 8642	(140) 15035	60 1.08N ^{1.0}
145	Realnetworks Inc	realnetworks	003	2019-06-12	93	102	82 1848 k	10 173	9 13	(135) 1145	(133) 1132	(107) 2142	(117) 5241	(118) 10495	123 0.21N ^{1.1}
146	Realnetworks Inc	realnetworks	004	2019-10-17	94	102	83 1848 1	9 171	83 11	(132) 1143	(134) 1137	(109) 2149	(110) 4740	(112) 9693	105 0.36N ^{1.0}
147	Realnetworks Inc	realnetworks	005	2021-06-23	168	209	172 2056 -	32 332	56 9	(153) 1654	(152) 1616	(131) 3030	(127) 6068	(127) 12134	41 1.01N ^{1.0}
148	Realnetworks Inc	realnetworks	006	2021-12-02	250	56	171 2056 -	36 348	45 8	(93) 543	(90) 531	(69) 996	(70) 1998	(64) 3991	40 0.33N ^{1.0}
149	Remark Holdings	remarkai	000	2019-06-12	234	1092	114 2048 k	112 650	94 12	(196) 5776	(198) 5703	(168) 11604	(174) 32133	(173) 91436	169 0.05N ^{1.3}
150	Remark Holdings	remarkai	0	2018-10-30	187	847	92 2048 k	94 593	114 14	(195) 5685	(197) 5723	-	-	-	-
151	Remark Holdings	remarkai	1	2018-10-30	187	847	89 2048 k	59 427	118 14	(194) 5680	(200) 5761	(171) 12475	(172) 28726	(170) 59618	158 0.37N ^{1.2}
152	Rendip	rendip	000	2021-05-21	0	416	113 2048 -	196 890	65 9	(47) 249	(68) 368	(56) 697	(56) 1452	(31) 2926	116 0.08N ^{1.1}
153	Reveal Media Ltd	revealmedia	000	2022-02-02	287	196	161 2052 -	45 383	72 10	(167) 2322	(166) 2019	(144) 3838	(142) 7816	(144) 16559	92 0.78N ^{1.0}
154	SQLsoft	sqisoft	001	2021-12-20	271	377	167 2056 -	69 462	63 9	(143) 1310	(142) 1319	(117) 2456	(111) 4906	(114) 9755	28 0.90N ^{1.0}
155	Samsung S1 Corp	s1	000	2021-06-03	257	196	198 4096 -	184 865	148 20	(203) 6715	(208) 6794	(175) 13032	(170) 26372	(169) 55723	84 2.82N ^{1.0}
156	Samsung S1 Corp	s1	001	2021-11-01	240	198	123 2048 -	168 813	51 8	(169) 2415	(178) 2491	(152) 4718	(150) 9614	(153) 24472	121 0.53N ^{1.1}

Notes
 1 Configuration size does not capture static data present in libraries. Libraries are included but the size also includes any ancillary libraries for image processing (e.g. openCV) or numerical computation (e.g. blas).
 2 Finalization is the processing of converting $N = 1600000$ templates into a searchable data structure an operation which can be a simple copy, or the building of an index or tree, for example. The duration of the operation may be data dependent, and may not be linear in the number of input templates.
 3 This multiplier expresses the increase in template size when k images are passed to the template generation function.
 4 All durations are measured on Intel®Xeon®CPU E5-2630 v4 @ 2.0GHz processors. Estimates are made by wrapping the API function call in calls to std::chrono::high_resolution_clock which on the machine in (3) counts 1ns clock ticks. Precision is somewhat worse than that however.
 5 Search durations are measured as in the prior note. The power-law model in the final column mostly fits the empirical results in Figure 134. However in certain cases the model is not correct and should not be used numerically.

Table 4: Summary of algorithms and properties included in this report. The blue superscripts give ranking for the quantity in that column. Missing search durations, denoted by “-”, are absent because those runs were not executed, usually because we did not run on the larger galleries. Caution: The power-law model is sometimes an incorrect model. It is included here only to show broad sublinear behavior, which is flagged in green. The models should not be used for prediction.

	DEVELOPER	SHORT NAME	SEQ. NUM.	VALIDATION DATE	CONFIG ¹	LIB ¹	TEMPLATE GENERATION SIZE (B)	FINALIZE ² TIME (S)	SEARCH DURATION ⁵ MILLISEC						POWER LAW (μ s)					
									L=1		L=50		L=50							
									N=1.6M	N=1.6M	N=1.6M	N=3M	N=6M	N=12M						
157	Scanovate Ltd	scanovate	000	2020-01-15	250	446	94	2048	-	135	705	118	14	(147) 1419	(146) 1412	(130) 3008	(152) 11616	(125) 12012	139 0.10 N ^{1.2}	
158	Scanovate Ltd	scanovate	001	2020-09-10	250	446	135	2048	-	121	675	100	13	(144) 1321	(143) 1320	(118) 2502	(114) 5047	(115) 10163	63 0.65 N ^{1.0}	
159	Sensetime Group	sensetime	0	2018-10-30	525	6	204	4104	k	131	693	184	41	(87) 498	(86) 501	(81) 1212	(73) 2281	(73) 5032	139 0.09 N ^{1.1}	
160	Sensetime Group	sensetime	1	2018-10-30	525	6	206	4104	k	104	628	189	48	(90) 516	(87) 502	(76) 1146	(75) 2301	(69) 4765	127 0.09 N ^{1.1}	
161	Sensetime Group	sensetime	002	2019-06-03	523	6	166	2056	k	97	603	141	18	(66) 359	(69) 370	(101) 1897	(106) 4508	(108) 9543	139 0.00 N ^{1.5}	
162	Sensetime Group	sensetime	003	2019-12-02	769	76	170	2056	1	205	910	148	19	(190) 4885	(195) 4988	(170) 12325	(167) 24712	(164) 49445	139 0.67 N ^{1.1}	
163	Sensetime Group	sensetime	004	2020-08-10	456	29	52	1032	-	128	690	93	12	(174) 2490	(175) 2477	(150) 4654	(149) 9402	(151) 19651	65 1.22 N ^{1.0}	
164	Sensetime Group	sensetime	005	2020-12-17	631	39	53	1032	-	217	980	82	11	(171) 2459	(189) 3939	(160) 7398	(158) 14768	(180) 19016	18 14.03 N ^{0.9}	
165	Sensetime Group	sensetime	006	2021-07-26	526	54	51	1032	-	207	929	39	7	(168) 2414	(174) 2422	(148) 4527	(146) 9128	(146) 18640	54 1.35 N ^{1.0}	
166	Sensetime Group	sensetime	007	2022-01-15	526	37	55	1032	-	209	935	52	8	(170) 2432	(173) 2406	(147) 4513	(145) 8998	(148) 18796	58 1.28 N ^{1.0}	
167	Shaman Software	shaman	6	2018-10-26	0	200	136	2048	k	136	706	115	14	(101) 603	(101) 612	-	-	-	-	
168	Shaman Software	shaman	7	2018-10-26	0	200	122	2048	k	137	707	117	14	(100) 602	(102) 614	(77) 1187	(80) 2448	(76) 5083	88 0.25 N ^{1.0}	
169	Shanghai Yitu Technology	yitu	4	2018-10-30	2119	136	177	2070	1	198	897	187	45	(141) 1288	(137) 1203	(114) 2440	(118) 5241	(111) 9671	83 0.52 N ^{1.0}	
170	Shanghai Yitu Technology	yitu	5	2018-10-30	2043	136	176	2070	1	180	853	188	44	(137) 1237	(136) 1199	(119) 2513	(113) 5013	(110) 9620	79 0.55 N ^{1.0}	
171	Smilart	smilart	4	2018-10-30	65	89	32	512	k	8	167	19	4	(209) 16137	(214) 15633	-	-	-	-	
172	Smilart	smilart	5	2018-10-30	562	89	107	2048	k	63	450	113	14	-	-	-	-	-	-	
173	Staqua Technologies	staqua	000	2021-08-30	1018	690	192	4096	-	171	826	159	24	(191) 4950	(194) 4933	-	-	-	-	
174	Synesis	synesis	3	2018-10-30	237	150	196	4096	k	5	99	167	29	(114) 789	(117) 801	(104) 1941	(98) 3888	(98) 8810	147 0.07 N ^{1.1}	
175	Synesis	synesis	003	2019-07-04	143	17	90	2048	k	18	211	95	12	(89) 507	(88) 502	(111) 2297	(107) 4564	(106) 9452	174 0.00 N ^{1.4}	
176	Synesis	synesis	005	2020-09-08	494	24	207	4104	-	150	756	157	24	(120) 877	(120) 865	(134) 3182	(109) 4658	(113) 9750	160 0.06 N ^{1.2}	
177	Tech5 SA	tech5	001	2019-08-19	1394	116	74	1536	k	195	887	71	10	(69) 383	(114) 766	(125) 2767	(128) 6149	(86) 6178	138 0.12 N ^{1.1}	
178	Tech5 SA	tech5	002	2021-04-07	727	112	35	513	-	211	940	15	4	(189) 4682	(206) 6689	(172) 12541	(168) 25145	(166) 50239	39 4.18 N ^{1.0}	
179	Tencent Deepsea Lab	deepsea	001	2019-07-29	250	323	88	2048	1	147	737	92	12	(128) 1021	(129) 1020	(126) 2774	(124) 5767	(128) 12341	165 0.06 N ^{1.2}	
180	Tevian	tevian	5	2018-10-30	773	15	87	2048	1	53	405	122	15	(74) 405	(76) 408	(61) 854	(64) 1757	(59) 3380	104 0.14 N ^{1.0}	
181	Tevian	tevian	006	2021-04-16	769	19	56	1032	-	95	597	70	10	(59) 295	(59) 295	(46) 578	(45) 1187	(47) 2741	117 0.06 N ^{1.1}	
182	Tevian	tevian	007	2021-10-12	703	19	58	1032	-	157	777	23	4	(60) 297	(47) 579	(44) 1179	(40) 2418	(41) 97	0.11 N ^{1.0}	
183	Thales	cogent	2	2018-10-30	681	39	61	1043	k	212	945	161	27	(164) 2017	(171) 2144	(146) 4298	(143) 8472	(143) 16429	64 1.08 N ^{1.0}	
184	Thales	cogent	3	2018-10-30	681	39	62	1043	k	210	940	67	9	(135) 1230	(141) 1311	(124) 2687	(119) 5398	(116) 10184	74 0.62 N ^{1.0}	
185	Thales	cogent	004	2021-02-10	1376	59	165	2053	-	214	947	107	14	(178) 2903	(163) 1911	(138) 3566	(139) 7498	(142) 16370	103 0.64 N ^{1.0}	
186	Thales	cogent	005	2021-09-13	1043	56	63	1062	-	155	769	27	5	(122) 912	(125) 996	(99) 1872	(97) 3845	(93) 7555	76 0.44 N ^{1.0}	
187	TigerIT Americas LLC	tiger	2	2018-10-29	416	518	157	2052	k	68	461	126	15	(160) 1816	(164) 1921	(143) 3833	(140) 7526	(138) 14820	81 0.83 N ^{1.0}	
188	TigerIT Americas LLC	tiger	3	2018-10-30	416	518	160	2052	k	67	461	216	10	(37) 3431	(39) 191	(37) 189	-	-	-	
189	Toshiba	toshiba	0	2018-10-30	961	105	79	1548	k	191	876	88	12	(209) 6153	(202) 6236	(169) 12221	(169) 25355	(165) 49448	154 0.36 N ^{1.2}	
190	Toshiba	toshiba	1	2018-10-30	961	105	174	2060	k	190	875	217	44701	(199) 6007	(204) 6355	-	-	-	-	
191	Triplezeize	aize	001	2021-08-06	262	150	132	2048	-	50	402	60	9	(181) 3087	(184) 3080	-	-	-	-	
192	Trueface.ai	trueface	000	2021-01-27	247	119	86	2000	-	37	363	98	13	(49) 271	(65) 327	(50) 614	(48) 1239	(43) 2678	71 0.15 N ^{1.0}	
193	Veridas Digital Authentication Solutions S.L.	veridas	001	2021-03-05	347	875	103	2048	-	187	872	91	13	(193) 5493	(197) 5469	(166) 10350	(160) 20655	(160) 41264	42 3.40 N ^{1.0}	
194	Veridas Digital Authentication Solutions S.L.	veridas	002	2021-07-06	347	870	143	2048	-	192	877	80	10	(63) 322	(63) 325	(55) 685	(53) 1365	(46) 2730	111 0.09 N ^{1.1}	
195	Veridas Digital Authentication Solutions S.L.	veridas	003	2021-11-09	346	870	118	2048	-	185	867	54	9	(82) 440	(64) 327	(57) 699	(54) 1401	(63) 3954	157 0.02 N ^{1.2}	
196	Viettel Group	vts	000	2021-03-12	250	257	95	2048	-	78	492	203	2295	(2) 4	(2) 4	(2) 6	(4) 11	-	13 0.61 N ^{0.6}	
197	Viettel Group	vts	001	2021-07-16	352	600	119	2048	-	197	891	153	21	(172) 2477	(177) 2487	(149) 4644	(147) 9313	(147) 18713	43 1.53 N ^{1.0}	
198	Viettel Group	vts	002	2022-02-08	244	600	145	2048	-	200	903	168	29	(173) 2485	(176) 2485	(151) 4678	(148) 9370	(149) 18833	47 1.49 N ^{1.0}	
199	Vigilant Solutions	vigilant	5	2018-10-30	335	122	78	1544	k	152	762	144	19	-	(157) 1720	-	-	-	-	-
200	Vigilant Solutions	vigilant	6	2018-10-30	337	122	77	1544	k	169	816	151	21	-	(156) 1713	-	-	-	-	-
201	Vigilant Solutions	vigilantsolutions	007	2021-01-08	340	51	75	1544	-	102	616	137	16	(146) 1354	(145) 1352	(128) 2911	(126) 5966	(122) 11466	122 0.27 N ^{1.1}	
202	Vigilant Solutions	vigilantsolutions	008	2021-07-23	340	51	76	1544	-	51	403	103	13	(130) 1062	(131) 1061	(112) 2330	(122) 5520	(107) 9499	143 0.11 N ^{1.1}	
203	Visidon	visidon	1	2018-10-30	166	42	151	2052	k	117	667	128	15	(187) 4370	(193) 4472	(163) 8454	(162) 17262	(158) 34288	57 2.40 N ^{1.0}	
204	Visidon	vd	002	2021-05-18	248	42	163	2052	-	127	687	35	9	(165) 2089	(172) 2336	-	-	-	-	
205	Visidon	vd	003	2021-10-12	497	43	152	2052	-	130	692	46	8	(166) 2095	(170) 2082	-	-	-	-	
206	Visiob-Box	visionbox	000	2021-09-17	252	274	173	2059	-	76	481	136	16	(77) 422	(67) 359	(62) 855	(26) 631	(37) 2096	16 2.46 N ^{0.8}	
207	VisionLabs	visionlabs	6	2018-10-30	360	17	51	512	1	29	289	213	20290	(14) 36	(14) 36	(12) 39	(11) 44	(9) 53	8 3211.93 N ^{0.2}	
208</td																				

	DEVELOPER	SHORT	SEQ.	VALIDATION	CONFIG ¹	LIB ¹	TEMPLATE GENERATION			FINALIZE ²	SEARCH DURATION ³ MILLISEC									
							NAME	NUM.	DATE	DATA (MB)	DATA (MB)	SIZE (B)	MULT ³	TIME (MS) ⁴	TIME (S)	L=1	L=50	L=50	L=50	POWER LAW
209	VisionLabs	visionlabs	008	2019-06-18	348	17	³³ 512	1	-	²⁵ 272	²¹¹ 12747	⁽⁹⁾ 23	⁽⁸⁾ 24	⁽⁷⁾ 26	⁽⁶⁾ 29	⁽⁵⁾ 33	⁶ 2539.61N ^{0.2}			
210	VisionLabs	visionlabs	009	2020-08-04	689	20	²⁶ 512	-	-	⁷¹ 467	²¹² 13245	⁽¹⁰⁾ 23	⁽⁹⁾ 29	⁽⁹⁾ 34	⁽¹²⁾ 61	⁽¹²⁾ 145	¹² 8.88N ^{0.6}			
211	VisionLabs	visionlabs	010	2021-02-05	1042	20	²⁵ 512	-	-	¹⁴⁴ 731	²⁰⁷ 11837	⁽⁷⁾ 21	⁽¹¹⁾ 32	⁽¹⁰⁾ 36	⁽⁸⁾ 39	⁽⁶⁾ 43	⁷ 3183.79N ^{0.2}			
212	VisionLabs	visionlabs	011	2021-10-20	1042	20	²⁸ 512	-	-	¹⁴⁶ 735	²¹⁰ 12255	⁽⁸⁾ 21	⁽⁷⁾ 23	⁽⁸⁾ 26	⁽⁷⁾ 34	⁽⁸⁾ 51	¹¹ 301.26N ^{0.3}			
213	Vocord	vocord	5	2018-10-30	1035	185	⁴⁴ 768	k	¹⁵⁹ 780	³⁷ 7	⁽³³⁾ 158	⁽³⁸⁾ 204	⁽³⁰⁾ 383	⁽³¹⁾ 767	⁽²⁶⁾ 1466	⁴⁵ 0.12N ^{1.0}				
214	Vocord	vocord	6	2018-10-30	1035	185	²¹⁷ 10240	k	¹⁶⁰ 785	²⁰² 243	⁽³⁴⁾ 170	⁽⁴¹⁾ 216	-	-	-	-				
215	Xforward AI Technology	xforwardai	000	2020-07-24	236	171	¹⁴² 2048	-	-	¹⁴⁹ 753	¹⁰⁸ 13	⁽¹⁸⁸⁾ 4603	⁽²¹⁰⁾ 7647	⁽¹⁷⁷⁾ 15723	⁽¹⁶⁶⁾ 23900	⁽¹⁶⁸⁾ 53729	¹⁴⁴ 0.56N ^{1.1}			
216	Xforward AI Technology	xforwardai	001	2021-01-21	332	50	¹⁰⁸ 2048	-	-	¹²³ 677	¹³⁴ 16	⁽¹⁹⁸⁾ 5887	⁽¹⁹²⁾ 4384	⁽¹⁶⁴⁾ 8798	⁽¹⁶³⁾ 18553	⁽¹⁵¹⁾ 48993	¹⁵¹ 0.32N ^{1.1}			
217	Xforward AI Technology	xforwardai	002	2021-05-24	691	50	¹⁹¹ 4096	-	-	²⁰⁸ 930	¹⁴² 18	⁽²⁰⁵⁾ 6957	⁽²⁰⁵⁾ 6400	⁽¹⁷³⁾ 12659	⁽¹⁷³⁾ 31077	⁽¹⁷¹⁾ 65158	¹⁴⁹ 0.52N ^{1.1}			

Notes

- Configuration size does not capture static data present in libraries. Libraries are included but the size also includes any ancillary libraries for image processing (e.g. openCV) or numerical computation (e.g. blas).
- Finalization is the processing of converting N = 1600000 templates into a searchable data structure an operation which can be a simple copy, or the building of an index or tree, for example. The duration of the operation may be data dependent, and may not be linear in the number of input templates.
- This multiplier expresses the increase in template size when k images are passed to the template generation function.
- All durations are measured on Intel®Xeon®CPU E5-2630 v4 @ 2.20GHz processors. Estimates are made by wrapping the API function call in calls to std::chrono::high_resolution_clock which on the machine in (3) counts 1ns clock ticks. Precision is somewhat worse than that however.
- Search durations are measured as in the prior note. The power-law model in the final column mostly fits the empirical results in Figure 134. However in certain cases the model is not correct and should not be used numerically.

Table 6: Summary of algorithms and properties included in this report. The blue superscripts give ranking for the quantity in that column. Missing search durations, denoted by “-”, are absent because those runs were not executed, usually because we did not run on the larger galleries. Caution: The power-law model is sometimes an incorrect model. It is included here only to show broad sublinear behavior, which is flagged in green. The models should not be used for prediction.

2022/03/30
17:50:48FNIR(N, R, T) = False neg. identification rate
FPFR(N, T) = False pos. identification rateN = Num. enrolled subjects
R = Num. candidates examined

T = Threshold

T = 0 → Investigation
T > 0 → Identification

#	ALGORITHM	INVESTIGATION ₁ FNIR(N, R = 1, T = 0)								IDENTIFICATION ₂ FNIR(N, R = L, T ≥ 0) FOR FPIR = 0.001								
		(0, 2]	(2, 4]	(4, 6]	(6, 8]	(8, 10]	(10, 12]	(12, 14]	(14, 18]	(0, 2]	(2, 4]	(4, 6]	(6, 8]	(8, 10]	(10, 12]	(12, 14]	(14, 18]	
1	3DIVI-005	97.0207	97.0304	97.0415	97.0533	97.0646	112.0735	112.0884	113.0148	107.01580	98.02316	98.03033	98.03740	98.04285	113.04742	111.05329	117.05975	
2	ANKE-000	95.0162	95.0245	95.0333	95.0428	95.0515	109.0615	109.0780	109.1028	96.01132	95.01761	95.02402	95.03057	95.03640	110.04200	110.04928	110.05680	
3	ANKE-002	4.0055	50.0074	50.0090	49.0103	48.00116	64.00135	63.00162	62.00202	54.00329	54.00560	56.00843	57.01169	57.01481	71.01820	72.02280	71.02831	
4	AWARE-005	106.0328	106.0519	106.0712	109.0910	109.01078	119.01235	119.01457	119.01831	108.03605	107.04949	107.05948	107.06783	108.07393	123.07905	123.08408	124.08831	
5	AWARE-006	110.0702	111.0110	111.01502	111.01899	111.02253	126.02614	125.03045	125.03659									
6	AYONIX-002	113.03360	114.04389	114.05144	114.05814	114.06340	129.06818	129.07297	130.07774	110.08288	111.09013	111.09375	111.09603	111.09744	127.09837	127.09893	127.09927	
7	CAMVI-004	109.0623	109.0944	109.01243	109.01548	109.01812	123.02056	123.02344	121.02672	91.0810	91.01267	88.02203	88.02619	101.03040	108.03543	96.04124		
8	CAMVI-005	111.0849	111.01255	111.01631	111.01989	111.02298	125.02585	124.02915	124.03246									
9	CANON-001						25.0052	22.0057	19.0042						27.00491	27.00606	28.00826	
10	CIB-000	114.0022	114.0030	115.0037	115.0044	117.00449	27.00557	27.0069	25.0062	25.0139	26.00240	27.00373	28.00525	28.00689	37.00859	38.01109	38.01454	
11	CLEARVIEWAI-000	1.0017	4.0023	4.0028	9.0034	11.0039	18.0046	21.0056	27.00407	16.00666	18.00121	18.00194	19.00287	19.00385	28.00493	30.00662	30.00873	
12	CLOUDWALK-HR-000	8.0019	7.0024	8.0029	6.0032	5.0032	5.0036	5.0041	3.0020	1.00029	1.00041	1.00054	1.00064	2.00073	4.00085	4.00102	4.00112	
13	CLOUDWALK-MT-000								1.0038	1.0013				1.0065	1.0072	1.0075		
14	COGENT-000	91.0128	99.0184	99.0250	92.0327	93.0407	108.0488	108.0611	105.0794	77.0559	79.0923	77.01342	78.01812	78.02243	99.02675	99.03240	92.03992	
15	COGENT-001	9.0128	91.0184	92.0250	93.0327	92.0407	102.0488	106.0611	104.0794	78.0559	78.0923	78.01342	77.01822	77.02243	88.02675	88.03240	93.03992	
16	COGENT-002	69.0081	66.0105	63.0123	64.0137	62.0157	77.0175	75.0215	75.0280	69.0499	68.0827	67.01207	66.01639	67.02037	81.02432	82.02972	83.03638	
17	COGENT-003	71.0082	67.0108	65.0128	67.0145	66.0168	83.0191	84.0239	81.0312	80.0582	80.0971	80.01417	80.1918	80.2380	98.02836	99.03440	99.04207	
18	COGENT-004	59.0066	59.0080	45.0085	39.00800	31.00883	45.00992	46.0106	49.0130	63.0410	65.0720	65.01099	65.01539	66.01974	82.02443	83.03043	85.03757	
19	COGNITEC-000	105.0265	103.0423	103.0588	103.0757	102.0894	117.01014	117.01169	116.01381	100.01522	99.02330	99.03051	99.03751	99.04300	114.04779	113.05307	111.05913	
20	COGNITEC-001	9.0149	99.0228	99.0312	94.0399	94.0479	105.0546	108.0656	106.0806	93.0963	93.01562	93.02157	93.02771	93.03287	108.03771	107.04343	108.04959	
21	COGNITEC-002	27.0101	80.0138	81.0170	81.0201	81.0237	95.0264	93.0309	92.0389	72.0517	71.0879	72.01269	73.01707	73.02098	83.02463	81.02919	81.03535	
22	COGNITEC-003	7.0104	81.0140	82.0174	82.0205	82.0238	96.0266	94.0311	94.0401	71.0504	70.0855	69.01235	68.01662	68.02045	80.02403	80.02854	79.03451	
23	COGNITEC-004	64.0073	63.0099	62.0118	59.0130	59.0147	76.0163	72.0189	71.0239	53.0325	53.0548	52.0798	51.074	50.01325	63.01591	62.01952	61.02414	
24	COGNITEC-006						39.0081	37.0086	38.0090				34.0777	34.0926	34.1274			
25	CUBOX-000	7.0019	5.0024	5.0028	4.0031	4.0032	6.0037	7.0044	7.0044	7.0027	6.0039	6.00559	7.0083	8.0111	8.0141	13.0185	13.0252	13.0339
26	CYBERLINK-002	5.0055	45.0068	41.0075	35.0078	32.0084	46.00994	47.0107	48.0114	32.0180	33.0302	33.0460	33.0643	33.0837	46.01058	45.01370	45.01787	
27	CYBERLINK-003	35.0041	34.0052	27.0057	25.0058	25.0061	36.0068	35.0078	35.0078	19.0109	19.0175	20.0259	21.0356	21.0468	31.0594	31.0787	32.01072	
28	DAHUA-002	3.0035	28.0047	28.0058	27.0067	28.0074	40.00882	43.0100	40.0108	30.0169	30.0294	31.0449	30.0635	30.0817	43.01013	42.01291	41.01638	
29	DAHUA-003	110.0026	19.0036	19.0043	20.0050	20.0055	29.0062	29.0080	31.0073	29.0160	30.0280	29.0432	29.0615	29.0794	41.0987	41.0987	39.01587	
30	DEEPLIGHT-001	17.0024	16.0032	14.0037	13.0040	13.0043	21.0049	23.0060	23.0052	12.0058	10.0087	11.0119	11.0195	11.0199	16.0249	16.0338	16.0463	
31	DEEPSEA-001	70.0081	70.0116	73.0149	76.0182	76.0216	94.0260	96.0332	96.0432	66.0458	66.0752	68.01086	68.01460	68.01812	78.02186	78.02663	77.03213	
32	DERMALOG-006	8.0113	82.0142	78.0163	77.0183	74.0200	88.0218	86.0251	84.0329	75.0545	73.0889	73.01271	73.01697	73.02090	84.02498	84.03028	84.03670	
33	DERMALOG-007	8.0125	88.0170	88.0214	88.0264	87.0309	101.0356	102.0432	102.0579	92.0910	92.1453	92.02009	92.2602	93.03134	10.03649	10.04289	10.05007	
34	DERMALOG-008	52.0057	52.0077	54.0095	54.0110	53.0128	70.0148	69.0180	70.0223	70.0501	69.0850	70.1247	71.01692	72.02105	86.02541	86.03102	86.03762	
35	FUJITSULAB-001						44.0089	42.0098	44.0111				59.01403	54.01723				
36	GORILLA-001	100.0213	100.0359	101.0528	102.0716	103.0895	118.01088	118.01367	118.01765	103.01828	104.02787	104.03654	104.04485	104.05168	117.05823	117.06508	117.07180	
37	GORILLA-005	38.0044	47.0070	58.0102	62.0136	67.0170	86.0204	89.0272	89.0373	79.0566	81.0973	82.01432	81.0937	81.02398	98.02862	97.03437	97.04150	
38	GORILLA-007						35.0108	52.0128	50.0145				73.01862	71.02198				
39	IDEMIA-003	81.0110	86.0151	86.0196	85.0238	84.0281	99.0313	99.0368	99.0504	87.0717	86.01147	86.01614	86.02113	85.02553	100.02976	99.03537	100.04334	
40	IDEMIA-004	80.0107	84.0148	88.0192	84.0233	83.0277	98.0312	98.0367	99.0512	88.0373	85.0587	84.0833	83.01100	82.01340	64.01580	61.01911	62.02482	
41	IDEMIA-005	8.0118	87.0167	90.0218	89.0270	88.0317	102.0357	101.0425	101.0579	65.0440	64.0689	64.0964	59.01254	56.01513	70.01762	65.02113	66.02698	
42	IDEMIA-006	87.0124	89.0171	89.0218	87.0263	86.0302	106.0321	97.0356	97.0471	62.0409	59.0620	57.0850	52.01097	49.01309	59.01486	56.01738	55.02200	
43	IDEMIA-007	4.0050	48.0071	48.0089	50.0106	51.0124	66.0142	66.0171	66.0220	36.0202	36.03235	34.0491	31.00663	31.00825	42.00999	39.01240	42.01645	
44	IDEMIA-008	1.0018	6.0024	6.0029	5.0032	7.00035	9.0039	12.0046	13.0033	3.0034	3.0051	3.0069	3.0087	3.0102	8.0123	7.0146	7.0186	

Table 7: Accuracy for the FRVT 2018 mugshot sets under ageing. The second row shows the time lapse between gallery and subsequent probe images, in years. The first two columns identify the algorithm. The next 8 values give rank-based FNIR with $R = 1$, $T = 0$ and FPIR = 1. All these are relevant to investigational uses where candidates from all searches would need human review. The second 8 values give threshold-based FNIR with $T \geq 0$, FPIR = 0.001 and no rank criterion. The shaded cells indicate the three most accurate algorithms for that elapsed time. The gallery size is 3068801. The total number of searches is 10951064.

2022/03/30

FNIR(N, R, T) =

False neg. identification rate

N = Num. enrolled subjects

R = Num. candidates examined

T = Threshold

T = 0 → Investigation

T > 0 → Identification

MISS RATES		INVESTIGATION, FNIR($N, R = 1, T = 0$)								IDENTIFICATION, FNIR($N, R = L, T \geq 0$) FOR FPIR = 0.001							
#	ALGORITHM	(0, 2]	(2, 4]	(4, 6]	(6, 8]	(8, 10]	(10, 12]	(12, 14]	(14, 18]	(0, 2]	(2, 4]	(4, 6]	(6, 8]	(8, 10]	(10, 12]	(12, 14]	(14, 18]
45	IDEMIA-009	³⁸ 0.0039	³⁷ 0.0052	³¹ 0.0061	²⁹ 0.0067	³⁰ 0.0077	⁴⁵ 0.0088	⁴⁴ 0.0103	⁴⁶ 0.0109	³⁹ 0.0212	³⁹ 0.0357	⁴⁰ 0.0539	⁴⁰ 0.0755	³⁸ 0.0967	⁵¹ 0.1183	⁵⁰ 0.1485	⁴⁸ 0.1893
46	IMAGUS-005	³⁴ 0.0040	³⁵ 0.0054	³⁶ 0.0067	³⁸ 0.0079	⁴⁰ 0.0093	⁵⁶ 0.0112	⁵⁵ 0.0139	⁵⁷ 0.0178	⁴⁹ 0.0286	⁵¹ 0.0503	⁵¹ 0.0779	⁵⁴ 0.1116	⁵⁶ 0.1455	⁷² 0.1844	⁷⁵ 0.2341	⁷⁴ 0.2951
47	IMPERIAL-000	⁹¹ 0.0155	⁹⁶ 0.0247	⁹⁶ 0.0348	⁹⁶ 0.0463	⁹⁶ 0.0571	¹¹¹ 0.0674	¹¹¹ 0.0856	¹¹² 0.1114	¹⁰² 0.1627	¹⁰² 0.2507	¹⁰² 0.3322	¹⁰⁰ 0.4122	¹⁰⁰ 0.4772	¹¹⁶ 0.5368	¹¹⁶ 0.6059	¹¹⁶ 0.6766
48	INCODE-003	⁵⁶ 0.0061	⁵⁹ 0.0087	⁵⁹ 0.0110	⁶¹ 0.0136	⁶⁴ 0.0161	⁷⁹ 0.0185	⁸² 0.0236	⁸⁰ 0.0309	⁷³ 0.0532	⁷⁴ 0.0908	⁷⁵ 0.1334	⁷⁷ 0.1809	⁷⁷ 0.2245	⁹¹ 0.2675	⁹⁰ 0.3249	⁸⁹ 0.3932
49	INCODE-004	¹¹⁴ 0.3594	¹¹³ 0.3629	¹¹¹ 0.3688	¹¹² 0.3754	¹¹² 0.3813	¹²⁷ 0.3870	¹²⁷ 0.3960	¹²⁷ 0.4135	¹⁰² 0.4234	¹⁰⁶ 0.4642	¹⁰⁶ 0.5073	¹⁰⁶ 0.5522	¹⁰⁵ 0.5902	¹²² 0.6274	¹¹⁶ 0.6736	¹¹⁶ 0.7253
50	INNOVATRICS-004	⁴¹ 0.0046	⁴¹ 0.0063	⁴² 0.0078	⁴⁵ 0.0092	⁴⁵ 0.0106	⁵⁸ 0.0124	⁵⁸ 0.0149	⁵⁸ 0.0178	³⁵ 0.0343	⁵⁶ 0.0590	⁵⁸ 0.0886	⁵⁸ 0.1222	⁵⁹ 0.1544	⁷³ 0.1881	⁷⁴ 0.2321	⁷² 0.2874
51	INNOVATRICS-005	²¹ 0.0031	²⁴ 0.0042	²⁵ 0.0051	²⁶ 0.0060	²⁶ 0.0068	³⁸ 0.0080	⁴⁰ 0.0095	⁴¹ 0.0107	⁵² 0.0313	⁵² 0.0539	⁵³ 0.0815	⁵⁶ 0.1137	⁵⁷ 0.1442	⁶⁹ 0.1755	⁷⁰ 0.2181	⁶⁸ 0.2718
52	IREX-000	⁷⁶ 0.0101	⁷⁹ 0.0135	⁸⁰ 0.0169	⁷⁹ 0.0197	⁸⁰ 0.0228	⁹² 0.0256	⁹² 0.0304	⁹³ 0.0398	⁹⁰ 0.0779	⁹⁸ 0.1258	⁹¹ 0.1759	⁹⁰ 0.2299	⁹⁰ 0.2758	¹⁰⁴ 0.3204	¹⁰⁴ 0.3763	¹⁰² 0.4401
53	ISYSTEMS-002	⁷⁷ 0.0089	⁶⁹ 0.0115	⁶⁹ 0.0139	⁶⁹ 0.0158	⁷⁰ 0.0177	⁸⁵ 0.0198	⁸¹ 0.0234	⁷⁸ 0.0303	⁸⁴ 0.0647	⁸⁴ 0.1056	⁸⁴ 0.1502	⁸¹ 0.1986	⁸¹ 0.2402	⁹⁴ 0.2819	⁹³ 0.3351	⁹¹ 0.3976
54	ISYSTEMS-003	⁸³ 0.0116	⁷⁵ 0.0130	⁶⁹ 0.0135	⁶⁹ 0.0133	⁵⁷ 0.0135	⁶⁵ 0.0141	⁵⁹ 0.0151	⁵⁶ 0.0176	⁴¹ 0.0241	⁴¹ 0.0360	³⁹ 0.0513	³⁴ 0.0689	³⁴ 0.0866	⁴⁷ 0.1060	⁴³ 0.1327	⁴³ 0.1694
55	KEDACOM-001	⁸⁸ 0.0123	⁸³ 0.0144	⁷⁷ 0.0158	⁷⁰ 0.0168	⁷¹ 0.0178	⁸¹ 0.0188	⁷⁴ 0.0212	⁷⁴ 0.0260	⁶⁴ 0.0438	⁶² 0.0687	⁶¹ 0.0978	⁶¹ 0.1296	⁶¹ 0.1581	⁷⁴ 0.1879	⁷³ 0.2294	⁷⁰ 0.2756
56	LOOKMAN-003	⁸⁸ 0.0118	⁷⁷ 0.0134	⁷⁰ 0.0142	⁶⁶ 0.0144	⁶¹ 0.0150	⁷⁵ 0.0160	⁶⁷ 0.0176	⁶⁵ 0.0213	⁵¹ 0.0310	⁴⁹ 0.0480	⁴⁶ 0.0698	⁴⁶ 0.0954	⁴⁶ 0.1216	⁶⁰ 0.1491	⁶⁰ 0.1890	⁶⁰ 0.2381
57	LOOKMAN-005	¹¹⁵ 0.4269	¹¹⁵ 0.5527	¹¹⁶ 0.6355	¹¹⁶ 0.7024	¹¹⁶ 0.7503	¹³¹ 0.7876	¹³¹ 0.8234	¹³² 0.8601	¹¹¹ 0.8338	¹¹² 0.9113	¹¹² 0.9468	¹¹² 0.9667	¹¹² 0.9771	¹²⁶ 0.9836	¹²⁶ 0.9880	¹²⁶ 0.9924
58	MICROFOCUS-005	²⁸ 0.0034	³² 0.0050	³³ 0.0064	³⁶ 0.0078	³⁸ 0.0092	⁵² 0.0107	⁵⁴ 0.0135	⁵⁵ 0.0166	⁵⁰ 0.0288	⁵⁰ 0.0503	⁵⁰ 0.0763	⁵⁰ 0.1067	⁵⁴ 0.1359	⁶⁷ 0.1680	⁶⁶ 0.2116	⁶⁴ 0.2644
59	MICROSOFT-003	²⁷ 0.0032	²⁷ 0.0047	²⁹ 0.0060	³² 0.0075	³⁵ 0.0087	⁴⁹ 0.0103	⁵³ 0.0131	⁵⁸ 0.0159	⁴⁷ 0.0268	⁴⁸ 0.0470	⁴⁷ 0.0716	⁴⁸ 0.1007	⁴⁷ 0.1291	⁶⁴ 0.1610	⁶³ 0.2052	⁶³ 0.2590
60	MICROSOFT-004	²² 0.0031	²⁹ 0.0047	³⁵ 0.0066	⁴³ 0.0084	⁴³ 0.0103	⁶² 0.0131	⁶⁴ 0.0164	⁶⁰ 0.0185	⁴³ 0.0243	⁴⁴ 0.0432	⁴⁴ 0.0658	⁴⁴ 0.0913	⁴⁷ 0.1172	⁵⁷ 0.1476	⁵⁹ 0.1874	⁵⁷ 0.2272
61	MICROSOFT-005	²² 0.0032	³¹ 0.0049	³⁴ 0.0065	⁴² 0.0081	⁴² 0.0096	⁵⁷ 0.0117	⁵⁶ 0.0144	⁵⁴ 0.0160	²⁴ 0.0134	²⁴ 0.0233	²⁵ 0.0346	²³ 0.0462	²² 0.0578	³³ 0.0713	³³ 0.0903	³³ 0.1156
62	MICROSOFT-006	⁹⁷ 0.0195	⁹⁹ 0.0316	⁹⁹ 0.0445	⁹⁹ 0.0581	⁹⁸ 0.0699	¹¹⁴ 0.0817	¹¹⁴ 0.0998	¹¹⁴ 0.1237	⁸⁹ 0.0759	⁸⁹ 0.1245	⁸⁹ 0.1729	⁸⁹ 0.2240	⁸⁷ 0.2671	¹⁰³ 0.3117	¹⁰³ 0.3639	¹⁰³ 0.4348
63	NEC-000	¹⁰⁴ 0.0246	¹⁰² 0.0382	¹⁰¹ 0.0524	¹⁰¹ 0.0672	¹⁰¹ 0.0793	¹¹⁶ 0.0904	¹¹⁵ 0.1076	¹¹⁵ 0.1317	⁹⁴ 0.1019	⁹⁴ 0.1623	⁹⁴ 0.2214	⁹⁴ 0.2834	⁹⁴ 0.3341	¹⁰⁹ 0.3844	¹⁰⁸ 0.4440	¹⁰⁸ 0.5183
64	NEC-001	¹⁰⁴ 0.0246	¹⁰² 0.0382	¹⁰¹ 0.0524	¹⁰¹ 0.0672	¹⁰¹ 0.0793	¹¹⁶ 0.0904	¹¹⁵ 0.1076	¹¹⁵ 0.1317	⁹⁴ 0.1019	⁹⁴ 0.1623	⁹⁴ 0.2214	⁹⁴ 0.2834	⁹⁴ 0.3341	¹⁰⁹ 0.3844	¹⁰⁸ 0.4440	¹⁰⁸ 0.5183
65	NEC-002	²² 0.0033	²² 0.0041	¹⁸ 0.0043	¹⁶ 0.0044	¹⁵ 0.0045	²⁰ 0.0049	²⁰ 0.0056	¹⁹ 0.0061	¹⁵ 0.0066	¹¹ 0.0090	¹⁰ 0.0111	¹⁰ 0.0131	⁹ 0.0149	¹¹ 0.0171	¹² 0.0207	¹² 0.0267
66	NEC-003	³¹ 0.0036	²⁶ 0.0046	²⁴ 0.0051	²⁴ 0.0055	²⁴ 0.0059	³¹ 0.0067	³¹ 0.0077	³³ 0.0073	⁹ 0.0056	⁹ 0.0076	⁹ 0.0091	⁷ 0.0105	⁶ 0.0119	¹⁰ 0.0137	⁹ 0.0162	⁹ 0.0209
67	NEC-004	³⁷ 0.0039	²⁵ 0.0045	²² 0.0047	¹⁸ 0.0046	¹⁴ 0.0044	¹⁹ 0.0046	¹⁸ 0.0052	¹⁸ 0.0052	⁷ 0.0046	⁵ 0.0057	⁴ 0.0063	⁴ 0.0066	² 0.0076	² 0.0090	² 0.0105	³ 0.0107
68	NEC-005								⁸ 0.0037	⁴ 0.0041	⁴ 0.0040				³ 0.0080	³ 0.0091	³ 0.0107
69	NEUROTECHNOLOGY-003	¹⁰¹ 0.0234	¹⁰¹ 0.0379	¹⁰² 0.0549	¹⁰¹ 0.0682	¹⁰⁰ 0.0720	¹¹³ 0.0747	¹¹³ 0.0886	¹¹¹ 0.1066	¹⁰⁹ 0.6802	¹⁰⁹ 0.8187	¹¹⁰ 0.8920	¹¹⁰ 0.9355	¹¹⁰ 0.9594	¹²⁰ 0.9738	¹²⁰ 0.9828	¹²⁰ 0.9885
70	NEUROTECHNOLOGY-004	⁷⁹ 0.0104	⁷⁸ 0.0134	⁷⁶ 0.0156	⁷³ 0.0173	⁷² 0.0195	⁸⁷ 0.0212	⁸⁵ 0.0245	⁸² 0.0320	⁸³ 0.0642	⁸² 0.1015	⁸¹ 0.1426	⁷⁹ 0.1881	⁷⁸ 0.2299	⁹² 0.2722	⁹¹ 0.3269	⁹⁰ 0.3943
71	NEUROTECHNOLOGY-005	⁷⁴ 0.0089	⁷¹ 0.0116	⁶⁸ 0.0136	⁶⁸ 0.0152	⁶⁹ 0.0173	⁸⁴ 0.0196	⁸⁰ 0.0233	⁷⁶ 0.0306	⁷⁶ 0.0556	⁷⁶ 0.0913	⁷⁴ 0.1315	⁷⁴ 0.1766	⁷¹ 0.2192	⁸⁸ 0.2617	⁸⁷ 0.3174	⁸⁸ 0.3843
72	NEUROTECHNOLOGY-007	⁶⁶ 0.0078	⁶⁹ 0.0103	⁶⁴ 0.0124	⁶⁵ 0.0140	⁶³ 0.0161	⁷⁸ 0.0185	⁷⁷ 0.0225	⁷⁶ 0.0290	⁸² 0.0641	⁸⁵ 0.1069	⁸⁵ 0.1546	⁸⁵ 0.2075	¹⁰² 0.3081	¹⁰³ 0.3713	¹⁰³ 0.4421	¹⁰³ 0.5133
73	NEUROTECHNOLOGY-010								²⁴ 0.0053	²⁴ 0.0061	²⁵ 0.0053				³⁸ 0.0863	³⁶ 0.1050	³⁶ 0.1333
74	NOBLIS-002	¹¹² 0.1520	¹¹² 0.2419	¹¹² 0.3296	¹¹³ 0.4114	¹¹² 0.4856	¹²⁸ 0.5528	¹²⁸ 0.6061	¹²⁸ 0.6532	¹¹³ 0.9984	¹¹³ 0.9996	¹¹³ 0.9998	¹¹³ 0.9999	¹²⁸ 1.0000	¹³² 1.0000	¹³² 1.0000	¹³² 1.0000
75	NTechLab-003	⁶⁵ 0.0078	⁷⁶ 0.0131	⁸² 0.0202	⁹⁰ 0.0295	⁹¹ 0.0405	¹⁰⁸ 0.0543	¹⁰⁹ 0.0761	¹¹⁰ 0.1035	⁶⁸ 0.0491	⁷² 0.0881	⁷⁹ 0.1384	⁸³ 0.1985	⁸⁷ 0.2594	¹⁰⁵ 0.3270	¹⁰⁵ 0.4065	¹⁰⁵ 0.4891
76	NTechLab-004	⁶² 0.0068	⁶⁸ 0.0110	⁷⁹ 0.0167	⁸⁶ 0.0239	⁸⁹ 0.0330	¹⁰⁵ 0.0471	¹⁰⁷ 0.0641	¹⁰⁸ 0.0891	⁶⁰ 0.0379	⁶³ 0.0688	⁶⁶ 0.1108	⁶⁹ 0.1629	⁷³ 0.2192	⁹² 0.2846	¹⁰⁵ 0.3657	¹⁰⁵ 0.4524
77	NTechLab-006	⁵¹ 0.0056	⁶² 0.0095	⁷² 0.0148	⁸³ 0.0218	⁸⁵ 0.0301	¹⁰³ 0.0413	¹⁰⁴ 0.0591	¹⁰⁷ 0.0814	⁵⁶ 0.0349	⁶⁰ 0.0636	⁶³ 0.1023	⁶⁴ 0.1506	⁶⁶ 0.2024	⁸⁷ 0.2617	⁹⁴ 0.3374	⁹⁸ 0.4185
78	NTechLab-007	¹⁷ 0.0044	⁴³ 0.0066	⁴⁹ 0.0089	⁵⁷ 0.0118	⁶⁰ 0.0150	⁸² 0.0189	⁸⁷ 0.0255	⁸⁷ 0.0342	⁴⁵ 0.0256	⁴⁶ 0.0450	⁴⁸ 0.0705	⁴⁹ 0.1012				

#	ALGORITHM	INVESTIGATION, FNIR(N, R = 1, T = 0)								IDENTIFICATION, FNIR(N, R = L, T ≥ 0) FOR FPIR = 0.001							
		(0, 2]	(2, 4]	(4, 6]	(6, 8]	(8, 10]	(10, 12]	(12, 14]	(14, 18]	(0, 2]	(2, 4]	(4, 6]	(6, 8]	(8, 10]	(10, 12]	(12, 14]	(14, 18]
89	PIXELLALL-002	⁷² 0.0085	⁷⁰ 0.0119	⁷¹ 0.0147	⁷² 0.0172	⁷³ 0.0198	⁸⁹ 0.0225	⁸⁸ 0.0270	⁸⁹ 0.0349	⁹⁷ 0.1193	⁹⁷ 0.1900	⁹⁷ 0.2601	⁹⁷ 0.3322	⁹⁷ 0.3955	¹¹² 0.4565	¹¹² 0.5268	¹¹¹ 0.6030
90	PIXELLALL-003	⁴⁶ 0.0050	⁴² 0.0063	³⁹ 0.0072	³⁴ 0.0077	³³ 0.0085	⁴⁷ 0.0095	⁴⁸ 0.0113	⁴⁶ 0.0119	⁴⁴ 0.0248	⁴³ 0.0418	⁴³ 0.0622	⁴³ 0.0861	⁴³ 0.1104	⁵³ 0.1364	⁵³ 0.1723	⁵³ 0.2167
91	PIXELLALL-004	⁴⁵ 0.0049	⁴⁰ 0.0063	⁴¹ 0.0072	³⁷ 0.0079	³⁶ 0.0089	⁵¹ 0.0103	⁵¹ 0.0127	⁵¹ 0.0146	³⁸ 0.0211	⁴⁰ 0.0360	⁴² 0.0553	⁴² 0.0792	³⁹ 0.1045	³⁷ 0.1317	⁵² 0.1700	⁵⁶ 0.2246
92	PTAKURATSATU-000	⁵⁴ 0.0061	⁵⁵ 0.0082	⁵⁵ 0.0097	⁵³ 0.0109	⁴⁹ 0.0120	⁶¹ 0.0131	⁵⁷ 0.0146	⁵⁹ 0.0180	⁵⁹ 0.0375	⁵⁷ 0.0596	⁵⁵ 0.0842	⁵⁵ 0.1116	⁵³ 0.1357	⁶³ 0.1553	⁵⁷ 0.1820	⁵⁹ 0.2326
93	RANKONE-002	⁹⁹ 0.0212	⁹⁸ 0.0313	⁹⁶ 0.0431	⁹⁸ 0.0562	⁹⁹ 0.0712	¹¹¹ 0.0881	¹¹⁶ 0.1130	¹¹⁷ 0.1543	⁹⁵ 0.1111	⁹⁵ 0.1707	⁹⁵ 0.2305	⁹⁵ 0.2968	⁹⁶ 0.3646	¹¹¹ 0.4345	¹¹¹ 0.5172	¹¹¹ 0.6110
94	RANKONE-004	¹⁰⁸ 0.0424	¹⁰⁷ 0.0643	¹⁰⁷ 0.0875	¹⁰⁷ 0.1127	¹⁰⁷ 0.1364	¹²⁰ 0.1579	¹²⁰ 0.1914	¹²⁰ 0.2378	¹⁰⁴ 0.1855	¹⁰³ 0.2681	¹⁰³ 0.3431	¹⁰¹ 0.4155	¹⁰¹ 0.4785	¹¹⁵ 0.5350	¹¹⁵ 0.5980	¹¹⁵ 0.6722
95	RANKONE-005	⁹² 0.0136	⁹³ 0.0192	⁹¹ 0.0246	⁹¹ 0.0303	⁹⁰ 0.0362	¹⁰⁴ 0.0422	¹⁰³ 0.0521	¹⁰³ 0.0694	⁸¹ 0.0582	⁷⁵ 0.0910	⁷¹ 0.1260	⁶⁸ 0.1645	⁶⁵ 0.2005	⁷⁹ 0.2353	⁸⁰ 0.2816	⁸⁰ 0.3522
96	RANKONE-007	⁶⁷ 0.0078	⁶⁹ 0.0099	⁶¹ 0.0113	⁵⁸ 0.0123	⁵⁸ 0.0139	⁷⁴ 0.0156	⁷³ 0.0191	⁷² 0.0242	⁴² 0.0242	⁴² 0.0376	⁴¹ 0.0542	³⁸ 0.0737	³⁷ 0.0935	⁴⁰ 0.1130	⁴⁷ 0.1416	⁴⁷ 0.1811
97	RANKONE-009	⁴⁸ 0.0054	⁴⁹ 0.0072	⁴⁶ 0.0085	⁴⁷ 0.0098	⁴⁷ 0.0113	⁶⁰ 0.0130	⁶⁵ 0.0169	⁶⁹ 0.0220	³⁷ 0.0208	³⁸ 0.0345	³⁷ 0.0504	³⁶ 0.0706	³⁶ 0.0930	⁵¹ 0.1174	⁵⁰ 0.2002	
98	RANKONE-010	⁴² 0.0047	³⁹ 0.0061	³⁶ 0.0070	³⁵ 0.0076	³⁴ 0.0087	⁴⁸ 0.0098	⁴⁹ 0.0113	⁴⁷ 0.0120	³¹ 0.0177	²⁹ 0.0269	²⁶ 0.0368	²⁶ 0.0479	²⁵ 0.0590	³⁹ 0.0688	³¹ 0.0991	
99	RANKONE-011	²³ 0.0031	²³ 0.0041	²³ 0.0047	²³ 0.0053	²² 0.0058	³⁴ 0.0067	³⁰ 0.0077	³² 0.0073	²³ 0.0127	²⁰ 0.0194	²¹ 0.0265	²⁰ 0.0345	²¹ 0.0422	²⁹ 0.0499	²⁸ 0.0611	²⁶ 0.0756
100	RANKONE-012						³⁰ 0.0065	²⁸ 0.0069	²³ 0.0053					²⁹ 0.0460	²⁴ 0.0540	²¹ 0.0672	
101	REALNETWORKS-002	¹⁰⁷ 0.0381	¹⁰⁸ 0.0687	¹⁰⁸ 0.1062	¹⁰⁸ 0.1495	¹⁰⁹ 0.1963	¹²⁴ 0.2513	¹²⁶ 0.3206	¹²⁶ 0.3927	¹⁰⁵ 0.2153	¹⁰⁵ 0.3323	¹⁰⁵ 0.4444	¹⁰⁵ 0.5485	¹⁰⁶ 0.6355	¹²¹ 0.7132	¹²² 0.7855	¹²³ 0.8437
102	REALNETWORKS-003	¹⁰³ 0.0245	¹⁰⁵ 0.0437	¹⁰⁵ 0.0686	¹⁰⁶ 0.0975	¹⁰⁶ 0.1312	¹²² 0.1719	¹²² 0.2294	¹²³ 0.2907	⁹⁸ 0.1468	¹⁰⁶ 0.2370	¹⁰¹ 0.3313	¹⁰³ 0.4269	¹⁰³ 0.5142	¹¹⁹ 0.5979	¹²⁰ 0.6815	¹²⁰ 0.7567
103	REALNETWORKS-004	¹⁰² 0.0244	¹⁰⁴ 0.0428	¹⁰⁴ 0.0663	¹⁰⁵ 0.0939	¹⁰⁵ 0.1251	¹²¹ 0.1634	¹²¹ 0.2170	¹²² 0.2785	⁹⁹ 0.1484	¹⁰¹ 0.2377	¹⁰⁰ 0.3303	¹⁰² 0.4249	¹⁰² 0.5106	¹¹⁸ 0.5924	¹¹⁹ 0.6758	¹¹⁹ 0.7534
104	REALNETWORKS-006								³⁷ 0.0069	³² 0.0077	³⁶ 0.0080			⁴⁴ 0.1022	⁴⁶ 0.1253	⁴⁰ 0.1622	
105	SCANOVATE-001	⁶⁸ 0.0079	⁷² 0.0117	⁷⁸ 0.0151	⁷⁸ 0.0185	⁷⁸ 0.0221	⁹³ 0.0259	⁹⁵ 0.0321	⁹⁵ 0.0427	⁸⁸ 0.0727	⁸⁸ 0.1169	⁸⁷ 0.1650	⁸⁷ 0.2115	⁸⁴ 0.2528	⁹⁰ 0.2925	⁹⁶ 0.3437	⁹⁵ 0.4084
106	SENSETIME-002	⁹⁵ 0.0186	⁹² 0.0191	⁸⁴ 0.0183	⁷³ 0.0179	⁶⁸ 0.0173	⁶³ 0.0133	³⁹ 0.0089	²⁶ 0.0059	⁴⁰ 0.0220	²⁵ 0.0236	¹⁹ 0.0237	¹⁸ 0.0240	¹² 0.0245	¹⁰ 0.0219	¹¹ 0.0195	¹⁰ 0.0222
107	SENSETIME-003	¹¹¹ 0.0021	¹² 0.0028	¹¹ 0.0031	⁷ 0.0033	⁶ 0.0035	¹⁰ 0.0040	¹³ 0.0047	¹² 0.0033	⁸ 0.0046	⁸ 0.0064	⁶ 0.0076	⁴ 0.0086	⁴ 0.0101	⁷ 0.0122	⁸ 0.0155	⁸ 0.0196
108	SENSETIME-004	³ 0.0016	³ 0.0022	³ 0.0025	³ 0.0028	³ 0.0030	⁴ 0.0035	⁸ 0.0043	⁷ 0.0025	⁴ 0.0036	⁴ 0.0052	³ 0.0066	³ 0.0081	³ 0.0099	⁹ 0.0126	¹¹ 0.0169	¹¹ 0.0230
109	SENSETIME-005	¹ 0.0015	² 0.0020	² 0.0024	² 0.0026	² 0.0029	³ 0.0035	³ 0.0043	¹⁰ 0.0028	⁵ 0.0036	⁵ 0.0059	⁸ 0.0089	⁸ 0.0128	¹⁰ 0.0177	¹⁰ 0.0240	¹⁷ 0.0345	¹⁷ 0.0493
110	SENSETIME-006	¹ 0.0015	¹ 0.0019	¹ 0.0022	¹ 0.0025	¹ 0.0027	¹ 0.0033	³ 0.0040	⁵ 0.0021	² 0.0031	² 0.0049	⁴ 0.0068	⁶ 0.0097	⁷ 0.0132	¹² 0.0184	¹⁴ 0.0262	¹⁴ 0.0359
111	SENSETIME-007						² 0.0035	¹ 0.0038	¹ 0.0015					⁶ 0.0112	⁶ 0.0140	⁶ 0.0176	
112	SIAT-002	¹¹⁷ 0.8309	¹¹⁷ 0.8310	¹¹⁷ 0.8311	¹¹⁷ 0.8306	¹¹⁷ 0.8296	¹³² 0.8302	¹³² 0.8300	¹³¹ 0.8301	¹¹² 0.8340	¹¹⁰ 0.8368	¹⁰⁹ 0.8404	¹⁰⁹ 0.8445	¹⁰⁹ 0.8480	¹²⁴ 0.8532	¹²⁴ 0.8595	¹²⁵ 0.8691
113	SYNSES-003	⁸⁹ 0.0125	⁸³ 0.0151	⁸¹ 0.0174	⁸⁰ 0.0199	⁷⁹ 0.0223	⁹⁰ 0.0240	⁹⁰ 0.0279	⁸⁵ 0.0331	⁸⁵ 0.0658	⁸³ 0.1052	⁸³ 0.1483	⁸² 0.1968	⁸² 0.2399	⁹⁵ 0.2834	⁹⁴ 0.3405	⁹⁴ 0.4046
114	SYNSES-005	⁴⁰ 0.0044	³⁷ 0.0058	³⁷ 0.0070	⁴⁰ 0.0080	³⁷ 0.0091	⁵⁰ 0.0103	⁵⁰ 0.0125	⁵² 0.0152	⁴⁶ 0.0262	⁴⁵ 0.0444	⁴⁵ 0.0666	⁴⁵ 0.0923	⁴⁴ 0.1156	⁵⁴ 0.1399	⁵⁵ 0.1736	⁵⁴ 0.2185
115	TECH-001	³ 0.0061	⁶ 0.0093	⁶ 0.0128	⁷¹ 0.0171	⁷⁷ 0.0221	⁹⁷ 0.0289	¹⁰⁶ 0.0412	¹⁰⁶ 0.0560	⁸⁶ 0.0660	⁸⁷ 0.1156	⁹⁰ 0.1733	⁹¹ 0.2385	⁹¹ 0.2998	¹⁰⁶ 0.3629	¹⁰⁸ 0.4424	¹⁰⁸ 0.5284
116	TOSHIBA-001	⁷³ 0.0086	⁷⁴ 0.0119	⁷⁴ 0.0150	⁷⁴ 0.0178	⁷⁵ 0.0209	⁹¹ 0.0241	⁹¹ 0.0292	⁹⁰ 0.0365								
117	TRUEFACE-000	⁴ 0.0043	³ 0.0057	³ 0.0061	²⁸ 0.0067	²⁷ 0.0073	⁴¹ 0.0084	⁴¹ 0.0097	³⁹ 0.0099	³⁵ 0.0200	³⁷ 0.0338	³⁸ 0.0504	³⁸ 0.0705	³⁸ 0.0904	⁴⁸ 0.1112	⁴⁶ 0.1401	⁴⁶ 0.1792
118	VERIDAS-001	⁵⁸ 0.0063	⁵⁶ 0.0083	⁵⁶ 0.0099	⁵⁶ 0.0113	⁵⁶ 0.0132	⁶⁹ 0.0148	⁷⁰ 0.0184	⁶⁷ 0.0219	⁶¹ 0.0403	⁶¹ 0.0684	⁶² 0.1012	⁶² 0.1386	⁶² 0.1741	⁷⁷ 0.2113	⁷⁷ 0.2611	⁷⁸ 0.3233
119	VISIONLABS-004	⁴³ 0.0048	⁴⁹ 0.0069	³⁹ 0.0091	⁵⁹ 0.0111	⁷² 0.0152	⁷¹ 0.0187	⁷³ 0.0242	⁷⁴ 0.0540	⁷⁷ 0.0916	⁷⁸ 0.1358	⁷⁸ 0.1855	⁷⁸ 0.2303	⁹² 0.2745	⁹² 0.3312	⁸⁸ 0.3913	
120	VISIONLABS-005	³⁹ 0.0044	³⁹ 0.0063	⁴³ 0.0081	⁴⁶ 0.0095	⁴⁶ 0.0109	⁵⁹ 0.0125	⁶⁰ 0.0151	⁶¹ 0.0187	⁶⁷ 0.0479	⁶⁷ 0.0812	⁶⁸ 0.1212	⁶⁹ 0.1664	⁶⁹ 0.2473	⁸³ 0.2999	⁸² 0.3577	
121	VISIONLABS-006	²⁹ 0.0035	³⁰ 0.0048	³⁰ 0.0061	³⁶ 0.0069	²⁹ 0.0077	⁴² 0.0087	⁴⁵ 0.0105	⁴⁸ 0.0120	⁴⁸ 0.0273	⁴⁷ 0.0465	⁴⁷ 0.0702	⁴⁷ 0.0970	⁴⁷ 0.1228	⁵⁶ 0.1847	⁵⁶ 0.2295	
122	VISIONLABS-008	²¹ 0.0028	²⁰ 0.0037	²¹ 0.0047	²² 0.0053	²³ 0.0058	³² 0.0067	³⁶ 0.0081	³⁷ 0.0085	²⁷ 0.0143	²⁷ 0.0241	²⁸ 0.0373	²⁷ 0.0519	²⁷ 0.0677	³⁰ 0.0850	³⁰ 0.1104	³⁰ 0.1444
123	VISIONLABS-009	¹⁰ 0.0020	¹¹ 0.0026	¹⁰ 0.0030	¹⁰ 0.0034	¹⁶ 0.0044	¹⁷ 0.0052	²⁰ 0.0046	¹⁴ 0.0065	¹⁵ 0.0105	¹⁵ 0.0156	¹⁵ 0.0217	¹⁶ 0.0289	²³ 0.0368	²² 0.0681		
124	VISIONLABS-010	⁹ 0.0020	⁹ 0.0025	⁹ 0.0030	¹¹ 0.0034	⁹ 0.0036	¹⁵ 0.0043	^{15</sup}									

#	ALGORITHM	INVESTIGATION MODE						IDENTIFICATION MODE						FAILURE TO EXTRACT FEATURES						
		RANK ONE MISS RATE, FNIR(N, 0, 1)						HIGH T → FPIR = 0.001, FNIR(N, T, L)												
		N=1.6M						N=1.6M												
GALLERY	MUGSHOT	MUGSHOT	MUGSHOT	VISA	BORDER	BOR ₁ 10YR	KIOSK	MUGSHOT	MUGSHOT	MUGSHOT	VISA	BORDER	BOR ₁ 10YR	KIOSK	MUGSHOT	MUGSHOT	MUGSHOT	VISA	BORDER	KIOSK
PROBE	MUGSHOT	WEBCAM	PROFILE	BORDER	BOR ₁ 10YR	KIOSK		MUGSHOT	WEBCAM	PROFILE	BORDER	BOR ₁ 10YR	KIOSK	MUGSHOT	WEBCAM	PROFILE	BORDER	BOR ₁ 10YR	KIOSK	
1	20FACE-000	²⁴ 0.055	²³³ 0.085	¹⁴⁴ 0.736	¹⁶⁵ 0.056	⁹⁵ 0.239	¹⁶³ 0.243	²⁴⁹ 0.348	²³⁶ 0.450	²⁰³ 1.000	¹⁷¹ 0.424	⁹⁹ 0.772	¹⁶⁶ 0.938	0.000	0.000	0.000	0.000	0.000		
2	3DIVI-003	²⁵³ 0.083	²⁴⁹ 0.206	¹⁸¹ 0.141		¹⁸⁷ 0.474	²⁴⁹ 0.400	²⁴⁹ 0.626		¹⁸³ 0.605		¹⁵¹ 0.821		0.002	0.005					
3	3DIVI-004	²¹² 0.018	²²¹ 0.062		¹⁶⁵ 0.035		¹⁶⁷ 0.279	²²⁶ 0.343		¹⁶⁵ 0.277		¹²⁷ 0.607		0.002	0.005					
4	3DIVI-005	²¹³ 0.018	²²⁰ 0.062	¹⁹⁰ 0.930	¹⁹⁹ 0.821		¹⁶⁸ 0.279	²¹⁷ 0.166	²²⁴ 0.339	¹³⁶ 0.996	¹⁸⁸ 0.864		¹²⁸ 0.597		0.002	0.005	0.442			
5	3DIVI-006	²² 0.024	²²⁸ 0.074		¹⁶⁵ 0.047		¹⁷⁶ 0.312	²¹⁷ 0.168	²²⁴ 0.342		¹⁶⁵ 0.283		¹³² 0.615		0.002	0.005				
6	ACER-000	¹⁹⁰ 0.011	¹⁸⁴ 0.036	¹⁷¹ 0.827	¹⁴⁷ 0.025		¹⁵¹ 0.209	²¹⁰ 0.146	²⁰³ 0.246	⁹¹ 0.981	¹⁵⁷ 0.201		¹¹⁶ 0.490		0.000	0.000	0.042			
7	ACER-001	¹⁴ 0.005	¹³⁶ 0.020	⁹⁰ 0.422	¹¹⁵ 0.008	⁸³ 0.050	⁶² 0.098	¹³⁵ 0.056	¹³⁵ 0.109	¹⁶⁸ 0.999	¹²⁸ 0.068	⁸⁶ 0.406	¹¹⁷ 0.479	0.001	0.001	0.041	0.000			
8	AIZE-001	¹⁵¹ 0.006	¹⁴⁹ 0.022	¹³⁴ 0.683	¹³⁸ 0.016	⁸⁵ 0.050	¹³⁵ 0.165	¹⁷⁰ 0.077	¹⁶² 0.143	¹¹⁶ 0.994	¹³³ 0.101	⁸⁰ 0.364	⁹⁷ 0.387	0.001	0.001	0.047				
9	ALCHERA-000	²⁰⁸ 0.016	²⁰⁸ 0.047	¹⁷⁸ 0.870	¹⁶³ 0.046		¹⁷³ 0.292	²⁰² 0.138	¹⁸⁹ 0.216	¹⁵² 0.999	¹⁵² 0.176		¹⁴⁷ 0.803		0.006	0.014	0.328			
10	ALCHERA-001	²⁷ 0.987	²⁷⁵ 1.000		²⁰¹ 1.000		²⁴⁸ 1.000	²⁷⁹ 0.999	²⁷⁵ 1.000		²⁶⁹ 1.000		²⁴⁹ 1.000		0.006	0.013	0.324			
11	ALCHERA-002	²⁵⁴ 0.095	²⁴⁶ 0.166	²⁰³ 0.954	¹⁹⁶ 0.668		¹⁸⁵ 0.446	²⁵⁶ 0.486	²⁴⁶ 0.591	¹⁷⁶ 1.000	¹⁸ 0.827		¹⁴⁸ 0.811		0.001	0.002	0.106			
12	ALCHERA-003	¹⁸ 0.010	¹⁸² 0.035	¹⁴⁵ 0.741	¹³⁷ 0.016		¹⁴⁹ 0.206	²¹¹ 0.155	²⁰⁰ 0.239	¹⁶³ 0.999	¹⁵¹ 0.172		¹¹⁷ 0.464		0.001	0.002	0.106			
13	ALCHERA-004	¹⁹² 0.011	¹⁸⁷ 0.038	⁸² 0.345	¹⁴⁰ 0.017	⁹¹ 0.088	¹²⁴ 0.144	²⁴⁸ 0.394	²⁴² 0.529	¹¹¹ 0.991	¹⁷³ 0.424	⁸⁹ 0.708	¹²⁵ 0.546	0.001	0.001	0.046	0.000			
14	ALLGOVISION-000	¹⁹ 0.011	¹⁷⁸ 0.033	¹⁸¹ 0.894	¹⁴⁴ 0.021		¹⁷⁰ 0.282	¹⁸⁸ 0.088	¹⁷⁸ 0.166	¹⁰⁸ 0.990	¹³⁶ 0.117		¹²⁷ 0.526		0.002	0.003	0.122			
15	ALLGOVISION-001	¹⁷⁸ 0.009	¹⁹³ 0.038	¹³⁰ 0.661	¹⁴⁴ 0.021		¹⁶¹ 0.241	¹⁸⁹ 0.102	¹⁹³ 0.221	⁹⁸ 0.986	¹⁴⁶ 0.150		¹¹⁷ 0.491		0.001	0.001	0.042			
16	ANKE-000	²⁰ 0.013	¹⁸⁹ 0.038	¹⁹³ 0.931	²¹⁷ 1.000		²⁴¹ 1.000	¹⁹⁴ 0.117	¹⁹² 0.220	¹¹⁷ 0.994	²⁷¹ 1.000		²³ 1.000		0.000	0.001	0.080			
17	ANKE-001	²⁰⁴ 0.013	¹⁸⁸ 0.038	¹⁹⁸ 0.946	²⁴⁷ 1.000		²¹⁹ 1.000	¹⁹⁸ 0.119	¹⁹¹ 0.220	¹²² 0.994	²³³ 1.000	¹⁹⁵ 1.000		0.000	0.001	0.080				
18	ANKE-002	¹⁶ 0.003	¹¹⁰ 0.016	¹⁰⁸ 0.522	⁸⁰ 0.005		¹⁰⁰ 0.119	¹¹⁸ 0.032	¹⁰¹ 0.079	⁶⁶ 0.948	⁸⁷ 0.034	⁶⁹ 0.245	0.001	0.001	0.049					
19	AWARE-003	²³⁰ 0.031	²³⁴ 0.090	²¹⁵ 0.966	¹⁸⁷ 0.316		¹⁷² 0.290	²⁰² 0.128	²¹⁸ 0.298	⁹⁵ 0.984	¹⁷⁴ 0.428		¹²⁵ 0.530		0.004	0.003	0.874			
20	AWARE-004	²⁴ 0.068	²⁴⁸ 0.176	²²³ 0.976	¹⁷⁷ 0.122		¹⁸³ 0.414	²³⁹ 0.269	²⁴¹ 0.509	¹⁸⁰ 1.000	¹⁶⁷ 0.397		¹⁴⁹ 0.816		0.003	0.003	0.776			
21	AWARE-005	²³¹ 0.031	²²² 0.067	²²⁴ 0.978	¹⁶⁶ 0.048		¹⁷⁵ 0.308	²⁴⁸ 0.364	²⁰⁵ 0.253	¹⁸⁴ 1.000	¹⁶¹ 0.255		¹⁶¹ 0.916		0.001	0.002	0.189			
22	AWARE-006	²⁵⁰ 0.070	²⁴² 0.128	²²⁶ 0.983	¹⁷⁸ 0.111		¹⁸⁴ 0.421	²³⁴ 0.276	²²⁹ 0.398	¹⁷³ 0.999	¹⁶¹ 0.368		¹⁴¹ 0.749		0.001	0.002	0.189			
23	AYONIX-000	²⁷ 0.450	²⁷⁰ 0.685	²³⁵ 0.996	¹⁹⁹ 0.607		¹⁹⁸ 0.867	²⁶⁸ 0.811	²⁶⁴ 0.939	¹⁴² 0.998	¹⁹² 0.954		¹⁷ 0.982		0.010	0.031	0.939			
24	AYONIX-001	²⁶⁸ 0.341	²⁶³ 0.527	²³⁰ 0.993	²⁰⁰ 0.994		¹⁹⁵ 0.778	²⁶⁷ 0.824	²⁵⁹ 0.920	¹⁷¹ 0.999	¹⁹⁶ 0.999		¹⁷⁰ 0.969		0.010	0.031	0.939			
25	AYONIX-002	²⁶ 0.341	²⁶⁴ 0.527	²³¹ 0.993	¹⁹⁷ 0.464		¹⁹⁶ 0.778	²⁶⁸ 0.824	²⁶⁰ 0.920	¹⁷⁰ 0.999	¹⁸⁸ 0.915		¹⁷ 0.969		0.010	0.031	0.939			
26	CAMVI-003	²⁴³ 0.052	²³⁵ 0.090	¹⁸³ 0.911	¹⁷⁵ 0.093		¹⁸⁰ 0.360	¹⁶⁷ 0.071	¹⁵⁴ 0.132	⁷⁴ 0.970	¹³⁸ 0.114		¹⁰⁰ 0.402		0.006	0.013	0.675			
27	CAMVI-004	²⁴ 0.047	²²⁹ 0.077	¹⁴⁷ 0.744	¹⁷⁷ 0.072		¹⁷⁴ 0.296	¹⁶⁸ 0.072	¹⁵⁶ 0.136	¹⁶⁶ 0.999	¹³⁵ 0.100		¹⁴ 0.787		0.000	0.000	0.000			
28	CAMVI-005	²⁴⁷ 0.065	²⁴⁰ 0.103	¹⁴⁹ 0.746	¹⁷⁶ 0.098		¹⁷⁹ 0.341	¹⁸⁸ 0.099	¹⁸⁵ 0.179	¹⁷⁷ 1.000	¹⁴⁵ 0.156		¹⁸² 0.999		0.000	0.000	0.000			
29	CANON-001	¹ 0.001	⁴ 0.006	²⁵ 0.088	¹² 0.001		¹² 0.007	¹¹ 0.062	³⁰ 0.005	²³ 0.023	¹⁴ 0.365	¹⁸ 0.008	²² 0.068	²⁸ 0.139	0.001	0.000	0.042	0.000		
30	CIB-000	³⁹ 0.002	²⁰ 0.008	²⁹ 0.100	²⁴ 0.002	³² 0.011	¹⁹ 0.069	⁵³ 0.012	⁵¹ 0.045	¹⁹² 1.000	⁴⁶ 0.017	⁴¹ 0.141	¹⁵⁸ 0.894		0.000	0.000	0.000	0.000		
31	CLEARVIEWAI-000	¹ 0.001	¹¹ 0.007	⁷ 0.062	¹¹ 0.001	⁹ 0.006	⁶ 0.056	³¹ 0.006	²⁶ 0.025	⁷⁹ 0.974	¹⁹ 0.008	¹⁸ 0.057	⁷ 0.268		0.000	0.000	0.037	0.000		
32	CLOUDWALK-HR-000	³⁵ 0.001	³⁶ 0.010	⁹ 0.064	²⁰ 0.002	¹¹ 0.006	⁷ 0.057	¹⁰ 0.002	¹⁰ 0.013	² 0.133	¹⁷ 0.005	⁷ 0.033	¹¹ 0.099		0.001	0.000	0.042	0.000		
33	CLOUDWALK-MT-000	⁵ 0.002	³⁵ 0.011	³ 0.057	⁴ 0.001	³ 0.004	² 0.004	² 0.005	⁷ 0.002	⁹ 0.013	¹ 0.109	¹ 0.002	¹ 0.018	¹ 0.072	0.001	0.000	0.042	0.000		
34	COGENT-000	¹⁸⁹ 0.010	²⁰⁵ 0.046	²¹⁴ 0.965						¹⁴² 0.053	¹⁵⁸ 0.140	¹²⁷ 0.995								
35	COGENT-001	¹⁸ 0.010	²⁰⁶ 0.046	²¹³ 0.965						¹⁴⁵ 0.053	¹⁵⁷ 0.140	¹²⁸ 0.995								
36	COGENT-002	¹²² 0.004	¹³⁸ 0.020	¹⁸⁸ 0.925						¹²⁸ 0.044	¹²⁶ 0.098	¹⁴¹ 0.998								
37	COGENT-003	¹²⁴ 0.004	¹⁴² 0.021	¹⁹⁷ 0.939						¹³⁴ 0.046	¹²⁹ 0.095	¹⁴⁴ 0.998								
38	COGENT-004	⁷ 0.002	²⁹ 0.013	¹⁸⁷ 0.922	²⁰ 0.004	⁸⁴ 0.019	⁹⁴ 0.113	¹¹ 0.033	³⁷ 0.051	¹³⁹ 0.997	⁵⁷ 0.022	³⁹ 0.126	¹⁰⁹ 0.456		0.000	0.000	0.000	0.000		
39	COGENT-005	⁴⁷ 0.002	⁴⁵ 0.010	³⁵ 0.126	²⁵ 0.002	³⁰ 0.010	¹⁰¹ 0.120	³⁹ 0.009	⁴¹ 0.037	¹⁰⁴ 0.989	³⁴ 0.011	²⁷ 0.082	¹⁵⁹ 0.905		0.000	0.000	0.000	0.000		
40	COGNITEC-000	²² 0.025	²¹⁶ 0.059	²¹¹ 0.964						²¹ 0.161	²¹⁹ 0.303	¹¹² 0.992				0.003	0.002	0.924		
41	COGNITEC-001	¹⁹⁶ 0.012	¹⁸⁰ 0.034	²⁰⁵ 0.958						¹⁹⁰ 0										

#	ALGORITHM	INVESTIGATION MODE						IDENTIFICATION MODE						FAILURE TO EXTRACT FEATURES							
		RANK ONE MISS RATE, FNIR(N, 0, 1)						HIGH T → FPIR = 0.001, FNIR(N, T, L)													
		N=1.6M						N=1.6M													
		MUGSHOT	MUGSHOT	MUGSHOT	VISA	BORDER	VISA	MUGSHOT	MUGSHOT	MUGSHOT	VISA	BORDER	VISA	MUGSHOT	MUGSHOT	MUGSHOT	VISA	BORDER	KIOSK		
	GALLERY	MUGSHOT	MUGSHOT	WEBCAM	PROFILE	BORDER	BOR ₁ 10YR	KIOSK	MUGSHOT	WEBCAM	PROFILE	BORDER	BOR ₁ 10YR	KIOSK	MUGSHOT	WEBCAM	PROFILE	BORDER	BOR ₁ 10YR	KIOSK	
47	CUBOX-000	³⁰ 0.001	40.010	⁴ 0.058	¹⁰ 0.002	⁵ 0.004	¹ 0.049	¹⁶ 0.003	¹⁷ 0.019	⁴ 0.168	⁷ 0.004	⁶ 0.028	² 0.073	0.001	0.000	0.042	0.000				
48	CYBERLINK-000	¹²⁶ 0.004	135.020	¹⁴³ 0.717	¹¹⁰ 0.007	116.034	¹⁵³ 0.056	¹³⁹ 0.116	¹³¹ 0.995	¹¹⁷ 0.063	⁹² 0.339	0.001	0.001	0.063							
49	CYBERLINK-001	¹²⁰ 0.004	123.018	¹⁴³ 0.731	¹⁰³ 0.007	115.013	¹⁴⁶ 0.054	¹³⁶ 0.109	¹²⁶ 0.995	¹¹¹ 0.062	¹³³ 0.652	0.000	0.000	0.040							
50	CYBERLINK-002	¹⁰⁶ 0.003	67.012	¹²² 0.577	⁶⁴ 0.004	⁸² 0.107	⁶² 0.015	⁶⁵ 0.053	¹⁰³ 0.988	⁶¹ 0.024	⁷⁹ 0.288	0.001	0.000	0.042							
51	CYBERLINK-003	⁴³ 0.002	27.009	⁹⁷ 0.474	⁴⁹ 0.003	³³ 0.012	⁴³ 0.082	³⁸ 0.008	⁷⁷ 0.972	³⁶ 0.012	³² 0.100	⁷⁴ 0.368	0.000	0.000	0.039	0.000					
52	CYBERLINK-004	⁴⁸ 0.002	63.011	⁹¹ 0.423	⁴³ 0.003	³¹ 0.011	⁷³ 0.104	³⁴ 0.007	³⁹ 0.036	²¹⁴ 1.000	³⁰ 0.013	³³ 0.109	¹⁶⁹ 0.954	0.000	0.000	0.011	0.000				
53	CYBERLINK-005	⁵⁹ 0.002	50.011	⁵² 0.209	²⁹ 0.002	²⁷ 0.010	⁶³ 0.098	⁴⁴ 0.010	⁴⁵ 0.041	¹⁸² 1.000	³⁶ 0.014	²⁸ 0.089	¹⁶⁵ 0.926	0.000	0.000	0.034					
54	DAHUA-000	¹⁸² 0.009	167.026					¹⁸⁰ 0.086	¹³⁵ 0.135					0.004	0.003						
55	DAHUA-001	¹⁶⁰ 0.007	159.024	¹³⁹ 0.703				¹²⁰ 0.073	¹⁴⁷ 0.122	⁸⁸ 0.980				0.002	0.002	0.346					
56	DAHUA-002	⁶³ 0.002	66.012	⁷² 0.304	⁴² 0.003	⁴⁵ 0.084	⁶³ 0.015	⁵³ 0.046	³⁴ 0.638	⁴⁸ 0.017	³⁸ 0.159	0.001	0.000	0.099							
57	DAHUA-003	²¹ 0.001	12.007	⁵⁰ 0.206	²² 0.002	²⁵ 0.009	²³ 0.073	⁵⁸ 0.014	⁴⁷ 0.041	²⁹ 0.579	³⁶ 0.013	²⁶ 0.081	²⁷ 0.134	0.000	0.000	0.000	0.000	0.000	0.000		
58	DAHUA-004	¹¹ 0.001	15.008	³⁹ 0.144	¹⁰ 0.002	¹⁵ 0.007	¹⁷ 0.069	³⁸ 0.007	²⁸ 0.26	²³ 0.485	² 0.008	¹⁴ 0.051	²¹ 0.113	0.000	0.000	0.000	0.000	0.000	0.000		
59	DAON-000	¹²⁹ 0.004	117.017	¹¹¹ 0.530	⁸¹ 0.005	⁵⁶ 0.020	¹⁰⁵ 0.125	⁹⁰ 0.023	⁷⁸ 0.061	¹⁸³ 1.000	⁶² 0.025	⁵⁸ 0.173	¹⁵⁴ 0.846	0.002	0.002	0.108	0.001				
60	DECATUR-000	⁸⁰ 0.002	65.011	⁵⁸ 0.229	⁷³ 0.004	⁵³ 0.019	⁸⁵ 0.109	⁹³ 0.023	⁸⁴ 0.066	³⁸ 0.675	⁶⁹ 0.027	⁵⁷ 0.173	⁶⁴ 0.239	0.001	0.000	0.044					
61	DEEPLINT-001	³³ 0.001	10.007	⁴⁸ 0.200	³⁶ 0.002	²⁴ 0.073	²⁰ 0.003	¹¹ 0.014	¹⁷⁴ 1.000	¹⁴ 0.006	³⁷ 0.159	0.000	0.000	0.038							
62	DEEPSA-001	¹³⁴ 0.004	107.016	¹⁶⁸ 0.814	¹¹⁸ 0.010	¹²² 0.140	¹³⁰ 0.046	¹²⁸ 0.101	⁹⁶ 0.985	¹² 0.077	⁸⁹ 0.326	0.000	0.001	0.047							
63	DERMALOG-003	²⁵⁸ 0.126	251.0217	¹⁹⁶ 0.296	¹⁹⁰ 0.560	²⁵⁵ 0.482	²⁵¹ 0.655	¹⁸⁰ 0.677	¹⁵⁶ 0.870					0.002	0.002	0.103					
64	DERMALOG-004	²⁵⁷ 0.125	250.215	¹⁹¹ 0.930	¹⁸¹ 0.135	¹⁸⁶ 0.467	²⁵² 0.480	¹³² 0.657	¹⁸² 0.995	¹⁸⁰ 0.603	¹⁵⁵ 0.856	0.001	0.002	0.107							
65	DERMALOG-005	²⁰⁷ 0.015	186.037	¹³⁷ 0.701	¹⁸⁵ 0.242	¹⁸² 0.384	¹⁸³ 0.088	¹⁶⁹ 0.154	¹⁰⁶ 0.990	¹⁶⁴ 0.300	¹³¹ 0.614	0.001	0.002	0.102							
66	DERMALOG-006	¹⁷³ 0.008	163.024	¹²⁸ 0.619	¹¹⁸ 0.010	¹³¹ 0.155	¹⁴⁰ 0.052	¹³¹ 0.105	⁹⁰ 0.981	¹¹² 0.059	⁸⁸ 0.318	0.003	0.006	0.181							
67	DERMALOG-007	¹⁸¹ 0.009	168.027	¹³² 0.675	¹³⁴ 0.014	¹³⁷ 0.170	¹⁸¹ 0.086	¹⁶⁷ 0.152	¹⁰⁷ 0.990	¹³¹ 0.099	¹²⁷ 0.557	0.001	0.002	0.102							
68	DERMALOG-008	¹⁰⁸ 0.003	99.015	¹⁰⁶ 0.516	¹⁰⁰ 0.007	⁷⁶ 0.029	¹²¹ 0.139	¹³¹ 0.045	¹¹⁷ 0.094	¹⁹⁸ 1.000	¹⁰⁹ 0.057	⁸⁴ 0.382	¹⁶⁷ 0.940	0.000	0.000	0.002	0.000	0.000	0.000		
69	DERMALOG-009	¹⁰⁷ 0.003	96.014	⁴⁵ 0.167	¹⁰³ 0.007	⁹⁷ 0.999	⁷⁶ 0.106	⁸⁵ 0.021	⁸⁵ 0.066	¹⁹⁴ 1.000	⁷⁸ 0.031	⁹⁵ 0.999	¹⁵³ 0.840	0.001	0.001	0.018	^{0.003}				
70	EYEDEA-003	²⁵² 0.080	244.0148	²⁰⁹ 0.960	¹⁷⁷ 0.101	¹⁸¹ 0.379	²⁴⁵ 0.388	²⁴⁴ 0.543	¹²³ 0.994	¹⁸⁰ 0.570	¹⁴⁶ 0.792	0.001	0.003	0.161							
71	F-001	²⁰⁰ 0.012	131	¹⁶⁶ 0.999	²⁴ 1.000	²⁵⁹ 1.000	²¹⁰ 0.166	¹⁵¹ 0.998				0.004	1.000	0.158							
72	FINCORE-000	¹⁹¹ 0.011	181.034	¹⁵⁸ 0.767	¹⁵⁶ 0.032	⁹² 0.117	¹⁴⁶ 0.191	²⁰⁶ 0.134	¹⁹⁰ 0.217	¹⁸⁷ 1.000	¹⁵³ 0.187	⁸⁸ 0.598	¹¹⁶ 0.458	0.000	0.001	0.043	0.000				
73	FUJITSULAB-000	⁸³ 0.002	89.014	⁹⁴ 0.440	⁶⁹ 0.004	⁵⁹ 0.023	⁶⁴ 0.098	⁸¹ 0.021	⁷¹ 0.056	⁵⁹ 0.024	⁸⁹ 0.177	⁶⁵ 0.240	0.000	0.001	0.016	0.000					
74	FUJITSULAB-001	⁶⁶ 0.002	82.013	⁹⁶ 0.455	⁷¹ 0.004	⁶⁶ 0.026	⁷⁸ 0.106	⁷⁵ 0.018	⁷³ 0.058	¹¹³ 0.992	⁶⁹ 0.024	⁹⁰ 0.739	⁶⁸ 0.247	1.000	1.000	1.000	1.000	1.000	1.000		
75	GLORY-000	²⁶² 0.178	257.030	²³⁴ 0.994	¹⁸¹ 0.228	¹⁹² 0.678	²⁴⁷ 0.547	¹²⁵ 0.995	¹⁷⁸ 0.453	¹⁵² 0.839	0.011	0.013	0.985								
76	GLORY-001	²⁵⁹ 0.127	254.0267	²²⁹ 0.992	¹⁸³ 0.178	¹⁹¹ 0.594	²³⁶ 0.305	²⁴³ 0.537	¹¹⁴ 0.993	¹⁷¹ 0.408	¹⁵⁰ 0.819	0.011	0.013	0.988							
77	GORILLA-001	²⁴⁵ 0.060	236.095	¹⁹⁵ 0.936	¹⁷⁶ 0.069	¹⁷⁷ 0.329	²⁴⁰ 0.406	¹⁹⁷ 0.453	¹⁹² 1.000	¹⁷⁷ 0.468	²²⁹ 1.000	0.001	0.001	0.069							
78	GORILLA-002	²¹⁹ 0.020	202.044	¹⁵¹ 0.753	¹⁵⁰ 0.027	¹⁵⁶ 0.214	²²³ 0.188	²¹² 1.000	¹⁶⁰ 0.250	¹⁸⁶ 1.000	0.001	0.001	0.069								
79	GORILLA-003	²³² 0.036	224.070	¹⁷⁶ 0.821	¹⁶ 0.048	¹⁶⁵ 0.265	²³⁸ 0.318	²³⁴ 0.434	²⁵¹ 1.000	¹⁷⁷ 0.407	¹⁹⁰ 1.000	0.001	0.001	0.069							
80	GORILLA-004	¹⁵⁷ 0.006	160.024	¹³⁶ 0.697	¹² 0.012	¹³⁴ 0.162	¹⁸⁶ 0.889	¹⁷⁵ 0.160	⁶⁸ 0.959	¹⁴⁴ 0.135	¹⁰⁶ 0.438	0.000	0.001	0.042							
81	GORILLA-005	¹¹⁴ 0.003	124.018	⁵¹ 0.209	⁹³ 0.006	¹⁰³ 0.124	¹³⁷ 0.058	¹⁶¹ 0.142	⁴⁰ 0.700	¹²⁹ 0.088	⁸⁶ 0.315	0.000	0.000	0.040							
82	GORILLA-006	⁸⁴ 0.002	69.012	³⁵ 0.122	³⁸ 0.003	⁴⁹ 0.018	⁷⁵ 0.105	¹⁰⁸ 0.027	¹¹² 0.089	²⁷ 0.531	⁶⁷ 0.028	⁸⁴ 0.166	⁸⁸ 0.218	0.000	0.001	0.041	0.000				
83	GORILLA-007	⁵¹ 0.002	49.011	³¹ 0.114	³³ 0.002	⁴⁷ 0.016	⁵⁰ 0.088	¹⁰³ 0.027	¹⁰⁰ 0.077	²⁸ 0.534	⁶³ 0.026	⁷² 0.264	⁴⁶ 0.178	1.000	1.000	1.000	1.000	1.000	1.000		
84	GRIAULE-000	⁹⁸ 0.002	83.014	⁷⁷ 0.327	¹² 0.011	⁷⁸ 0.031	¹⁰⁶ 0.126	⁸¹ 0.020	¹²⁹ 0.995	⁸⁴ 0.033	⁶³ 0.185	⁵⁴ 0.198	0.000	0.002	0.090	0.001	0.001	0.001			
85	HIK-003	¹⁹⁷ 0.012	171.027	¹³⁸ 0.689	¹²⁶ 0.012	¹²⁸ 0.151	¹⁹¹ 0.103	¹⁷¹ 0.158	⁷² 0.969	¹⁴⁴ 0.142	¹⁰⁸ 0.445	0.000	0.000	0.048							

#	ALGORITHM	INVESTIGATION MODE						IDENTIFICATION MODE						FAILURE TO EXTRACT FEATURES							
		RANK ONE MISS RATE, FNIR(N, 0, 1)						HIGH T → FPIR = 0.001, FNIR(N, T, L)						N=1.6M							
		GALLERY	MUGSHOT	MUGSHOT	MUGSHOT	VISA	BORDER	BOR _{10YR}	KIOSK	MUGSHOT	MUGSHOT	MUGSHOT	VISA	BORDER	BOR _{10YR}	KIOSK	MUGSHOT	MUGSHOT	KIOSK		
93	IDEMLA-006	185	0.010	226	0.072	217	0.969	152	0.030	164	0.253	128	0.043	158	0.226	92	0.982	148	0.144	138	0.733
94	IDEMLA-007	95	0.003	104	0.015	261	1.000	94	0.006	79	0.036	117	0.131	74	0.018	68	0.055	243	1.000	105	0.052
95	IDEMLA-008	10	0.001	6	0.007	22	0.079	15	0.001	16	0.007	29	0.075	8	0.002	8	0.013	6	0.204	10	0.005
96	IDEMLA-009	4	0.001	7	0.006	11	0.065	3	0.001	3	0.005	7	0.051	2	0.002	3	0.011	3	0.141	3	0.003
97	IMAGUS-002	265	0.220	255	0.301	228	0.988					26	0.749	256	0.816	210	1.000				0.004
98	IMAGUS-003	27	0.356	26	0.513	232	0.993					26	0.807	258	0.909	195	1.000				0.004
99	IMAGUS-005	71	0.002	68	0.012	74	0.319	92	0.006	37	0.022	114	0.132	78	0.018	83	0.066	53	0.838	69	0.029
100	IMAGUS-006	77	0.002	86	0.014	70	0.293	72	0.004	56	0.019	92	0.112	80	0.019	86	0.069	61	0.897	68	0.028
101	IMAGUS-007	77	0.002	80	0.013	75	0.321	65	0.004	38	0.022	93	0.117	92	0.023	99	0.073	76	0.031	70	0.265
102	IMPERIAL-000	95	0.002	101	0.015	67	0.280	77	0.004			60	0.097	98	0.026	87	0.068	155	0.999	94	0.042
103	INCODE-000	24	0.049	238	0.100	201	0.951					23	0.310	23	0.420	147	0.998				0.001
104	INCODE-001	210	0.017	207	0.046	152	0.762					226	0.212	215	0.296	207	1.000				0.001
105	INCODE-002	21	0.018	209	0.048	173	0.843					222	0.184	216	0.269	115	0.993				0.000
106	INCODE-003	202	0.013	196	0.040	153	0.764					218	0.167	209	0.264	169	0.999				0.000
107	INCODE-004	12	0.004	12	0.017	100	0.475	116	0.008	118	0.135	148	0.054	146	0.120	124	0.995	116	0.063	84	0.313
108	INCODE-005	47	0.002	61	0.011	41	0.147	35	0.002	38	0.013	38	0.079	48	0.011	50	0.043	25	0.528	45	0.017
109	INNOVATRICS-002	24	0.045	227	0.074	176	0.853					23	0.234	228	0.310	199	1.000				0.000
110	INNOVATRICS-003	229	0.026	212	0.055	175	0.845					222	0.221	216	0.297	181	1.000				0.000
111	INNOVATRICS-004	201	0.012	198	0.040	206	0.958					204	0.132	194	0.222	86	0.980				0.000
112	INNOVATRICS-005	97	0.002	95	0.014	89	0.407	79	0.005	84	0.109	115	0.034	111	0.089	84	0.846	101	0.047	69	0.251
113	INNOVATRICS-007	50	0.002	60	0.011	62	0.248	38	0.002	40	0.013	32	0.077	54	0.013	58	0.051	42	0.743	44	0.017
114	INTELLIVISION-001	23	0.036	239	0.102	219	0.972	169	0.057	97	0.222	170	0.333	238	0.279	23	0.404	185	1.000	165	0.328
115	INTSYSMSU-000	260	0.146	158	0.023	121	0.562	174	0.072			113	0.132	274	0.998	269	1.000	179	0.999	199	0.999
116	IREX-000	13	0.004	30	0.010	133	0.681	34	0.002	34	0.012	41	0.082	108	0.028	77	0.060	67	0.957	97	0.044
117	ISYSTEMS-002	158	0.006	166	0.026	174	0.844					174	0.078	150	0.126	140	0.998				0.002
118	ISYSTEMS-003	14	0.005	155	0.023	158	0.791					158	0.059	137	0.107	186	1.000				0.002
119	KAKAO-000	34	0.001	48	0.011	32	0.119	39	0.002	37	0.013	34	0.078	69	0.015	70	0.056	20	0.468	49	0.019
120	KEDACOM-001	16	0.008	185	0.036	220	0.972	158	0.034			158	0.237	91	0.023	92	0.072	100	0.986	108	0.055
121	KNERON-000	153	0.006	176	0.027	119	0.552	151	0.028			147	0.195								0.000
122	KNERON-001	22	0.030	269	0.621	61	0.237	182	0.144	93	0.207	169	0.280								0.000
123	LINE-000	84	0.002	87	0.014	57	0.223	89	0.005	74	0.029	79	0.107	111	0.031	121	0.095	99	0.046	78	0.278
124	LINE-001	1	0.001	14	0.007	8	0.063	19	0.002	23	0.008	4	0.085	25	0.005	29	0.027	211	1.000	29	0.009
125	LOOKMAN-003	177	0.009	192	0.038	161	0.035					160	0.239	127	0.044	138	0.112	128	0.084	93	0.355
126	LOOKMAN-004	17	0.009	195	0.039	222	0.973					136	0.045	138	0.105	81	0.977				0.000
127	LOOKMAN-005	171	0.008	185	0.036	221	0.972	160	0.035			159	0.237	118	0.030	107	0.086	83	0.978	115	0.062
128	MANTRA-000	56	0.002	41	0.010	140	0.709	101	0.007	64	0.024	90	0.112	45	0.010	46	0.041	246	1.000	70	0.029
129	MEGVII-001	199	0.012	120	0.017	214	1.000					169	0.072	123	0.097						0.002
130	MEGVII-002	199	0.012	122	0.017	95	0.450	237	1.000			173	0.077	123	0.096	150	0.998				0.002
131	MICROFOCUS-003	27	0.594	275	0.781	198	0.708					208	0.907	279	0.931	268	0.979	194	0.982	178	0.991
132	MICROFOCUS-004	275	0.576	272	0.758	197	0.701					199	0.904	273	0.999	266	0.975	193	0.974	176	0.989
133	MICROFOCUS-005	27	0.424	267	0.601	193	0.494					197	0.777	268	0.835	262	0.928	191	0.935	177	0.985
134	MICROFOCUS-006	272	0.427	266	0.583	192	0.490					197	0.782	272	0.978	261	0.923	190	0.923	172	0.971
135	MICROFOCUS-003	4	0.002	72	0.012	62	0.004					80	0.109	106	0.028	111	0.091	87	0.036	6	0.233
136	MICROSOFT-004	36	0.001	71	0.012	40	0.144	50	0.003			87	0.109	99	0.026	109	0.087	83	0.033	59	0.222
137	MICROSOFT-005	6	0.002	34	0.011	40	0.144	50	0.003			69	0.099	96	0.026	107	0.070	30	0.587	64	0.027
138	MICROSOFT-006	73	0.002	64	0.011	43	0.150	60	0.004			67	0.100	49	0.012	40	0.037	15	0.386	79	0.032

Table 12: **Miss rates by dataset:** At left, rank 1 miss rates relevant to investigations; at right, with threshold set to target FPIR = 0.01 for higher volume, low prior, uses. Yellow indicates most accurate algorithm. Throughout blue superscripts indicate the rank of the algorithm for that column.

2022/03/30

FNIR(N, R, T) = False neg. identification rate

N = Num. enrolled subjects

R = Num. candidates examined

T = Threshold

T = 0 → Investigation

T > 0 → Identification

#	ALGORITHM	INVESTIGATION MODE						IDENTIFICATION MODE						FAILURE TO EXTRACT FEATURES															
		RANK ONE MISS RATE, FNIR(N, 0, 1)						HIGH T → FPIR = 0.001, FNIR(N, T, L)						N=1.6M															
		GALLERY		MUGSHOT	MUGSHOT	WEBCAM	PROFILE	BORDER	BOR _L 10YR	KIOSK	MUGSHOT	MUGSHOT	MUGSHOT	VISA	BORDER	BOR _L 10YR	KIOSK	MUGSHOT	MUGSHOT	MUGSHOT	VISA	BORDER	KIOSK						
139	NEC-000	211	0.017	200	0.041	209	0.959	14	0.025	162	0.243	176	0.079	160	0.140	88	0.979	114	0.474	0.001	0.002	0.890							
140	NEC-001	220	0.021	213	0.056	216	0.967	157	0.033	166	0.277	193	0.106	187	0.197	99	0.986	140	0.133	113	0.468	0.005	0.003	0.934					
141	NEC-002	9	0.001	26	0.009	8	0.363	35	0.003	97	0.117	14	0.003	20	0.020	165	0.999	2	0.008	135	0.676	0.000	0.001	0.041					
142	NEC-003	26	0.001	38	0.010	84	0.352	59	0.004	36	0.013	102	0.120	12	0.002	16	0.017	50	0.824	24	0.008	12	0.036	134	0.668	0.000	0.001		
143	NEC-004	31	0.001	24	0.009	117	0.538	48	0.003	19	0.007	28	0.075	6	0.002	7	0.013	33	0.622	3	0.004	13	0.019	13	0.100	0.000	0.001		
144	NEC-005	19	0.001	16	0.008	29	0.081	18	0.002	7	0.005	25	0.073	3	0.002	3	0.012	37	0.673	2	0.003	10	0.019	10	0.099	0.000	0.001		
145	NEUROTECHNOLOGY-003	221	0.022	201	0.042	210	0.961					261	0.636	211	0.266	240	1.000					0.000	0.001	0.131					
146	NEUROTECHNOLOGY-004	148	0.006	134	0.020	210	0.970					163	0.063	140	0.117	120	0.994					0.000	0.001	0.131					
147	NEUROTECHNOLOGY-005	133	0.004	162	0.024	180	0.893					150	0.054	152	0.130	143	0.998					0.000	0.000	0.030					
148	NEUROTECHNOLOGY-006	215	0.018	204	0.045	120	0.606					232	0.249	231	0.418							0.000	0.000						
149	NEUROTECHNOLOGY-007	125	0.004	141	0.021	161	0.796	117	0.009			143	0.180	162	0.062	181	0.173	190	1.000	166	0.339	234	1.000	0.001	0.001	0.041			
150	NEUROTECHNOLOGY-008	82	0.002	94	0.014	9	0.457	6	0.004	61	0.023	69	0.101	144	0.053	103	0.080	208	1.000	80	0.035	76	0.293	35	0.203	0.000	0.052		
151	NEUROTECHNOLOGY-009	32	0.001	51	0.011	47	0.179	28	0.002	39	0.013	37	0.079	66	0.015	62	0.052	31	0.588	91	0.020	49	0.153	40	0.165	0.001	0.000		
152	NEUROTECHNOLOGY-010	22	0.001	29	0.009	17	0.070	8	0.001	18	0.007	16	0.068	43	0.010	42	0.037	11	0.277	32	0.010	25	0.075	24	0.126	0.000	0.041		
153	NEWLAND-002	251	0.079	241	0.117	194	0.936					252	0.438	238	0.466	159	0.999					0.007	0.012	0.200					
154	NOBLIS-001	267	0.249	262	0.522	233	0.993					277	1.000	277	1.000	215	1.000					0.000	0.000	0.000					
155	NOBLIS-002	263	0.179	259	0.392	227	0.982					273	0.997	274	1.000	202	1.000					0.000	0.000	0.000					
156	NOTIONTAG-000	96	0.002	73	0.012	47	0.204	68	0.004	45	0.016	57	0.095	69	0.017	76	0.059	32	0.611	54	0.021	47	0.150	44	0.176	0.000	0.000		
157	NTECHLAB-003	154	0.006	152	0.023	105	0.504					148	0.054	141	0.118	52	0.837					0.000	0.000	0.040					
158	NTECHLAB-004	142	0.005	129	0.019	103	0.506	112	0.008			109	0.129	123	0.041	132	0.105	51	0.833	107	0.053	73	0.263	0.000	0.000	0.040			
159	NTECHLAB-005	140	0.005	125	0.018	80	0.367	114	0.008			99	0.118	124	0.042	130	0.102	45	0.771	12	0.073	80	0.294	0.000	0.040				
160	NTECHLAB-006	130	0.004	116	0.017	83	0.347	109	0.007			95	0.113	118	0.037	118	0.094	44	0.754	110	0.057	72	0.260	0.000	0.000	0.040			
161	NTECHLAB-007	101	0.003	74	0.012	70	0.326	76	0.004			80	0.107	75	0.026	86	0.067	45	0.750	78	0.032	60	0.223	0.000	0.000	0.042			
162	NTECHLAB-008	32	0.002	31	0.010	47	0.157	51	0.003			46	0.084	59	0.014	52	0.045	26	0.529	84	0.033	30	0.183	0.000	0.000	0.044			
163	NTECHLAB-009	24	0.001	18	0.008	3	0.138	25	0.002	41	0.013	27	0.074	20	0.005	22	0.022	17	0.430	37	0.015	34	0.109	29	0.142	0.000	0.041		
164	NTECHLAB-010	14	0.001	21	0.008	21	0.085	17	0.002	22	0.008	8	0.057	13	0.003	14	0.015	10	0.252	15	0.007	19	0.059	9	0.098	0.001	0.043		
165	NTECHLAB-011	8	0.001	8	0.007	18	0.072	10	0.001	21	0.007	4	0.051	17	0.003	13	0.015	8	0.228	28	0.009	24	0.074	7	0.091	0.000	0.040		
166	PANGIAM-000	20	0.001	17	0.008	29	0.074	21	0.002	20	0.007	14	0.065	32	0.006	34	0.030	13	0.318	31	0.009	39	0.136	16	0.105	1.000	1.000		
167	PARAVISION-000	216	0.019	191	0.038	117	0.534	190	0.423			189	0.529	185	0.089	179	0.170	161	0.999	178	0.470	164	0.926	0.000	0.000				
168	PARAVISION-001	123	0.004	139	0.020	70	0.329	18	0.414			188	0.484	137	0.049	131	0.128	153	0.999	17	0.444	140	0.739	0.000	0.000				
169	PARAVISION-002	128	0.004	145	0.022	80	0.335	136	0.015			139	0.175	138	0.050	144	0.119	93	0.983	125	0.080	118	0.497	0.000	0.000	0.032			
170	PARAVISION-003	113	0.003	131	0.019	61	0.252	137	0.015			136	0.167	116	0.035	122	0.096	121	0.994	11	0.058	81	0.296	0.000	0.000	0.032			
171	PARAVISION-004	45	0.002	44	0.010	30	0.104	90	0.006			91	0.112	47	0.010	43	0.038	200	1.000	47	0.018	160	0.908	0.000	0.000	0.032			
172	PARAVISION-005	38	0.002	33	0.010	27	0.079	104	0.007			77	0.106	22	0.004	24	0.024	8	0.980	3	0.011	25	0.132	0.000	0.000	0.038			
173	PARAVISION-007	17	0.001	19	0.008	12	0.066	83	0.005	28	0.010	68	0.101	21	0.004	25	0.025	209	1.000	27	0.009	35	0.113	268	1.000	0.000	0.000		
174	PARAVISION-009	7	0.001	13	0.007	17	0.067	7	0.001	4	0.004	5	0.054	15	0.003	18	0.019	41	0.735	0	0.003	8	0.033	3	0.073	0.000	0.025		
175	PIXELALL-002	137	0.005	148	0.022	166	0.810	121	0.011			144	0.187	192	0.105	228	0.388	215	1.000	18	0.602	243	1.000	0.000	0.000				
176	PIXELALL-003	81	0.002	93	0.014	105	0.515	99	0.006			127	0.151	82	0.022	93	0.073	178	1.000	90	0.037	126	0.554	0.000	0.000				
177	PIXELALL-004	78	0.002	109	0.015	105	0.523	87	0.005			129	0.152	77	0.018	102	0.079	193	1.000	103	0.051	179	0.994	0.000	0.000				
178	PIXELALL-005	68	0.002	53	0.011	65	0.264	125	0.012			71	0.028	125	0.146	51	0.012	56	0.050	206	1.000	65	0.027	65	0.203	184	1.000	0.000	0.000
179	PTAKURATSATU-000	111	0.003	115	0.017	121	0.605	80	0.005	69	0.027	74	0.105	117	0.037	149	0.124	63	0.924	103	0.046	67	0.206	62	0.232	0.000	0.001		
180	QNAP-000	169	0.008	173	0.027	107	0.522	132	0.013	86	0.054	132	0.158	203	0.129	199	0.238	217	1.000	134	0.191	87	0.539	181	0.998	0.001	0.000		
181	QNAP-001	131	0.004	146	0.022	101	0.498	98	0.006	82	0.041	93	0.112	147	0.054	157	0.137	64	0.928	120	0.081	82	0.368	91	0.331	0.000	0.004		
18																													

#	ALGORITHM	INVESTIGATION MODE						IDENTIFICATION MODE						FAILURE TO EXTRACT FEATURES					
		RANK ONE MISS RATE, FNIR(N, 0, 1)						HIGH T → FPIR = 0.001, FNIR(N, T, L)											
		N=1.6M						N=1.6M											
		MUGSHOT	MUGSHOT	MUGSHOT	VISA	BORDER	VISA	MUGSHOT	MUGSHOT	MUGSHOT	VISA	BORDER	VISA	MUGSHOT	MUGSHOT	MUGSHOT	VISA	BORDER	KIOSK
PROBE		MUGSHOT	WEBCAM	PROFILE	BORDER	BOR _i 10YR	KIOSK	MUGSHOT	WEBCAM	PROFILE	BORDER	BOR _i 10YR	KIOSK	MUGSHOT	WEBCAM	PROFILE	BORDER	BOR _i 10YR	KIOSK
185	RANKONE-004	²³⁹ 0.041	²⁴³ 0.141	²²⁷ 0.986				²³⁴ 0.193	²³³ 0.426					0.000	0.000				
186	RANKONE-005	¹⁸³ 0.009	¹⁹⁹ 0.041	¹⁶³ 0.797				¹⁵⁹ 0.059	¹⁸² 0.173	¹⁴⁵ 0.998	⁸² 0.977			0.000	0.000	0.489			
187	RANKONE-006	¹⁴⁴ 0.005	¹²⁷ 0.019	¹⁶⁶ 0.796				¹¹⁹ 0.037	⁹⁸ 0.022	¹¹⁹ 0.095	⁷¹ 0.967			0.002	0.167				
188	RANKONE-007	¹¹⁷ 0.003	¹²⁷ 0.019	¹⁶⁶ 0.796				¹¹⁷ 0.134	⁷² 0.018	⁹⁷ 0.076	⁷³ 0.969	¹¹³ 0.062	⁹⁰ 0.328	0.001	0.001	0.102			
189	RANKONE-009	⁹¹ 0.002	⁷⁶ 0.013	¹¹⁸ 0.549	⁸⁹ 0.006			¹⁰⁷ 0.126	⁵⁷ 0.014	⁷⁴ 0.058	⁴⁸ 0.802	¹⁰⁶ 0.052	⁶⁸ 0.208	⁷⁰ 0.259	0.000	0.000	0.000	0.000	
190	RANKONE-010	⁸⁵ 0.002	³⁵ 0.010	⁸⁷ 0.374	⁸² 0.005	⁶⁷ 0.027		²¹ 0.142	¹¹⁹ 0.037	⁸⁶ 0.095	⁸⁰ 0.037	⁶⁰ 0.182	¹⁷³ 0.977	0.000	0.000	0.000	0.000	0.000	
191	RANKONE-011	³⁷ 0.002	⁶² 0.011	⁵⁶ 0.223	⁵⁸ 0.004	⁵² 0.019	⁴⁴ 0.082	³⁸ 0.009	⁵⁴ 0.048	⁷¹ 0.029	⁴³ 0.144	¹¹² 0.465	0.000	0.000	0.000	0.000	0.000		
192	RANKONE-012	²⁵ 0.001	⁴⁷ 0.010	³⁶ 0.127	⁴⁹ 0.003	⁴³ 0.014	¹⁸ 0.069	³⁵ 0.008	⁶⁶ 0.053										
193	REALNETWORKS-000	²³⁷ 0.040	²³² 0.078					²³¹ 0.234	²²³ 0.319					0.001	0.000				
194	REALNETWORKS-001	²³⁸ 0.040	²³¹ 0.078					²²⁹ 0.234	²²² 0.319					0.001	0.000				
195	REALNETWORKS-002	²³⁴ 0.039	²³⁰ 0.078					²²⁸ 0.231	²²¹ 0.315					0.001	0.000				
196	REALNETWORKS-003	²²⁴ 0.024	²¹⁹ 0.062	¹⁵⁶ 0.771	¹⁵⁵ 0.031			¹⁵⁰ 0.209	²¹⁴ 0.159	²¹⁰ 0.266	¹⁴⁹ 0.998	¹⁴⁹ 0.164	¹¹⁹ 0.500	0.001	0.000	0.009			
197	REALNETWORKS-004	²²² 0.024	²¹⁷ 0.059	¹⁶² 0.797	¹⁵⁹ 0.031			¹⁵⁵ 0.213	²¹¹ 0.158	²⁰⁸ 0.263	¹⁶² 0.999	¹⁵⁹ 0.170	¹³⁰ 0.613	0.001	0.000	0.009			
198	REALNETWORKS-005	⁸⁷ 0.002	⁸¹ 0.013	⁹³ 0.433	⁷⁴ 0.004	⁶⁰ 0.023	⁷¹ 0.102	¹⁰⁵ 0.028	⁹⁵ 0.074	⁷⁵ 0.971	⁸⁸ 0.037	⁶⁹ 0.223	⁵⁷ 0.215	0.000	0.000	0.006	0.000		
199	REALNETWORKS-006	²⁹ 0.001	³⁷ 0.010	⁶⁹ 0.287	⁴⁰ 0.002	²⁹ 0.010	³⁵ 0.078	⁶⁰ 0.015	⁶⁴ 0.053	⁸⁹ 0.980	⁴⁰ 0.016	³⁶ 0.120	³⁴ 0.154	0.000	0.000	0.009	0.000		
200	REMARKAI-000	¹⁷⁶ 0.009	¹⁷⁶ 0.030					²⁰¹ 0.128	¹⁸⁸ 0.203					0.000	0.001				
201	REMARKAI-000	¹¹⁹ 0.003	¹²⁶ 0.018	¹²⁹ 0.660	¹¹¹ 0.008			¹²⁶ 0.148	¹⁵¹ 0.055	¹⁴⁵ 0.120	¹⁶⁰ 0.999	¹²¹ 0.069	¹³⁸ 0.717	0.000	0.000	0.000			
202	REMARKAI-002	¹⁷⁴ 0.008	¹⁷⁵ 0.029	¹⁶⁴ 0.802				²⁰⁰ 0.124	¹⁸⁶ 0.196	¹¹⁰ 0.991				0.000	0.001	0.017			
203	RENDIP-000	⁴¹ 0.002	¹⁰⁰ 0.015	⁹² 0.424	⁹⁵ 0.006	⁷⁰ 0.028	⁴⁷ 0.084	⁵⁰ 0.012	⁷⁵ 0.059	⁶⁰ 0.894	⁵⁵ 0.022	⁶² 0.185	⁴¹ 0.167	0.000	0.000	0.041	0.000		
204	REVEALMEDIA-000	⁶⁵ 0.002	³² 0.010	⁶⁶ 0.275	²⁹ 0.002	³⁵ 0.012	²⁶ 0.074	³² 0.012	⁴⁹ 0.042	³⁹ 0.680	⁵⁰ 0.021	³¹ 0.093	³⁰ 0.143	0.000	0.000	0.041	0.000		
205	S1-000	⁹³ 0.002	¹¹⁴ 0.017	⁶¹ 0.258	⁸⁸ 0.005	⁶⁵ 0.025	⁵² 0.090	¹⁰⁷ 0.028	¹⁰⁶ 0.085	²¹⁸ 1.000	¹⁰² 0.047	²⁵¹ 1.000	²⁷³ 1.000	0.000	0.000	0.040	0.000		
206	S1-001	¹¹² 0.003	⁹⁰ 0.014	⁵⁶ 0.215	⁴¹ 0.003	⁵⁰ 0.018	³⁰ 0.077	⁶² 0.016	⁶¹ 0.052	⁹⁷ 0.985	⁴¹ 0.019	³⁸ 0.136	³¹ 0.148	0.001	0.000	0.035	0.000		
207	SCANOVATE-000	¹⁴³ 0.005	²⁰³ 0.045	¹²⁰ 0.560	¹⁵⁹ 0.035			¹⁵⁴ 0.211	¹⁶⁶ 0.067	²⁰² 0.240	⁸⁸ 0.893	¹⁵⁸ 0.215	⁹⁹ 0.400	0.000	0.001	0.057			
208	SCANOVATE-001	¹⁴⁷ 0.005	¹⁹⁷ 0.040	¹²⁴ 0.585	¹⁵³ 0.031			¹⁴² 0.178	¹⁷ 0.081	¹⁹⁶ 0.227	⁶² 0.911	¹⁵³ 0.192	¹⁰² 0.404	0.000	0.001	0.044			
209	SENSETIME-000	⁸⁹ 0.002	¹⁰⁶ 0.016	¹¹⁰ 0.528				⁸⁵ 0.021	⁸⁰ 0.063	²³³ 1.000				0.004	0.000	0.042			
210	SENSETIME-001	⁹⁰ 0.002	¹⁰⁵ 0.016					⁸⁰ 0.022	⁸² 0.064					0.004	0.000				
211	SENSETIME-002	²⁰⁵ 0.014	¹³² 0.020	⁸⁸ 0.384	¹²⁰ 0.011			⁷² 0.104	⁶¹ 0.015	³² 0.028	¹¹⁸ 0.994	⁷⁸ 0.032	¹²¹ 0.523	0.009	0.000	0.040			
212	SENSETIME-003	⁶ 0.001	⁷ 0.007	⁴² 0.150	⁴¹ 0.003			⁵³ 0.091	⁷ 0.002	⁴ 0.012	²¹ 0.477	²² 0.008	²⁶ 0.133	0.000	0.000	0.041			
213	SENSETIME-004	⁵ 0.001	⁹ 0.007	¹⁹ 0.072	³² 0.002			⁴⁸ 0.084	¹ 0.002	⁶ 0.013	⁹ 0.229	¹ 0.006	²⁰ 0.113	0.000	0.000	0.041			
214	SENSETIME-005	³ 0.001	³ 0.006	⁶ 0.059	³¹ 0.002	¹⁷ 0.007	⁴⁰ 0.082	¹¹ 0.002	¹² 0.014	⁵ 0.173	¹⁶ 0.007	¹⁵ 0.051	¹⁵ 0.104	0.000	0.000	0.041	0.000		
215	SENSETIME-006	² 0.001	² 0.006	² 0.055	² 0.001	² 0.004	¹³ 0.064	⁵ 0.002	⁵ 0.012	¹⁴⁸ 0.998	⁹ 0.004	⁹ 0.034	⁸ 0.093	0.000	0.000	0.025	0.000		
216	SENSETIME-007	¹ 0.001	¹ 0.006	¹ 0.052	¹ 0.001	¹ 0.003	¹⁰ 0.062	¹ 0.001	¹ 0.009	¹⁶⁷ 0.999	² 0.003	⁴ 0.024	⁵ 0.085	0.000	0.000	0.025	0.000		
217	SHAMAN-003	²⁵⁵ 0.124	²⁴⁷ 0.172					²⁵ 0.451	²⁴⁷ 0.597					0.020	0.011				
218	SHAMAN-004	²⁶⁶ 0.222	²⁵⁶ 0.319					²⁶⁰ 0.615	²⁵⁴ 0.754					0.020	0.011				
219	SHAMAN-006	²³⁴ 0.040	²¹⁵ 0.058	¹⁹⁶ 0.938				²⁶⁸ 0.141	¹⁹⁸ 0.237	⁷⁶ 0.972				0.020	0.011	^{0.869}			
220	SHAMAN-007	²³⁵ 0.040	²¹⁴ 0.057					²⁶⁹ 0.141	²⁰¹ 0.240					0.020	0.010				
221	SIAT-001	⁸⁸ 0.002	²⁵⁸ 0.333		⁷⁵ 0.004			⁶⁶ 0.099	²⁰ 0.018	²²⁷ 0.365	⁷⁴ 0.031			0.000	0.000				
222	SIAT-002	⁶¹ 0.002	²⁶⁰ 0.446	¹⁸⁸ 0.348				⁷⁰ 0.102	⁸⁶ 0.022	²³⁹ 0.478	¹⁶⁸ 0.372	¹⁶³ 0.923	0.000	0.000					
223	SMILART-004	²⁷⁸ 0.965	²⁷⁴ 0.974					²⁷¹ 0.968	²⁶⁷ 0.976					0.011	0.013				
224	SMILART-005													0.011	0.013				
225	SQISOFT-001	¹³² 0.004	¹³⁰ 0.019	⁶⁸ 0.282	⁸⁴ 0.005	⁶⁸ 0.027	⁶¹ 0.097	²⁰⁵ 0.132	²⁰⁴ 0.252	⁴⁶ 0.797	⁹² 0.040	⁷⁹ 0.317	¹⁰⁴ 0.420	0.000	0.000	0.039	0.000		
226	STAQU-000	¹⁶⁵ 0.007	¹³⁷ 0.020	¹²⁷ 0.613	¹⁴³ 0.020	⁸⁷ 0.055	¹³³ 0.159	¹⁶⁰ 0.062	²³⁵ 0.443	¹⁸⁸ 1.000	¹⁷⁵ 0.535	⁹⁴ 0.961	²⁵⁹ 1.000	0.000	0.000	0.000	0.000		
227	SYNESIS-003	²⁶¹ 0.170	²⁵² 0.235					²⁵⁸ 0.582	²⁵⁰ 0.646					0.006	0.015				
228	SYNESIS-003	²⁰⁹ 0.016	¹⁵⁶ 0.023	¹⁷² 0.827	¹²⁸ 0.013			¹¹⁹ 0.136	¹⁶⁴ 0.065	¹⁴⁸ 0.123	⁶⁹ 0.960	¹²³ 0.075	⁸⁵ 0.314	0.000	0.001	0.063			
229	SYNESIS-005	¹⁷⁵ 0.009	⁷⁷ 0.013	^{148</}															

#	ALGORITHM	INVESTIGATION MODE						IDENTIFICATION MODE						FAILURE TO EXTRACT FEATURES							
		RANK ONE MISS RATE, FNIR(N, 0, 1)						HIGH T → FPIR = 0.001, FNIR(N, T, L)													
	GALLERY	MUGSHOT	MUGSHOT	MUGSHOT	VISA	BORDER	VISA	MUGSHOT	MUGSHOT	MUGSHOT	VISA	BORDER	BOR _L 10YR	KIOSK	MUGSHOT	MUGSHOT	MUGSHOT	VISA	BORDER	BOR _L 10YR	KIOSK
	PROBE	MUGSHOT	WEBCAM	PROFILE	BORDER	BOR _L 10YR	KIOSK	MUGSHOT	WEBCAM	PROFILE	BORDER	BOR _L 10YR	KIOSK	MUGSHOT	WEBCAM	PROFILE	BORDER	BOR _L 10YR	KIOSK		
231	TECH5-002	102.003	32.011	73.032	51.003	75.029	31.089	102.027	39.070	49.085	91.039	66.205	107.440	0.001	0.000	0.041	0.000	0.000	0.000	0.000	
232	TEVIAN-003	20.015	210.052					22.177	217.298					0.001	0.002						
233	TEVIAN-004	19.011	190.038					19.117	183.076					0.001	0.002						
234	TEVIAN-005	166.007	174.028	98.047				182.087	163.0144	70.962				0.001	0.002	0.116					
235	TEVIAN-006	91.002	38.011	34.0123	45.0003	42.013	22.071	40.010	36.032	16.0425	41.016	29.093	168.951	0.001	0.000	0.062	0.000	0.000	0.000	0.000	
236	TEVIAN-007	57.002	28.009	28.093	23.002	26.009	15.067	29.005	21.022	12.301	30.009	21.065	22.0122	0.000	0.000	0.062	0.000	0.000	0.000	0.000	
237	TIGER-000	240.062	237.095					24.390	240.500					0.000	0.000						
238	TIGER-002	149.006	153.023	104.0514				178.086	172.0158	157.0999				0.000	0.000	0.056					
239	TIGER-003	150.006	154.023					17.086	173.0158					0.000	0.000						
240	TONGYITRANS-000	161.007	150.022					171.074	137.0112					0.003	0.001						
241	TONGYITRANS-001	160.007	151.022					163.066	129.0101					0.003	0.001						
242	TOSHIBA-000	136.004	143.022	154.0766				161.062	142.0118	130.0995				0.000	0.000	0.070					
243	TOSHIBA-001	141.005	147.022					150.058	116.0092					0.000	0.000						
244	TRUEFACE-000	118.003	84.014	59.0230	108.0007	62.024	35.0092	28.018	29.0062	35.0882	72.030	64.0194	82.0188	0.001	0.001	0.047	0.003				
245	VD-000	274.474	265.051					269.017	265.0946					0.111	0.13						
246	VD-001	228.028	211.053					22.201	214.0281					0.005	0.001						
247	VD-002	184.010	172.027	179.0893	131.0013	84.0050	140.0176	175.079	165.0148	133.0996	130.0095	81.0367	95.0372	0.004	0.003	0.156	0.002				
248	VD-003	167.008	144.022	157.0773	115.0008	7.0030	120.0137	13.046	127.0100	158.099	104.0051	7.0244	8.0315	0.003	0.003	0.144	0.002				
249	VERIDAS-001	105.003	91.014	112.050	97.006	73.028	110.131	121.037	104.0082	101.0987	93.0044	73.0266	75.0264	0.000	0.002	0.093	0.001				
250	VERIDAS-002	101.003	92.014	118.0550	96.006	72.0028	111.131	122.037	105.0082	102.0987	96.0044	74.0266	74.0264	0.000	0.002	0.093	0.001				
251	VERIDAS-003	60.002	57.011	71.0297	66.0004	46.0016	83.0108	68.017	69.0055	137.0997	50.020	46.0150	47.0178	0.000	0.002	0.093	0.001				
252	VIGILANTSOLUTIONS-003	249.069	245.0151	207.0958				25.0408	253.0660	154.0999				0.000	0.001	0.127					
253	VIGILANTSOLUTIONS-004	256.0125	253.0244	212.0965				257.0549	257.0817	135.0996				0.000	0.001	0.127					
254	VIGILANTSOLUTIONS-005	189.009		185.0920				24.0388		204.0000				0.000	0.001	0.127					
255	VIGILANTSOLUTIONS-006	189.010		186.0921				24.0353		205.0000				0.000	0.001	0.127					
256	VIGILANTSOLUTIONS-007	118.003	118.017	189.0925	129.0013	89.0068	138.0175	109.028	110.0088	134.0996	127.0081	83.0371	98.0391	0.000	0.001	0.127	0.001				
257	VIGILANTSOLUTIONS-008	111.003	119.017	184.0913	135.0014	90.0072	141.0178	81.021	98.0077	136.0999	134.0104	85.0398	12.0511	0.000	0.001	0.127	0.001				
258	VISIONBOX-000	69.002	59.011	150.0752	78.0005	48.0017	36.0078	73.0018	72.0057	109.0990	58.0023	45.0146	39.0162	0.000	0.001	0.043	0.001				
259	VISIONLABS-004	101.003	133.020	81.0343				15.058	174.0159	57.0890				0.001	0.001	0.046					
260	VISIONLABS-005	92.002	128.019	79.0334				139.050	164.0147	56.0888				0.001	0.001	0.046					
261	VISIONLABS-006	62.002	103.015	54.0211	61.0004			10.027	114.0090	35.0672				0.001	0.001	0.051					
262	VISIONLABS-007	56.002	102.015	53.0211	57.0004			38.095	100.027	113.0090	36.0672	77.031	31.0185	0.001	0.001	0.051					
263	VISIONLABS-008	70.002	85.014	38.0141	30.0002			39.081	50.013	69.0051	22.0481	42.017	32.0151	0.001	0.000	0.075					
264	VISIONLABS-009	16.001	23.008	27.0901	9.0001			21.071	24.0005	27.0205	47.0799	26.0008	19.0113	0.000	0.000	0.060					
265	VISIONLABS-010	28.001	46.010	16.069	9.0001	10.0006	20.069	28.0005	31.0027	20.008	17.0055	18.0109	0.000	0.000	0.040	0.000					
266	VISIONLABS-011	18.001	25.009	10.064	3.001	6.0004	12.063	12.0003	19.0020	9.004	10.034	6.0090	0.000	0.000	0.032	0.000					
267	VOCORD-003	158.006	161.024	168.0804	171.061			145.0188	199.0122	170.0155	146.0998	148.0157	101.0404	0.001	0.011	0.425					
268	VOCORD-004	171.008	140.021	159.0792	122.0012			108.0127	24.0355	180.0173	189.0100	156.0193	17.0991	0.000	0.000						
269	VOCORD-005	164.007	152.023	167.0812	167.0055			148.0206	212.0158	153.0130	138.0997	143.0138	96.0381	0.001	0.009	0.554					
270	VOCORD-006	28.000	279.000	247.0000	20.0000			153.0000	27.0000	278.0000	27.0000	27.0000	27.0000	0.001	0.009	0.554					
271	VTS-000	276.0594	268.0608	182.0909	194.0607	96.0724	193.0739	259.0598	248.0619	164.0999	184.0613	92.0760	142.0761	0.000	0.001	0.047	0.000				
272	VTS-001	40.002	39.010	46.0167	9.0006	31.0018	33.0077	50.0013	29.0051	119.0994	56.022	42.0141	33.0192	0.000	0.040						
273	VTS-002	70.002	78.013	60.0233	135.0014	81.0038	104.0125	9.0026	36.0075	175.0000	98.0045	70.0231	103.0417	0.000	0.000	0.029	0.000				
274	XFORWARDAI-000	86.002	88.014	26.089	63.0004	44.0015	36.0094	64.0015	67.0053	18.0440	52.021	31.059	42.0169	0.000	0.000	0.000	0.000				
275	XFORWARDAI-001	70.002	75.013	14.0067	47.0003	28.0009	42.0082	20.0005	33.0028	19.0448	23.0008	20.0062	25.0123	0.000	0.000	0.000	0.000				
276	XFORWARDAI-002	72.002	70.012	5.059	37.0002	14.0007	31.0077	18.0003	15.0016	24.0525	12.0005	13.0041	12.0099	0.000	0.000	0.000	0.000				

Table 15: **Miss rates by dataset**: At left, rank 1 miss rates relevant to investigations; at right, with threshold set to target FPIR = 0.01 for higher volume, low prior, uses. Yellow indicates most accurate algorithm. Throughout blue superscripts indicate the rank of the algorithm for that column.

2022/03/30
17:50:48

FN(R, R, T) = False neg. identification rate
 FPIR(N, T) = False pos. identification rate

N = Num. enrolled subjects
R = Num. candidates examined

T = Threshold

$T = 0 \rightarrow$ Investigation
 $T > 0 \rightarrow$ Identification

#	ALGORITHM	INVESTIGATION MODE						IDENTIFICATION MODE						FAILURE TO EXTRACT FEATURES					
		RANK ONE MISS RATE, FNIR(N, 0, 1)						HIGH T → FPIR = 0.001, FNIR(N, T, L)											
		N=1.6M						N=1.6M											
GALLERY	MUGSHOT	MUGSHOT	MUGSHOT	VISA	BORDER	VISA	MUGSHOT	MUGSHOT	MUGSHOT	VISA	BORDER	VISA	MUGSHOT	MUGSHOT	MUGSHOT	VISA	BORDER	KIOSK	
PROBE	MUGSHOT	WEBCAM	PROFILE	BORDER	BOR _L 10YR	KIOSK	MUGSHOT	WEBCAM	PROFILE	BORDER	BOR _L 10YR	KIOSK	MUGSHOT	WEBCAM	PROFILE	BORDER	BOR _L 10YR	KIOSK	
277	YISHENG-001	²²⁷ 0.027	²¹⁹ 0.060		¹⁷⁰ 0.058		¹⁷¹ 0.287	²³⁹ 0.346	²⁵⁵ 0.808	¹⁸⁵ 0.666	¹⁶² 0.919		0.002	0.005					
278	YITU-002	⁶⁴ 0.002	⁴³ 0.010					⁷¹ 0.018	⁵⁵ 0.049					0.000	0.000				
279	YITU-003	¹⁰⁹ 0.003	¹⁰⁸ 0.016					⁷⁹ 0.019	⁶³ 0.052					0.003	0.001				
280	YITU-004	²³ 0.001	²² 0.008	¹⁷⁷ 0.866				⁴⁰ 0.010	³⁰ 0.027	⁶⁵ 0.936				0.000	0.000	0.000			
281	YITU-005	⁸⁸ 0.002	⁹⁷ 0.014					⁴⁶ 0.010	³⁷ 0.032					0.003	0.001				

Table 16: **Miss rates by dataset:** At left, rank 1 miss rates relevant to investigations; at right, with threshold set to target FPIR = 0.01 for higher volume, low prior, uses. Yellow indicates most accurate algorithm. Throughout blue superscripts indicate the rank of the algorithm for that column.

#	ALGORITHM	MISSES BELOW THRESHOLD, T	ENROL MOST RECENT			
		DATASET: FRVT 2018 MUGSHOTS				
		N=0.64M	N=1.6M	N=3.0M	N=6.0M	N=12.0M
1	3DIVI-005	²¹⁷ 0.1358	²¹⁷ 0.1664	¹⁹⁸ 0.1915	¹⁸¹ 0.2370	¹⁷³ 0.3054
2	ACER-000	²¹¹ 0.1185	²¹⁰ 0.1455	¹⁸⁴ 0.1714	¹⁷⁴ 0.2074	¹⁶⁶ 0.2537
3	ALCHERA-003	²⁰⁹ 0.1176	²¹¹ 0.1553	¹⁸⁸ 0.1853	¹⁸² 0.2409	¹⁸⁸ 0.3553
4	ALLGOVISION-000	¹⁸³ 0.0688	¹⁸⁴ 0.0881	¹⁶⁷ 0.1084	¹⁵⁹ 0.1389	¹⁴⁶ 0.2129
5	ALLGOVISION-001	¹⁸⁹ 0.0785	¹⁸⁹ 0.1017	¹⁷⁴ 0.1218	¹⁶⁶ 0.1584	¹⁵⁵ 0.2273
6	ANKE-000	¹⁹⁶ 0.0942	¹⁹⁴ 0.1169	¹⁷⁹ 0.1404	¹⁷¹ 0.1776	¹⁶⁷ 0.2559
7	ANKE-002	¹¹³ 0.0229	¹¹³ 0.0318	¹¹³ 0.0406	¹⁰⁸ 0.0605	⁹⁴ 0.1466
8	AWARE-003	²⁰⁶ 0.1098	²⁰² 0.1283	¹⁸⁹ 0.1447	¹⁶⁹ 0.1768	¹⁵⁸ 0.2364
9	AWARE-005	²⁴ 0.3389	²⁴³ 0.3643	¹⁹ 0.3993	¹⁹⁰ 0.4526	¹⁶ 0.2531
10	AYONIX-002	²⁶⁶ 0.7862	²⁶⁶ 0.8242	²⁰³ 0.8508	¹⁹⁵ 0.8704	¹⁸⁹ 0.8939
11	CAMVI-004	¹³ 0.0367	¹⁶⁸ 0.0716	¹⁶ 0.0983	¹⁸⁴ 0.2508	¹⁷ 0.2701
12	CANON-001	³⁰ 0.0039	³⁰ 0.0054	³⁰ 0.0074	²⁷ 0.0158	³⁴ 0.0924
13	CB-000	³⁸ 0.0086	⁵³ 0.0125	⁵⁰ 0.0160	⁴⁶ 0.0303	²⁴ 0.1251
14	CLEARVIEWAI-000	³¹ 0.0040	³¹ 0.0058	³¹ 0.0078	²⁸ 0.0159	³⁷ 0.0971
15	CLOUDWALK-HR-000	¹⁰ 0.0019	¹⁰ 0.0020	⁸ 0.0023	¹² 0.0072	¹⁶ 0.0701
16	CLOUDWALK-MT-000	¹¹ 0.0019	⁹ 0.0020	⁷ 0.0022	⁵ 0.0049	⁸ 0.0466
17	COGENT-000	¹⁵ 0.0430	¹⁴² 0.0527	¹⁴⁵ 0.0695	¹⁴⁵ 0.1133	¹³ 0.1960
18	COGENT-001	¹⁵⁸ 0.0430	¹⁴³ 0.0527	¹⁴⁴ 0.0695	¹⁴⁴ 0.1133	¹³⁴ 0.1960
19	COGENT-002	¹² 0.0322	¹²⁹ 0.0444	¹²⁴ 0.0610	¹⁴² 0.1116	¹⁴ 0.2180
20	COGENT-003	¹²⁶ 0.0328	¹³⁴ 0.0463	¹⁴⁴ 0.0683	¹⁵² 0.1294	¹⁶⁰ 0.2445
21	COGENT-004	¹¹⁰ 0.0210	¹¹⁴ 0.0331	¹²⁴ 0.0527	¹⁴⁷ 0.1138	¹⁴⁵ 0.2119
22	COGENT-005	⁴⁰ 0.0064	³⁹ 0.0091	³⁹ 0.0123	³⁷ 0.0303	²⁰ 0.1233
23	COGNITEC-000	²¹⁹ 0.1377	²¹⁵ 0.1606	¹⁸⁹ 0.1870	¹⁷⁶ 0.2176	¹⁷² 0.2831
24	COGNITEC-001	¹⁹ 0.0807	¹⁹⁰ 0.1017	¹⁷⁷ 0.1214	¹⁶² 0.1513	¹⁵ 0.2238
25	COGNITEC-002	¹⁵⁰ 0.0406	¹⁴⁵ 0.0531	¹³⁷ 0.0666	¹³⁰ 0.0935	¹³⁰ 0.1874
26	COGNITEC-003	¹⁴ 0.0400	¹⁴¹ 0.0526	¹³⁶ 0.0650	¹²⁵ 0.0895	¹² 0.1772
27	COGNITEC-004	¹¹² 0.0222	¹¹² 0.0313	¹¹⁰ 0.0388	¹⁰¹ 0.0540	⁹³ 0.1103
28	COGNITEC-005	³⁹ 0.0063	⁴¹ 0.0096	⁴⁶ 0.0144	⁵¹ 0.0287	³⁶ 0.0967
29	COGNITEC-006	³⁵ 0.0053	³⁶ 0.0077	³⁶ 0.0117	⁴¹ 0.0254	³⁰ 0.0919
30	CYBERLINK-000	¹⁵² 0.0414	¹⁵³ 0.0565	¹⁴⁸ 0.0707	¹³⁸ 0.1031	¹⁴¹ 0.2050
31	CYBERLINK-001	¹⁴³ 0.0392	¹⁴⁶ 0.0536	¹⁴⁵ 0.0695	¹³⁵ 0.0973	¹² 0.1794
32	CYBERLINK-002	⁵⁹ 0.0105	⁶² 0.0148	⁶⁷ 0.0202	⁷⁸ 0.0399	⁷⁵ 0.1255
33	CYBERLINK-003	³⁶ 0.0056	³⁷ 0.0077	³⁶ 0.0100	³⁷ 0.0235	²¹ 0.1237
34	CYBERLINK-004	³⁴ 0.0051	³⁴ 0.0071	³⁶ 0.0102	³² 0.0199	²⁸ 0.1269
35	CYBERLINK-005	⁴² 0.0067	⁴⁴ 0.0099	⁴⁴ 0.0138	⁴⁵ 0.0394	¹⁶ 0.1566
36	DAHUA-001	¹⁷² 0.0569	¹⁷⁰ 0.0727	¹⁵⁸ 0.0878	¹⁴⁸ 0.1148	¹²⁹ 0.1867
37	DAHUA-002	⁶ 0.0108	⁶³ 0.0151	⁶ 0.0191	⁵³ 0.0291	⁶ 0.1153
38	DAHUA-003	³⁷ 0.0100	³⁸ 0.0139	³⁹ 0.0180	³⁴ 0.0296	³⁸ 0.1130
39	DAHUA-004	³³ 0.0048	³³ 0.0069	³³ 0.0090	³⁰ 0.0164	²⁴ 0.0853
40	DAON-000	⁹⁰ 0.0161	⁹⁰ 0.0226	⁹² 0.0293	¹⁰⁷ 0.0562	¹¹⁷ 0.1702
41	DECATUR-000	⁹² 0.0173	⁹³ 0.0229	⁹³ 0.0305	⁸⁷ 0.0464	⁹¹ 0.1433
42	DEEPLINT-001	²⁰ 0.0027	²⁰ 0.0033	¹⁹ 0.0043	²¹ 0.0121	³³ 0.0922
43	DEEPSEA-001	¹³⁵ 0.0347	¹³³ 0.0462	¹²⁸ 0.0586	¹²³ 0.0802	¹¹⁹ 0.1708
44	DERMALOG-005	¹⁸ 0.0700	¹⁸³ 0.0880	¹⁶⁹ 0.1144	¹⁶⁵ 0.1578	¹⁶ 0.2451
45	DERMALOG-006	¹⁴⁴ 0.0395	¹⁴⁰ 0.0517	¹³³ 0.0659	¹³⁴ 0.0973	¹²² 0.1745
46	DERMALOG-007	¹⁸ 0.0691	¹⁸¹ 0.0863	¹⁶⁸ 0.1107	¹⁶¹ 0.1504	¹⁵ 0.2299
47	DERMALOG-008	¹³¹ 0.0338	¹³¹ 0.0455	¹³¹ 0.0626	¹³⁹ 0.1060	¹⁵⁴ 0.2276
48	DERMALOG-009	⁸⁸ 0.0148	⁸³ 0.0206	⁸⁴ 0.0268	⁸¹ 0.0416	⁸⁰ 0.1374
49	FUJITSULAB-000	⁸⁴ 0.0148	⁸⁴ 0.0206	⁸⁸ 0.0277	¹⁰³ 0.0541	¹²¹ 0.1739
50	FUJITSULAB-001	⁶ 0.0126	⁷⁵ 0.0182	⁸⁰ 0.0251	¹¹¹ 0.0646	¹⁴ 0.2079
51	GORILLA-002	²²⁵ 0.1539	²²³ 0.1880	¹⁹³ 0.2184	¹⁸⁵ 0.2596	¹⁸⁰ 0.3398
52	GORILLA-004	¹⁸ 0.0699	¹⁸⁶ 0.0892	¹⁶⁷ 0.1048	¹⁵⁷ 0.1370	¹³⁰ 0.1969
53	GORILLA-005	¹⁶² 0.0453	¹⁵⁷ 0.0583	¹⁴⁷ 0.0704	¹³⁶ 0.0974	⁹⁵ 0.1474
54	GORILLA-006	¹⁰⁵ 0.0196	¹⁰⁴ 0.0275	⁹⁷ 0.0331	⁹⁴ 0.0516	⁵⁶ 0.1113
55	GORILLA-007	¹⁰² 0.0190	¹⁰³ 0.0271	¹⁰⁵ 0.0348	⁹⁷ 0.0520	⁵⁷ 0.1129
56	GRIAULE-000	⁸⁰ 0.0145	⁸¹ 0.0201	⁸¹ 0.0253	⁸⁰ 0.0407	⁹² 0.1440
57	HIK-003	¹⁹² 0.0828	¹⁹¹ 0.1028	¹⁷⁸ 0.1202	¹⁶⁴ 0.1525	¹⁶ 0.2480
58	HIK-004	¹⁹⁰ 0.0796	¹⁸⁷ 0.0988	¹⁷⁰ 0.1147	¹⁶⁰ 0.1474	¹⁶⁴ 0.2483
59	HIK-005	¹² 0.0312	¹²⁶ 0.0436	¹² 0.0560	¹²⁷ 0.0911	¹⁴ 0.2129
60	HYPERVERGE-001	²³ 0.0033	²³ 0.0045	²³ 0.0059	¹⁸ 0.0117	²⁶ 0.0872
61	IDEARIA-003	¹³ 0.0346	¹³⁶ 0.0471	¹⁵ 0.0892	¹⁸ 0.2789	¹⁸ 0.4311
62	IDEARIA-004	¹²² 0.0300	¹²² 0.0373	¹¹⁶ 0.0447	¹⁰⁹ 0.0617	¹¹⁶ 0.1635
63	IDEARIA-005	¹³ 0.0360	¹²⁸ 0.0440	¹²⁸ 0.0537	¹²² 0.0764	¹³ 0.1915
64	IDEARIA-006	¹³⁶ 0.0351	¹²⁵ 0.0433	¹²³ 0.0525	¹¹⁹ 0.0734	¹⁴⁹ 0.2201
65	IDEARIA-007	²⁶ 0.0136	⁷⁴ 0.0181	⁶⁹ 0.0228	⁶⁸ 0.0357	⁸⁹ 0.1402
66	IDEARIA-008	³ 0.0016	⁸ 0.0019	¹⁰ 0.0024	⁶ 0.0053	³ 0.0470
67	IDEARIA-009	² 0.0013	² 0.0016	² 0.0018	⁹ 0.0061	¹² 0.0550
68	IMAGUS-005	⁷ 0.0137	⁷⁸ 0.0185	⁷⁵ 0.0237	⁷⁰ 0.0368	⁴ 0.1067
69	IMAGUS-006	⁷⁸ 0.0137	⁸⁰ 0.0190	⁷⁸ 0.0244	⁷⁶ 0.0396	⁶⁵ 0.1159
70	IMAGUS-007	⁸⁸ 0.0160	⁹² 0.0228	⁹⁶ 0.0284	⁸⁴ 0.0444	⁶ 0.1179
71	IMPERIAL-000	⁹⁸ 0.0187	⁹⁸ 0.0259	¹⁰⁷ 0.0358	¹¹⁸ 0.0733	¹²⁵ 0.1794
72	INCODE-003	²¹⁶ 0.1324	²¹⁸ 0.1672	¹⁹¹ 0.1961	¹⁷⁹ 0.2345	¹⁷⁵ 0.3123

Table 17: **Identification-mode: Effect of N on FNIR at high threshold.** Values are threshold-based miss rates i.e. FNIR at FPIR = 0.001 for five enrollment population sizes, N. The right six columns apply for enrollment of one image. Missing entries usually apply because another algorithm from the same developer was run instead. Some developers are missing because less accurate algorithms were not run on galleries with $N \geq 3\,000\,000$. Throughout blue superscripts indicate the rank of the algorithm for that column.

#	ALGORITHM	MISSES BELOW THRESHOLD, T		ENROL MOST RECENT					
		FNIR(N, T > 0, R > L)		DATASET: FRVT 2018 MUGSHOTS					
73	INCODE-004	¹⁴⁸ 0.0403	¹⁴⁹ 0.0538	N=0.64M	N=1.6M	N=3.0M	N=6.0M	N=12.0M	
74	INCODE-005	⁴⁸ 0.0083	⁴⁸ 0.0113	⁴⁷ 0.0145	³⁸ 0.0247	²⁹ 0.0912			
75	INNOVATRICS-007	⁵⁴ 0.0093	⁵⁴ 0.0125	⁵² 0.0159	⁴³ 0.0259	⁵⁰ 0.1092			
76	INTSYSMSU-000	²⁷ 0.0982	²⁷ 0.0984	²⁰ 0.0985	¹⁹ 0.9987	¹⁹ 0.9988			
77	IREX-000	¹⁰³ 0.0190	¹⁰⁸ 0.0280	¹¹¹ 0.0391	¹¹⁴ 0.0677	⁹⁸ 0.1479			
78	ISYSTEMS-002	¹⁷ 0.0584	¹⁷ 0.0783	¹⁶ 0.0973	¹⁸ 0.1373	¹⁵ 0.2295			
79	ISYSTEMS-003	¹⁶⁰ 0.0438	¹⁵⁸ 0.0590	¹⁵⁴ 0.0807	¹⁵⁰ 0.1259	¹⁵⁷ 0.2357			
80	KAKAO-000	⁶⁵ 0.0109	⁶⁵ 0.0151	⁶⁴ 0.0196	⁶³ 0.0324	⁴⁹ 0.1010			
81	KEDACOM-001	⁹⁴ 0.0181	⁹¹ 0.0227	⁸² 0.0265	⁸³ 0.0422	⁸⁵ 0.1340			
82	LOOKMAN-003	¹³ 0.0346	¹² 0.0437	¹² 0.0514	¹¹ 0.0724	¹¹ 0.1620			
83	LOOKMAN-005	¹¹⁴ 0.0240	¹¹⁰ 0.0301	¹⁰⁶ 0.0356	⁹³ 0.0512	⁸⁴ 0.1334			
84	MANTRA-000	⁴ 0.0065	⁴⁵ 0.0101	⁴⁸ 0.0151	³⁸ 0.0308	⁴¹ 0.1035			
85	MEGVII-001	¹²⁰ 0.0562	¹⁶⁹ 0.0722	¹⁵⁹ 0.0872	¹⁵⁴ 0.1309	¹⁷¹ 0.2713			
86	MICROFOCUS-005	²⁷ 0.9732	²⁶ 0.8354	²⁰ 0.8555	¹⁶ 0.8755	¹⁹ 0.8954			
87	MICROSOFT-003	¹⁰⁶ 0.0198	¹⁰⁶ 0.0278	¹⁰⁵ 0.0356	¹⁰⁰ 0.0538	¹⁰⁴ 0.1539			
88	MICROSOFT-004	⁹ 0.0185	⁹⁹ 0.0259	⁹⁶ 0.0333	⁹⁵ 0.0517	¹⁰ 0.1510			
89	MICROSOFT-005	⁹⁵ 0.0181	⁹⁶ 0.0256	⁹⁶ 0.0320	⁹² 0.0512	¹⁰⁰ 0.1491			
90	MICROSOFT-006	⁵³ 0.0091	⁴⁹ 0.0120	⁵⁴ 0.0162	⁵⁵ 0.0301	⁹⁹ 0.1482			
91	NEC-000	¹⁷⁸ 0.0637	¹⁷⁶ 0.0789	¹⁶⁰ 0.0933	¹⁴⁹ 0.1163	¹³⁵ 0.1941			
92	NEC-001	¹⁹³ 0.0863	¹⁹³ 0.1055	¹⁷³ 0.1249	¹⁶³ 0.1519	¹⁵² 0.2253			
93	NEC-002	¹⁴ 0.0020	¹⁴ 0.0026	¹⁵ 0.0033	²³ 0.0135	¹⁴ 0.0653			
94	NEC-003	¹⁵ 0.0021	¹² 0.0024	¹¹ 0.0028	⁸ 0.0059	¹¹ 0.0540			
95	NEC-004	⁷ 0.0017	⁶ 0.0018	⁴ 0.0020	² 0.0037	³ 0.0329			
96	NEC-005	⁴ 0.0015	³ 0.0017	³ 0.0019	¹⁰ 0.0065	¹ 0.0307			
97	NEUROTECHNOLOGY-003	²⁶ 0.5698	²⁶ 0.6362	²⁰ 0.7035	¹⁹ 0.7602	¹⁸ 0.8224			
98	NEUROTECHNOLOGY-004	¹⁶⁴ 0.0466	¹⁶³ 0.0629	¹⁴⁹ 0.0779	¹⁴⁶ 0.1135	¹⁴⁴ 0.2102			
99	NEUROTECHNOLOGY-005	¹⁴ 0.0396	¹⁵⁰ 0.0538	¹³⁹ 0.0675	¹³³ 0.0950	¹³ 0.1966			
100	NEUROTECHNOLOGY-007	¹⁵⁹ 0.0436	¹⁶² 0.0623	¹⁵¹ 0.0802	¹⁵⁵ 0.1320	¹⁵⁹ 0.2393			
101	NEUROTECHNOLOGY-008	¹³² 0.0339	¹⁴⁴ 0.0530	¹⁵⁸ 0.0893	¹⁷⁰ 0.1769	¹⁷⁸ 0.3288			
102	NEUROTECHNOLOGY-009	⁶⁵ 0.0108	⁶⁶ 0.0152	⁶⁷ 0.0196	⁶¹ 0.0324	⁵⁹ 0.1102			
103	NEUROTECHNOLOGY-010	⁴⁴ 0.0069	⁴³ 0.0099	⁴⁵ 0.0138	³⁶ 0.0449	¹²⁰ 0.1727			
104	NOTIONTAG-000	²⁰ 0.0128	⁶⁹ 0.0175	²⁰ 0.0228	⁶⁹ 0.0357	²⁹ 0.1270			
105	NTECHLAB-003	¹⁵⁴ 0.0421	¹⁴⁸ 0.0537	¹³⁸ 0.0674	¹²⁶ 0.0907	¹¹⁰ 0.1582			
106	NTECHLAB-004	¹² 0.0312	¹²³ 0.0405	¹² 0.0519	¹¹⁶ 0.0722	¹⁰ 0.1503			
107	NTECHLAB-005	¹²⁸ 0.0334	¹²⁴ 0.0424	¹²⁸ 0.0537	¹²¹ 0.0760	¹⁰⁷ 0.1543			
108	NTECHLAB-006	¹² 0.0288	¹¹⁸ 0.0367	¹¹ 0.0471	¹¹ 0.0670	¹⁰ 0.1523			
109	NTECHLAB-007	⁹⁹ 0.0188	⁹⁵ 0.0256	⁹⁴ 0.0317	⁹¹ 0.0495	⁸³ 0.1306			
110	NTECHLAB-008	⁶² 0.0107	⁵⁹ 0.0145	⁶¹ 0.0187	⁵⁰ 0.0286	³⁹ 0.0995			
111	NTECHLAB-009	²⁷ 0.0037	²⁷ 0.0049	²⁸ 0.0062	²² 0.0125	¹⁹ 0.0735			
112	NTECHLAB-010	¹² 0.0020	¹³ 0.0025	¹² 0.0030	¹⁴ 0.0077	¹⁸ 0.0710			
113	NTECHLAB-011	¹⁰ 0.0022	¹⁷ 0.0030	¹⁸ 0.0038	¹³ 0.0075	¹³ 0.0625			
114	PANGIAM-000	³² 0.0042	³² 0.0060	³² 0.0080	²⁹ 0.0160	²⁷ 0.0876			
115	PARAVISION-003	¹¹⁶ 0.0260	¹¹⁶ 0.0351	¹¹⁷ 0.0447	¹¹² 0.0657	¹¹⁵ 0.1630			
116	PARAVISION-004	⁴⁵ 0.0074	⁴⁷ 0.0101	⁴³ 0.0136	⁴⁶ 0.0267	²⁶ 0.1256			
117	PARAVISION-005	²¹ 0.0032	²² 0.0041	²⁵ 0.0057	³¹ 0.0174	⁴¹ 0.1037			
118	PARAVISION-007	²¹ 0.0030	²¹ 0.0040	²¹ 0.0055	³³ 0.0211	³¹ 0.1097			
119	PARAVISION-009	¹² 0.0020	¹⁵ 0.0026	¹⁷ 0.0038	¹⁷ 0.0098	²⁸ 0.0857			
120	PIXELALL-002	¹⁸⁸ 0.0716	¹⁹² 0.1052	¹⁸⁸ 0.1475	¹⁸³ 0.2489	¹⁸³ 0.3904			
121	PIXELALL-003	⁸⁷ 0.0158	⁸⁷ 0.0218	⁹¹ 0.0288	⁸⁸ 0.0474	⁶² 0.1138			
122	PIXELALL-004	⁷² 0.0129	⁷⁷ 0.0183	⁷⁹ 0.0245	⁷¹ 0.0378	⁸⁷ 0.1375			
123	PIXELALL-005	⁵¹ 0.0087	⁵¹ 0.0121	⁵⁶ 0.0171	⁴⁰ 0.0250	⁴⁶ 0.1052			
124	PTAKURATSATU-000	¹¹ 0.0275	¹¹⁷ 0.0366	¹¹⁸ 0.0458	⁹⁸ 0.0523	¹⁰ 0.0523			
125	QNAP-001	¹⁴⁹ 0.0404	¹⁴⁷ 0.0536	¹³⁸ 0.0661	¹²⁸ 0.0916	¹¹¹ 0.1595			
126	QUANTASOFT-001	²⁶² 0.6387	²⁶² 0.6387	²⁰ 0.6387		¹⁸ 0.6387			
127	RANKONE-002	²⁰¹ 0.0973	¹⁹⁶ 0.1175	¹⁷⁶ 0.1359	¹⁶⁸ 0.1718	¹⁶⁹ 0.2613			
128	RANKONE-003	²⁰² 0.0973	¹⁹⁷ 0.1175	¹⁷⁷ 0.1359	¹⁶⁷ 0.1718	¹⁶⁸ 0.2613			
129	RANKONE-005	¹⁶⁵ 0.0473	¹⁵⁹ 0.0592	¹⁴⁵ 0.0700	¹³¹ 0.0944	¹³⁹ 0.1998			
130	RANKONE-007	⁹ 0.0168	⁸⁹ 0.0222	⁸⁰ 0.0266	⁷³ 0.0381	⁵⁹ 0.1132			
131	RANKONE-009	⁷⁵ 0.0132	⁷² 0.0177	⁷² 0.0230	⁶⁵ 0.0344	³² 0.0921			
132	RANKONE-010	⁶⁰ 0.0106	⁵⁷ 0.0136	⁵⁶ 0.0174	⁴⁵ 0.0265	²¹ 0.0785			
133	RANKONE-011	³⁸ 0.0063	³⁸ 0.0087	³⁷ 0.0115	³⁷ 0.0269	⁶¹ 0.1135			
134	RANKONE-012	³⁷ 0.0058	³⁵ 0.0077	³⁵ 0.0100	³⁴ 0.0220	⁵⁵ 0.1111			
135	REALNETWORKS-002	²² 0.1943	²²⁸ 0.2314	¹⁹⁶ 0.2656	¹⁸⁹ 0.3134	¹⁷ 0.3208			
136	REALNETWORKS-003	²¹⁵ 0.1300	²¹⁴ 0.1594	¹⁸⁸ 0.1858	¹⁷⁷ 0.2246	¹⁷⁴ 0.3076			
137	REALNETWORKS-004	²¹ 0.1279	²¹³ 0.1581	¹⁸⁷ 0.1857	¹⁷⁸ 0.2329	¹⁷⁶ 0.3179			
138	REALNETWORKS-005	¹⁰⁷ 0.0202	¹⁰⁵ 0.0277	¹⁰⁴ 0.0355	¹⁰⁶ 0.0560	⁹⁰ 0.1431			
139	REALNETWORKS-006	⁵⁶ 0.0097	⁶⁰ 0.0145	⁶⁰ 0.0182	³⁷ 0.0308	³⁸ 0.0991			
140	REMARKAI-000	¹⁵¹ 0.0406	¹⁵¹ 0.0552	¹⁴⁸ 0.0676	¹³⁷ 0.1028	¹⁴⁰ 0.2003			
141	RENDDIP-000	⁴⁸ 0.0085	⁵⁰ 0.0121	⁵⁰ 0.0156	⁴⁹ 0.0277	⁶⁸ 0.1182			
142	REVEALMEDIA-000	⁵² 0.0090	⁵² 0.0122	⁵¹ 0.0158	⁴⁸ 0.0277	⁴¹ 0.1019			
143	S1-000	¹⁰ 0.0204	¹⁰⁷ 0.0279	¹⁰⁷ 0.0382	¹¹⁰ 0.0630	¹¹ 0.1707			
144	S1-001	⁶⁶ 0.0115	⁶⁷ 0.0156	⁶⁶ 0.0199	⁷⁴ 0.0392	⁷⁷ 0.1256			

Table 18: Identification-mode: Effect of N on FNIR at high threshold. Values are threshold-based miss rates i.e. FNIR at FPIR = 0.001 for five enrollment population sizes, N. The right six columns apply for enrollment of one image. Missing entries usually apply because another algorithm from the same developer was run instead. Some developers are missing because less accurate algorithms were not run on galleries with $N \geq 3\,000\,000$. Throughout blue superscripts indicate the rank of the algorithm for that column.

#	ALGORITHM	ENROL MOST RECENT				
		DATASET: FRVT 2018 MUGSHOTS				
		N=0.64M	N=1.6M	N=3.0M	N=6.0M	N=12.0M
145	SCANOVATE-000	¹⁶⁶ 0.0498	¹⁶⁶ 0.0667	¹⁵² 0.0804	¹⁴¹ 0.1097	⁵⁴ 0.1109
146	SCANOVATE-001	¹⁷ 0.0630	¹⁷⁷ 0.0815	¹⁶ 0.0993	¹³¹ 0.1292	¹³⁶ 0.1960
147	SENSETIME-000	⁸⁶ 0.0158	⁸⁵ 0.0208	⁸⁶ 0.0270	⁷⁷ 0.0398	⁶⁹ 0.1232
148	SENSETIME-001	⁸⁹ 0.0161	⁸⁸ 0.0219	⁸⁹ 0.0277	⁸² 0.0420	⁸¹ 0.1304
149	SENSETIME-002	⁸¹ 0.0146	⁶¹ 0.0148	⁴⁹ 0.0153	³⁶ 0.0234	¹⁵ 0.0657
150	SENSETIME-003	⁶ 0.0016	⁷ 0.0018	⁶ 0.0021	⁷ 0.0054	⁶ 0.0451
151	SENSETIME-004	⁵ 0.0015	⁴ 0.0018	³ 0.0021	³ 0.0040	⁴ 0.0354
152	SENSETIME-005	⁷ 0.0016	¹¹ 0.0022	¹³ 0.0031	¹⁶ 0.0089	⁷ 0.0454
153	SENSETIME-006	¹ 0.0014	⁵ 0.0018	⁷ 0.0023	⁴ 0.0047	⁷ 0.0372
154	SENSETIME-007	¹ 0.0012	¹ 0.0014	¹ 0.0016	¹ 0.0036	² 0.0316
155	SHAMAN-007	²¹³ 0.1212	²⁰⁹ 0.1413	¹⁸⁰ 0.1587	¹⁷² 0.1879	¹⁶² 0.2460
156	SIAT-001	⁷⁵ 0.0136	⁷⁰ 0.0176	⁷³ 0.0230	⁶⁴ 0.0344	⁴² 0.1035
157	SIAT-002	⁸⁵ 0.0154	⁸⁶ 0.0216	⁸⁷ 0.0273	⁷⁹ 0.0404	⁸⁰ 0.1283
158	SQISOFT-001	¹⁹⁴ 0.0921	²⁰⁵ 0.1322	¹⁸⁸ 0.1781	¹⁸⁰ 0.2348	¹⁹¹ 0.9271
159	SYNESSIS-003	²⁵ 0.5341	²⁸ 0.5821	²⁰ 0.6113	¹⁹³ 0.6479	¹⁸ 0.6822
160	SYNESSIS-003	¹⁶⁷ 0.0499	¹⁶⁴ 0.0652	¹⁵³ 0.0804	¹⁴⁰ 0.1095	¹³² 0.1916
161	SYNESSIS-005	⁹³ 0.0181	⁹⁴ 0.0248	⁹⁵ 0.0319	⁹⁶ 0.0518	¹⁰ 0.1580
162	TECH5-001	¹⁵³ 0.0420	¹⁵⁴ 0.0574	¹⁵⁹ 0.0911	¹⁷⁵ 0.2106	¹⁸² 0.3725
163	TECH5-002	¹⁰³ 0.0194	¹⁰² 0.0269	¹⁰⁵ 0.0346	⁹⁹ 0.0537	¹¹² 0.1607
164	TEVIAN-005	¹⁸⁵ 0.0692	¹⁸² 0.0873	¹⁶⁶ 0.1066	¹⁵³ 0.1301	¹²⁷ 0.1840
165	TEVIAN-006	⁴⁷ 0.0078	⁴² 0.0098	⁴¹ 0.0130	⁴⁴ 0.0261	⁸² 0.1305
166	TEVIAN-007	²⁹ 0.0038	²⁹ 0.0052	²⁷ 0.0065	²⁶ 0.0154	³⁵ 0.0957
167	TIGER-002	¹⁸⁰ 0.0647	¹⁷⁸ 0.0861	¹⁶¹ 0.1036	¹⁵⁶ 0.1332	¹⁵⁰ 0.2231
168	TOSHIBA-000	¹⁶³ 0.0460	¹⁶¹ 0.0620	¹⁵⁹ 0.0780	¹⁴³ 0.1117	¹⁴³ 0.2082
169	TRUEFACE-000	⁷⁴ 0.0134	⁷⁶ 0.0182	⁷⁶ 0.0238	⁷² 0.0380	⁸⁸ 0.1385
170	VD-001	²²⁵ 0.1642	²²⁵ 0.2015	¹⁹⁹ 0.2351	¹⁸⁶ 0.2736	¹⁷⁹ 0.3293
171	VERIDAS-001	¹¹⁸ 0.0278	¹²¹ 0.0373	¹²⁰ 0.0491	¹²⁰ 0.0753	¹⁰⁵ 0.1541
172	VERIDAS-002	¹¹⁹ 0.0278	¹²⁰ 0.0373	¹⁰⁸ 0.0373	⁹⁰ 0.0491	²⁰ 0.0753
173	VERIDAS-003	⁶⁷ 0.0117	⁶⁸ 0.0166	⁶⁸ 0.0219	⁸⁵ 0.0446	¹⁰⁶ 0.1543
174	VIGILANTSOLUTIONS-008	⁸² 0.0146	⁸² 0.0205	⁸⁷ 0.0269	⁸⁹ 0.0489	⁶⁶ 0.1164
175	VISIONBOX-000	⁶⁸ 0.0122	⁷³ 0.0177	⁷⁷ 0.0239		¹⁹² 0.9538
176	VISIONLABS-004	¹⁵⁶ 0.0427	¹⁵⁵ 0.0578	¹⁴⁶ 0.0703	¹³² 0.0949	¹²⁸ 0.1853
177	VISIONLABS-005	¹⁴¹ 0.0369	¹³⁹ 0.0502	¹³⁰ 0.0626	¹²⁴ 0.0847	¹²⁶ 0.1815
178	VISIONLABS-006	¹⁰ 0.0188	¹⁰¹ 0.0267	¹⁰⁸ 0.0336	¹⁰⁴ 0.0542	⁹⁶ 0.1478
179	VISIONLABS-007	¹⁰⁰ 0.0188	¹⁰⁰ 0.0266	⁹⁹ 0.0335	¹⁰² 0.0540	⁹⁷ 0.1479
180	VISIONLABS-008	⁵⁵ 0.0096	⁵⁵ 0.0131	⁵⁶ 0.0166	⁵² 0.0291	⁷³ 0.1247
181	VISIONLABS-009	²⁵ 0.0034	²⁴ 0.0046	²⁴ 0.0060	²⁴ 0.0140	²⁸ 0.0881
182	VISIONLABS-010	²⁸ 0.0038	²⁸ 0.0051	²⁹ 0.0070	²⁵ 0.0149	³¹ 0.0920
183	VISIONLABS-011	¹⁸ 0.0025	¹⁹ 0.0033	²⁰ 0.0044	²⁰ 0.0120	²³ 0.0825
184	VCORD-005	²¹⁰ 0.1179	²¹² 0.1577	¹⁹² 0.2183	¹⁸⁸ 0.3122	¹⁸⁵ 0.4490
185	VTS-001	³⁸ 0.0102	⁵⁶ 0.0133	⁵⁶ 0.0175	⁶⁰ 0.0322	⁷² 0.1243
186	VTS-002	⁹⁶ 0.0185	⁹⁷ 0.0259	¹⁰¹ 0.0344	¹⁰⁵ 0.0549	⁹³ 0.1447
187	XFORWARDAI-000	⁶¹ 0.0107	⁶⁴ 0.0151	⁶⁷ 0.0195	⁶² 0.0324	⁴⁷ 0.1057
188	XFORWARDAI-001	²⁶ 0.0037	²⁶ 0.0049	²⁵ 0.0060	¹⁹ 0.0120	²² 0.0800
189	XFORWARDAI-002	¹⁹ 0.0026	¹⁸ 0.0030	¹⁶ 0.0035	¹⁵ 0.0078	¹⁷ 0.0706
190	YITU-002	⁷¹ 0.0129	⁷¹ 0.0177	⁷¹ 0.0228	⁶⁶ 0.0345	⁶⁰ 0.1133
191	YITU-003	⁷⁰ 0.0138	⁷⁹ 0.0185	⁷¹ 0.0236	⁶⁷ 0.0353	⁶⁸ 0.1148
192	YITU-004	⁴³ 0.0067	⁴⁰ 0.0096	⁴⁰ 0.0129	³⁵ 0.0232	⁴⁵ 0.1046
193	YITU-005	⁴⁶ 0.0074	⁴⁶ 0.0101	⁴² 0.0135	⁴² 0.0255	⁴⁸ 0.1057

Table 19: Identification-mode: Effect of N on FNIR at high threshold. Values are threshold-based miss rates i.e. FNIR at FPIR = 0.001 for five enrollment population sizes, N. The right six columns apply for enrollment of one image. Missing entries usually apply because another algorithm from the same developer was run instead. Some developers are missing because less accurate algorithms were not run on galleries with $N \geq 3\,000\,000$. Throughout blue superscripts indicate the rank of the algorithm for that column.

MISSES AT GIVEN RANK		ENROL MOST RECENT																							
#	ALGORITHM	RANK 1					aN ^b	RANK 50																	
	FNIR(N, T= 0, R)	N=0.64M	N=1.6M	N=3.0M	N=6.0M	N=12.0M	aN ^b	N=0.64M	N=1.6M	N=3.0M	N=6.0M	N=12.0M	aN ^b												
1	3DIVI-005	215	0.0137	213	0.0176	183	0.0210	177	0.0253	172	0.0302	140	0.0004 N ^{0.271} 154	197	0.0040	196	0.0049	173	0.0057	169	0.0068	164	0.0081	48	0.0002 N ^{-0.240} 159
2	ACER-000	184	0.0081	196	0.0106	171	0.0128	169	0.0157	168	0.0195	61	0.0001 N ^{0.299} 178	143	0.0020	162	0.0026	151	0.0031	151	0.0037	146	0.0045	19	0.0000 N ^{-0.284} 172
3	ALCHERA-003	180	0.0079	187	0.0104	167	0.0123	168	0.0147	163	0.0180	89	0.0002 N ^{0.278} 165	178	0.0027	176	0.0032	159	0.0035	158	0.0042	14	0.0048	56	0.0002 N ^{-0.199} 149
4	ALLGOVISION-000	198	0.0101	195	0.0114	170	0.0127	167	0.0145	162	0.0166	170	0.0010 N ^{0.171} 92	216	0.0063	212	0.0067	178	0.0071	172	0.0075	163	0.0081	176	0.0020 N ^{-0.086} 107
5	ALLGOVISION-001	172	0.0069	176	0.0096	164	0.0107	162	0.0128	159	0.0157	75	0.0002 N ^{0.277} 163	165	0.0023	166	0.0027	152	0.0031	146	0.0036	143	0.0043	41	0.0001 N ^{-0.211} 154
6	ANKE-000	201	0.0102	203	0.0132	179	0.0155	174	0.0188	168	0.0225	123	0.0003 N ^{0.270} 153	187	0.0032	189	0.0040	169	0.0046	167	0.0056	155	0.0066	40	0.0001 N ^{-0.247} 161
7	ANKE-002	107	0.0024	106	0.0028	107	0.0032	103	0.0037	99	0.0043	69	0.0002 N ^{0.203} 107	117	0.0016	110	0.0017	101	0.0018	94	0.0019	104	0.0006 N ^{-0.067} 95		
8	AWARE-003	232	0.0238	239	0.0306	194	0.0361	188	0.0431	180	0.0506	167	0.0008 N ^{0.258} 148	210	0.0055	218	0.0075	188	0.0092	188	0.0113	182	0.0143	39	0.0001 N ^{-0.323} 182
9	AWARE-005	233	0.0245	231	0.0311	195	0.0366	189	0.0434	176	0.0312	186	0.0056 N ^{0.118} 50	214	0.0062	224	0.0082	190	0.0101	186	0.0128	128	0.0007 N ^{-0.169} 144		
10	AYONIX-002	268	0.2935	269	0.3414	205	0.3736	197	0.4101	191	0.4465	191	0.0440 N ^{0.143} 65	267	0.0950	269	0.1274	205	0.1524	198	0.1828	190	0.2150	178	0.0233 N ^{-0.279} 170
11	CAMVI-004	208	0.0124	241	0.0468	199	0.0719	196	0.2363	190	0.2367	123	0.0000 N ^{0.155} 192	240	0.0117	259	0.0464	201	0.0715	197	0.2361	191	0.2364	3	0.0000 N ^{-0.171} 192
12	CANON-001	14	0.0011	12	0.0011	19	0.0012	15	0.0013	13	0.0014	108	0.0002 N ^{0.113} 43	18	0.0009	17	0.0009	17	0.0009	16	0.0010	103	0.0006 N ^{-0.026} 43		
13	CIB-000	42	0.0014	39	0.0015	39	0.0017	42	0.0019	153	0.0131	40	0.0000 N ^{0.385} 191	56	0.0012	48	0.0012	48	0.0012	128	0.0122	4	0.0000 N ^{-0.647} 191		
14	CLEARVIEWAI-000	11	0.0010	13	0.0011	14	0.0012	16	0.0013	16	0.0015	89	0.0002 N ^{0.129} 58	19	0.0009	16	0.0009	16	0.0009	14	0.0010	118	0.0007 N ^{-0.19} 34		
15	CLOUDWALK-HR-000	47	0.0015	35	0.0015	32	0.0015	27	0.0016	22	0.0017	163	0.0007 N ^{0.054} 10	103	0.0014	90	0.0014	89	0.0014	73	0.0014	161	0.0012 N ^{-0.12} 15		
16	CLOUDWALK-MT-000	73	0.0018	55	0.0018	49	0.0018	38	0.0019	30	0.0020	121	0.0011 N ^{0.035} 5	130	0.0018	125	0.0018	114	0.0018	97	0.0018	173	0.0017 N ^{-0.002} 4		
17	COGENT-000	199	0.0101	189	0.0105	166	0.0109	158	0.0115	150	0.0125	184	0.0038 N ^{0.071} 16	153	0.0021	138	0.0024	146	0.0028	148	0.0036	8	0.0000 N ^{-0.466} 188		
18	COGENT-001	200	0.0101	188	0.0105	165	0.0109	157	0.0115	151	0.0125	188	0.0038 N ^{0.071} 17	154	0.0021	154	0.0024	144	0.0028	149	0.0036	170	0.0095	0	0.0000 N ^{-0.466} 187
19	COGENT-002	119	0.0029	122	0.0036	120	0.0041	118	0.0049	114	0.0059	43	0.0001 N ^{0.244} 124	100	0.0014	102	0.0015	106	0.0019	106	0.0021	53	0.0002 N ^{-0.144} 138		
20	COGENT-003	125	0.0031	124	0.0032	123	0.0043	121	0.0051	117	0.0060	57	0.0001 N ^{0.230} 129	111	0.0015	118	0.0017	122	0.0018	118	0.0020	112	0.0022	56	0.0002 N ^{-0.143} 137
21	COGENT-004	75	0.0018	74	0.0020	72	0.0022	70	0.0025	62	0.0028	95	0.0002 N ^{0.159} 81	91	0.0013	88	0.0014	84	0.0014	78	0.0015	67	0.0015	111	0.0007 N ^{-0.050} 76
22	COGENT-005	84	0.0016	49	0.0017	48	0.0018	45	0.0020	39	0.0021	139	0.0004 N ^{0.108} 38	94	0.0013	82	0.0013	73	0.0014	68	0.0014	59	0.0014	139	0.0011 N ^{-0.017} 27
23	COGNITEC-000	226	0.0252	197	0.0295	186	0.0352	180	0.0417	176	0.0447	160	0.0006 N ^{0.259} 149	208	0.0050	210	0.0065	185	0.0077	178	0.0097	177	0.0122	37	0.0001 N ^{-0.305} 176
24	COGNITEC-001	194	0.0090	196	0.0117	176	0.0139	172	0.0166	166	0.0199	113	0.0002 N ^{0.271} 156	183	0.0030	182	0.0034	166	0.0040	161	0.0054	54	0.0002 N ^{-0.207} 153		
25	COGNITEC-002	154	0.0048	152	0.0057	144	0.0067	138	0.0079	137	0.0094	97	0.0002 N ^{0.232} 131	167	0.0024	163	0.0026	149	0.0028	144	0.0030	131	0.0034	89	0.0005 N ^{-0.117} 124
26	COGNITEC-003	157	0.0053	156	0.0062	147	0.0072	144	0.0085	140	0.0100	120	0.0003 N ^{0.222} 120	180	0.0028	174	0.0030	154	0.0032	144	0.0035	136	0.0037	135	0.0008 N ^{-0.097} 115
27	COGNITEC-004	114	0.0027	113	0.0032	115	0.0037	113	0.0045	111	0.0056	33	0.0001 N ^{0.233} 146	90	0.0013	91	0.0014	92	0.0015	89	0.0019	62	0.0002 N ^{-0.123} 129		
28	COGNITEC-005	44	0.0014	46	0.0016	50	0.0018	48	0.0021	49	0.0024	62	0.0001 N ^{0.169} 89	44	0.0011	45	0.0011	42	0.0012	40	0.0012	34	0.0012	109	0.0007 N ^{-0.037} 56
29	COGNITEC-006	40	0.0014	40	0.0016	38	0.0017	41	0.0019	41	0.0022	78	0.0002 N ^{0.154} 73	46	0.0011	44	0.0011	41	0.0012	36	0.0012	36	0.0007 N ^{-0.036} 55		
30	CYBERLINK-000	131	0.0034	126	0.0040	128	0.0046	124	0.0054	119	0.0063	91	0.0002 N ^{0.209} 115	151	0.0021	145	0.0022	138	0.0023	134	0.0025	125	0.0027	103	0.0006 N ^{-0.092} 112
31	CYBERLINK-001	122	0.0030	124	0.0035	122	0.0042	120	0.0050	116	0.0060	44	0.0001 N ^{0.243} 139	119	0.0016	122	0.0017	115	0.0018	111	0.0020	107	0.0022	78	0.0004 N ^{-0.109} 119
32	CYBERLINK-002	106	0.0024	106	0.0026	98	0.0031	92	0.0033	82	0.0035	154	0.0005 N ^{0.121} 52	146	0.0020	140	0.0021	135	0.0021	129	0.0022	111	0.0022	164	0.0012 N ^{-0.035} 34
33	CYBERLINK-003	45	0.0015	41	0.0016	41	0.0017	39	0.0018	31	0.0020	130	0.0003 N ^{0.110} 40	48	0.0011	47	0.0012	44	0.0012	41	0.0013	36	0.0003 N ^{-0.047} 32		
34	CYBERLINK-004	58	0.0016	48	0.0017	46	0.0018	39	0.0019	34	0.0021	154	0.0005 N ^{0.088} 35	101	0.0014	93	0.0014	83	0.0014	71	0.0014	62	0.0015	158	0.0010 N ^{-0.022} 37
35	CYBERLINK-005	68	0.0017	59	0.0018	58	0.0019	50	0.0021	44	0.0023	77	0.0004 N ^{0.099} 35	106	0.0014	94	0.0014	91	0.0015	81	0.0015	68	0.0015	148	0.0009 N ^{-0.032} 52
36	DAHUA-001	159	0.0053	161	0.0067	151	0.0079	149	0.0093	144	0.0112	77	0.0002 N ^{0.236} 147	177	0.0027	169	0.0029	153	0.0031	143	0.0038	92	0.0005 N ^{-0.121} 127		
37	DAHUA-002	65	0.0017	63	0.0018	63	0.0021	59	0.0023	56	0.0027	90	0.0002 N ^{0.156} 75	82	0.0013	80	0.0013	76	0.0014	69	0.0015	123	0.0007 N ^{-0.043} 68		
38	DAHUA-003	13	0.0010	21	0.0012	23	0.0014	25	0.0016	27	0.0018	24	0.0001 N ^{0.199} 104	14	0.0009	12	0.0009	11	0.0009	10	0.0009	98	0.0006 N ^{-0.027} 44		
39	DAHUA-004	12	0.0010	11	0.0011	12	0.0012	11	0.0013	14	0.0014	101	0.0002 N ^{0.113} 46	16	0.										

MISSES AT GIVEN RANK FNIR(N, T= 0, R)		ENROL MOST RECENT										
#	ALGORITHM	RANK 1					aN^b	RANK 50				
		N=0.64M	N=1.6M	N=3.0M	N=6.0M	N=12.0M		N=0.64M	N=1.6M	N=3.0M	N=6.0M	N=12.0M
73	INCODE-004	120.0029	121.0035	121.0041	119.0049	115.0060	42.00001 $N^{0.244}$ 141	133.0018	129.0019	128.0020	122.0021	110.0022
74	INCODE-005	50.0015	47.00017	45.00018	46.00020	46.00023	106.00002 $N^{0.240}$ 63	69.00012	60.00013	59.00013	53.00014	120.0007 $N^{0.041}$ 60
75	INNOVATRICS-007	56.0016	50.0017	52.0019	49.0021	50.0024	103.00002 $N^{0.243}$ 67	67.00012	59.00012	52.00013	46.00013	126.0007 $N^{0.037}$ 57
76	INTSYSMU-000	260.1395	260.1457	261.1498	193.1544	187.1591	193.0768 $N^{0.045}$ 7	269.01098	267.01163	264.01206	195.01252	189.01296
77	IREX-000	146.0043	135.0044	126.0044	114.0046	105.0048	180.0028 $N^{0.204}$ 4	201.00443	192.00443	167.00443	156.00443	142.00443
78	ISYSTEMS-002	158.0053	158.0064	148.0072	145.0083	138.0096	136.00033 $N^{0.204}$ 109	189.00333	183.00334	159.00336	152.00338	140.00401
79	ISYSTEMS-003	149.0046	146.0052	137.0057	137.0066	126.0076	146.00004 $N^{0.174}$ 94	185.00311	179.00333	155.00344	145.00353	138.00307
80	KAKAO-000	28.0013	34.0015	30.0016	46.0019	42.0022	37.00001 $N^{0.192}$ 103	25.00099	23.00010	22.00010	23.00010	83.00005 $N^{0.050}$ 77
81	KEDACOM-001	178.0076	168.0077	152.0079	141.0083	131.0087	188.00400 $N^{0.147}$ 8	221.00711	214.00722	182.00722	170.0073	188.00603 $N^{0.049}$ 13
82	KNERON-000	153.0048	153.0059	145.0067	139.0079	136.0093	108.00002 $N^{0.226}$ 125	205.00488	205.00559	177.00667	175.00709	168.00993
83	LOOKMAN-003	186.0083	177.0088	160.0091	152.0096	142.0104	181.00300 $N^{0.076}$ 19	225.00727	184.00757	173.00767	161.0077	186.00554 $N^{0.022}$ 36
84	LOOKMAN-005	179.0078	171.0080	155.0083	145.0086	137.0092	182.00338 $N^{0.053}$ 9	222.00722	215.00722	183.00723	171.00723	188.0074
85	MANTRA-000	51.0015	53.0017	55.0019	54.0022	52.0025	65.00002 $N^{0.171}$ 91	60.00122	53.00122	51.00122	48.0013	42.0013
86	MEGVII-001	203.0105	198.0118	174.0128	168.0142	167.0161	176.0015 $N^{0.143}$ 66	227.00777	223.00808	186.00808	188.00886	167.00889
87	MICROFOCUS-005	271.0370	271.0424	266.0460	198.0500	192.05391	192.0674 $N^{0.128}$ 57	273.01300	272.01724	206.0246	198.02425	192.02810
88	MICROSOFT-003	26.0013	44.0016	51.0018	57.0022	61.0028	14.00000 $N^{0.217}$ 157	2.00006	4.00007	7.00008	9.00009	28.00001 $N^{0.158}$ 143
89	MICROSOFT-004	25.0012	36.0015	44.0018	53.0021	59.0028	13.00000 $N^{0.281}$ 166	1.00006	1.00006	1.00007	1.00007	5.00009
90	MICROSOFT-005	49.0015	67.0019	70.0023	88.0030	88.0037	9.00000 $N^{0.320}$ 183	3.00006	3.00006	2.00007	2.00008	3.00009
91	MICROSOFT-006	53.0016	73.0020	85.0025	89.0030	92.0038	12.00000 $N^{0.305}$ 179	4.00006	4.00007	3.00007	8.00009	19.00010
92	NEC-000	211.0131	211.0170	188.0203	178.0244	174.0294	134.00003 $N^{0.276}$ 162	182.00299	188.00338	170.00448	160.00509	159.0074
93	NEC-001	223.0180	220.0209	186.0233	180.0266	173.0304	177.0016 $N^{0.179}$ 96	238.01099	231.01131	191.01116	184.01211	179.0129
94	NEC-002	5.0009	9.0010	9.0011	9.0012	7.0013	93.00002 $N^{0.113}$ 45	5.00008	5.00008	4.00008	4.00008	8.00005 $N^{0.038}$ 38
95	NEC-003	30.0013	26.0014	23.0015	29.0016	19.0016	148.00005 $N^{0.079}$ 21	56.00122	46.00122	45.00122	37.0012	147.00009 $N^{0.119}$ 33
96	NEC-004	37.0014	31.0014	27.0015	21.0016	20.0017	159.00006 $N^{0.059}$ 12	89.00133	68.00133	64.00133	44.0013	157.0010 $N^{0.016}$ 25
97	NEC-005	23.0011	19.0012	18.0012	15.0013	11.0014	150.00005 $N^{0.066}$ 14	41.00111	38.00111	34.00111	26.00111	146.00009 $N^{0.113}$ 19
98	NEUROTECHNOLOGY-003	222.0179	221.0225	188.0263	183.0306	178.0361	166.00007 $N^{0.239}$ 137	200.00442	204.00577	181.00722	181.00722	21.00000 $N^{0.134}$ 183
99	NEUROTECHNOLOGY-004	151.0046	148.0056	145.0064	137.0074	132.0084	114.00002 $N^{0.220}$ 119	157.00222	156.00225	148.00228	142.00331	133.0034
100	NEUROTECHNOLOGY-005	135.0035	133.0043	131.0049	129.0057	121.0068	81.00002 $N^{0.223}$ 122	159.00211	150.00233	140.00244	135.00252	127.0028
101	NEUROTECHNOLOGY-007	128.0032	125.0039	12.0044	122.0052	118.0062	71.00002 $N^{0.222}$ 121	147.00200	143.00222	137.00233	128.00244	120.0026
102	NEUROTECHNOLOGY-008	79.0019	82.0022	82.0025	80.0029	80.0034	45.00001 $N^{0.205}$ 111	88.00133	76.00133	72.00133	61.0015	125.0007 $N^{0.143}$ 65
103	NEUROTECHNOLOGY-009	31.0013	32.0014	33.0016	35.0018	32.0021	60.00001 $N^{0.162}$ 83	42.00111	41.00111	38.00111	34.00112	31.0012
104	NEUROTECHNOLOGY-010	22.0011	22.0012	21.0013	20.0015	18.0016	96.00002 $N^{0.125}$ 85	33.00100	31.00110	23.00100	22.00100	21.00014
105	NOTIONTAG-000	104.0023	96.0024	89.0026	83.0029	73.0032	149.00005 $N^{0.117}$ 48	140.00199	136.00209	119.00202	105.00202	167.00027 $N^{0.027}$ 45
106	NTECHLAB-003	152.0046	154.0062	150.0076	151.0094	145.00114	29.00001 $N^{0.310}$ 180	86.00133	111.00166	121.00166	125.00222	121.0026
107	NTECHLAB-004	138.0037	142.0048	138.0058	134.0071	130.0085	28.00001 $N^{0.291}$ 171	50.00111	78.00103	95.00105	93.00107	103.0021
108	NTECHLAB-005	132.0035	140.0047	132.0058	130.0073	132.0092	16.00000 $N^{0.344}$ 186	10.00088	35.00111	50.00112	84.00115	11.00000 $N^{0.285}$ 171
109	NTECHLAB-006	121.0030	130.0041	132.0050	128.0062	127.0078	15.00000 $N^{0.326}$ 185	6.00008	18.00099	35.00111	50.00113	13.00000 $N^{0.253}$ 162
110	NTECHLAB-007	96.0022	101.0027	101.0031	102.0037	104.0044	36.00001 $N^{0.245}$ 142	45.00111	54.00112	59.00113	69.00115	60.00003 $N^{0.109}$ 120
111	NTECHLAB-008	43.0014	52.0017	58.0020	69.0024	57.0027	23.00001 $N^{0.222}$ 124	32.00100	33.00100	31.00111	33.00111	77.00004 $N^{0.065}$ 93
112	NTECHLAB-009	24.0012	24.0013	23.0014	22.0015	21.0016	24.00000 $N^{0.140}$ 62	23.00009	22.00009	21.00010	20.00010	20.00005 $N^{0.041}$ 61
113	NTECHLAB-010	15.0011	14.0011	11.0012	12.0013	12.0014	128.00003 $N^{0.091}$ 30	34.00100	29.00100	25.00100	21.00010	151.00009 $N^{0.005}$ 10
114	NTECHLAB-011	10.0010	8.0010	7.0011	7.0012	8.00103	111.00002 $N^{0.103}$ 36	15.00099	13.00099	15.00099	12.00099	10.00009 $N^{0.017}$ 28
115	PANGAM-000	21.0011	20.0012	20.0013	17.0014	17.0016	102.00002 $N^{0.118}$ 51	31.00010	32.00010	27.00010	25.00011	113.00021
116	PARAVISION-003	113.0026	113.0031	112.0035	109.0042	107.0048	67.00002 $N^{0.210}$ 114	123.00166	121.00171	120.00188	115.00200	104.00211
117	PARAVISION-004	52.0015	45.0016	45.0017	39.0019	36.0021	134.00003 $N^{0.111}$ 41	83.00123	74.00116	65.00116	57.00116	24.00001 $N^{0.237}$ 158
118	PARAVISION-005	46.0015	38.0015	35.0016	32.0018	28.0019	143.00004 $N^{0.094}$ 32	87.00113	77.00103	70.00103	61.00103	50.00114
119	PARAVISION-007	20.0011	17.0012	17.0013	18.0013	15.0015	130.00003 $N^{0.091}$ 29	38.00100	26.00100	24.00100	22.00100	138.00008 $N^{0.018}$ 31
120	PARAVISION-009	9.0010	7.0010	8.0011	8.0012	9.0014	88.00002 $N^{0.118}$ 49	22.00009	20.00009	19.00010	17.00010	97.00006 $N^{0.032}$ 51
121	PIXELALL-002	140.0037	137.0045	135.0052	128.0062	122.0075	64.00002 $N^{0.238}$ 135	128.00017	135.00199	132.00211	130.00224	125.00227
122	PIXELALL-003	81.0019	81.0021	80.0024	77.0028	76.0032	72.00002 $N^{0.182}$ 98	99.00144	92.00144	85.00144	80.00145	72.00016
123	PIXELALL-004	67.0017	78.0020	70.0023	73.0026	69.0030	54.00001 $N^{0.192}$ 102	80.00113	71.00113	77.00114	63.00115	114.00007 $N^{0.045}$ 70
124	PIXELALL-005	72.0018	68.0019	59.0020	59.0021	47.0024	152.00005 $N^{0.098}$ 34	114.00105	110.00116	100.00116	88.00116	78.00116
125	PTAKURATSATU-000	109.0025	111.0030	114.0036	108.0040	94.0040	124.00003 $N^{0.167}$ 87	113.00155	112.00166	123.00188	113.00200	99.00200
126	QNAP-001	133.0035	131.0041	129.0047	125.0054	120.0063	111.00002 $N^{0.200}$ 105	158.00222	153.00223	142.00244	136.00205	126.00228
127	QUANTASOFT-001	267.0217	264.0217	261.0217	188.02177	188.02177	194.02177 $N^{0.001}$ 1	270.01116	266.01116	203.01116	188.01116	194.00000 $N^{0.001}$ 1
128	RANKONE-002	218.0155	218.0194	185.0224								

#	ALGORITHM	MISSES AT GIVEN RANK FNIR(N, T= 0, R)					ENROL MOST RECENT						
		RANK 1					RANK 50						
		N=0.64M	N=1.6M	N=3.0M	N=6.0M	N=12.0M	aN^b	N=0.64M	N=1.6M	N=3.0M	N=6.0M	N=12.0M	aN^b
145	s1-001	¹²⁶ 0.0031	¹¹² 0.0031	¹¹⁰ 0.0034	⁹⁹ 0.0036	⁹⁸ 0.0040	¹⁶⁸ 0.0009 N ^{0.052 31}	¹⁶⁴ 0.0023	¹⁵² 0.0023	¹³⁹ 0.0024	¹³¹ 0.0024	¹¹⁹ 0.0025	¹⁷² 0.0017 N ^{0.023 40}
146	SCANOVATE-000	¹⁴¹ 0.0038	¹⁴³ 0.0050	¹⁴¹ 0.0059	¹³⁹ 0.0073	¹²⁴ 0.0073	⁷⁸ 0.0002 N ^{0.235 133}	¹⁰⁸ 0.0014	¹⁰⁹ 0.0015	¹⁰⁹ 0.0017	¹²⁰ 0.0020	¹⁰¹ 0.0020	³⁵ 0.0002 N ^{0.142 136}
147	SCANOVATE-001	¹⁴⁴ 0.0041	¹⁴⁷ 0.0053	¹⁴² 0.0064	¹⁴⁰ 0.0079	¹³⁹ 0.0098	²⁷ 0.0001 N ^{0.299 176}	⁹⁷ 0.0013	¹⁰⁶ 0.0015	¹⁰⁸ 0.0017	¹²¹ 0.0021	¹¹⁸ 0.0024	³⁶ 0.0001 N ^{0.207 152}
148	SENSETIME-000	⁹⁵ 0.0022	⁸⁹ 0.0023	⁸⁹ 0.0026	⁸¹ 0.0028	⁷⁴ 0.0032	¹³⁷ 0.0003 N ^{0.135 60}	¹²⁸ 0.0016	¹²⁴ 0.0017	¹¹⁶ 0.0018	¹⁰³ 0.0018	⁹⁷ 0.0020	¹³⁰ 0.0007 N ^{0.060 87}
149	SENSETIME-001	⁹⁴ 0.0022	⁹⁰ 0.0023	⁸⁶ 0.0025	⁸⁵ 0.0029	⁸⁷ 0.0037	⁸⁷ 0.0002 N ^{0.177 95}	¹²² 0.0016	¹¹⁵ 0.0016	¹⁰⁷ 0.0017	¹⁰¹ 0.0018	¹¹⁶ 0.0024	⁶⁶ 0.0003 N ^{0.125 130}
150	SENSETIME-002	²¹⁴ 0.0136	²⁰⁵ 0.0137	¹⁷ 0.0137	¹⁶⁸ 0.0138	¹⁵ 0.0139	¹⁸⁹ 0.0124 N ^{0.007 2}	²⁴⁷ 0.0136	²³⁷ 0.0136	¹⁹³ 0.0136	¹⁸⁷ 0.0136	¹⁸¹ 0.0136	¹⁹⁸ 0.0135 N ^{0.001 3}
151	SENSETIME-003	⁸ 0.010	⁶ 0.010	⁶ 0.010	⁶ 0.011	⁶ 0.012	¹²⁷ 0.0003 N ^{0.085 26}	²³ 0.0009	²¹ 0.0009	¹⁸ 0.0009	¹⁸ 0.0010	¹⁵ 0.0010	¹³⁷ 0.0008 N ^{0.013 17}
152	SENSETIME-004	⁶ 0.010	⁵ 0.010	⁴ 0.010	³ 0.011	⁴ 0.012	¹²⁹ 0.0003 N ^{0.081 22}	¹¹ 0.0008	⁹ 0.0009	¹⁰ 0.0009	¹⁰ 0.0009	⁸ 0.0009	¹⁰⁷ 0.0007 N ^{0.018 32}
153	SENSETIME-005	² 0.0008	³ 0.0009	³ 0.0009	³ 0.0010	³ 0.0011	¹¹⁸ 0.0003 N ^{0.085 25}	⁷ 0.0008	⁶ 0.0008	⁵ 0.0008	⁴ 0.0008	⁴ 0.0008	¹³⁹ 0.0008 N ^{0.002 6}
154	SENSETIME-006	³ 0.0008	² 0.0009	² 0.0009	² 0.0010	² 0.0010	¹³¹ 0.0003 N ^{0.069 15}	⁸ 0.0008	⁸ 0.0008	⁷ 0.0008	⁶ 0.0008	⁵ 0.0008	¹¹⁹ 0.0007 N ^{0.011 14}
155	SENSETIME-007	¹ 0.0008	¹ 0.0008	¹ 0.0009	¹ 0.0009	¹ 0.0010	¹³⁸ 0.0004 N ^{0.061 13}	⁹ 0.0008	⁸ 0.0008	⁸ 0.0008	⁵ 0.0008	² 0.0008	¹²⁹ 0.0007 N ^{0.008 12}
156	SHAMAN-007	²⁴² 0.0371	²³⁸ 0.0396	¹⁹⁶ 0.0416	¹⁸⁴ 0.0443	¹⁸⁸ 0.0473	¹⁸⁸ 0.0122 N ^{0.083 23}	²⁵⁷ 0.0308	²⁵¹ 0.0314	¹⁹⁹ 0.0319	¹⁹¹ 0.0326	¹⁸⁵ 0.0337	¹⁹¹ 0.0207 N ^{0.029 50}
157	SIAT-001	⁶¹ 0.0017	⁵⁸ 0.0018	⁶¹ 0.0020	⁶¹ 0.0023	⁵⁸ 0.0027	⁶⁸ 0.0002 N ^{0.173 93}	³⁹ 0.0010	⁴⁰ 0.0011	⁴³ 0.0012	⁴⁷ 0.0013	⁴⁵ 0.0013	⁷⁰ 0.0003 N ^{0.085 106}
158	SIAT-002	⁵⁹ 0.0016	⁶¹ 0.0018	⁶² 0.0020	⁶² 0.0023	⁵⁵ 0.0027	⁷⁰ 0.0002 N ^{0.171 90}	⁵² 0.0011	⁵⁶ 0.0012	⁵⁶ 0.0013	⁵⁵ 0.0013	⁵¹ 0.0014	⁸⁹ 0.0005 N ^{0.062 90}
159	SQISOFT-001	¹¹⁸ 0.0028	¹³² 0.0042	¹⁴⁰ 0.0059	¹⁴⁵ 0.0084	¹⁹³ 0.0207	² 0.0000 N ^{1.674 193}	²⁷ 0.0010	³⁴ 0.0010	³⁶ 0.0011	⁴¹ 0.0012	¹⁹³ 0.9198	² 0.0000 N ^{0.883 193}
160	SYNESIS-003	²⁶¹ 0.1456	²⁶¹ 0.1700	²⁰² 0.1876	¹⁹⁴ 0.2088	¹⁸⁹ 0.2317	¹⁹⁰ 0.0177 N ^{0.158 79}	²⁶³ 0.0828	²⁶ 0.0869	²⁰² 0.0920	¹⁹⁴ 0.0998	¹⁸⁷ 0.1104	¹⁹² 0.0218 N ^{0.098 116}
161	SYNESIS-003	²²⁰ 0.0161	²⁰⁹ 0.0162	¹⁸⁸ 0.0163	¹⁷¹ 0.0165	¹⁷⁰ 0.0254	¹⁷⁹ 0.0002 N ^{0.127 36}	²⁴ 0.0160	²⁴² 0.0160	¹⁸⁹ 0.0160	¹⁸⁴ 0.0245	¹⁵² 0.0009 N ^{0.192 147}	
162	SYNESIS-005	¹⁸⁹ 0.0085	¹⁷⁵ 0.0085	¹⁵⁸ 0.0085	¹⁴⁶ 0.0086	¹³³ 0.0088	¹⁸⁰ 0.0072 N ^{0.102 3}	²³¹ 0.0085	²²⁵ 0.0085	¹⁸⁷ 0.0085	¹⁸⁵ 0.0085	¹⁸⁹ 0.0085 N ^{0.000 2}	
163	TECH5-001	¹²⁷ 0.0032	¹²⁷ 0.0040	¹³⁰ 0.0047	¹²⁵ 0.0057	¹²² 0.0071	³¹ 0.0001 N ^{0.271 155}	¹¹⁸ 0.0016	¹²⁰ 0.0017	¹¹⁹ 0.0018	¹¹² 0.0020	¹¹³ 0.0023	⁶⁸ 0.0003 N ^{0.119 125}
164	TECH5-002	⁸⁷ 0.0020	¹⁰² 0.0027	¹⁰⁵ 0.0031	¹⁰¹ 0.0037	¹⁰³ 0.0047	¹⁷ 0.0000 N ^{0.285 169}	²⁹ 0.0009	²⁷ 0.0010	³³ 0.0011	³⁵ 0.0012	⁴³ 0.0013	⁴⁹ 0.0002 N ^{0.122 132}
165	TEVIAN-005	¹⁶⁴ 0.0056	¹⁶⁶ 0.0073	¹⁵⁹ 0.0084	¹⁵⁶ 0.0105	¹⁵² 0.0130	⁵⁶ 0.0001 N ^{0.283 168}	¹⁴⁶ 0.0020	¹⁴⁹ 0.0023	¹⁴⁴ 0.0025	¹³⁸ 0.0028	¹³² 0.0034	³⁰ 0.0002 N ^{0.178 145}
166	TEVIAN-006	¹⁰² 0.0023	⁹⁴ 0.0024	⁹² 0.0026	⁷⁹ 0.0028	⁷² 0.0031	¹⁵⁷ 0.0005 N ^{0.106 37}	¹¹⁸ 0.0016	¹¹⁵ 0.0017	¹⁰⁵ 0.0017	⁹⁶ 0.0017	⁸⁸ 0.0018	¹⁴⁹ 0.0009 N ^{0.041 62}
167	TEVIAN-007	⁶⁹ 0.0017	⁴⁹ 0.0018	⁴⁹ 0.0018	⁴⁹ 0.0020	³⁷ 0.0021	¹⁶¹ 0.0000 N ^{0.073 18}	⁷⁵ 0.0013	⁶⁴ 0.0013	⁶³ 0.0013	⁵⁸ 0.0013	⁴⁷ 0.0013	¹⁴⁴ 0.0009 N ^{0.026 42}
168	TIGER-002	¹⁴⁷ 0.0044	¹⁴⁹ 0.0056	¹⁴⁶ 0.0068	¹⁴⁷ 0.0086	¹⁴³ 0.0105	²⁹ 0.0001 N ^{0.299 177}	⁷⁸ 0.0013	¹⁰³ 0.0015	¹¹³ 0.0018	¹²³ 0.0021	¹²² 0.0027	¹⁸ 0.0000 N ^{0.253 163}
169	TOSHIBA-000	¹³⁴ 0.0035	¹³⁶ 0.0045	¹³² 0.0052	¹²⁶ 0.0061	¹⁵⁹ 0.0154	⁹⁰ 0.0000 N ^{0.449 189}	¹²⁹ 0.0016	¹²⁷ 0.0018	¹²⁶ 0.0019	¹²⁴ 0.0021	¹⁷⁵ 0.0105	⁷⁰ 0.0000 N ^{0.539 190}
170	TRUEFACE-000	¹²⁴ 0.0031	¹¹⁶ 0.0033	¹¹³ 0.0035	¹⁰⁸ 0.0039	⁹⁷ 0.0043	¹⁶² 0.0006 N ^{0.115 47}	¹⁷² 0.0025	¹⁵⁹ 0.0026	¹⁴⁵ 0.0026	¹³⁷ 0.0027	¹²⁸ 0.0028	¹⁷⁰ 0.0015 N ^{0.038 59}
171	VDI-001	²³¹ 0.0230	²²⁸ 0.0276	¹⁹² 0.0315	¹⁸³ 0.0363	¹⁸⁴ 0.0418	¹⁷⁸ 0.0015 N ^{0.204 110}	²⁴¹ 0.0120	²³⁶ 0.0130	¹⁹⁴ 0.0140	¹⁸⁸ 0.0154	¹⁸³ 0.0170	¹⁷⁹ 0.0024 N ^{0.120 126}
172	VERIDAS-001	¹⁰³ 0.0023	¹⁰⁵ 0.0028	¹⁰⁶ 0.0032	¹⁰⁴ 0.0037	¹⁰¹ 0.0045	⁴⁰ 0.0001 N ^{0.231 130}	¹⁰⁸ 0.0014	⁹⁹ 0.0015	⁹³ 0.0015	⁹¹ 0.0016	⁸⁶ 0.0018	⁸¹ 0.0005 N ^{0.083 105}
173	VERIDAS-002	¹⁰¹ 0.0023	¹⁰⁴ 0.0028	⁹⁸ 0.0028	⁹¹ 0.0032	⁸⁹ 0.0037	¹²² 0.0003 N ^{0.158 77}	¹⁰⁴ 0.0014	⁹⁸ 0.0015	⁸⁷ 0.0015	⁸⁷ 0.0015	⁷⁷ 0.0016	¹³² 0.0007 N ^{0.047 73}
174	VERIDAS-003	⁶² 0.0017	⁶⁰ 0.0018	⁵⁶ 0.0020	⁵⁶ 0.0022	⁵³ 0.0026	⁹⁸ 0.0002 N ^{0.150 70}	⁷⁹ 0.0013	⁷¹ 0.0013	⁶⁷ 0.0013	⁶² 0.0014	⁵⁷ 0.0014	¹¹⁷ 0.0007 N ^{0.043 67}
175	VIGILANTSOLUTIONS-008	¹⁰⁸ 0.0025	¹¹⁰ 0.0029	¹¹¹ 0.0034	¹⁰⁸ 0.0040	¹⁰² 0.0047	⁵¹ 0.0001 N ^{0.224 123}	⁵⁸ 0.0012	⁶⁶ 0.0013	⁶² 0.0013	⁶⁹ 0.0013	⁸¹ 0.0017	⁵⁴ 0.0002 N ^{0.130 133}
176	VISIONBOX-000	⁷⁰ 0.0017	⁶⁹ 0.0019	⁷⁴ 0.0022	²⁵¹ 0.0000	¹⁹⁴ 0.9526	¹ 0.0000 N ^{2.570 194}	⁷⁰ 0.0012	⁶³ 0.0013	⁶⁹ 0.0013	²⁰⁰ 1.0000	¹⁹⁴ 0.9525	¹ 0.0000 N ^{2.710 194}
177	VISIONLABS-004	⁹⁷ 0.0022	¹⁰³ 0.0027	¹⁰⁸ 0.0032	¹¹⁰ 0.0044	¹²² 0.0070	⁷ 0.0000 N ^{0.387 187}	⁷¹ 0.0012	⁸⁷ 0.0014	¹⁰⁶ 0.0017	¹³³ 0.0025	¹⁴⁵ 0.0045	⁶ 0.0000 N ^{0.435 186}
178	VISIONLABS-005	⁸⁴ 0.0020	⁹² 0.0024	¹⁰⁸ 0.0029	¹⁰⁹ 0.0037	¹⁰⁹ 0.0051	¹¹ 0.0000 N ^{0.322 184}	⁶⁹ 0.0012	⁷⁰ 0.0013	⁹⁹ 0.0016	¹¹⁰ 0.0019	¹²⁹ 0.0029	¹² 0.0000 N ^{0.298 174}
179	VISIONLABS-006	⁶⁰ 0.0016	⁶² 0.0018	⁷³ 0.0022	⁸⁰ 0.0028	⁹⁶ 0.0041	¹⁰ 0.0000 N ^{0.314 182}	⁶³ 0.0012	⁶⁵ 0.0013	⁸⁸ 0.0015	¹⁰⁴ 0.0019	¹²⁴ 0.0027	¹⁴ 0.0000 N ^{0.275 168}
180	VISIONLABS-007	⁵⁷ 0.0016	⁵⁶ 0.0018	⁶⁰ 0.0020	⁶⁰ 0.0023	⁵⁸ 0.0034	¹⁰ 0.0001 N ^{0.248 143}	⁵⁷ 0.0012	⁵⁵ 0.0013	⁵³ 0.0013	⁵⁵ 0.0020	⁴³ 0.0001 N ^{0.152 139}	
181	VISIONLABS-008	⁷⁸ 0.0019	⁷⁶ 0.0020	⁶⁹ 0.0021	⁷¹ 0.0025	⁷⁰ 0.0030	⁸⁴ 0.0002 N ^{0.169 88}	¹²⁶ 0.0016	¹²³ 0.0017	¹¹¹ 0.0017	¹¹⁴ 0.0020	¹¹⁴ 0.0023	⁷¹ 0.0003 N ^{0.114 122}
182	VISIONLABS-009	¹⁷ 0.0011	¹⁶ 0.0011	¹⁶ 0.0012	¹⁸ 0.0014	²⁰ 0.0017	⁴⁷ 0.0001 N ^{0.160 82}	²⁸ 0.0010	²⁶ 0.0010	²¹ 0.0011	⁵⁴ 0.0014	³⁹ 0.0002 N ^{0.109 118}	
183	VISIONLABS-010	³⁴ 0.0014											

#	ALGORITHM	MISSES OUTSIDE RANK R		RESOURCE USAGE		ENROL MOST RECENT, N = 1.6M						
		FNIR(N, T=0, R)		TEMPLATE		FRVT 2018 MUGSHOTS						
		BYTES	MSEC	R=1	R=5	R=10	R=20	R=50	WORK-10			
1	20FACE-000	¹³⁴ 2048	⁴⁵ 247	²⁴ 0.0552	²³⁸ 0.0269	²³⁷ 0.0198	²³⁴ 0.0146	²²⁸ 0.0099	²³⁹ 1.275			
2	3DIVI-003	⁴⁷ 512	¹⁴⁶ 625	²⁵³ 0.0833	²⁴⁸ 0.0444	²⁴⁶ 0.0349	²⁴⁴ 0.0270	²⁴⁴ 0.0191	²⁴⁹ 1.447			
3	3DIVI-004	²⁵⁴ 4096	¹⁴⁷ 628	²¹ 0.0175	²⁰⁵ 0.0091	²⁰¹ 0.0075	²⁰⁰ 0.0061	¹⁹⁵ 0.0049	²⁰⁷ 1.092			
4	3DIVI-005	²⁵⁹ 4096	¹⁵⁵ 653	²¹³ 0.0176	²⁰⁶ 0.0091	²⁰¹ 0.0074	¹⁹⁹ 0.0061	¹⁹⁶ 0.0049	²¹⁰ 1.092			
5	3DIVI-006	⁹⁹ 528	¹⁵⁴ 653	²²³ 0.0240	²²⁹ 0.0171	²³³ 0.0160	²³⁵ 0.0154	²⁴⁰ 0.0148	²²⁸ 1.162			
6	ACER-000	⁴⁸ 512	³⁵ 201	¹⁹⁴ 0.0106	¹⁷⁴ 0.0051	¹⁷¹ 0.0041	¹⁶⁹ 0.0034	¹⁶² 0.0026	¹⁷⁷ 1.053			
7	ACER-001	¹²⁹ 2048	²⁶ 184	¹⁴⁵ 0.0051	¹⁴⁸ 0.0032	¹⁴⁷ 0.0028	¹⁴⁶ 0.0025	¹⁴⁶ 0.0022	¹⁴⁷ 1.031			
8	AIZE-001	¹⁷ 2048	⁸⁵ 403	¹⁵ 0.0056	¹⁵² 0.0037	¹⁵ 0.0033	¹⁵⁸ 0.0030	¹⁶⁵ 0.0027	¹⁵¹ 1.035			
9	ALCHERA-000	¹⁷¹ 2048	⁴⁹ 263	²⁰⁸ 0.0161	²¹⁷ 0.0124	²²² 0.0117	²²⁷ 0.0111	²³⁰ 0.0105	²¹⁶ 1.116			
10	ALCHERA-001	¹⁸⁸ 2048	¹¹ 66	²⁷ 0.9869	²⁹ 0.9782	²⁷⁹ 0.9735	²⁷⁹ 0.9679	²⁷⁸ 0.9590	²⁷⁷ 9.811			
11	ALCHERA-002	¹⁵¹ 2048	¹⁹ 115	²⁵⁴ 0.0949	²⁵³ 0.0555	²⁵¹ 0.0443	²⁵¹ 0.0354	²⁴⁶ 0.0254	²⁵³ 1.544			
12	ALCHERA-003	¹⁹ 2048	¹³⁰ 548	¹⁸ 0.0104	¹⁷⁷ 0.0054	¹⁷⁷ 0.0045	¹⁷⁷ 0.0038	¹⁷⁶ 0.0032	¹⁷⁹ 1.055			
13	ALCHERA-004	¹⁸⁹ 2048	²³⁸ 854	¹⁹² 0.0110	¹⁷³ 0.0049	¹⁶⁷ 0.0038	¹⁶¹ 0.0032	¹⁵⁸ 0.0025	¹⁷³ 1.051			
14	ALLGOVISION-000	¹⁸ 2048	⁹⁵ 425	¹⁹ 0.0114	²⁰⁰ 0.0084	²⁰⁶ 0.0078	²⁰⁷ 0.0073	²¹² 0.0067	²⁰⁰ 1.079			
15	ALLGOVISION-001	¹⁷⁴ 2048	²¹⁷ 792	¹⁷⁸ 0.0090	¹⁷¹ 0.0048	¹⁷⁰ 0.0040	¹⁶⁸ 0.0033	¹⁶⁶ 0.0027	¹⁷¹ 1.048			
16	ANKE-000	²³⁸ 2072	⁹⁷ 431	²⁰ 0.0132	¹⁹¹ 0.0073	¹⁹⁶ 0.0060	¹⁸⁹ 0.0050	¹⁸⁹ 0.0040	¹⁹⁶ 1.072			
17	ANKE-001	²³ 2072	⁹⁸ 433	²⁰⁴ 0.0132	¹⁹² 0.0073	¹⁹² 0.0061	¹⁹⁰ 0.0050	¹⁹⁰ 0.0040	¹⁹⁷ 1.073			
18	ANKE-002	²³ 2056	¹⁵⁰ 641	¹⁰⁶ 0.0028	¹⁰⁷ 0.0020	¹⁰⁸ 0.0018	¹¹³ 0.0018	¹¹⁷ 0.0017	¹⁰⁸ 1.019			
19	AWARE-003	²³⁵ 2076	¹⁹¹ 716	²³ 0.0306	²²⁷ 0.0162	²²³ 0.0127	²²¹ 0.0100	²¹⁸ 0.0075	²²⁹ 1.163			
20	AWARE-004	⁷ 92	¹⁸⁸ 712	²⁴⁸ 0.0679	²⁴⁵ 0.0348	²⁴⁷ 0.0274	²⁴² 0.0208	²³⁹ 0.0145	²⁴⁵ 1.354			
21	AWARE-005	²⁴⁵ 3100	²²⁴ 827	²³ 0.0311	²²⁸ 0.0167	²²⁵ 0.0134	²²³ 0.0107	²²⁴ 0.0082	²³⁹ 1.167			
22	AWARE-006	⁸ 124	²²¹ 818	²⁵⁰ 0.0697	²⁴⁷ 0.0369	²⁴³ 0.0288	²⁴³ 0.0223	²⁴¹ 0.0158	²⁴⁷ 1.371			
23	AYONIX-000	⁸⁷ 1036	⁶ 10	²⁷ 0.4505	²⁷⁴ 0.3540	²⁷⁷ 0.3176	²⁷⁴ 0.2834	²⁷⁴ 0.2381	²⁷⁷ 4.288			
24	AYONIX-001	⁹⁰ 1036	⁸ 12	²⁶⁸ 0.3414	²⁶⁸ 0.2338	²⁶⁸ 0.1977	²⁶⁹ 0.1652	²⁶⁸ 0.1274	²⁶⁸ 3.226			
25	AYONIX-002	⁸⁹ 1036	⁷ 11	²⁶ 0.3414	²⁶⁹ 0.2338	²⁶⁷ 0.1977	²⁶⁸ 0.1652	²⁶⁹ 0.1274	²⁶⁷ 3.226			
26	CAMVI-003	⁷³ 1024	¹⁸⁴ 707	²⁴³ 0.0520	²⁵² 0.0517	²⁵³ 0.0517	²⁵⁶ 0.0517	²⁵⁶ 0.0517	²⁵¹ 1.466			
27	CAMVI-004	⁷³ 1024	¹⁹³ 718	²⁴ 0.0468	²⁵⁰ 0.0465	²⁵³ 0.0465	²⁵³ 0.0464	²⁵⁵ 0.0464	²⁴⁶ 1.419			
28	CAMVI-005	⁷³ 1024	²⁰⁸ 769	²⁷ 0.6652	²⁵⁴ 0.0648	²⁵⁷ 0.0648	²⁵⁸ 0.0648	²⁶⁰ 0.0647	²⁵¹ 1.584			
29	CANON-001	²⁶⁰ 4096	²⁵⁴ 893	¹² 0.0011	¹⁹ 0.0010	¹⁷ 0.0010	¹⁷ 0.0009	¹⁷ 0.0009	¹³ 1.009			
30	CIB-000	²⁷ 8196	¹⁶³ 674	³⁹ 0.0015	⁴⁶ 0.0013	⁴⁴ 0.0012	⁴⁵ 0.0012	⁴⁸ 0.0012	⁴⁴ 1.012			
31	CLEARVIEWAI-000	²⁵² 4096	²⁰⁵ 765	¹² 0.0011	¹⁷ 0.0010	¹⁹ 0.0010	¹⁶ 0.0009	¹⁶ 0.0009	¹³ 1.009			
32	CLOUDWALK-HR-000	¹³⁰ 2048	²⁶¹ 908	³⁵ 0.0015	⁶³ 0.0014	⁷⁰ 0.0014	⁸¹ 0.0014	⁹⁰ 0.0014	⁵⁶ 1.013			
33	CLOUDWALK-MT-000	¹⁵ 2048	²⁴⁵ 870	³² 0.0018	⁸⁹ 0.0018	¹⁰⁸ 0.0018	¹⁰⁹ 0.0018	¹²⁵ 0.0018	⁸⁷ 1.016			
34	COGENT-000	⁵⁵ 525	¹³¹ 551	¹⁸⁹ 0.0105	²¹⁰ 0.0096	²¹⁹ 0.0095	¹⁶³ 0.0032	¹⁵⁵ 0.0024	²⁰⁷ 1.088			
35	COGENT-001	⁵⁶ 525	¹³² 552	¹⁸⁸ 0.0105	²¹¹ 0.0096	²¹⁶ 0.0095	¹⁶² 0.0032	¹⁵⁴ 0.0024	²⁰⁸ 1.088			
36	COGENT-002	⁹² 1043	²²⁹ 987	¹² 0.0036	¹¹⁷ 0.0022	¹¹⁵ 0.0020	¹¹¹ 0.0018	¹⁰⁷ 0.0015	¹¹⁸ 1.021			
37	COGENT-003	⁹¹ 1043	²⁷⁶ 960	¹²⁴ 0.0038	¹²⁸ 0.0024	¹²⁴ 0.0021	¹²⁶ 0.0019	¹¹⁸ 0.0017	¹²⁸ 1.023			
38	COGENT-004	²¹⁷ 2053	²⁷³ 952	²⁷ 0.0020	⁷⁷ 0.0016	⁷⁷ 0.0015	⁸⁶ 0.0015	⁸⁸ 0.0014	⁷⁷ 1.015			
39	COGENT-005	⁹³ 1062	²¹¹ 774	⁴⁹ 0.0017	⁶² 0.0014	⁶² 0.0014	⁷² 0.0014	⁸² 0.0013	⁶¹ 1.013			
40	COGNITEC-000	²⁰ 2052	²⁴ 176	²² 0.0252	²²³ 0.0136	²²¹ 0.0107	²²⁰ 0.0085	²¹⁰ 0.0065	²²¹ 1.136			
41	COGNITEC-001	²⁰⁷ 2052	³⁶ 202	¹⁹⁶ 0.0117	¹⁸⁴ 0.0062	¹⁸⁸ 0.0051	¹⁸⁵ 0.0042	¹⁸² 0.0034	¹⁸⁴ 1.062			
42	COGNITEC-002	¹⁹⁷ 2052	⁴¹ 227	¹⁵⁹ 0.0057	¹⁵¹ 0.0037	¹⁵² 0.0032	¹⁵⁴ 0.0029	¹⁶³ 0.0026	¹⁵² 1.035			
43	COGNITEC-003	²⁰⁹ 2052	⁵⁹ 297	¹⁵⁶ 0.0062	¹⁶⁰ 0.0040	¹⁶¹ 0.0036	¹⁶⁷ 0.0033	¹⁷⁴ 0.0030	¹⁵⁹ 1.039			
44	COGNITEC-004	²¹³ 2052	³² 192	¹¹⁵ 0.0032	¹¹⁰ 0.0020	¹⁰¹ 0.0018	⁹³ 0.0015	⁹¹ 0.0014	¹¹² 1.020			
45	COGNITEC-005	²⁰⁸ 2052	⁷³ 367	⁴⁰ 0.0016	⁴¹ 0.0013	⁴⁰ 0.0012	⁴¹ 0.0012	⁴⁵ 0.0011	⁴⁰ 1.012			
46	COGNITEC-006	²¹² 2052	¹⁰⁷ 463	⁴² 0.0016	⁴⁰ 0.0013	³⁷ 0.0012	⁴⁰ 0.0012	⁴⁴ 0.0011	³⁸ 1.012			
47	CUBOX-000	¹⁵ 2048	²⁶⁵ 918	³⁶ 0.0014	⁵² 0.0014	⁶⁴ 0.0014	⁷³ 0.0014	⁸⁴ 0.0014	⁴⁹ 1.012			
48	CYBERLINK-000	²⁰⁵ 2052	¹⁷⁹ 699	¹²⁶ 0.0040	¹³⁸ 0.0028	¹⁴³ 0.0026	¹⁴⁴ 0.0024	¹⁴⁵ 0.0022	¹³⁷ 1.027			
49	CYBERLINK-001	¹⁹⁷ 2052	⁹⁹ 433	¹²³ 0.0035	¹²⁵ 0.0023	¹²² 0.0021	¹¹⁷ 0.0018	¹²² 0.0017	¹²¹ 1.022			
50	CYBERLINK-002	²⁷³ 4140	²⁰⁰ 738	¹⁰⁶ 0.0026	¹¹⁹ 0.0023	¹²⁹ 0.0022	¹³⁶ 0.0021	¹⁴⁰ 0.0021	¹¹⁸ 1.021			
51	CYBERLINK-003	²⁷ 6212	¹⁷⁷ 696	⁴ 0.0016	⁴⁵ 0.0013	⁴⁶ 0.0013	⁴⁶ 0.0012	⁴⁷ 0.0012	⁴⁶ 1.012			
52	CYBERLINK-004	²⁷ 6212	²⁰¹ 738	⁴⁸ 0.0017	⁶⁹ 0.0015	⁷⁶ 0.0015	⁸² 0.0014	⁹³ 0.0014	⁶⁹ 1.014			
53	CYBERLINK-005	²⁷⁶ 6212	²⁰² 739	⁵⁹ 0.0018	⁷⁶ 0.0016	⁸³ 0.0015	⁹⁰ 0.0015	⁹⁴ 0.0014	⁷² 1.015			
54	DAHUA-000	¹⁶⁰ 2048	³⁷⁸ 378	¹⁸² 0.0093	¹⁸⁷ 0.0066	¹⁹¹ 0.0061	¹⁹⁷ 0.0057	²⁰⁰ 0.0054	¹⁸⁸ 1.062			
55	DAHUA-001	¹⁷⁸ 2048	⁷⁵ 371	¹⁶⁰ 0.0067	¹⁶¹ 0.0040	¹⁵⁹ 0.0036	¹⁶⁵ 0.0033	¹⁶⁹ 0.0029	¹⁶¹ 1.040			
56	DAHUA-002	¹⁵⁰ 2048	⁶⁹ 699	⁶⁸ 0.0018	⁶⁶ 0.0015	⁷² 0.0014	⁷⁷ 0.0014	⁸⁰ 0.0013	⁶⁶ 1.014			
57	DAHUA-003	¹⁵⁷ 2048	¹⁹⁶ 725	²¹ 0.0012	¹¹ 0.0010	¹³ 0.0009	¹² 0.0009	¹² 0.0009	¹² 1.009			
58	DAHUA-004	¹⁹⁸ 2048	²⁰⁴ 759	¹ 0.0011	¹⁴ 0.0010	¹⁴ 0.0009	¹⁴ 0.0009	¹⁴ 0.0009	¹¹ 1.009			
59	DAON-000	²²⁶ 2069	¹³⁷ 584	¹²⁹ 0.0041	¹⁵³ 0.0038	¹⁶⁴ 0.0037	¹⁷⁴ 0.0037	¹⁸⁵ 0.0036	¹⁴⁹ 1.034			
60	DECATAR-000	²⁰⁹ 2052	²⁴⁸ 874	⁸⁸ 0.0021	⁷⁸ 0.0016	⁸¹ 0.0015	⁷⁸ 0.0014	⁷³ 0.0013	⁷⁸ 1.015			
61	DEEPLINT-001	²⁵ 4096	⁶⁸⁷ 687	³⁵ 0.0014	⁵¹ 0.0014	⁵						

MISSES OUTSIDE RANK R		RESOURCE USAGE		ENROL MOST RECENT, N = 1.6M						
FNIR(N, T=0, R)		TEMPLATE		FRVT 2018 MUGSHOTS						
#	ALGORITHM	BYTES	MSEC	R=1	R=5	R=10	R=20	R=50	WORK-10	
73	FUJITSULAB-000	80	1032	272	950	83	0.0022	84	0.0015	
74	FUJITSULAB-001	10	2	1	66	0.0019	72	0.0015	82	0.0014
75	GLORY-000	37	418	20	160	26	0.1781	264	0.1391	
76	GLORY-001	116	1726	87	405	259	0.1268	259	0.0967	
77	GORILLA-001	235	2156	22	169	245	0.0603	240	0.0304	
78	GORILLA-002	97	1132	68	341	219	0.0197	207	0.0092	
79	GORILLA-003	236	2156	134	563	232	0.0361	225	0.0146	
80	GORILLA-004	237	2192	83	395	19	0.0063	147	0.0032	
81	GORILLA-005	278	6288	115	483	114	0.0032	96	0.0019	
82	GORILLA-006	280	8336	207	768	39	0.0017	39	0.0013	
83	GORILLA-007	3	0	5	6	81	0.0017	35	0.0012	
84	GRIAULE-000	210	2052	94	419	98	0.0025	103	0.0020	
85	HIK-003	105	1408	148	633	197	0.0117	182	0.0060	
86	HIK-004	98	1152	120	510	194	0.0113	180	0.0059	
87	HIK-005	103	1408	145	619	139	0.0046	130	0.0025	
88	HIK-006	104	1408	61	610	138	0.0046	131	0.0025	
89	HYPERVERGE-001	75	1024	236	846	27	0.0014	42	0.0013	
90	IDEMIA-003	58	528	169	689	163	0.0069	167	0.0045	
91	IDEMIA-004	58	528	161	669	159	0.0066	157	0.0038	
92	IDEMIA-005	36	352	77	374	172	0.0081	165	0.0044	
93	IDEMIA-006	37	352	76	373	18	0.0096	175	0.0052	
94	IDEMIA-007	68	860	219	807	99	0.0026	79	0.0016	
95	IDEMIA-008	31	300	102	451	10	0.0011	8	0.0009	
96	IDEMIA-009	4	0	1	10	4	0.0010	4	0.0009	
97	IMAGUS-002	45	512	12	76	26	0.2023	263	0.1342	
98	IMAGUS-003	41	512	10	57	270	0.3559	270	0.2491	
99	IMAGUS-005	156	2048	216	788	21	0.0019	80	0.0016	
100	IMAGUS-006	128	2048	259	905	75	0.0020	84	0.0016	
101	IMAGUS-007	138	2048	138	590	77	0.0020	68	0.0015	
102	IMPERIAL-000	162	2048	157	654	95	0.0024	98	0.0019	
103	INCODE-000	71	1024	29	190	242	0.0489	237	0.0261	
104	INCODE-001	154	2048	171	690	210	0.166	201	0.0084	
105	INCODE-002	143	2048	56	291	214	0.0178	204	0.0090	
106	INCODE-003	163	2048	181	704	202	0.0129	186	0.0064	
107	INCODE-004	123	2048	119	508	121	0.0035	124	0.0024	
108	INCODE-005	188	2048	118	500	47	0.0017	53	0.0014	
109	INNOVATRICS-002	60	530	46	255	240	0.0451	242	0.0342	
110	INNOVATRICS-003	61	530	47	255	226	0.0263	218	0.0126	
111	INNOVATRICS-004	94	1076	406	201	0.0123	185	0.0063	187	0.0050
112	INNOVATRICS-005	62	538	233	842	97	0.0024	92	0.0018	
113	INNOVATRICS-007	63	538	215	785	30	0.0017	57	0.0014	
114	INTELLIVISION-001	5	0	3	2	233	0.0365	235	0.0199	
115	INTSYSMSU-000	152	2048	164	675	260	0.1457	262	0.1320	
116	IREX-000	244	3080	281	2379	135	0.0044	162	0.0043	
117	ISYSTEMS-002	194	2048	64	316	158	0.0064	163	0.0043	
118	ISYSTEMS-003	172	2048	239	856	146	0.0052	158	0.0039	
119	KAKAO-000	204	2052	231	840	34	0.0015	27	0.0011	
120	KEDACOM-001	33	292	126	537	168	0.0077	193	0.0074	
121	KNERON-000	183	2048	123	530	153	0.0059	181	0.0059	
122	KNERON-001	142	2048	111	468	229	0.0295	239	0.0295	
123	LINE-000	158	2048	113	482	84	0.0022	74	0.0015	
124	LINE-001	181	2048	263	910	15	0.0011	18	0.0010	
125	LOOKMAN-003	32	292	69	342	17	0.0088	197	0.0078	
126	LOOKMAN-004	60	548	63	325	179	0.0091	198	0.0079	
127	LOOKMAN-005	65	548	121	514	121	0.0080	195	0.0075	
128	MANTRA-000	202	2052	90	412	53	0.0017	48	0.0013	
129	MEGVII-001	262	4096	153	652	198	0.0118	208	0.0093	
130	MEGVII-002	253	4096	159	656	199	0.0118	209	0.0093	
131	MICROFOCUS-003	22	256	52	269	277	0.5942	276	0.4692	
132	MICROFOCUS-004	21	256	53	270	277	0.5763	275	0.4519	
133	MICROFOCUS-005	26	256	51	266	271	0.4242	271	0.3028	
134	MICROFOCUS-006	27	256	50	265	272	0.4268	272	0.3049	
135	MICROSOFT-003	76	1024	86	404	44	0.0016	16	0.0010	
136	MICROSOFT-004	131	2048	210	773	36	0.0015	9	0.0009	
137	MICROSOFT-005	74	1024	162	673	67	0.0019	12	0.0010	
138	MICROSOFT-006	72	1024	175	695	23	0.0020	18	0.0011	
139	NEC-000	243	2592	13	82	211	0.0170	203	0.0086	
140	NEC-001	242	2592	14	88	220	0.0209	224	0.0141	
141	NEC-002	114	1616	156	653	3	0.0010	5	0.0009	
142	NEC-003	115	1712	172	690	26	0.0014	38	0.0012	
143	NEC-004	96	1104	278	967	31	0.0014	49	0.0013	
144	NEC-005	95	1104	27	964	19	0.0012	28	0.0011	

Table 24: Rank-based accuracy for the FRVT 2018 mugshot sets. In columns 3 and 4 are template size and template generation duration. Thereafter values are rank-based FNIR with $T = 0$ and FPIR = 1. This is appropriate to investigational uses but not those with higher volumes where candidates from all searches would need review. The next column is a workload statistic, a small value shows an algorithm front-loads mates into the first 10 candidates. Throughout, blue superscripts indicate the rank of the algorithm for that column, and the best value is highlighted in yellow.

MISSES OUTSIDE RANK R		RESOURCE USAGE		ENROL MOST RECENT, N = 1.6M					
FNIR(N, T=0, R)		TEMPLATE		R=1	R=5	R=10	R=20	R=50	WORK=10
#	ALGORITHM	BYTES	MSEC						
145	NEUROTECHNOLOGY-003	¹⁴ 2048	¹² 547	221.0225	²¹ 0.0126	²¹ 0.0100	²¹ 0.0078	²⁰ 0.0057	²² 0.1.125
146	NEUROTECHNOLOGY-004	¹⁴ 2048	¹² 543	148.0056	¹⁵⁰ 0.0036	¹⁵⁵ 0.0032	¹⁵⁷ 0.0029	¹⁵⁶ 0.0025	¹⁵¹ 1.035
147	NEUROTECHNOLOGY-005	¹⁹ 256	⁹ 412	133.0043	¹⁴⁷ 0.0029	¹⁴⁴ 0.0027	¹⁴⁵ 0.0024	¹⁵⁰ 0.0023	¹⁴¹ 1.028
148	NEUROTECHNOLOGY-006	²³ 256	²⁰ 746	215.0180	¹⁹⁹ 0.0079	¹⁸⁷ 0.0059	¹⁸⁷ 0.0046	¹⁸⁰ 0.0033	²⁰¹ 1.083
149	NEUROTECHNOLOGY-007	²⁷ 256	²¹ 169	125.0039	¹³ 0.0027	¹⁴⁰ 0.0025	¹⁴¹ 0.0023	¹⁴³ 0.0022	¹³³ 1.026
150	NEUROTECHNOLOGY-008	³⁴ 514	²¹ 804	82.0022	⁷⁰ 0.0015	⁷³ 0.0014	⁷⁴ 0.0014	⁷⁶ 0.0013	⁷³ 1.015
151	NEUROTECHNOLOGY-009	³² 513	¹⁶ 686	32.0014	³⁶ 0.0012	³⁶ 0.0012	³⁷ 0.0011	⁴ 0.0011	³³ 1.011
152	NEUROTECHNOLOGY-010	¹⁸ 256	¹⁶ 663	22.0012	²¹ 0.0011	²³ 0.0010	²⁴ 0.0010	³¹ 0.0010	²² 1.010
153	NEWLAND-002	¹⁵ 2048	²⁴ 868	251.0786	²⁵¹ 0.0480	²⁵⁰ 0.0397	²⁵⁰ 0.0332	²⁴⁷ 0.0263	²⁵² 1.468
154	NOBLIS-001	¹⁹ 2048	³⁹ 211	267.02492	²⁶⁷ 0.1772	²⁶⁷ 0.1542	²⁶⁷ 0.1339	²⁶⁵ 0.1112	²⁶⁷ 2.679
155	NOBLIS-002	²⁷ 6144	¹² 535	263.01794	²⁶⁰ 0.1108	²⁶⁰ 0.0903	²⁵⁹ 0.0722	²⁵⁸ 0.0535	²⁶⁰ 2.077
156	NOTIONTAG-000	²³ 2120	¹⁰ 461	96.0024	¹¹⁷ 0.0021	¹²¹ 0.0021	¹³² 0.0020	¹³⁶ 0.0019	¹¹⁰ 1.019
157	NTECHLAB-003	²⁴ 3484	²² 831	154.0062	¹⁴³ 0.0029	¹³⁶ 0.0023	¹²⁷ 0.0019	¹¹¹ 0.0016	¹⁴⁶ 1.030
158	NTECHLAB-004	²⁴ 3484	²⁶ 929	142.0048	¹²⁴ 0.0023	¹⁰⁹ 0.0019	¹⁰¹ 0.0016	⁷⁸ 0.0013	¹²⁹ 1.024
159	NTECHLAB-005	¹¹ 1940	¹⁹ 717	140.0047	¹¹⁶ 0.0022	⁹⁸ 0.0017	⁶³ 0.0013	³⁵ 0.0011	¹²⁴ 1.023
160	NTECHLAB-006	¹² 1940	²³ 841	130.0041	⁹⁷ 0.0019	⁸⁰ 0.0015	⁴⁴ 0.0012	¹⁸ 0.0009	¹¹¹ 1.019
161	NTECHLAB-007	²⁴ 3348	²³ 834	101.0027	⁸⁵ 0.0017	⁷¹ 0.0014	⁶⁸ 0.0013	⁵⁴ 0.0012	⁸⁷ 1.016
162	NTECHLAB-008	¹⁰ 1300	¹³ 562	52.0017	³⁸ 0.0012	³⁴ 0.0012	³⁴ 0.0011	³⁸ 0.0010	³⁶ 1.012
163	NTECHLAB-009	¹⁰ 1300	²⁵ 900	24.0013	²⁵ 0.0011	²² 0.0010	²¹ 0.0010	²² 0.0009	²⁵ 1.010
164	NTECHLAB-010	⁹ 1280	²⁴ 875	14.0011	²⁰ 0.0010	²¹ 0.0010	²³ 0.0010	¹⁸ 0.0010	
165	NTECHLAB-011	¹⁰ 1280	²⁴ 865	8.0010	⁷ 0.0009	¹¹ 0.0009	¹³ 0.0009	¹³ 0.0009	⁷ 1.008
166	PANGIAM-000	² 0	⁴ 2	20.0012	²⁴ 0.0011	²⁶ 0.0011	²⁷ 0.0010	³² 0.0010	²⁴ 1.010
167	PARAVISION-000	¹⁸ 2048	¹⁰ 438	216.0188	²³⁸ 0.0171	²³⁵ 0.0167	²³⁸ 0.0165	²⁴ 0.0164	²²⁶ 1.156
168	PARAVISION-001	¹⁶ 2048	¹³ 590	123.0038	¹²⁷ 0.0024	¹²⁷ 0.0022	¹³³ 0.0020	¹³⁰ 0.0019	¹²⁷ 1.023
169	PARAVISION-002	¹² 2048	⁷ 377	128.0040	¹³⁷ 0.0025	¹³² 0.0022	¹³⁵ 0.0021	¹³⁵ 0.0019	¹³⁰ 1.025
170	PARAVISION-003	¹⁶ 2048	¹⁹ 735	113.0031	¹¹⁵ 0.0022	¹²⁰ 0.0020	¹²¹ 0.0019	¹²¹ 0.0017	¹¹⁵ 1.021
171	PARAVISION-004	²⁵ 4096	¹⁹ 720	45.0016	⁵⁶ 0.0014	⁵⁸ 0.0013	⁶⁶ 0.0013	⁷⁴ 0.0013	⁵⁵ 1.013
172	PARAVISION-005	²⁶ 4096	²⁴ 558	38.0015	⁵⁴ 0.0014	⁵⁹ 0.0013	⁶² 0.0013	⁷⁷ 0.0013	⁵⁰ 1.013
173	PARAVISION-007	²⁵ 4096	¹⁸ 706	17.0012	²⁵ 0.0011	²⁵ 0.0010	²⁶ 0.0010	²⁶ 0.0010	²¹ 1.010
174	PARAVISION-009	²⁶ 4100	¹⁴ 638	7.0010	¹³ 0.0010	¹⁸ 0.0010	²⁰ 0.0009	²⁰ 0.0009	⁹ 1.009
175	PIXELALL-002	²⁴ 2560	³ 198	137.0045	¹⁴² 0.0029	¹⁴¹ 0.0025	¹³⁸ 0.0022	¹³⁵ 0.0019	¹⁴² 1.028
176	PIXELALL-003	²⁴ 2560	¹⁹ 719	81.0021	⁸¹ 0.0016	⁸⁵ 0.0015	⁸³ 0.0014	⁸² 0.0014	⁸¹ 1.015
177	PIXELALL-004	²³ 2560	¹⁰ 453	78.0020	⁷³ 0.0015	⁷⁵ 0.0015	⁸⁰ 0.0014	⁸¹ 0.0013	⁷¹ 1.014
178	PIXELALL-005	²³ 2560	²³ 845	68.0019	⁸⁸ 0.0017	⁸⁸ 0.0016	¹⁰⁸ 0.0016	¹¹⁰ 0.0016	⁸⁰ 1.015
179	PTAKURATSATU-000	⁶ 4538	²⁶ 910	111.0030	¹¹³ 0.0021	¹¹⁴ 0.0019	¹⁰⁸ 0.0018	¹¹² 0.0016	¹¹³ 1.020
180	QNAP-000	¹⁴ 2048	¹⁰ 457	169.0078	¹⁶⁵ 0.0044	¹⁶⁵ 0.0037	¹⁶⁶ 0.0028	¹⁶⁵ 0.0028	¹⁶⁵ 1.043
181	QNAP-001	¹⁴ 2048	¹⁴ 615	131.0041	¹⁴¹ 0.0029	¹⁴⁵ 0.0027	¹⁴⁶ 0.0025	¹⁵³ 0.0023	¹³⁹ 1.028
182	QUANTASOFT-001	¹⁷ 2048	⁸ 396	264.0177	²⁶ 0.1643	²⁶ 0.1468	²⁶ 0.1312	²⁶ 0.1116	²⁶ 2.539
183	RANKONE-002	¹³ 133	¹⁷ 113	218.0194	²¹³ 0.0112	²¹² 0.0093	²¹³ 0.0077	²⁰⁸ 0.0060	²¹⁴ 1.111
184	RANKONE-003	¹⁵ 133	¹⁸ 114	217.0194	²¹⁸ 0.0112	²¹⁵ 0.0093	²¹² 0.0077	²⁰⁷ 0.0060	²¹³ 1.111
185	RANKONE-004	⁶ 85	⁹ 36	239.0145	²³⁶ 0.0226	²³⁶ 0.0177	²³² 0.0141	²²⁹ 0.0102	²³⁶ 1.225
186	RANKONE-005	¹⁴ 133	¹⁵ 94	183.0094	¹⁷⁸ 0.0054	¹⁷⁸ 0.0046	¹⁸⁰ 0.0039	¹⁷ 0.0032	¹⁷⁸ 1.054
187	RANKONE-006	¹⁶ 165	⁴⁸ 261	144.0050	¹⁴⁶ 0.0030	¹⁴⁶ 0.0027	¹⁴³ 0.0024	¹³⁹ 0.0021	¹⁴⁵ 1.030
188	RANKONE-007	¹⁷ 165	⁵⁵ 278	117.0034	¹²² 0.0023	¹²³ 0.0021	¹¹⁸ 0.0018	¹¹⁶ 0.0017	¹¹⁹ 1.022
189	RANKONE-009	²⁸ 260	³¹ 191	91.0024	⁸⁹ 0.0016	⁸⁷ 0.0015	⁸⁹ 0.0014	⁸⁴ 0.0014	⁸¹ 1.015
190	RANKONE-010	³⁰ 261	³⁴ 200	85.0022	⁹⁰ 0.0018	⁹¹ 0.0016	⁹² 0.0015	⁹⁷ 0.0015	⁸⁹ 1.016
191	RANKONE-011	²⁹ 261	¹³ 567	37.0015	³⁷ 0.0012	³⁹ 0.0012	⁴² 0.0012	⁴⁶ 0.0012	³⁵ 1.011
192	RANKONE-012	³¹ 261	¹³ 563	25.0014	³² 0.0012	³³ 0.0011	³⁶ 0.0011	⁴³ 0.0011	²⁹ 1.011
193	REALNETWORKS-000	²⁶ 4100	⁴ 244	237.0042	²³⁸ 0.0195	²³⁹ 0.0149	²²⁵ 0.0111	²²³ 0.0077	²³⁴ 1.201
194	REALNETWORKS-001	²⁶ 4104	⁴² 243	238.00402	²³⁵ 0.0195	²³⁹ 0.0149	²²⁸ 0.0111	²²¹ 0.0077	²³⁵ 1.201
195	REALNETWORKS-002	²⁶ 4104	⁴¹ 245	234.00393	²³⁶ 0.0189	²²⁸ 0.0142	²²⁴ 0.0108	²¹⁹ 0.0076	²³² 1.195
196	REALNETWORKS-003	¹⁷ 1848	²³ 178	224.00242	²¹⁹ 0.0117	²¹¹ 0.0090	²⁰⁸ 0.0070	²⁰¹ 0.0054	²¹⁸ 1.120
197	REALNETWORKS-004	¹⁸ 1848	²⁷ 185	222.00236	²¹⁵ 0.0112	²⁰⁹ 0.0087	²⁰³ 0.0068	¹⁹⁷ 0.0050	²¹⁵ 1.116
198	REALNETWORKS-005	²¹ 2056	⁶ 337	87.00203	⁷⁹ 0.0016	⁶⁷ 0.0014	⁷⁰ 0.0013	⁵⁸ 0.0012	⁷⁷ 1.015
199	REALNETWORKS-006	²¹ 2056	⁷¹ 350	29.0014	³¹ 0.0012	³¹ 0.0011	²⁹ 0.0011	²⁸ 0.0010	³⁰ 1.011
200	REMARKAI-000	¹⁸ 2048	¹⁴ 615	176.0086	¹⁶⁵ 0.0044	¹⁶⁰ 0.0036	¹⁶⁰ 0.0031	¹⁵⁹ 0.0025	¹⁶⁸ 1.045
201	REMARKAI-000	¹² 2048	¹⁷ 691	119.0034	¹¹² 0.0021	¹⁰⁷ 0.0019	¹⁰⁵ 0.0017	¹⁰⁸ 0.0015	¹¹⁴ 1.020
202	REMARKAI-002	¹⁸ 2048	¹⁰ 434	174.0081	¹⁵⁹ 0.0040	¹⁵¹ 0.0031	¹⁴⁸ 0.0026	¹³⁸ 0.0021	¹⁶² 1.041
203	RENDIP-000	¹³ 2048	²⁵ 894	41.0015	⁴³ 0.0013	⁴³ 0.0012	⁴⁷ 0.0012	⁵² 0.0012	⁴⁵ 1.012
204	REVEALMEDIA-000	²⁰ 2052	⁸ 385	65.0019	⁴⁹ 0.0013	⁵³ 0.0013	⁵⁴ 0.0013	⁵⁴ 0.0012	⁵⁴ 1.013
205	S1-000	²⁵ 4096	²⁴ 865	93.0024	⁸⁸ 0.0018	⁹² 0.0017	⁹² 0.0016	¹⁰⁴ 0.0015	⁹¹ 1.017
206	S1-001	¹⁷ 2048	²² 814	112.0031	¹²⁰ 0.0025	¹³⁹ 0.0024	¹⁴² 0.0024	¹³² 0.0023	¹²⁵ 1.023
207	SCANOVATE-000	¹⁴ 2048	¹⁸ 712	143.0050	¹³⁹ 0.0026	¹²⁸ 0.0022	¹¹⁶ 0.0018	¹⁰⁹ 0.0015	¹³⁶ 1.026
208	SCANOVATE-001	¹³ 2048	¹⁶ 675	147.0053	¹⁴³ 0.0027	¹³³ 0.0022	¹¹⁹ 0.0018	¹⁰⁶ 0.0015	¹⁴⁰ 1.028
209	SENSETIME-000	²⁶ 4104	¹⁹ 715	89.00203	¹⁰⁸ 0.0020	¹¹² 0.0019	¹¹⁵ 0.0018	¹²⁴ 0.0017	¹⁰³ 1.018
210	SENSETIME-001	²⁷ 4104	¹⁵ 656	90.0023	¹⁰⁵ 0.0020	¹¹⁰ 0.0019	¹⁰⁷ 0.0017	¹¹³ 0.0016	¹⁰⁰ 1.018
211	SENSETIME-002	²² 2056	¹⁵ 650	205.0137	²² 0.0136	²⁷ 0.0136	²³ 0.0136	²	

#	ALGORITHM	MISSES OUTSIDE RANK R FNIR(N, T=0, R)		RESOURCE USAGE TEMPLATE		ENROL MOST RECENT, N = 1.6M FRVT 2018 MUGSHOTS					
		BYTES	MSEC	R=1	R=5	R=10	R=20	R=50	WORK=10		
217	SHAMAN-003	126	2048	180 ⁷⁰⁴	255 ^{0.1243}	258 ^{0.0823}	258 ^{0.0708}	257 ^{0.0616}	259 ^{0.0518}	258 ^{1.789}	
218	SHAMAN-004	182	2048	151 ⁶⁴²	266 ^{0.2221}	265 ^{0.1473}	263 ^{0.1241}	263 ^{0.1049}	262 ^{0.0825}	265 ^{2.411}	
219	SHAMAN-006	145	2048	185 ⁷⁰⁶	236 ^{0.0398}	248 ^{0.0344}	247 ^{0.0332}	249 ^{0.0323}	252 ^{0.0315}	243 ^{1.316}	
220	SHAMAN-007	175	2048	185 ⁷⁰⁹	235 ^{0.0396}	248 ^{0.0342}	246 ^{0.0331}	248 ^{0.0322}	251 ^{0.0314}	241 ^{1.315}	
221	SIAT-001	214	2052	238 ⁸⁴²	58 ^{0.0018}	57 ^{0.0014}	48 ^{0.0013}	45 ^{0.0012}	40 ^{0.0011}	57 ^{1.013}	
222	SIAT-002	196	2052	260 ⁹⁰⁶	610 ^{0.0018}	56 ^{0.0014}	57 ^{0.0013}	60 ^{0.0013}	56 ^{0.0012}	60 ^{1.013}	
223	SMILART-004	56	512	21 ¹⁶⁷	278 ^{0.9648}	278 ^{0.9641}	278 ^{0.9640}	278 ^{0.9639}	278 ^{0.9638}	278 ^{9.678}	
224	SMILART-005	177	2048	110 ⁴⁶⁴						281 ^{10.000}	
225	SQISOFT-001	222	2056	168 ⁴⁶⁰	132 ^{0.0042}	64 ^{0.0014}	45 ^{0.0013}	39 ^{0.0012}	34 ^{0.0010}	88 ^{1.016}	
226	STAQU-000	258	4096	225 ⁸²⁷	165 ^{0.0071}	183 ^{0.0060}	183 ^{0.0057}	193 ^{0.0055}	198 ^{0.0053}	180 ^{1.056}	
227	SYNESIS-003	257	4096	18 ¹⁰³	261 ^{0.1700}	26 ^{0.1172}	261 ^{0.1047}	26 ^{0.0953}	26 ^{0.0869}	261 ^{2.120}	
228	SYNESIS-003	136	2048	40 ²¹⁵	209 ^{0.0162}	220 ^{0.0160}	232 ^{0.0160}	237 ^{0.0160}	242 ^{0.0160}	225 ^{1.144}	
229	SYNESIS-005	269	4104	209 ⁷⁷²	175 ^{0.0085}	202 ^{0.0085}	207 ^{0.0085}	219 ^{0.0085}	225 ^{0.0085}	199 ^{1.076}	
230	TECH5-001	106	1536	259 ⁸⁹⁸	127 ^{0.0040}	128 ^{0.0024}	125 ^{0.0021}	129 ^{0.0018}	120 ^{0.0017}	128 ^{1.024}	
231	TECH5-002	53	513	21 ⁹⁴¹	102 ^{0.0027}	61 ^{0.0014}	42 ^{0.0012}	35 ^{0.0011}	27 ^{0.0010}	70 ^{1.014}	
232	TEVIAN-003	125	2048	61 ³⁰⁰	206 ^{0.0147}	194 ^{0.0074}	186 ^{0.0059}	188 ^{0.0047}	185 ^{0.0037}	198 ^{1.075}	
233	TEVIAN-004	147	2048	60 ²⁹⁹	193 ^{0.0113}	179 ^{0.0057}	179 ^{0.0047}	176 ^{0.0037}	171 ^{0.0030}	181 ^{1.058}	
234	TEVIAN-005	168	2048	97 ⁴¹⁶	166 ^{0.0073}	159 ^{0.0038}	180 ^{0.0031}	151 ^{0.0027}	149 ^{0.0023}	158 ^{1.038}	
235	TEVIAN-006	82	1032	140 ⁵⁹⁹	94 ^{0.0024}	93 ^{0.0018}	99 ^{0.0018}	108 ^{0.0017}	115 ^{0.0017}	93 ^{1.017}	
236	TEVIAN-007	84	1032	21 ⁷⁷⁹	57 ^{0.0018}	56 ^{0.0014}	56 ^{0.0013}	64 ^{0.0013}	64 ^{0.0013}	52 ^{1.013}	
237	TIGER-000	211	2052	96 ⁴²⁸	246 ^{0.0616}	241 ^{0.0310}	240 ^{0.0236}	248 ^{0.0178}	234 ^{0.0120}	242 ^{1.315}	
238	TIGER-002	201	2052	108 ⁴⁶⁴	149 ^{0.0056}	144 ^{0.0029}	138 ^{0.0024}	122 ^{0.0019}	103 ^{0.0015}	143 ^{1.030}	
239	TIGER-003	199	2052	109 ⁴⁶⁴	150 ^{0.0056}	148 ^{0.0029}	137 ^{0.0024}	121 ^{0.0019}	102 ^{0.0015}	144 ^{1.030}	
240	TONGYITRANS-000	230	2070	30 ¹⁹⁰	161 ^{0.0069}	154 ^{0.0038}	156 ^{0.0032}	153 ^{0.0029}	161 ^{0.0026}	156 ^{1.038}	
241	TONGYITRANS-001	229	2070	28 ¹⁸⁹	162 ^{0.0069}	159 ^{0.0038}	154 ^{0.0032}	156 ^{0.0029}	160 ^{0.0026}	157 ^{1.038}	
242	TOSHIBA-000	113	1548	267 ⁹³⁰	136 ^{0.0045}	133 ^{0.0026}	131 ^{0.0022}	131 ^{0.0020}	127 ^{0.0018}	134 ^{1.026}	
243	TOSHIBA-001	225	2060	26 ⁹³¹	141 ^{0.0048}	137 ^{0.0027}	134 ^{0.0023}	134 ^{0.0020}	125 ^{0.0018}	138 ^{1.027}	
244	TRUEFACE-000	121	2000	72 ³⁶⁵	116 ^{0.0033}	139 ^{0.0028}	148 ^{0.0028}	150 ^{0.0026}	159 ^{0.0026}	135 ^{1.026}	
245	VD-000	79	1028	66 ³³⁷	274 ^{0.4737}	27 ^{0.3204}	273 ^{0.2695}	27 ^{0.2215}	27 ^{0.1678}	273 ^{4.058}	
246	VD-001	215	2052	176 ⁶⁹⁵	228 ^{0.0276}	231 ^{0.0181}	234 ^{0.0162}	233 ^{0.0146}	236 ^{0.0130}	231 ^{1.174}	
247	VD-002	216	2052	170 ⁶⁸⁹	184 ^{0.0095}	194 ^{0.0077}	200 ^{0.0073}	204 ^{0.0070}	213 ^{0.0068}	193 ^{1.071}	
248	VD-003	198	2052	174 ⁶⁹³	167 ^{0.0076}	189 ^{0.0069}	196 ^{0.0067}	202 ^{0.0066}	211 ^{0.0066}	187 ^{1.063}	
249	VERIDAS-001	165	2048	25 ⁸⁸⁵	105 ^{0.0028}	101 ^{0.0019}	96 ^{0.0017}	96 ^{0.0015}	99 ^{0.0015}	101 ^{1.018}	
250	VERIDAS-002	169	2048	252 ⁸⁸⁸	104 ^{0.0028}	100 ^{0.0019}	94 ^{0.0017}	94 ^{0.0015}	98 ^{0.0015}	99 ^{1.018}	
251	VERIDAS-003	140	2048	250 ⁸⁷⁷	60 ^{0.0018}	67 ^{0.0015}	68 ^{0.0014}	67 ^{0.0013}	71 ^{0.0013}	64 ^{1.014}	
252	VIGILANTSOLUTIONS-003	111	1544	228 ⁸³²	249 ^{0.0694}	246 ^{0.0349}	241 ^{0.0262}	241 ^{0.0201}	238 ^{0.0140}	246 ^{1.355}	
253	VIGILANTSOLUTIONS-004	108	1544	226 ⁸³⁰	256 ^{0.1249}	258 ^{0.0706}	254 ^{0.0557}	252 ^{0.0434}	250 ^{0.0305}	255 ^{1.699}	
254	VIGILANTSOLUTIONS-005	107	1544	212 ⁷⁷⁸	180 ^{0.0092}	183 ^{0.0045}	188 ^{0.0036}	157 ^{0.0029}	144 ^{0.0022}	169 ^{1.046}	
255	VIGILANTSOLUTIONS-006	109	1544	229 ⁸³⁴	186 ^{0.0099}	170 ^{0.0048}	166 ^{0.0038}	159 ^{0.0030}	148 ^{0.0022}	172 ^{1.049}	
256	VIGILANTSOLUTIONS-007	110	1544	14 ⁶¹⁸	118 ^{0.0034}	10 ^{0.0020}	97 ^{0.0017}	92 ^{0.0015}	70 ^{0.0013}	109 ^{1.019}	
257	VIGILANTSOLUTIONS-008	112	1544	88 ⁴⁰⁵	110 ^{0.0029}	95 ^{0.0018}	89 ^{0.0016}	83 ^{0.0015}	66 ^{0.0013}	98 ^{1.018}	
258	VISIONBOX-000	224	2059	114 ⁴⁸²	69 ^{0.0019}	70 ^{0.0015}	74 ^{0.0014}	71 ^{0.0013}	63 ^{0.0013}	68 ^{1.014}	
259	VISIONLABS-004	20	256	63 ³¹⁵	103 ^{0.0027}	91 ^{0.0018}	90 ^{0.0016}	91 ^{0.0015}	87 ^{0.0014}	95 ^{1.017}	
260	VISIONLABS-005	46	512	62 ³⁰⁰	92 ^{0.0024}	87 ^{0.0017}	82 ^{0.0015}	75 ^{0.0014}	86 ^{0.0013}	86 ^{1.016}	
261	VISIONLABS-006	45	512	57 ²⁹²	62 ^{0.0018}	66 ^{0.0015}	62 ^{0.0014}	63 ^{0.0013}	65 ^{0.0013}	63 ^{1.014}	
262	VISIONLABS-007	42	512	58 ²⁹³	56 ^{0.0018}	60 ^{0.0014}	52 ^{0.0013}	52 ^{0.0013}	57 ^{0.0012}	59 ^{1.013}	
263	VISIONLABS-008	36	512	51 ²⁷⁷	76 ^{0.0020}	99 ^{0.0018}	102 ^{0.0018}	118 ^{0.0018}	12 ^{0.0017}	90 ^{1.017}	
264	VISIONLABS-009	41	512	117 ⁴⁹⁴	16 ^{0.0011}	23 ^{0.0011}	24 ^{0.0010}	25 ^{0.0010}	24 ^{0.0010}	20 ^{1.010}	
265	VISIONLABS-010	40	512	19 ⁷³²	28 ^{0.0014}	48 ^{0.0013}	49 ^{0.0013}	55 ^{0.0013}	62 ^{0.0013}	42 ^{1.012}	
266	VISIONLABS-011	51	512	199 ⁷³⁶	18 ^{0.0012}	26 ^{0.0011}	30 ^{0.0011}	30 ^{0.0011}	37 ^{0.0011}	26 ^{1.010}	
267	VOCORD-003	70	896	18 ⁷¹⁴	155 ^{0.0062}	149 ^{0.0035}	149 ^{0.0030}	148 ^{0.0026}	151 ^{0.0023}	150 ^{1.035}	
268	VOCORD-004	69	896	127 ⁵⁹⁸	170 ^{0.0079}	172 ^{0.0049}	175 ^{0.0043}	175 ^{0.0038}	181 ^{0.0035}	166 ^{1.044}	
269	VOCORD-005	67	768	22 ⁸²²	164 ^{0.0070}	16 ^{0.0046}	172 ^{0.0041}	178 ^{0.0038}	184 ^{0.0035}	170 ^{1.044}	
270	VOCORD-006	280	10240	22 ⁸²⁵	280 ^{1.0000}	281 ^{0.0000}	281 ^{0.0000}	280 ^{1.0000}	280 ^{1.0000}	280 ^{10.000}	
271	VTS-000	137	2048	116 ⁴⁹²	276 ^{0.5937}	277 ^{0.5936}	277 ^{0.5936}	277 ^{0.5936}	277 ^{0.5936}	277 ^{6.343}	
272	VTS-001	176	2048	25 ⁸⁹¹	40 ^{0.0015}	39 ^{0.0012}	28 ^{0.0011}	29 ^{0.0011}	25 ^{0.0010}	31 ^{1.011}	
273	VTS-002	164	2048	258 ⁹⁰³	70 ^{0.0019}	58 ^{0.0014}	47 ^{0.0013}	49 ^{0.0012}	42 ^{0.0011}	62 ^{1.013}	
274	XFORWARDAI-000	124	2048	208 ⁷⁶⁸	86 ^{0.0023}	107 ^{0.0020}	116 ^{0.0020}	128 ^{0.0019}	133 ^{0.0019}	104 ^{1.018}	
275	XFORWARDAI-001	192	2048	166 ⁶⁸¹	79 ^{0.0020}	102 ^{0.0019}	113 ^{0.0019}	128 ^{0.0019}	133 ^{0.0019}	96 ^{1.018}	
276	XFORWARDAI-002	263	4096	269 ⁹³⁵	72 ^{0.0020}	99 ^{0.0019}	111 ^{0.0019}	124 ^{0.0019}	131 ^{0.0019}	94 ^{1.017}	
277	YISHENG-001	249	3704	82 ³⁸⁷	227 ^{0.0265}	221 ^{0.0130}	218 ^{0.0102}	216 ^{0.0080}	206 ^{0.0059}	222 ^{1.134}	
278	YITU-002	271	4138	248 ⁸⁷⁰	64 ^{0.0018}	36 ^{0.0012}	32 ^{0.0011}	31 ^{0.0011}	30 ^{0.0010}	41 ^{1.012}	
279	YITU-003	272	4138	247 ⁸⁷¹	109 ^{0.0029}	120 ^{0.0023}	130 ^{0.0022}	137 ^{0.0021}	142 ^{0.0021}	117 ^{1.021}	
280	YITU-004	227	2070	26 ⁹¹⁰	23 ^{0.0013}	10 ^{0.0009}	10 ^{0.0009}	11 ^{0.0009}	11 ^{0.0009}	14 ^{1.009}	
281	YITU-005	228	2070	241 ⁸⁶¹	88 ^{0.0023</sup}						

MISSES BELOW THRESHOLD, T		ENROL RECENT MUGSHOT, N = 1.6M												ENROL APPLICATION PORTRAIT, N = 1.6M																	
#	ALGORITHM	ENROL: MUGSHOT			ENROL: MUGSHOT			ENROL: MUGSHOT			ENROL: VISA			ENROL: BORDER			ENROL: BORDER 10+YR			ENROL: KIOSK											
		FPIR=0.0003	FPIR=0.001	FPIR=0.01	FPIR=0.0003	FPIR=0.001	FPIR=0.01	FPIR=0.0003	FPIR=0.001	FPIR=0.01	FPIR=0.0001	FPIR=0.001	FPIR=0.01	FPIR=0.001	FPIR=0.001	FPIR=0.01	FPIR=0.001	FPIR=0.001	FPIR=0.01	FPIR=0.001	FPIR=0.001	FPIR=0.01	FPIR=0.001	FPIR=0.01							
1	20FACE-000	231	0.462	240	0.348	247	0.230	242	0.763	236	0.450	235	0.301	191	1.000	203	1.000	214	1.000	172	0.424	171	0.255	93	0.772	94	0.599	166	0.938	178	0.836
2	3DIVI-003	233	0.482	249	0.400	253	0.282	237	0.685	249	0.626	251	0.497							183	0.605	188	0.445			151	0.821	168	0.717		
3	3DIVI-004	204	0.256	220	0.169	224	0.093	208	0.400	226	0.343	230	0.237							162	0.277	165	0.172			129	0.607	149	0.485		
4	3DIVI-005	203	0.255	217	0.166	222	0.093	207	0.395	223	0.339	229	0.234	134	0.998	136	0.996	148	0.990	188	0.864	198	0.846			128	0.597	148	0.484		
5	3DIVI-006	202	0.253	219	0.168	226	0.096	211	0.403	225	0.342	231	0.238							163	0.283	166	0.174			132	0.615	150	0.490		
6	ACER-000	188	0.208	210	0.146	215	0.074	192	0.300	203	0.246	205	0.157	84	0.987	91	0.981	113	0.955	157	0.201	161	0.114			116	0.490	134	0.363		
7	ACER-001	134	0.109	152	0.056	156	0.026	130	0.136	138	0.109	138	0.069	161	1.000	168	0.999	193	0.998	120	0.068	120	0.036	86	0.406	87	0.250	115	0.479	90	0.206
8	AIZE-001	145	0.127	172	0.077	174	0.034	158	0.187	162	0.143	161	0.087	107	0.995	116	0.994	138	0.983	133	0.101	138	0.052	80	0.364	81	0.216	97	0.387	118	0.289
9	ALCHERA-000	195	0.231	207	0.138	208	0.070	181	0.259	189	0.216	199	0.146	145	0.999	152	0.999	176	0.996	152	0.176	159	0.111			147	0.803	144	0.456		
10	ALCHERA-001	276	1.000	276	0.999	277	0.999	271	1.000	274	1.000									269	1.000	259	1.000			149	1.000	275	1.000		
11	ALCHERA-002	258	0.807	256	0.486	256	0.302	236	0.685	246	0.591	246	0.442	178	1.000	176	1.000	198	0.999	187	0.827	187	0.770			148	0.811	168	0.705		
12	ALCHERA-003	227	0.450	211	0.155	209	0.070	193	0.304	200	0.239	204	0.152	174	1.000	163	0.999	181	0.997	151	0.172	155	0.097			111	0.464	133	0.362		
13	ALCHERA-004	238	0.520	248	0.394	246	0.211	233	0.642	242	0.529	240	0.327	108	0.995	111	0.991	79	0.813	173	0.424	169	0.232	89	0.708	92	0.515	125	0.546	144	0.398
14	ALLGOVISION-000	154	0.138	184	0.088	190	0.045	169	0.202	178	0.166	185	0.106	94	0.993	108	0.990	137	0.982	136	0.117	141	0.066			122	0.526	141	0.396		
15	ALLGOVISION-001	163	0.155	189	0.102	196	0.053	186	0.275	193	0.221	198	0.141	98	0.993	98	0.986	99	0.933	146	0.150	148	0.081			117	0.491	140	0.389		
16	ANKE-000	174	0.184	194	0.117	205	0.063	179	0.256	192	0.220	202	0.151	104	0.995	117	0.994	146	0.990	272	1.000	245	1.000			139	1.000	279	1.000		
17	ANKE-001	172	0.183	198	0.119	206	0.063	180	0.256	191	0.220	203	0.151	109	0.995	122	0.994	159	0.992	233	1.000	201	1.000			195	1.000	218	1.000		
18	ANKE-002	99	0.062	113	0.032	112	0.014	96	0.103	101	0.079	103	0.050	64	0.975	66	0.948	74	0.795	85	0.034	87	0.018			66	0.245	81	0.190		
19	AWARE-003	171	0.174	202	0.128	216	0.082	201	0.351	218	0.298	223	0.204	81	0.987	95	0.984	137	0.977	174	0.428	177	0.378			123	0.530	143	0.443		
20	AWARE-004	219	0.355	233	0.269	242	0.175	229	0.619	241	0.509	244	0.375	176	1.000	180	1.000	202	0.999	169	0.397	173	0.279			149	0.816	160	0.631		
21	AWARE-005	244	0.608	243	0.364	218	0.085	198	0.342	207	0.253	207	0.163	173	1.000	184	1.000	206	0.999	161	0.255	165	0.122			161	0.916	167	0.714		
22	AWARE-006	232	0.475	234	0.276	243	0.175	220	0.466	229	0.398	234	0.283	158	1.000	173	0.999	194	0.999	167	0.368	170	0.254			141	0.749	157	0.623		
23	AYONIX-000	258	0.846	265	0.811	274	0.724	259	0.956	264	0.939	266	0.892	135	0.998	142	0.998	172	0.995	192	0.954	199	0.891			174	0.982	184	0.959		
24	AYONIX-001	259	0.875	267	0.824	268	0.701	250	0.946	259	0.920	262	0.845	168	1.000	171	0.999	178	0.996	196	0.999	196	0.998			170	0.969	181	0.926		
25	AYONIX-002	260	0.876	266	0.824	269	0.702	251	0.946	260	0.920	261	0.845	170	1.000	170	0.999	177	0.996	189	0.915	188	0.821			171	0.969	180	0.926		
26	CAMVI-003	123	0.094	167	0.071	201	0.058	130	0.152	154	0.132	186	0.108	70	0.979	74	0.970	10	0.940	135	0.114	159	0.100			100	0.402	137	0.377		
27	CAMVI-004	132	0.107	168	0.072	199	0.054	176	0.240	156	0.136	175	0.100	160	1.000	166	0.999	184	0.998	132	0.100	147	0.081			145	0.787	151	0.507		
28	CAMVI-005	158	0.139	188	0.099	217	0.076	185	0.241	179	0.179	193	0.132	163	1.000	177	1.000	199	0.998	147	0.156	167	0.112			182	0.999	196	0.983		
29	CANON-001	241	0.012	30	0.005	28	0.002	23	0.031	223	0.023	23	0.015	24	0.633	14	0.365	22	0.217	18	0.008	19	0.004	22	0.068	24	0.034	28	0.139	19	0.092
30	CIB-000	72	0.044	53	0.012	48	0.005	69	0.077	51	0.045	48	0.025	199	1.000	192	1.000	210	1.000	46	0.017	38	0.008	41	0.141	39	0.068	188	0.894	152	0.521
31	CLEARVIEWAI-000	26	0.013	31	0.006	27	0.002	30	0.036	26	0.025	26	0.016	147	0.999	79	0.974	10	0.149	19	0.008	14	0.004	18	0.057	18	0.027	77	0.268	11	0.080
32	CLOUDWALK-HR-000	8	0.004	10	0.002	17	0.002	8	0.015	10	0.013	13	0.012	208	1.000	208	1.000	191	1.000	114	0.956										
33	CLOUDWALK-MT-000	4	0.003	9	0.002	17	0.002	5	0.015	9	0.013	15	0.012	116	0.999	122	0.999	144	0.998	172	0.995										
34	COGENT-000	159	0.143	142	0.053	161	0.029	149	0.175	159	0.140	177	0.100	115	0.996	128	0.995	154	0.991												
35	COGENT-001	158	0.143	143	0.053	162	0.029	149	0.175	159	0.140	177	0.100	115	0.996	128	0.995	154	0.991												
36	COGENT-002	168	0.159	129	0.044	12	0.017	116	0.124	126	0.098	130	0.063	139	0.998	141	0.998	16	0.994												
37	COGENT-003	186	0.203	134	0.046	117	0.016	114	0.121	120	0.095	122	0.061	140	0.999	127	0.998	144	0.998	172	0.995										
38	COGENT-004	190	0.209	114	0.033	56	0.006	39	0.067	37	0.051	59	0.031	133	0.998	139	0.997	172	0.995	57	0										

Table 28: **Threshold-based accuracy**. Values are $FNIR(N, T, L)$ with $N = 1.6$ million with thresholds set to produce $FPIR = 0.0003, 0.001$, and 0.01 in non-mate searches. Throughout blue superscripts indicate the rank of the algorithm for that column. Caution: The Power-low models are mostly intended to draw attention to the kind of behavior, not as a model to be used for prediction.

17:50:48
2022/03/30

$\text{FNIR}(N, k, \beta) =$ False neg. identification rate
 $\text{FPIR}(N, T) =$ False pos. identification rate

N = Num. enrolled subjects
 R = Num. candidates examined

T = Threshold

$T = 0 \rightarrow$ Investigation
 $T > 0 \rightarrow$ Identification

MISSES BELOW THRESHOLD, T		ENROL RECENT MUGSHOT, N = 1.6M												ENROL APPLICATION PORTRAIT, N = 1.6M																							
#	ALGORITHM	ENROL: MUGSHOT			ENROL: MUGSHOT			ENROL: WEBCAM			ENROL: MUGSHOT			ENROL: VISA			ENROL: BORDER			ENROL: BORDER 10+YR			ENROL: VISA														
		FPIR=0.0003	FPIR=0.001	FPIR=0.01	FPIR=0.0003	FPIR=0.001	FPIR=0.01	FPIR=0.0003	FPIR=0.001	FPIR=0.01	FPIR=0.0003	FPIR=0.001	FPIR=0.01	FPIR=0.001	FPIR=0.01	FPIR=0.001	FPIR=0.01	FPIR=0.001	FPIR=0.01	FPIR=0.001	FPIR=0.01	FPIR=0.001	FPIR=0.01	FPIR=0.001	FPIR=0.01												
93	IDEMIA-006	104	0.065	125	0.043	152	0.025	184	0.266	195	0.226	206	0.161	80	0.984	92	0.982	135	0.980	145	0.144	159	0.090	139	0.733	153	0.531										
94	IDEMIA-007	60	0.035	74	0.018	77	0.008	67	0.073	68	0.055	67	0.033	220	1.000	242	1.000	254	1.000	105	0.052	100	0.022	61	0.182	66	0.109	200	1.000	188	0.982						
95	IDEMIA-008	6	0.004	8	0.002	9	0.001	10	0.016	8	0.013	50	0.009	7	0.276	6	0.204	7	0.136	10	0.005	9	0.003	11	0.036	12	0.019	17	0.106	18	0.092						
96	IDEMIA-009	5	0.004	2	0.002	3	0.001	2	0.012	2	0.011	2008	0.008	3	0.202	3	0.141	4	0.099	3	0.003	4	0.002	5	0.027	5	0.013	4	0.074	4	0.064						
97	IMAGUS-002	263	0.908	263	0.749	267	0.564	247	0.944	259	0.816	258	0.645	208	1.000	210	1.000	218	1.000																		
98	IMAGUS-003	262	0.898	264	0.807	267	0.669	254	0.954	258	0.909	260	0.809	203	1.000	195	1.000	212	1.000																		
99	IMAGUS-005	58	0.034	78	0.018	78	0.008	88	0.088	83	0.066	83	0.040	49	0.926	53	0.838	69	0.647	69	0.029	79	0.016	53	0.161	61	0.094	61	0.231	82	0.189						
100	IMAGUS-006	65	0.039	80	0.019	79	0.008	84	0.093	88	0.069	91	0.042	74	0.980	61	0.897	55	0.621	68	0.028	73	0.015	52	0.161	57	0.092	71	0.260	78	0.181						
101	IMAGUS-007	70	0.044	92	0.023	92	0.010	94	0.073	95	0.045	61	0.973	59	0.893	61	0.651	76	0.031	70	0.016	55	0.169	63	0.098	76	0.265	77	0.181								
102	IMPERIAL-000	162	0.154	98	0.026	88	0.009	82	0.089	87	0.068	88	0.041	204	1.000	155	0.999	167	0.995	94	0.042	96	0.020			67	0.245	69	0.168								
103	INCODE-000	225	0.423	237	0.310	24	0.199	222	0.486	232	0.420	237	0.304	167	1.000	147	0.998	16	0.994																		
104	INCODE-001	214	0.319	229	0.212	231	0.112	202	0.348	215	0.296	219	0.198	186	1.000	207	1.000	209	1.000																		
105	INCODE-002	211	0.285	222	0.184	229	0.100	196	0.333	213	0.269	215	0.176	130	0.998	115	0.993	131	0.976																		
106	INCODE-003	212	0.286	218	0.167	217	0.084	206	0.372	209	0.264	209	0.164	175	1.000	169	0.999	170	0.996																		
107	INCODE-004	128	0.099	149	0.054	145	0.023	146	0.167	146	0.120	142	0.070	126	0.997	124	0.995	97	0.929	116	0.063	112	0.031			84	0.313	99	0.226								
108	INCODE-005	34	0.021	48	0.011	46	0.005	43	0.055	50	0.043	51	0.026	22	0.614	25	0.528	30	0.372	45	0.017	40	0.009	44	0.145	40	0.073	35	0.155	32	0.116						
109	INNOVATRICS-002	223	0.379	231	0.234	239	0.139	210	0.403	220	0.209	189	1.000	199	1.000	206	0.999																				
110	INNOVATRICS-003	213	0.297	227	0.221	238	0.132	206	0.351	210	0.297	222	0.203	177	1.000	181	1.000	187	0.998																		
111	INNOVATRICS-004	177	0.184	204	0.132	218	0.074	182	0.262	194	0.222	200	0.149	79	0.984	86	0.980	125	0.973																		
112	INNOVATRICS-005	96	0.057	115	0.034	111	0.014	107	0.114	111	0.089	109	0.052	45	0.890	54	0.846	66	0.723	101	0.047	99	0.022			69	0.251	79	0.182								
113	INNOVATRICS-007	39	0.024	54	0.013	53	0.005	51	0.065	58	0.051	60	0.032	39	0.806	42	0.743	51	0.567	44	0.017	46	0.009	30	0.093	38	0.053	33	0.154	40	0.120						
114	INTELLIVISION-001	236	0.508	235	0.279	241	0.158	219	0.459	230	0.404	236	0.302	181	1.000	185	1.000	204	0.999	165	0.328	168	0.219	91	0.749	93	0.598	137	0.685	155	0.562						
115	INTSYSMSU-000	272	0.999	274	0.998	276	0.990	269	1.000	270	0.998	171	1.000	179	1.000	185	0.998	195	0.999	198	0.989			183	0.999	192	0.988										
116	IREE-000	108	0.068	108	0.028	76	0.008	91	0.099	77	0.060	62	0.032	80	0.988	67	0.957	65	0.680	97	0.044	94	0.011	77	0.302	37	0.062	43	0.170	49	0.135						
117	ISYSTEMS-002	164	0.155	174	0.078	167	0.032	142	0.161	150	0.126	156	0.080	137	0.998	140	0.998	159	0.993																		
118	ISYSTEMS-003	187	0.204	158	0.059	148	0.024	129	0.135	134	0.107	137	0.068	183	1.000	186	1.000	183	0.997																		
119	KAKAO-000	49	0.028	65	0.015	64	0.006	65	0.071	70	0.056	72	0.034	15	0.539	20	0.468	30	0.327	49	0.019	49	0.010	40	0.141	41	0.075	36	0.158	39	0.120						
120	KEDACOM-001	67	0.041	91	0.023	111	0.013	87	0.096	92	0.072	113	0.054	89	0.989	100	0.986	127	0.973	108	0.055	128	0.043			82	0.305	111	0.264								
121	KNERON-000																																				
122	KNERON-001																																				
123	LINE-000	100	0.062	111	0.031	110	0.012	126	0.132	121	0.095	115	0.054					221	1.000	99	0.046	99	0.021	75	0.278	79	0.151	188	1.000	113	0.268						
124	LINE-001	52	0.030	25	0.005	22	0.002	52	0.066	29	0.027	25	0.015	198	1.000	211	1.000	227	1.000	29	0.009	20	0.004	23	0.072	25	0.034	252	1.000	179	0.858						
125	LOOKMAN-003	105	0.066	127	0.044	119	0.025	12	0.131	138	0.112	157	0.082							128	0.084	130	0.061							93	0.355	129	0.304				
126	LOOKMAN-004	112	0.074	130	0.045	146	0.024	115	0.123	133	0.105	148	0.075	69	0.979	81	0.977	129	0.974											85	0.308	115	0.273				
127	LOOKMAN-005	85	0.050	110	0.030	124	0.017	94	0.102	10	0.086	131	0.063	73	0.980	83	0.978	12	0.973	115	0.062	139	0.047														
128	MANTRA-000	107	0.066	45	0.010	39	0.004	47	0.063	46	0.041	38	0.022	226	1.000	246	1.000	201	0.999	70	0.029	68	0.014	48	0.152	50	0.081	188	1.000	59	0.151						
129	MEGVII-001	191	0.210	169	0.072	173	0.037	111	0.119	125	0.097	124	0.061																								
130	MEGVII-002	205	0.258	173	0.077	175	0.037	112	0.120	123	0.096	121	0.059	144	0.999	150	0.998	86	0.872																		
131	MICROFOCUS-003	266	0.958	270																																	

MISSSES BELOW THRESHOLD, T		ENROL RECENT MUGSHOT, N = 1.6M												ENROL APPLICATION PORTRAIT, N = 1.6M													
#	ALGORITHM	ENROL: MUGSHOT			ENROL: MUGSHOT			ENROL: MUGSHOT			ENROL: VISA			ENROL: BORDER			ENROL: VISA										
		FPIR=0.0003	FPIR=0.001	FPIR=0.01	FPIR=0.0003	FPIR=0.001	FPIR=0.01	FPIR=0.0003	FPIR=0.001	FPIR=0.01	FPIR=0.0001	FPIR=0.01	FPIR=0.01	FPIR=0.0001	FPIR=0.01	FPIR=0.0001	FPIR=0.01	FPIR=0.0001	FPIR=0.01								
139	NEC-000	¹³⁷ 0.113	¹⁷⁶ 0.079	¹⁹¹ 0.047	¹⁴⁷ 0.171	¹⁶⁰ 0.140	¹⁶⁷ 0.093	⁷⁶ 0.983	⁸⁵ 0.979	¹²⁰ 0.969	¹⁴⁰ 0.133	¹⁴⁹ 0.082	¹¹⁴ 0.474	¹³⁸ 0.377													
140	NEC-001	¹⁶¹ 0.148	¹⁹³ 0.106	²⁰⁴ 0.060	¹⁷¹ 0.238	¹⁸⁷ 0.197	¹⁹⁴ 0.133	⁹⁰ 0.991	⁹⁹ 0.986	¹²² 0.972	¹⁷⁰ 0.095	²¹ 0.008	³⁰ 0.005	¹¹⁷ 0.468	¹³⁹ 0.378												
141	NEC-002	³¹ 0.018	¹⁴ 0.003	¹² 0.002	²² 0.029	²⁰ 0.020	¹⁷ 0.013	¹⁶² 1.000	¹⁶⁵ 0.999	¹⁷⁰ 0.995	²¹ 0.008	³⁰ 0.005	¹³⁵ 0.676	¹²² 0.292													
142	NEC-003	¹⁰ 0.005	¹² 0.002	¹⁶ 0.002	¹⁶ 0.021	¹⁶ 0.017	¹⁶ 0.013	⁴⁷ 0.902	⁵⁰ 0.824	⁵⁷ 0.628	²⁴ 0.008	³¹ 0.006	¹² 0.036	¹³ 0.023	¹³ 0.668	¹¹⁰ 0.261											
143	NEC-004	¹ 0.003	⁶ 0.002	¹¹ 0.002	⁷ 0.015	⁷ 0.013	¹⁰ 0.010	²⁶ 0.654	³³ 0.622	⁵² 0.575	⁸ 0.004	¹² 0.004	³ 0.019	⁴ 0.012	¹³ 0.100	¹⁵ 0.088											
144	NEC-005	¹⁵ 0.007	³ 0.002	³ 0.001	³ 0.014	³ 0.012	⁶ 0.009	⁴⁶ 0.901	³⁷ 0.673	¹⁷ 0.177	⁵ 0.003	⁶ 0.002	² 0.019	² 0.011	¹⁰ 0.099	¹⁴ 0.087											
145	NEUROTECHNOLOGY-003	²⁷³ 0.999	²⁶¹ 0.636	²²⁸ 0.099	²⁴⁸ 0.773	²¹¹ 0.266	²⁰⁸ 0.164	²¹⁸ 1.000	²⁴⁰ 1.000	²⁵² 1.000	¹⁶⁶ 0.339	¹¹⁹ 0.036	²³⁴ 1.000	¹⁹³ 0.989													
146	NEUROTECHNOLOGY-004	¹³⁹ 0.120	¹⁶³ 0.063	¹⁵⁹ 0.028	¹³⁸ 0.146	¹⁴⁶ 0.117	¹⁴⁴ 0.073	¹¹⁸ 0.996	¹²⁰ 0.994	¹⁴⁷ 0.990	¹⁶ 0.008	²⁰ 0.005	¹¹ 0.005	¹¹ 0.005	¹¹ 0.005	¹¹ 0.005	¹¹ 0.005	¹¹ 0.005	¹¹ 0.005	¹¹ 0.005	¹¹ 0.005	¹¹ 0.005	¹¹ 0.005				
147	NEUROTECHNOLOGY-005	¹³⁸ 0.117	¹⁵⁰ 0.054	¹⁴⁶ 0.022	¹⁷⁸ 0.252	¹⁵⁷ 0.130	¹⁴⁷ 0.074	¹⁴² 0.999	¹⁴³ 0.998	¹⁴⁴ 0.989	¹⁶ 0.008	²⁰ 0.005	¹¹ 0.005	¹¹ 0.005	¹¹ 0.005	¹¹ 0.005	¹¹ 0.005	¹¹ 0.005	¹¹ 0.005	¹¹ 0.005	¹¹ 0.005	¹¹ 0.005	¹¹ 0.005				
148	NEUROTECHNOLOGY-006	²⁷¹ 0.987	²³² 0.249	²³³ 0.121	²⁷⁹ 1.000	²³¹ 0.418	²²⁴ 0.206	¹⁶ 0.008	¹⁶ 0.007	¹⁶ 0.006	²⁰⁰ 1.000	¹⁹⁰ 1.000	¹⁸² 0.997	¹⁶⁶ 0.339	¹¹⁹ 0.036	²³⁴ 1.000	¹⁹³ 0.989										
149	NEUROTECHNOLOGY-007	²⁰¹ 0.252	¹⁶² 0.062	¹³⁷ 0.021	²⁶ 0.996	¹⁸¹ 0.173	¹³⁶ 0.068	²⁰⁶ 1.000	¹⁹⁰ 1.000	¹⁸² 0.997	¹⁶⁶ 0.339	¹¹⁹ 0.036	²³⁴ 1.000	¹⁹³ 0.989													
150	NEUROTECHNOLOGY-008	²⁵⁴ 0.797	¹⁴⁴ 0.053	¹⁰⁹ 0.012	¹⁰⁰ 0.110	¹⁰³ 0.080	¹⁰⁰ 0.047	²⁰⁶ 1.000	²⁰⁸ 1.000	²²⁴ 1.000	⁸⁶ 0.035	⁸⁴ 0.017	⁷⁶ 0.293	⁷⁷ 0.149	⁵⁵ 0.203	⁶⁰ 0.152											
151	NEUROTECHNOLOGY-009	⁴⁷ 0.027	⁶⁶ 0.015	⁵⁹ 0.006	⁵⁴ 0.066	⁶² 0.052	⁶¹ 0.032	²⁷ 0.661	³¹ 0.588	³⁷ 0.436	⁵¹ 0.020	⁴⁹ 0.010	⁴⁰ 0.153	⁵² 0.082	⁴¹ 0.165	⁴⁵ 0.129											
152	NEUROTECHNOLOGY-010	²¹⁶ 0.346	⁴³ 0.010	³⁶ 0.003	⁴⁶ 0.047	⁴² 0.037	⁴⁴ 0.023	¹¹ 0.377	¹¹ 0.277	¹⁵ 0.170	³² 0.010	²⁶ 0.005	²⁵ 0.075	²⁷ 0.039	²⁴ 0.126	²⁴ 0.097											
153	NEWLAND-002	²³⁹ 0.523	²⁵² 0.438	²⁵⁴ 0.294	²²² 0.535	²³⁸ 0.466	²⁴¹ 0.335	¹⁵⁰ 0.999	¹⁵⁹ 0.999	¹⁸⁸ 0.998	¹⁶ 0.008	²⁰ 0.005	¹¹ 0.005	¹¹ 0.005	¹¹ 0.005	¹¹ 0.005	¹¹ 0.005	¹¹ 0.005	¹¹ 0.005	¹¹ 0.005	¹¹ 0.005	¹¹ 0.005	¹¹ 0.005				
154	NOBLIS-001	²⁷⁷ 1.000	²⁷⁷ 1.000	²⁷⁷ 1.000	²⁷⁸ 1.000	²⁷⁷ 1.000	²⁷⁶ 1.000	²⁰² 1.000	²¹⁵ 1.000	²²⁶ 1.000	¹⁶ 0.008	²⁰ 0.005	¹¹ 0.005	¹¹ 0.005	¹¹ 0.005	¹¹ 0.005	¹¹ 0.005	¹¹ 0.005	¹¹ 0.005	¹¹ 0.005	¹¹ 0.005	¹¹ 0.005	¹¹ 0.005				
155	NOBLIS-002	²⁷⁵ 1.000	²⁷³ 0.997	²⁶ 0.488	²⁷⁸ 1.000	²⁷⁴ 1.000	²⁷⁸ 1.000	¹⁹² 1.000	²⁰² 1.000	²¹⁸ 1.000	¹⁶ 0.008	²⁰ 0.005	¹¹ 0.005	¹¹ 0.005	¹¹ 0.005	¹¹ 0.005	¹¹ 0.005	¹¹ 0.005	¹¹ 0.005	¹¹ 0.005	¹¹ 0.005	¹¹ 0.005	¹¹ 0.005				
156	NOTIONTAG-000	⁵⁶ 0.032	⁶⁹ 0.017	⁷⁴ 0.007	⁶⁸ 0.076	⁷⁶ 0.059	⁷⁷ 0.036	²⁸ 0.671	³² 0.611	³⁹ 0.467	⁵⁴ 0.021	⁵⁵ 0.011	⁴⁷ 0.150	⁵³ 0.084	⁴⁴ 0.176	⁵² 0.140	¹¹ 0.005	¹¹ 0.005	¹¹ 0.005	¹¹ 0.005	¹¹ 0.005	¹¹ 0.005	¹¹ 0.005	¹¹ 0.005			
157	NTECHLAB-003	¹¹⁵ 0.080	¹⁴⁸ 0.054	¹⁶⁰ 0.028	¹³⁶ 0.148	¹⁴¹ 0.118	¹⁴⁹ 0.075	⁴⁵ 0.873	⁵² 0.837	⁷³ 0.752	¹⁶ 0.008	²⁰ 0.005	¹¹ 0.005	¹¹ 0.005	¹¹ 0.005	¹¹ 0.005	¹¹ 0.005	¹¹ 0.005	¹¹ 0.005	¹¹ 0.005	¹¹ 0.005	¹¹ 0.005	¹¹ 0.005				
158	NTECHLAB-004	¹⁰² 0.063	¹²³ 0.041	¹³⁸ 0.021	¹²¹ 0.131	¹³² 0.105	¹³³ 0.065	⁴² 0.868	⁵¹ 0.833	⁷¹ 0.746	¹⁰⁷ 0.053	¹¹⁰ 0.030	¹⁶ 0.008	²⁰ 0.005	¹¹ 0.005	¹¹ 0.005	¹¹ 0.005	¹¹ 0.005	¹¹ 0.005	¹¹ 0.005	¹¹ 0.005	¹¹ 0.005	¹¹ 0.005	¹¹ 0.005			
159	NTECHLAB-005	¹⁰¹ 0.062	¹²⁴ 0.042	¹³⁶ 0.021	¹²² 0.130	¹³⁰ 0.102	¹³² 0.063	⁴⁰ 0.816	⁴⁵ 0.771	⁶² 0.661	¹²² 0.073	¹²³ 0.039	¹⁶ 0.008	²⁰ 0.005	¹¹ 0.005	¹¹ 0.005	¹¹ 0.005	¹¹ 0.005	¹¹ 0.005	¹¹ 0.005	¹¹ 0.005	¹¹ 0.005	¹¹ 0.005	¹¹ 0.005			
160	NTECHLAB-006	⁹⁵ 0.056	¹¹⁸ 0.037	¹²⁵ 0.018	¹¹¹ 0.121	¹¹⁹ 0.094	¹²⁰ 0.059	³⁸ 0.802	⁴⁴ 0.754	⁵⁸ 0.635	¹¹⁰ 0.057	¹¹⁴ 0.032	¹⁶ 0.008	²⁰ 0.005	¹¹ 0.005	¹¹ 0.005	¹¹ 0.005	¹¹ 0.005	¹¹ 0.005	¹¹ 0.005	¹¹ 0.005	¹¹ 0.005	¹¹ 0.005	¹¹ 0.005			
161	NTECHLAB-007	⁶⁶ 0.040	⁹⁵ 0.026	¹⁰⁶ 0.012	⁷⁷ 0.085	⁸⁶ 0.067	⁸⁷ 0.041	³⁷ 0.796	⁴³ 0.750	⁵⁹ 0.642	⁸⁰ 0.032	⁸³ 0.017	⁶⁰ 0.391	⁸⁴ 0.033	⁸⁹ 0.018	⁶¹ 0.183	⁵³ 0.140	¹¹ 0.005	¹¹ 0.005	¹¹ 0.005	¹¹ 0.005	¹¹ 0.005	¹¹ 0.005	¹¹ 0.005	¹¹ 0.005		
162	NTECHLAB-008	⁴¹ 0.024	⁵⁹ 0.014	⁴⁴ 0.007	⁵² 0.045	³⁵ 0.029	³⁵ 0.015	¹⁹ 0.601	¹⁴ 0.522	¹⁷ 0.430	²⁶ 0.311	³⁹ 0.015	⁴⁰ 0.008	³⁴ 0.109	³⁶ 0.061	²⁹ 0.142	²⁹ 0.114	¹⁴ 0.739	¹⁵⁶ 0.573								
163	NTECHLAB-009	¹⁸ 0.010	²⁷ 0.005	³⁰ 0.003	²¹ 0.028	²² 0.022	²¹ 0.014	¹⁴ 0.522	¹⁷ 0.430	²⁶ 0.311	³⁹ 0.015	⁴⁰ 0.008	²¹ 0.005	²¹ 0.031	¹⁷ 0.098	⁸ 0.077	¹¹ 0.008	¹¹ 0.005	¹¹ 0.005	¹¹ 0.005	¹¹ 0.005	¹¹ 0.005	¹¹ 0.005	¹¹ 0.005	¹¹ 0.005		
164	NTECHLAB-010	¹² 0.005	¹⁵ 0.003	¹⁶ 0.002	¹² 0.018	¹⁴ 0.015	¹² 0.011	¹⁰ 0.334	¹⁰ 0.252	¹⁴ 0.169	¹⁵ 0.007	¹⁷ 0.004	¹⁷ 0.059	²¹ 0.031	²¹ 0.013	¹⁷ 0.098	⁸ 0.077	¹¹ 0.008	¹¹ 0.005	¹¹ 0.005	¹¹ 0.005	¹¹ 0.005	¹¹ 0.005	¹¹ 0.005	¹¹ 0.005		
165	NTECHLAB-011	¹³ 0.006	¹⁷ 0.003	¹³ 0.002	¹² 0.018	¹³ 0.015	¹¹ 0.010	⁸ 0.291	⁸ 0.228	¹² 0.150	²⁸ 0.009	²⁴ 0.004	²⁴ 0.074	²⁶ 0.038	¹⁷ 0.091	¹⁷ 0.057	¹⁷ 0.024	¹⁷ 0.013	¹⁷ 0.008								

MISSES BELOW THRESHOLD, T		ENROL RECENT MUGSHOT, N = 1.6M												ENROL APPLICATION PORTRAIT, N = 1.6M													
#	ALGORITHM	ENROL: MUGSHOT			ENROL: MUGSHOT			ENROL: WEBCAM			PROBE: PROFILE			ENROL: VISA			ENROL: BORDER			ENROL: BORDER 10+YR			ENROL: VISA				
		FPIR=0.0003	FPIR=0.001	FPIR=0.01	FPIR=0.0003	FPIR=0.001	FPIR=0.01	FPIR=0.0003	FPIR=0.001	FPIR=0.01	FPIR=0.0003	FPIR=0.001	FPIR=0.01	FPIR=0.001	FPIR=0.01	FPIR=0.001	FPIR=0.01	FPIR=0.001	FPIR=0.01	FPIR=0.001	FPIR=0.01	FPIR=0.001	FPIR=0.01	FPIR=0.001	FPIR=0.01		
185	RANKONE-004	200	0.250	224	0.193	234	0.124	221	0.482	233	0.426	239	0.324	152	0.999	148	0.998	166	0.994	113	0.062	109	0.029	90	0.328	91	0.206
186	RANKONE-005	125	0.096	150	0.059	168	0.033	171	0.212	182	0.173	190	0.119	82	0.987	82	0.977	101	0.937	89	0.037	88	0.017	60	0.182	56	0.092
187	RANKONE-006	98	0.061	119	0.037	128	0.020	102	0.118	119	0.095	126	0.061	66	0.975	71	0.967	94	0.924	71	0.029	70	0.014	43	0.144	41	0.072
188	RANKONE-007	57	0.034	89	0.022	102	0.011	110	0.118	119	0.095	126	0.061	75	0.983	73	0.969	81	0.859	106	0.052	106	0.027	68	0.208	69	0.119
189	RANKONE-009	53	0.031	72	0.018	81	0.008	88	0.098	97	0.076	94	0.045	48	0.905	48	0.802	62	0.652	89	0.037	88	0.017	60	0.182	56	0.092
190	RANKONE-010	36	0.023	57	0.014	72	0.007	70	0.077	74	0.058	76	0.036	21	0.905	21	0.802	62	0.652	71	0.029	70	0.014	43	0.144	41	0.072
191	RANKONE-011	135	0.109	38	0.009	42	0.004	74	0.079	73	0.048	56	0.029	11	0.975	11	0.967	94	0.924	71	0.029	70	0.014	43	0.144	41	0.072
192	RANKONE-012	33	0.020	35	0.008	40	0.004	66	0.072	66	0.053	57	0.030	11	0.975	11	0.967	94	0.924	71	0.029	70	0.014	43	0.144	41	0.072
193	REALNETWORKS-000	221	0.374	230	0.234	238	0.138	213	0.433	223	0.319	226	0.209	11	0.975	11	0.967	94	0.924	71	0.029	70	0.014	43	0.144	41	0.072
194	REALNETWORKS-001	222	0.374	229	0.234	237	0.138	214	0.433	222	0.319	227	0.209	11	0.975	11	0.967	94	0.924	71	0.029	70	0.014	43	0.144	41	0.072
195	REALNETWORKS-002	220	0.370	228	0.231	236	0.137	212	0.416	221	0.315	228	0.209	11	0.975	11	0.967	94	0.924	71	0.029	70	0.014	43	0.144	41	0.072
196	REALNETWORKS-003	208	0.273	214	0.159	224	0.090	194	0.342	210	0.266	214	0.172	149	0.999	149	0.998	141	0.987	149	0.164	153	0.103	119	0.500	135	0.364
197	REALNETWORKS-004	198	0.242	213	0.158	219	0.090	205	0.353	208	0.263	211	0.169	166	1.000	162	0.999	158	0.992	150	0.170	153	0.103	130	0.613	136	0.370
198	REALNETWORKS-005	88	0.052	105	0.028	106	0.012	88	0.094	95	0.074	99	0.047	78	0.984	75	0.971	89	0.896	88	0.037	88	0.017	69	0.223	72	0.123
199	REALNETWORKS-006	45	0.025	60	0.015	56	0.006	60	0.068	64	0.053	65	0.032	93	0.993	89	0.980	81	0.838	40	0.016	43	0.008	36	0.120	38	0.063
200	REMARKAI-000	185	0.197	201	0.128	205	0.059	181	0.263	192	0.203	192	0.123	157	0.999	160	0.999	169	0.995	121	0.069	116	0.033	138	0.717	128	0.315
201	REMARKAI-000	144	0.125	151	0.055	144	0.023	148	0.173	145	0.120	140	0.070	97	0.993	110	0.991	137	0.980	121	0.069	116	0.033	138	0.717	128	0.315
202	REMARKAI-002	181	0.188	200	0.124	202	0.059	172	0.248	186	0.196	191	0.122	97	0.993	110	0.991	137	0.980	121	0.069	116	0.033	138	0.717	128	0.315
203	RENDIP-000	37	0.023	50	0.012	51	0.005	160	0.189	75	0.059	71	0.034	56	0.945	60	0.894	70	0.744	55	0.022	63	0.013	62	0.185	59	0.089
204	REVEALMEDIA-000	38	0.024	52	0.012	55	0.006	42	0.054	49	0.042	49	0.025	31	0.755	39	0.680	48	0.539	53	0.021	50	0.011	31	0.093	34	0.051
205	S1-000	152	0.137	107	0.028	101	0.011	121	0.129	106	0.085	101	0.048	211	1.000	218	1.000	53	0.596	102	0.047	90	0.018	251	1.000	71	0.123
206	S1-001	91	0.054	67	0.016	69	0.007	53	0.066	61	0.052	70	0.033	91	0.992	97	0.985	111	0.952	48	0.019	48	0.010	38	0.136	45	0.075
207	SCANOVATE-000	130	0.103	166	0.067	164	0.030	190	0.296	202	0.240	201	0.150	51	0.931	58	0.893	78	0.803	158	0.215	168	0.118	99	0.400	121	0.299
208	SCANOVATE-001	146	0.128	177	0.081	176	0.037	189	0.281	196	0.227	197	0.140	52	0.935	62	0.911	81	0.834	135	0.192	156	0.103	102	0.404	120	0.290
209	SENSETIME-000	61	0.036	85	0.021	89	0.009	71	0.078	88	0.063	84	0.040	248	1.000	235	1.000	142	0.988	121	0.523	66	0.160	26	0.133	30	0.115
210	SENSETIME-001	62	0.036	88	0.022	91	0.010	75	0.080	82	0.064	90	0.041	121	0.997	118	0.994	133	0.979	78	0.032	83	0.017	121	0.523	66	0.160
211	SENSETIME-002	63	0.037	61	0.015	115	0.014	117	0.124	32	0.028	42	0.023	121	0.997	118	0.994	133	0.979	78	0.032	83	0.017	121	0.523	66	0.160
212	SENSETIME-003	7	0.004	7	0.002	6	0.001	4	0.014	4	0.012	4	0.009	21	0.607	21	0.477	27	0.311	22	0.008	29	0.005	20	0.113	25	0.100
213	SENSETIME-004	3	0.003	4	0.002	3	0.001	1	0.015	1	0.013	9	0.010	9	0.301	9	0.229	11	0.149	13	0.006	14	0.004	15	0.051	11	0.023
214	SENSETIME-005	21	0.011	11	0.002	4	0.001	15	0.018	12	0.014	7	0.010	4	0.259	5	0.173	10	0.103	16	0.007	14	0.004	15	0.051	11	0.023
215	SENSETIME-006	9	0.005	5	0.002	1	0.001	9	0.016	5	0.012	3	0.009	141	0.999	148	0.998	64	0.680	6	0.004	5	0.002	9	0.034	8	0.093
216	SENSETIME-007	2	0.003	1	0.001	1	0.001	1	0.012	1	0.009	10	0.007	165	1.000	167	0.999	4	0.538	2	0.003	1	0.001	4	0.024	3	0.011
217	SHAMAN-003	235	0.506	253	0.451	257	0.347	234	0.650	247	0.597	250	0.472	59	0.956	46	0.797	54	0.608	92	0.040	92	0.019	79	0.317	70	0.150
218	SHAMAN-004	249	0.679	260	0.615	262	0.488	24	0.812	25	0.754	257	0.639	59	0.956	46	0.797	54	0.608	92	0.040	92	0.019	79	0.317	70	0.150
219	SHAMAN-006	178	0.185	208	0.141	222	0.092	187	0.278	198	0.237	210	0.168	68	0.978	76	0.972	116	0.960	121	0.309	124	0.039	94	0.961	81	0.183
220	SHAMAN-007	173	0.183	209	0.141	222	0.092	187	0.278	198	0.237	210	0.168	68	0.978	76	0.972	116	0.960	121	0.309	124	0.039	94	0.961	81	0.183
221	SIAT-001	149	0.132	70	0.018	68	0.007	232	0.641	227	0.365	242	0.348	74	0.031	69	0.014	168	0.372	170	0.356	163	0.923	70	0.169		
222	SIAT-002	224	0.417	86	0.022	70	0.007	24	0.942	24	0.478	248	0.460	105	0.995	94	0.984	70	0.795	81	0.032	77	0.016	180	0.994	177	0.817
223	SMILART-004	268	0.970	271	0.968	275	0.965	258	0.977	267	0.976	269	0.973	11	0.055	215	1.000</td										

MISSES BELOW THRESHOLD, T			ENROL RECENT MUGSHOT, N = 1.6M												ENROL APPLICATION PORTRAIT, N = 1.6M									
			ENROL: MUGSHOT			ENROL: MUGSHOT			ENROL: WEBCAM			PROBE: PROFILE			ENROL: VISA		ENROL: BORDER		ENROL: KIOSK					
#	ALGORITHM	FPIR=0.0003	FPIR=0.001	FPIR=0.01	FPIR=0.0003	FPIR=0.001	FPIR=0.01	FPIR=0.0003	FPIR=0.001	FPIR=0.01	FPIR=0.0003	FPIR=0.001	FPIR=0.01	FPIR=0.001	FPIR=0.01	FPIR=0.001	FPIR=0.01	FPIR=0.001	FPIR=0.01	FPIR=0.001	FPIR=0.01	FPIR=0.001		
231	TECH5-002	⁹⁰ 0.053	¹⁰² 0.027	¹⁰⁷ 0.012	⁸⁷ 0.094	⁸⁷ 0.070	⁸⁶ 0.040	⁴⁴ 0.874	⁴⁹ 0.805	⁵⁶ 0.627	⁹¹ 0.039	⁹¹ 0.019	⁶⁶ 0.205	⁶⁷ 0.111	¹⁰⁷ 0.440	⁸⁰ 0.182								
232	TEVIAN-003	¹⁰⁷ 0.239	²²¹ 0.177	²²³ 0.096	²⁰¹ 0.346	²¹⁷ 0.298	²²⁰ 0.198																	
233	TEVIAN-004	¹⁷⁰ 0.170	¹⁹⁵ 0.117	²⁰⁷ 0.063	¹⁷⁷ 0.216	¹⁸⁸ 0.115																		
234	TEVIAN-005	¹⁴⁸ 0.129	¹⁸² 0.087	¹⁸⁸ 0.045	¹⁵⁴ 0.180	¹⁶³ 0.144	¹⁶⁴ 0.089	⁸⁸ 0.988	⁷⁰ 0.962	⁷⁶ 0.796														
235	TEVIAN-006	⁴⁰ 0.024	⁴² 0.010	⁵⁰ 0.005	³⁴ 0.041	³⁶ 0.032	³⁶ 0.021	¹⁷ 0.562	¹⁶ 0.425	²⁵ 0.291	⁴¹ 0.016	⁴⁴ 0.009	²⁹ 0.093	³² 0.050	¹⁶⁸ 0.951	³³⁰ 0.117								
236	TEVIAN-007	²² 0.011	²⁹ 0.005	³¹ 0.003	²⁰ 0.028	²¹ 0.022	²² 0.015	¹³ 0.504	¹² 0.301	¹⁹ 0.183	³⁰ 0.009	²² 0.005	²¹ 0.065	²² 0.033	²² 0.122	²⁷ 0.102								
237	TIGER-000	²³⁰ 0.462	²⁴⁷ 0.390	²⁵⁹ 0.261	²²² 0.565	²⁴⁹ 0.500	²⁴³ 0.366																	
238	TIGER-002	¹⁶⁶ 0.158	¹⁷⁸ 0.086	¹⁷⁹ 0.039	¹⁶⁸ 0.202	¹⁷² 0.158	¹⁷¹ 0.095	¹⁵⁶ 0.999	¹⁵⁷ 0.999	¹⁵⁰ 0.975														
239	TIGER-003	¹⁶⁷ 0.158	¹⁷⁹ 0.086	¹⁷⁸ 0.039	¹⁶⁷ 0.202	¹⁷⁸ 0.158	¹⁷⁰ 0.095																	
240	TONGYITRANS-000	¹³³ 0.107	¹⁷¹ 0.074	¹⁷⁷ 0.038	¹³⁵ 0.141	¹³⁷ 0.112	¹³⁹ 0.069																	
241	TONGYITRANS-001	¹⁴⁵ 0.124	¹⁶⁵ 0.066	¹⁶⁶ 0.032	¹²⁵ 0.128	¹²¹ 0.101	¹²⁹ 0.062																	
242	TOSHIBA-000	¹⁴² 0.123	¹⁶¹ 0.062	¹⁵⁸ 0.027	¹³⁷ 0.150	¹⁴⁴ 0.118	¹⁴⁵ 0.074	¹²³ 0.997	¹³⁰ 0.995	¹⁴³ 0.988														
243	TOSHIBA-001	¹⁹² 0.225	¹⁵⁶ 0.058	¹²⁶ 0.019	¹²⁸ 0.133	¹¹⁸ 0.092	¹¹⁶ 0.054																	
244	TRUEFACE-000	⁷⁷ 0.046	⁷⁶ 0.018	⁸⁰ 0.008	⁷² 0.079	⁷⁹ 0.062	⁸¹ 0.039	¹¹⁰ 0.995	⁵⁵ 0.882	⁴⁰ 0.499	⁷² 0.030	⁸⁰ 0.016	⁶⁴ 0.194	⁶⁸ 0.111	⁵² 0.188	⁵⁶ 0.145								
245	VD-000	²⁶⁵ 0.950	²⁶⁹ 0.917	²⁷² 0.827	²⁵⁹ 0.968	²⁶⁴ 0.946	²⁶⁵ 0.871																	
246	VD-001	²⁰⁹ 0.278	²²⁵ 0.201	²³⁹ 0.116	¹⁹⁹ 0.331	²¹⁷ 0.281	²¹⁷ 0.188																	
247	VD-002	¹⁶⁰ 0.144	¹⁷⁵ 0.079	¹⁷² 0.036	¹⁵⁹ 0.188	¹⁶⁵ 0.148	¹⁶⁸ 0.092	¹³² 0.998	¹³³ 0.996	¹⁴⁰ 0.987	¹³⁰ 0.095	¹³³ 0.048	⁸¹ 0.367	⁸⁴ 0.220	⁹⁵ 0.372	¹¹⁶ 0.280								
248	VD-003	¹⁹⁶ 0.234	¹³² 0.046	¹²⁷ 0.020	¹²⁷ 0.133	¹²⁷ 0.100	¹²⁸ 0.061	¹⁵⁴ 0.999	¹⁵⁸ 0.999	¹⁶² 0.994	¹⁰⁴ 0.051	¹⁰⁵ 0.027	⁷¹ 0.244	⁷³ 0.133	⁸ 0.315	⁸⁷ 0.203								
249	VERIDAS-001	¹¹⁶ 0.080	¹²¹ 0.037	¹¹⁸ 0.016	⁹⁸ 0.106	¹⁰⁴ 0.082	¹⁰⁴ 0.051	⁹⁵ 0.993	¹⁰¹ 0.987	¹⁰² 0.938	⁹⁵ 0.044	¹⁰² 0.023	⁷³ 0.266	⁷³ 0.146	⁷⁵ 0.264	⁸⁹ 0.204								
250	VERIDAS-002	¹¹⁷ 0.080	¹²⁰ 0.037	¹¹⁹ 0.016	⁹⁹ 0.106	¹⁰⁵ 0.082	¹⁰⁵ 0.051	⁹⁶ 0.993	¹⁰² 0.987	¹⁰⁵ 0.938	⁹⁶ 0.044	¹⁰¹ 0.023	⁷⁴ 0.266	⁷⁶ 0.146	⁷⁴ 0.264	⁸⁸ 0.204								
251	VERIDAS-003	¹⁰⁹ 0.072	⁶⁸ 0.017	⁶² 0.006	⁶³ 0.071	⁶⁹ 0.055	⁶⁸ 0.033	¹³⁸ 0.998	¹³⁷ 0.997	⁹⁶ 0.927	⁵⁰ 0.020	⁵¹ 0.011	⁴⁶ 0.150	⁴⁶ 0.078	⁴⁷ 0.178	⁵⁴ 0.142								
252	VIGILANTSOLUTIONS-003	²³⁴ 0.482	²⁵¹ 0.408	²⁵⁹ 0.282	²⁴¹ 0.730	²⁵⁷ 0.660	²⁵⁴ 0.526	¹⁵¹ 0.999	¹⁵⁴ 0.999	¹⁷¹ 0.995														
253	VIGILANTSOLUTIONS-004	²⁴⁵ 0.624	²⁵⁷ 0.549	²⁶⁰ 0.422	²⁴⁷ 0.858	²⁵⁷ 0.817	²³⁶ 0.998	¹³⁵ 0.996	¹³⁷ 0.991															
254	VIGILANTSOLUTIONS-005	²⁶⁴ 0.936	²⁴⁶ 0.388	¹⁸¹ 0.043				¹⁹⁴ 1.000	²⁰⁴ 1.000	²¹⁹ 1.000														
255	VIGILANTSOLUTIONS-006	²⁶⁷ 0.959	²⁴¹ 0.353	¹⁸⁰ 0.043				¹⁸⁵ 1.000	²⁰⁵ 1.000	²²² 1.000														
256	VIGILANTSOLUTIONS-007	¹¹³ 0.076	¹⁰⁹ 0.028	¹⁰³ 0.011	¹⁰⁴ 0.113	¹¹⁰ 0.088	¹¹¹ 0.053	¹²⁸ 0.997	¹³⁴ 0.996	¹⁵³ 0.991	¹²⁷ 0.081	¹³¹ 0.047	⁸³ 0.371	⁸⁶ 0.242	⁹⁸ 0.391	¹²³ 0.295								
257	VIGILANTSOLUTIONS-008	⁸⁷ 0.051	⁸² 0.021	⁹⁰ 0.010	⁹⁷ 0.105	⁹⁹ 0.077	⁹⁷ 0.046	¹⁵⁹ 1.000	¹⁵⁶ 0.999	¹⁵¹ 0.991	¹³⁴ 0.104	¹³⁶ 0.054	⁸⁵ 0.398	⁸⁸ 0.259	¹²⁰ 0.511	¹²⁹ 0.316								
258	VISIONBOX-000	¹¹⁰ 0.073	⁷³ 0.018	⁷⁰ 0.007	⁶⁴ 0.071	⁷² 0.057	⁷⁵ 0.035	¹⁰² 0.995	¹⁰⁹ 0.990	¹²⁸ 0.974	⁵⁸ 0.023	⁵⁹ 0.012	⁴⁵ 0.146	⁴⁸ 0.081	³⁹ 0.162	⁴² 0.126								
259	VISIONLABS-004	¹²² 0.091	¹³⁵ 0.058	¹⁴⁷ 0.024	¹⁶³ 0.199	¹⁷¹ 0.159	¹⁷³ 0.097	³⁴ 0.944	³⁷ 0.890	⁶⁷ 0.742														
260	VISIONLABS-005	¹¹⁸ 0.080	¹³⁹ 0.050	¹³¹ 0.020	¹⁵⁷ 0.183	¹⁶⁴ 0.147	¹⁶² 0.087	³⁵ 0.945	³⁶ 0.888	⁶⁸ 0.736														
261	VISIONLABS-006	⁷⁴ 0.044	¹⁰¹ 0.027	⁹⁵ 0.010	¹⁰⁸ 0.117	¹¹¹ 0.090	¹⁰⁷ 0.051	³⁴ 0.764	³⁵ 0.672	⁴⁵ 0.511														
262	VISIONLABS-007	⁷³ 0.044	¹⁰⁰ 0.027	⁹⁴ 0.010	¹⁰⁷ 0.117	¹¹³ 0.090	¹⁰⁶ 0.051	³³ 0.764	³⁶ 0.672	⁴⁴ 0.511	²⁷ 0.031	²² 0.014												
263	VISIONLABS-008	⁴⁸ 0.028	⁵⁵ 0.013	⁵⁴ 0.006	⁵⁶ 0.068	⁶⁰ 0.051	⁶³ 0.032	¹⁸ 0.574	²² 0.481	²⁶ 0.317	⁴² 0.017	³⁹ 0.008												
264	VISIONLABS-009	²⁵ 0.012	²⁴ 0.005	²¹ 0.002	²⁷ 0.032	²⁹ 0.025	²⁹ 0.017	⁵⁰ 0.930	⁴⁷ 0.799	²¹ 0.196	²⁶ 0.008	²³ 0.004												
265	VISIONLABS-010	²³ 0.011	¹⁹ 0.003	¹⁹ 0.002	¹⁹ 0.024	²⁰ 0.020	¹⁹ 0.014				²⁰ 0.194	⁹ 0.004	⁷ 0.002	¹⁰ 0.034	⁹ 0.017	¹⁸ 0.109	¹⁷ 0.089							
266	VISIONLABS-011	²¹⁷ 0.354	¹⁹⁹ 0.122	¹⁹² 0.048	¹⁶² 0.195	¹⁷⁰ 0.155	¹⁶⁸ 0.093	¹⁴³ 0.999	¹⁴⁶ 0.998	¹⁴⁹ 0.991	¹⁴⁸ 0.157	¹⁵¹ 0.105												
267	VOCORD-003	²⁵⁷ 0.826	²⁴² 0.355	¹⁹⁷ 0.051	²⁰⁹ 0.401	¹⁸⁰ 0.173	¹⁶⁶ 0.093	²⁰¹ 1.000	¹⁸⁹ 1.000	¹⁹⁶ 0.999	¹⁵⁶ 0.193	¹⁴⁶ 0.065												
268	VOCORD-004	²⁵⁰ 0.689	²¹² 0.158	¹⁸⁸ 0.044	¹⁴³ 0.161	¹⁵³ 0.130	¹⁵⁵ 0.080	¹⁴⁸ 0.999	¹³⁸ 0.997	¹¹⁹ 0.968	¹⁴³ 0.138	¹⁵¹ 0.090												
269	VOCORD-005	²⁷⁹ 1.000	²⁷⁹ 1.000	²⁸¹ 1.000	²⁷¹ 1.000	²⁷⁹ 1.000	²⁶⁴ 1.000	²⁷⁶ 1.000	²⁶															

MISSES BELOW THRESHOLD, T		ENROL RECENT MUGSHOT, N = 1.6M									ENROL APPLICATION PORTRAIT, N = 1.6M						
#	ALGORITHM	ENROL: MUGSHOT			ENROL: MUGSHOT			ENROL: MUGSHOT			ENROL: VISA			ENROL: BORDER		ENROL: VISA	
		FPIR=0.0003	FPIR=0.001	FPIR=0.01	FPIR=0.0003	FPIR=0.001	FPIR=0.01	FPIR=0.0003	FPIR=0.001	FPIR=0.01	FPIR=0.001	FPIR=0.001	FPIR=0.01	FPIR=0.001	FPIR=0.01	FPIR=0.001	FPIR=0.01
277	YISHENG-001	²²⁸ 0.452	²³⁹ 0.346	²⁴⁵ 0.206	²³⁹ 0.983	²³⁵ 0.808	²³³ 0.269				¹⁸⁵ 0.666	¹⁸⁰ 0.396				¹⁶² 0.919	¹⁶¹ 0.695
278	YITU-002	⁵⁴ 0.031	⁷¹ 0.018	⁷⁰ 0.008	⁴⁸ 0.063	³⁵ 0.049	⁵³ 0.028										
279	YITU-003	³⁵ 0.032	⁷⁹ 0.019	⁸³ 0.009	³⁵ 0.067	⁶³ 0.052	⁶⁹ 0.033										
280	YITU-004	³² 0.019	⁴⁰ 0.010	⁴¹ 0.004	²⁵ 0.035	³⁰ 0.027	³⁰ 0.017	³⁸ 0.948	⁶⁵ 0.936	⁹² 0.913							
281	YITU-005	³⁵ 0.022	⁴⁶ 0.010	⁴⁹ 0.005	³² 0.039	³⁷ 0.032	⁴¹ 0.023										

Table 33: **Threshold-based accuracy.** Values are FNIR(N, T, L) with $N = 1.6$ million with thresholds set to produce FPIR = 0.0003, 0.001, and 0.01 in non-mate searches. Throughout blue superscripts indicate the rank of the algorithm for that column. Caution: The Power-low models are mostly intended to draw attention to the kind of behavior, not as a model to be used for prediction.

Appendices

Appendix A Accuracy on large-population FRVT 2018 mugshots

2022/03/30 17:50:48	$\text{FNIR}(N, R, T) =$ $\text{FPTR}(N, T) =$	False neg. identification rate False pos. identification rate	$N =$ Num. enrolled subjects $R =$ Num. candidates examined	$T =$ Threshold $T > 0 \rightarrow$ Identification	$T = 0 \rightarrow$ Investigation
------------------------	---	--	--	---	-----------------------------------

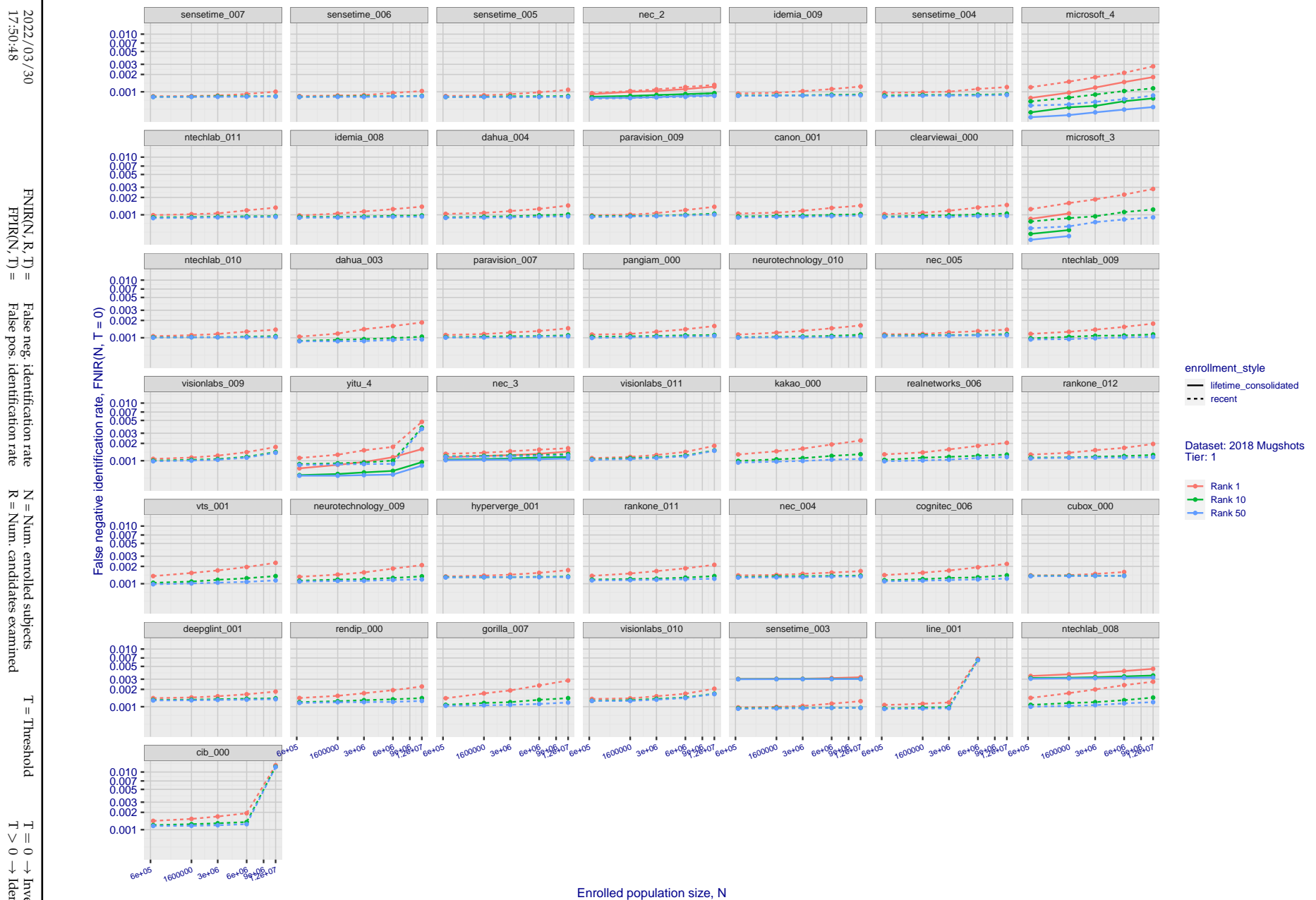


Figure 20: [FRVT-2018 Mugshot Dataset] Rank-based identification miss rates vs. number of enrolled subjects. The figure shows false negative identification rates, $\text{FNIR}(N, R)$, across various gallery sizes and ranks 1, 10 and 50. The threshold is set to zero, so this metric rewards even weak scoring rank 1 mates. This also means $\text{FPFR} = 1$, so any search without an enrolled mate will return non-mated candidates. For clarity, results are sorted and reported into tiers spanning multiple pages, the tiering criteria being rank 1 hit rate on a gallery size of 640 000.

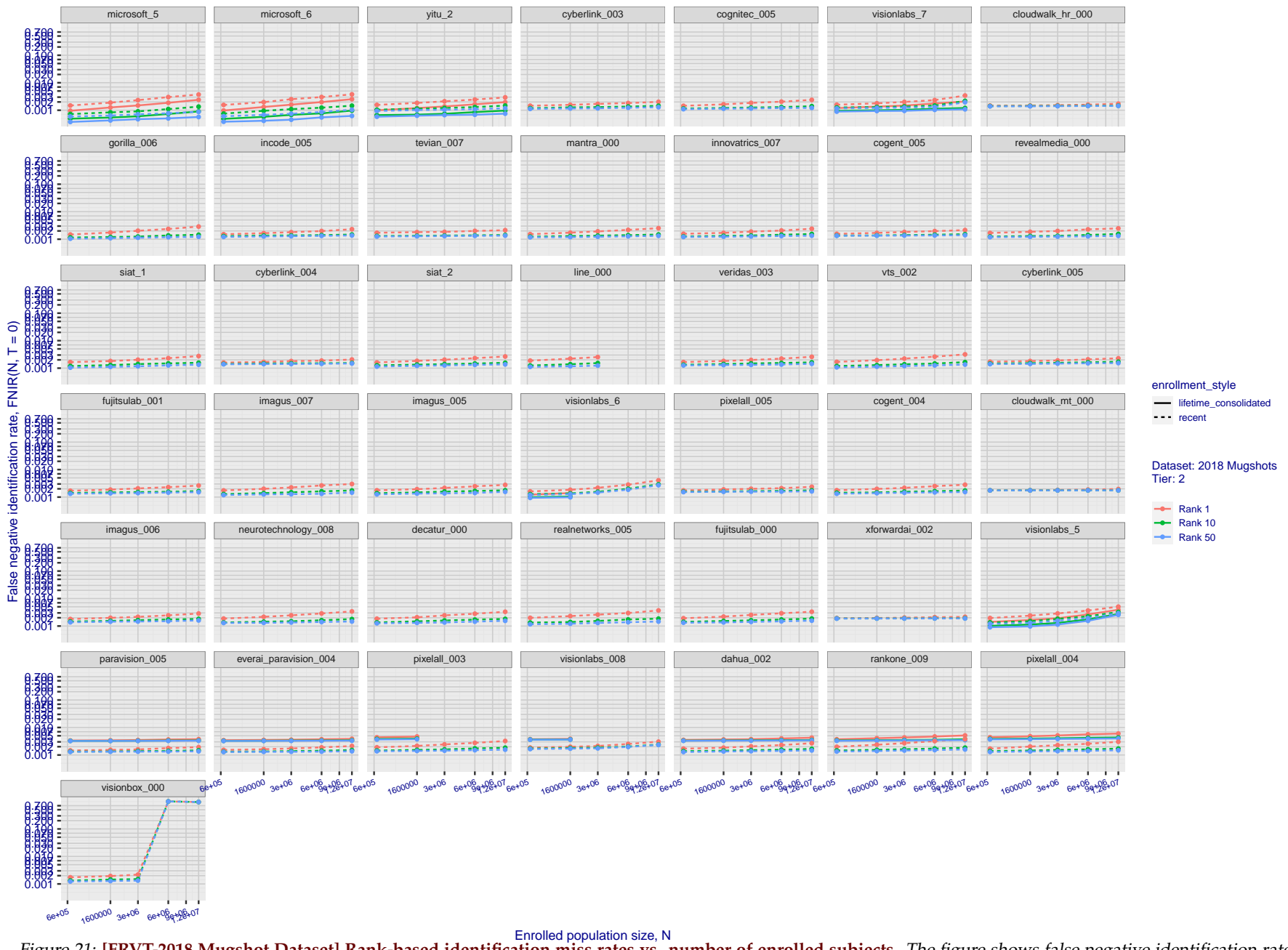


Figure 21: [FRVT-2018 Mugshot Dataset] Rank-based identification miss rates vs. number of enrolled subjects. The figure shows false negative identification rates, $\text{FNIR}(N, R)$, across various gallery sizes and ranks 1, 10 and 50. The threshold is set to zero, so this metric rewards even weak scoring rank 1 mates. This also means $\text{FPIR} = 1$, so any search without an enrolled mate will return non-mated candidates. For clarity, results are sorted and reported into tiers spanning multiple pages, the tiering criteria being rank 1 hit rate on a gallery size of 640 000.

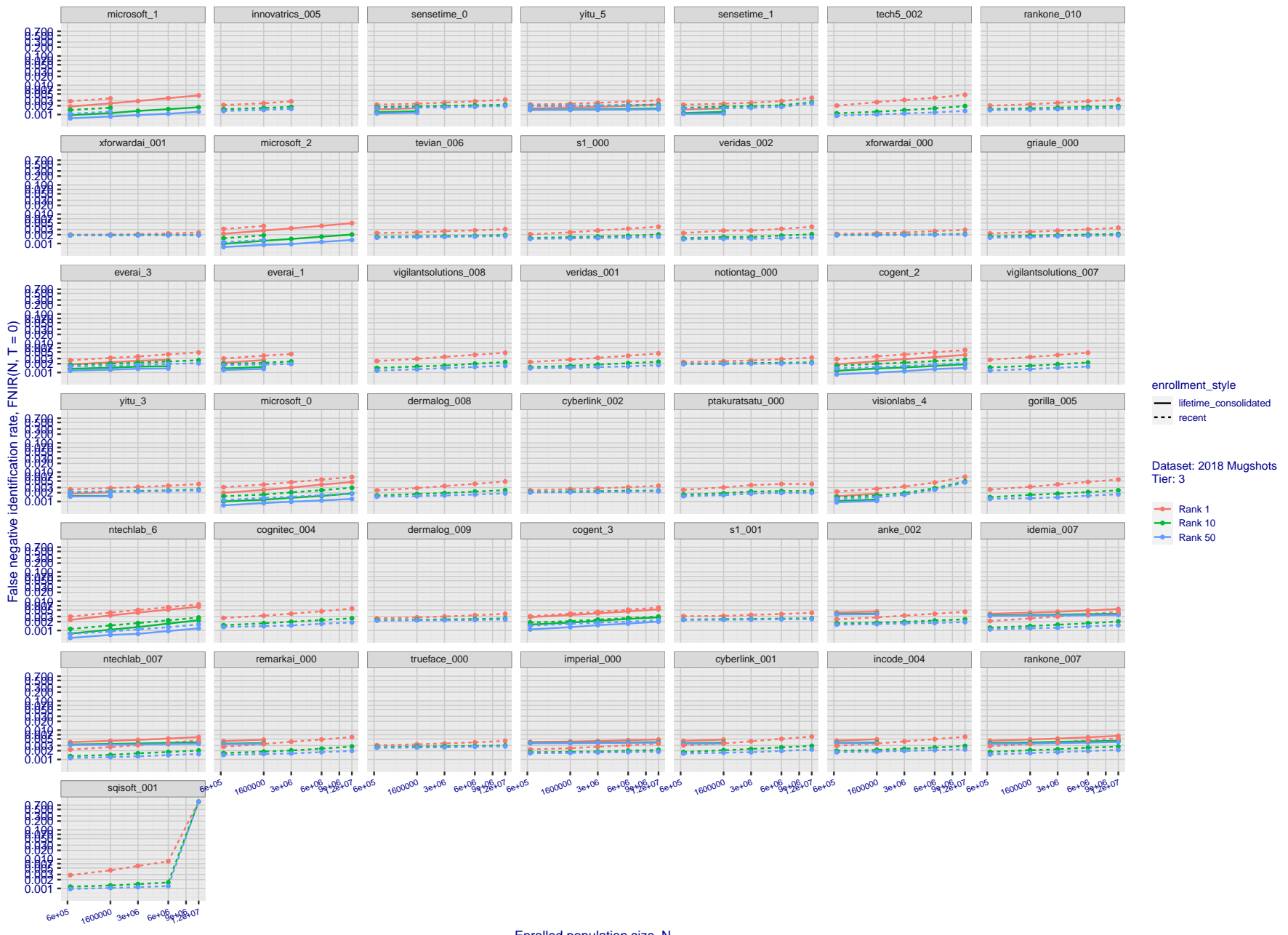


Figure 22: [FRVT-2018 Mugshot Dataset] Rank-based identification miss rates vs. number of enrolled subjects. The figure shows false negative identification rates, $\text{FNIR}(N, R)$, across various gallery sizes and ranks 1, 10 and 50. The threshold is set to zero, so this metric rewards even weak scoring rank 1 mates. This also means $\text{FPIR} = 1$, so any search without an enrolled mate will return non-mated candidates. For clarity, results are sorted and reported into tiers spanning multiple pages, the tiering criteria being rank 1 hit rate on a gallery size of 640 000.

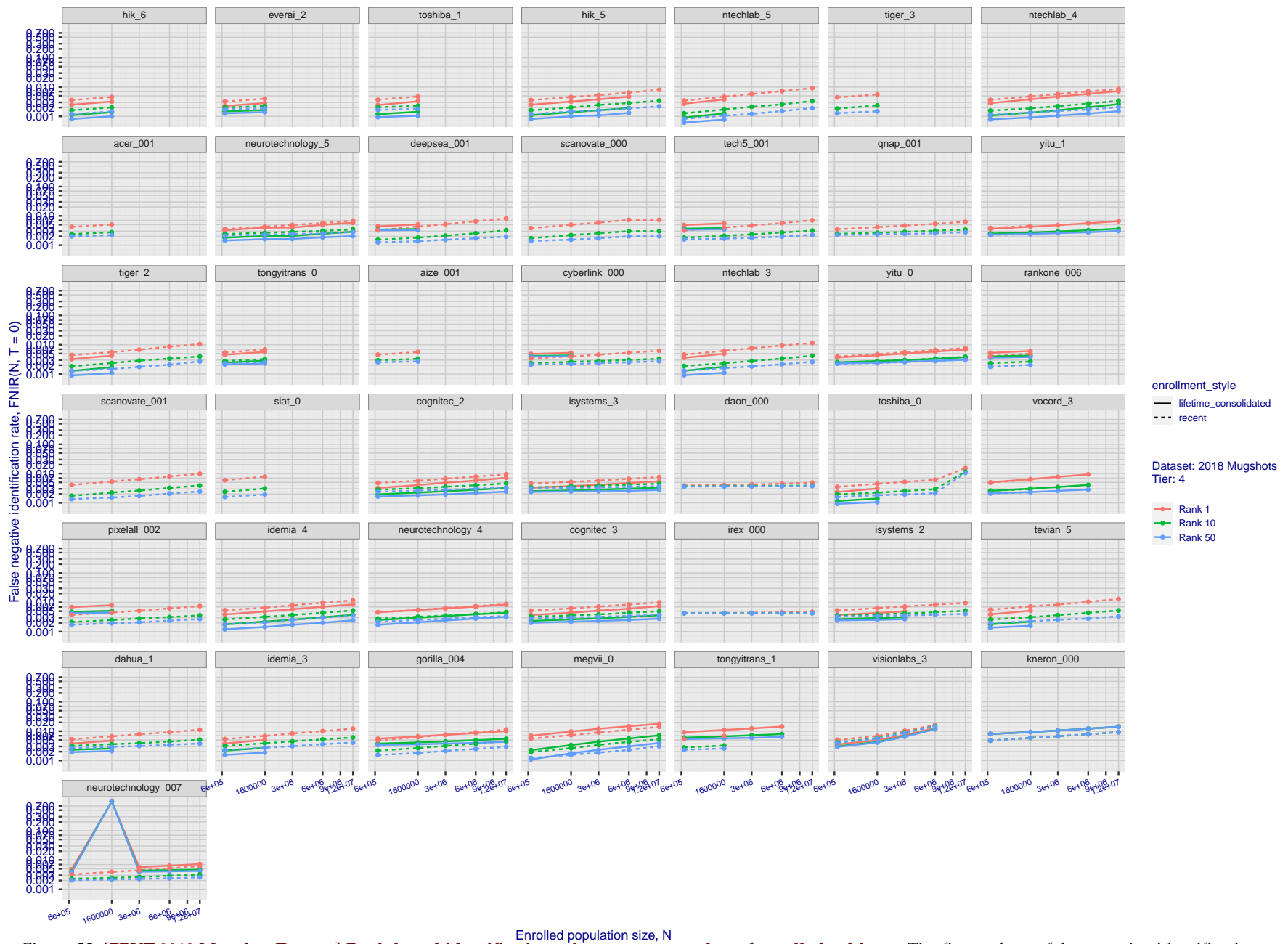


Figure 23: [FRVT-2018 Mugshot Dataset] Rank-based identification miss rates vs. number of enrolled subjects. The figure shows false negative identification rates, $\text{FNIR}(N, R)$, across various gallery sizes and ranks 1, 10 and 50. The threshold is set to zero, so this metric rewards even weak scoring rank 1 mates. This also means $\text{FPIR} = 1$, so any search without an enrolled mate will return non-mated candidates. For clarity, results are sorted and reported into tiers spanning multiple pages, the tiering criteria being rank 1 hit rate on a gallery size of 640 000.

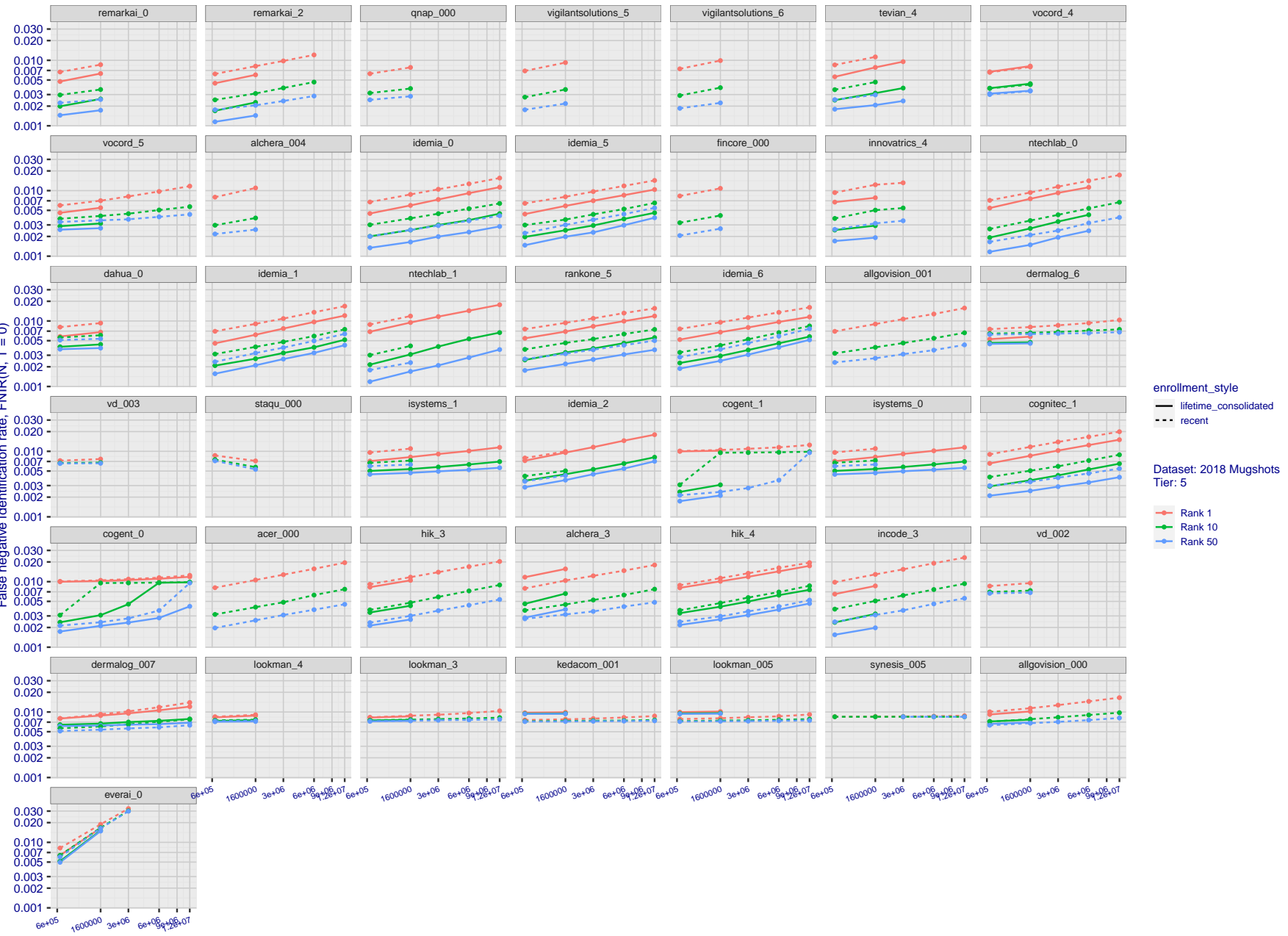
2022 /03 /30
17:50:48FNIR(N, R, T) = False neg. identification rate
FPIR(N, T) = False pos. identification rateN = Num. enrolled subjects
R = Num. candidates examinedT = Threshold
 $T = 0 \rightarrow$ Investigation
 $T > 0 \rightarrow$ Identification

Figure 24: [FRVT-2018 Mugshot Dataset] Rank-based identification miss rates vs. number of enrolled subjects. The figure shows false negative identification rates, $\text{FNIR}(N, R)$, across various gallery sizes and ranks 1, 10 and 50. The threshold is set to zero, so this metric rewards even weak scoring rank 1 mates. This also means $\text{FPIR} = 1$, so any search without an enrolled mate will return non-mated candidates. For clarity, results are sorted and reported into tiers spanning multiple pages, the tiering criteria being rank 1 hit rate on a gallery size of 640 000.

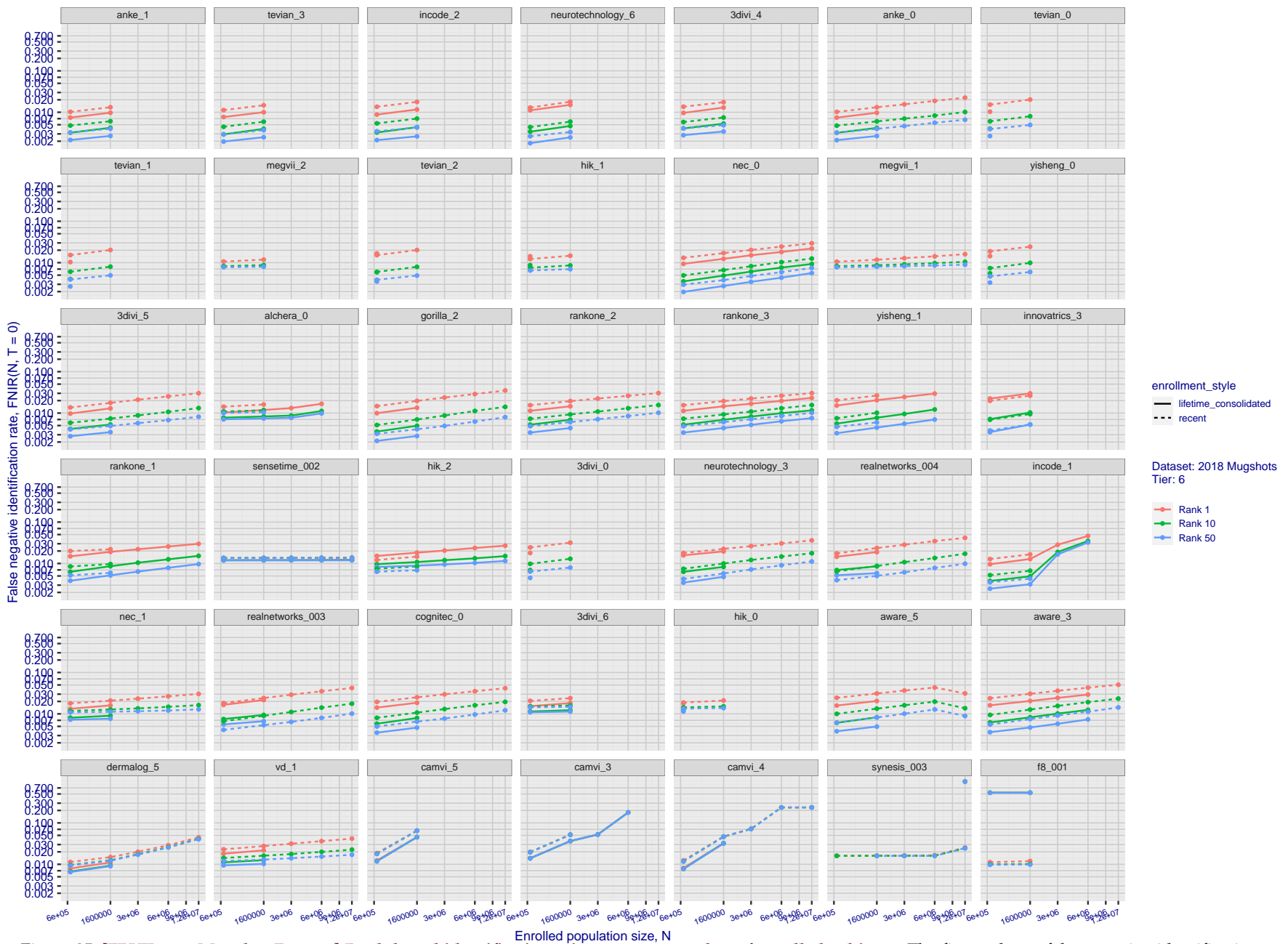


Figure 25: [FRVT-2018 Mugshot Dataset] Rank-based identification miss rates vs. number of enrolled subjects. The figure shows false negative identification rates, $FNIR(N, R)$, across various gallery sizes and ranks 1, 10 and 50. The threshold is set to zero, so this metric rewards even weak scoring rank 1 mates. This also means $FPIR = 1$, so any search without an enrolled mate will return non-mated candidates. For clarity, results are sorted and reported into tiers spanning multiple pages, the tiering criteria being rank 1 hit rate on a gallery size of 640 000.

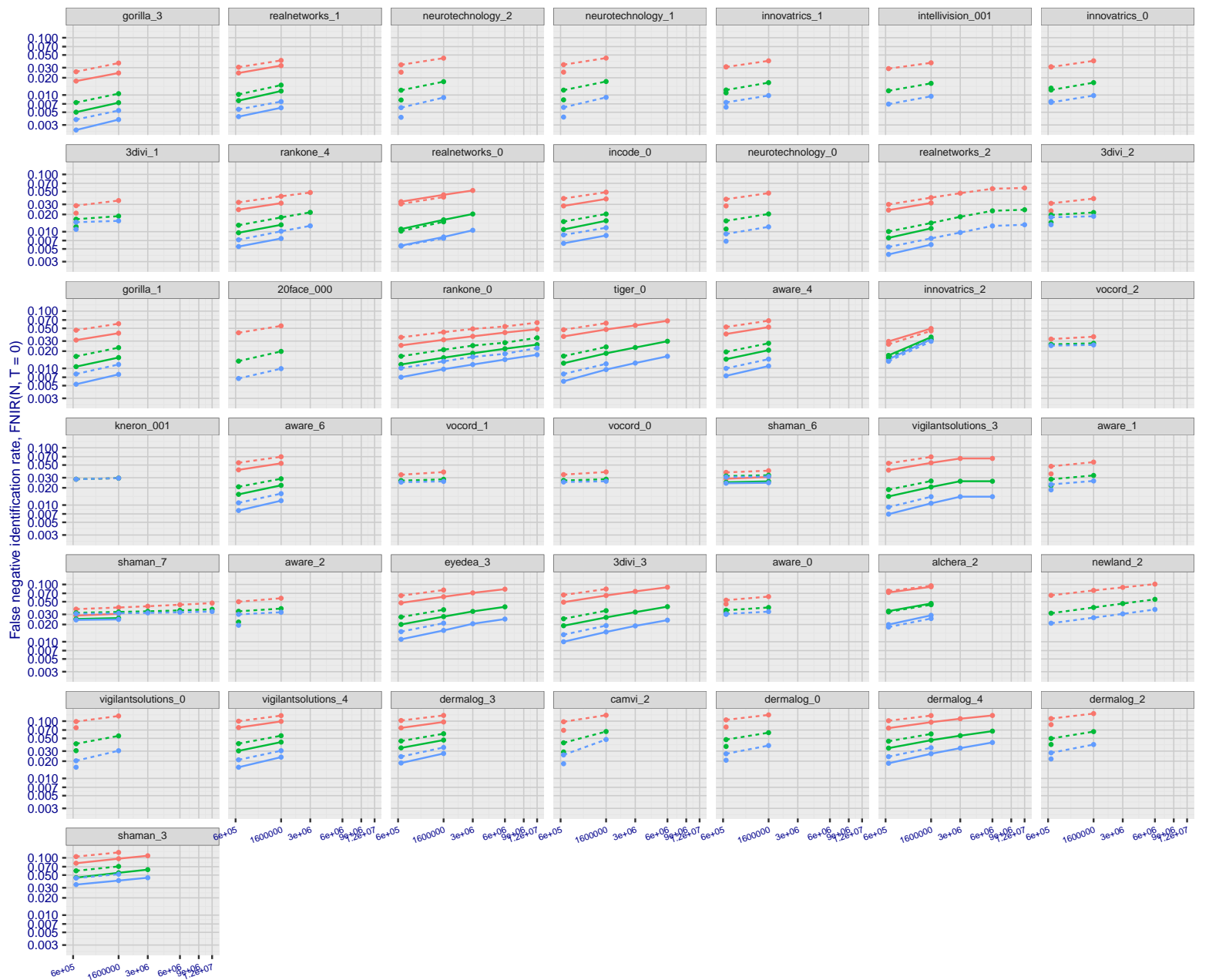


Figure 26: [FRVT-2018 Mugshot Dataset] Rank-based identification miss rates vs. number of enrolled subjects. The figure shows false negative identification rates, $\text{FNIR}(N, R)$, across various gallery sizes and ranks 1, 10 and 50. The threshold is set to zero, so this metric rewards even weak scoring rank 1 mates. This also means $\text{FPIR} = 1$, so any search without an enrolled mate will return non-mated candidates. For clarity, results are sorted and reported into tiers spanning multiple pages, the tiering criteria being rank 1 hit rate on a gallery size of 640 000.

2022/03/30
17:50:48

$FNI(N, R, T) =$ False neg. identification rate
 $FPI(N, T) =$ False pos. identification rate

N = Num. enrolled subjects
R = Num. candidates examined

$I = 0 \rightarrow$ Investigation
 $T > 0 \rightarrow$ Identification

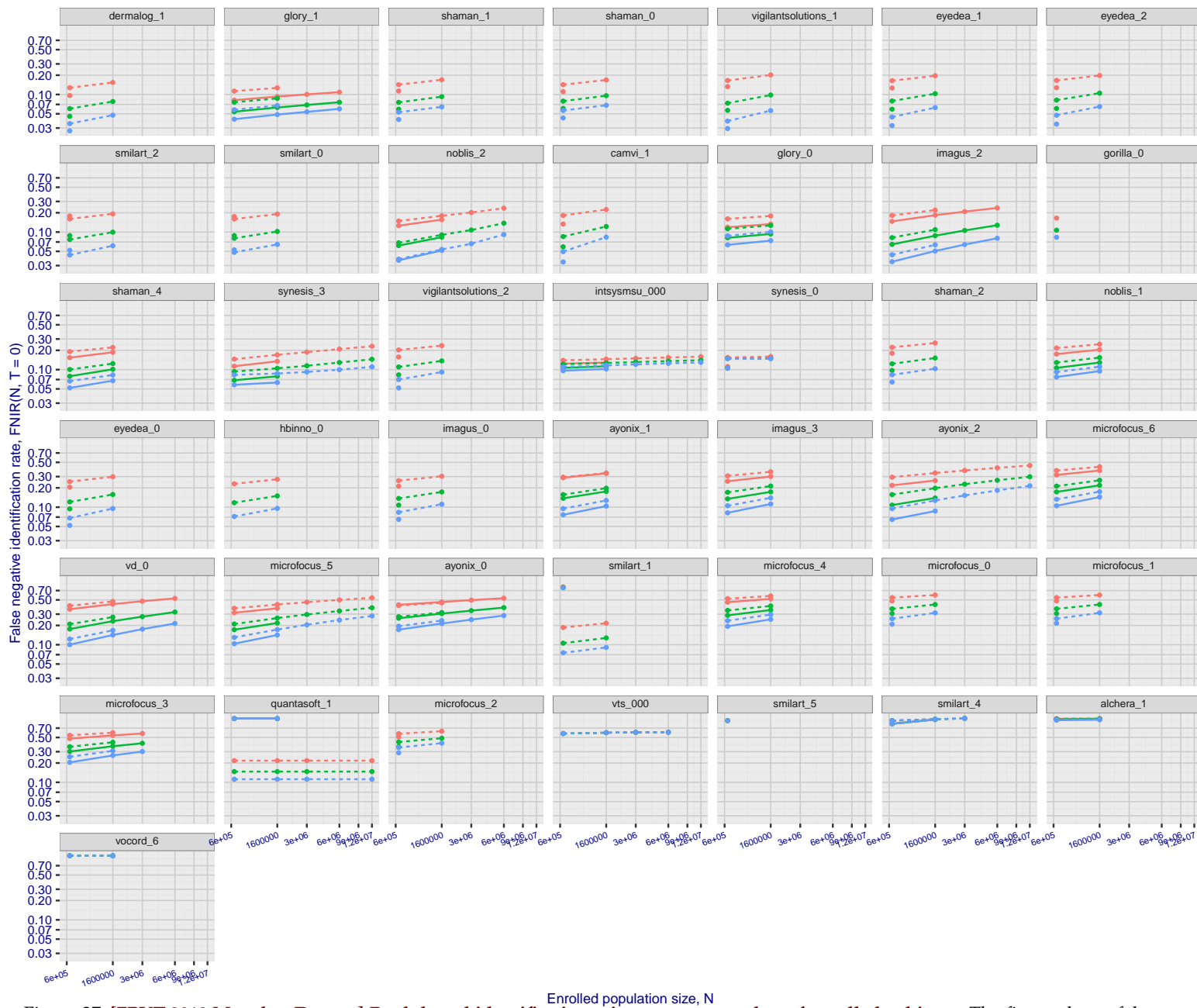


Figure 27: [FRVT-2018 Mugshot Dataset] Rank-based identification miss rates vs. number of enrolled subjects. The figure shows false negative identification rates, FNIR(N, R), across various gallery sizes and ranks 1, 10 and 50. The threshold is set to zero, so this metric rewards even weak scoring rank 1 mates. This also means FPIR = 1, so any search without an enrolled mate will return non-mated candidates. For clarity, results are sorted and reported into tiers spanning multiple pages, the tiering criteria being rank 1 hit rate on a gallery size of 640 000.

2022/03/30 17:50:48	$\text{FNIR}(N, R, T) =$ $\text{FPTR}(N, T) =$	False neg. identification rate False pos. identification rate	$N =$ Num. enrolled subjects $R =$ Num. candidates examined	$T =$ Threshold	$T = 0 \rightarrow$ Investigation $T > 0 \rightarrow$ Identification
------------------------	---	--	--	-----------------	---

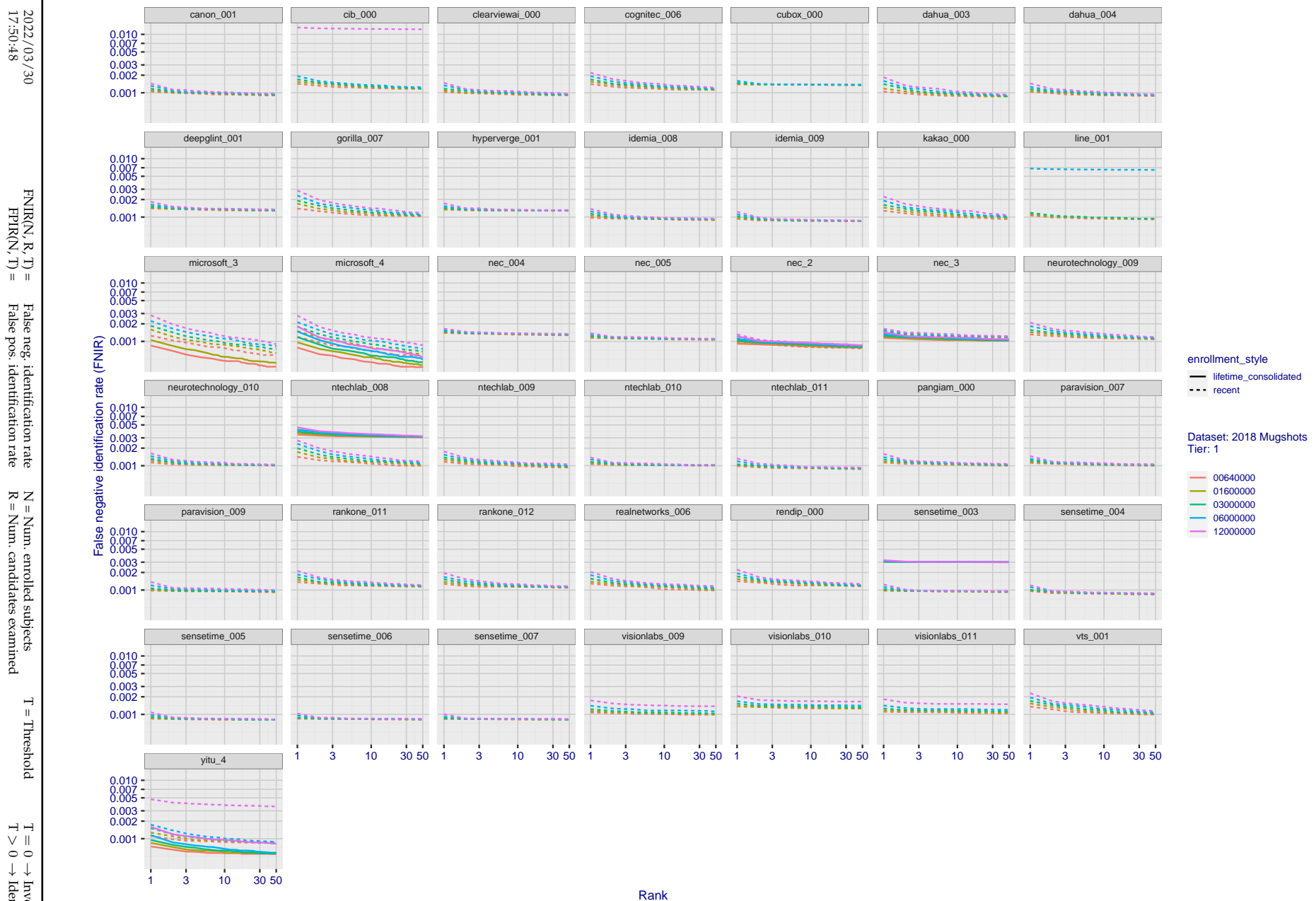


Figure 28: [FRVT-2018 Mugshot Dataset] Rank-based identification miss rates vs. rank. The figure shows false negative identification rates (FNIR) for ranks up to 50. This metric is appropriate to investigational applications where human reviewers will adjudicate sorted candidate lists. Note that with threshold set to zero, FPIR = 1, i.e. any search without an enrolled mate will return non-mated candidates. Results are sorted and reported into tiers for clarity, with the tiering criteria being rank 1 hit rate on a gallery size of $N = 640\,000$ subjects.

2022 /03 /30
17:50:48

 $\text{FNIR}(N, R, T) = \text{False neg. identification rate}$
 $\text{FPIR}(N, T) = \text{False pos. identification rate}$

 $N = \text{Num. enrolled subjects}$
 $R = \text{Num. candidates examined}$

 $T = \text{Threshold}$
 $T = 0 \rightarrow \text{Investigation}$
 $T > 0 \rightarrow \text{Identification}$

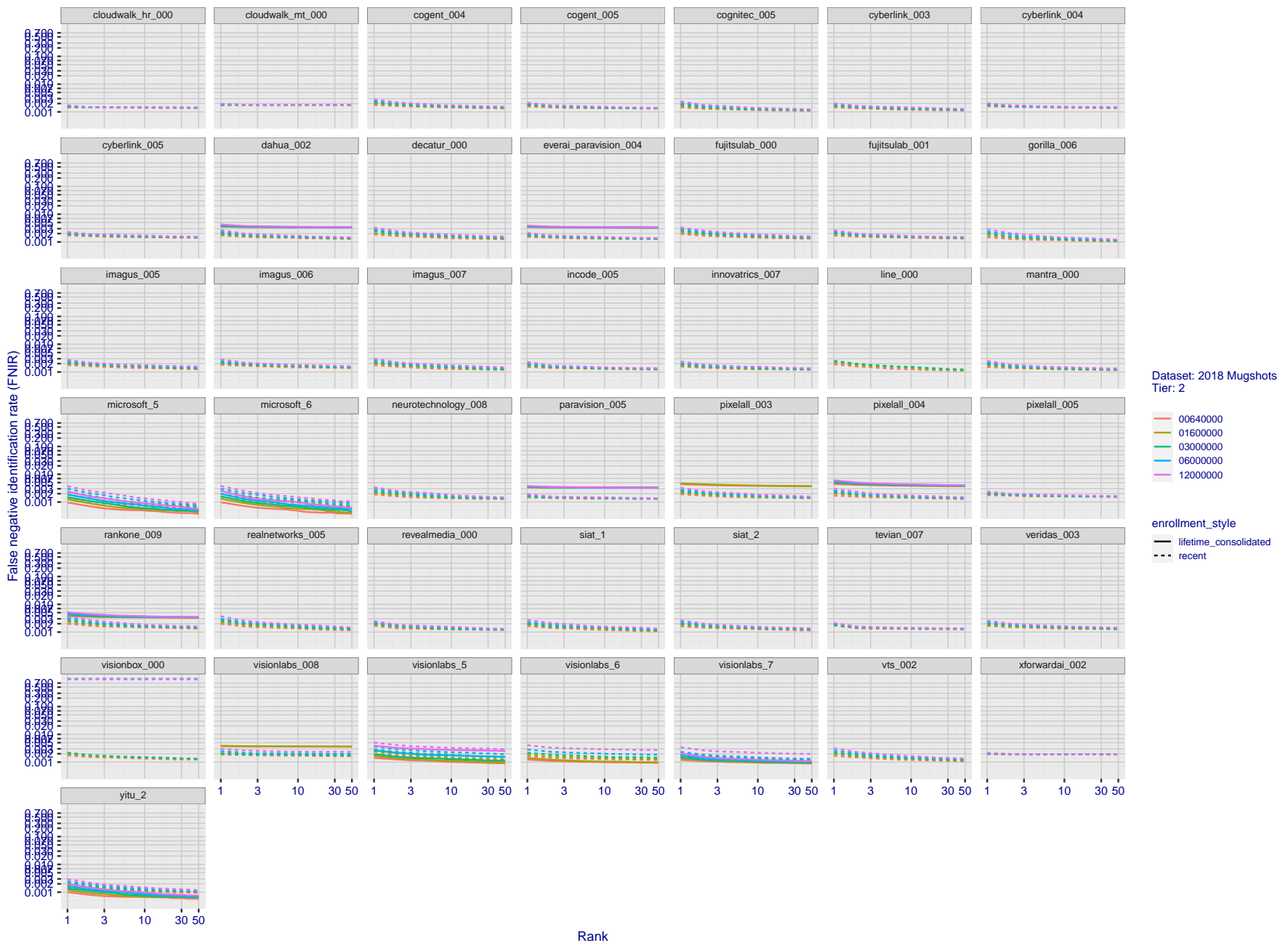


Figure 29: [FRVT-2018 Mugshot Dataset] Rank-based identification miss rates vs. rank. The figure shows false negative identification rates (FNIR) for ranks up to 50. This metric is appropriate to investigational applications where human reviewers will adjudicate sorted candidate lists. Note that with threshold set to zero, FPIR = 1, i.e. any search without an enrolled mate will return non-mated candidates. Results are sorted and reported into tiers for clarity, with the tiering criteria being rank 1 hit rate on a gallery size of $N = 640\,000$ subjects.

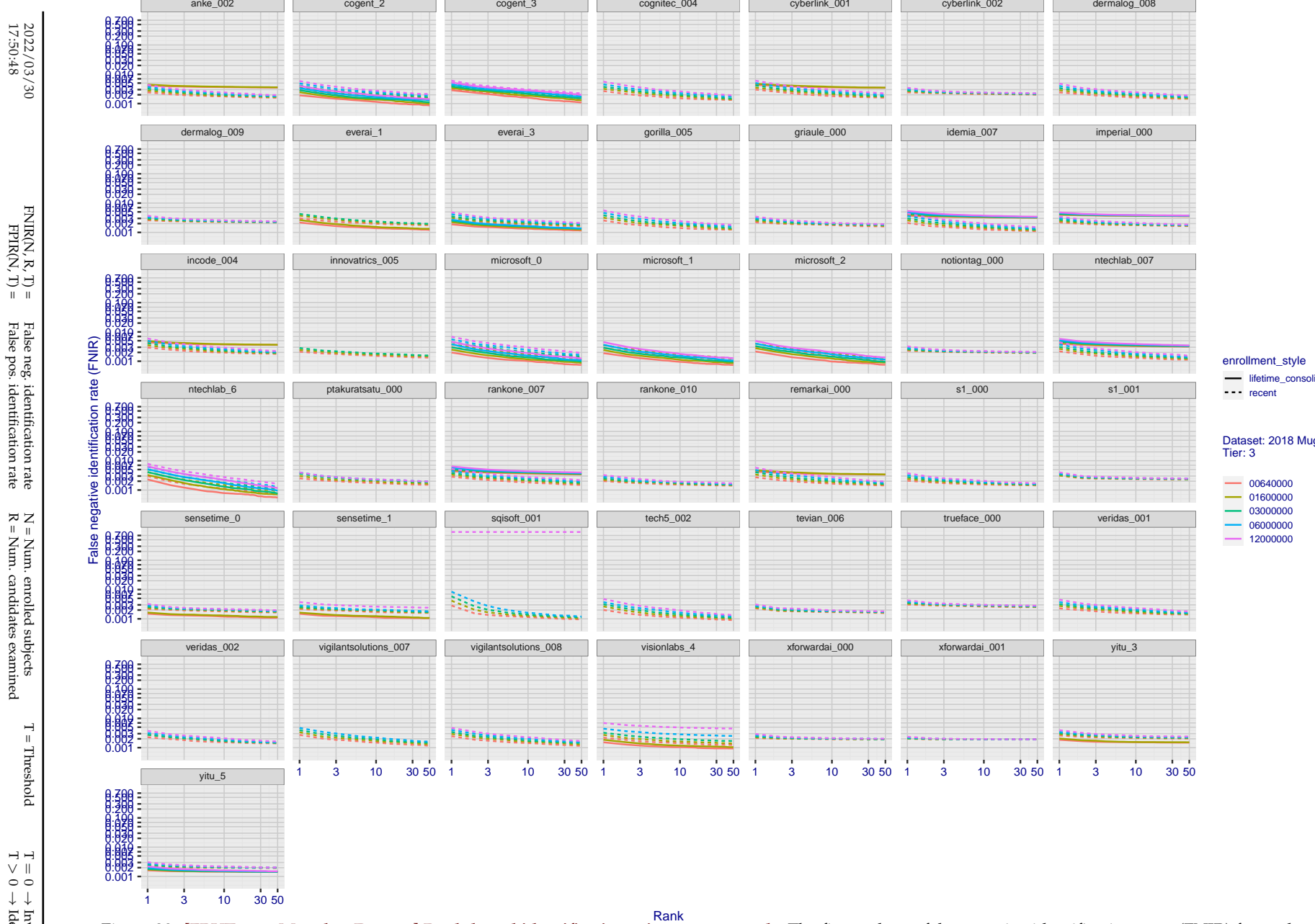


Figure 30: [FRVT-2018 Mugshot Dataset] Rank-based identification miss rates vs. rank. The figure shows false negative identification rates (FNIR) for ranks up to 50. This metric is appropriate to investigational applications where human reviewers will adjudicate sorted candidate lists. Note that with threshold set to zero, FPIR = 1, i.e. any search without an enrolled mate will return non-mated candidates. Results are sorted and reported into tiers for clarity, with the tiering criteria being rank 1 hit rate on a gallery size of N = 640 000 subjects.

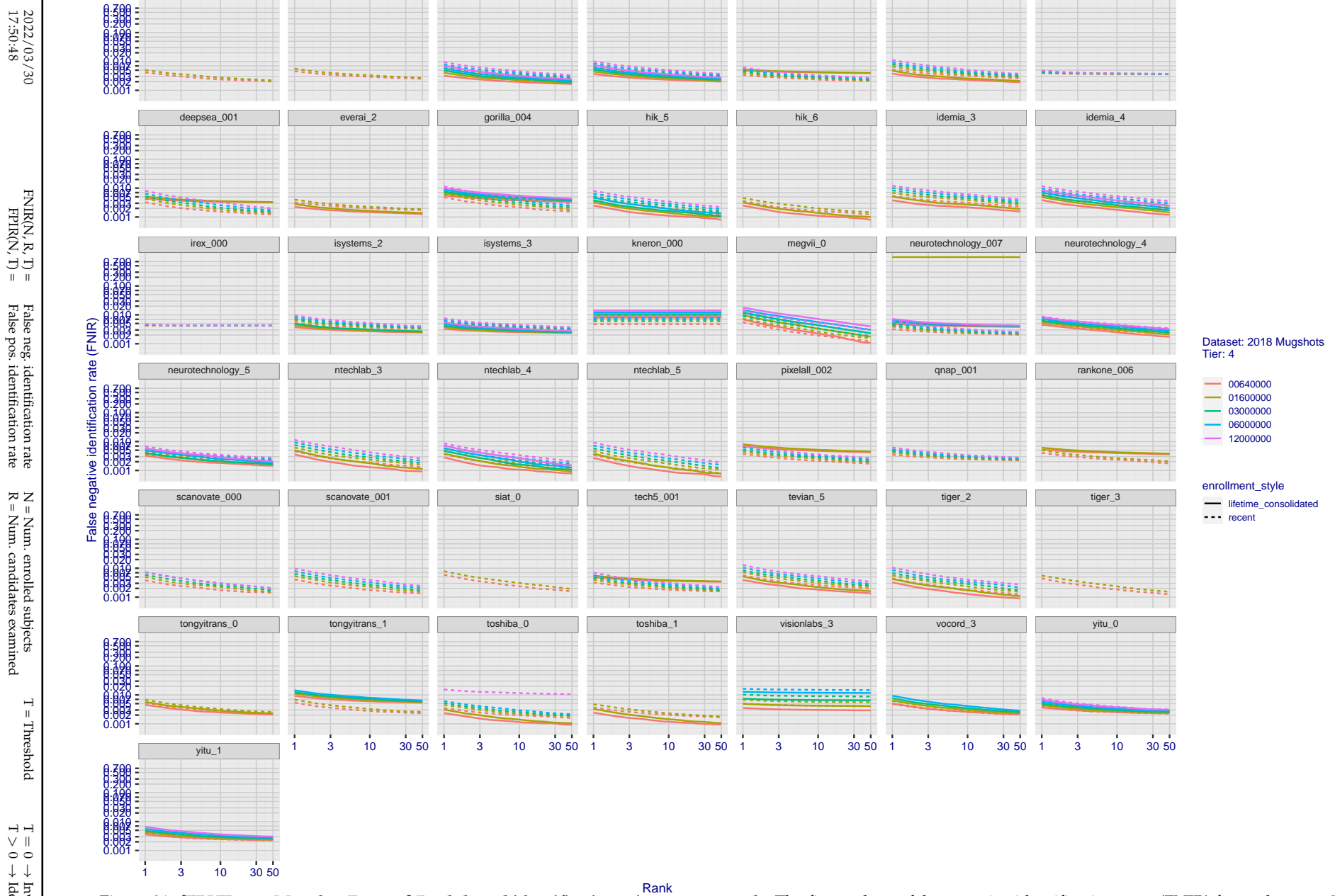


Figure 31: [FRVT-2018 Mugshot Dataset] Rank-based identification miss rates vs. rank. The figure shows false negative identification rates (FNIR) for ranks up to 50. This metric is appropriate to investigational applications where human reviewers will adjudicate sorted candidate lists. Note that with threshold set to zero, FPIR = 1, i.e. any search without an enrolled mate will return non-mated candidates. Results are sorted and reported into tiers for clarity, with the tiering criteria being rank 1 hit rate on a gallery size of N = 640 000 subjects.

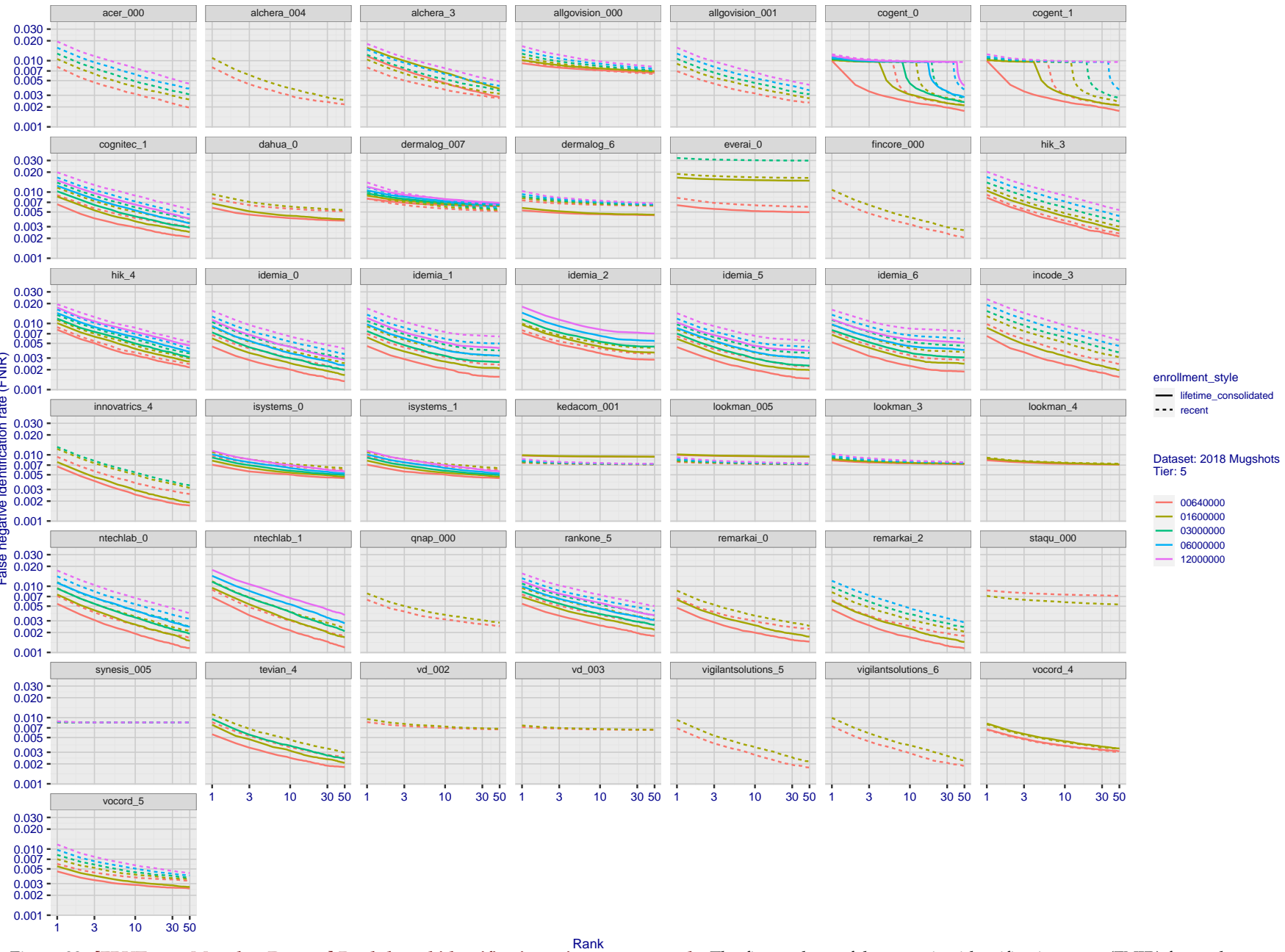
2022 / 03 / 30
17:50:48FNIR(N, R, T) = False neg. identification rate
FPIR(N, T) = False pos. identification rateN = Num. enrolled subjects
R = Num. candidates examined
T = ThresholdT = 0 → Investigation
 $T > 0 \rightarrow$ Identification

Figure 32: [FRVT-2018 Mugshot Dataset] Rank-based identification miss rates vs. rank. The figure shows false negative identification rates (FNIR) for ranks up to 50. This metric is appropriate to investigational applications where human reviewers will adjudicate sorted candidate lists. Note that with threshold set to zero, FPIR = 1, i.e. any search without an enrolled mate will return non-mated candidates. Results are sorted and reported into tiers for clarity, with the tiering criteria being rank 1 hit rate on a gallery size of N = 640 000 subjects.

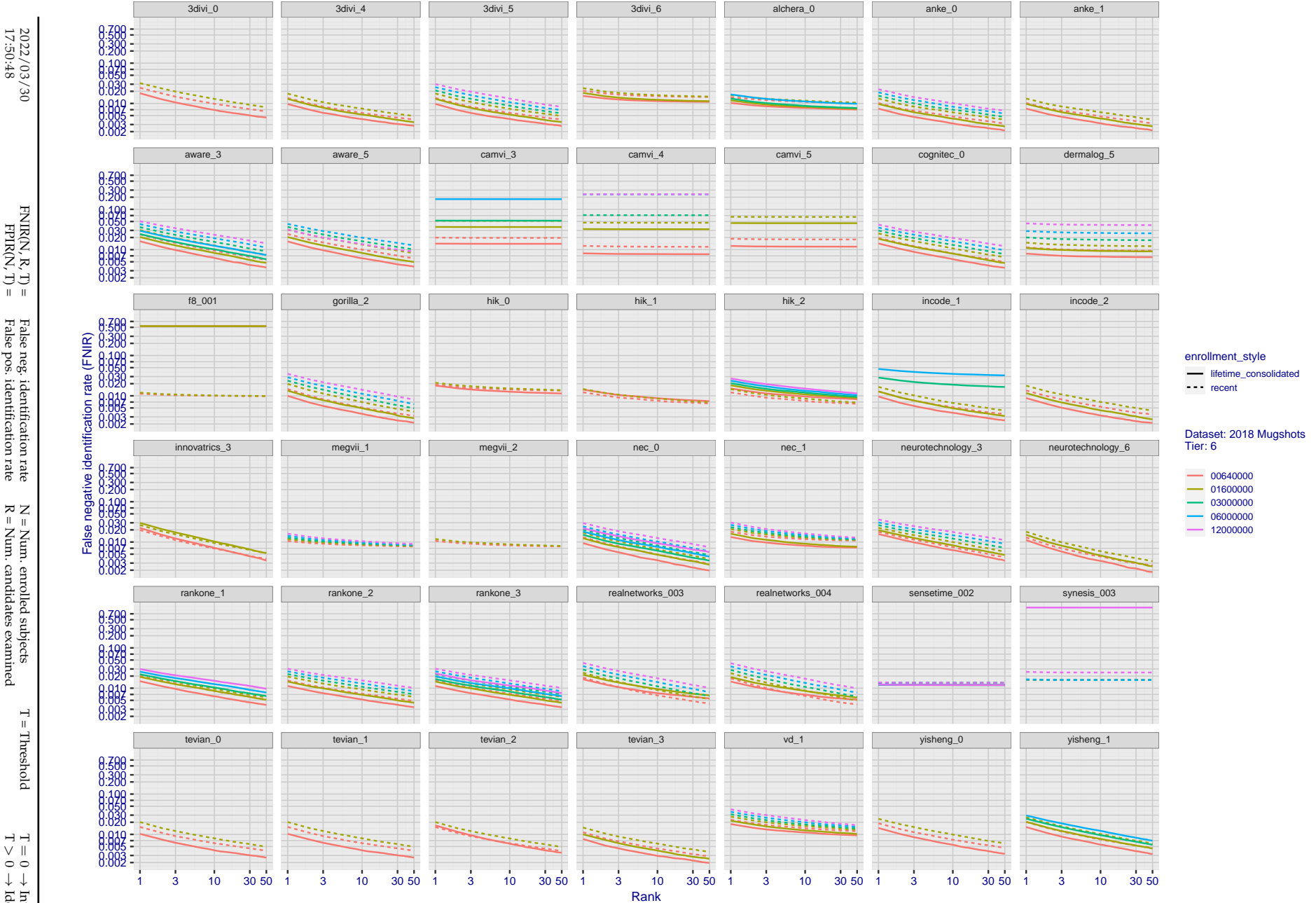


Figure 33: [FRVT-2018 Mugshot Dataset] Rank-based identification miss rates vs. rank. The figure shows false negative identification rates (FNIR) for ranks up to 50. This metric is appropriate to investigational applications where human reviewers will adjudicate sorted candidate lists. Note that with threshold set to zero, FPIR = 1, i.e. any search without an enrolled mate will return non-mated candidates. Results are sorted and reported into tiers for clarity, with the tiering criteria being rank 1 hit rate on a gallery size of $N = 640\,000$ subjects.

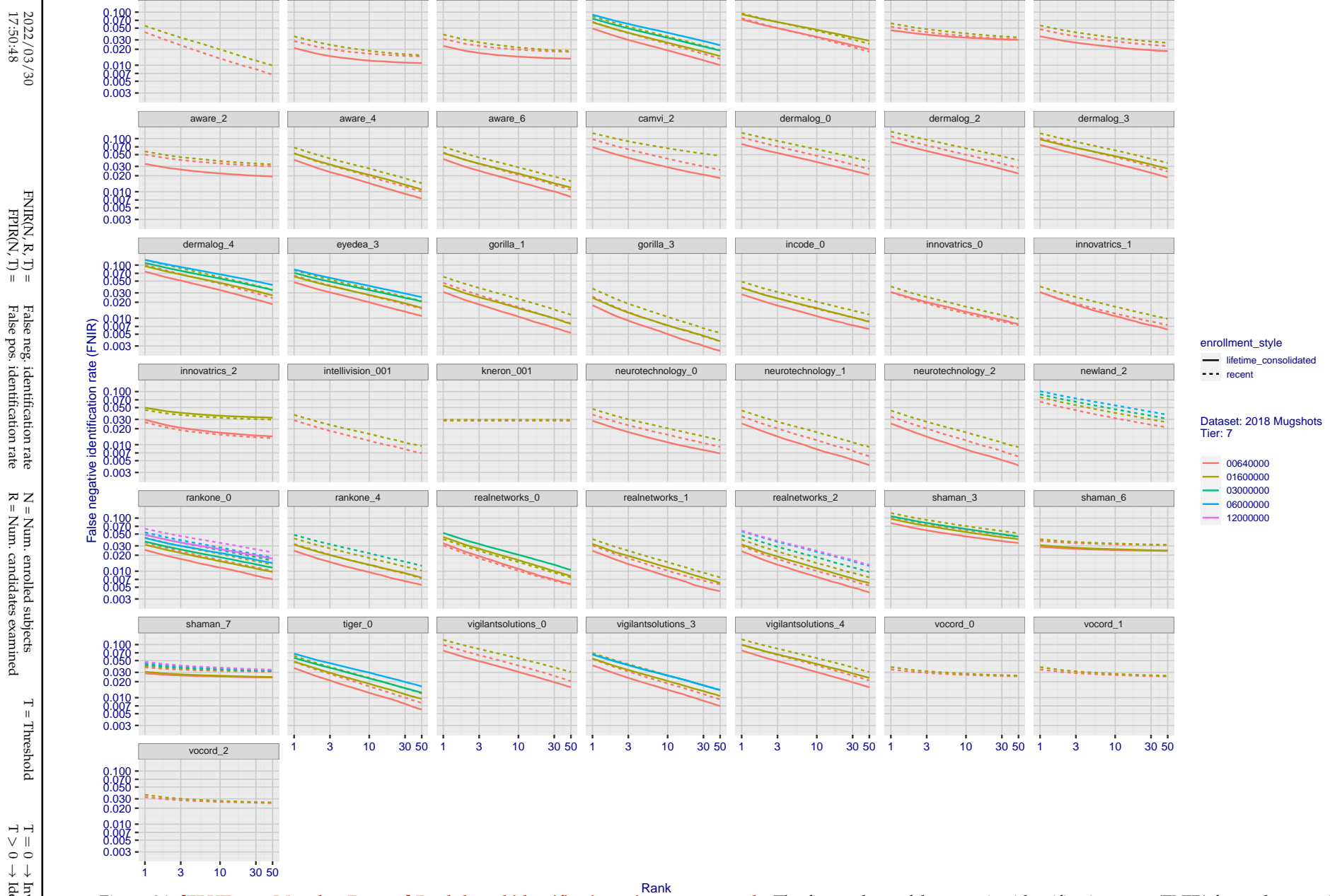


Figure 34: [FRVT-2018 Mugshot Dataset] Rank-based identification miss rates vs. rank. The figure shows false negative identification rates (FNIR) for ranks up to 50. This metric is appropriate to investigational applications where human reviewers will adjudicate sorted candidate lists. Note that with threshold set to zero, FPIR = 1, i.e. any search without an enrolled mate will return non-mated candidates. Results are sorted and reported into tiers for clarity, with the tiering criteria being rank 1 hit rate on a gallery size of N = 640 000 subjects.

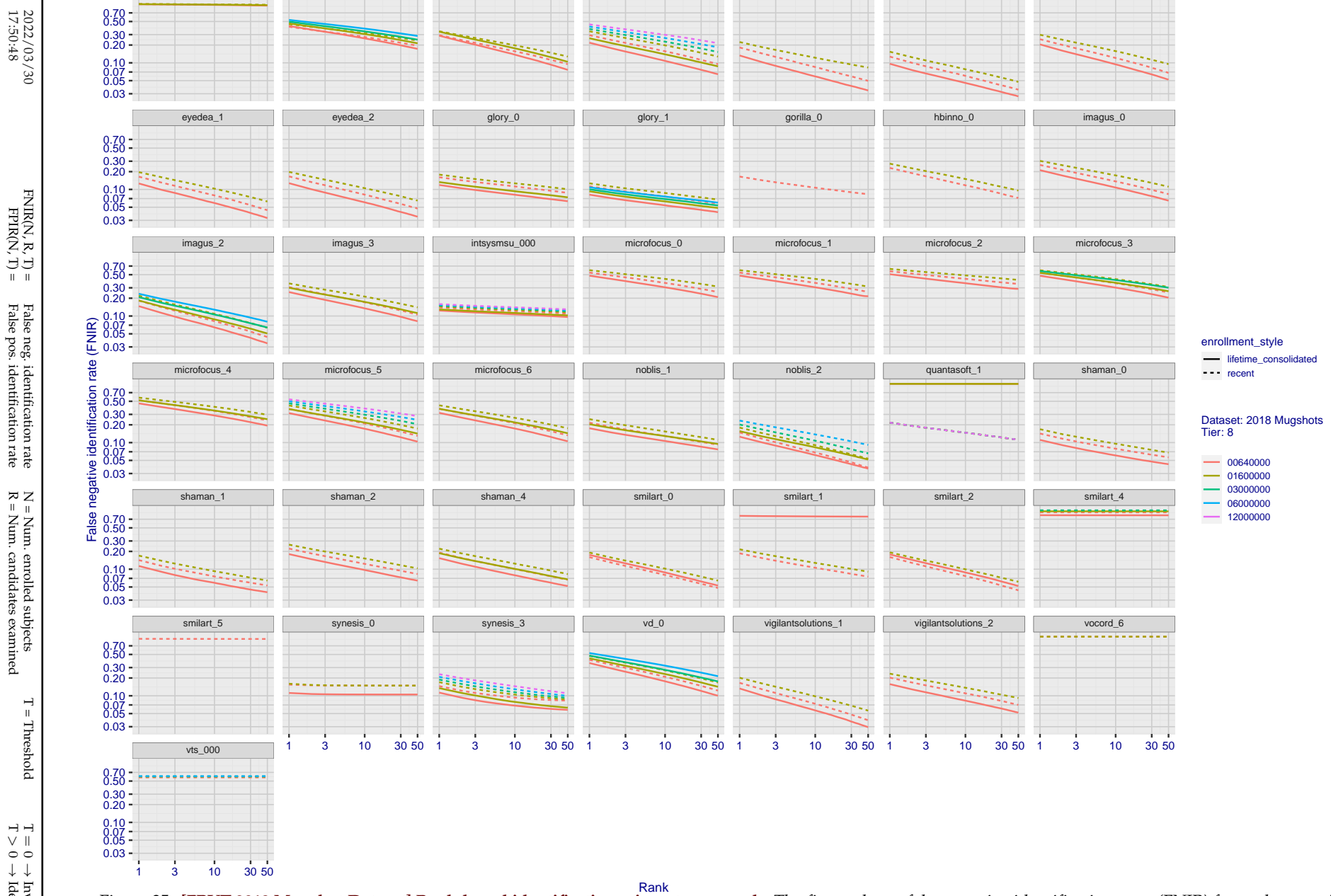


Figure 35: [FRVT-2018 Mugshot Dataset] Rank-based identification miss rates vs. rank. The figure shows false negative identification rates (FNIR) for ranks up to 50. This metric is appropriate to investigational applications where human reviewers will adjudicate sorted candidate lists. Note that with threshold set to zero, FPIR = 1, i.e. any search without an enrolled mate will return non-mated candidates. Results are sorted and reported into tiers for clarity, with the tiering criteria being rank 1 hit rate on a gallery size of N = 640 000 subjects.

2022/03/30 17:50:48	$\text{FNIR}(N, R, T) =$ $\text{FPTR}(N, T) =$	False neg. identification rate False pos. identification rate	$N =$ Num. enrolled subjects $R =$ Num. candidates examined	$T =$ Threshold $T > 0 \rightarrow$ Identification	$T = 0 \rightarrow$ Investigation
------------------------	---	--	--	---	-----------------------------------

2022/03/30
17:50:48FNIR(N, R, T) = False neg. identification rate
FPIR(N, T) = False pos. identification rateN = Num. enrolled subjects
R = Num. candidates examined

T = Threshold

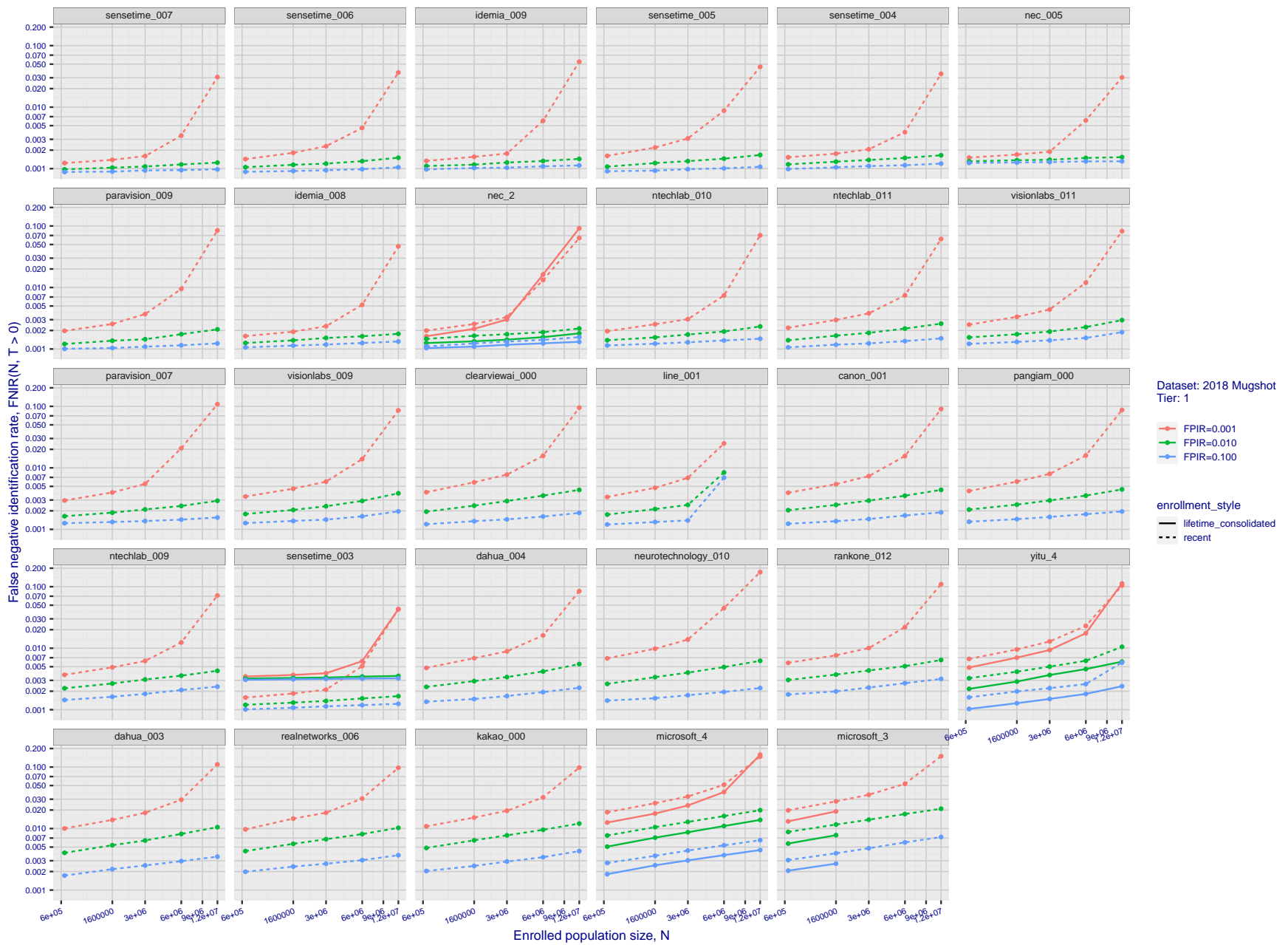
T = 0 → Investigation
T > 0 → Identification

Figure 36: [FRVT-2018 Mugshot Dataset] Threshold-based identification miss rates vs. number of enrolled subjects. The figure shows FNIR(N, T) across various gallery sizes when the threshold is set to achieve the given FPIRs. The rank criterion is irrelevant at high thresholds as mates are always at rank 1. The results are computed from the trials listed in rows 1-10 of Table 1. Less accurate algorithms were not run on large N , so results are missing. For clarity, results are sorted and reported into tiers spanning multiple pages. The tiering criteria is complicated: First paging by FNIR($N_b, 1, 0$), then sorting by median FNIR(N_b, T), $N_b = 640\,000$.

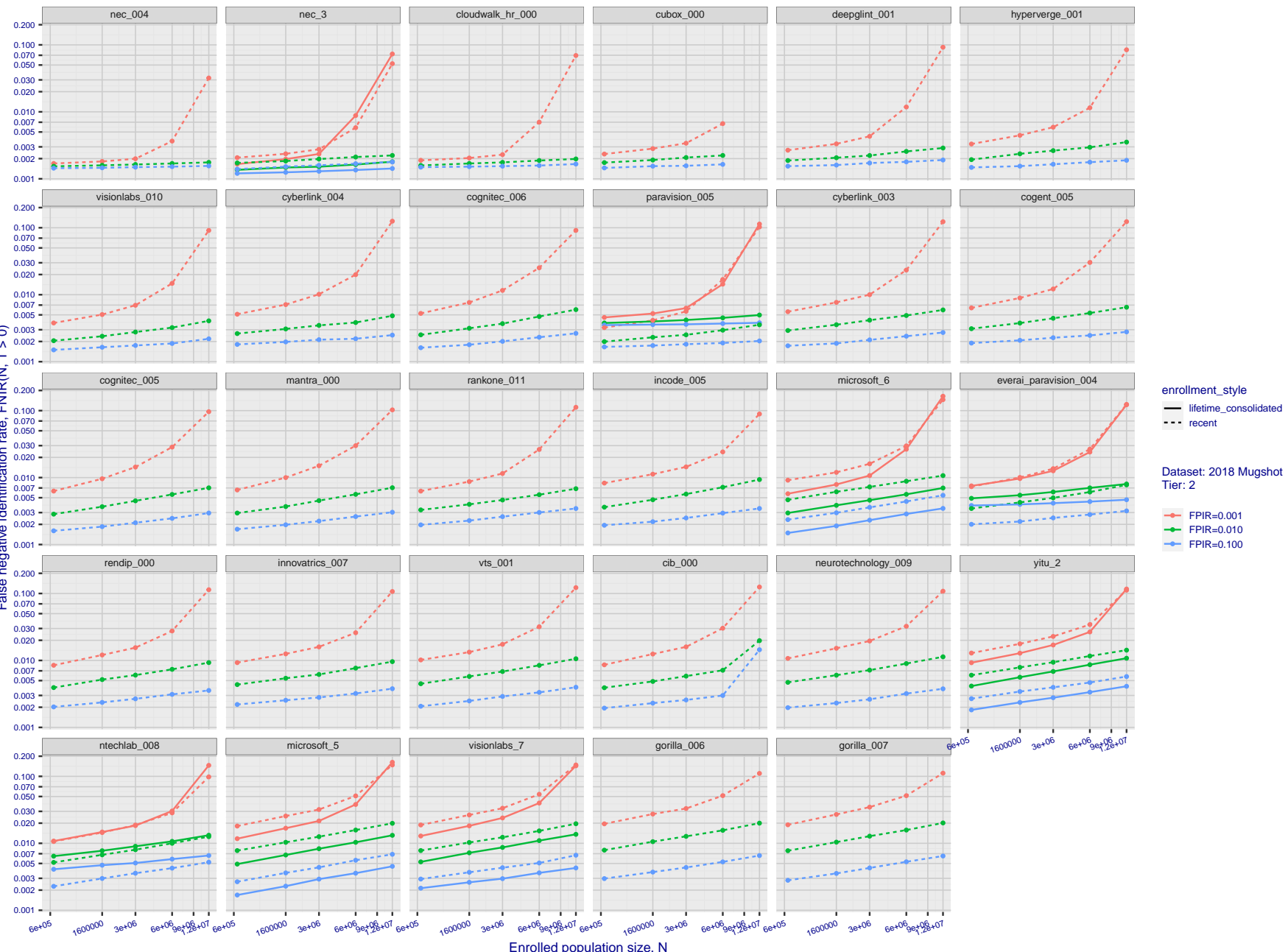
2022 /03 /30
17:50:48

Figure 37: [FRVT-2018 Mugshot Dataset] Threshold-based identification miss rates vs. number of enrolled subjects. The figure shows FNIR(N, T) across various gallery sizes when the threshold is set to achieve the given FPIRs. The rank criterion is irrelevant at high thresholds as mates are always at rank 1. The results are computed from the trials listed in rows 1-10 of Table 1. Less accurate algorithms were not run on large N , so results are missing. For clarity, results are sorted and reported into tiers spanning multiple pages. The tiering criteria is complicated: First paging by $\text{FNIR}(N_b, 1, 0)$, then sorting by median $\text{FNIR}(N_b, T)$, $N_b = 640\,000$.

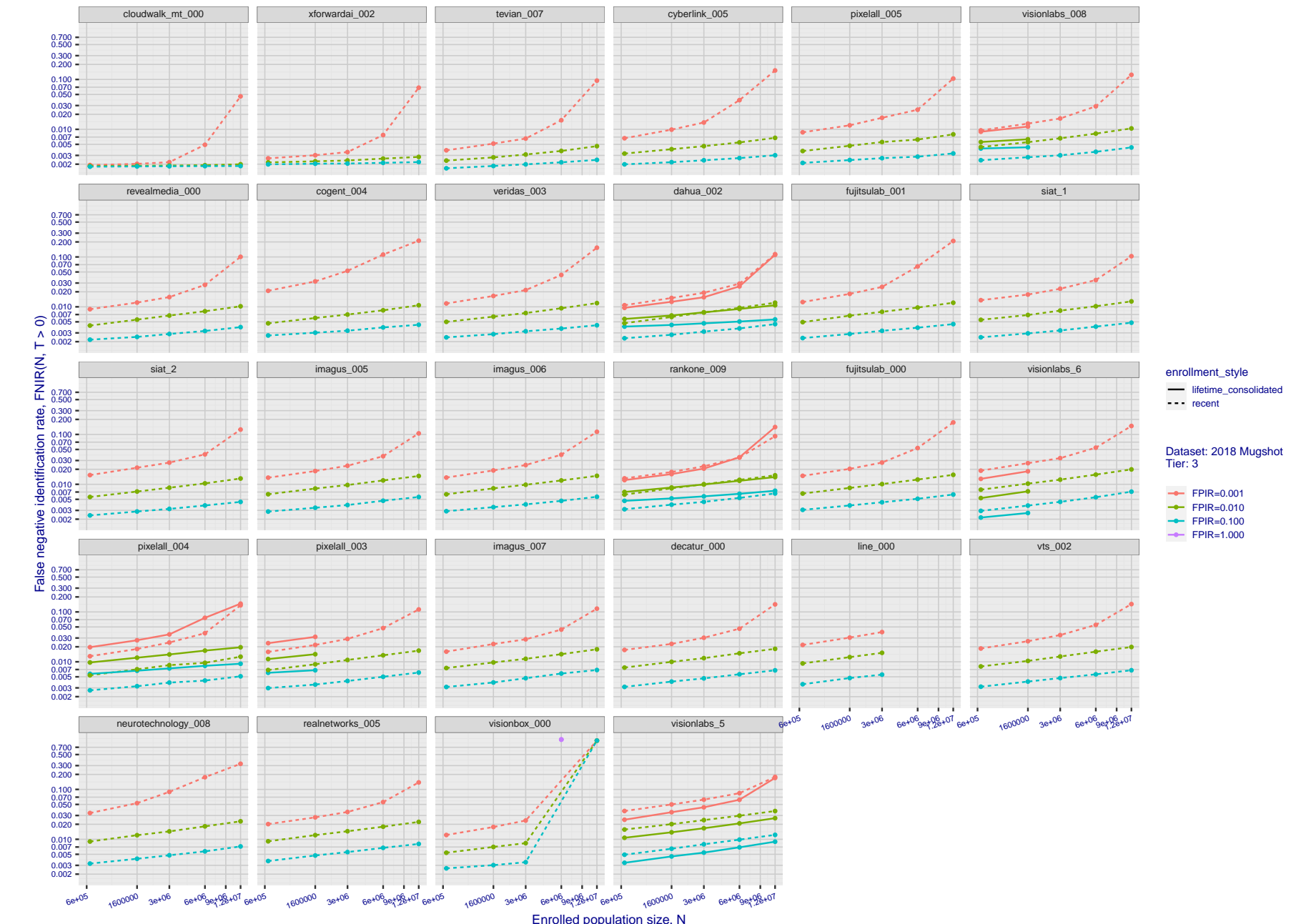
2022 /03 /30
17:50:48

Figure 38: [FRVT-2018 Mugshot Dataset] Threshold-based identification miss rates vs. number of enrolled subjects. The figure shows FNIR(N, T) across various gallery sizes when the threshold is set to achieve the given FPIRs. The rank criterion is irrelevant at high thresholds as mates are always at rank 1. The results are computed from the trials listed in rows 1-10 of Table 1. Less accurate algorithms were not run on large N , so results are missing. For clarity, results are sorted and reported into tiers spanning multiple pages. The tiering criteria is complicated: First paging by FNIR($N_b, 1, 0$), then sorting by median FNIR(N_b, T), $N_b = 640\,000$.

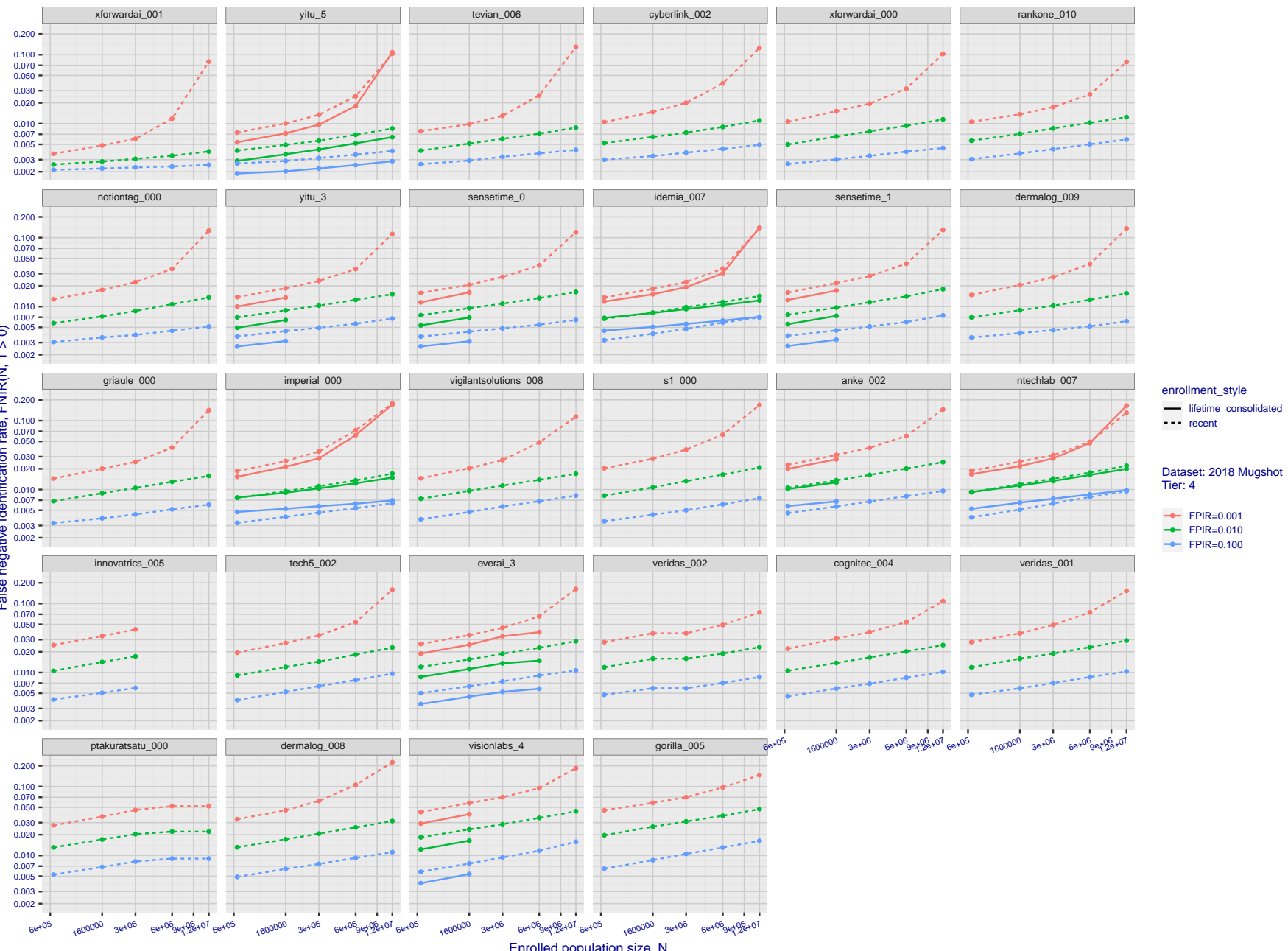
2022/03/30
17:50:48

Figure 39: [FRVT-2018 Mugshot Dataset] Threshold-based identification miss rates vs. number of enrolled subjects. The figure shows FNIR(N, T) across various gallery sizes when the threshold is set to achieve the given FPIRs. The rank criterion is irrelevant at high thresholds as mates are always at rank 1. The results are computed from the trials listed in rows 1-10 of Table 1. Less accurate algorithms were not run on large N , so results are missing. For clarity, results are sorted and reported into tiers spanning multiple pages. The tiering criteria is complicated: First paging by FNIR($N_b, 1, 0$), then sorting by median FNIR(N_b, T), $N_b = 640\,000$.

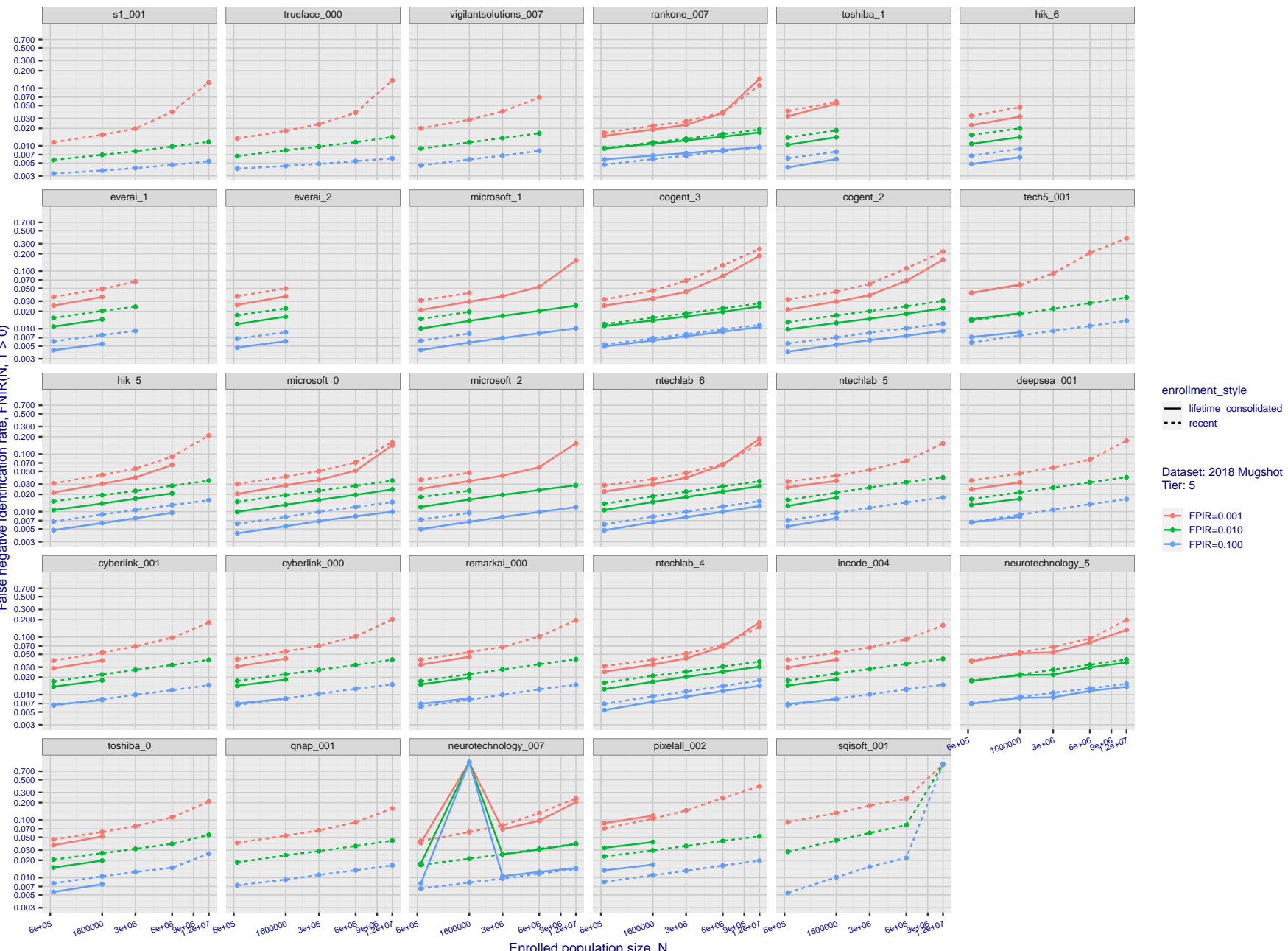
2022/03/30
17:50:48

Figure 40: [FRVT-2018 Mugshot Dataset] Threshold-based identification miss rates vs. number of enrolled subjects. The figure shows FNIR(N, T) across various gallery sizes when the threshold is set to achieve the given FPIRs. The rank criterion is irrelevant at high thresholds as mates are always at rank 1. The results are computed from the trials listed in rows 1-10 of Table 1. Less accurate algorithms were not run on large N , so results are missing. For clarity, results are sorted and reported into tiers spanning multiple pages. The tiering criteria is complicated: First paging by $\text{FNIR}(N_b, 1, 0)$, then sorting by median $\text{FNIR}(N_b, T)$, $N_b = 640\,000$.

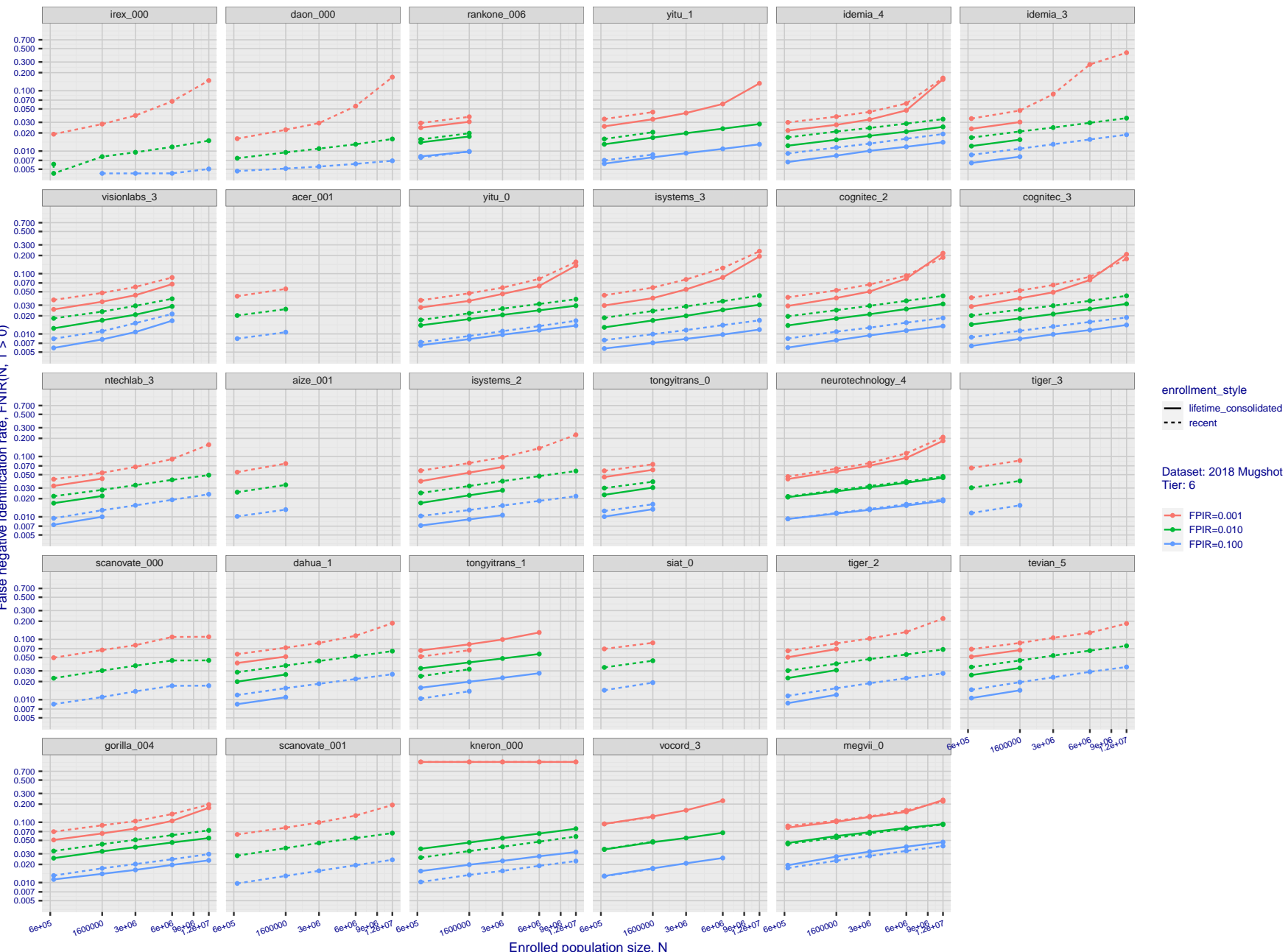
2022/03/30
17:50:48

Figure 41: [FRVT-2018 Mugshot Dataset] Threshold-based identification miss rates vs. number of enrolled subjects. The figure shows FNIR(N, T) across various gallery sizes when the threshold is set to achieve the given FPIRs. The rank criterion is irrelevant at high thresholds as mates are always at rank 1. The results are computed from the trials listed in rows 1-10 of Table 1. Less accurate algorithms were not run on large N , so results are missing. For clarity, results are sorted and reported into tiers spanning multiple pages. The tiering criteria is complicated: First paging by FNIR($N_b, 1, 0$), then sorting by median FNIR(N_b, T), $N_b = 640\,000$.

2022 /03 /30
17:50:48FNIR(N, R, T) = False neg. identification rate
FPIR(N, T) = False pos. identification rate
N = Num. enrolled subjects
R = Num. candidates examined

T = Threshold

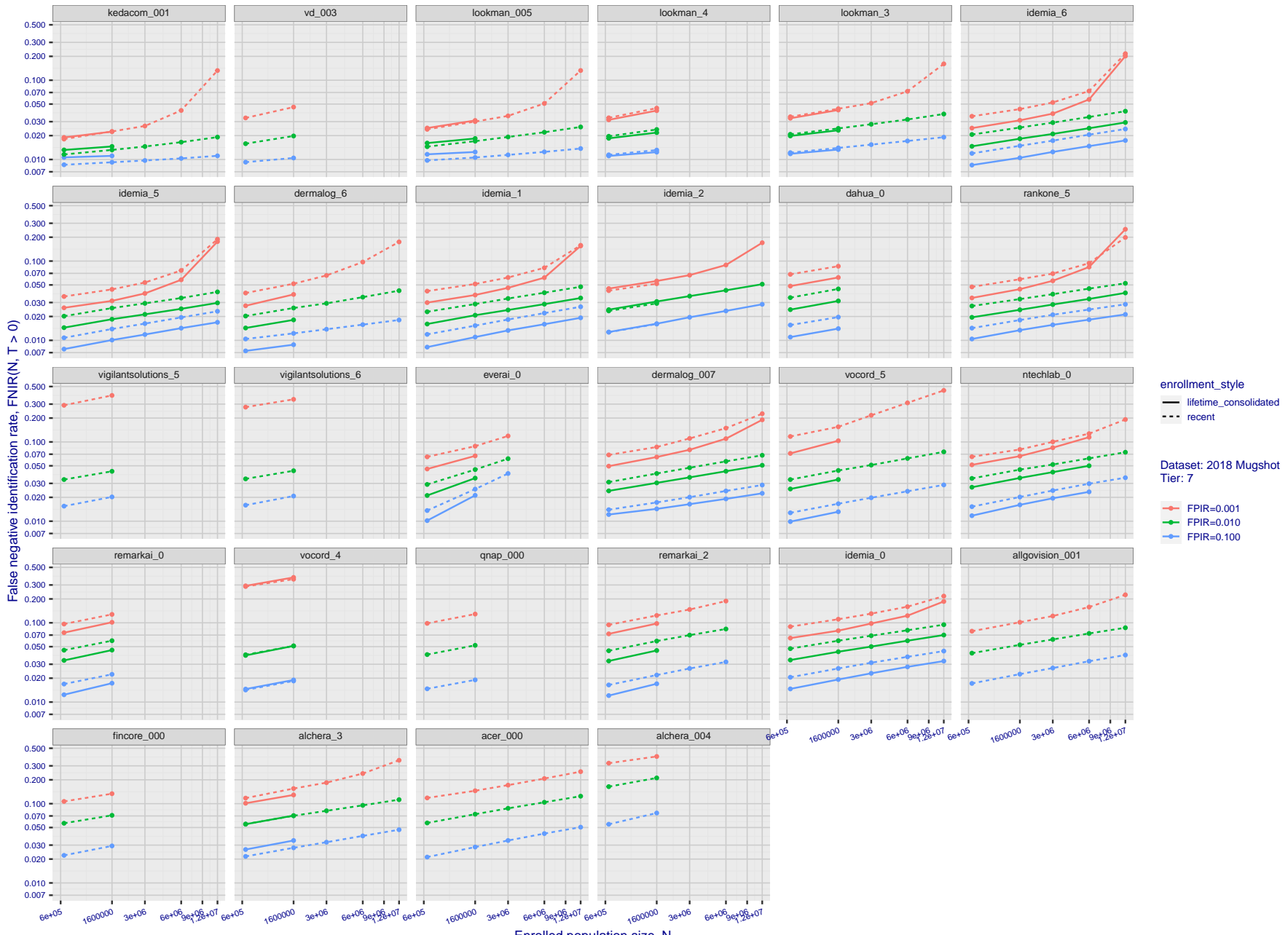
T = 0 → Investigation
T > 0 → Identification

Figure 42: [FRVT-2018 Mugshot Dataset] Threshold-based identification miss rates vs. number of enrolled subjects. The figure shows FNIR(N, T) across various gallery sizes when the threshold is set to achieve the given FPIRs. The rank criterion is irrelevant at high thresholds as mates are always at rank 1. The results are computed from the trials listed in rows 1-10 of Table 1. Less accurate algorithms were not run on large N, so results are missing. For clarity, results are sorted and reported into tiers spanning multiple pages. The tiering criteria is complicated: First paging by FNIR(N_b , 1, 0), then sorting by median FNIR(N_b , T), $N_b = 640\,000$.

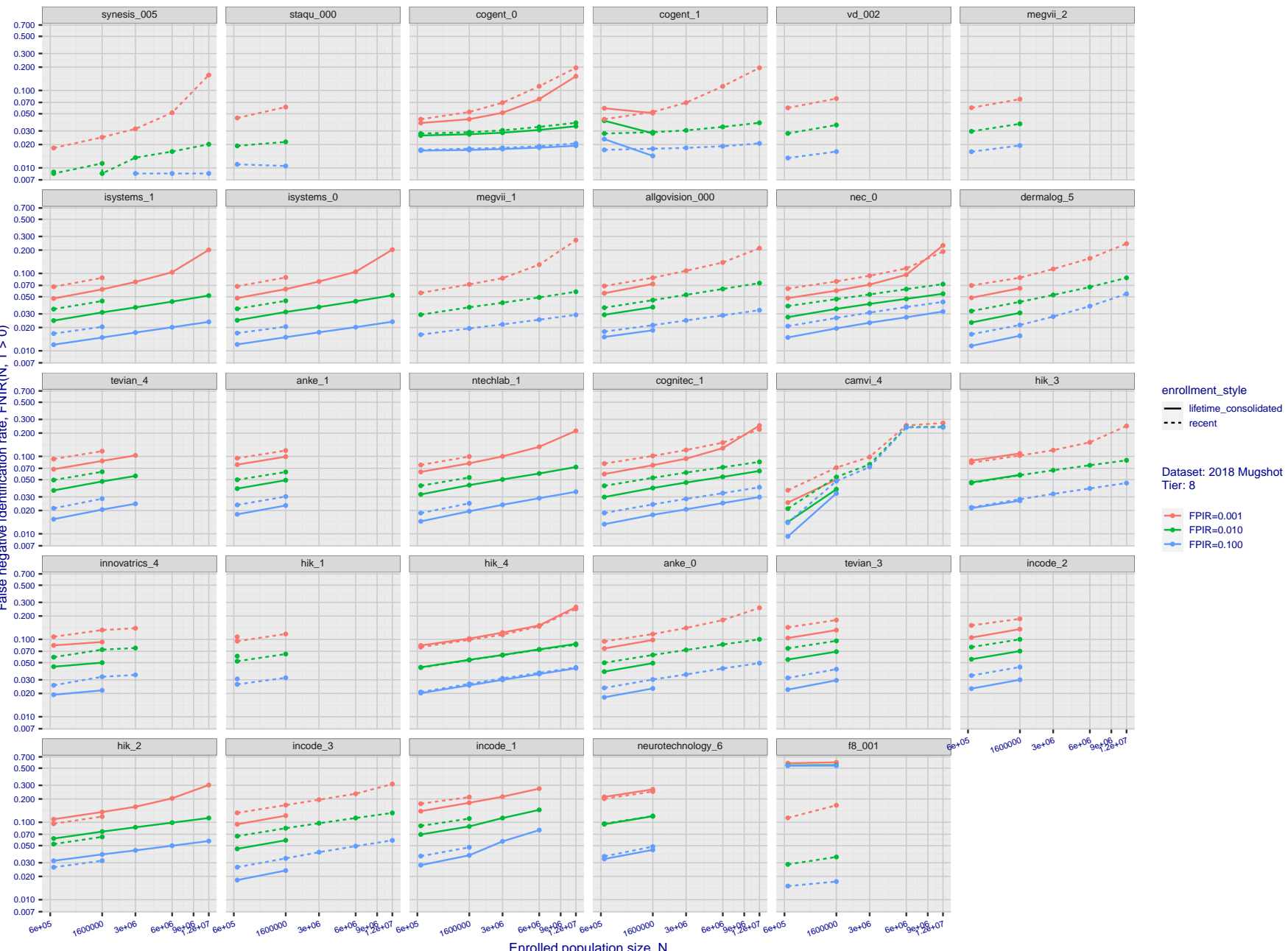
2022/03/30
17:50:48

Figure 43: [FRVT-2018 Mugshot Dataset] Threshold-based identification miss rates vs. number of enrolled subjects. The figure shows FNIR(N, T) across various gallery sizes when the threshold is set to achieve the given FPIRs. The rank criterion is irrelevant at high thresholds as mates are always at rank 1. The results are computed from the trials listed in rows 1-10 of Table 1. Less accurate algorithms were not run on large N , so results are missing. For clarity, results are sorted and reported into tiers spanning multiple pages. The tiering criteria is complicated: First paging by FNIR($N_b, 1, 0$), then sorting by median FNIR(N_b, T), $N_b = 640\,000$.

2022/03/
17:50:48

$FNI(N, K, T) = \text{False neg. identification rate}$
 $FPIR(N, T) = \text{False pos. identification rate}$

$N = \text{Num. enrolled subjects}$
 $R = \text{Num. candidates examined}$

N = Null. effited subjects
 R = Num. candidates examined

1
Introduction

$I = 0 \rightarrow$ Investigation
 $T > 0 \rightarrow$ Identification

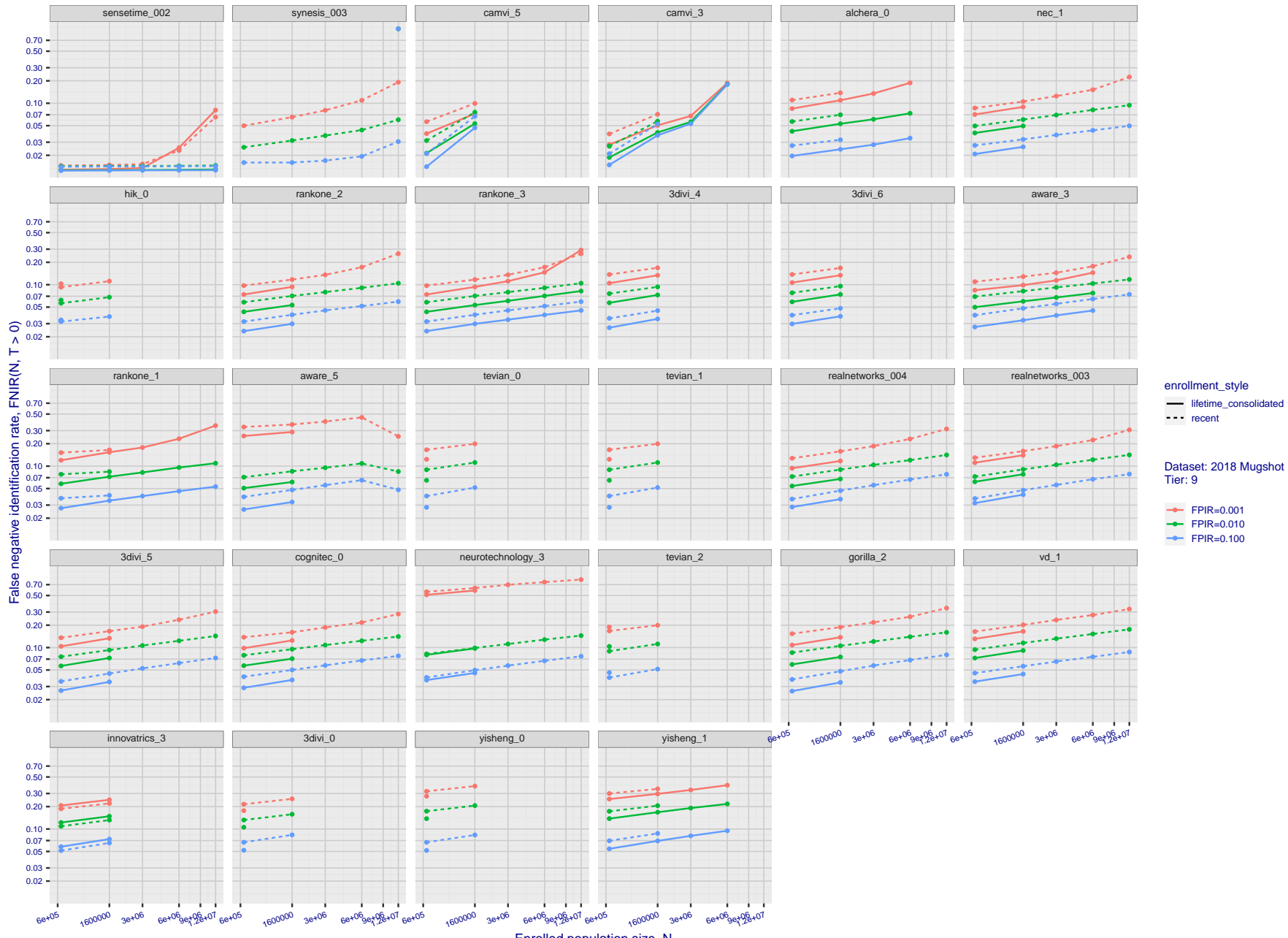


Figure 44: [FRVT-2018 Mugshot Dataset] Threshold-based identification miss rates vs. number of enrolled subjects. The figure shows FNIR(N, T) across various gallery sizes when the threshold is set to achieve the given FPIRs. The rank criterion is irrelevant at high thresholds as mates are always at rank 1. The results are computed from the trials listed in rows 1-10 of Table 1. Less accurate algorithms were not run on large N , so results are missing. For clarity, results are sorted and reported into tiers spanning multiple pages. The tiering criteria is complicated: First paging by $\text{FNIR}(N_b, 1, 0)$, then sorting by median $\text{FNIR}(N_b, T)$, $N_b = 640\,000$.

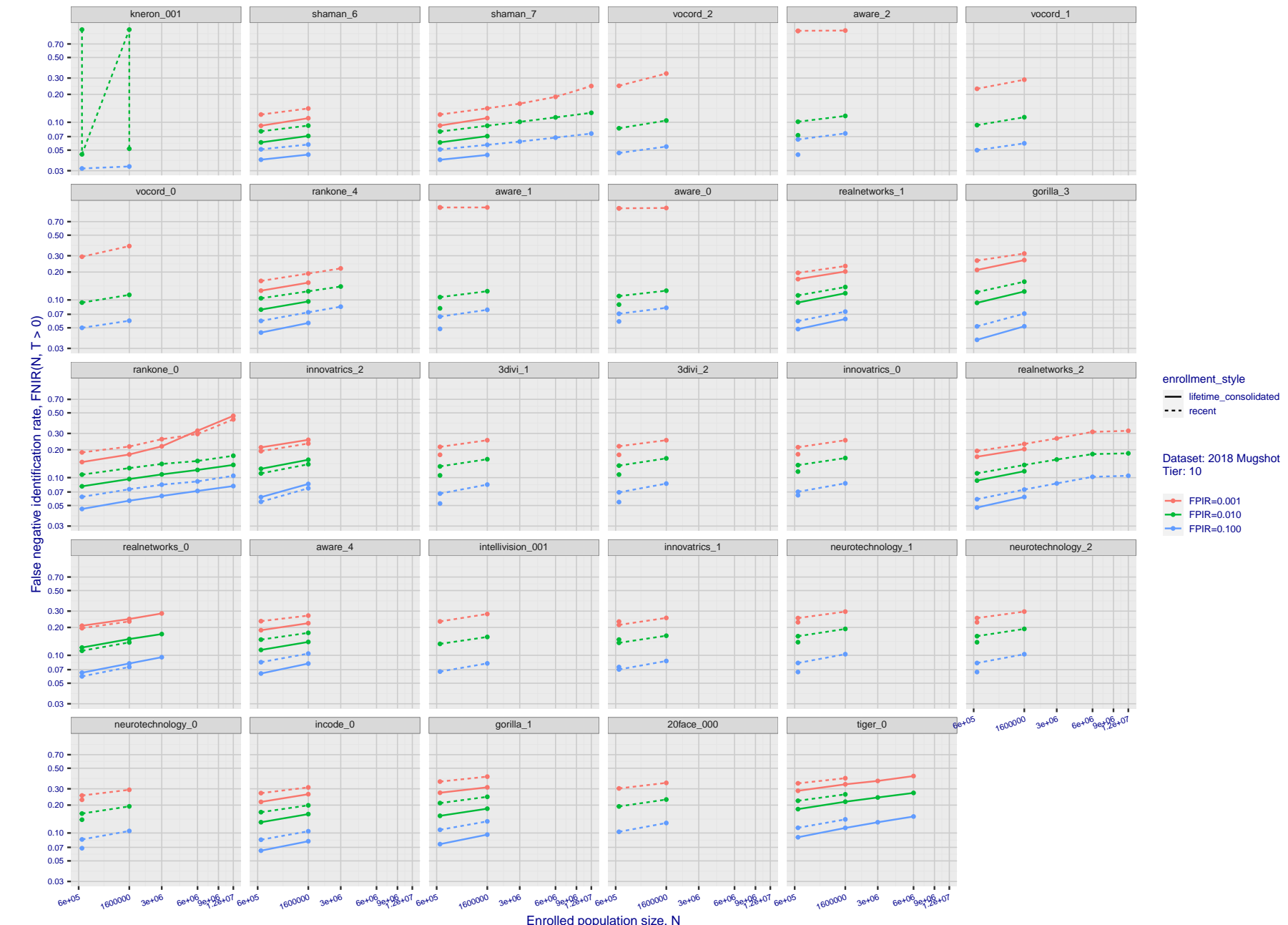


Figure 45: [FRVT-2018 Mugshot Dataset] Threshold-based identification miss rates vs. number of enrolled subjects. The figure shows $\text{FNIR}(N, T)$ across various gallery sizes when the threshold is set to achieve the given FPIRs. The rank criterion is irrelevant at high thresholds as mates are always at rank 1. The results are computed from the trials listed in rows 1-10 of Table 1. Less accurate algorithms were not run on large N , so results are missing. For clarity, results are sorted and reported into tiers spanning multiple pages. The tiering criteria is complicated: First paging by $\text{FNIR}(N_b, 1, 0)$, then sorting by median $\text{FNIR}(N_b, T)$, $N_b = 640\,000$.

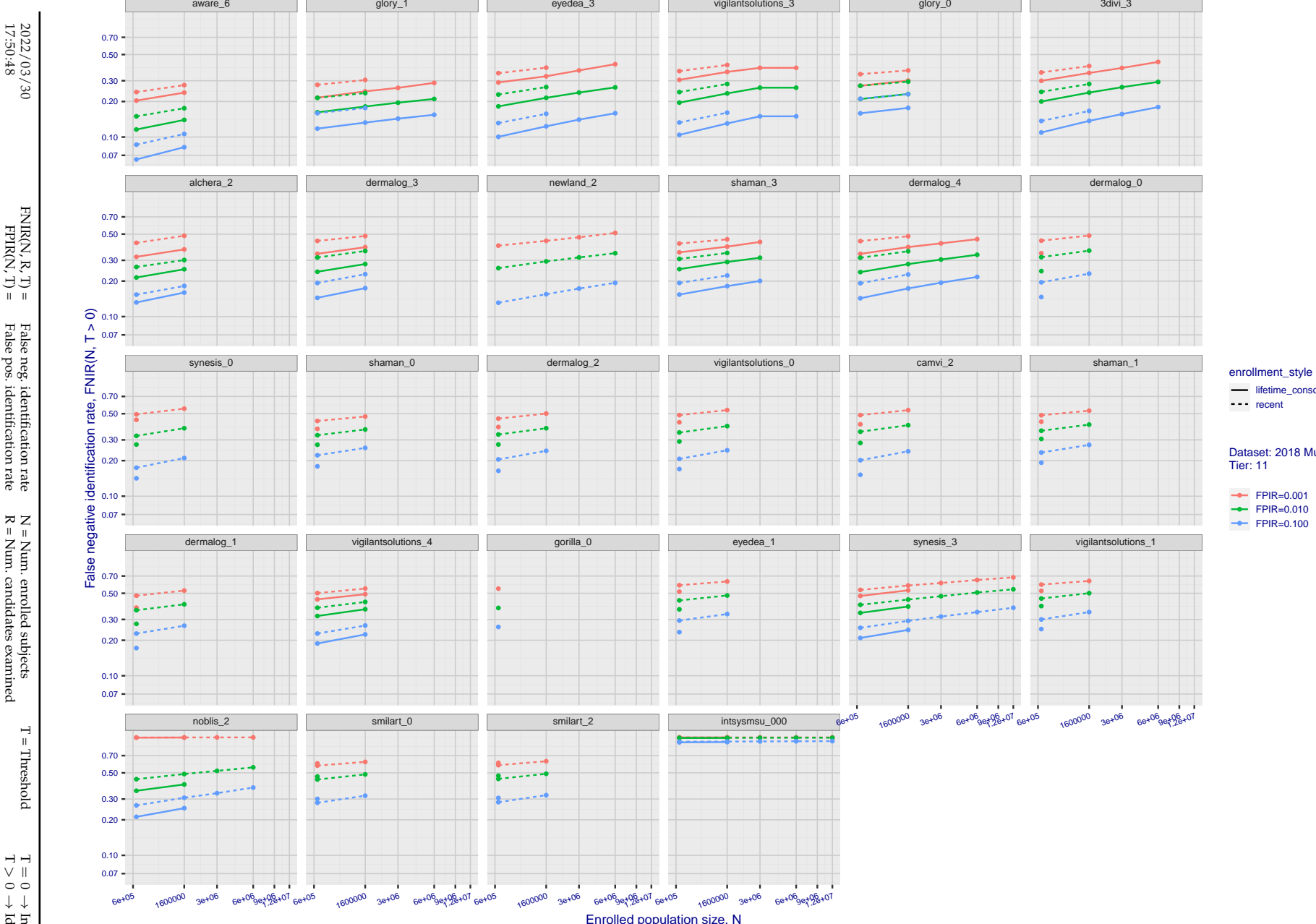


Figure 46: [FRVT-2018 Mugshot Dataset] Threshold-based identification miss rates vs. number of enrolled subjects. The figure shows $\text{FNIR}(N, T)$ across various gallery sizes when the threshold is set to achieve the given FPIRs. The rank criterion is irrelevant at high thresholds as mates are always at rank 1. The results are computed from the trials listed in rows 1-10 of Table 1. Less accurate algorithms were not run on large N , so results are missing. For clarity, results are sorted and reported into tiers spanning multiple pages. The tiering criteria is complicated: First paging by $\text{FNIR}(N_b, 1, 0)$, then sorting by median $\text{FNIR}(N_b, T)$, $N_b = 640\,000$.

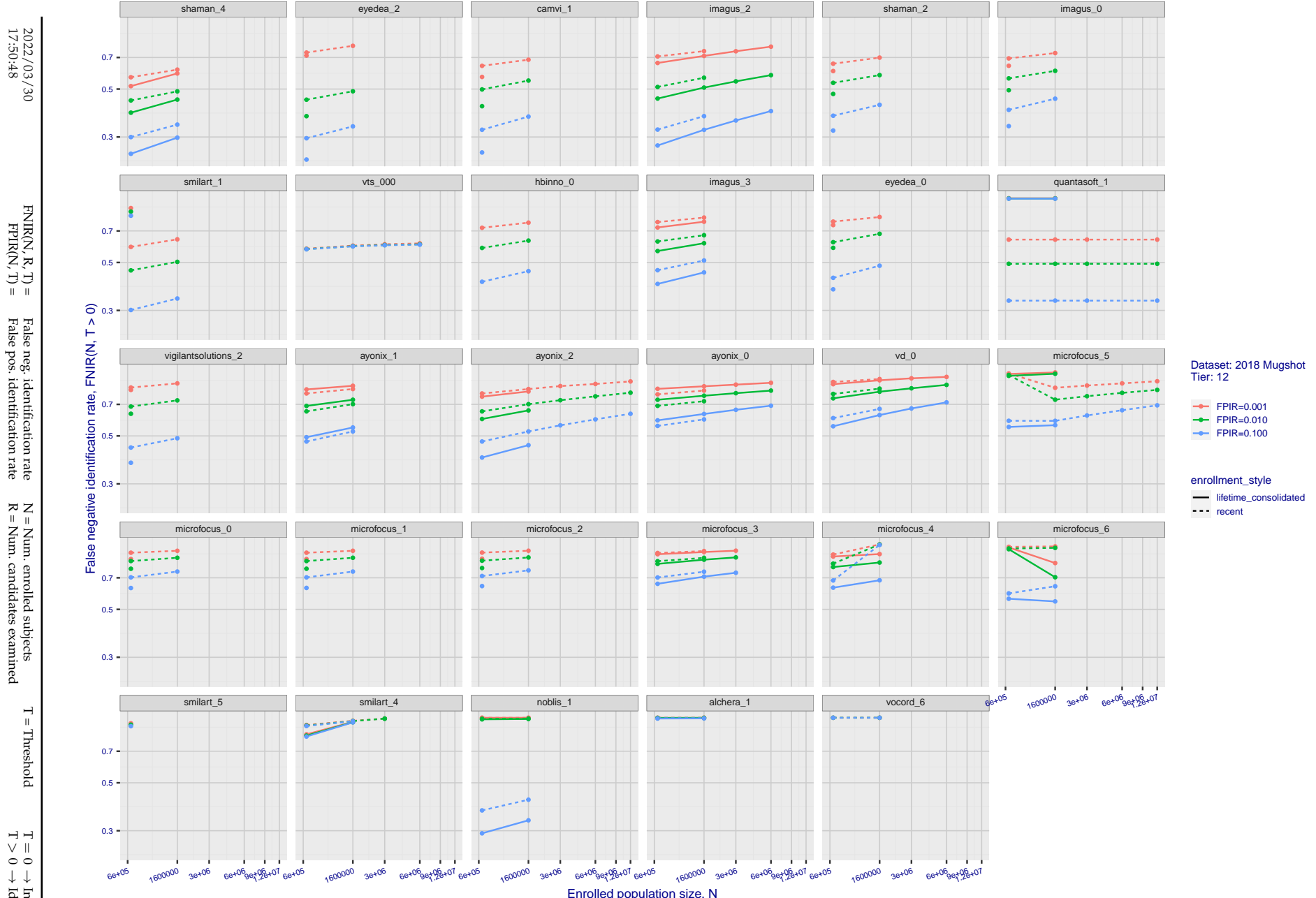


Figure 47: [FRVT-2018 Mugshot Dataset] Threshold-based identification miss rates vs. number of enrolled subjects. The figure shows FNIR(N, T) across various gallery sizes when the threshold is set to achieve the given FPIRs. The rank criterion is irrelevant at high thresholds as mates are always at rank 1. The results are computed from the trials listed in rows 1-10 of Table 1. Less accurate algorithms were not run on large N, so results are missing. For clarity, results are sorted and reported into tiers spanning multiple pages. The tiering criteria is complicated: First paging by FNIR(N_b , 1, 0), then sorting by median FNIR(N_b , T), $N_b = 640\,000$.

2022/03/30 17:50:48	FNIR(N, R, T) = FPTR(N, T) =	False neg. identification rate False pos. identification rate	N = Num. enrolled subjects R = Num. candidates examined	T = Threshold	T = 0 → Investigation T > 0 → Identification
------------------------	---------------------------------	--	--	---------------	---

2022/03/30
17:50:48FNIR(N, R, T) = False neg. identification rate
FPIR(N, T) = False pos. identification rate
N = Num. enrolled subjects
R = Num. candidates examined

T = Threshold

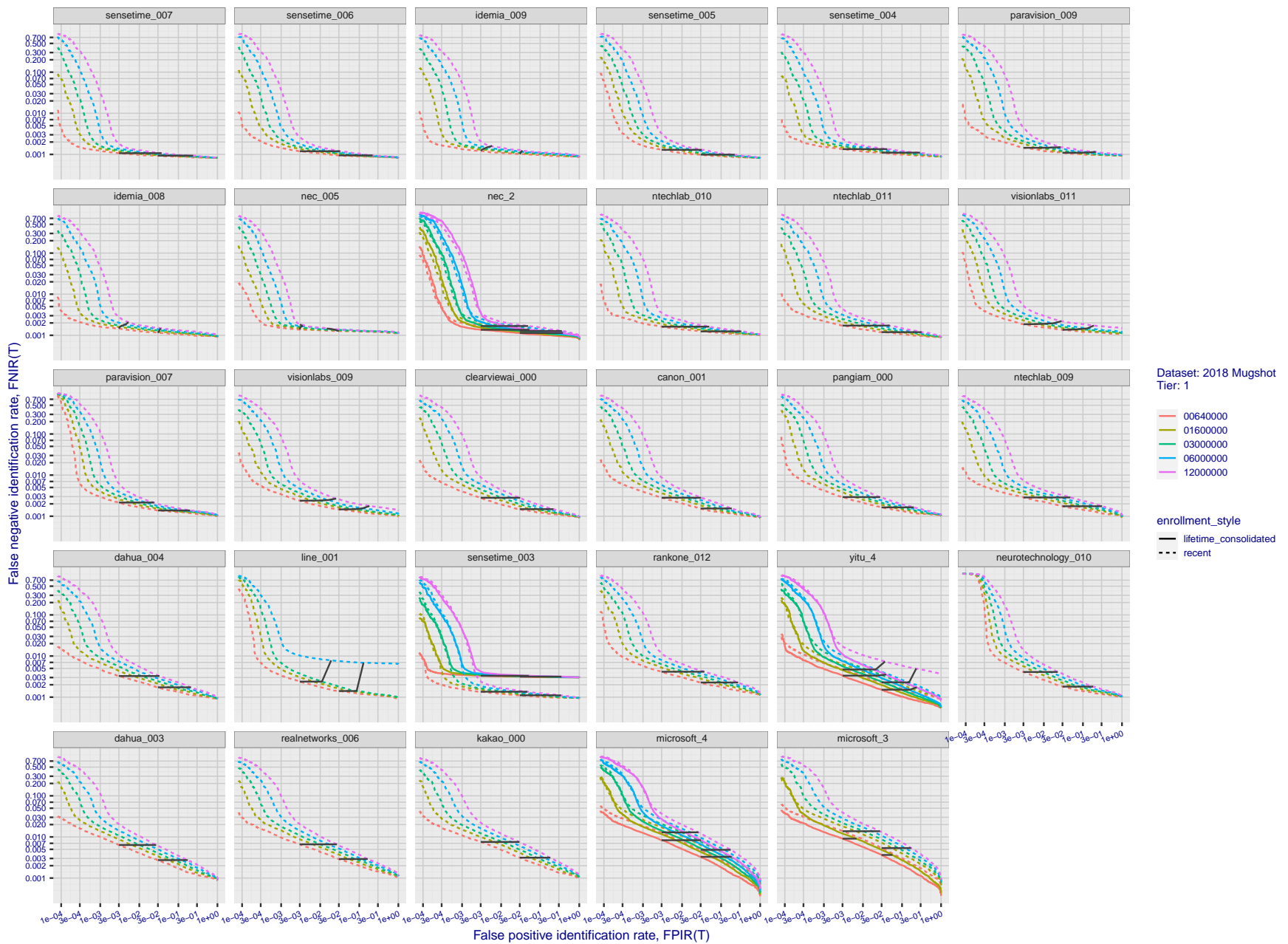
T = 0 → Investigation
 $T > 0 \rightarrow$ Identification

Figure 48: [FRVT-2018 Mugshot Dataset] Identification miss rates vs. false positive rates. The figure shows miss rates $\text{FNIR}(N, L, T)$ as a function of $\text{FPIR}(N, T)$, with N ranging from 640 000 to 12 000 000 as noted in rows 1-10 of Table 1. These error tradeoff characteristics are useful for applications where a threshold must be elevated to limit false positives, such as when human reviewer labor is not matched to the volume of searches. Dark lines join points of equal threshold: If horizontal, $\text{FPIR}(T)$ rises with N , and mate scores are independent of N . Other algorithms adjust scores in an attempt to make FPIR independent of N .

2022 /03 /30
17:50:48FNIR(N, R, T) = False neg. identification rate
FPIR(N, T) = False pos. identification rateN = Num. enrolled subjects
R = Num. candidates examined

T = Threshold

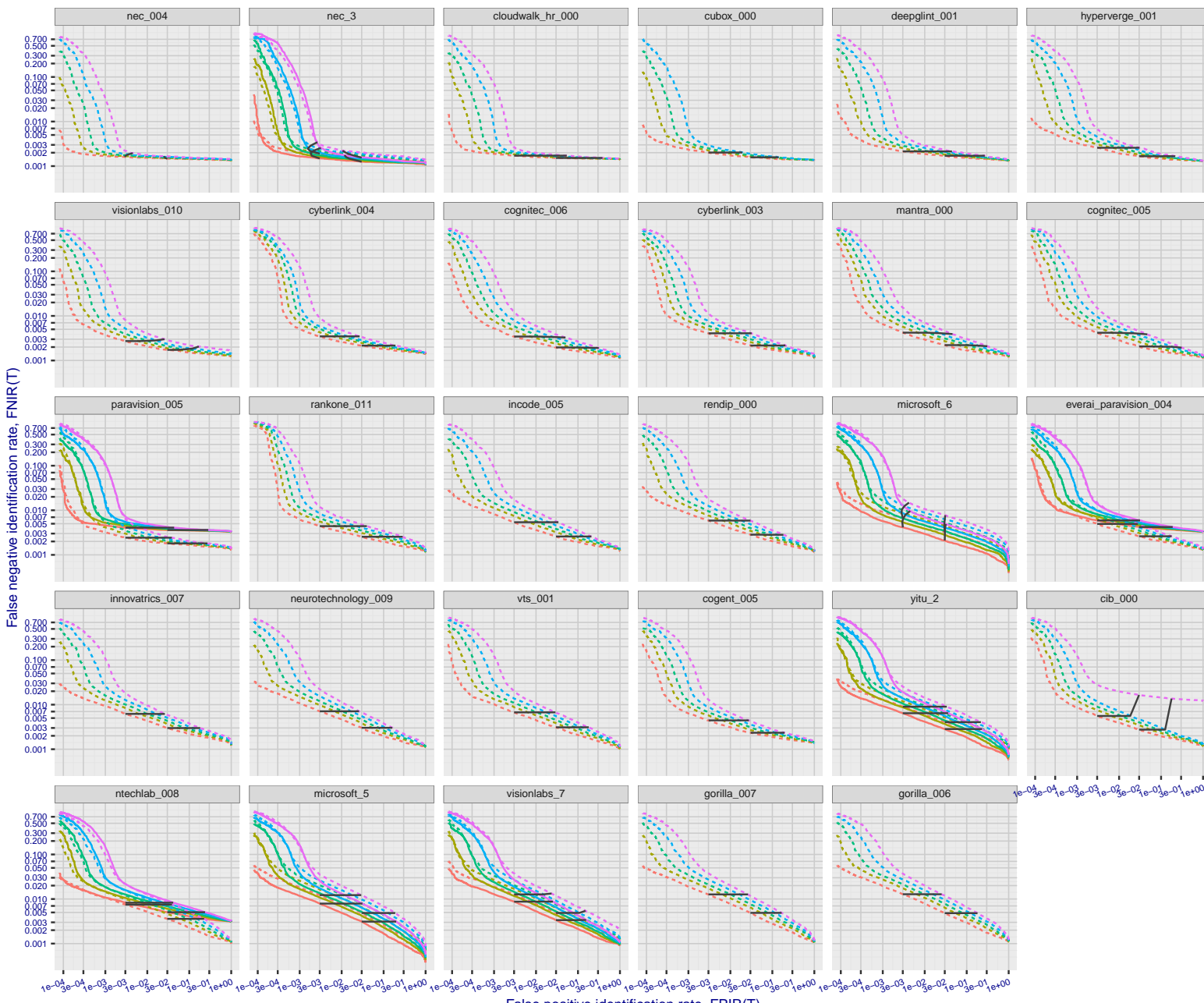
T = 0 → Investigation
 $T > 0 \rightarrow$ Identification

Figure 49: [FRVT-2018 Mugshot Dataset] Identification miss rates vs. false positive rates. The figure shows miss rates $\text{FNIR}(N, L, T)$ as a function of $\text{FPIR}(N, T)$, with N ranging from 640 000 to 12 000 000 as noted in rows 1-10 of Table 1. These error tradeoff characteristics are useful for applications where a threshold must be elevated to limit false positives, such as when human reviewer labor is not matched to the volume of searches. Dark lines join points of equal N . If horizontal, $\text{FPIR}(T)$ rises with N , and mate scores are independent of N . Other algorithms adjust scores in an attempt to make FPIR independent of N .

2022 /03 /30
17:50:48FNIR(N, R, T) = False neg. identification rate
FPIR(N, T) = False pos. identification rateN = Num. enrolled subjects
R = Num. candidates examined

T = Threshold

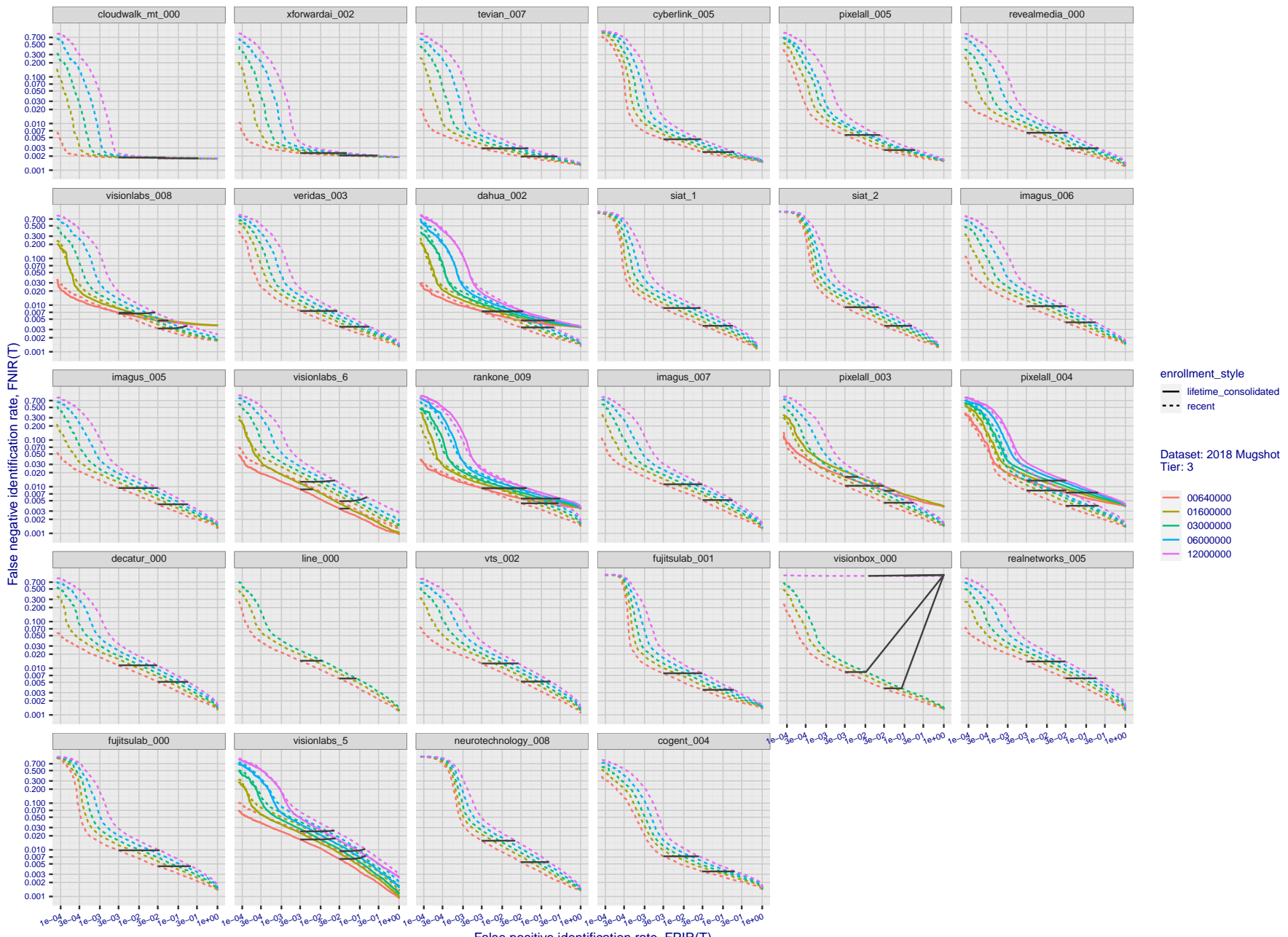
T = 0 → Investigation
 $T > 0 \rightarrow$ Identification

Figure 50: [FRVT-2018 Mugshot Dataset] Identification miss rates vs. false positive rates. The figure shows miss rates $\text{FNIR}(N, L, T)$ as a function of $\text{FPIR}(N, T)$, with N ranging from 640 000 to 12 000 000 as noted in rows 1-10 of Table 1. These error tradeoff characteristics are useful for applications where a threshold must be elevated to limit false positives, such as when human reviewer labor is not matched to the volume of searches. Dark lines join points of equal N . If horizontal, $\text{FPIR}(T)$ rises with N , and mate scores are independent of N . Other algorithms adjust scores in an attempt to make FPIR independent of N .

2022 /03 /30
17:50:48

 $\text{FNIR}(N, R, T) =$
 $\text{False neg. identification rate}$
 $\text{FPIR}(N, T) =$
 $\text{False pos. identification rate}$
 $N = \text{Num. enrolled subjects}$
 $R = \text{Num. candidates examined}$
 $T = \text{Threshold}$
 $T = 0 \rightarrow \text{Investigation}$
 $T > 0 \rightarrow \text{Identification}$

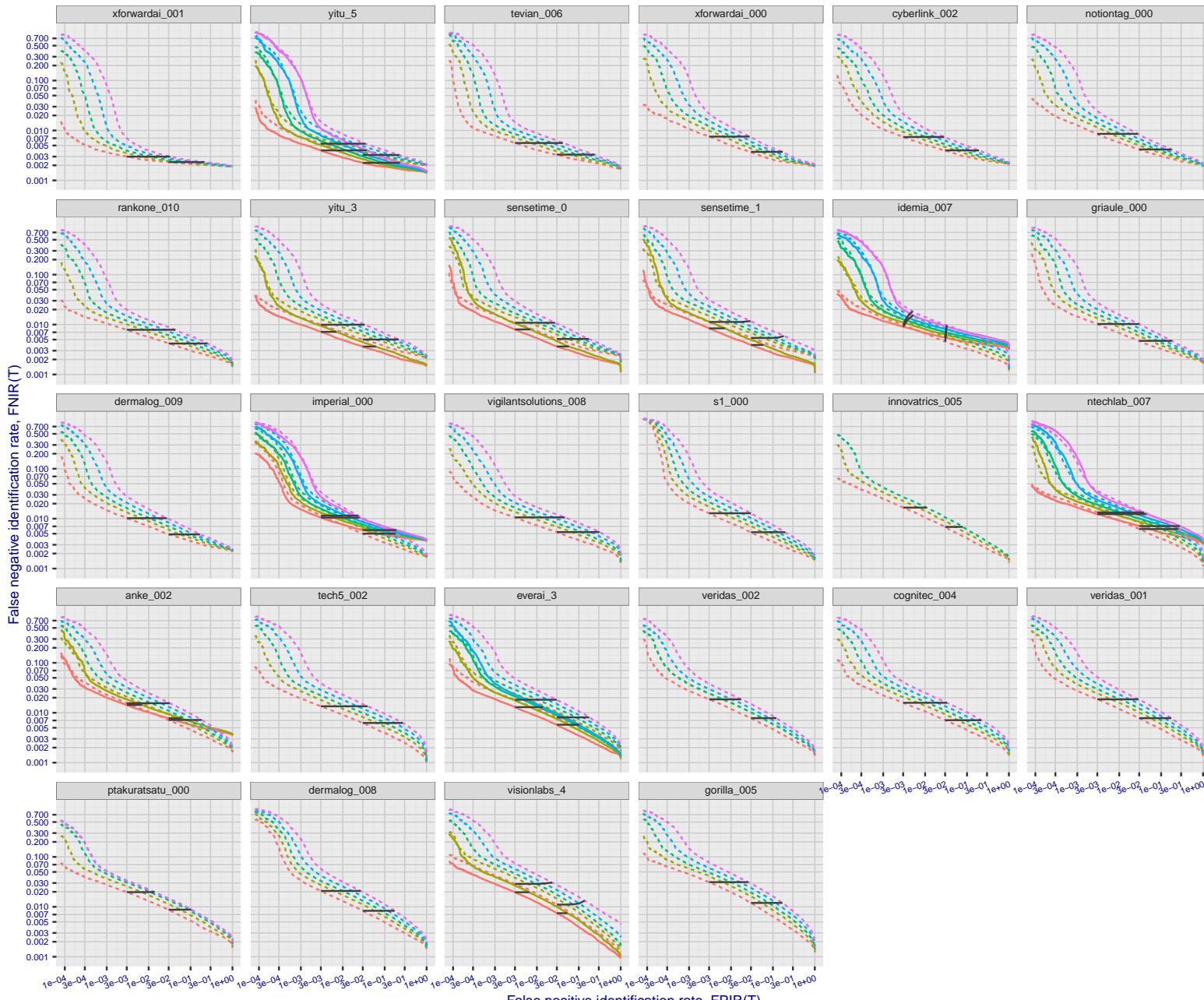


Figure 51: [FRVT-2018 Mugshot Dataset] Identification miss rates vs. false positive rates. The figure shows miss rates $\text{FNIR}(N, L, T)$ as a function of $\text{FPIR}(N, T)$, with N ranging from 640 000 to 12 000 000 as noted in rows 1-10 of Table 1. These error tradeoff characteristics are useful for applications where a threshold must be elevated to limit false positives, such as when human reviewer labor is not matched to the volume of searches. Dark lines join points of equal threshold: If horizontal, $\text{FPIR}(T)$ rises with N , and mate scores are independent of N . Other algorithms adjust scores in an attempt to make FPIR independent of N .

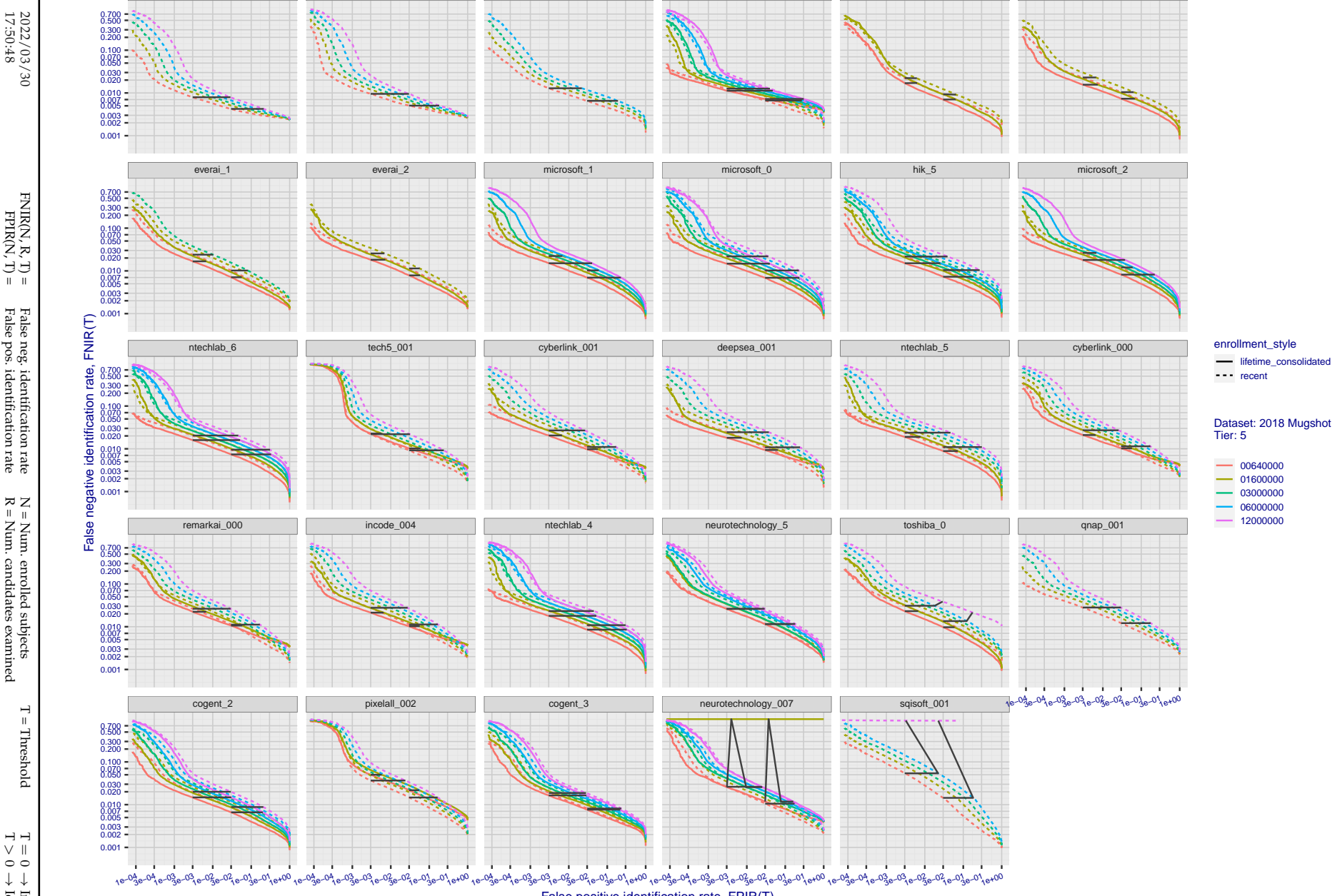


Figure 52: [FRVT-2018 Mugshot Dataset] Identification miss rates vs. false positive rates. The figure shows miss rates $\text{FNIR}(N, L, T)$ as a function of $\text{FPIR}(N, T)$, with N ranging from 640 000 to 12 000 000 as noted in rows 1-10 of Table 1. These error tradeoff characteristics are useful for applications where a threshold must be elevated to limit false positives, such as when human reviewer labor is not matched to the volume of searches. Dark lines join points of equal threshold: If horizontal, $\text{FPIR}(T)$ rises with N , and mate scores are independent of N . Other algorithms adjust scores in an attempt to make FPIR independent of N .

2022 /03 /30
17:50:48FNIR(N, R, T) = False neg. identification rate
FPIR(N, T) = False pos. identification rateN = Num. enrolled subjects
R = Num. candidates examined

T = Threshold

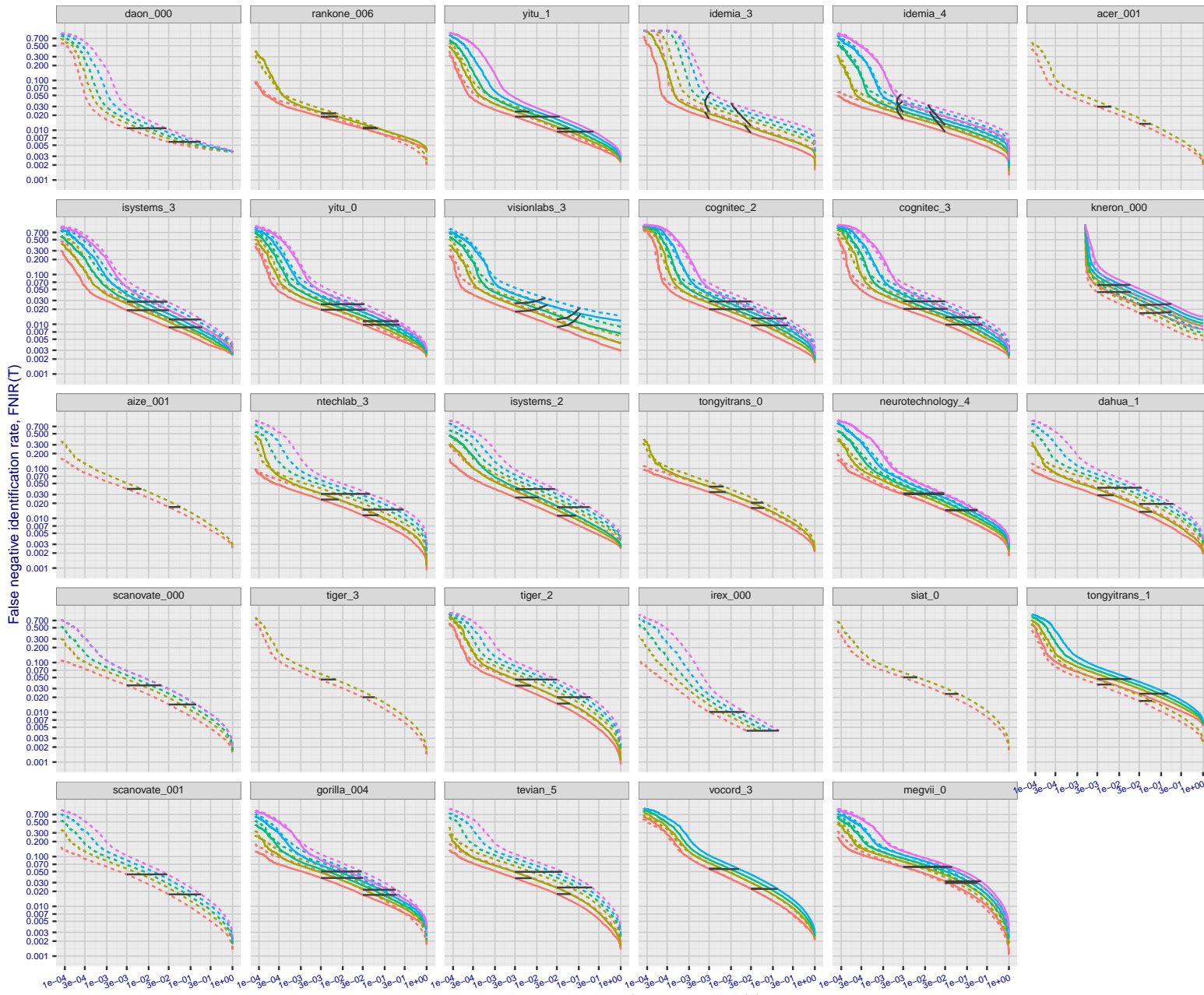
T = 0 → Investigation
 $T > 0 \rightarrow$ Identification

Figure 53: [FRVT-2018 Mugshot Dataset] Identification miss rates vs. false positive rates. The figure shows miss rates $\text{FNIR}(N, L, T)$ as a function of $\text{FPIR}(N, T)$, with N ranging from 640 000 to 12 000 000 as noted in rows 1-10 of Table 1. These error tradeoff characteristics are useful for applications where a threshold must be elevated to limit false positives, such as when human reviewer labor is not matched to the volume of searches. Dark lines join points of equal threshold: If horizontal, $\text{FPIR}(T)$ rises with N , and mate scores are independent of N . Other algorithms adjust scores in an attempt to make FPIR independent of N .

2022 /03 /30
17:50:48FNIR(N, R, T) = False neg. identification rate
FPIR(N, T) = False pos. identification rate
N = Num. enrolled subjects
R = Num. candidates examined

T = Threshold

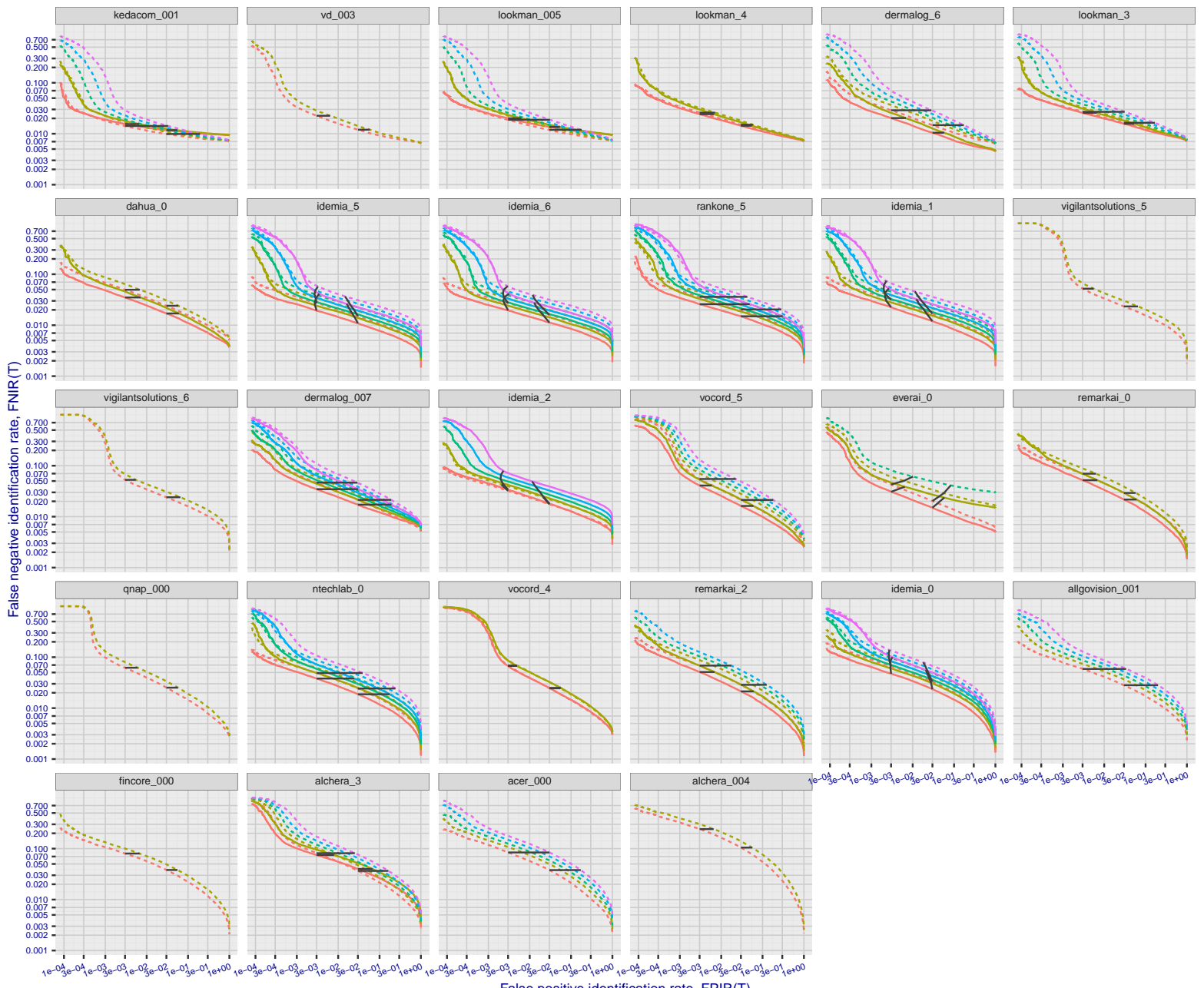
T = 0 → Investigation
 $T > 0 \rightarrow$ Identification

Figure 54: [FRVT-2018 Mugshot Dataset] Identification miss rates vs. false positive rates. The figure shows miss rates $\text{FNIR}(N, L, T)$ as a function of $\text{FPIR}(N, T)$, with N ranging from 640 000 to 12 000 000 as noted in rows 1-10 of Table 1. These error tradeoff characteristics are useful for applications where a threshold must be elevated to limit false positives, such as when human reviewer labor is not matched to the volume of searches. Dark lines join points of equal threshold: If horizontal, $\text{FPIR}(T)$ rises with N , and mate scores are independent of N . Other algorithms adjust scores in an attempt to make FPIR independent of N .

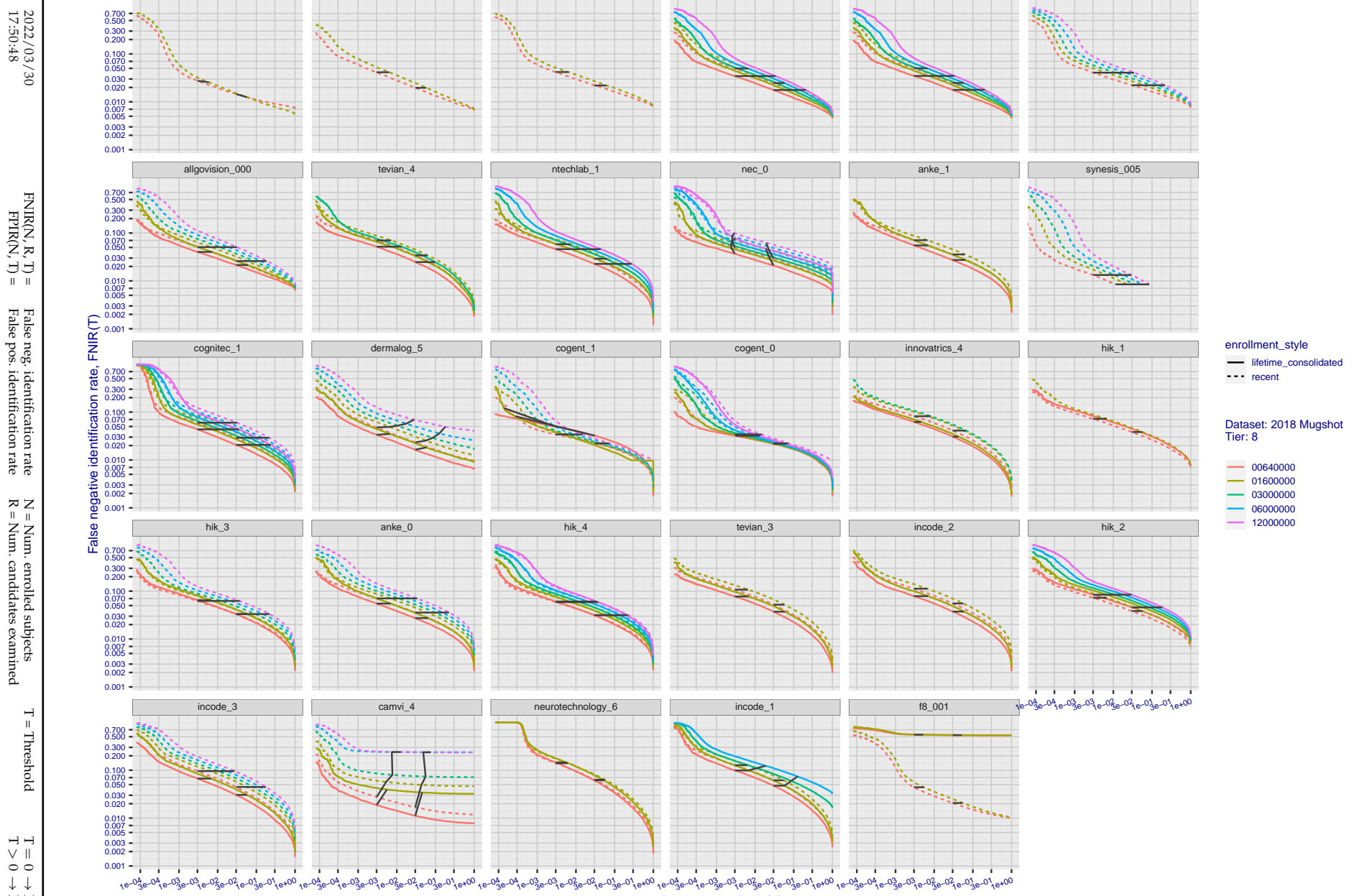


Figure 55: [FRVT-2018 Mugshot Dataset] Identification miss rates vs. false positive rates. The figure shows miss rates $\text{FNIR}(N, L, T)$ as a function of $\text{FPIR}(N, T)$, with N ranging from 640 000 to 12 000 000 as noted in rows 1-10 of Table 1. These error tradeoff characteristics are useful for applications where a threshold must be elevated to limit false positives, such as when human reviewer labor is not matched to the volume of searches. Dark lines join points of equal threshold: If horizontal, $\text{FPIR}(T)$ rises with N , and mate scores are independent of N . Other algorithms adjust scores in an attempt to make FPIR independent of N .

2022/03/30

FNIR(N, R, T) = False neg. identification rate
FPIR(N, T) = False pos. identification rateN = Num. enrolled subjects
R = Num. candidates examined

T = Threshold

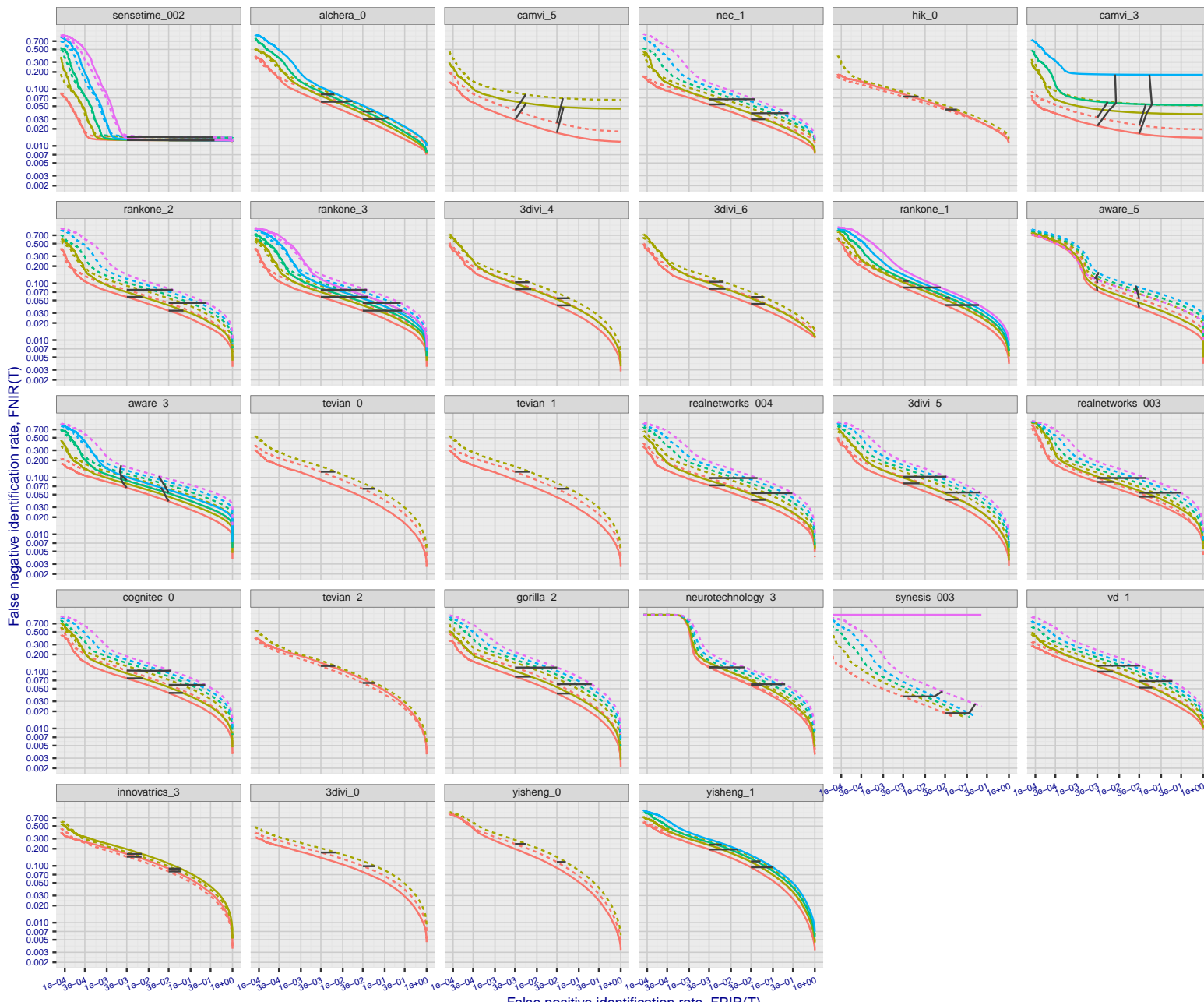
T = 0 → Investigation
T > 0 → Identification

Figure 56: [FRVT-2018 Mugshot Dataset] Identification miss rates vs. false positive rates. The figure shows miss rates $\text{FNIR}(N, L, T)$ as a function of $\text{FPIR}(N, T)$, with N ranging from 64 000 to 12 000 000 as noted in rows 1-10 of Table 1. These error tradeoff characteristics are useful for applications where a threshold must be elevated to limit false positives, such as when human reviewer labor is not matched to the volume of searches. Dark lines join points of equal N . Other algorithms adjust scores in an attempt to make FPIR independent of N .

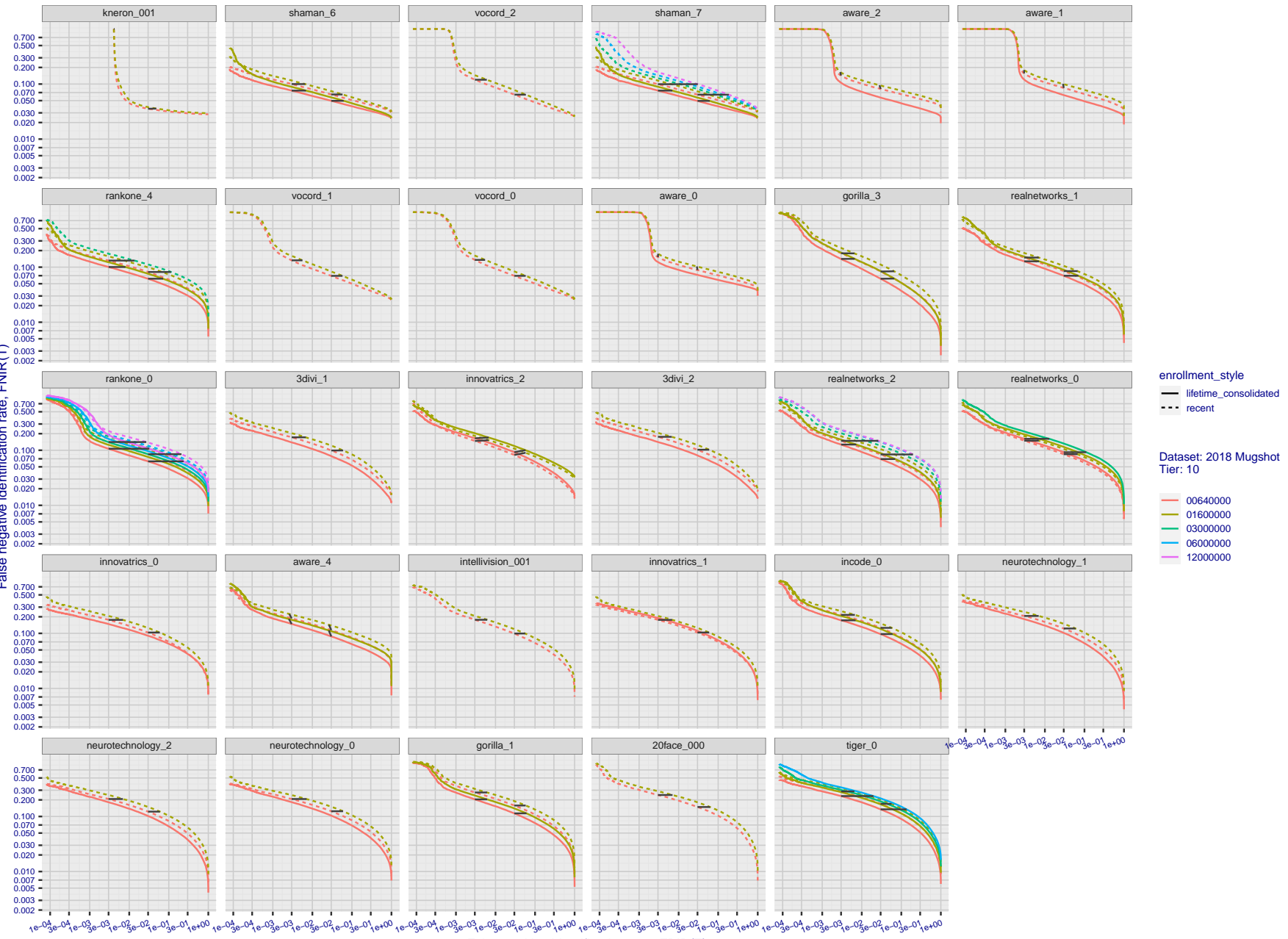
2022/03/30
17:50:48FNIR(N, R, T) = False neg. identification rate
FPIR(N, T) = False pos. identification rate
N = Num. enrolled subjects
R = Num. candidates examinedT = Threshold
T = 0 → Investigation
T > 0 → Identification

Figure 57: [FRVT-2018 Mugshot Dataset] Identification miss rates vs. false positive rates. The figure shows miss rates $\text{FNIR}(N, L, T)$ as a function of $\text{FPIR}(N, T)$, with N ranging from 640 000 to 12 000 000 as noted in rows 1-10 of Table 1. These error tradeoff characteristics are useful for applications where a threshold must be elevated to limit false positives, such as when human reviewer labor is not matched to the volume of searches. Dark lines join points of equal threshold: If horizontal, $\text{FPIR}(T)$ rises with N , and mate scores are independent of N . Other algorithms adjust scores in an attempt to make FPIR independent of N .

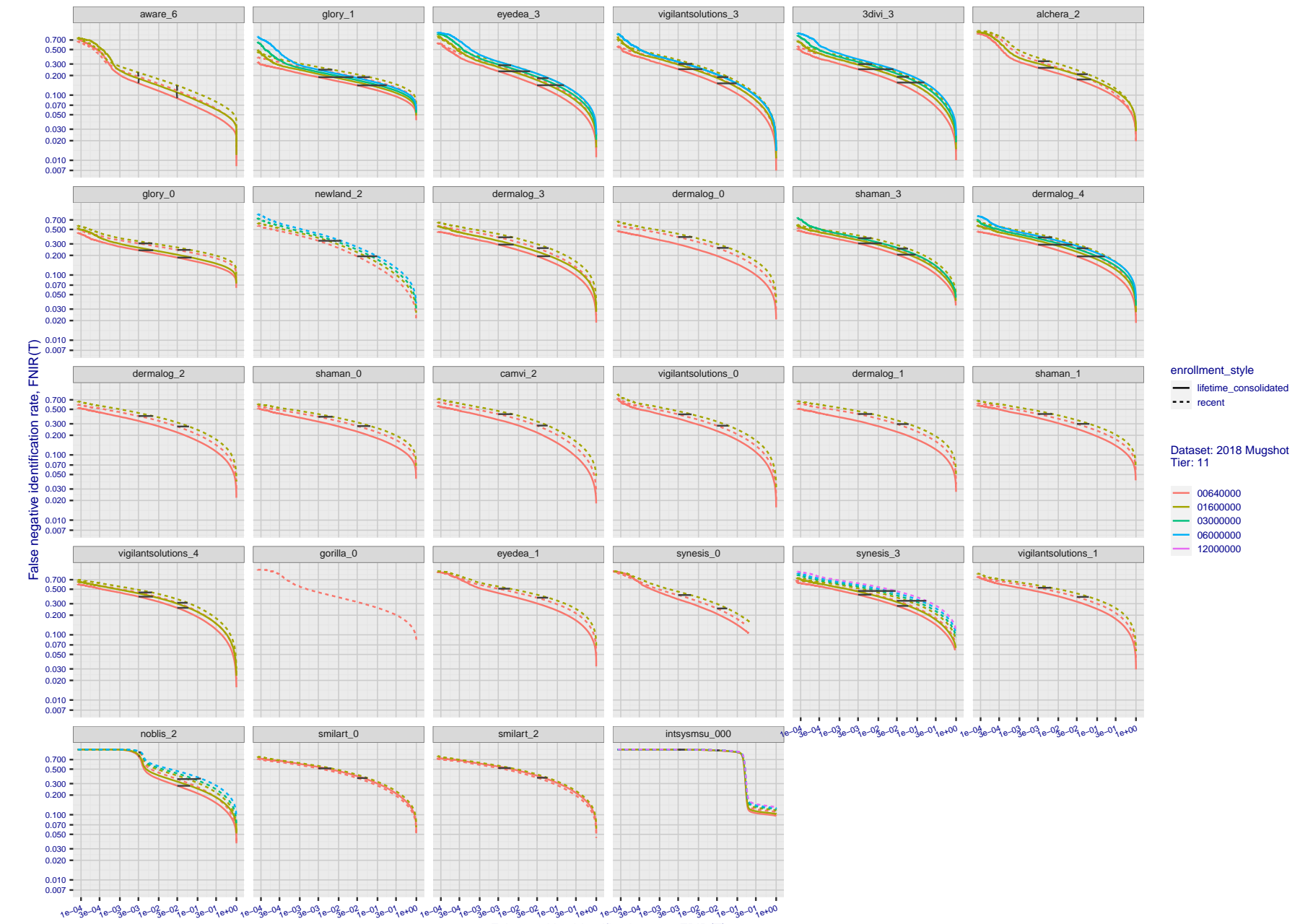


Figure 58: [FRVT-2018 Mugshot Dataset] Identification miss rates vs. false positive rates. The figure shows miss rates $\text{FNIR}(N, L, T)$ as a function of $\text{FPIR}(N, T)$, with N ranging from 640 000 to 12 000 000 as noted in rows 1-10 of Table 1. These error tradeoff characteristics are useful for applications where a threshold must be elevated to limit false positives, such as when human reviewer labor is not matched to the volume of searches. Dark lines join points of equal threshold: If horizontal, $\text{FPIR}(T)$ rises with N , and mate scores are independent of N . Other algorithms adjust scores in an attempt to make FPIR independent of N .

2022/03/30
17:50:48FNIR(N, R, T) = False neg. identification rate
FPIR(N, T) = False pos. identification rate
N = Num. enrolled subjects
R = Num. candidates examined

T = Threshold

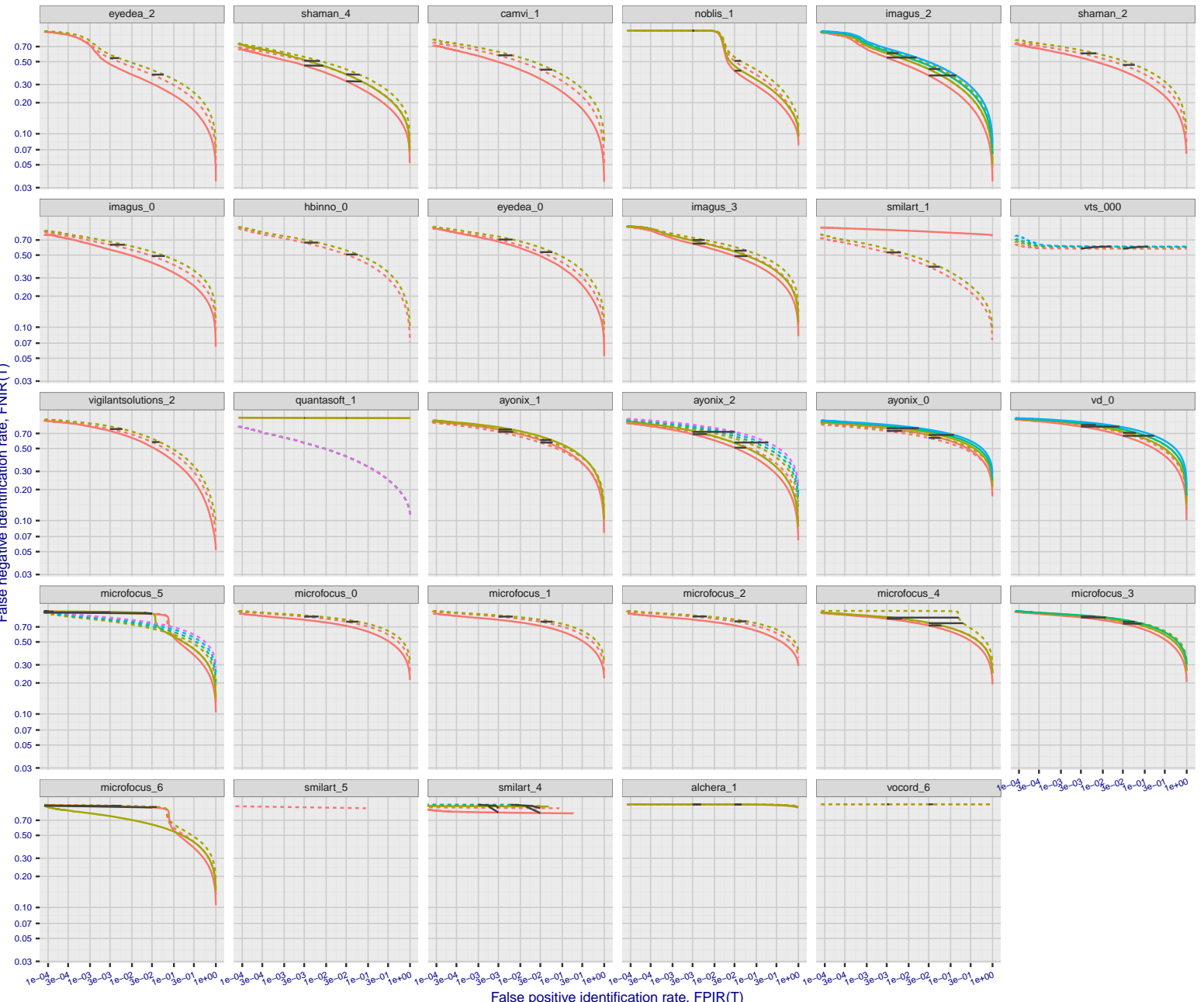
T = 0 → Investigation
T > 0 → Identification

Figure 59: [FRVT-2018 Mugshot Dataset] Identification miss rates vs. false positive rates. The figure shows miss rates $\text{FNIR}(N, L, T)$ as a function of $\text{FPIR}(N, T)$, with N ranging from 640 000 to 12 000 000 as noted in rows 1-10 of Table 1. These error tradeoff characteristics are useful for applications where a threshold must be elevated to limit false positives, such as when human reviewer labor is not matched to the volume of searches. Dark lines join points of equal threshold: If horizontal, $\text{FPIR}(T)$ rises with N , and mate scores are independent of N . Other algorithms adjust scores in an attempt to make FPIR independent of N .

Appendix B Effect of time-lapse: Accuracy after face ageing

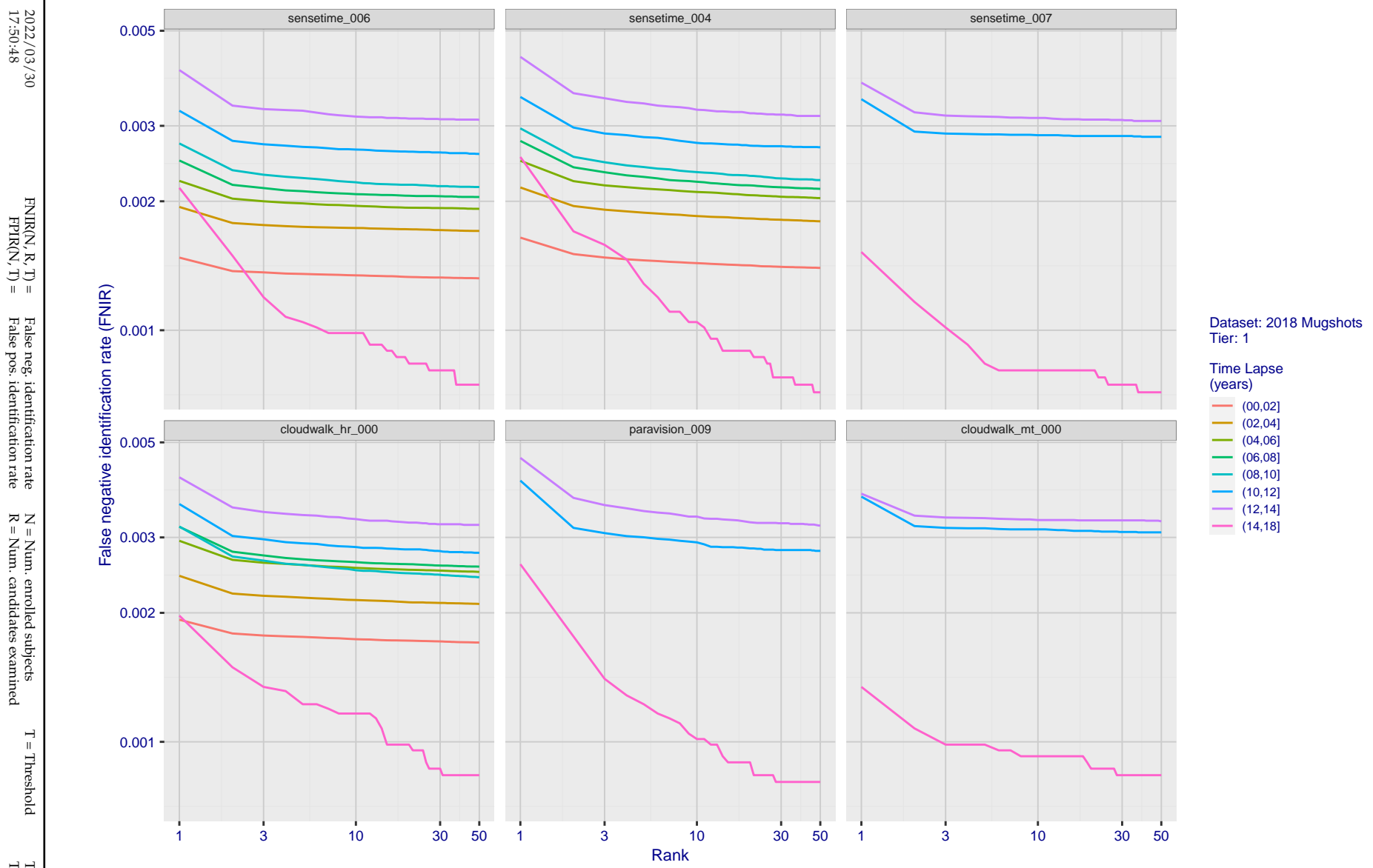


Figure 60: [FRVT-2018 Mugshot Ageing Dataset] Identification miss rates vs. rank by time-elapsed. The oldest image of each individual is enrolled. Thereafter, all more recent images are searched. Miss rates are computed over all searches noted in row 17 of Table 1 and binned by number of years between search and initial enrollment.

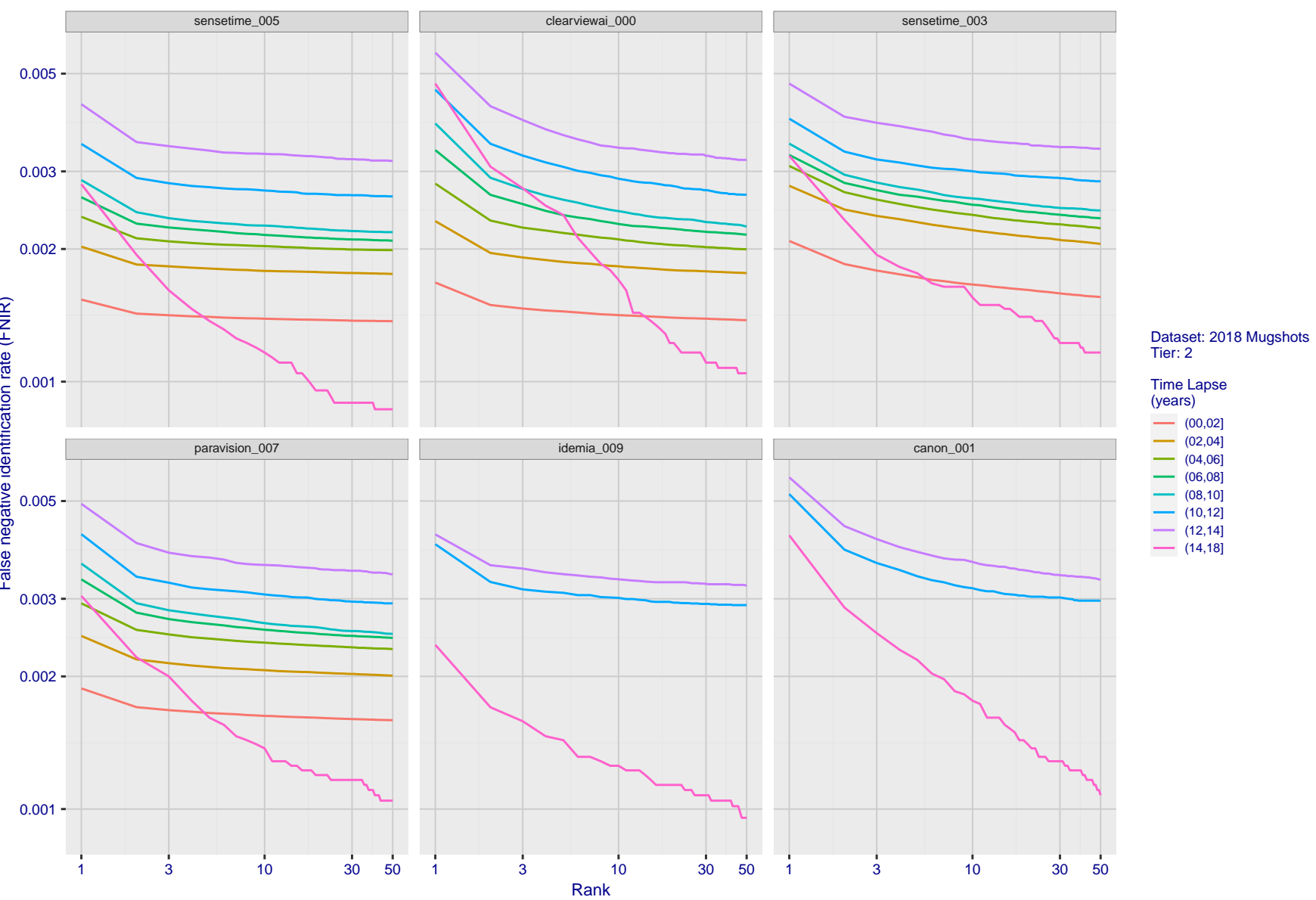
2022/03/30
17:50:48

Figure 61: [FRVT-2018 Mugshot Ageing Dataset] Identification miss rates vs. rank by time-elapsed. The oldest image of each individual is enrolled. Thereafter, all more recent images are searched. Miss rates are computed over all searches noted in row 17 of Table 1 and binned by number of years between search and initial enrollment.

2022/03/30
17:50:48FNIR(N, R, T) = False neg. identification rate
FPIR(N, T) = False pos. identification rateN = Num. enrolled subjects
R = Num. candidates examinedT = Threshold
T = 0 → Investigation

T > 0 → Identification

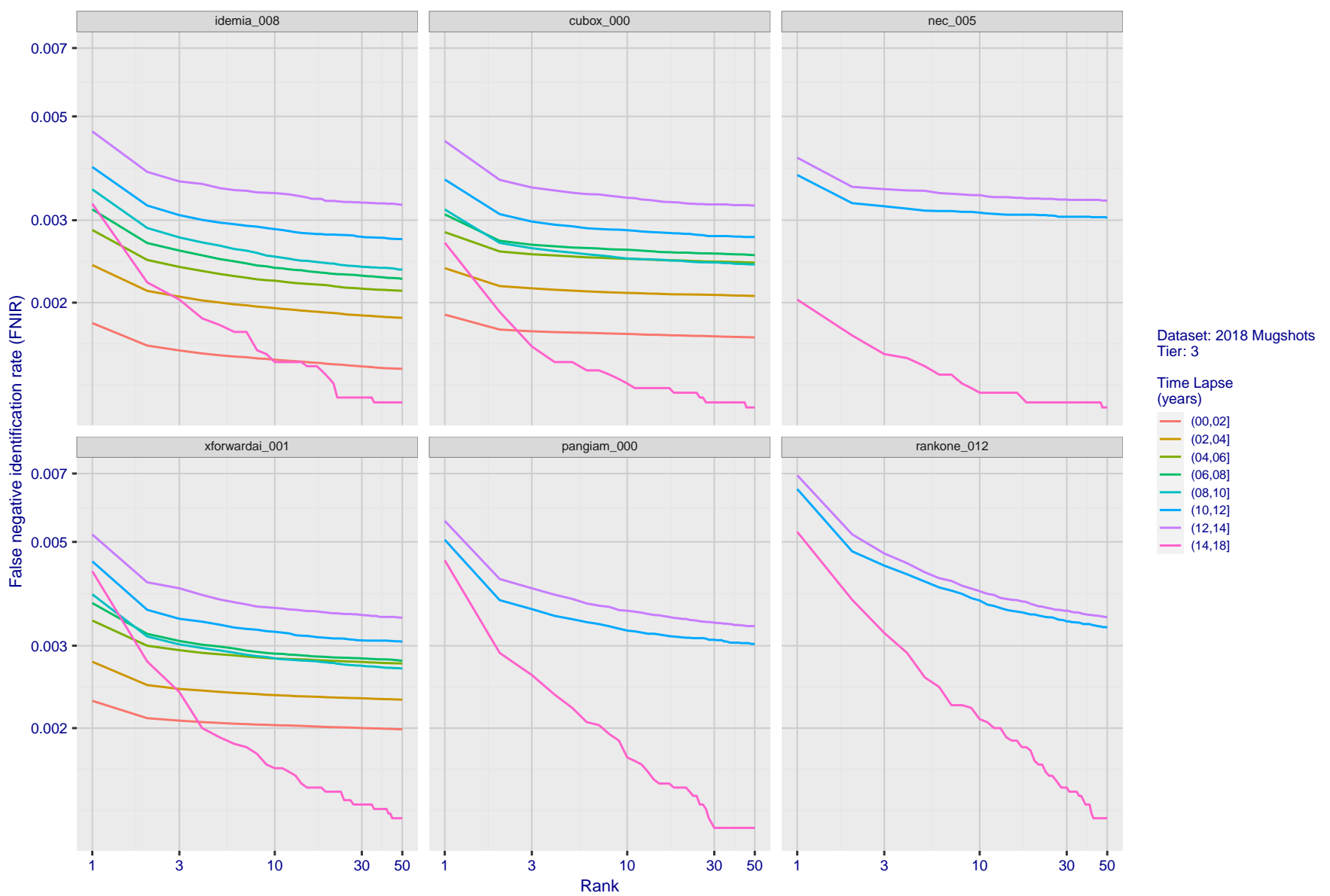


Figure 62: [FRVT-2018 Mugshot Ageing Dataset] Identification miss rates vs. rank by time elapsed. The oldest image of each individual is enrolled. Thereafter, all more recent images are searched. Miss rates are computed over all searches noted in row 17 of Table 1 and binned by number of years between search and initial enrollment.

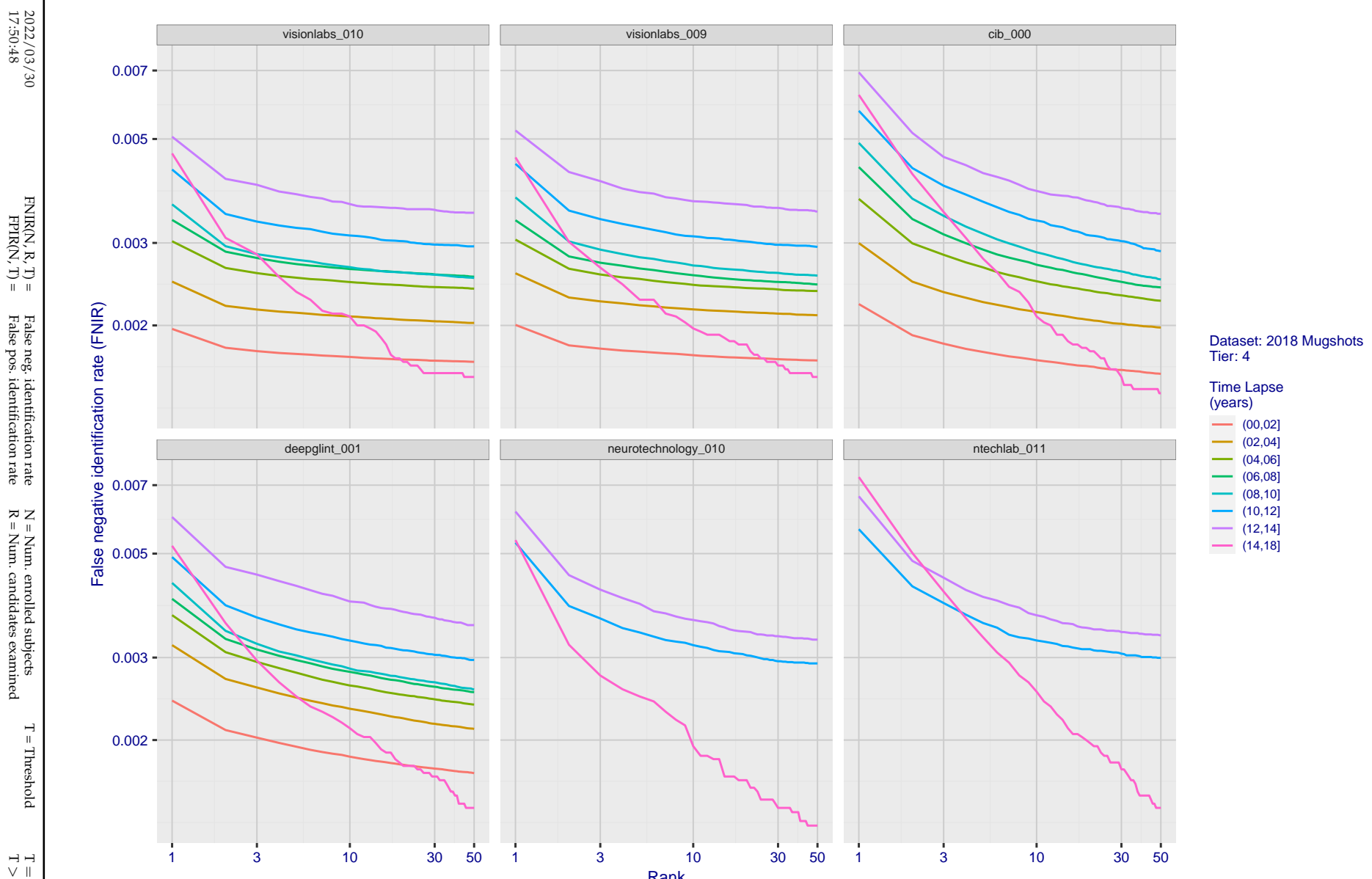


Figure 63: [FRVT-2018 Mugshot Ageing Dataset] Identification miss rates vs. rank by time-elapsed. The oldest image of each individual is enrolled. Thereafter, all more recent images are searched. Miss rates are computed over all searches noted in row 17 of Table 1 and binned by number of years between search and initial enrollment.

2022/03/30
17:50:48FNIR(N, R, T) = False neg. identification rate
FPIR(N, T) = False pos. identification rateN = Num. enrolled subjects
R = Num. candidates examined

T = Threshold

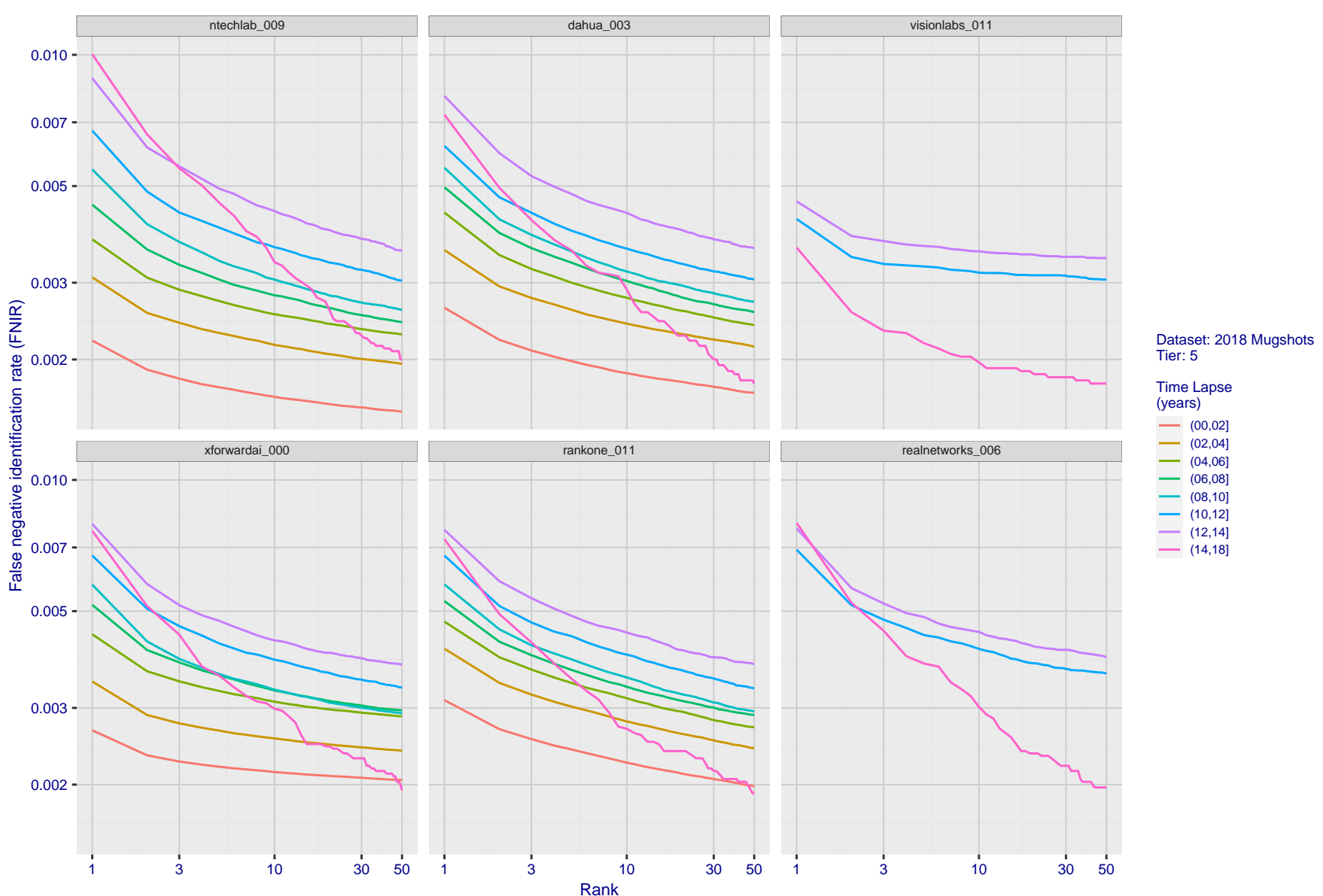
T = 0 → Investigation
T > 0 → Identification

Figure 64: [FRVT-2018 Mugshot Ageing Dataset] Identification miss rates vs. rank by time-elapsed. The oldest image of each individual is enrolled. Thereafter, all more recent images are searched. Miss rates are computed over all searches noted in row 17 of Table 1 and binned by number of years between search and initial enrollment.

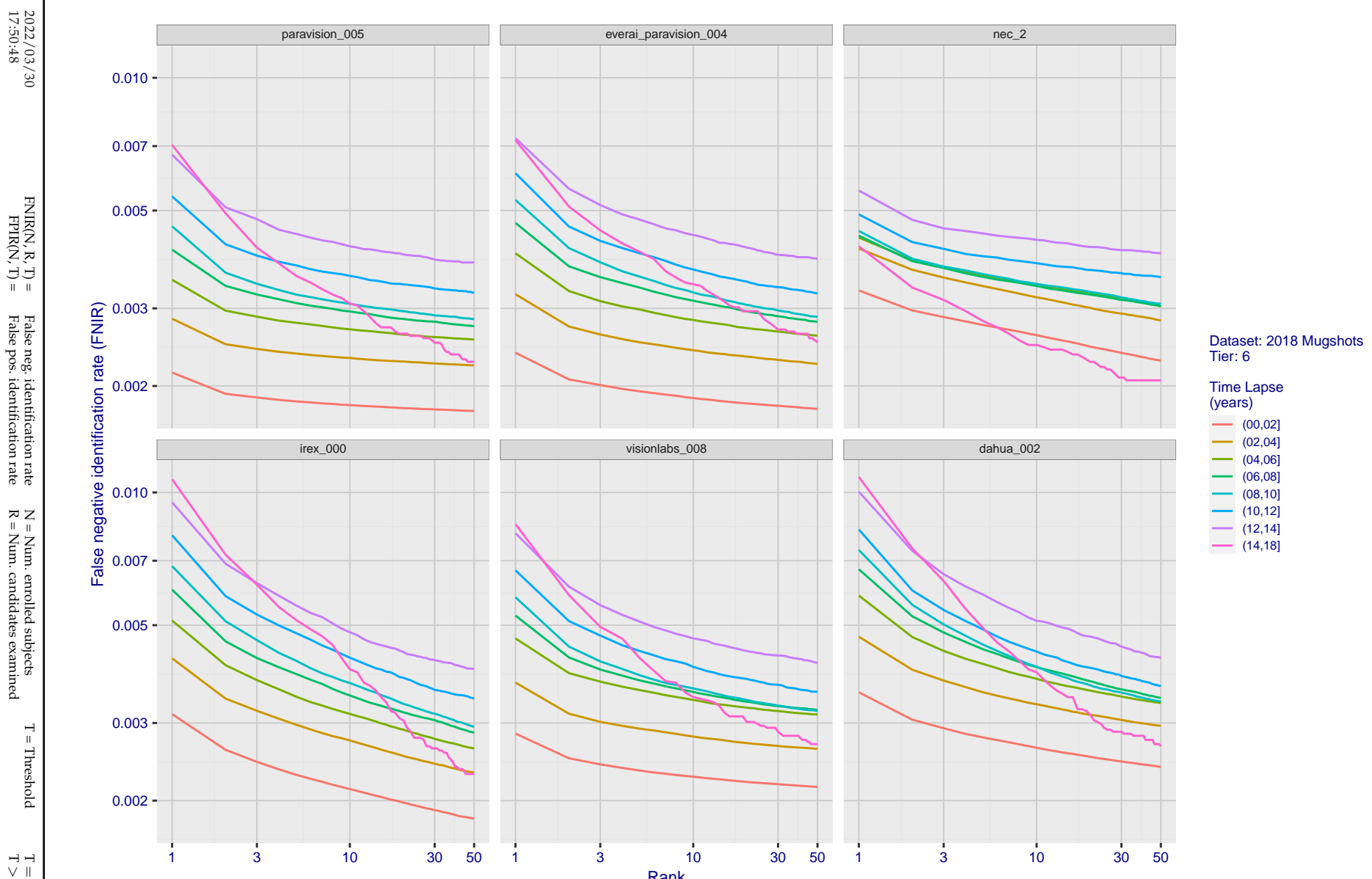


Figure 65: [FRVT-2018 Mugshot Ageing Dataset] Identification miss rates vs. rank by time-elapsed. The oldest image of each individual is enrolled. Thereafter, all more recent images are searched. Miss rates are computed over all searches noted in row 17 of Table 1 and binned by number of years between search and initial enrollment.

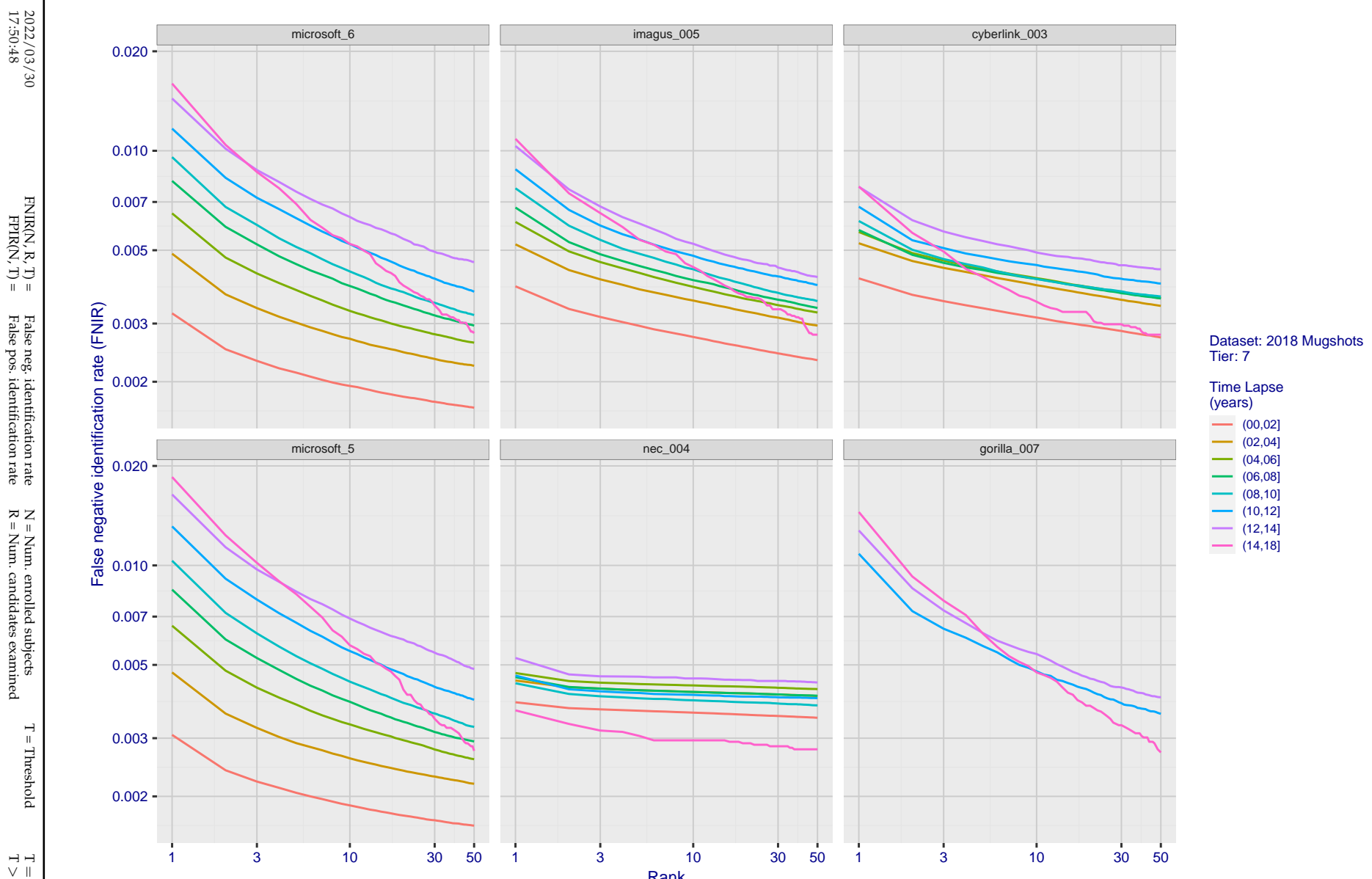


Figure 66: [FRVT-2018 Mugshot Ageing Dataset] Identification miss rates vs. rank by time-elapsed. The oldest image of each individual is enrolled. Thereafter, all more recent images are searched. Miss rates are computed over all searches noted in row 17 of Table 1 and binned by number of years between search and initial enrollment.

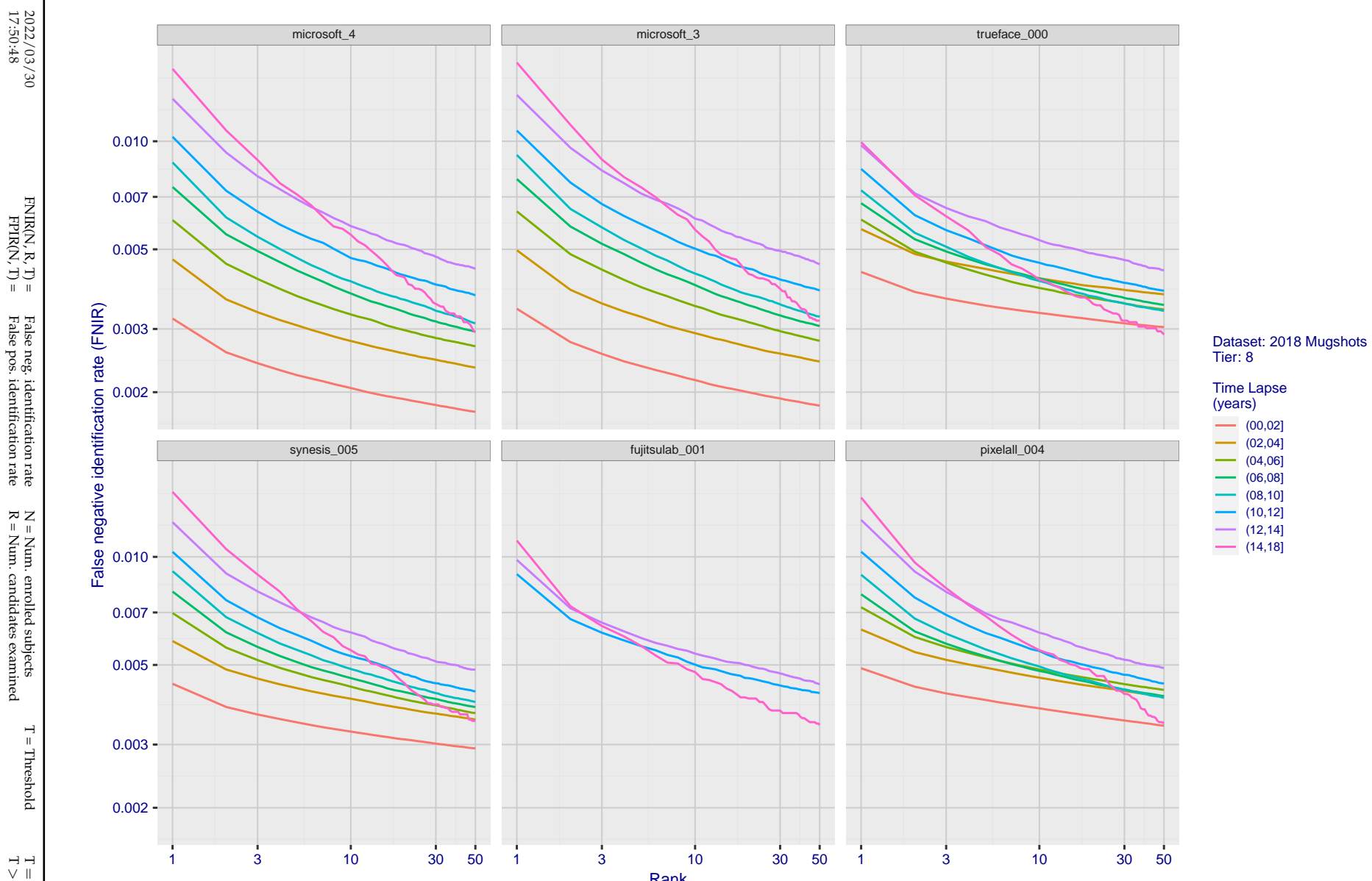


Figure 67: [FRVT-2018 Mugshot Ageing Dataset] Identification miss rates vs. rank by time-elapsed. The oldest image of each individual is enrolled. Thereafter, all more recent images are searched. Miss rates are computed over all searches noted in row 17 of Table 1 and binned by number of years between search and initial enrollment.

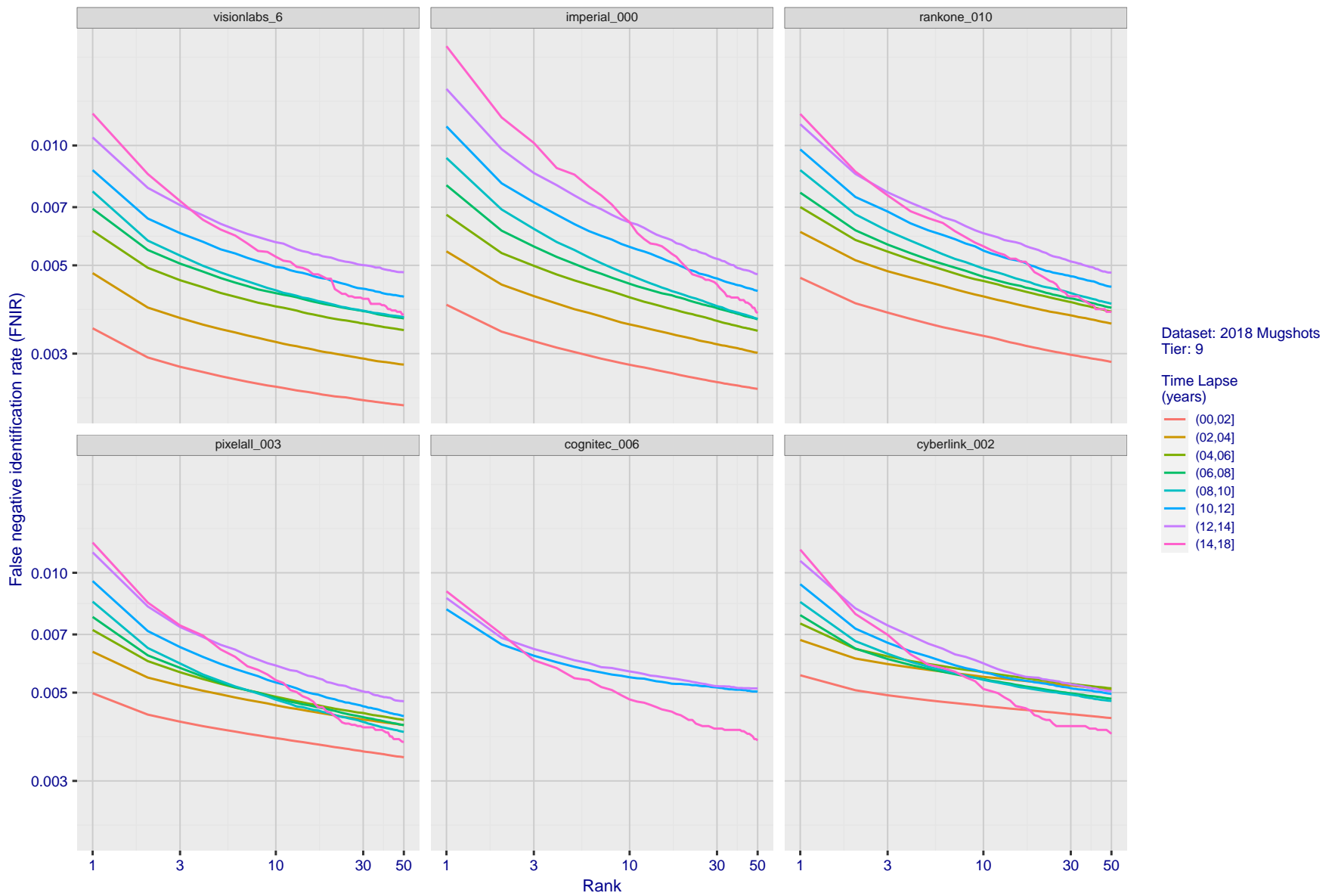


Figure 68: [FRVT-2018 Mugshot Ageing Dataset] Identification miss rates vs. rank by time-elapsed. The oldest image of each individual is enrolled. Thereafter, all more recent images are searched. Miss rates are computed over all searches noted in row 17 of Table 1 and binned by number of years between search and initial enrollment.

2022/03/30
17:50:48FNIR(N, R, T) = False neg. identification rate
FPIR(N, T) = False pos. identification rateN = Num. enrolled subjects
R = Num. candidates examinedT = Threshold
T = 0 → Investigation

T > 0 → Identification

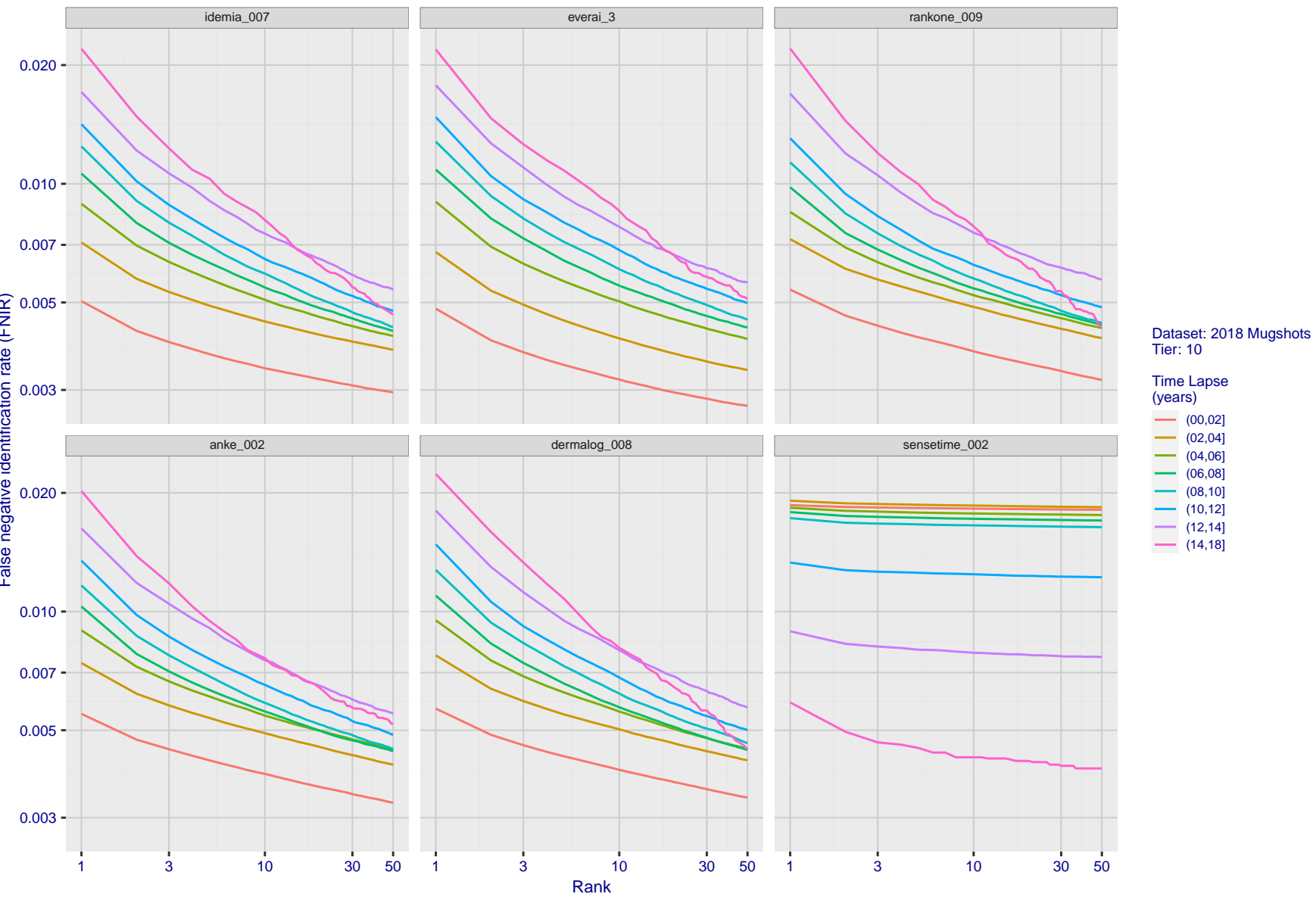


Figure 69: [FRVT-2018 Mugshot Ageing Dataset] Identification miss rates vs. rank by time-elapsed. The oldest image of each individual is enrolled. Thereafter, all more recent images are searched. Miss rates are computed over all searches noted in row 17 of Table 1 and binned by number of years between search and initial enrollment.

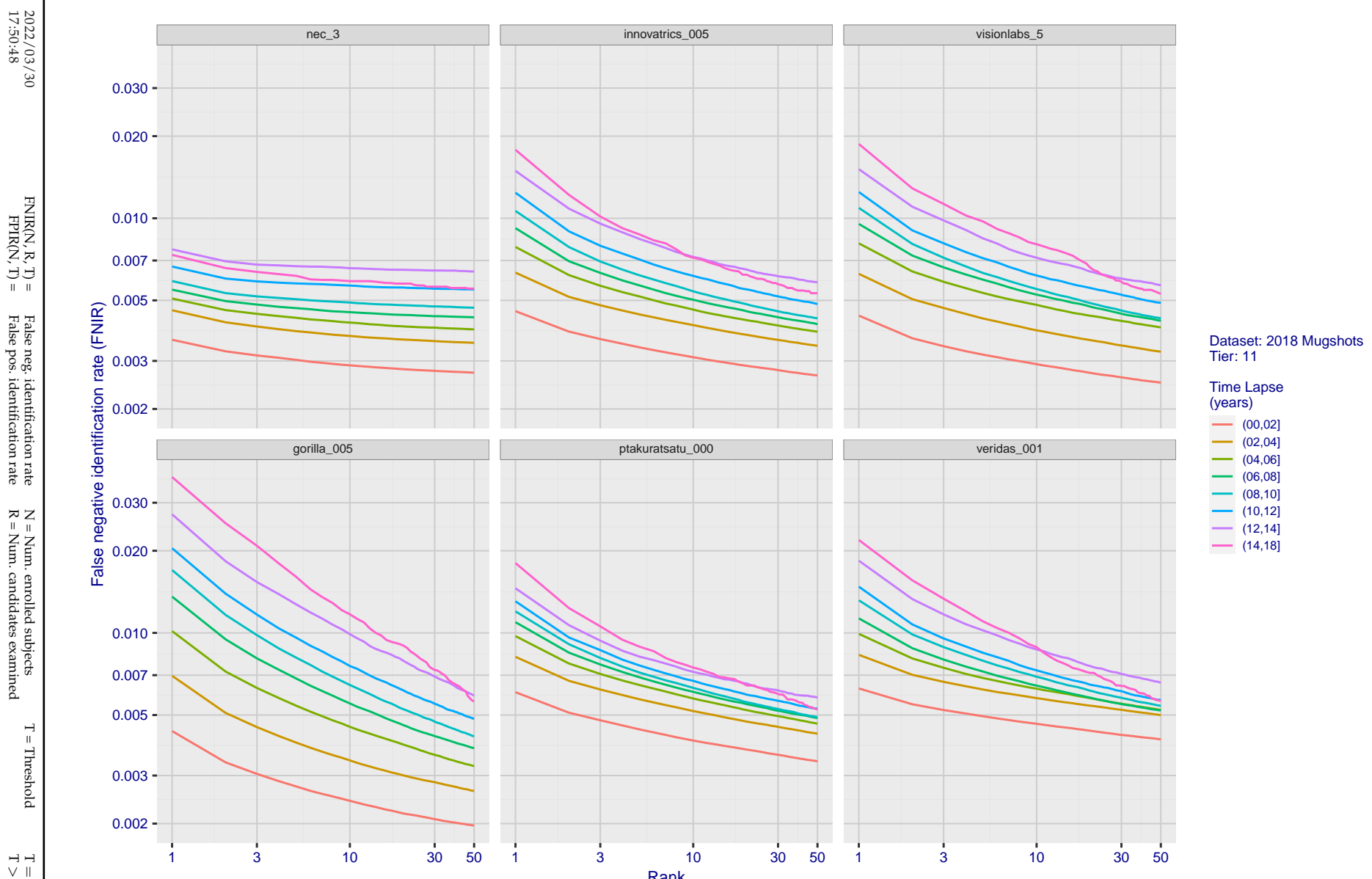


Figure 70: [FRVT-2018 Mugshot Ageing Dataset] Identification miss rates vs. rank by time-elapsed. The oldest image of each individual is enrolled. Thereafter, all more recent images are searched. Miss rates are computed over all searches noted in row 17 of Table 1 and binned by number of years between search and initial enrollment.

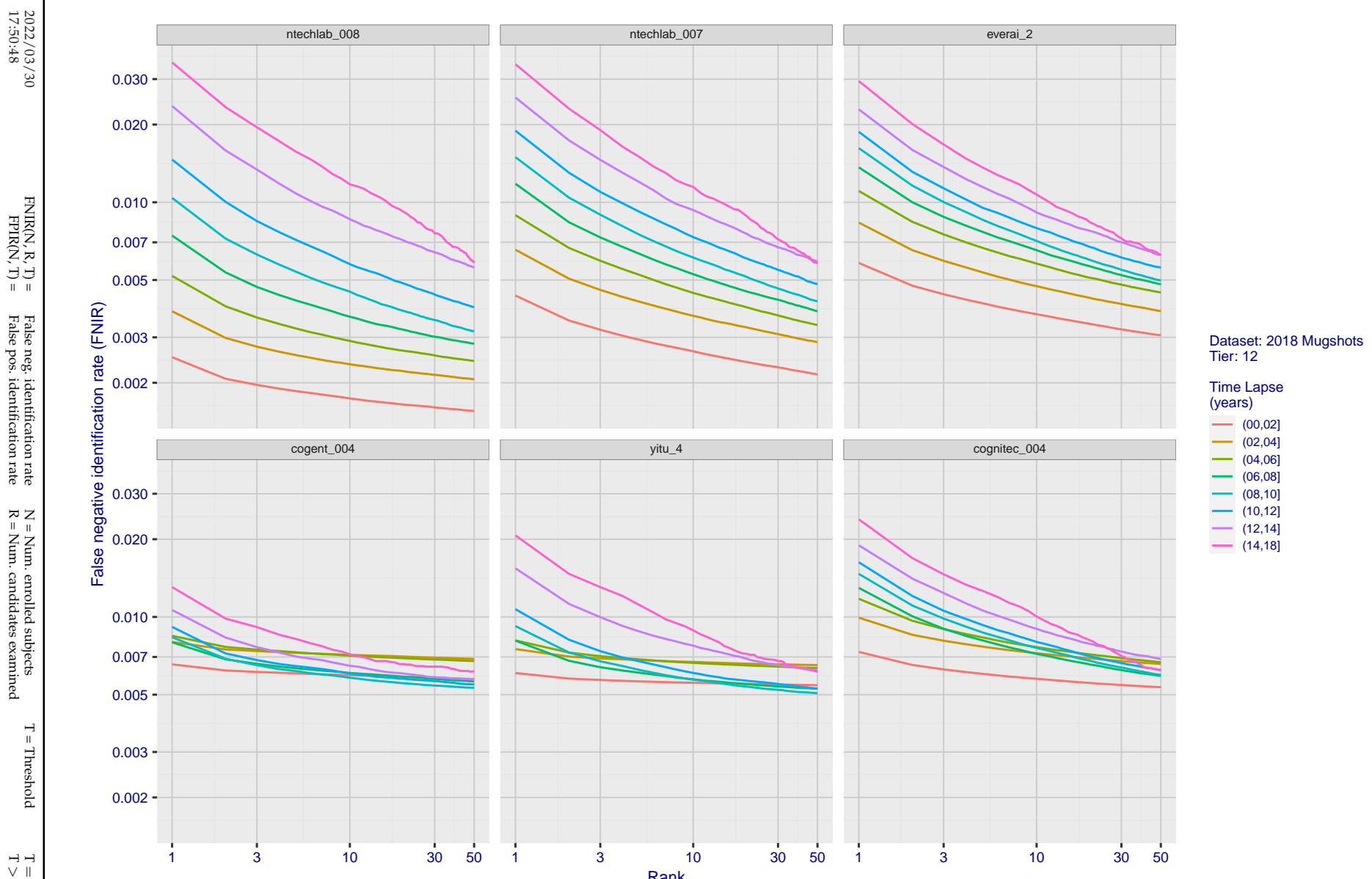


Figure 71: [FRVT-2018 Mugshot Ageing Dataset] Identification miss rates vs. rank by time-elapsed. The oldest image of each individual is enrolled. Thereafter, all more recent images are searched. Miss rates are computed over all searches noted in row 17 of Table 1 and binned by number of years between search and initial enrollment.

2022/03/30
17:50:48FNIR(N, R, T) = False neg. identification rate
FPIR(N, T) = False pos. identification rateN = Num. enrolled subjects
R = Num. candidates examinedT = Threshold
T = 0 → Investigation

T > 0 → Identification

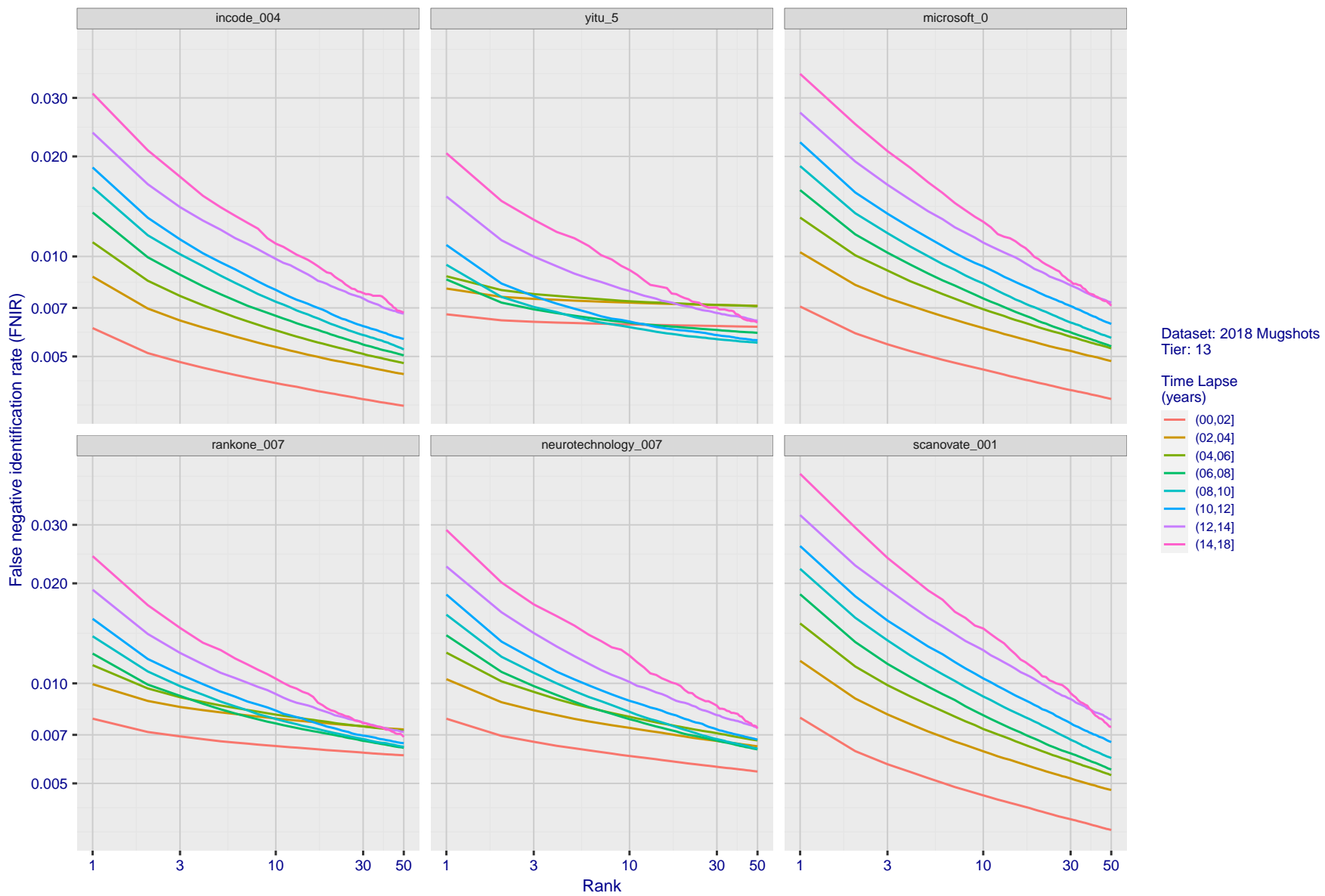


Figure 72: [FRVT-2018 Mugshot Ageing Dataset] Identification miss rates vs. rank by time elapsed. The oldest image of each individual is enrolled. Thereafter, all more recent images are searched. Miss rates are computed over all searches noted in row 17 of Table 1 and binned by number of years between search and initial enrollment.

2022/03/30
17:50:48FNIR(N, R, T) = False neg. identification rate
FPIR(N, T) = False pos. identification rateN = Num. enrolled subjects
R = Num. candidates examinedT = Threshold
T = 0 → Investigation

T > 0 → Identification

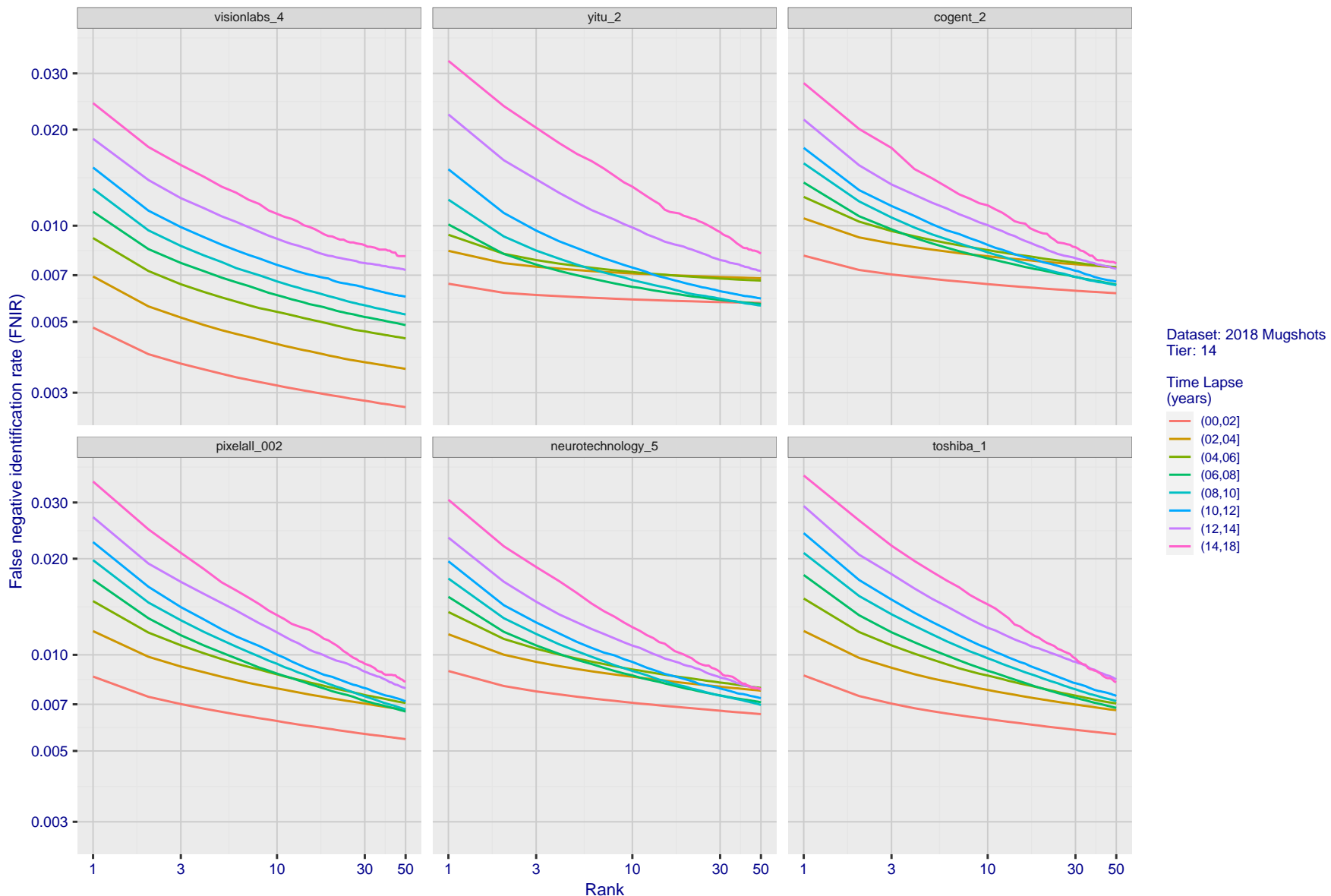


Figure 73: [FRVT-2018 Mugshot Ageing Dataset] Identification miss rates vs. rank by time elapsed. The oldest image of each individual is enrolled. Thereafter, all more recent images are searched. Miss rates are computed over all searches noted in row 17 of Table 1 and binned by number of years between search and initial enrollment.

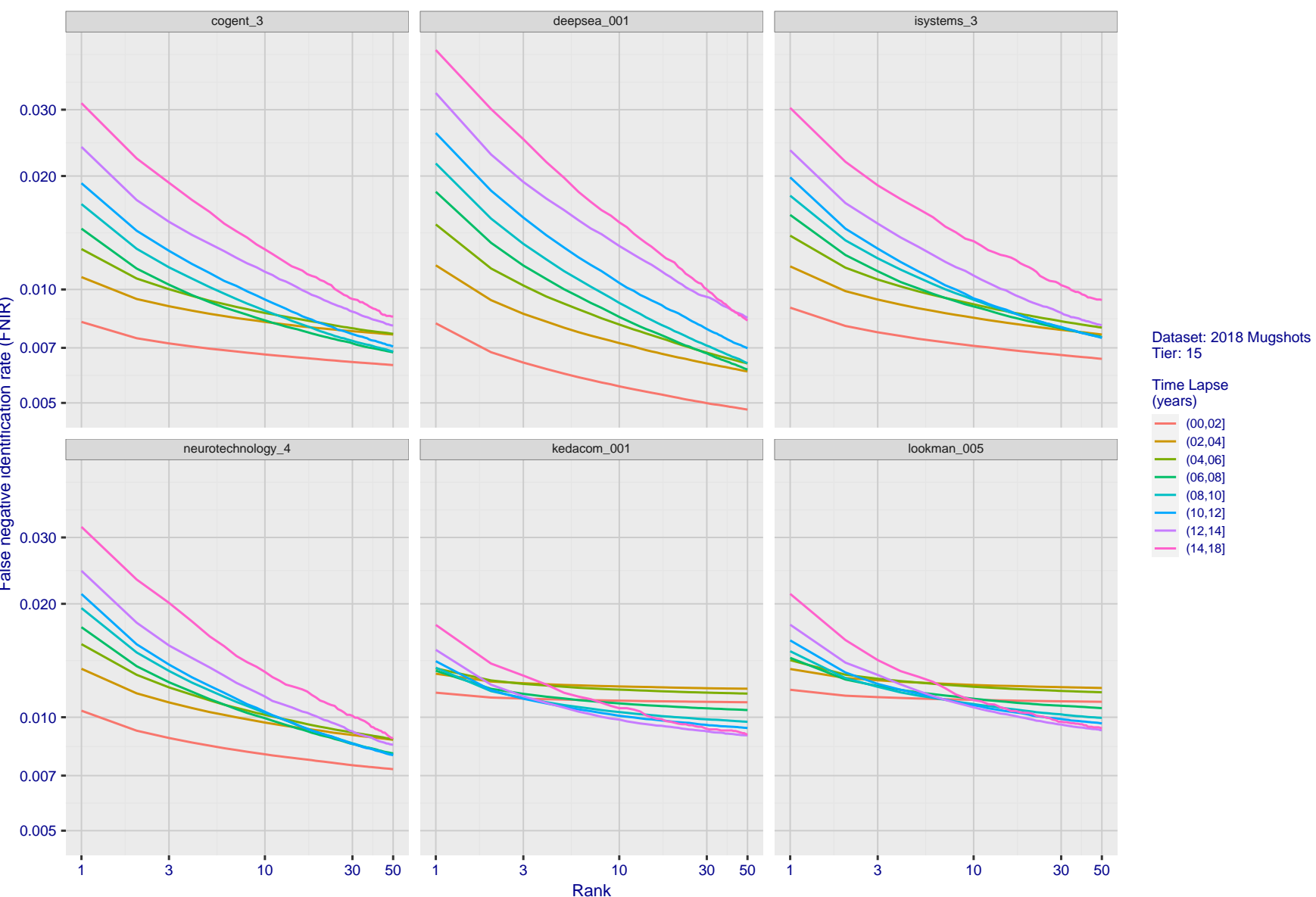
2022/03/30
17:50:48

Figure 74: [FRVT-2018 Mugshot Ageing Dataset] Identification miss rates vs. rank by time-elapsed. The oldest image of each individual is enrolled. Thereafter, all more recent images are searched. Miss rates are computed over all searches noted in row 17 of Table 1 and binned by number of years between search and initial enrollment.

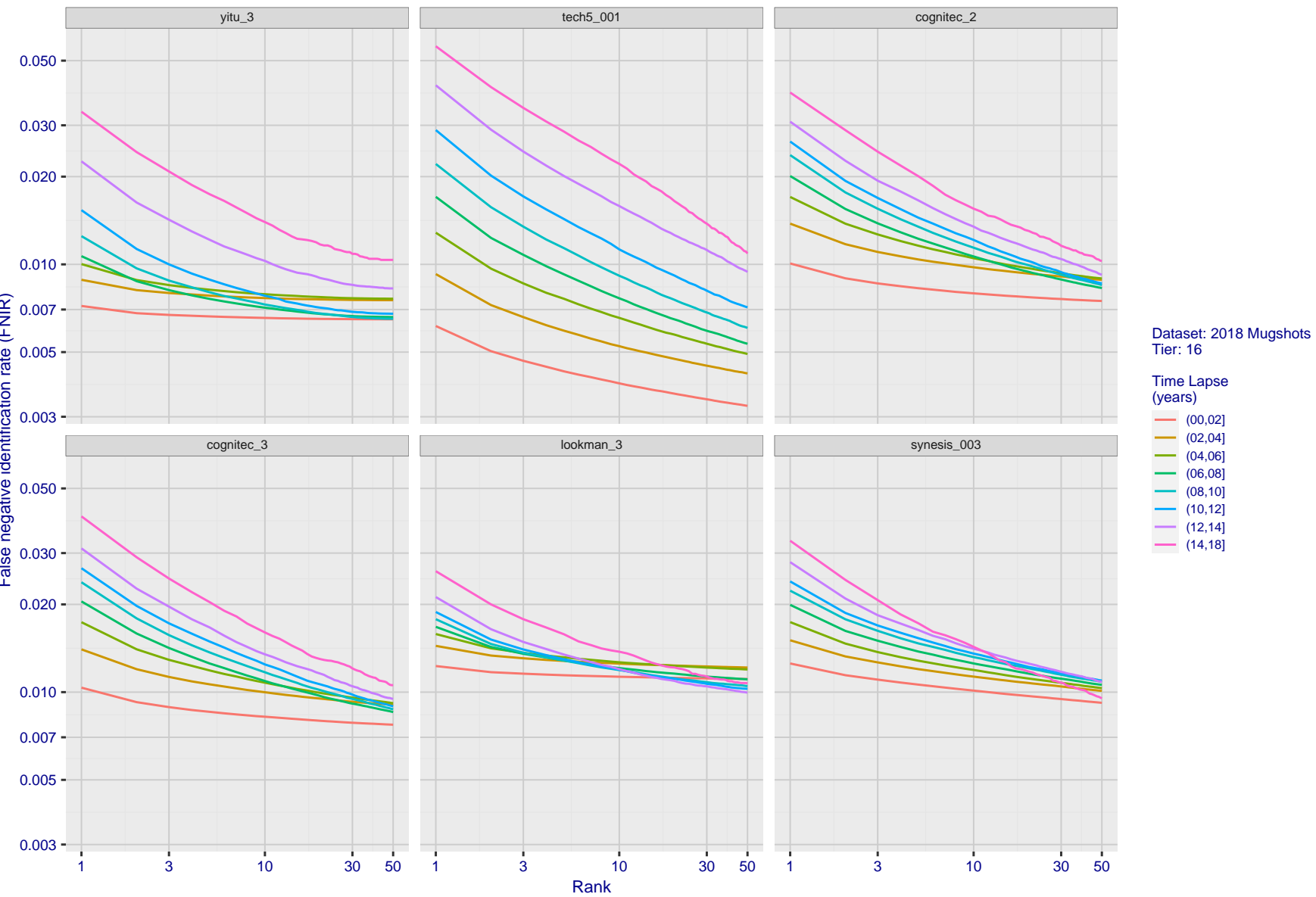
2022/03/30
17:50:48FNIR(N, R, T) = False neg. identification rate
FPFR(N, T) = False pos. identification rate
N = Num. enrolled subjects
R = Num. candidates examined
T = Threshold
T = 0 → Investigation
T > 0 → Identification

Figure 75: [FRVT-2018 Mugshot Ageing Dataset] Identification miss rates vs. rank by time-elapsed. The oldest image of each individual is enrolled. Thereafter, all more recent images are searched. Miss rates are computed over all searches noted in row 17 of Table 1 and binned by number of years between search and initial enrollment.

2022/03/30
17:50:48FNIR(N, R, T) = False neg. identification rate
FPIR(N, T) = False pos. identification rateN = Num. enrolled subjects
R = Num. candidates examinedT = Threshold
T = 0 → Investigation

T > 0 → Identification

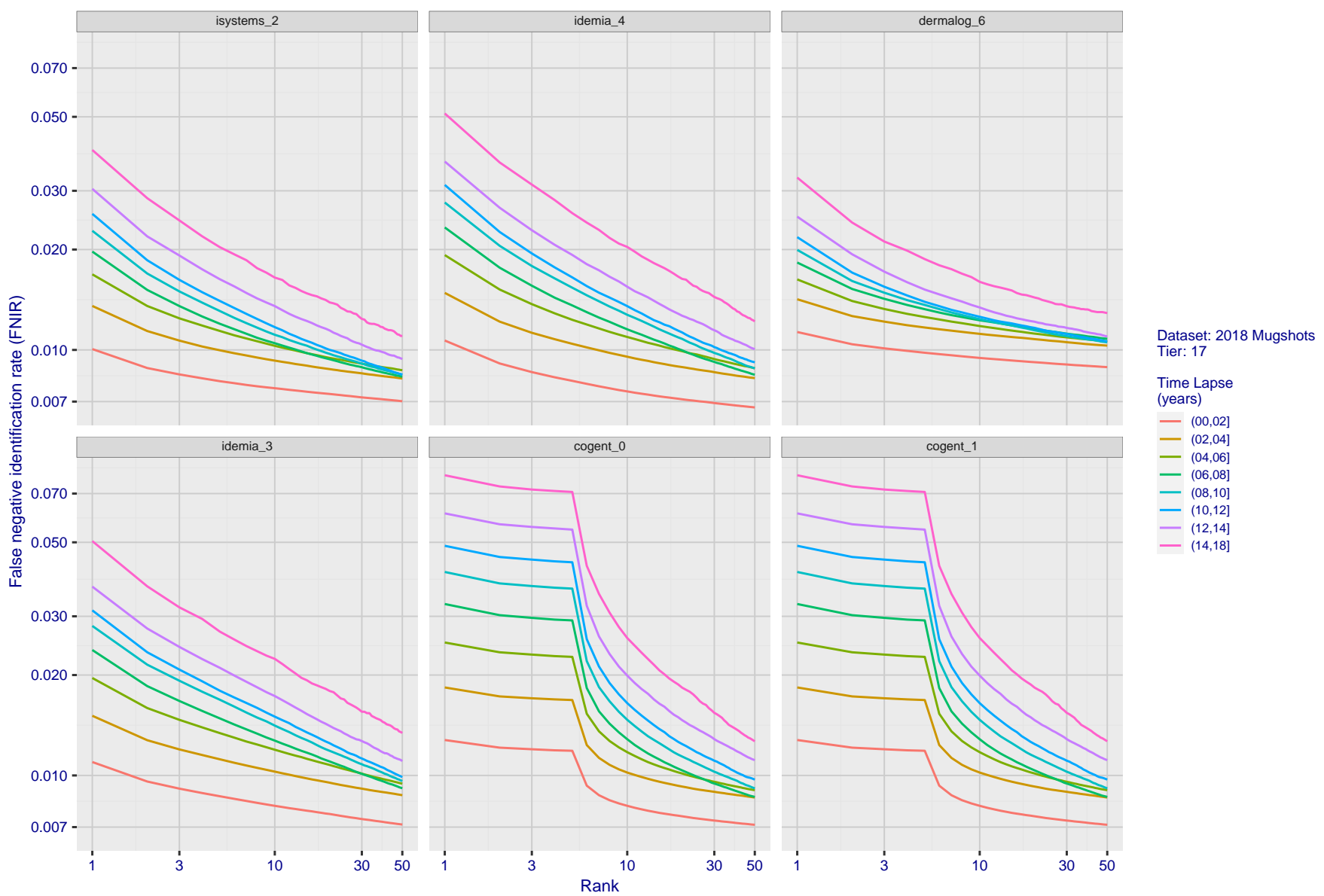
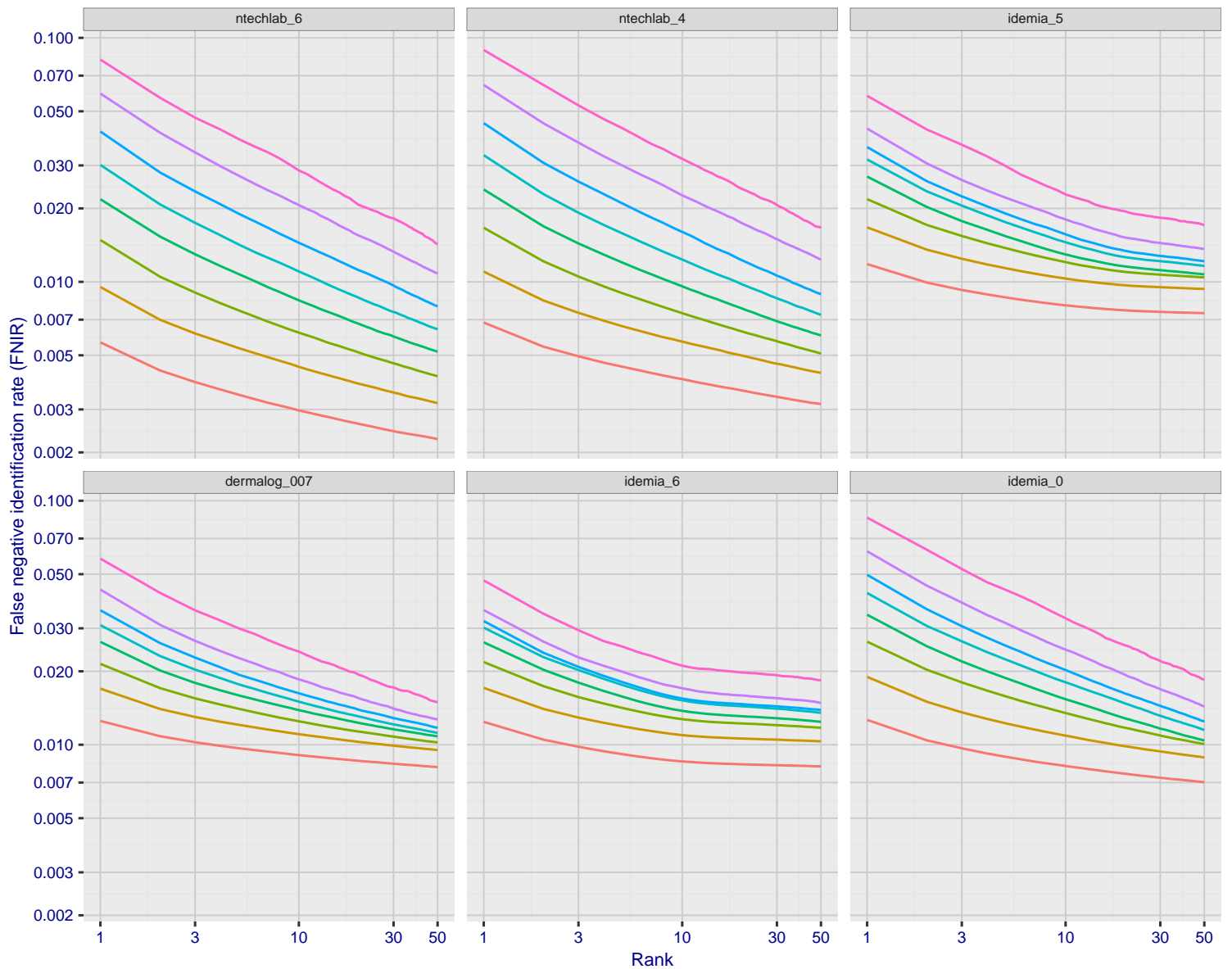


Figure 76: [FRVT-2018 Mugshot Ageing Dataset] Identification miss rates vs. rank by time elapsed. The oldest image of each individual is enrolled. Thereafter, all more recent images are searched. Miss rates are computed over all searches noted in row 17 of Table 1 and binned by number of years between search and initial enrollment.

2022/03/30
17:50:48

 $\text{FNIR}(N, R, T) =$
False neg. identification rate
 $\text{FPIR}(N, T) =$
False pos. identification rate
 $N = \text{Num. enrolled subjects}$
 $R = \text{Num. candidates examined}$
 $T = \text{Threshold}$
 $T = 0 \rightarrow \text{Investigation}$
 $T > 0 \rightarrow \text{Identification}$



Dataset: 2018 Mugshots
Tier: 18

Time Lapse
(years)

(00,02]
(02,04]
(04,06]
(06,08]
(08,10]
(10,12]
(12,14]
(14,18]

Figure 77: [FRVT-2018 Mugshot Ageing Dataset] Identification miss rates vs. rank by time-elapsed. The oldest image of each individual is enrolled. Thereafter, all more recent images are searched. Miss rates are computed over all searches noted in row 17 of Table 1 and binned by number of years between search and initial enrollment.

2022/03/30
17:50:48FNIR(N, R, T) = False neg. identification rate
FPFR(N, T) = False pos. identification rateN = Num. enrolled subjects
R = Num. candidates examinedT = Threshold
T = 0 → Investigation

T > 0 → Identification

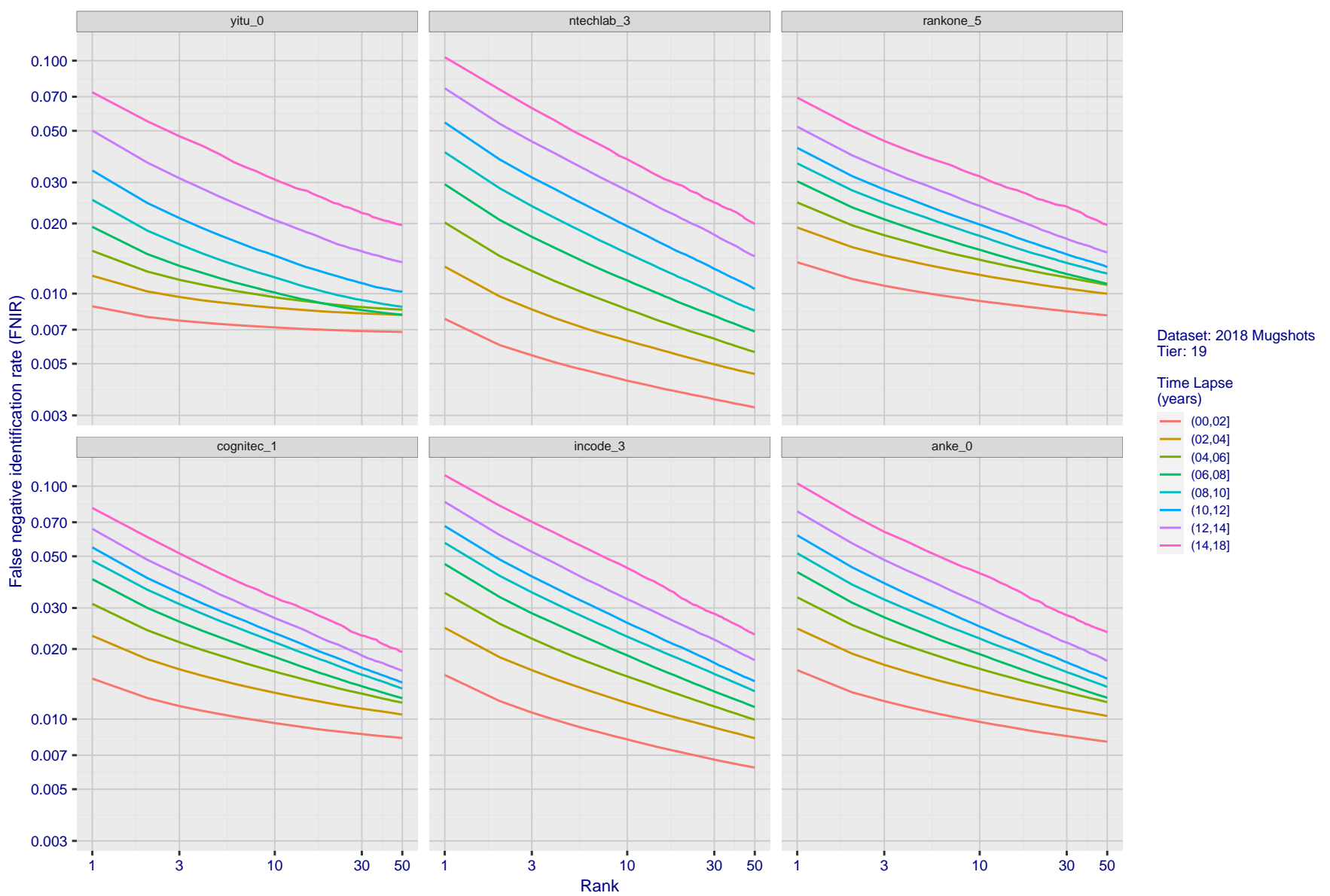


Figure 78: [FRVT-2018 Mugshot Ageing Dataset] Identification miss rates vs. rank by time elapsed. The oldest image of each individual is enrolled. Thereafter, all more recent images are searched. Miss rates are computed over all searches noted in row 17 of Table 1 and binned by number of years between search and initial enrollment.

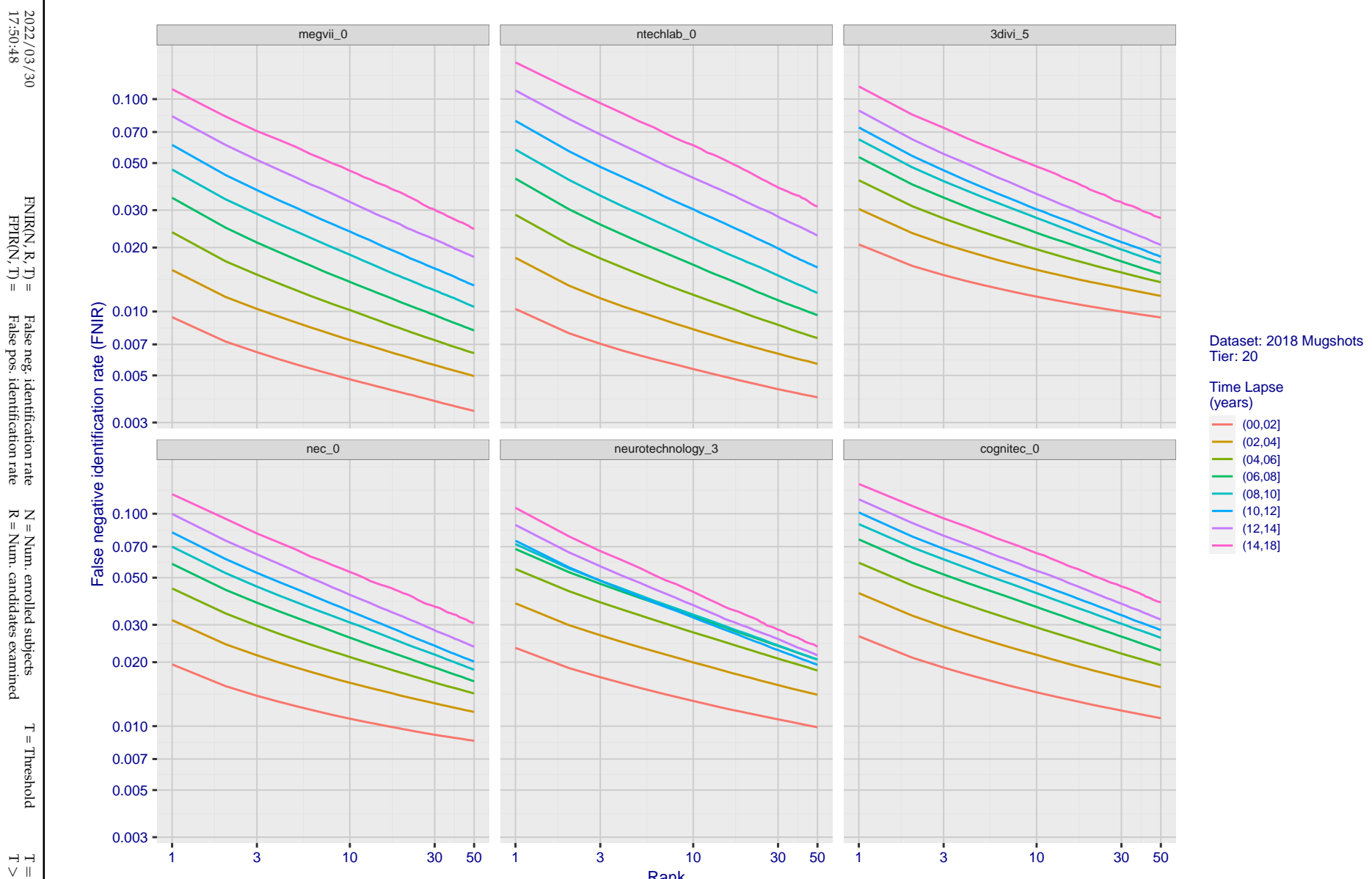


Figure 79: [FRVT-2018 Mugshot Ageing Dataset] Identification miss rates vs. rank by time-elapsed. The oldest image of each individual is enrolled. Thereafter, all more recent images are searched. Miss rates are computed over all searches noted in row 17 of Table 1 and binned by number of years between search and initial enrollment.

2022/03/30
17:50:48FNIR(N, R, T) = False neg. identification rate
FPIR(N, T) = False pos. identification rateN = Num. enrolled subjects
R = Num. candidates examinedT = Threshold
T = 0 → Investigation

T > 0 → Identification

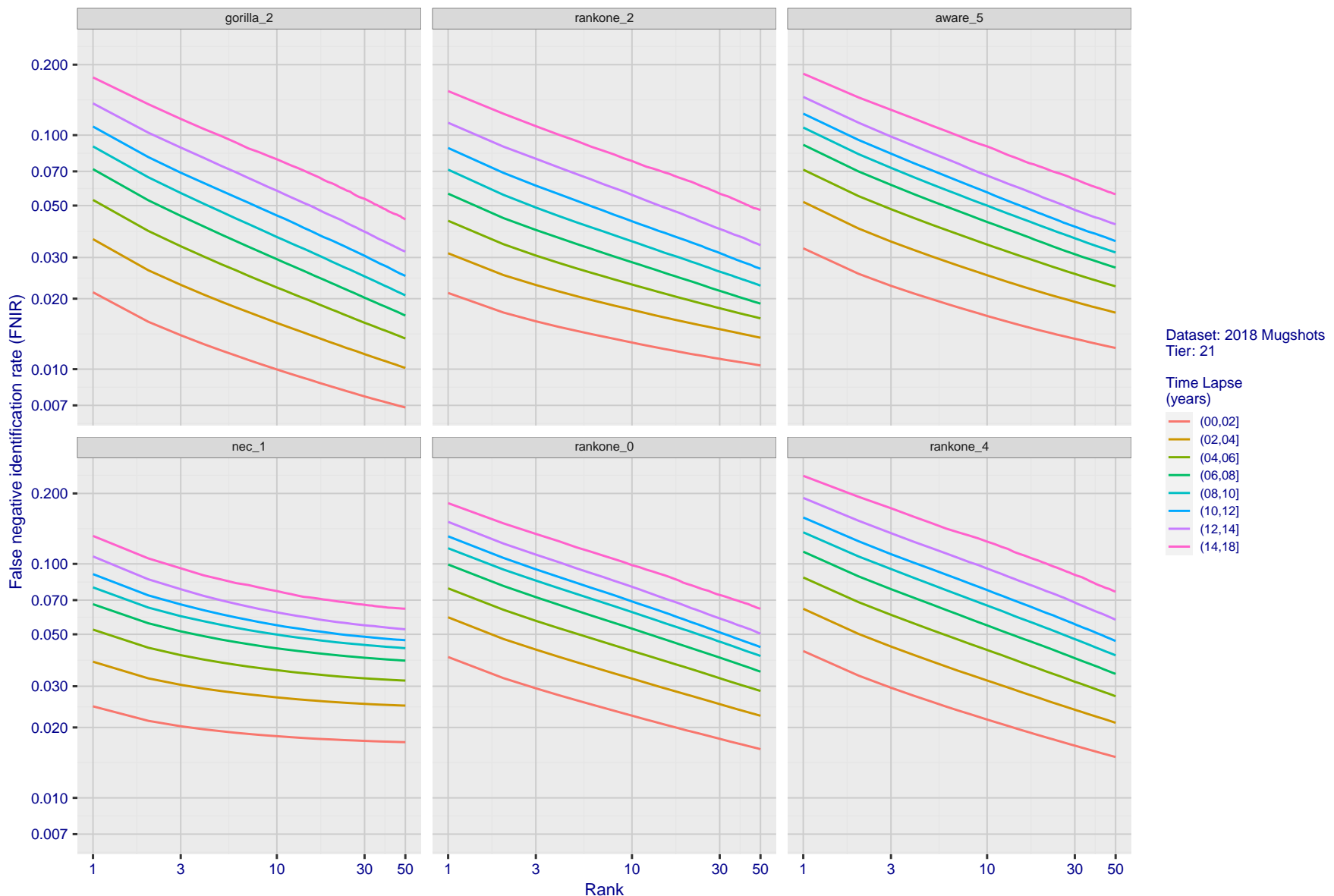


Figure 80: [FRVT-2018 Mugshot Ageing Dataset] Identification miss rates vs. rank by time-elapsed. The oldest image of each individual is enrolled. Thereafter, all more recent images are searched. Miss rates are computed over all searches noted in row 17 of Table 1 and binned by number of years between search and initial enrollment.

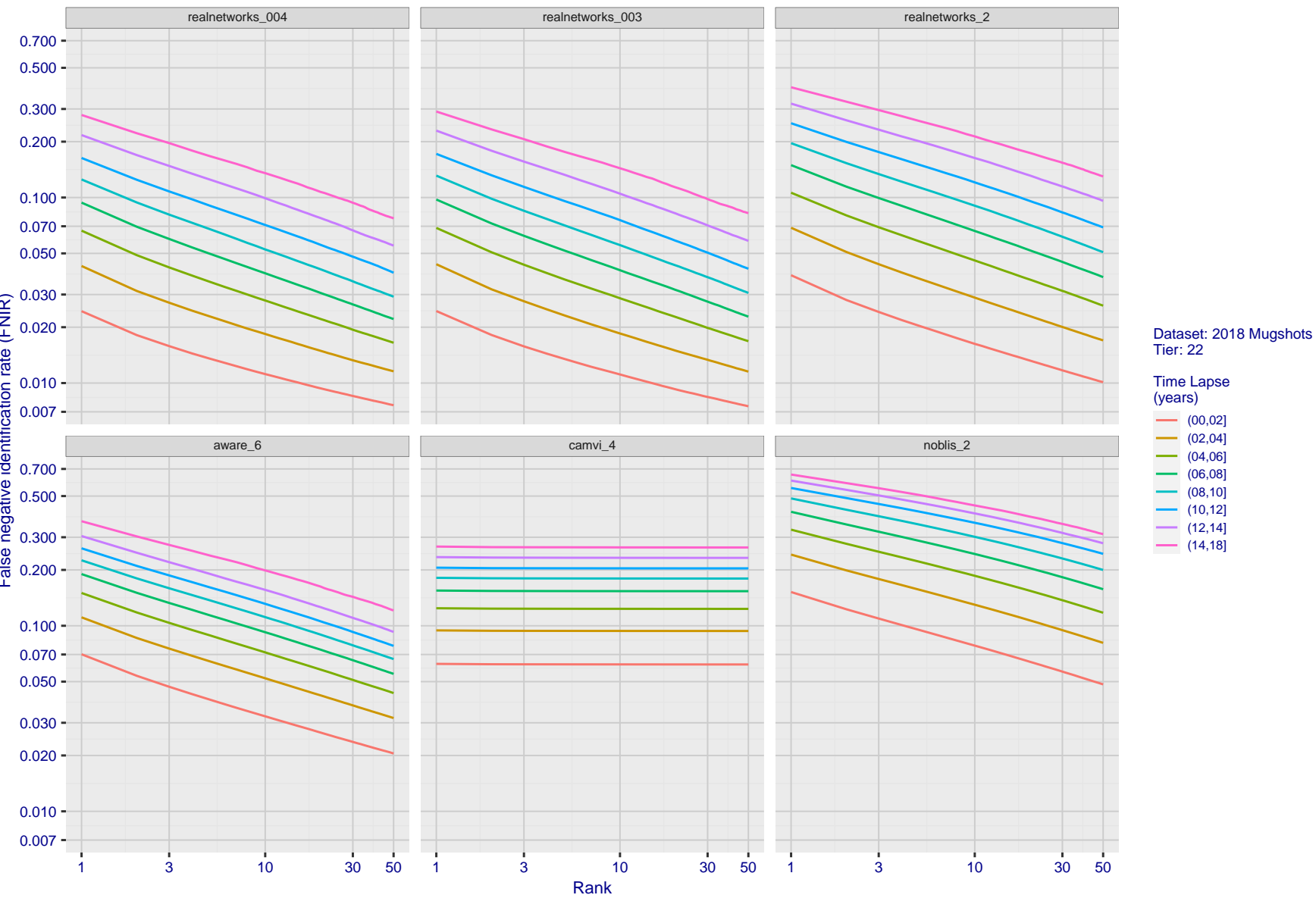
2022/03/30
17:50:48FNIR(N, R, T) = False neg. identification rate
FPIR(N, T) = False pos. identification rate
N = Num. enrolled subjects
R = Num. candidates examined
T = Threshold
T = 0 → Investigation
T > 0 → Identification

Figure 81: [FRVT-2018 Mugshot Ageing Dataset] Identification miss rates vs. rank by time-elapsed. The oldest image of each individual is enrolled. Thereafter, all more recent images are searched. Miss rates are computed over all searches noted in row 17 of Table 1 and binned by number of years between search and initial enrollment.

2022/03/30
17:50:48FNIR(N, R, T) = False neg. identification rate
FPIR(N, T) = False pos. identification rateN = Num. enrolled subjects
R = Num. candidates examinedT = Threshold
T = 0 → Investigation

T > 0 → Identification

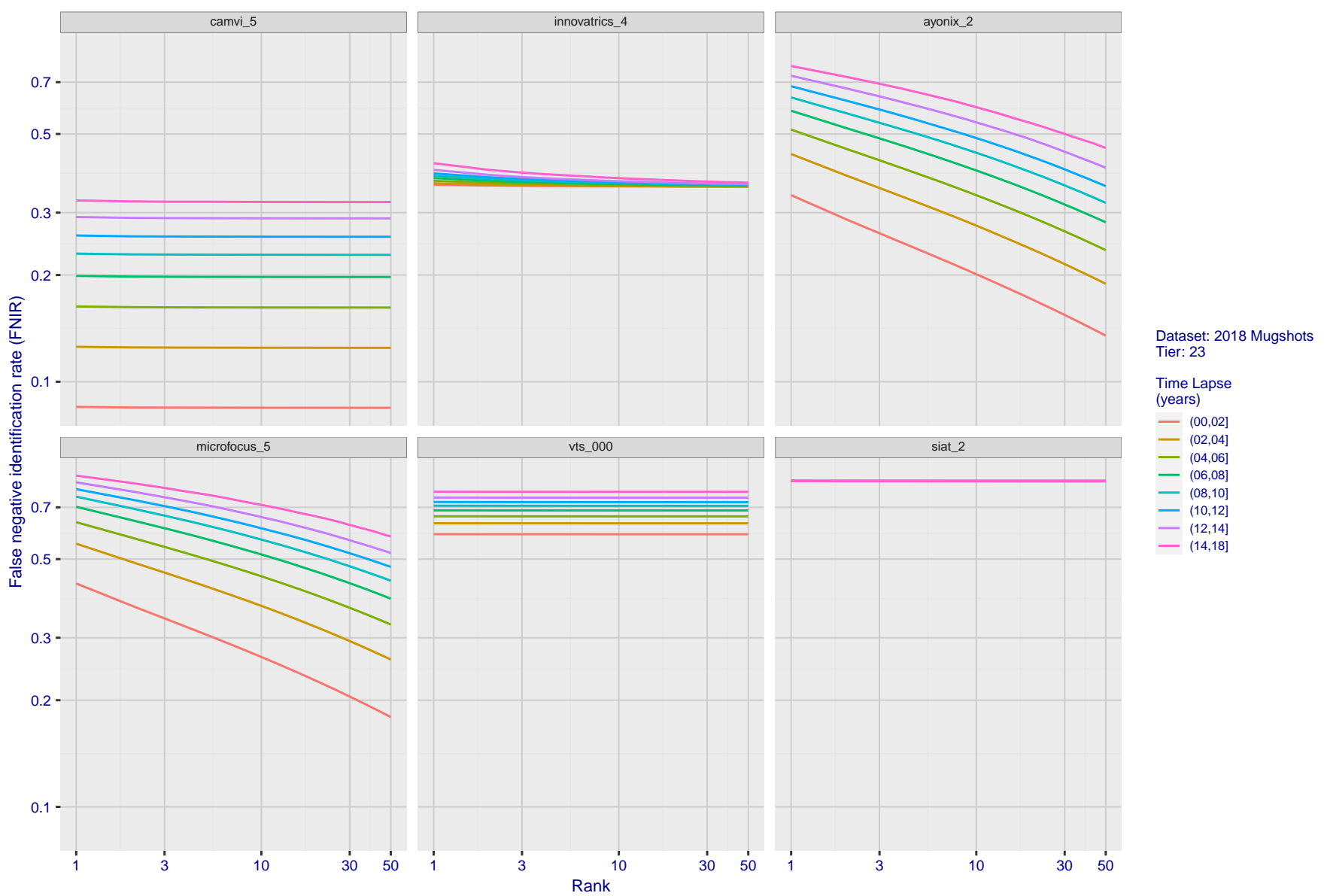


Figure 82: [FRVT-2018 Mugshot Ageing Dataset] Identification miss rates vs. rank by time-elapsed. The oldest image of each individual is enrolled. Thereafter, all more recent images are searched. Miss rates are computed over all searches noted in row 17 of Table 1 and binned by number of years between search and initial enrollment.

2022/03/30 17:50:48	$\text{FNIR}(N, R, T) =$ $\text{FPTR}(N, T) =$	False neg. identification rate False pos. identification rate	$N =$ Num. enrolled subjects $R =$ Num. candidates examined	$T =$ Threshold $T > 0 \rightarrow$ Identification	$T = 0 \rightarrow$ Investigation
------------------------	---	--	--	---	-----------------------------------

2022/03/30
17:50:48

 $FNIR(N, R, T)$ = False neg. identification rate
 $FPIR(N, T)$ = False pos. identification rate

 N = Num. enrolled subjects
 R = Num. candidates examined

 T = Threshold

 $T = 0 \rightarrow$ Investigation
 $T > 0 \rightarrow$ Identification

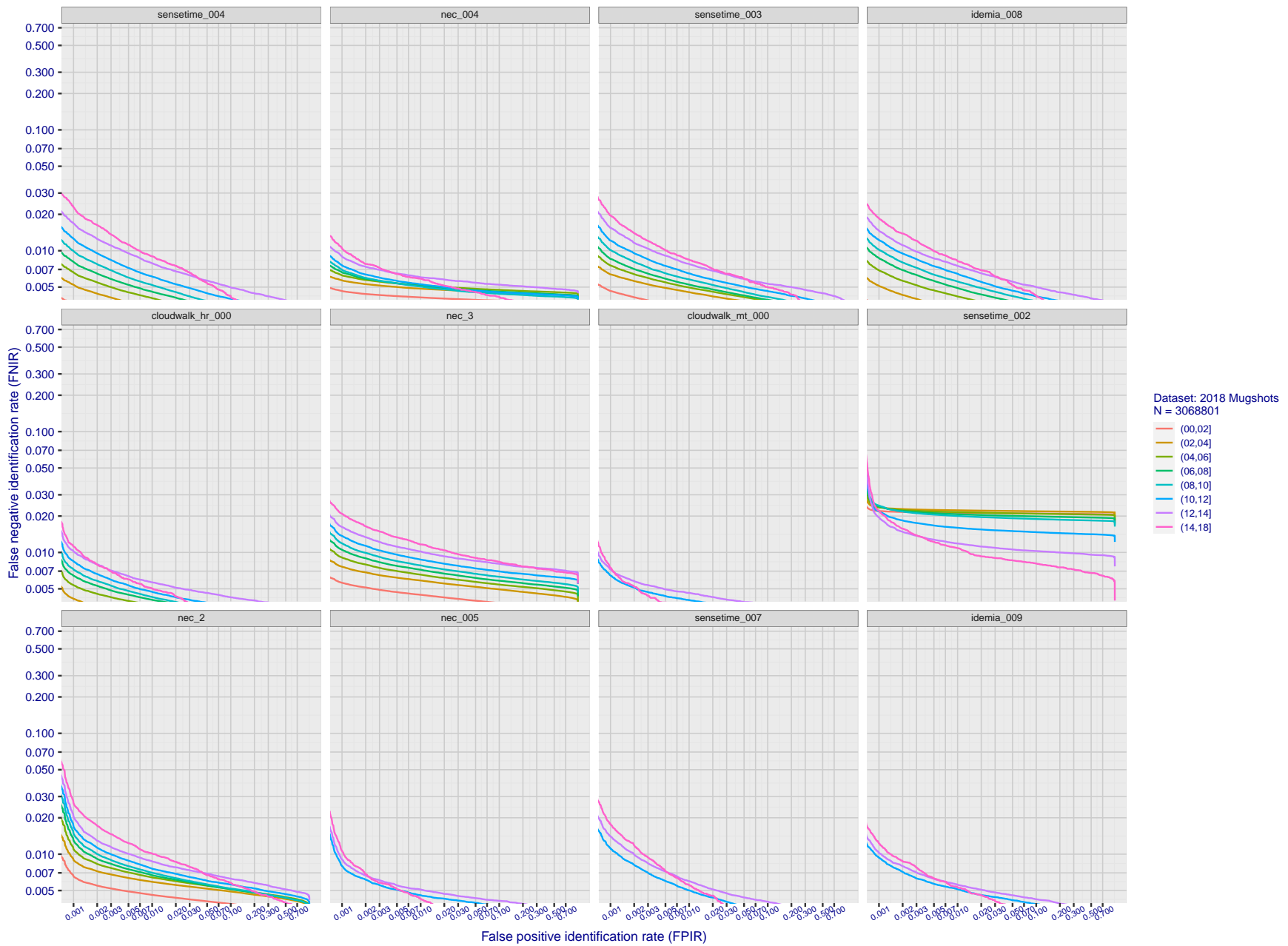


Figure 83: [FRVT-2018 Mugshot Ageing Dataset] Identification miss rates vs. FPIR by time-elapsed. The oldest image of each individual is enrolled. Thereafter, all more recent images are searched. Miss rates are computed over all searches noted in row 17 of Table 1 and binned by number of years between search and initial enrollment. FPIR is computed from the same FRVT 2018 non-mates noted in row 3 of Table 1 with $N = 3000\,000$.

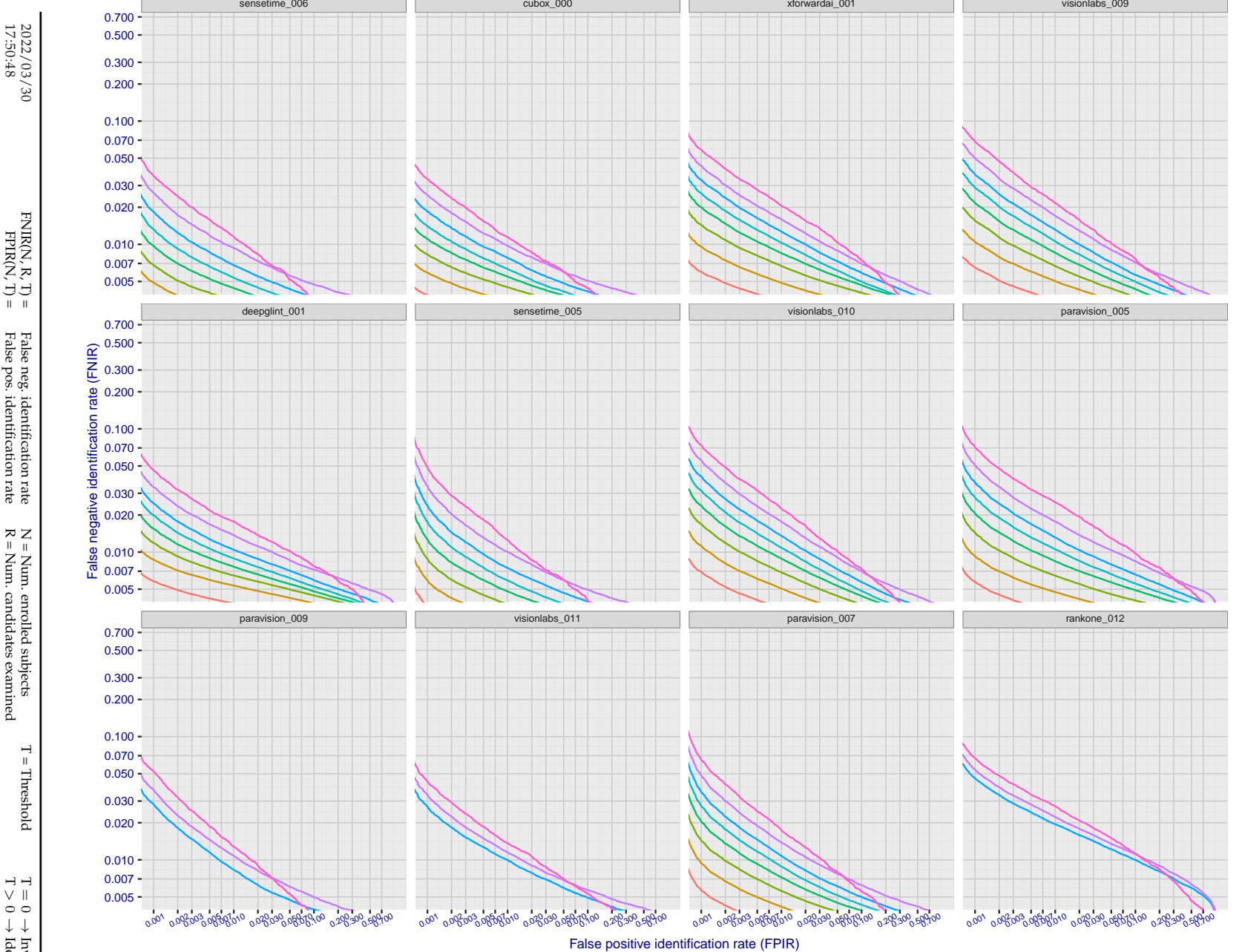


Figure 84: [FRVT-2018 Mugshot Ageing Dataset] Identification miss rates vs. FPIR by time-elapsed. The oldest image of each individual is enrolled. Thereafter, all more recent images are searched. Miss rates are computed over all searches noted in row 17 of Table 1 and binned by number of years between search and initial enrollment. FPIR is computed from the same FRVT 2018 non-mates noted in row 3 of Table 1 with $N = 3\,000\,000$.

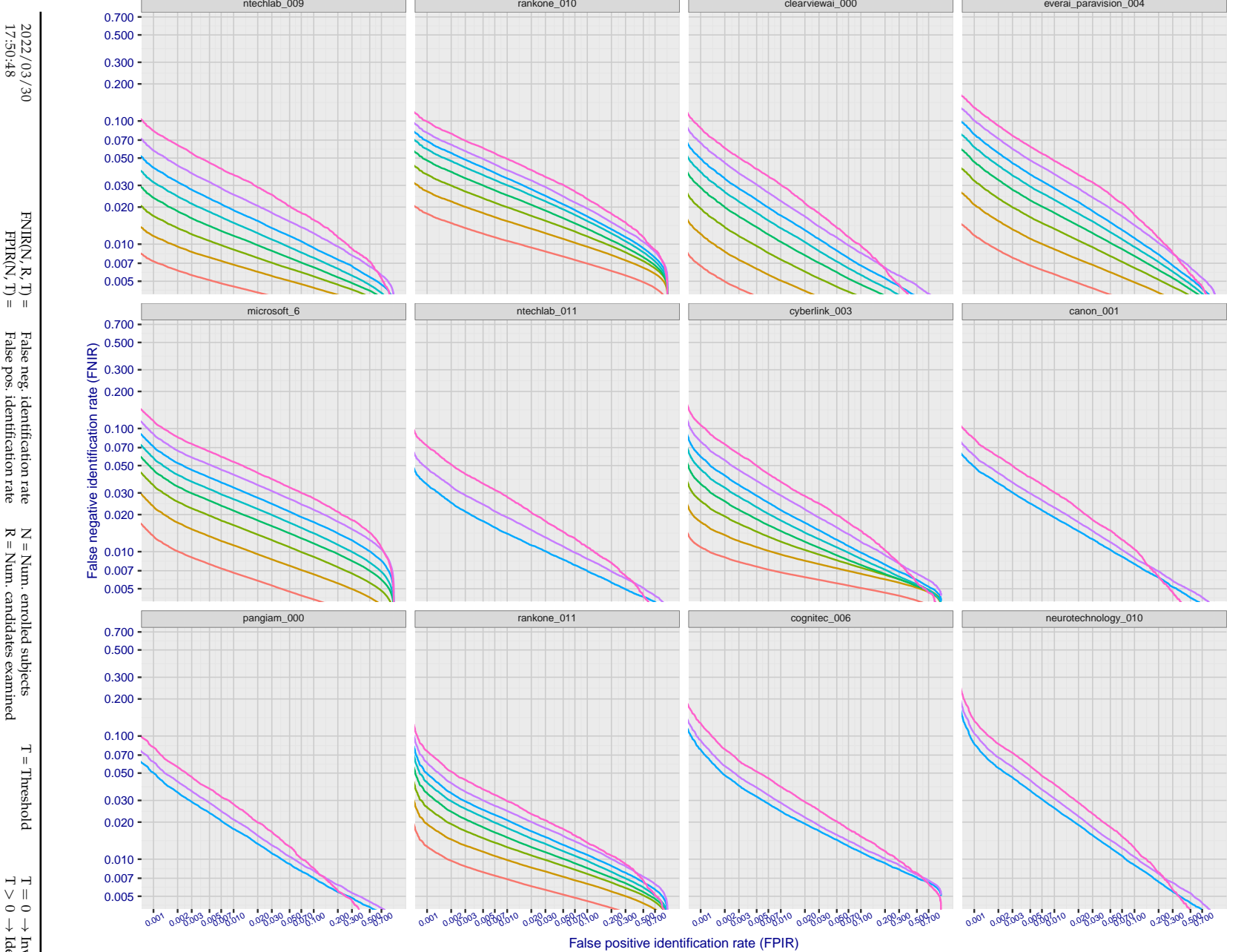


Figure 85: [FRVT-2018 Mugshot Ageing Dataset] Identification miss rates vs. FPIR by time-elapsed. The oldest image of each individual is enrolled. Thereafter, all more recent images are searched. Miss rates are computed over all searches noted in row 17 of Table 1 and binned by number of years between search and initial enrollment. FPIR is computed from the same FRVT 2018 non-mates noted in row 3 of Table 1 with $N = 3\,000\,000$.

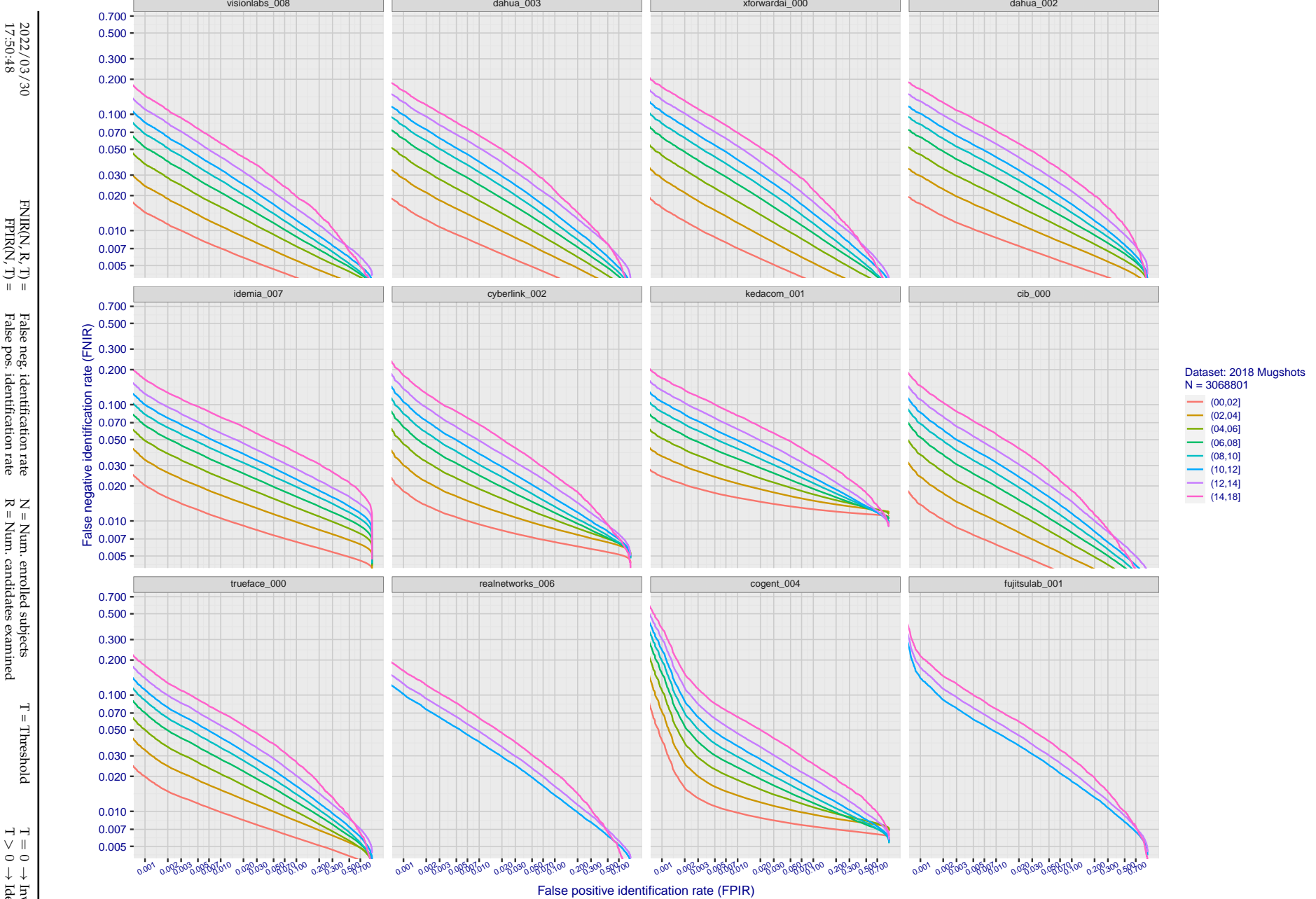


Figure 86: [FRVT-2018 Mugshot Ageing Dataset] Identification miss rates vs. FPIR by time-elapsed. The oldest image of each individual is enrolled. Thereafter, all more recent images are searched. Miss rates are computed over all searches noted in row 17 of Table 1 and binned by number of years between search and initial enrollment. FPIR is computed from the same FRVT 2018 non-mates noted in row 3 of Table 1 with $N = 3\,000\,000$.

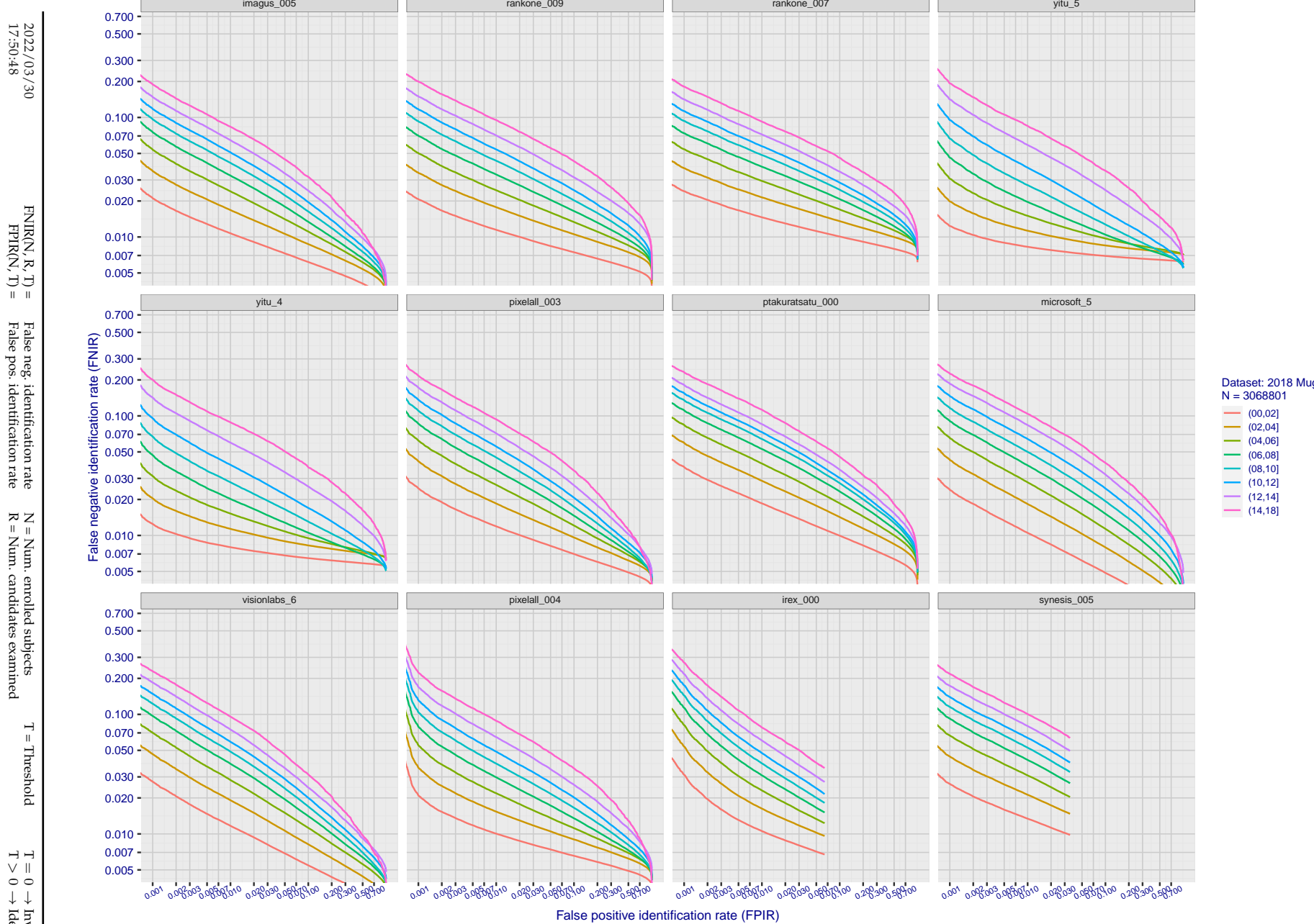


Figure 87: [FRVT-2018 Mugshot Ageing Dataset] Identification miss rates vs. FPIR by time-elapsed. The oldest image of each individual is enrolled. Thereafter, all more recent images are searched. Miss rates are computed over all searches noted in row 17 of Table 1 and binned by number of years between search and initial enrollment. FPIR is computed from the same FRVT 2018 non-mates noted in row 3 of Table 1 with $N = 3\,000\,000$.

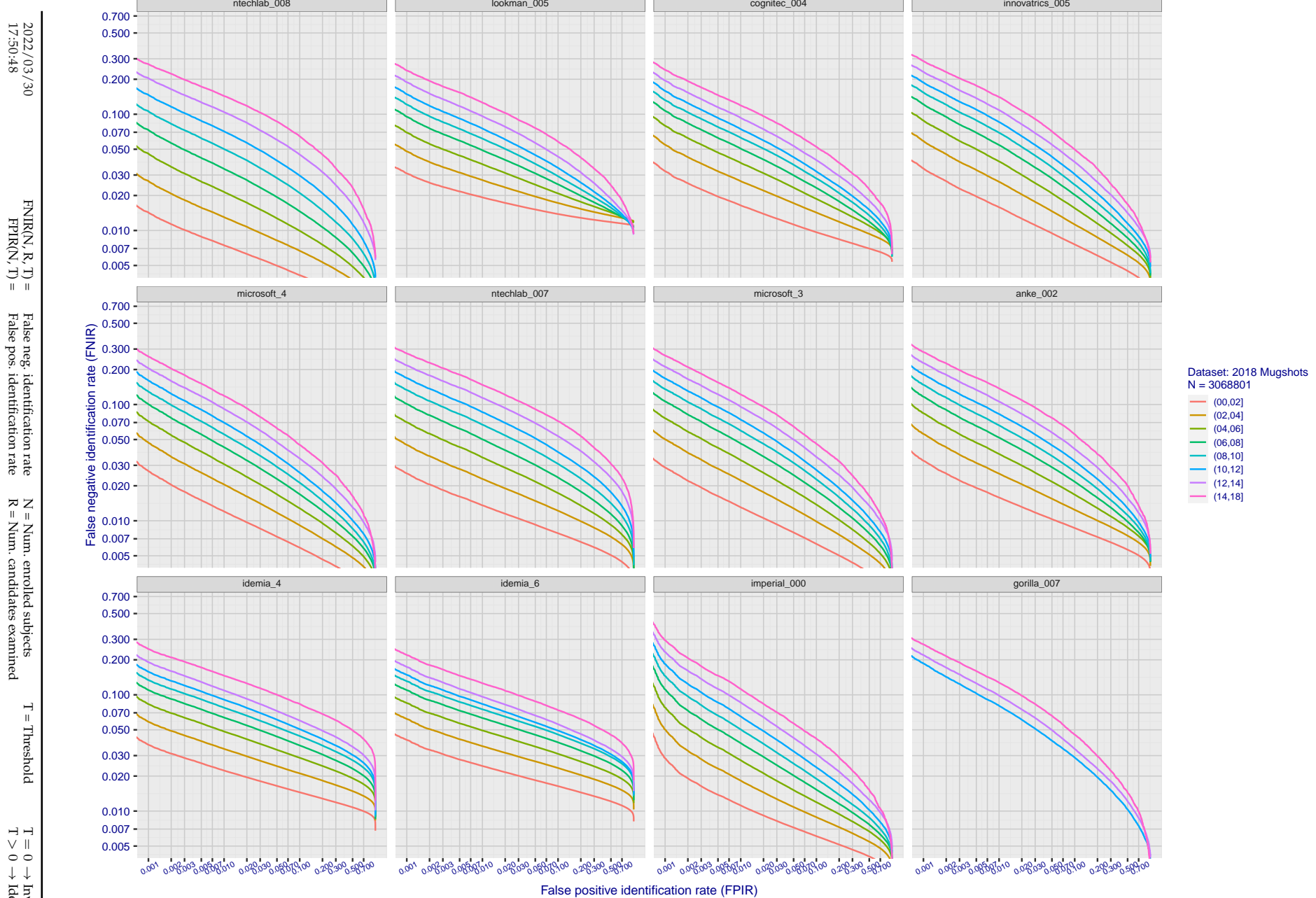


Figure 88: [FRVT-2018 Mugshot Ageing Dataset] Identification miss rates vs. FPIR by time elapsed. The oldest image of each individual is enrolled. Thereafter, all more recent images are searched. Miss rates are computed over all searches noted in row 17 of Table 1 and binned by number of years between search and initial enrollment. FPIR is computed from the same FRVT 2018 non-mates noted in row 3 of Table 1 with $N = 3\,000\,000$.

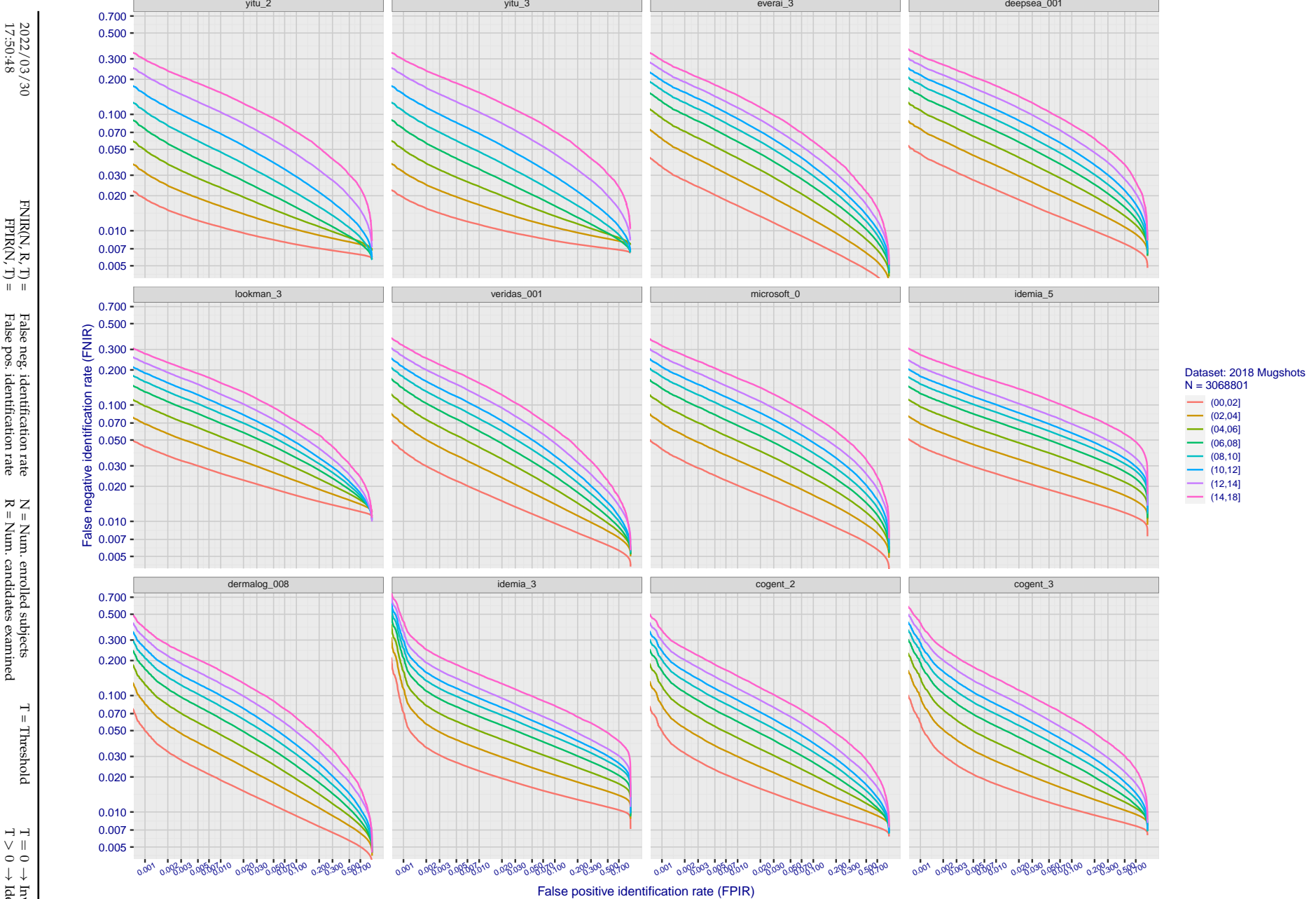


Figure 89: [FRVT-2018 Mugshot Ageing Dataset] Identification miss rates vs. FPIR by time elapsed. The oldest image of each individual is enrolled. Thereafter, all more recent images are searched. Miss rates are computed over all searches noted in row 17 of Table 1 and binned by number of years between search and initial enrollment. FPIR is computed from the same FRVT 2018 non-mates noted in row 3 of Table 1 with $N = 3\,000\,000$.

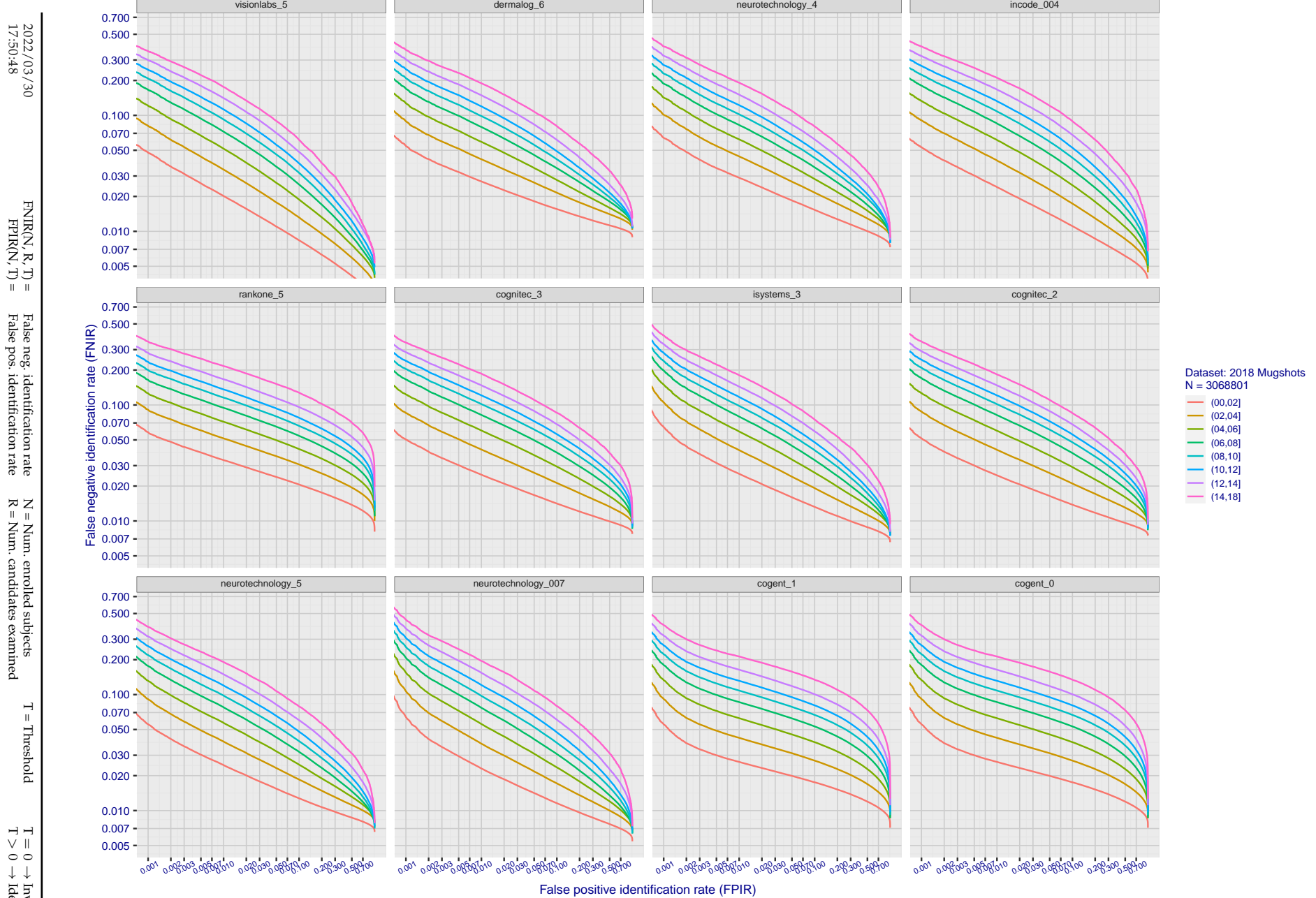


Figure 90: [FRVT-2018 Mugshot Ageing Dataset] Identification miss rates vs. FPIR by time-elapsed. The oldest image of each individual is enrolled. Thereafter, all more recent images are searched. Miss rates are computed over all searches noted in row 17 of Table 1 and binned by number of years between search and initial enrollment. FPIR is computed from the same FRVT 2018 non-mates noted in row 3 of Table 1 with N = 3 000 000.

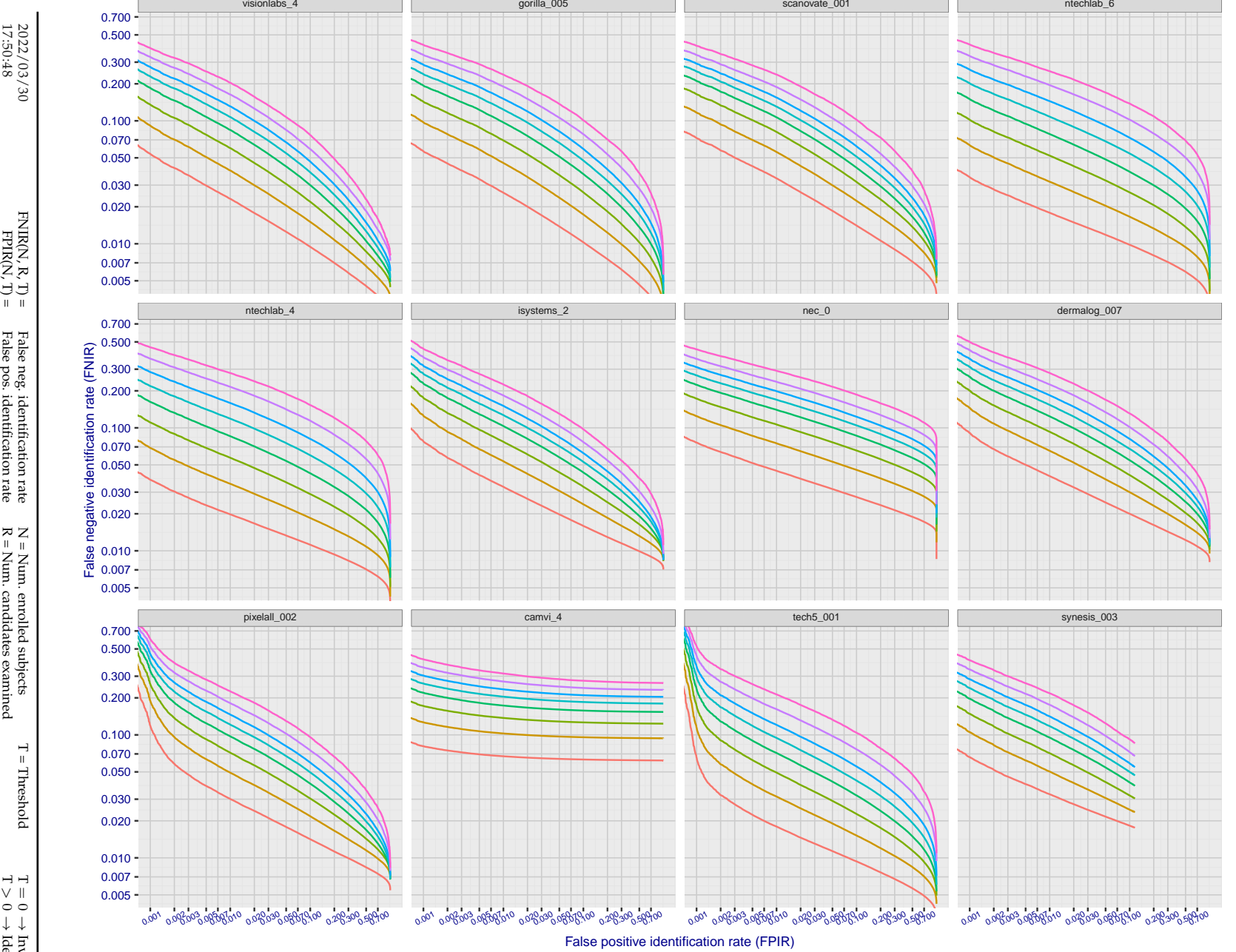


Figure 91: [FRVT-2018 Mugshot Ageing Dataset] Identification miss rates vs. FPIR by time-elapsed. The oldest image of each individual is enrolled. Thereafter, all more recent images are searched. Miss rates are computed over all searches noted in row 17 of Table 1 and binned by number of years between search and initial enrollment. FPIR is computed from the same FRVT 2018 non-mates noted in row 3 of Table 1 with $N = 3000\,000$.

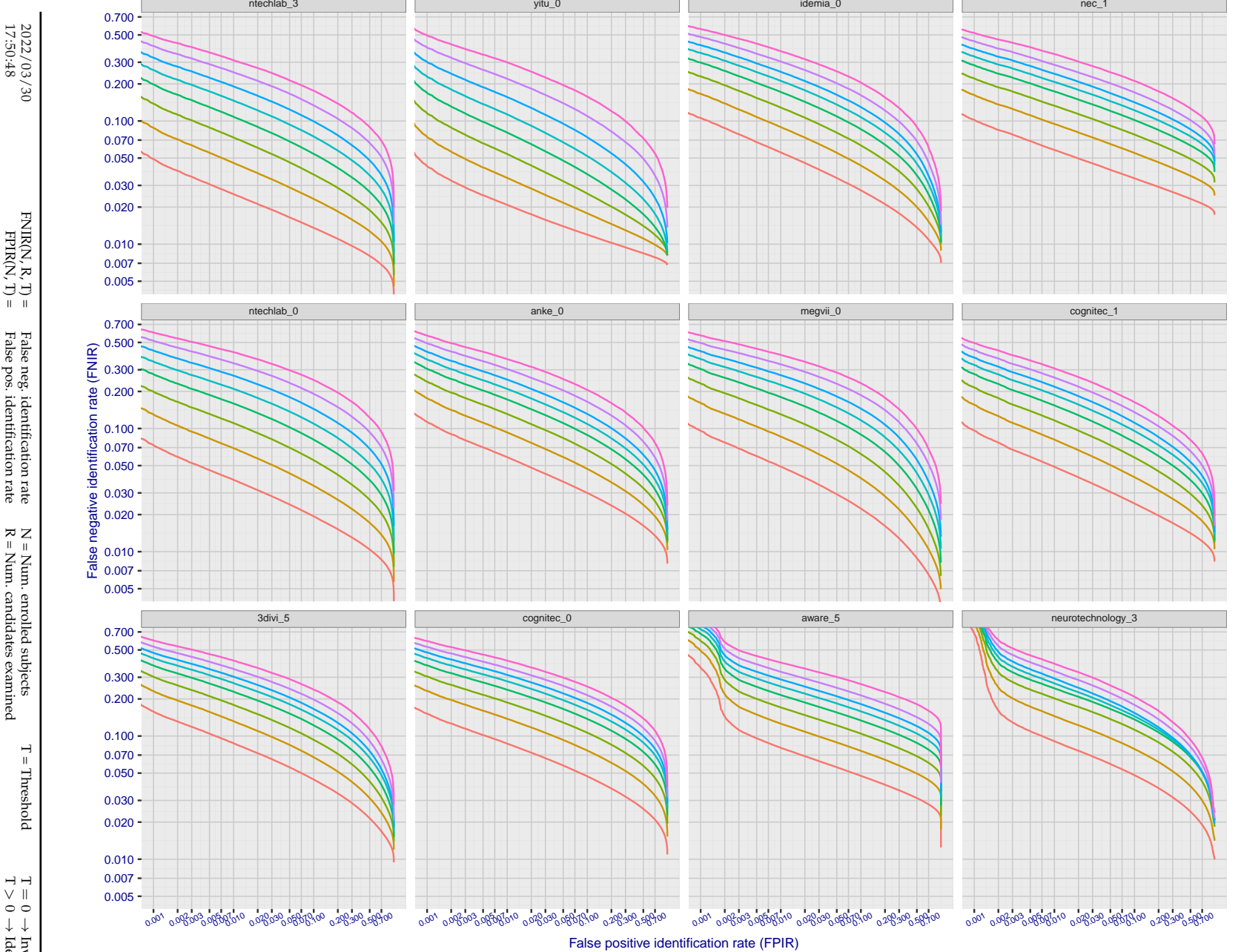


Figure 92: [FRVT-2018 Mugshot Ageing Dataset] Identification miss rates vs. FPIR by time-elapsed. The oldest image of each individual is enrolled. Thereafter, all more recent images are searched. Miss rates are computed over all searches noted in row 17 of Table 1 and binned by number of years between search and initial enrollment. FPIR is computed from the same FRVT 2018 non-mates noted in row 3 of Table 1 with $N = 3\,000\,000$.

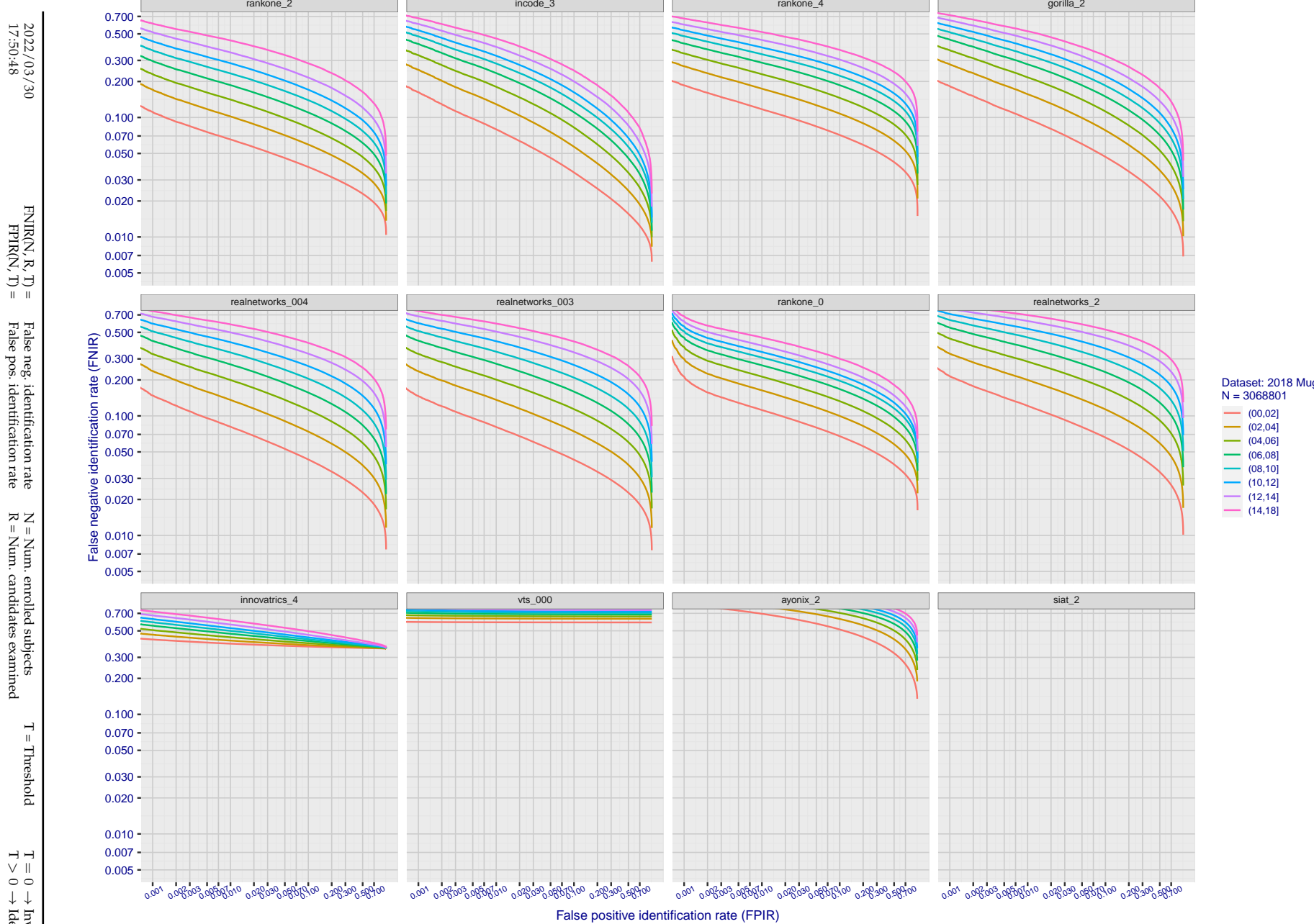


Figure 93: [FRVT-2018 Mugshot Ageing Dataset] Identification miss rates vs. FPIR by time-elapsed. The oldest image of each individual is enrolled. Thereafter, all more recent images are searched. Miss rates are computed over all searches noted in row 17 of Table 1 and binned by number of years between search and initial enrollment. FPIR is computed from the same FRVT 2018 non-mates noted in row 3 of Table 1 with $N = 3\,000\,000$.

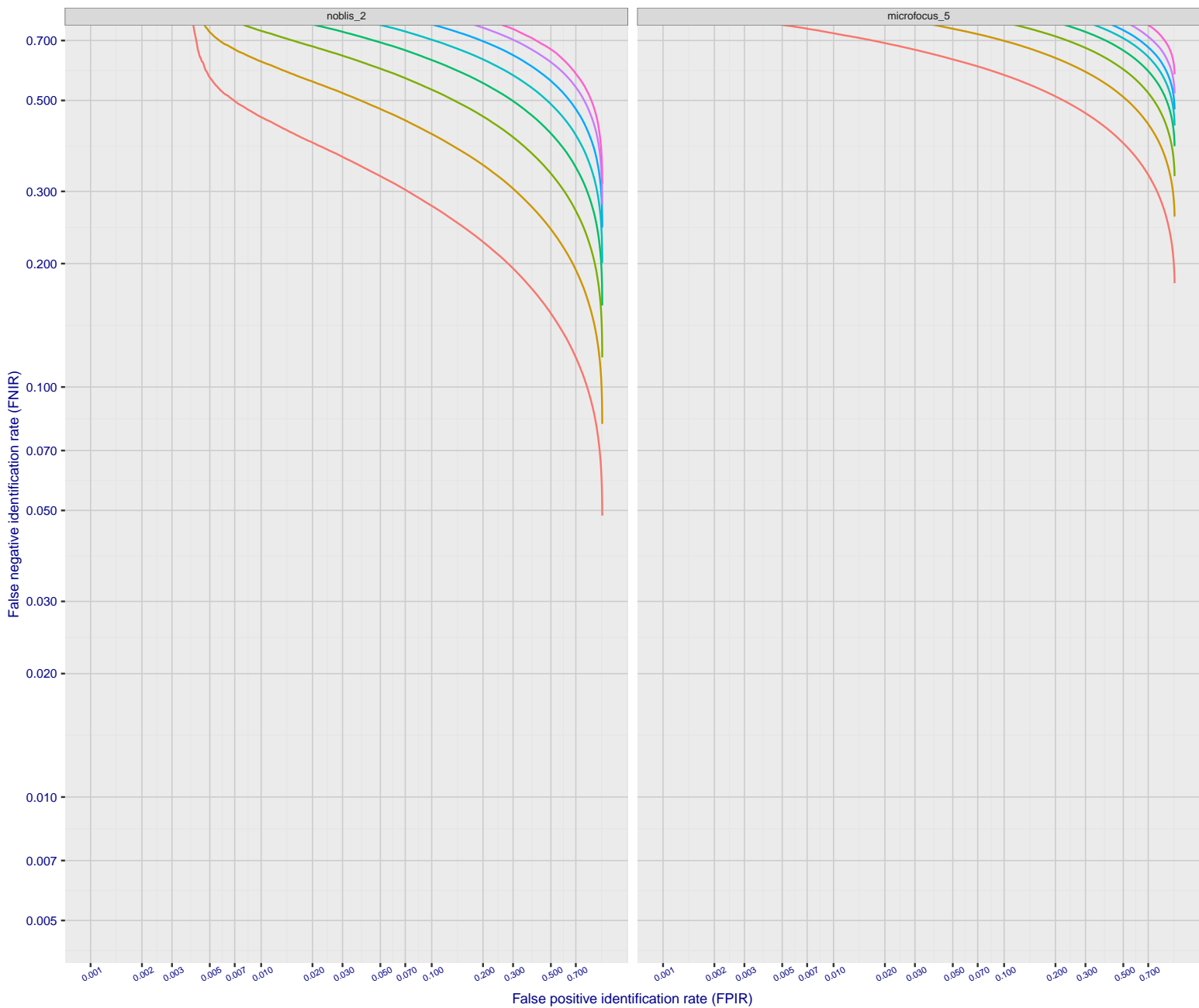
2022/03/30
17:50:48

 $\text{FNIR}(N, R, T) =$
False neg. identification rate
 $\text{FPIR}(N, T) =$
False pos. identification rate

 $N = \text{Num. enrolled subjects}$
 $R = \text{Num. candidates examined}$

 $T = \text{Threshold}$

 $T = 0 \rightarrow \text{Investigation}$
 $T > 0 \rightarrow \text{Identification}$



Dataset: 2018 Mugshots
 $N = 3068801$

(00,02]
(02,04]
(04,06]
(06,08]
(08,10]
(10,12]
(12,14]
(14,18]

Figure 94: [FRVT-2018 Mugshot Ageing Dataset] Identification miss rates vs. FPIR by time elapsed. The oldest image of each individual is enrolled. Thereafter, all more recent images are searched. Miss rates are computed over all searches noted in row 17 of Table 1 and binned by number of years between search and initial enrollment. FPIR is computed from the same FRVT 2018 non-mates noted in row 3 of Table 1 with $N = 3\,000\,000$.

2022/03/30 17:50:48	$\text{FNIR}(N, R, T) =$ $\text{FPTR}(N, T) =$	False neg. identification rate False pos. identification rate	$N =$ Num. enrolled subjects $R =$ Num. candidates examined	$T =$ Threshold $T > 0 \rightarrow$ Identification	$T = 0 \rightarrow$ Investigation
------------------------	---	--	--	---	-----------------------------------

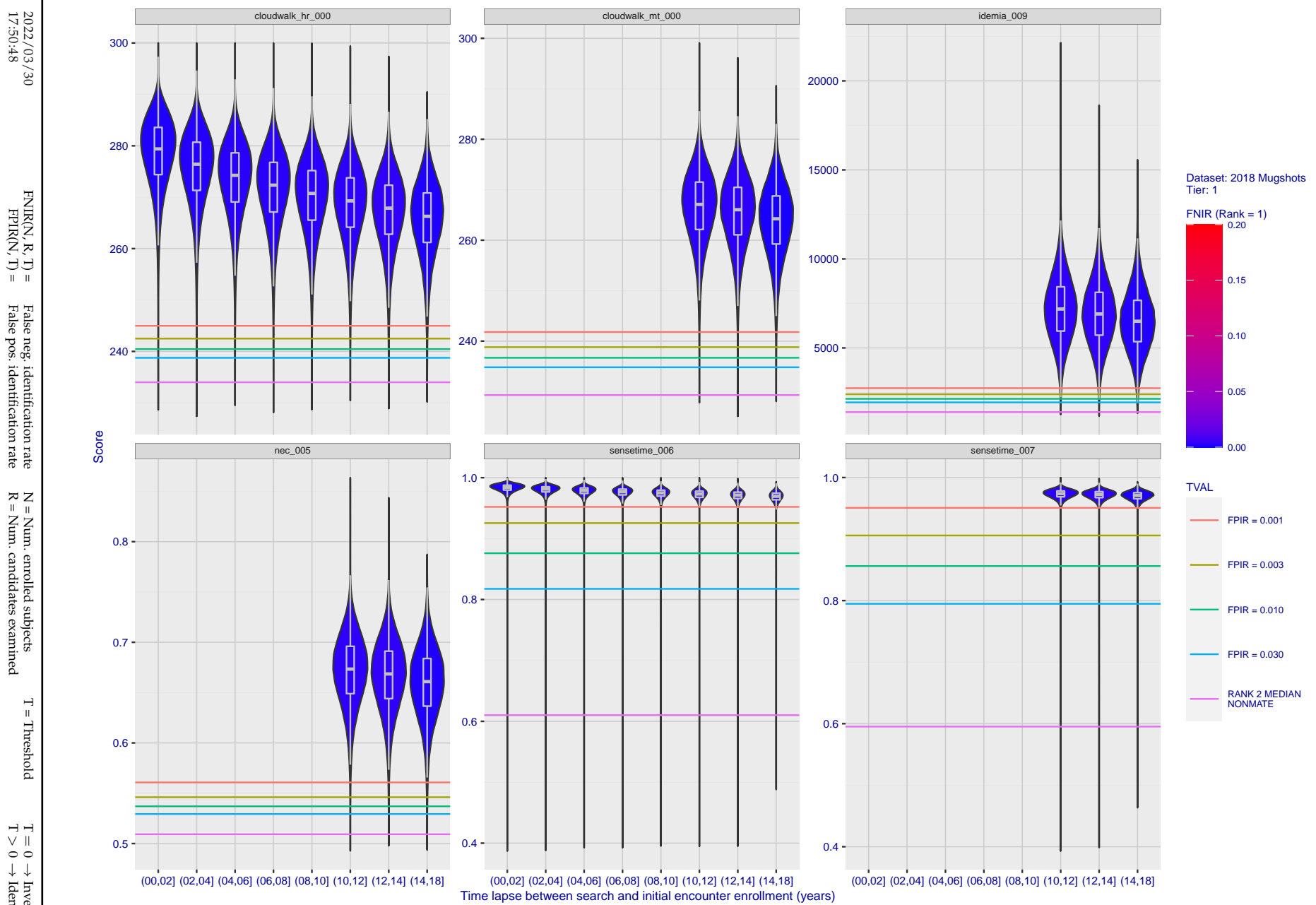


Figure 95: [FRVT-2018 Mugshot Ageing Dataset] Native mate scores vs. time-elapsed. The oldest image of each individual is enrolled. Thereafter, all more recent images are searched. Mated score distributions are computed over all searches noted in row 17 of Table 1 binned by number of years between search and initial enrollment.

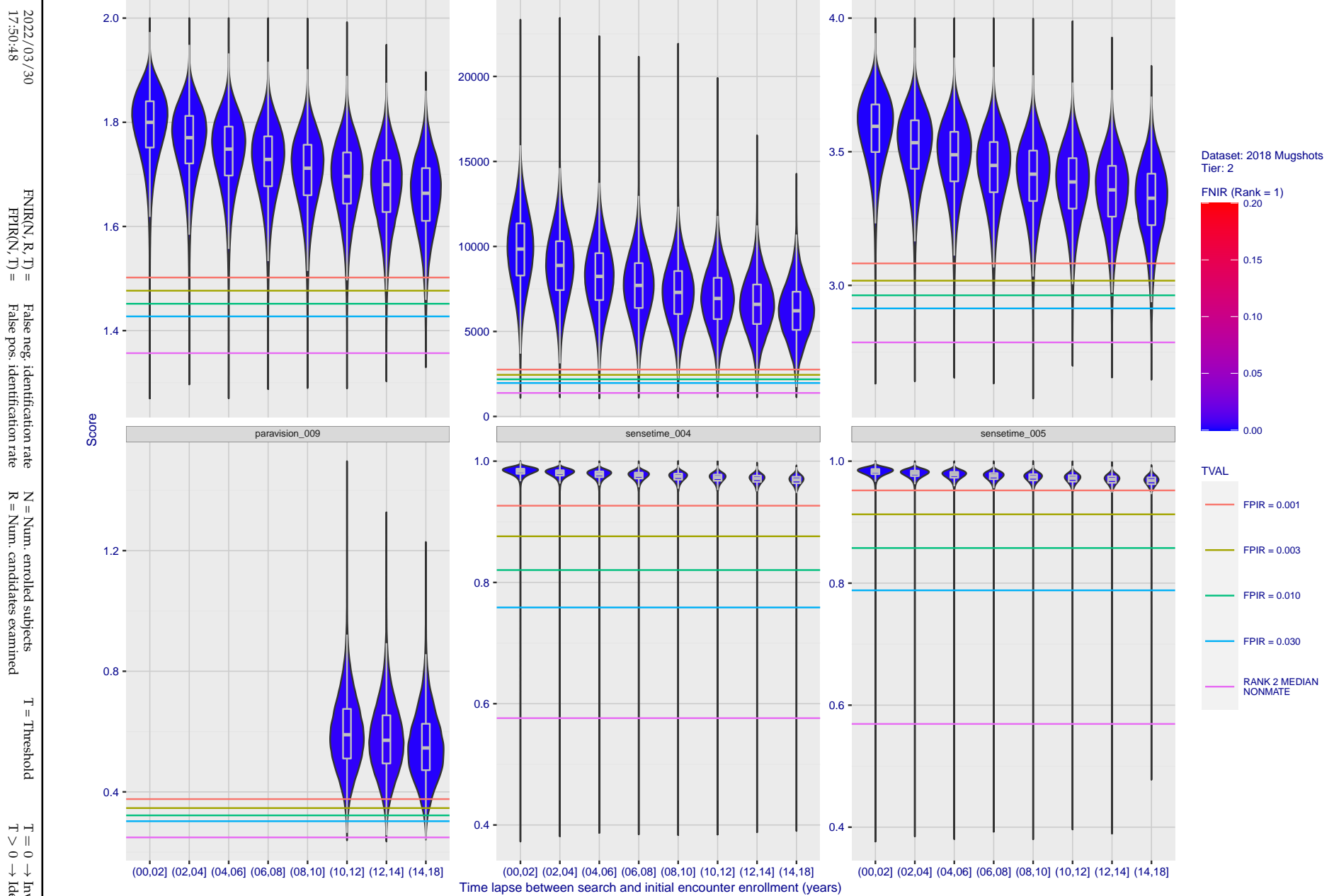


Figure 96: [FRVT-2018 Mugshot Ageing Dataset] Native mate scores vs. time-elapsed. The oldest image of each individual is enrolled. Thereafter, all more recent images are searched. Mated score distributions are computed over all searches noted in row 17 of Table 1 binned by number of years between search and initial enrollment.

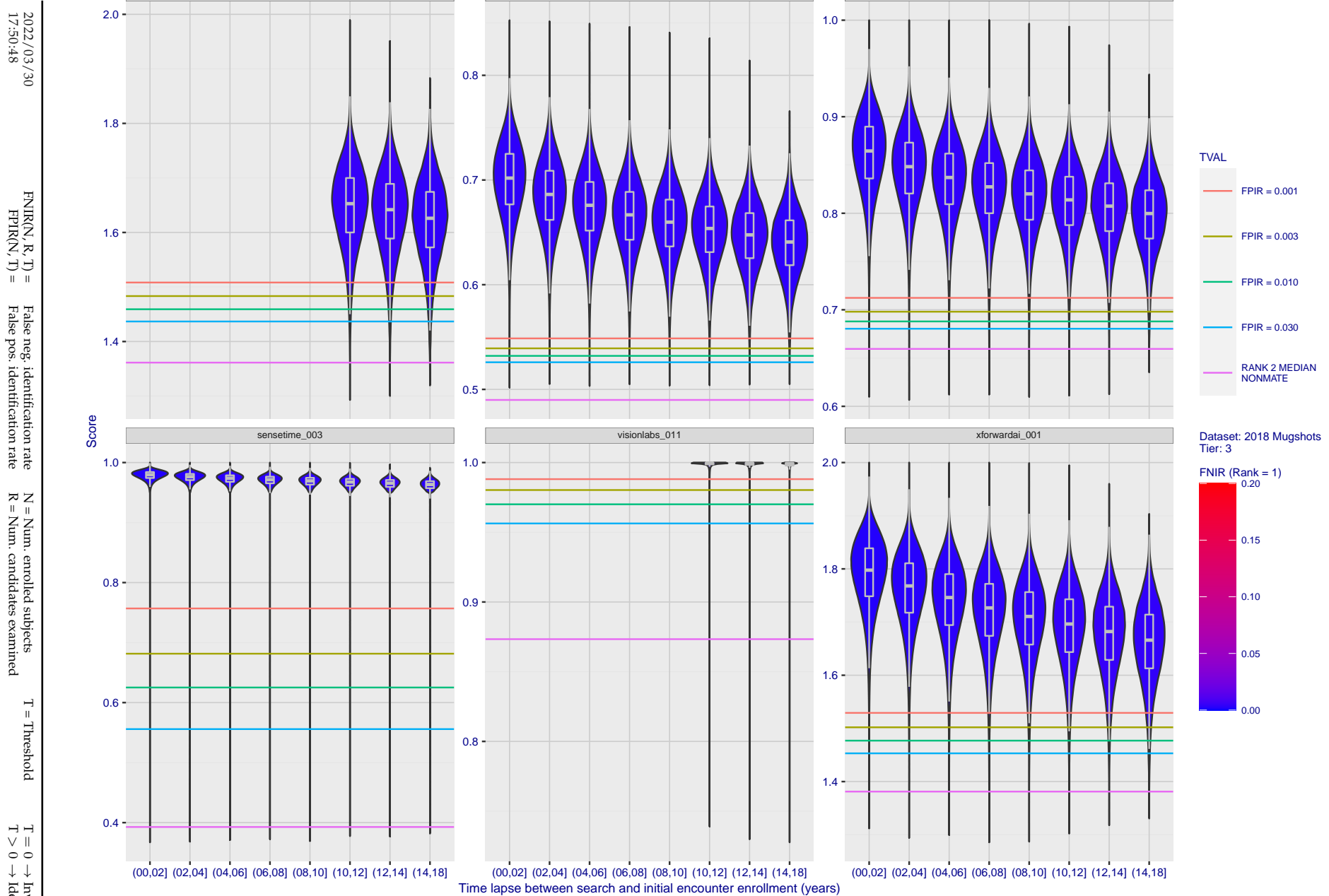


Figure 97: [FRVT-2018 Mugshot Ageing Dataset] Native mate scores vs. time-elapsed. The oldest image of each individual is enrolled. Thereafter, all more recent images are searched. Mated score distributions are computed over all searches noted in row 17 of Table 1 binned by number of years between search and initial enrollment.

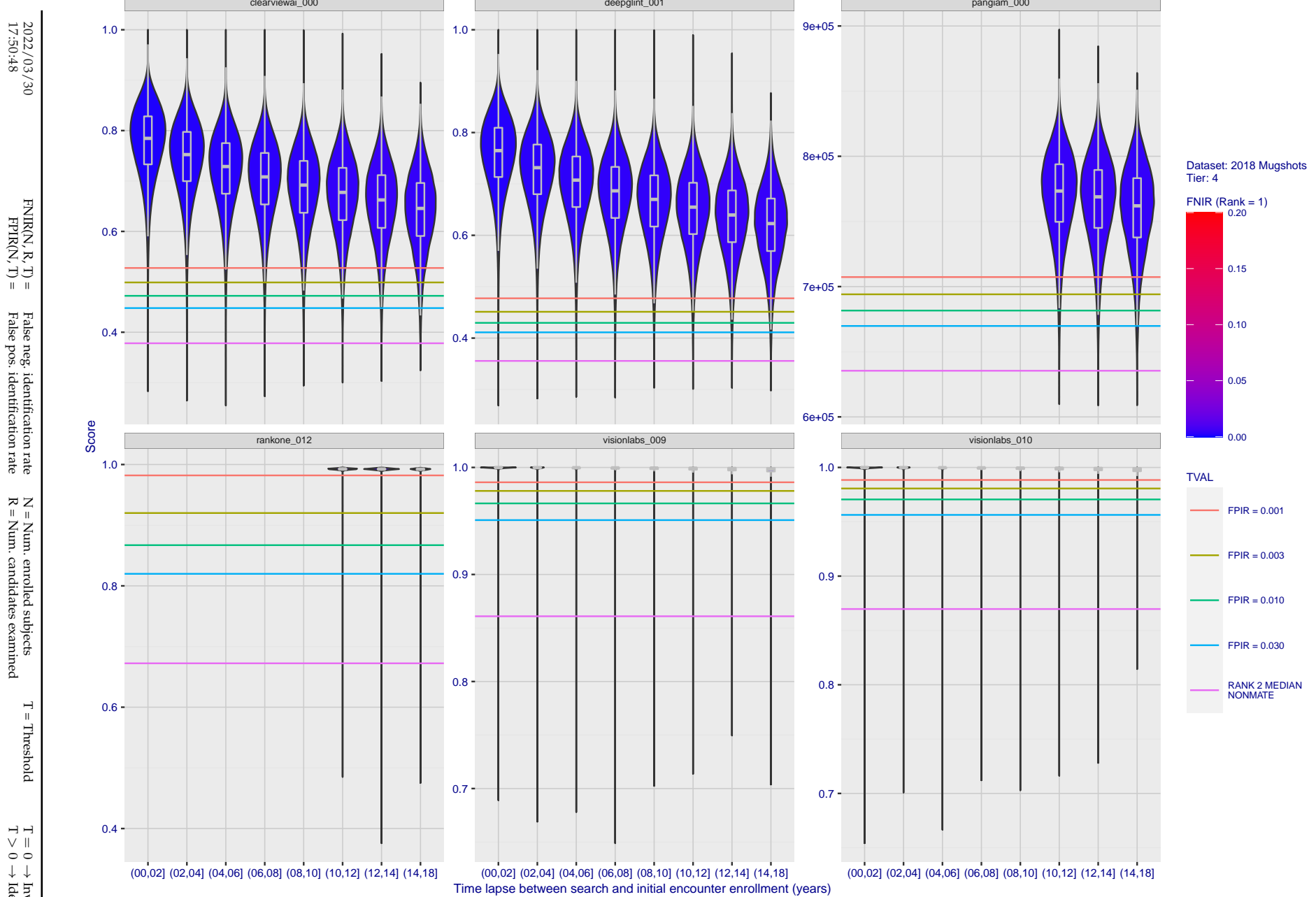


Figure 98: [FRVT-2018 Mugshot Ageing Dataset] Native mate scores vs. time-elapsed. The oldest image of each individual is enrolled. Thereafter, all more recent images are searched. Mated score distributions are computed over all searches noted in row 17 of Table 1 binned by number of years between search and initial enrollment.

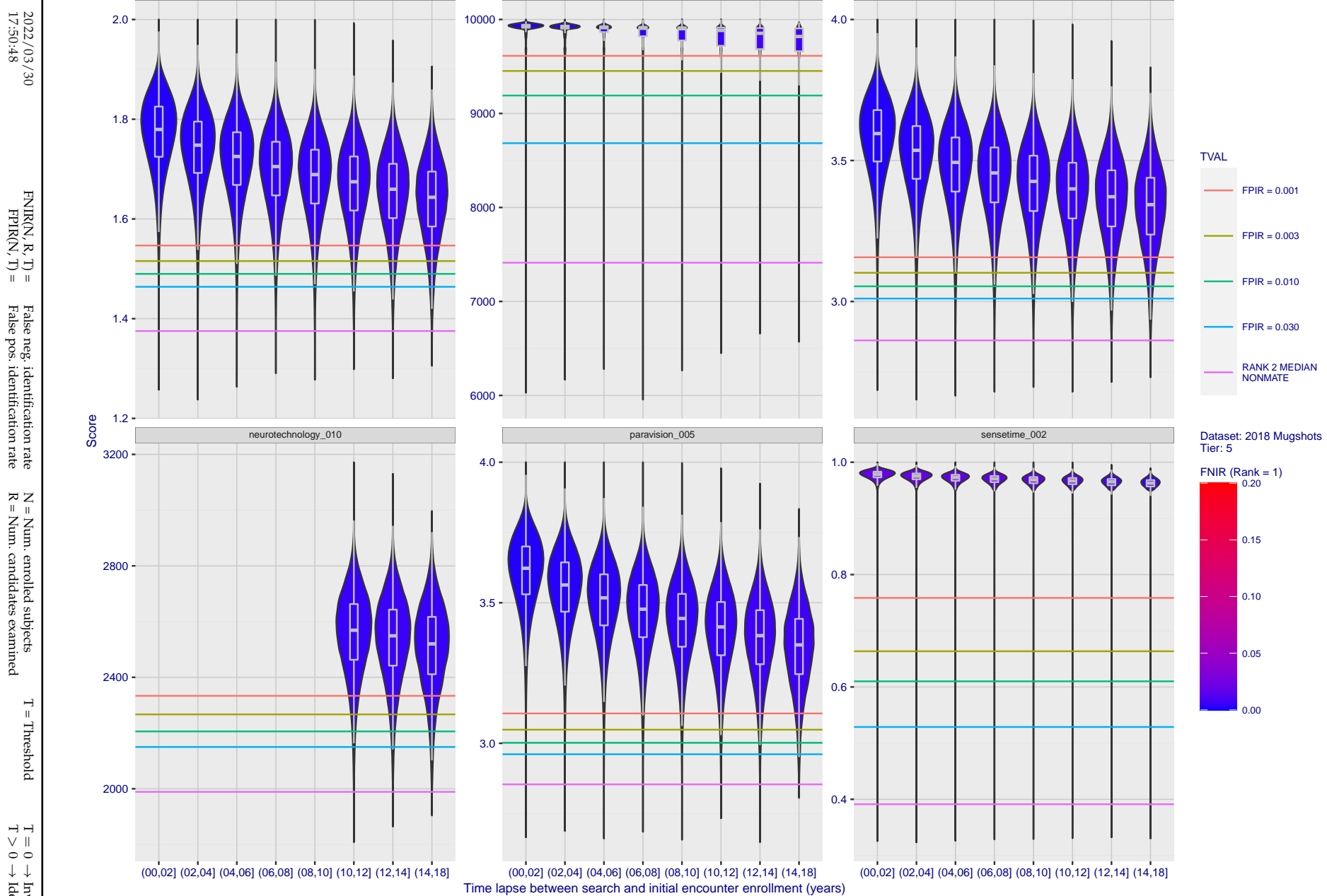


Figure 99: [FRVT-2018 Mugshot Ageing Dataset] Native mate scores vs. time-elapsed. The oldest image of each individual is enrolled. Thereafter, all more recent images are searched. Mated score distributions are computed over all searches noted in row 17 of Table 1 binned by number of years between search and initial enrollment.

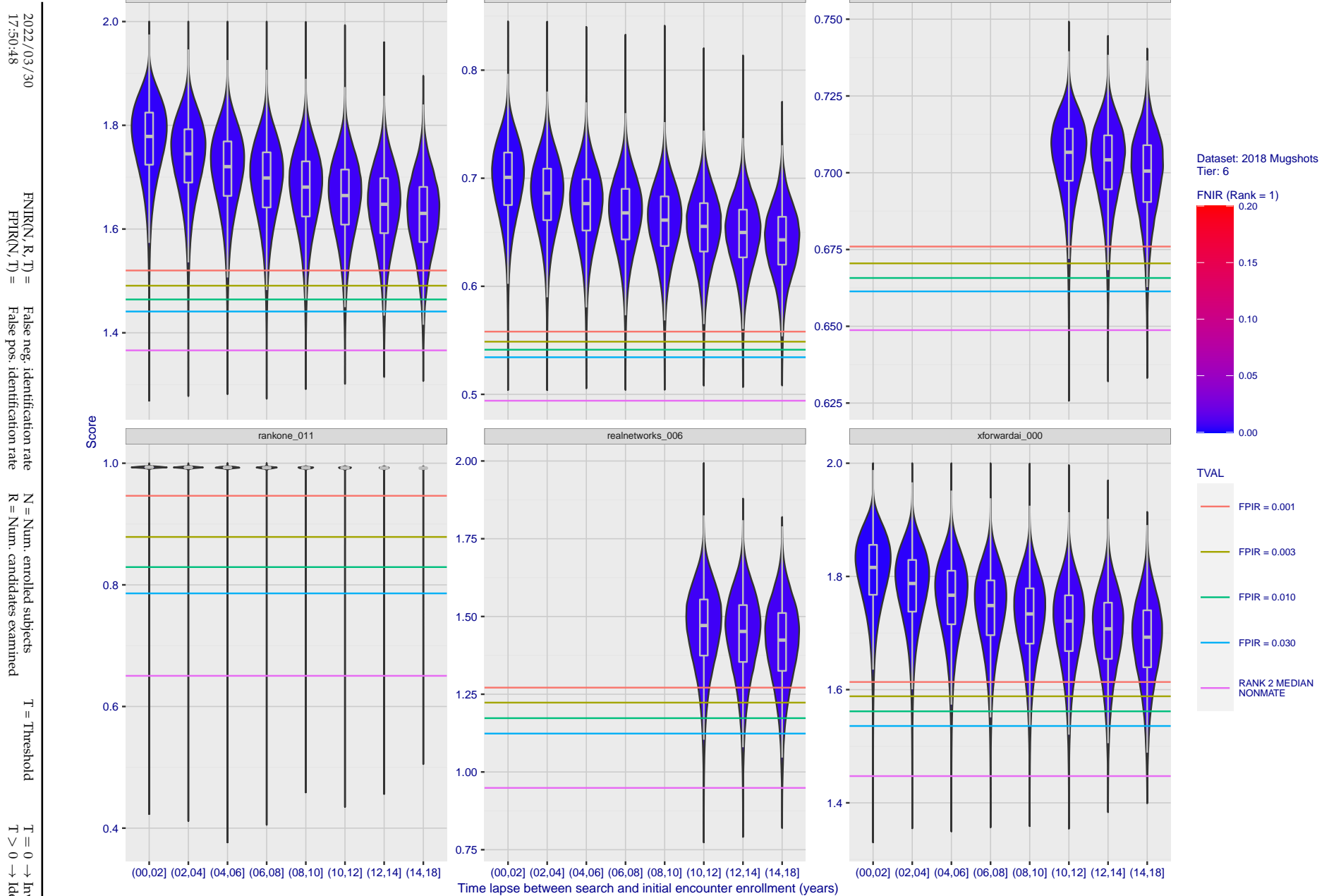


Figure 100: [FRVT-2018 Mugshot Ageing Dataset] Native mate scores vs. time-elapsed. The oldest image of each individual is enrolled. Thereafter, all more recent images are searched. Mated score distributions are computed over all searches noted in row 17 of Table 1 binned by number of years between search and initial enrollment.

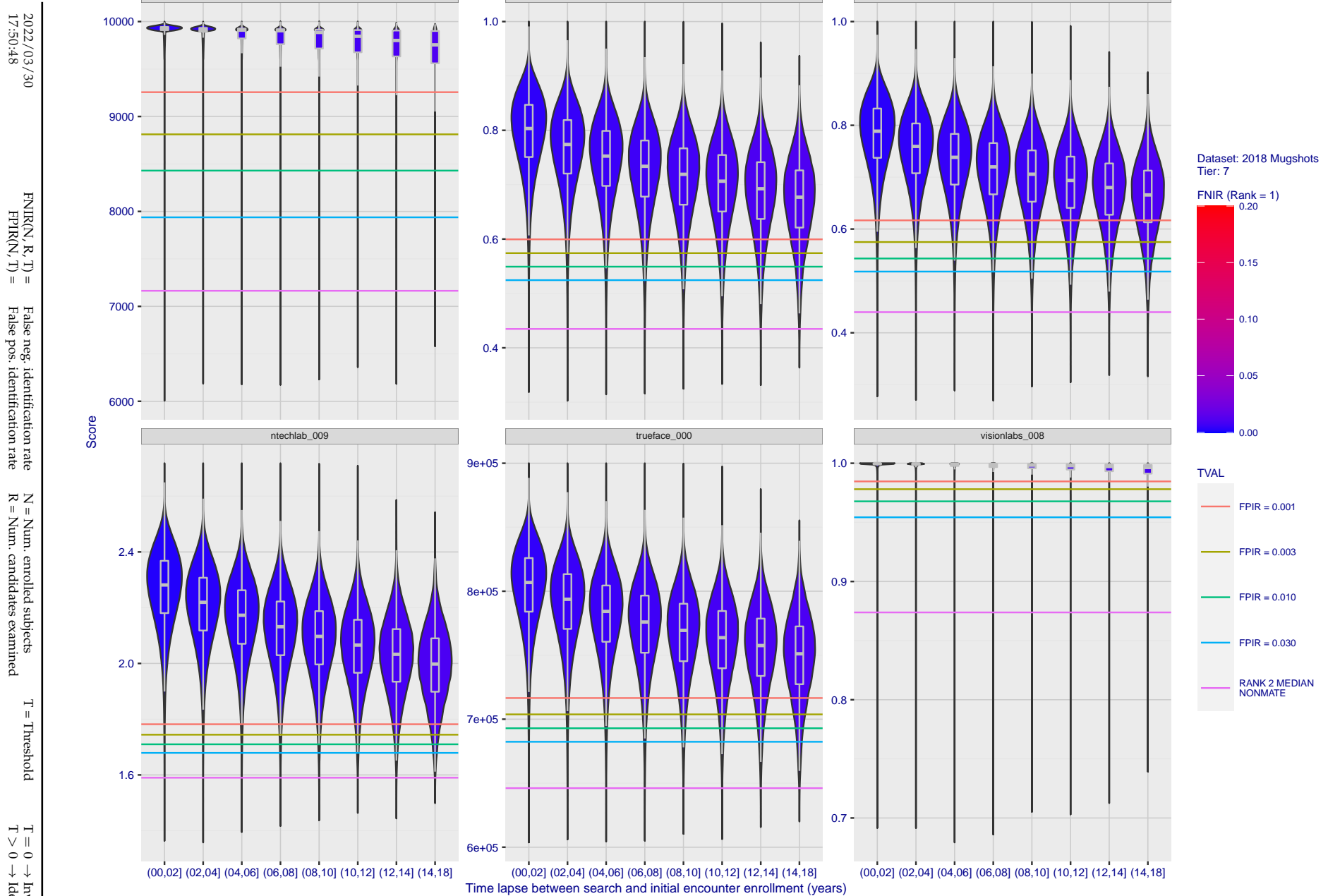


Figure 101: [FRVT-2018 Mugshot Ageing Dataset] Native mate scores vs. time-elapsed. The oldest image of each individual is enrolled. Thereafter, all more recent images are searched. Mated score distributions are computed over all searches noted in row 17 of Table 1 binned by number of years between search and initial enrollment.

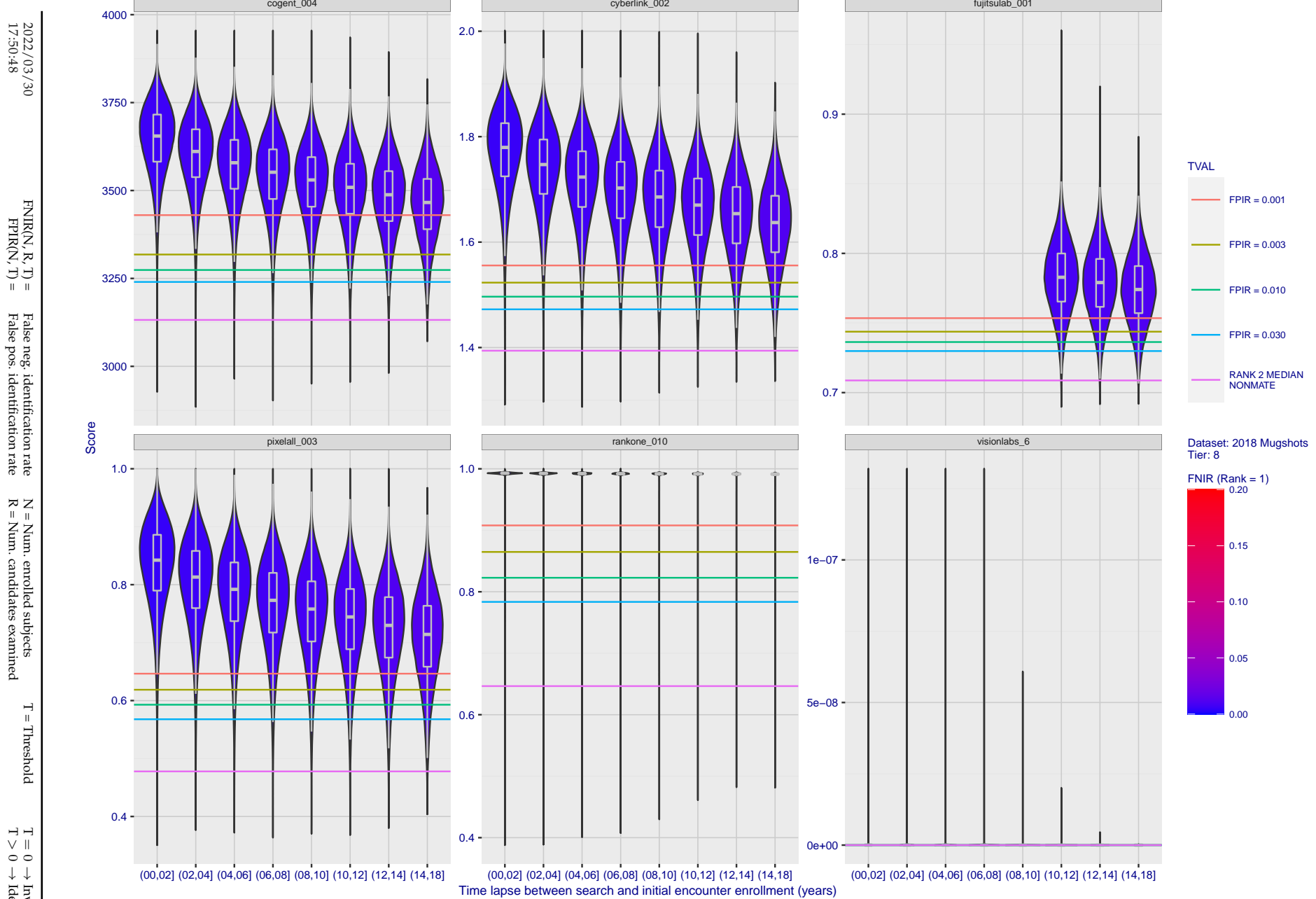


Figure 102: [FRVT-2018 Mugshot Ageing Dataset] Native mate scores vs. time-elapsed. The oldest image of each individual is enrolled. Thereafter, all more recent images are searched. Mated score distributions are computed over all searches noted in row 17 of Table 1 binned by number of years between search and initial enrollment.

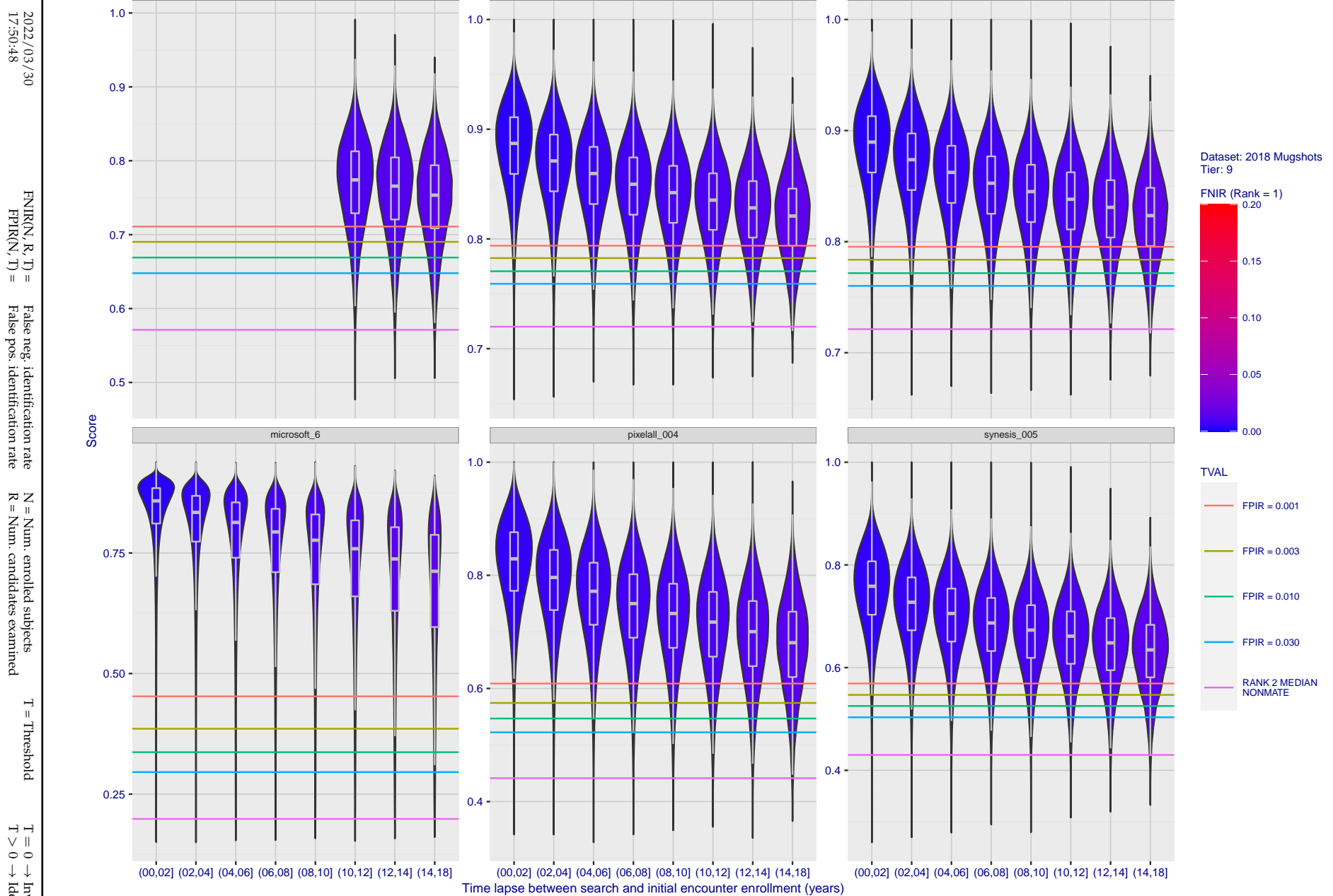


Figure 103: [FRVT-2018 Mugshot Ageing Dataset] Native mate scores vs. time-elapsed. The oldest image of each individual is enrolled. Thereafter, all more recent images are searched. Mated score distributions are computed over all searches noted in row 17 of Table 1 binned by number of years between search and initial enrollment.

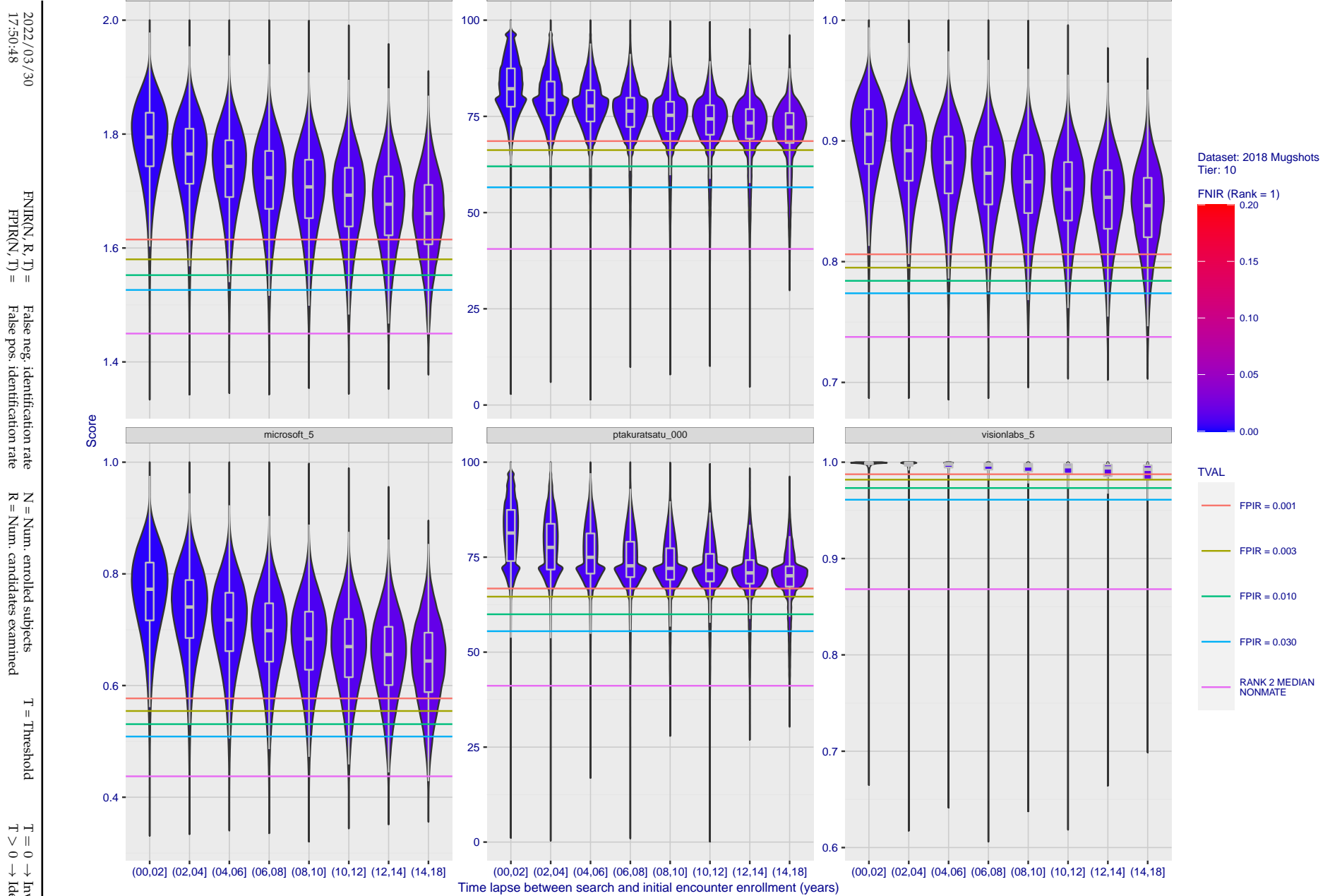


Figure 104: [FRVT-2018 Mugshot Ageing Dataset] Native mate scores vs. time-elapsed. The oldest image of each individual is enrolled. Thereafter, all more recent images are searched. Mated score distributions are computed over all searches noted in row 17 of Table 1 binned by number of years between search and initial enrollment.

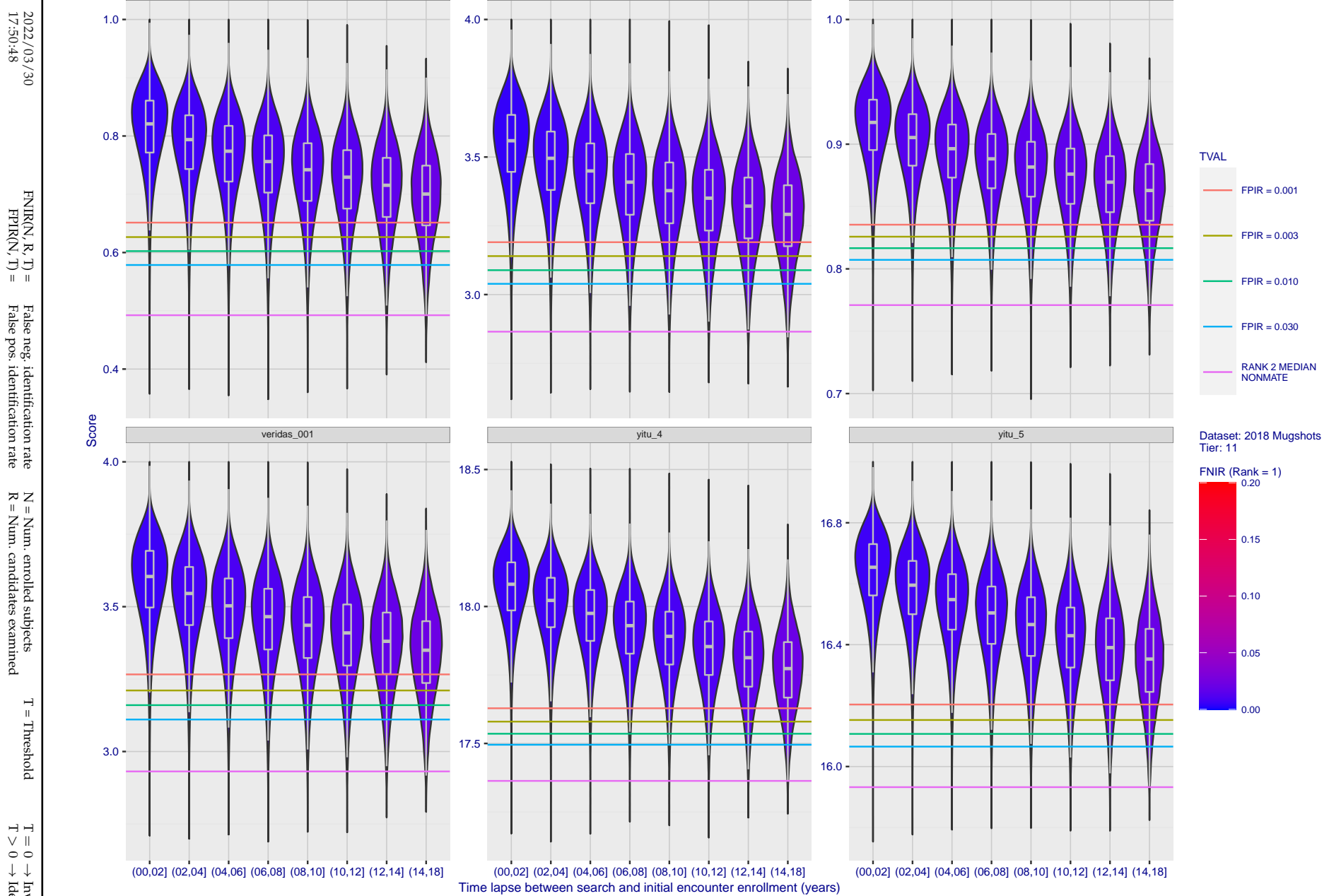


Figure 105: [FRVT-2018 Mugshot Ageing Dataset] Native mate scores vs. time-elapsed. The oldest image of each individual is enrolled. Thereafter, all more recent images are searched. Mated score distributions are computed over all searches noted in row 17 of Table 1 binned by number of years between search and initial enrollment.

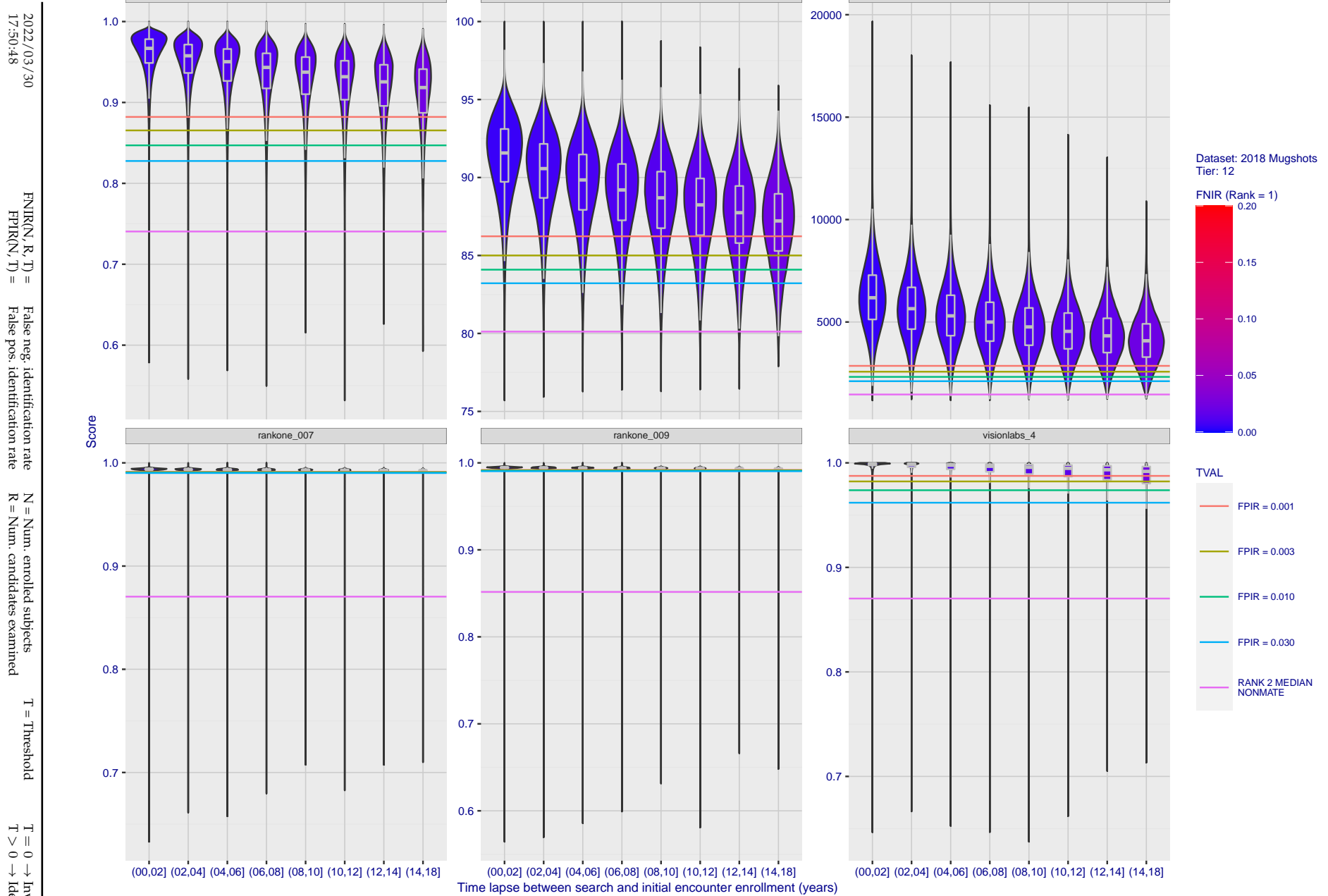


Figure 106: [FRVT-2018 Mugshot Ageing Dataset] Native mate scores vs. time-elapsed. The oldest image of each individual is enrolled. Thereafter, all more recent images are searched. Mated score distributions are computed over all searches noted in row 17 of Table 1 binned by number of years between search and initial enrollment.

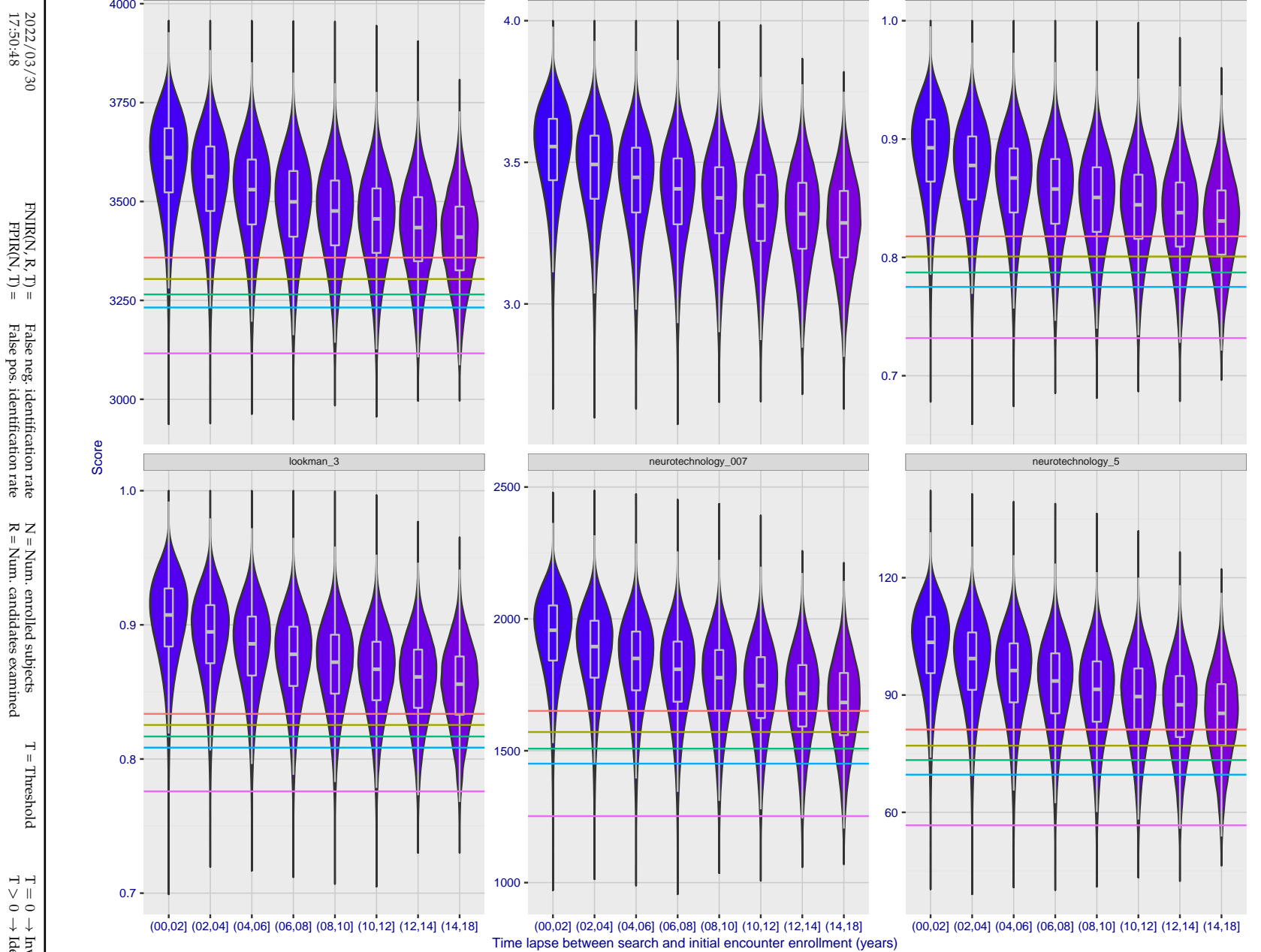


Figure 107: [FRVT-2018 Mugshot Ageing Dataset] Native mate scores vs. time-elapsed. The oldest image of each individual is enrolled. Thereafter, all more recent images are searched. Mated score distributions are computed over all searches noted in row 17 of Table 1 binned by number of years between search and initial enrollment.

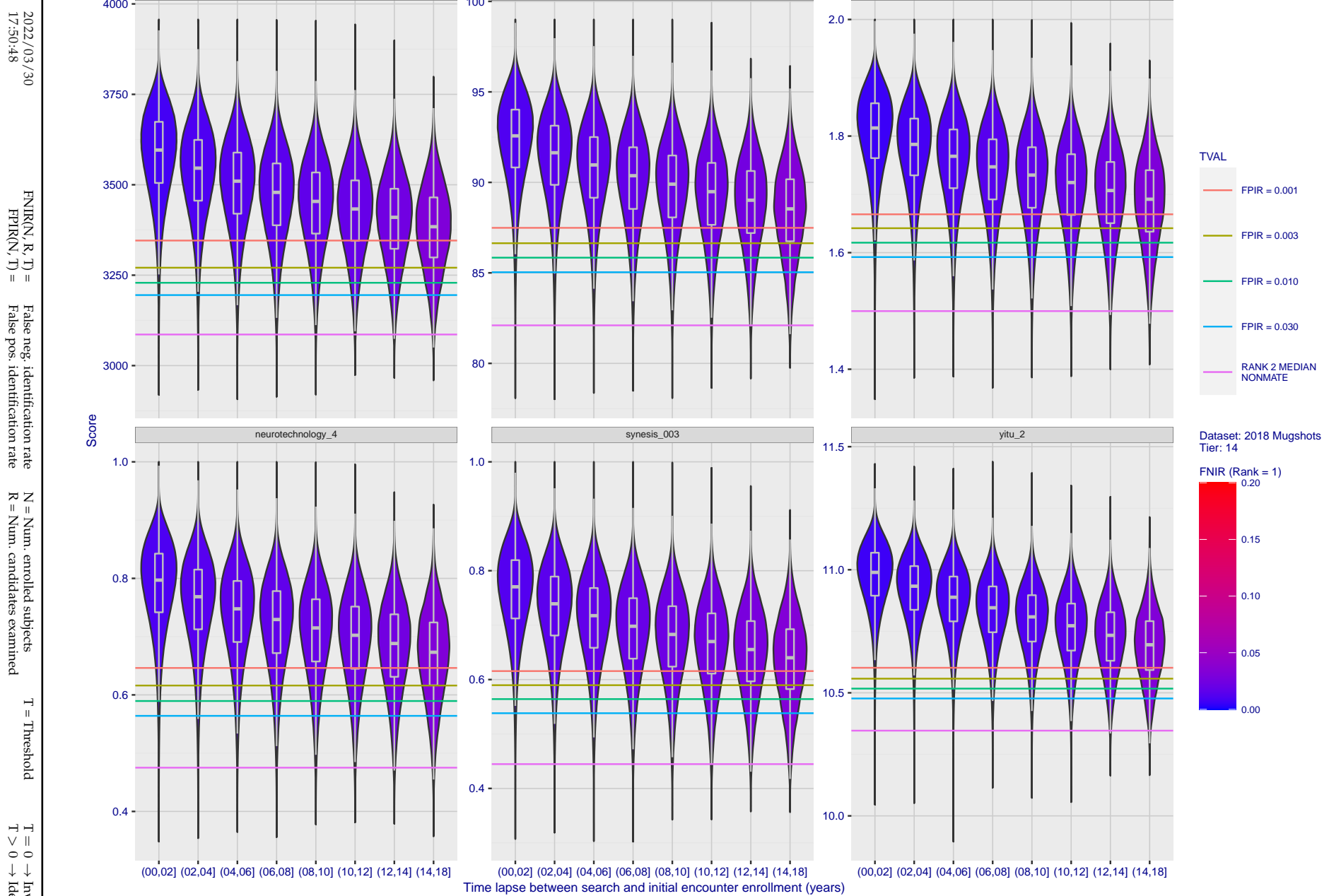


Figure 108: [FRVT-2018 Mugshot Ageing Dataset] Native mate scores vs. time-elapsed. The oldest image of each individual is enrolled. Thereafter, all more recent images are searched. Mated score distributions are computed over all searches noted in row 17 of Table 1 binned by number of years between search and initial enrollment.

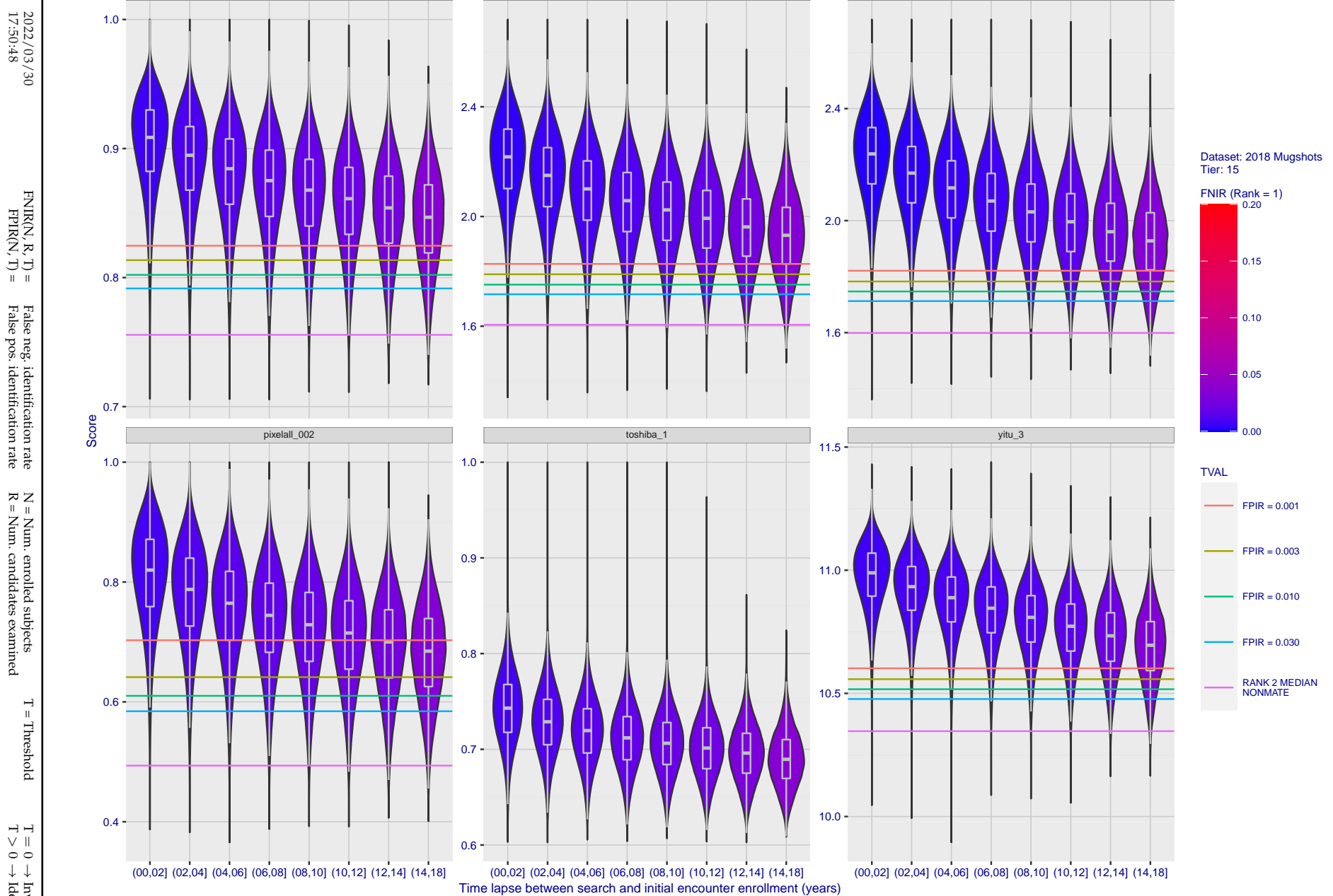


Figure 109: [FRVT-2018 Mugshot Ageing Dataset] Native mate scores vs. time-elapsed. The oldest image of each individual is enrolled. Thereafter, all more recent images are searched. Mated score distributions are computed over all searches noted in row 17 of Table 1 binned by number of years between search and initial enrollment.

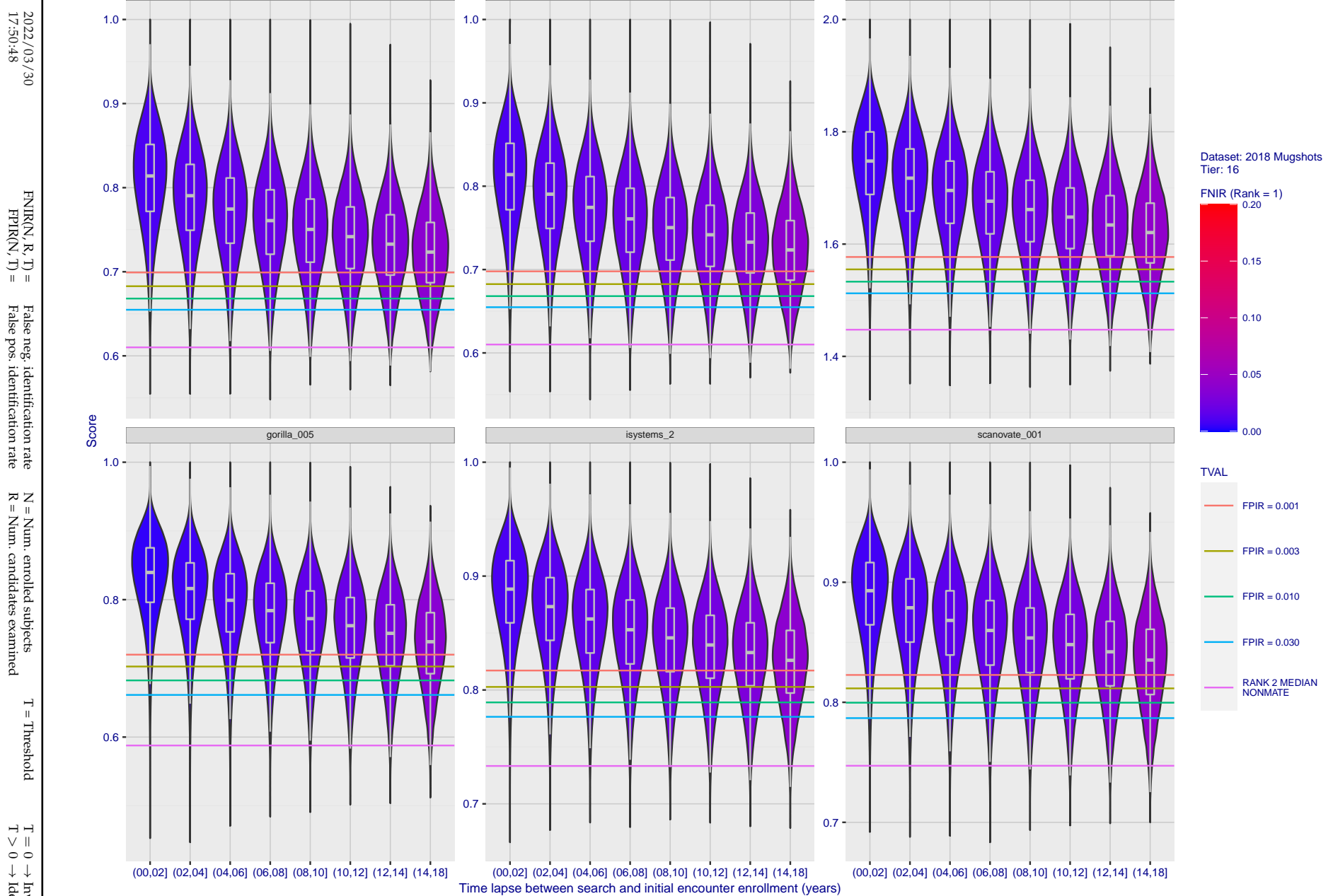


Figure 110: [FRVT-2018 Mugshot Ageing Dataset] Native mate scores vs. time-elapsed. The oldest image of each individual is enrolled. Thereafter, all more recent images are searched. Mated score distributions are computed over all searches noted in row 17 of Table 1 binned by number of years between search and initial enrollment.

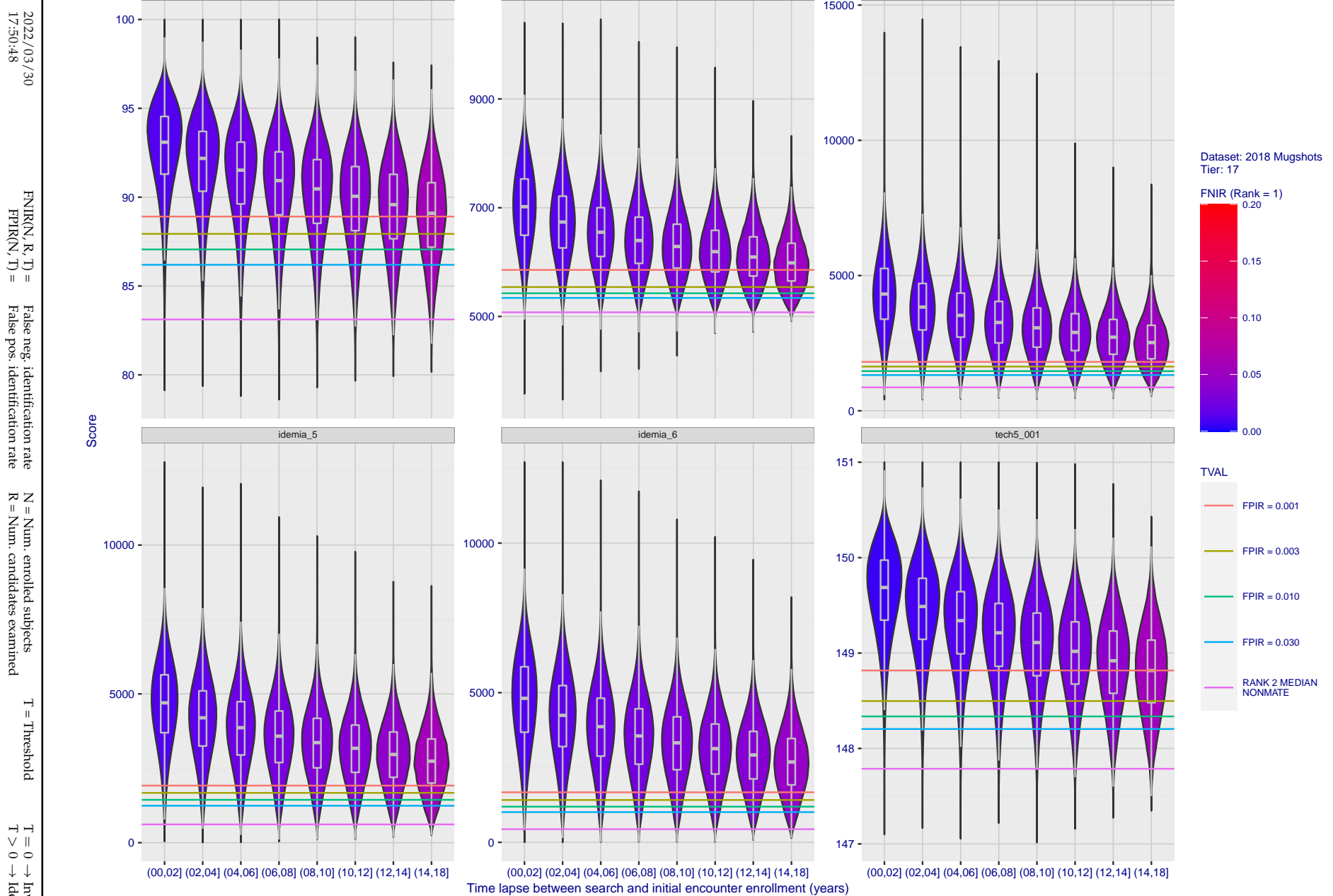


Figure 111: [FRVT-2018 Mugshot Ageing Dataset] Native mate scores vs. time-elapsed. The oldest image of each individual is enrolled. Thereafter, all more recent images are searched. Mated score distributions are computed over all searches noted in row 17 of Table 1 binned by number of years between search and initial enrollment.

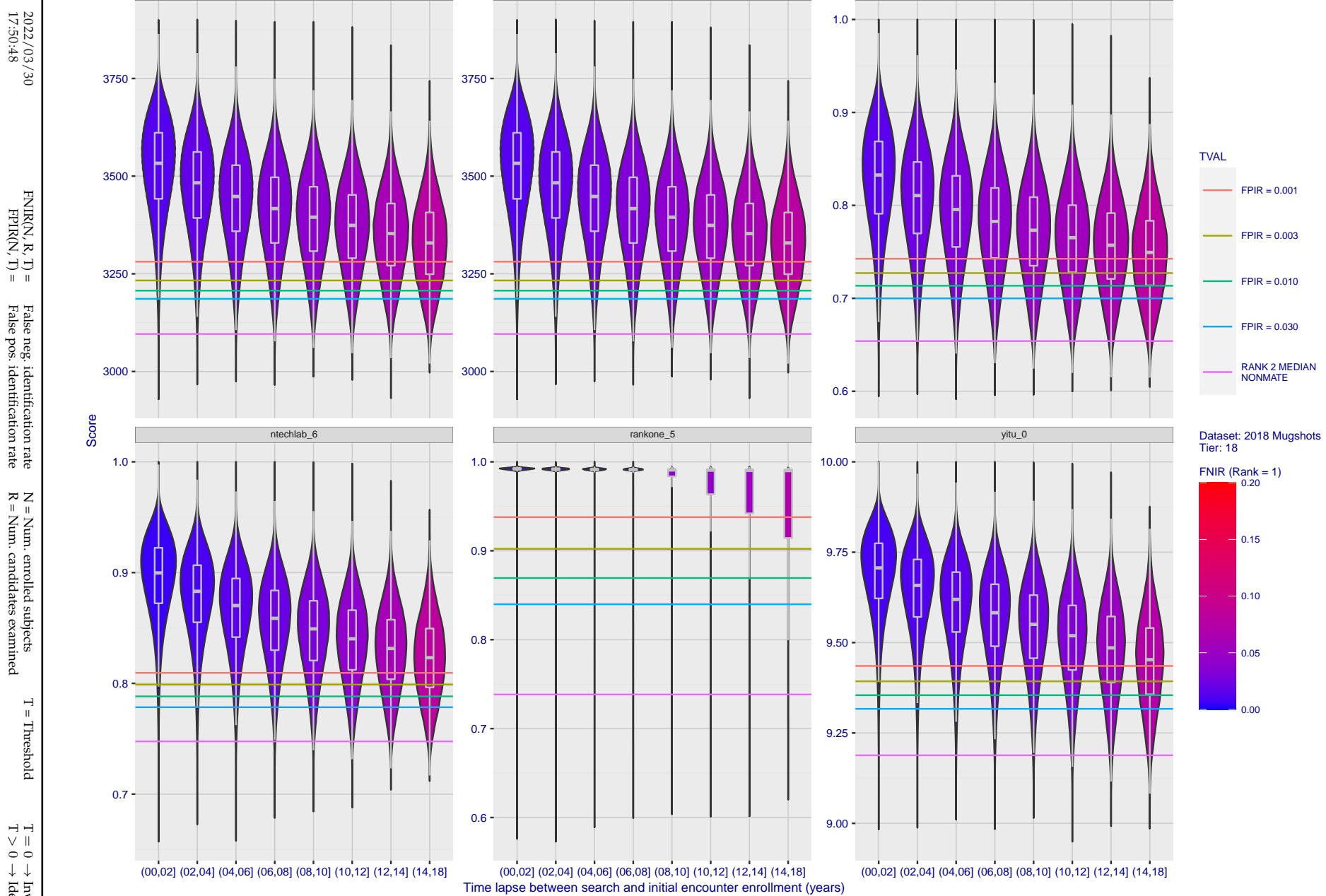


Figure 112: [FRVT-2018 Mugshot Ageing Dataset] Native mate scores vs. time-elapsed. The oldest image of each individual is enrolled. Thereafter, all more recent images are searched. Mated score distributions are computed over all searches noted in row 17 of Table 1 binned by number of years between search and initial enrollment.

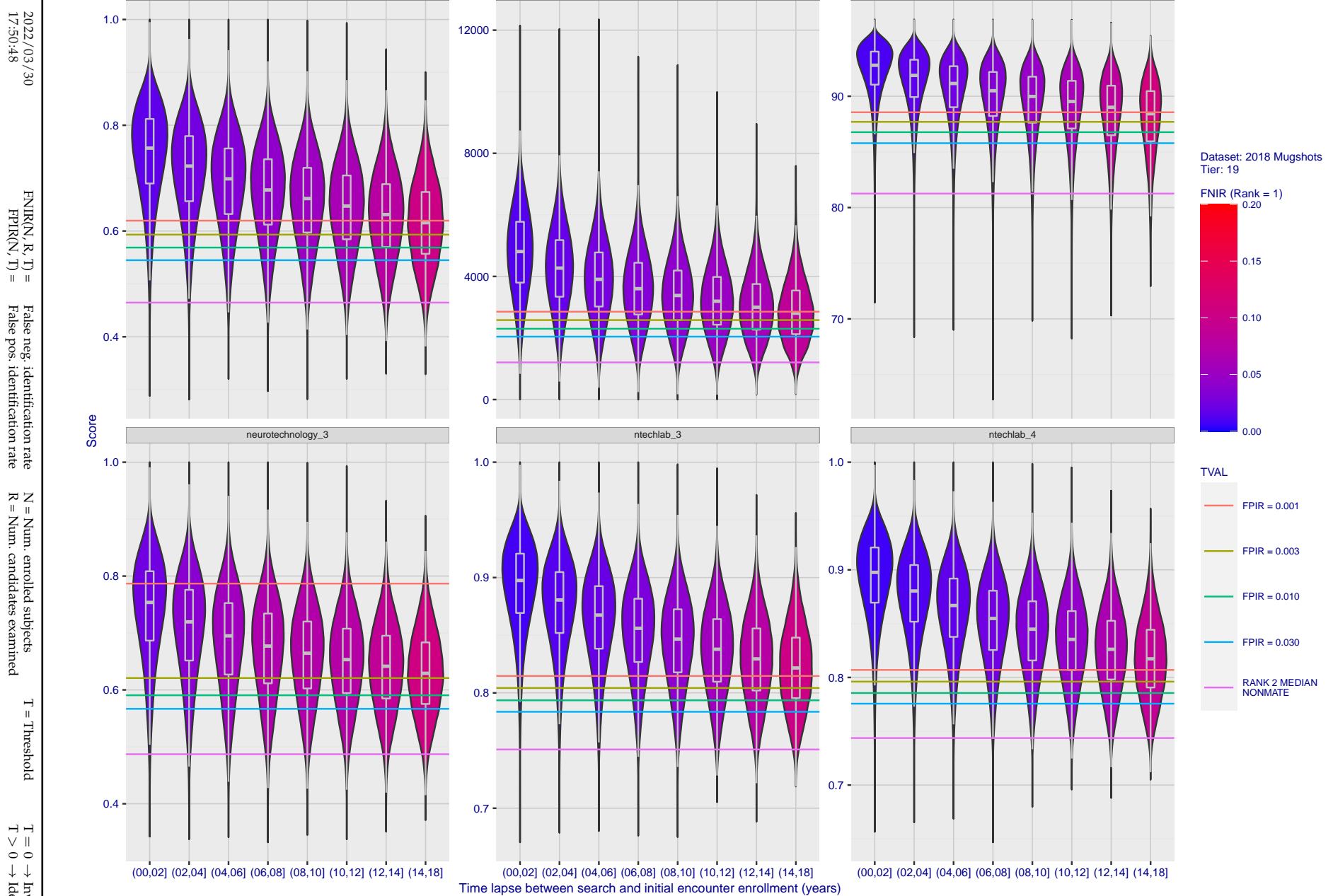


Figure 113: [FRVT-2018 Mugshot Ageing Dataset] Native mate scores vs. time-elapsed. The oldest image of each individual is enrolled. Thereafter, all more recent images are searched. Mated score distributions are computed over all searches noted in row 17 of Table 1 binned by number of years between search and initial enrollment.

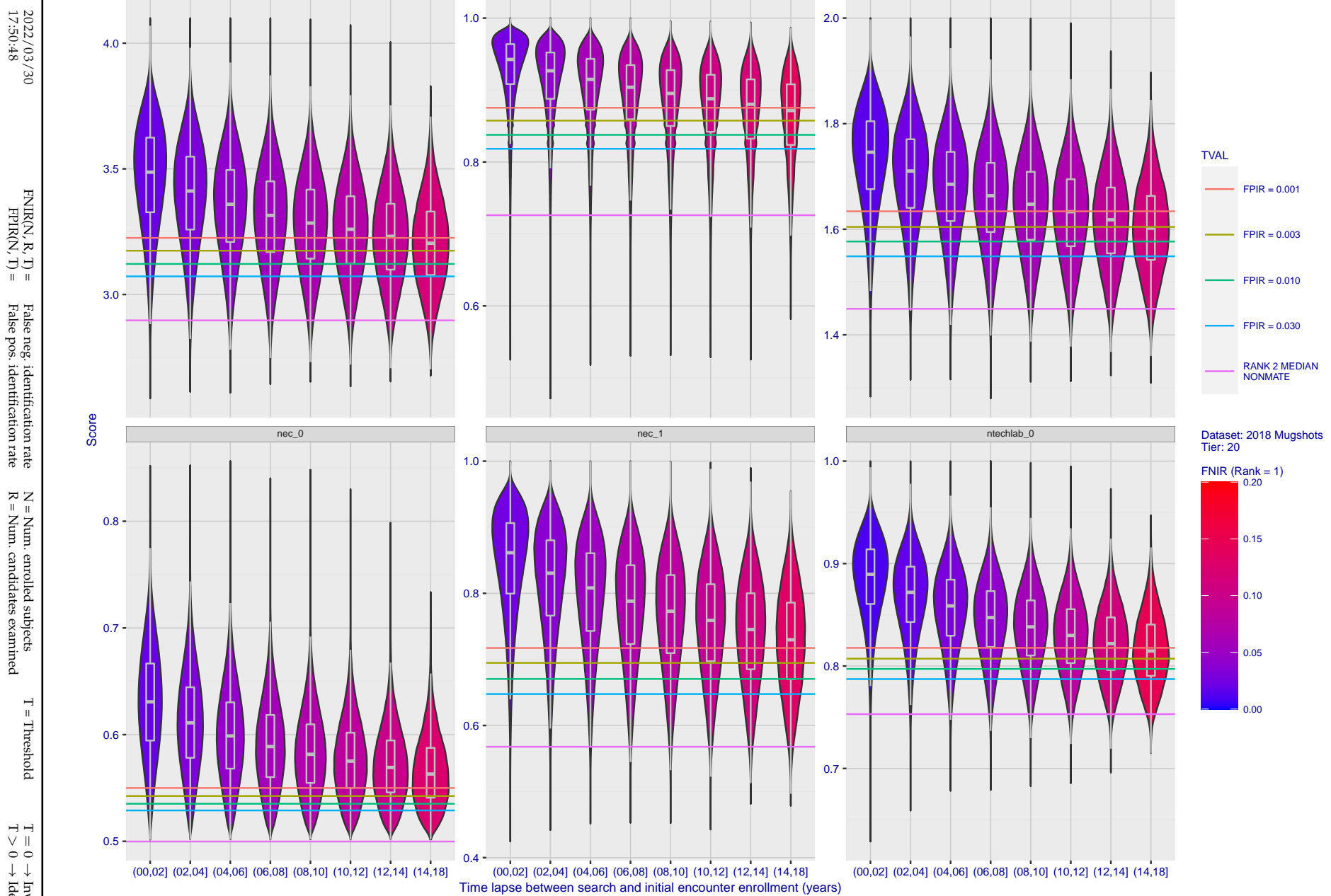


Figure 114: [FRVT-2018 Mugshot Ageing Dataset] Native mate scores vs. time-elapsed. The oldest image of each individual is enrolled. Thereafter, all more recent images are searched. Mated score distributions are computed over all searches noted in row 17 of Table 1 binned by number of years between search and initial enrollment.

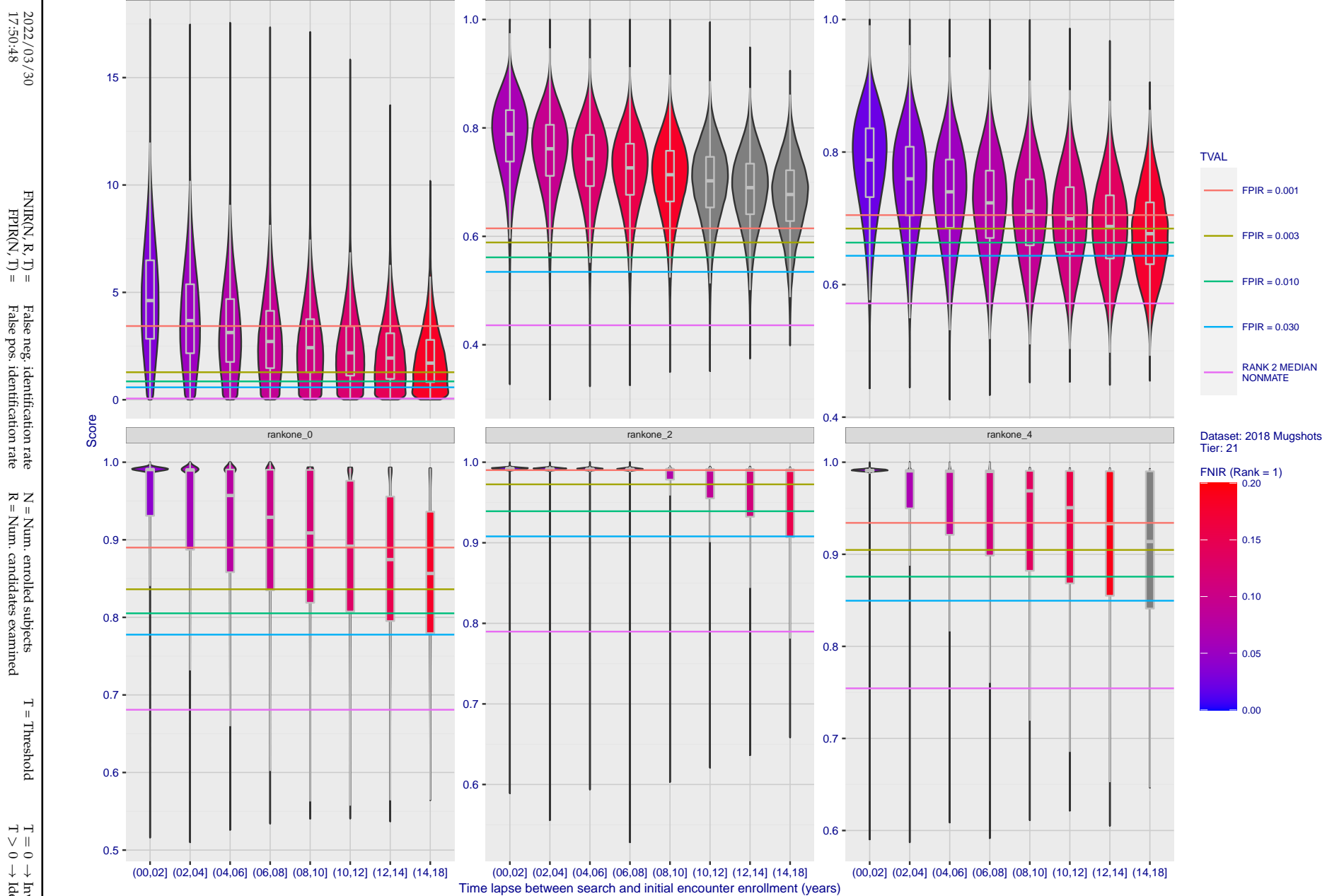


Figure 115: [FRVT-2018 Mugshot Ageing Dataset] Native mate scores vs. time-elapsed. The oldest image of each individual is enrolled. Thereafter, all more recent images are searched. Mated score distributions are computed over all searches noted in row 17 of Table 1 binned by number of years between search and initial enrollment.

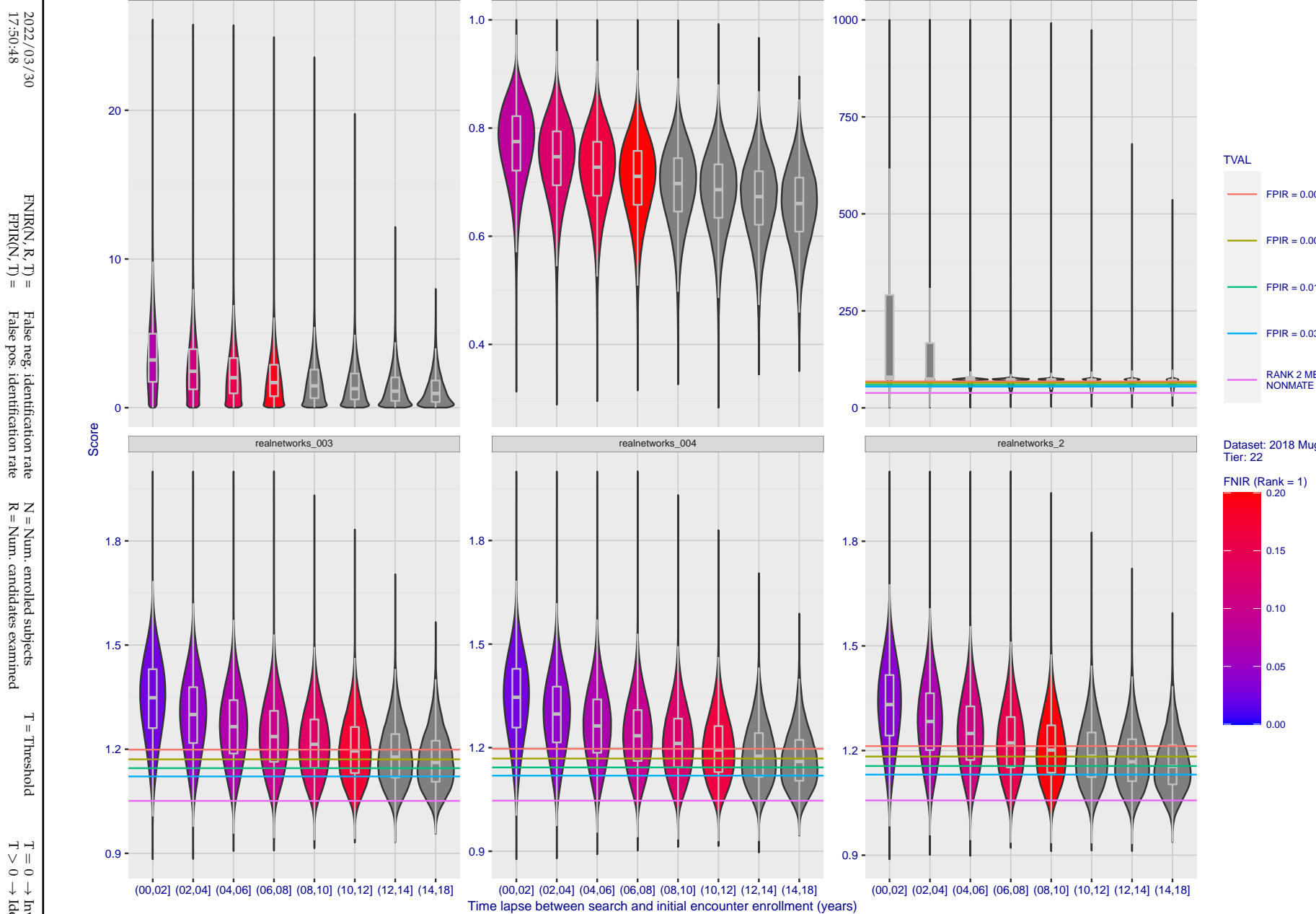


Figure 116: [FRVT-2018 Mugshot Ageing Dataset] Native mate scores vs. time-elapsed. The oldest image of each individual is enrolled. Thereafter, all more recent images are searched. Mated score distributions are computed over all searches noted in row 17 of Table 1 binned by number of years between search and initial enrollment.

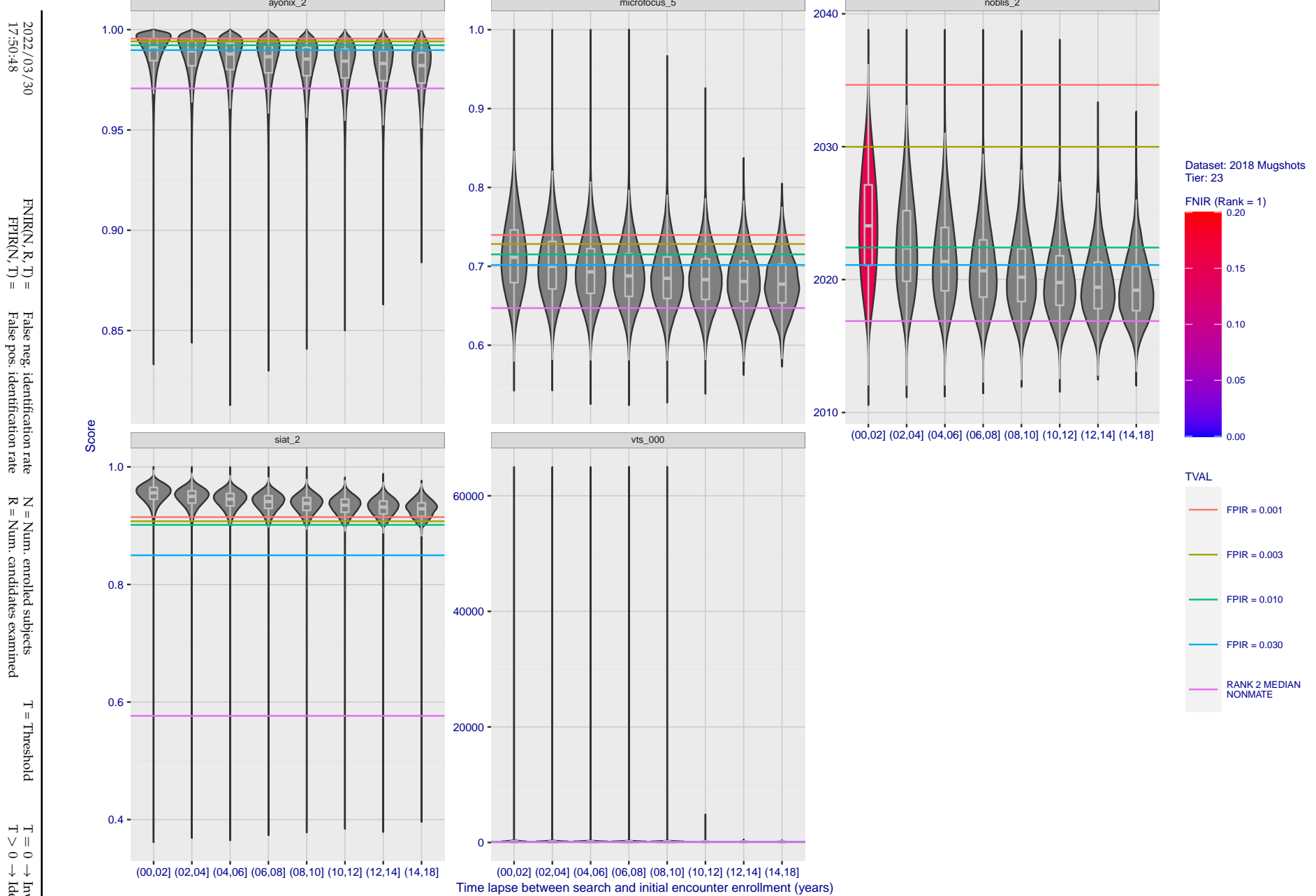


Figure 117: [FRVT-2018 Mugshot Ageing Dataset] Native mate scores vs. time-elapsed. The oldest image of each individual is enrolled. Thereafter, all more recent images are searched. Mated score distributions are computed over all searches noted in row 17 of Table 1 binned by number of years between search and initial enrollment.

Appendix C Effect of enrolling multiple images

2022/03/30
17:50:48FNIR(N, R, T) = False neg. identification rate
FPIR(N, T) = False pos. identification rateN = Num. enrolled subjects
R = Num. candidates examined

T = Threshold

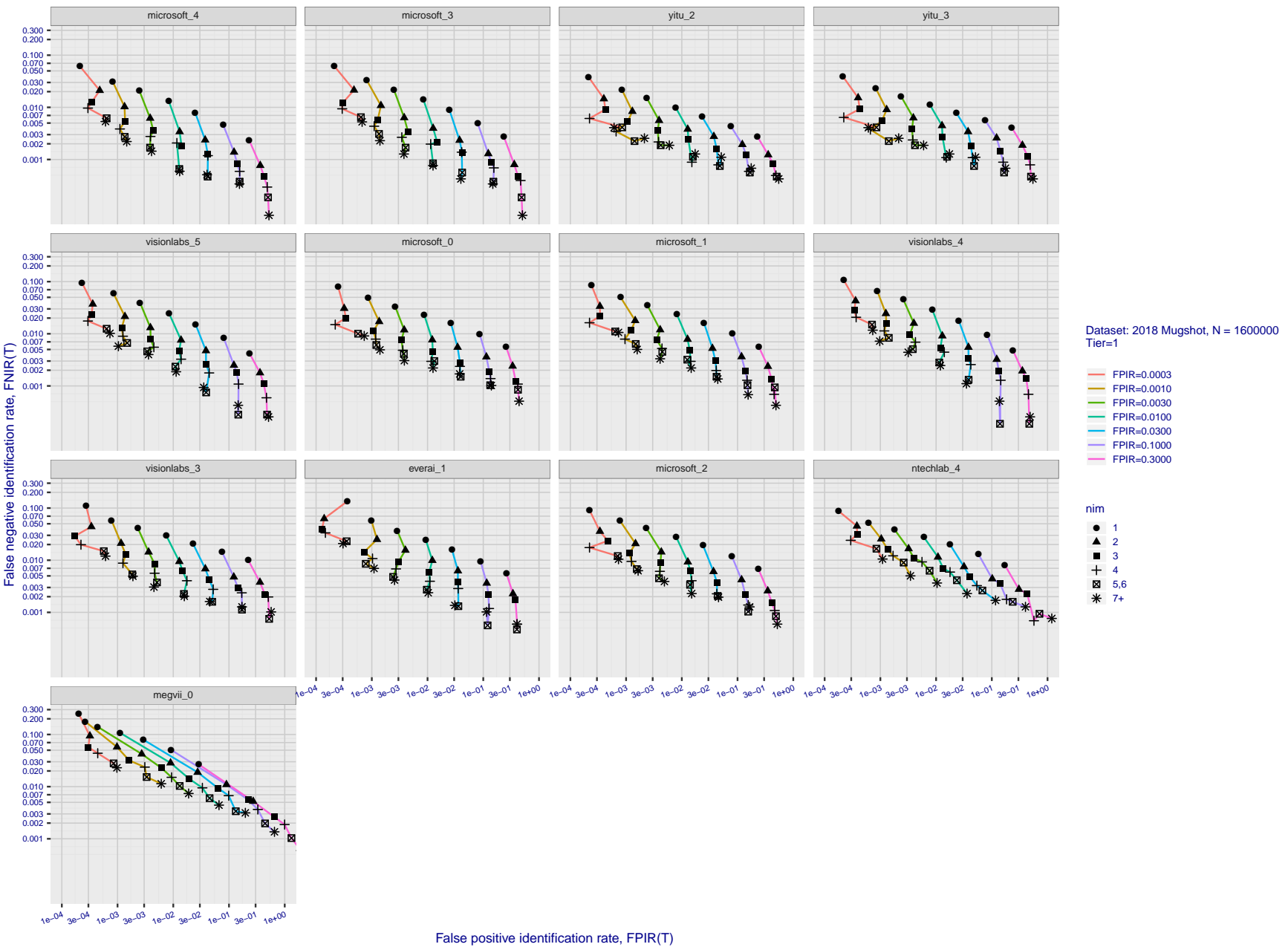
T = 0 → Investigation
T > 0 → Identification

Figure 118: [FRVT-2018 Mugshot Dataset] Effect of enrolling multiple images for each identity. The plot shows an identification miss rates vs. false positive rates, at seven operating thresholds. The enrolled population size is fixed. The images are enrolled with lifetime-consolidation - see section 2.3.

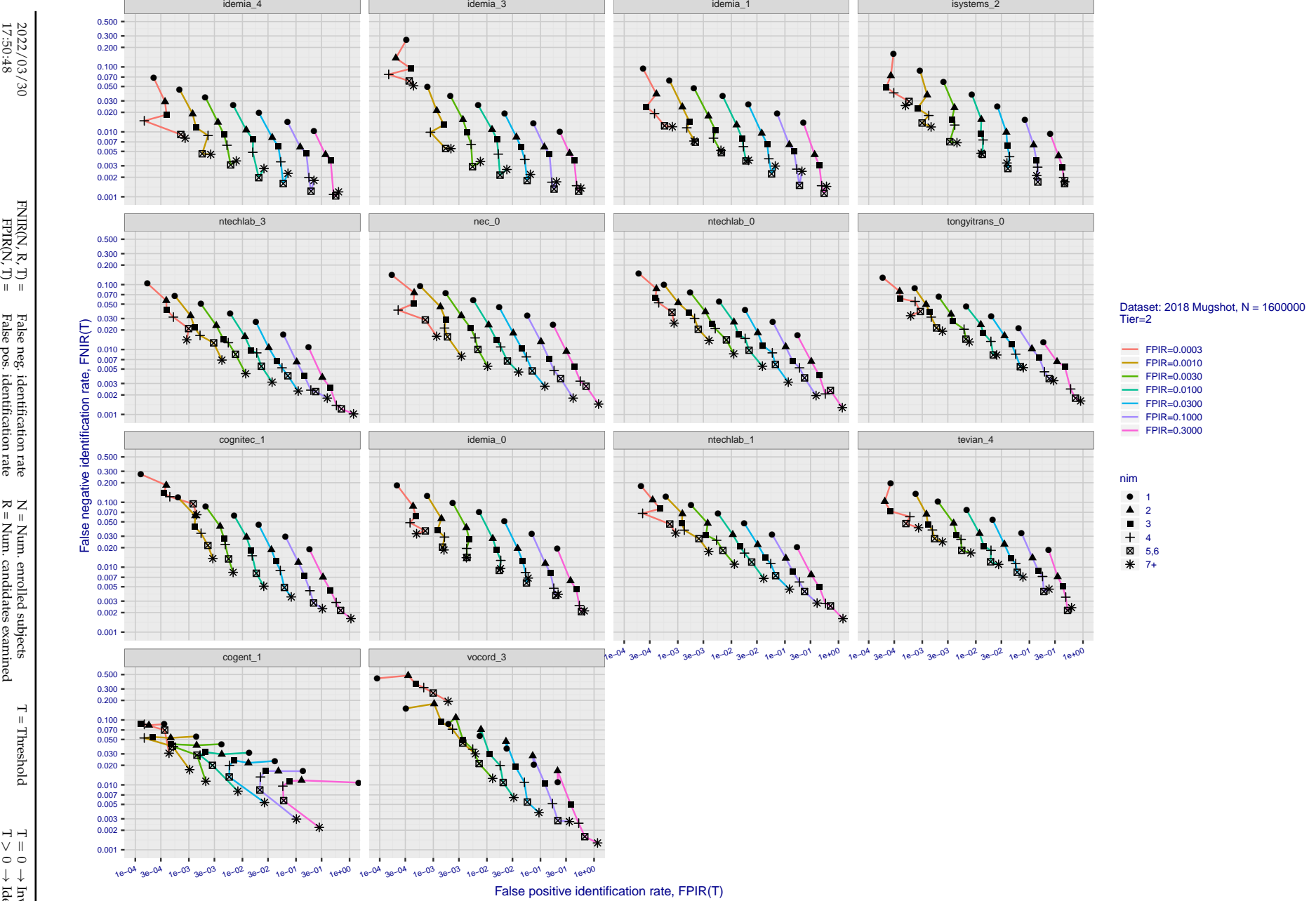


Figure 119: [FRVT-2018 Mugshot Dataset] Effect of enrolling multiple images for each identity. The plot shows an identification miss rates vs. false positive rates, at seven operating thresholds. The enrolled population size is fixed. The images are enrolled with lifetime-consolidation - see section 2.3.

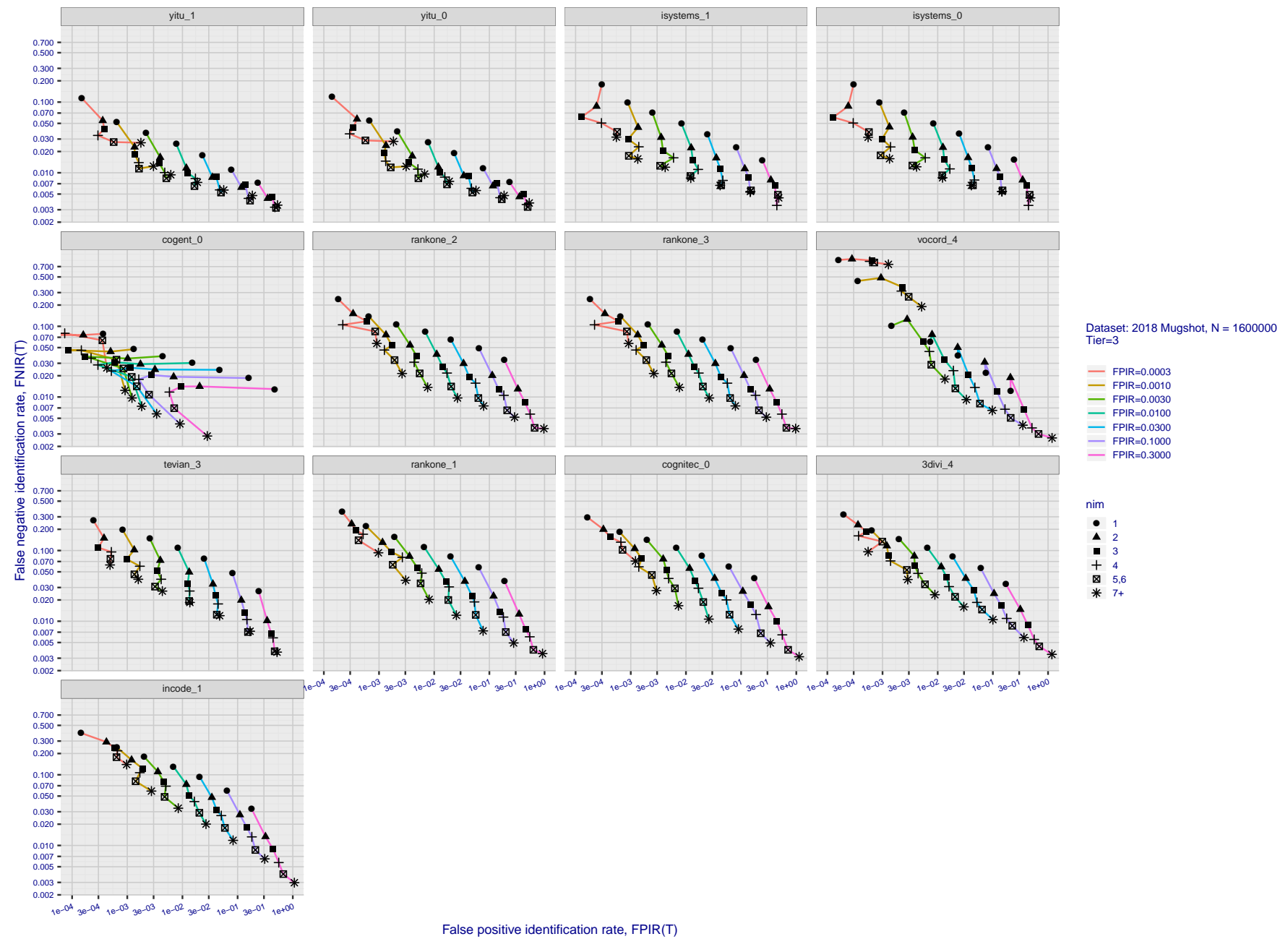


Figure 120: [FRVT-2018 Mugshot Dataset] Effect of enrolling multiple images for each identity. The plot shows an identification miss rates vs. false positive rates, at seven operating thresholds. The enrolled population size is fixed. The images are enrolled with lifetime-consolidation - see section 2.3.

2022/03/30
17:50:48

 $FNIR(N, R, T)$ = False neg. identification rate
 $FPIR(N, T)$ = False pos. identification rate

 N = Num. enrolled subjects
 R = Num. candidates examined

 T = Threshold
 $T = 0 \rightarrow$ Investigation
 $T > 0 \rightarrow$ Identification

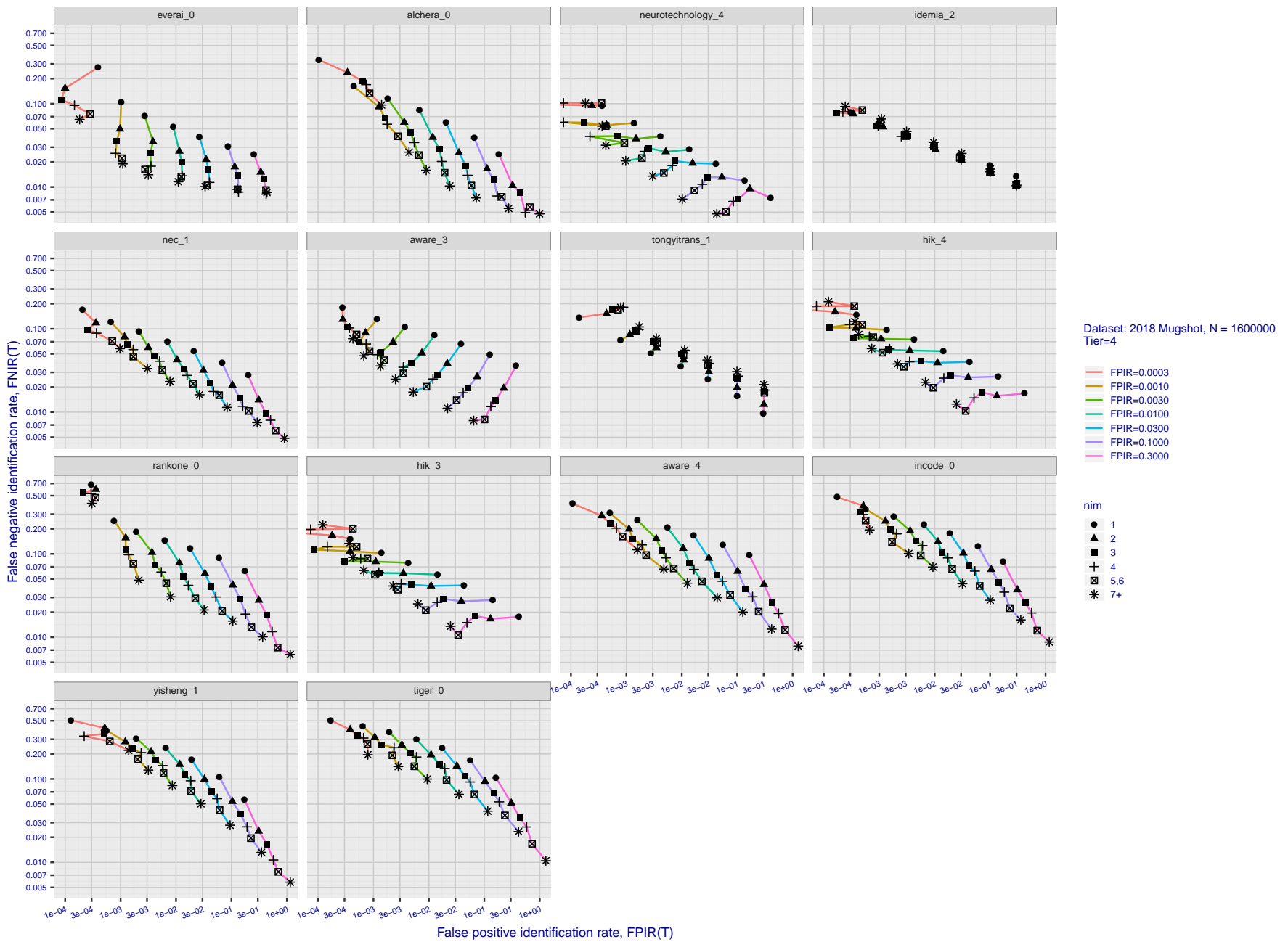


Figure 121: [FRVT-2018 Mugshot Dataset] Effect of enrolling multiple images for each identity. The plot shows an identification miss rates vs. false positive rates, at seven operating thresholds. The enrolled population size is fixed. The images are enrolled with lifetime-consolidation - see section 2.3.

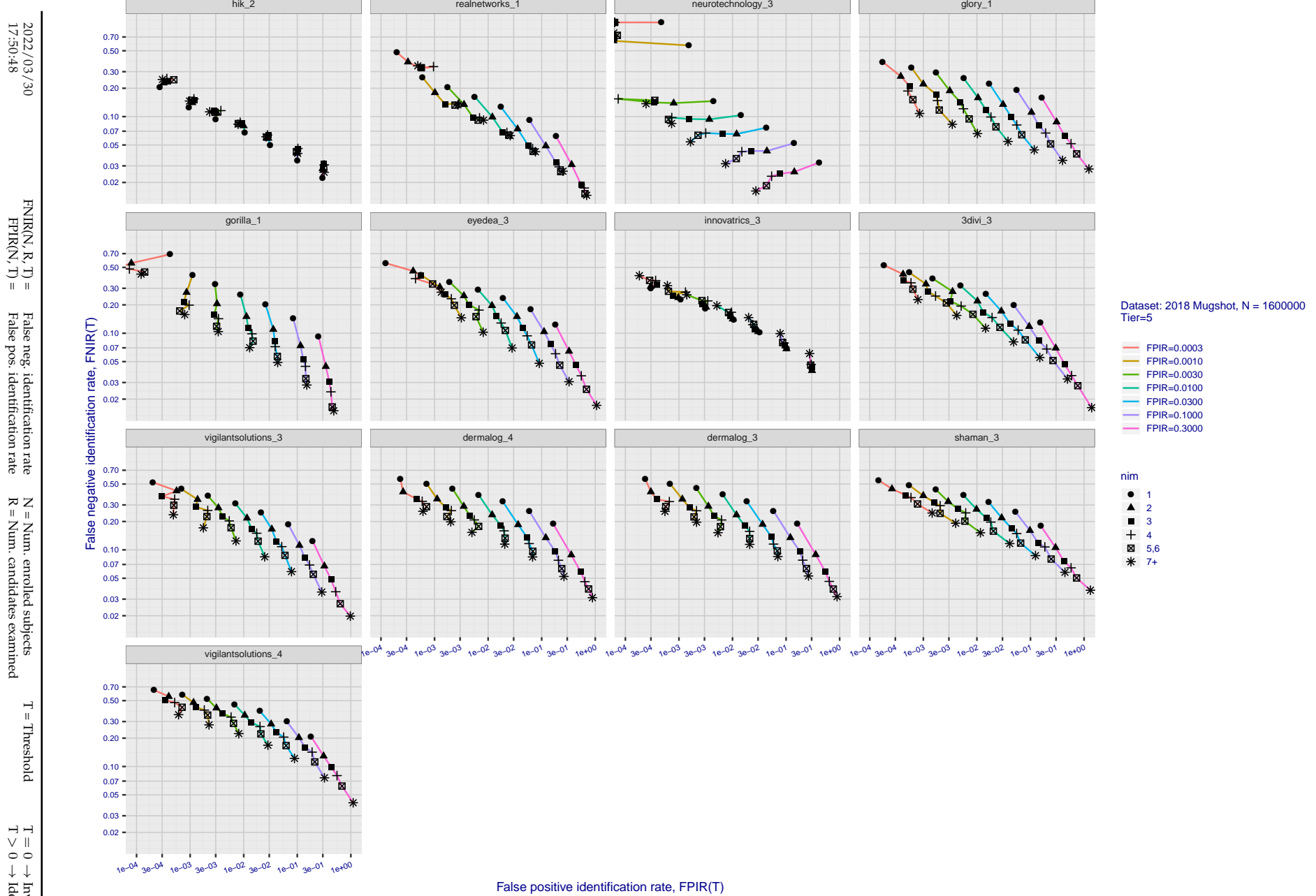


Figure 122: [FRVT-2018 Mugshot Dataset] Effect of enrolling multiple images for each identity. The plot shows an identification miss rates vs. false positive rates, at seven operating thresholds. The enrolled population size is fixed. The images are enrolled with lifetime-consolidation - see section 2.3.

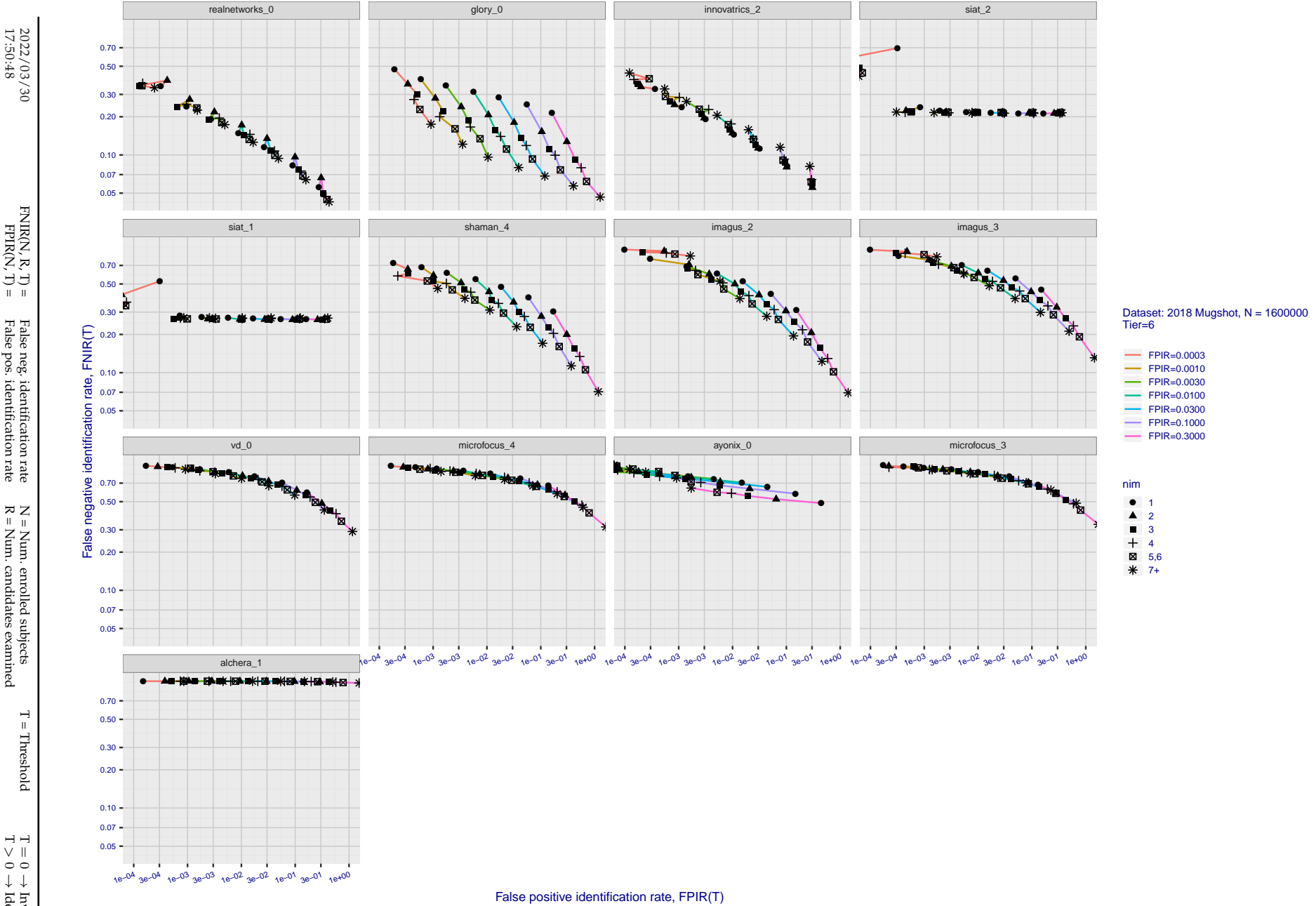


Figure 123: [FRVT-2018 Mugshot Dataset] Effect of enrolling multiple images for each identity. The plot shows an identification miss rates vs. false positive rates, at seven operating thresholds. The enrolled population size is fixed. The images are enrolled with lifetime-consolidation - see section 2.3.

Appendix D Accuracy with poor quality webcam images

2022/03/30 17:50:48	$\text{FNIR}(N, R, T) =$ $\text{FPTR}(N, T) =$	False neg. identification rate False pos. identification rate	$N =$ Num. enrolled subjects $R =$ Num. candidates examined	$T =$ Threshold $T > 0 \rightarrow$ Identification	$T = 0 \rightarrow$ Investigation
------------------------	---	--	--	---	-----------------------------------

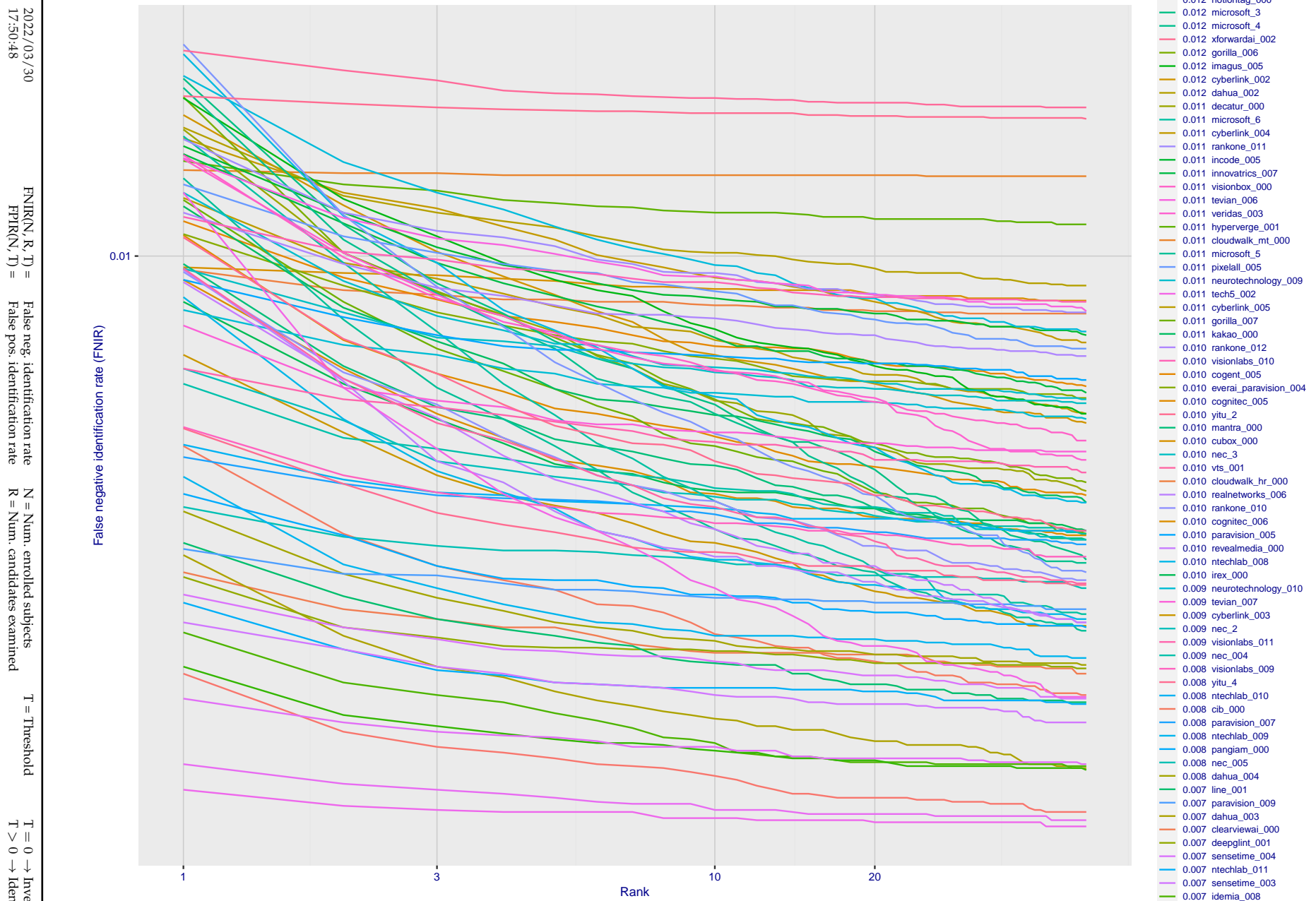


Figure 124: [Webcam Dataset] Identification miss rates vs. rank. The results apply to cross-domain recognition in which webcams are searched against enrolled mugshots. The FNIR values are higher than those for mugshot-mugshot identification due to low image resolution, lighting and less constrained subject pose in webcam images - see Figure 6.

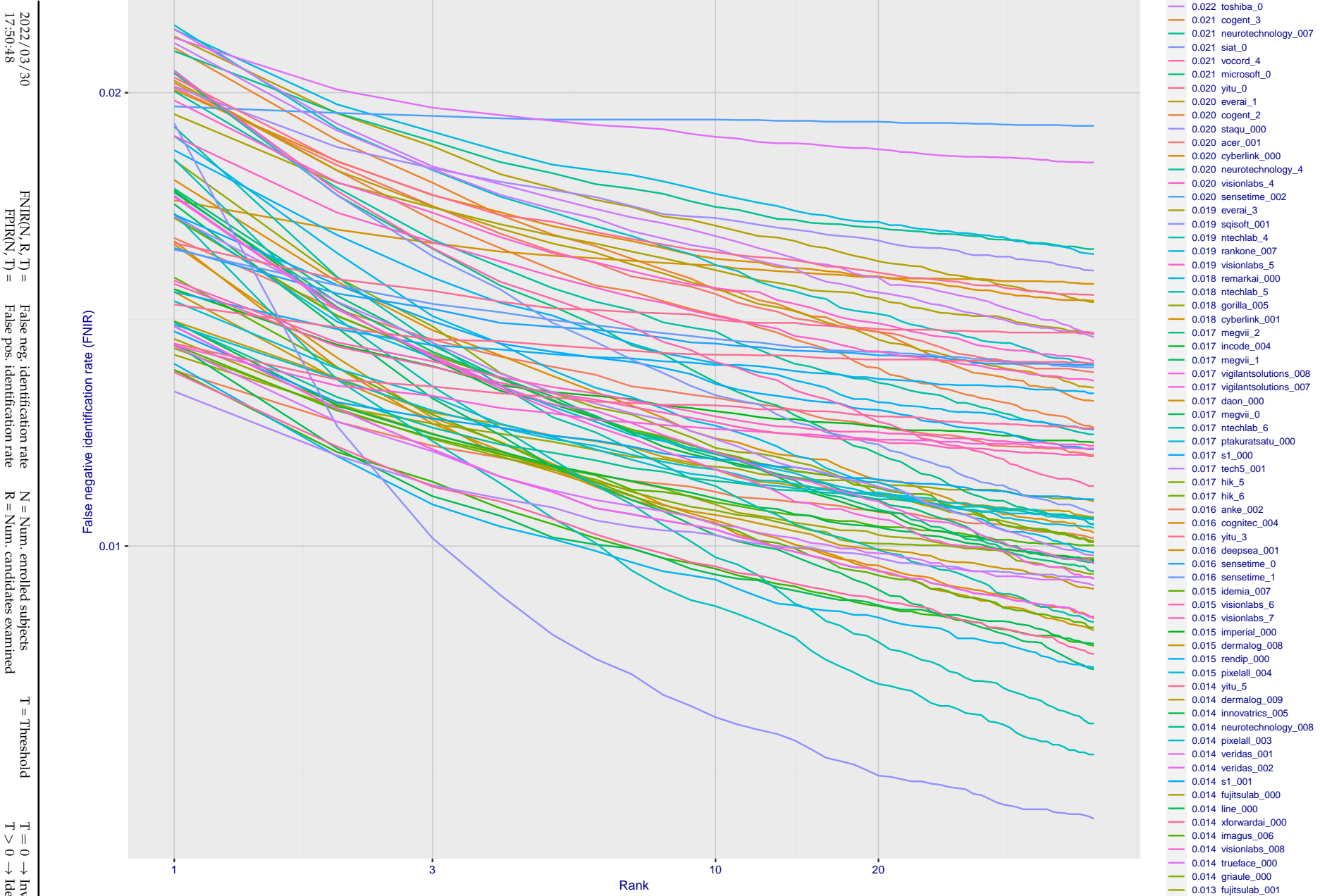


Figure 125: [Webcam Dataset] Identification miss rates vs. rank. The results apply to cross-domain recognition in which webcams are searched against enrolled mugshots. The FNIR values are higher than those for mugshot-mugshot identification due to low image resolution, lighting and less constrained subject pose in webcam images - see Figure 6.

2022/03/30
17:50:48
FNIR(N, R, T) = False neg. identification rate
FPR(N, T) = False pos. identification rate
N = Num. enrolled subjects
R = Num. candidates examined
T = Threshold
T = 0 → Investigation
T > 0 → Identification

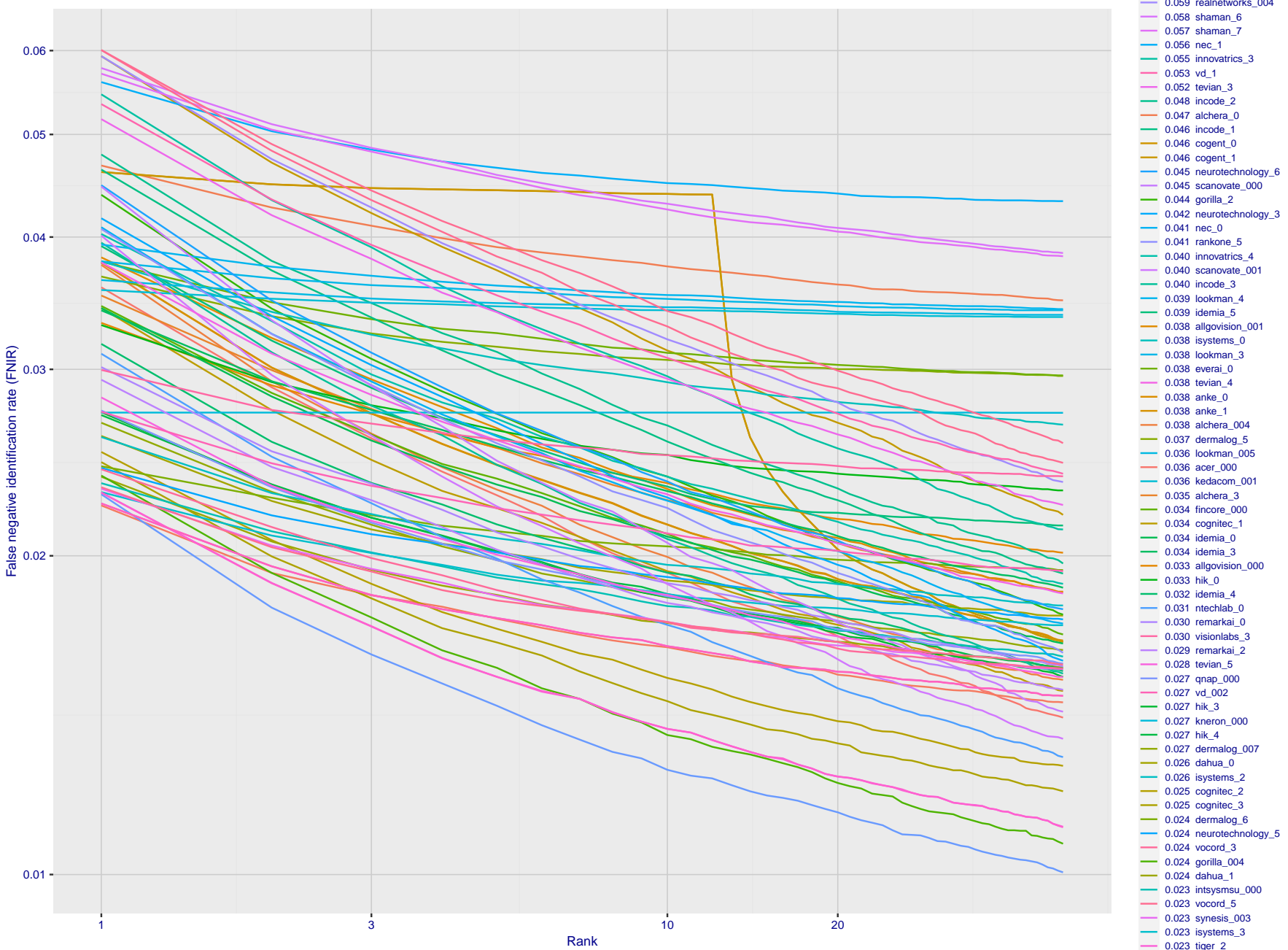


Figure 126: [Webcam Dataset] Identification miss rates vs. rank. The results apply to cross-domain recognition in which webcams are searched against enrolled mugshots. The FNIR values are higher than those for mugshot-mugshot identification due to low image resolution, lighting and less constrained subject pose in webcam images - see Figure 6.

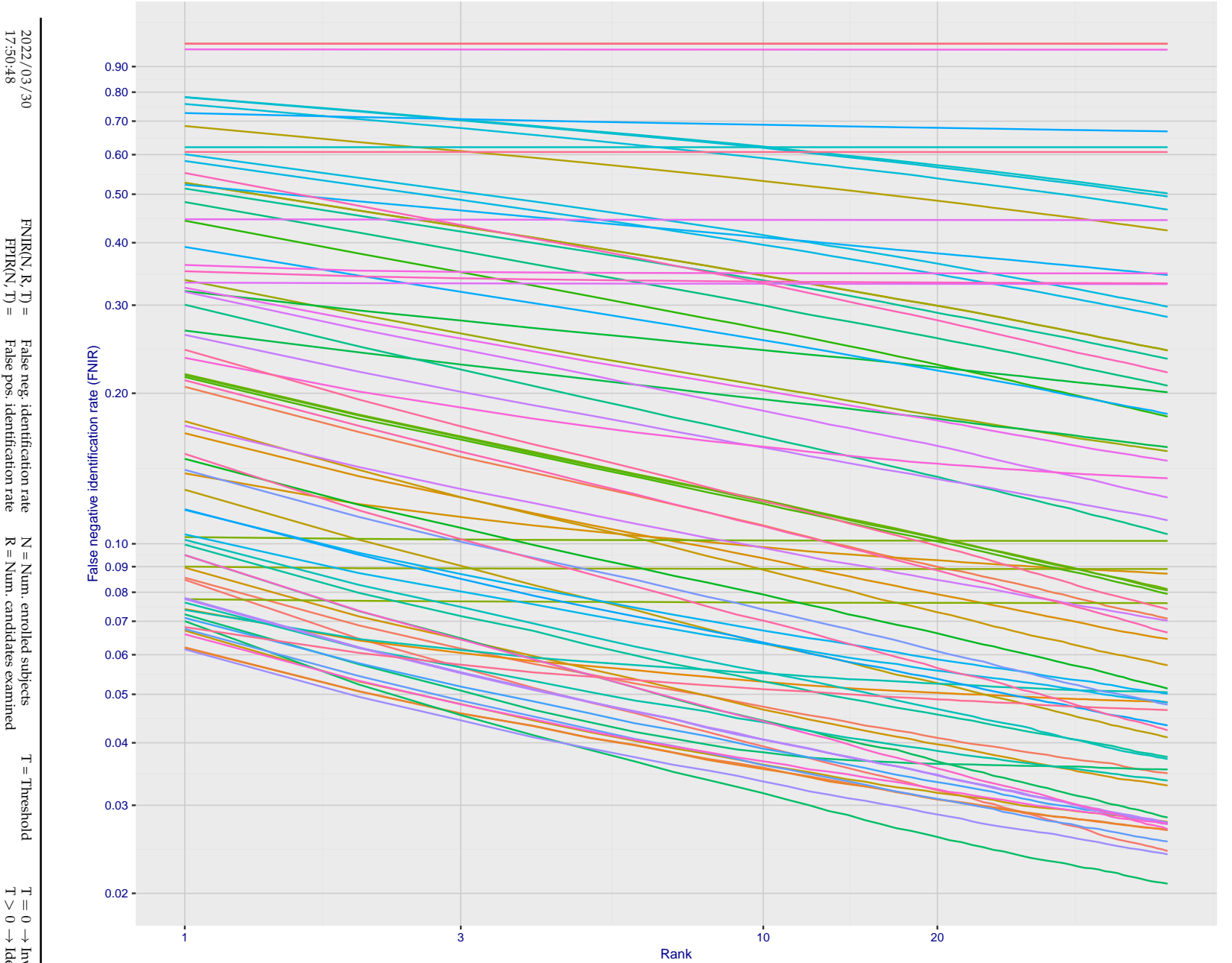


Figure 127: [Webcam Dataset] Identification miss rates vs. rank. The results apply to cross-domain recognition in which webcams are searched against enrolled mugshots. The FNIR values are higher than those for mugshot-mugshot identification due to low image resolution, lighting and less constrained subject pose in webcam images - see Figure 6.

2022/03/30 17:50:48	FNIR(N, R, T) = FPTR(N, T) =	False neg. identification rate False pos. identification rate	N = Num. enrolled subjects R = Num. candidates examined	T = Threshold	T = 0 → Investigation T > 0 → Identification
------------------------	---------------------------------	--	--	---------------	---

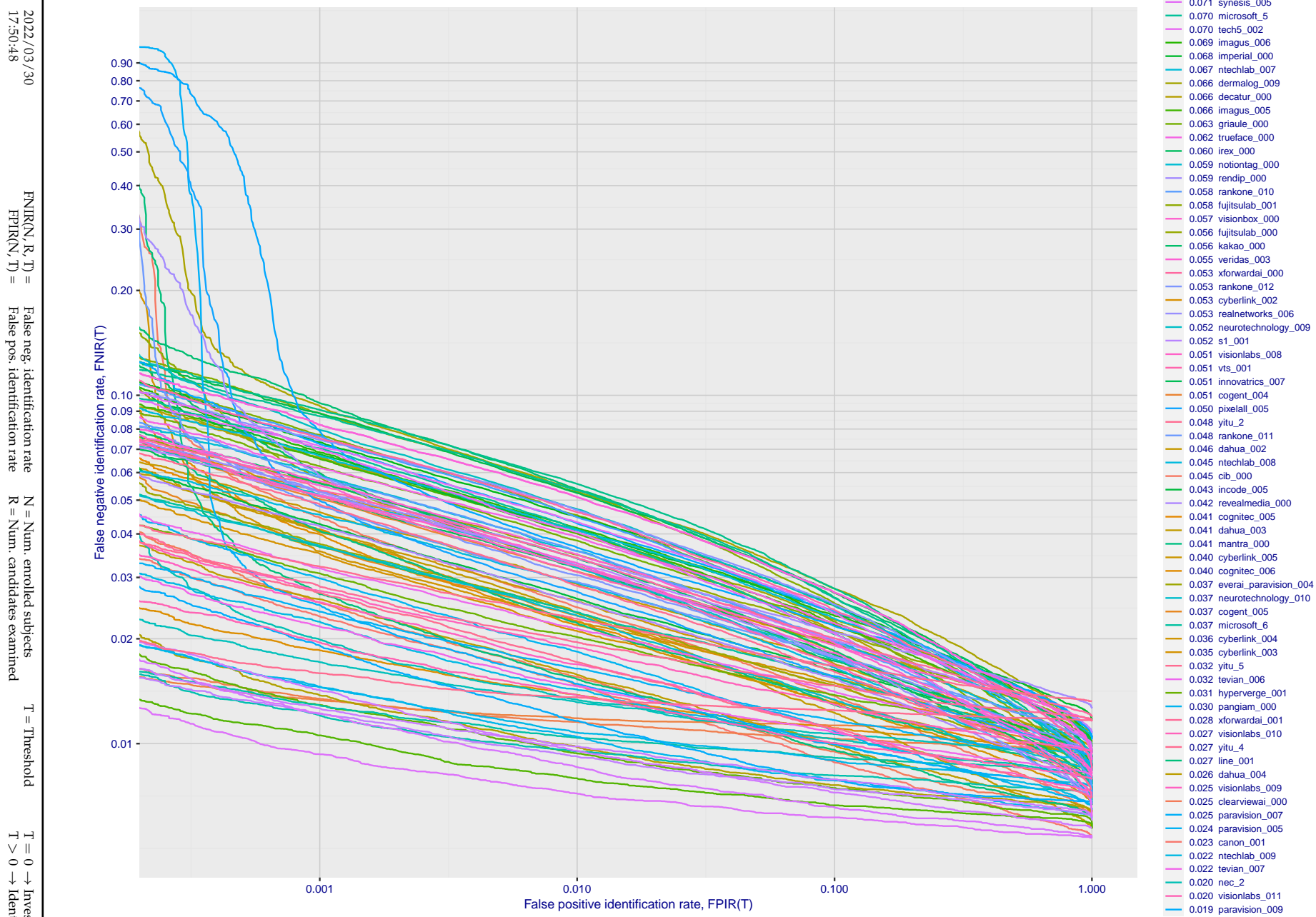


Figure 128: [Webcam Dataset] Identification miss rates vs. false positive rates. The results apply to cross-domain recognition in which webcams are searched against enrolled mugshots. The FNIR values are higher than those for mugshot-mugshot identification due to low image resolution, lighting and less constrained subject pose in webcam images - see Figure 6.

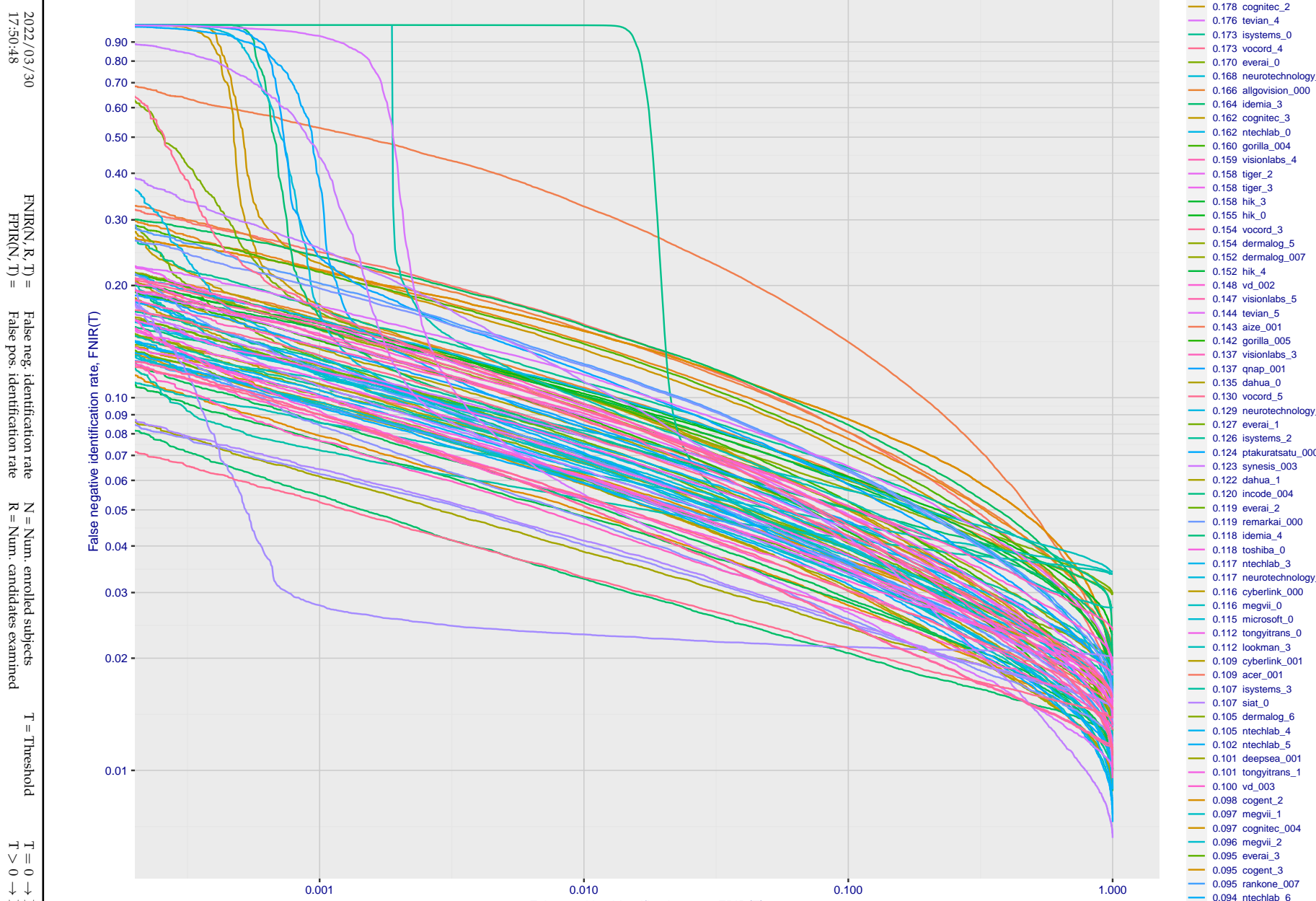


Figure 129: [Webcam Dataset] Identification miss rates vs. false positive rates. The results apply to cross-domain recognition in which webcams are searched against enrolled mugshots. The FNIR values are higher than those for mugshot-mugshot identification due to low image resolution, lighting and less constrained subject pose in webcam images - see Figure 6.

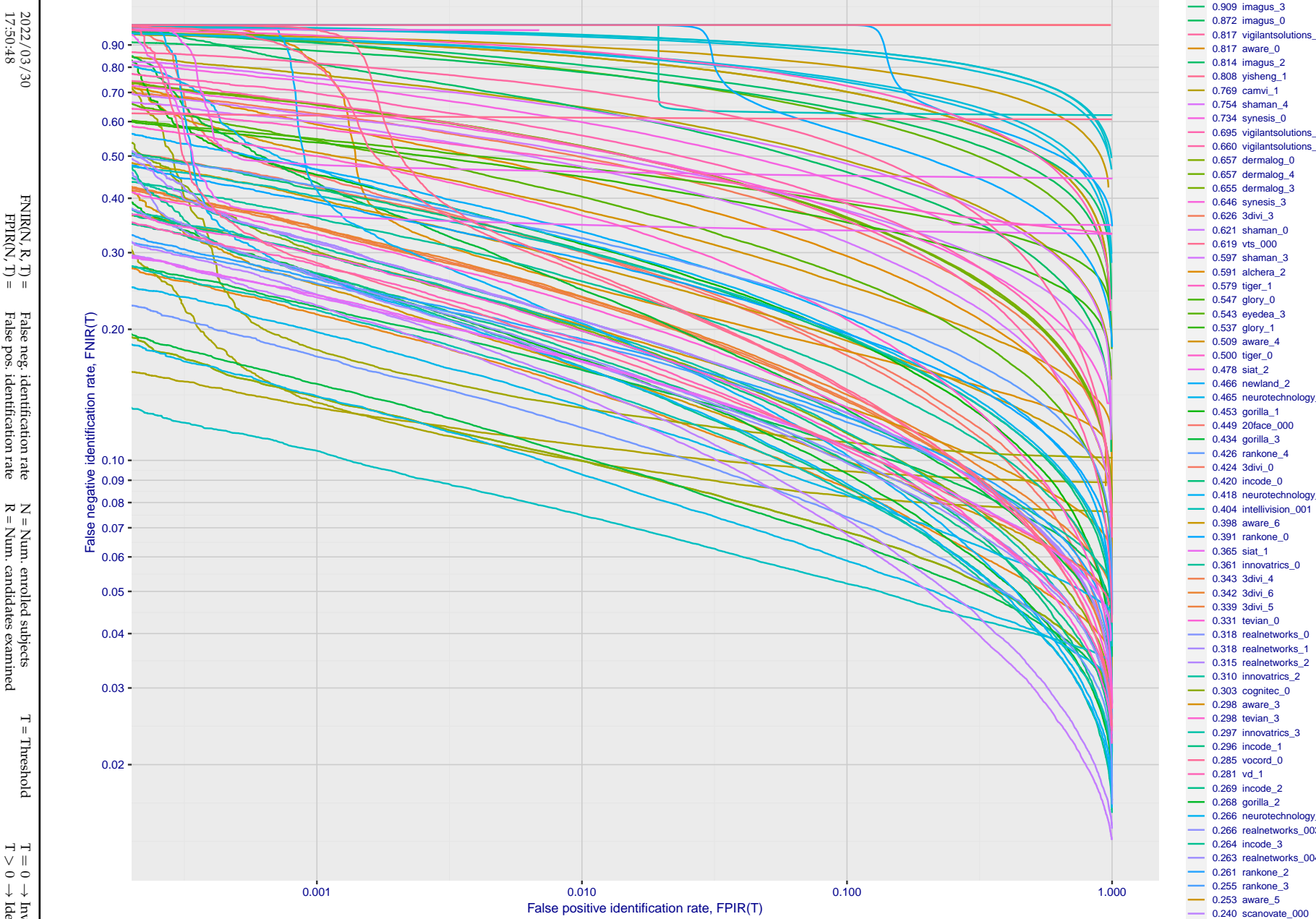


Figure 130: [Webcam Dataset] Identification miss rates vs. false positive rates. The results apply to cross-domain recognition in which webcams are searched against enrolled mugshots. The FNIR values are higher than those for mugshot-mugshot identification due to low image resolution, lighting and less constrained subject pose in webcam images - see Figure 6.

Appendix E Accuracy for profile-view to frontal recognition

Figures 131 - 133 gives accuracy results for searching 100 000 mated and 100 000 non-mated profile-view images against the same FRVT 2018 frontal enrollment dataset, $N = 1\,600\,000$, used in the main mugshot trials. This experiment corresponds to row-13 of Table 1. An example of profile-view image is given in Figure 7.

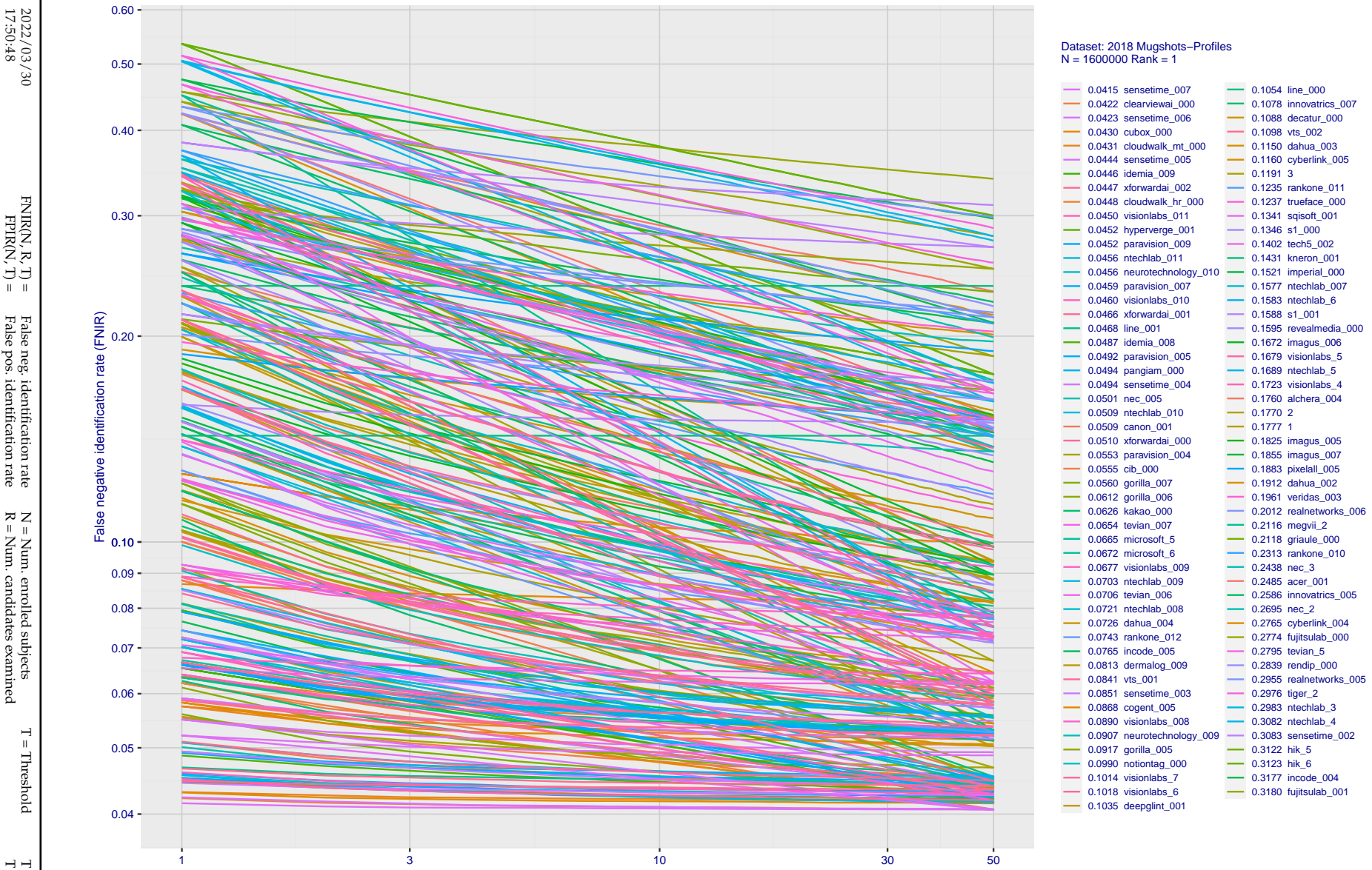


Figure 131: [Mugshot and profile-view dataset] Rank-based accuracy. For some of the more accurate Phase 3 algorithms the figure plots error tradeoff characteristics for frontal and profile-view searches into an enrolled set of $N = 1\,600\,000$ frontal images. Note that some algorithms fail on profile-view images with $\text{FNIR} \rightarrow 1$ - this evaluation did not ask developers to provide profile-view capability. Some algorithms, on the other hand, give FNIR approaching that for frontal-view searches using c. 2010 algorithms. The best result is that 91% of profile-view searches yield the correct mate at rank 1, and better than 94% in the top-50 candidates.

2022/03/30
17:50:48
FNIR(N, R, T) = False neg. identification rate
FPIR(N, T) = False pos. identification rate
N = Num. enrolled subjects
R = Num. candidates examined
T = Threshold
T = 0 → Investigation
T > 0 → Identification

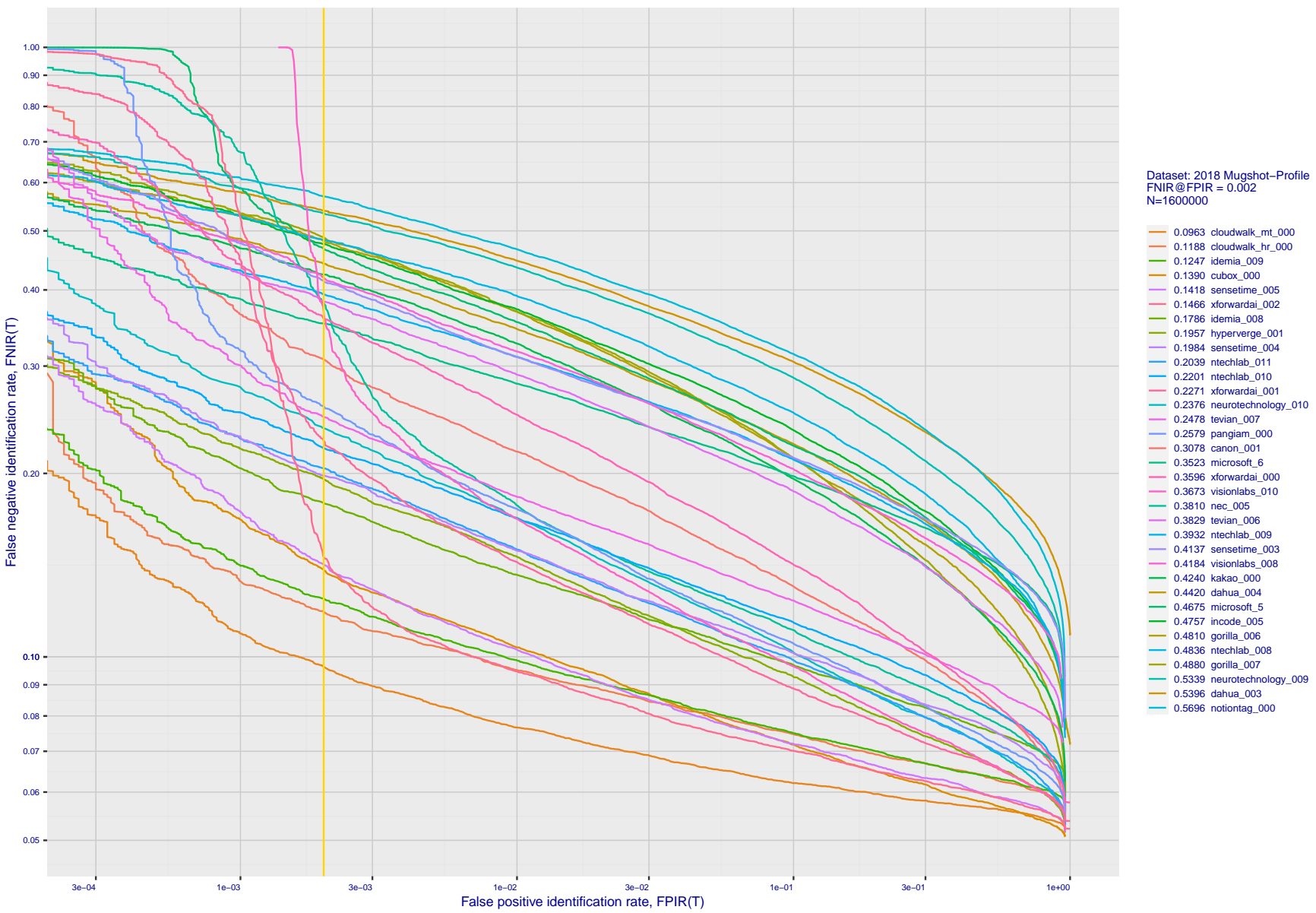


Figure 132: [Mugshot and profile-view dataset] Threshold-based accuracy. For some of the more accurate Phase 3 algorithms the figure plots error tradeoff characteristics for frontal and profile-view searches into an enrolled set of $N = 1\,600\,000$ frontal images. Note that some algorithms fail on profile-view images with $\text{FNIR} \rightarrow 1$ - this evaluation did not ask developers to provide profile-view capability. Some algorithms, on the other hand, give FNIR approaching that for frontal-view searches using c. 2010 algorithms.

2022/03/30
17:50:48FNIR(N, R, T) = False neg. identification rate
FPIR(N, T) = False pos. identification rateN = Num. enrolled subjects
R = Num. candidates examined

T = Threshold

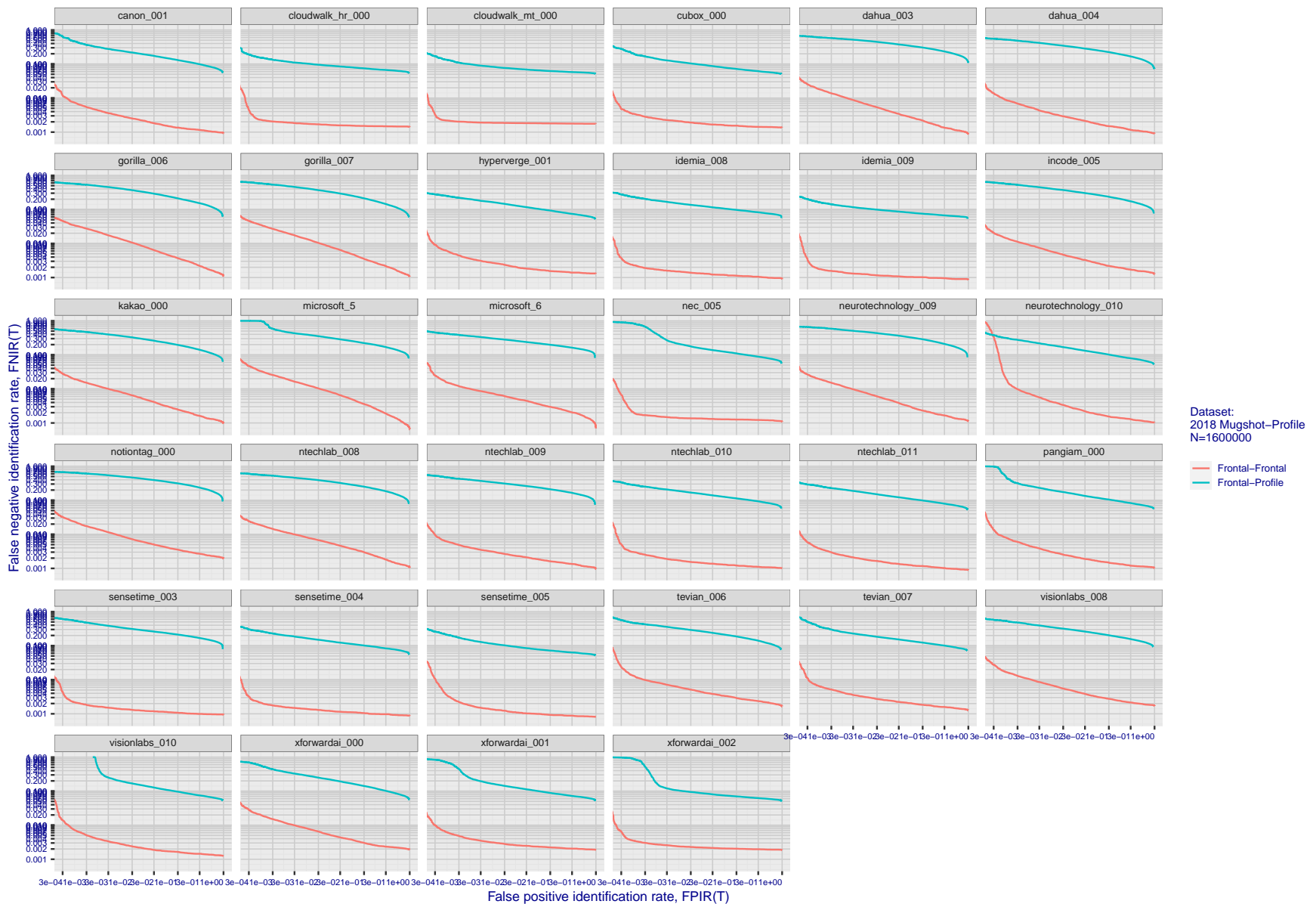
T = 0 → Investigation
T > 0 → Identification

Figure 133: [Mugshot and profile-view dataset] Speed-accuracy tradeoff. For some of the more accurate Phase 3 algorithms the figure plots error tradeoff characteristics for frontal and profile-view searches into an enrolled set of $N = 1600000$ frontal images. Some algorithms fail on profile-view images with $\text{FNIR} \rightarrow 1$ - this evaluation did not ask developers to provide profile-view capability. Some algorithms, on the other hand, give FNIR approaching that for frontal-view searches using c. 2010 algorithms. Blue lines connect points of equal threshold from which it is evident that some algorithms would give markedly higher false positive outcomes if profile-view images were searched in a system configured for frontal searches. This would be a vulnerability in an access control system.

Appendix F Search duration

As in and prior tests, this section documents search speeds spanning three orders of magnitude. In applications where search volumes are high enough, this will have implications for hardware requirements especially for large N or when search duration is appreciably larger than the time it takes to prepare a template from the search image(s). Further, given very large (and growing) operational databases, the scalability of algorithms is important. It has been reported previously [8] that search duration can scale sublinearly with enrolled population size N. Further there has been considerable recent research on indexing, exact [13] and approximate nearest neighbor search [1,13] and fast-search [14,16].

Figure 134 charts the search duration measurements presented earlier in Tables 2 - 4.

- ▷ Most algorithms scale linearly. For those in that category, there is a wide range in speed with search durations ranging from 82 milliseconds for a 12 million gallery (for NEC-3) to more than 40 seconds (for Yitu-3, Toshiba-2) and even higher for less accurate algorithms.
- ▷ Some developers (Camvi, Dermalog, EverAI, Innovatrics, and Visionlabs) provide algorithms whose template search durations grow approximately logarithmically i.e. $T(N) \sim \log N$ with the constant a varying between implementations. In the figure this model is fit using the point $T(1) = 0$, and $T(640\,000)$. This very sublinear behaviour affords extremely fast search times in very large galleries. One caveat for the sublinear algorithms is that their fast-search data structures can require considerable computation time - on the order of hours - for N in the millions, and this scales mildly super-linearly, i.e. $O(N^b)$, $b > 1$. There are exceptions: the Camvi algorithms take minutes; and Innovatrics' scale sublinearly.

2022/03/30 17:50:48	$\text{FNIR}(N, R, T) =$ $\text{FPTR}(N, T) =$	False neg. identification rate False pos. identification rate	$N =$ Num. enrolled subjects $R =$ Num. candidates examined	$T =$ Threshold	$T = 0 \rightarrow$ Investigation $T > 0 \rightarrow$ Identification
------------------------	---	--	--	-----------------	---

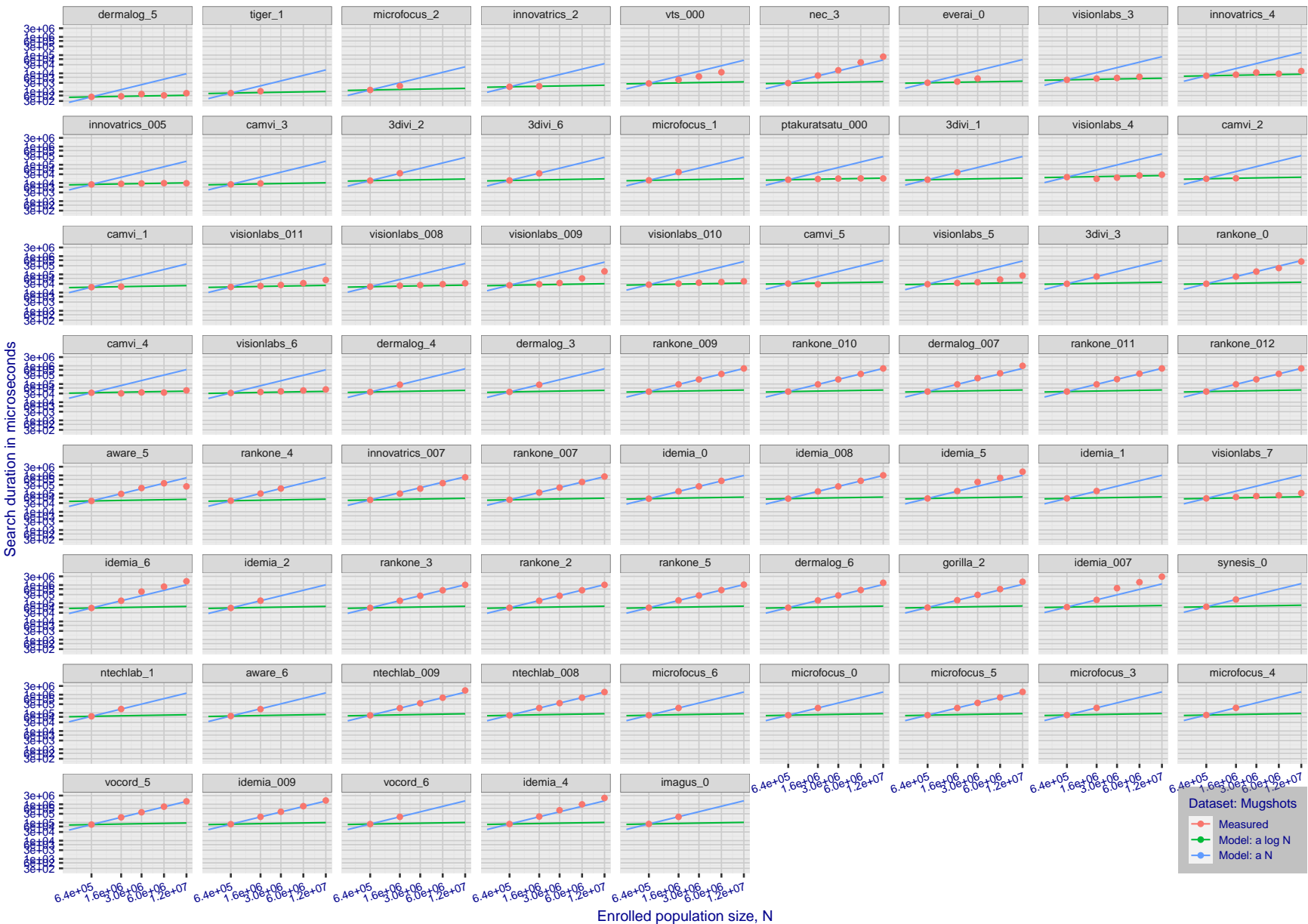
2022/03/30
17:50:48FNIR(N, R, T) = False neg. identification rate
FPFR(N, T) = False pos. identification rateN = Num. enrolled subjects
R = Num. candidates examined
T = ThresholdT = 0 → Investigation
T > 0 → Identification

Figure 134: [Mugshot Dataset] Search duration vs. enrolled population size. In red are the actual point durations measured on a single c. 2016 core. The blue shows linear growth from $N = 640\,000$. The green line shows logarithmic growth from that point to $N = 1\,600\,000$. Note the sublinear growth from algorithms from Camvi, Dermalog, EverAI, Innovatrics, and Visionlabs. The tiger_1 algorithm is also sublinear, but inaccurate and inoperable at $N \geq 3\,000\,000$. This capability sometimes comes at the additional expense of converting a linear gallery data structure into whatever fast-search data structure is used. Note that search times are sometimes dominated by the template generation times shown in Table 23.

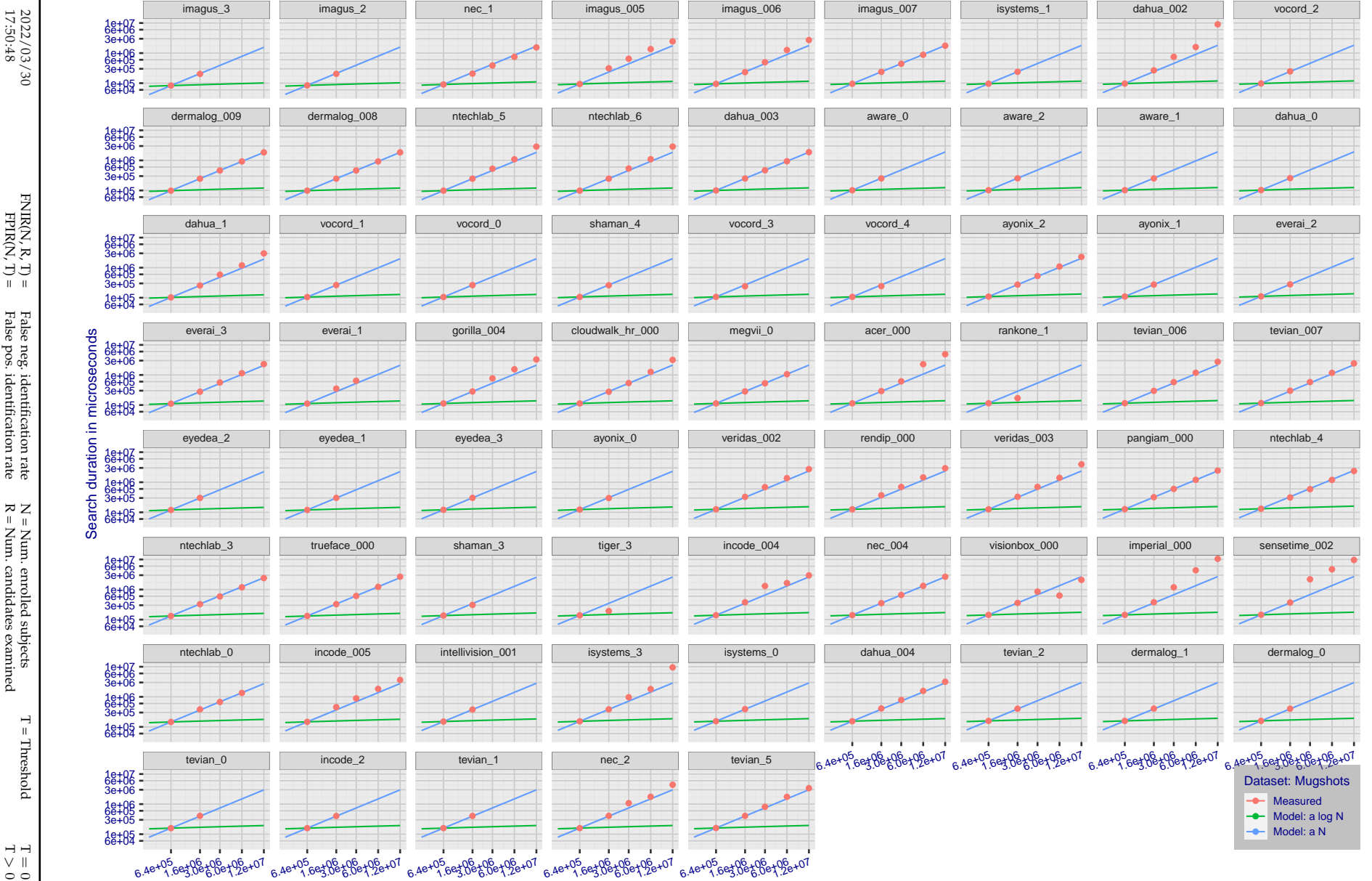


Figure 135: [Mugshot Dataset] Search duration vs. enrolled population size. In red are the actual point durations measured on a single c. 2016 core. The blue shows linear growth from $N = 640\,000$. The green line shows logarithmic growth from that point to $N = 1\,600\,000$. Note the sublinear growth from algorithms from Camvi, Dermalog, EverAI, Innovatrics, and Visionlabs. The tiger_1 algorithm is also sublinear, but inaccurate and inoperable at $N \geq 3000000$. This capability sometimes comes at the additional expense of converting a linear gallery data structure into whatever fast-search data structure is used. Note that search times are sometimes dominated by the template generation times shown in Table 23.

2022/03/30
17:50:48FNIR(N, R, T) = False neg. identification rate
FPTR(N, T) = False pos. identification rateN = Num. enrolled subjects
R = Num. candidates examined

T = Threshold

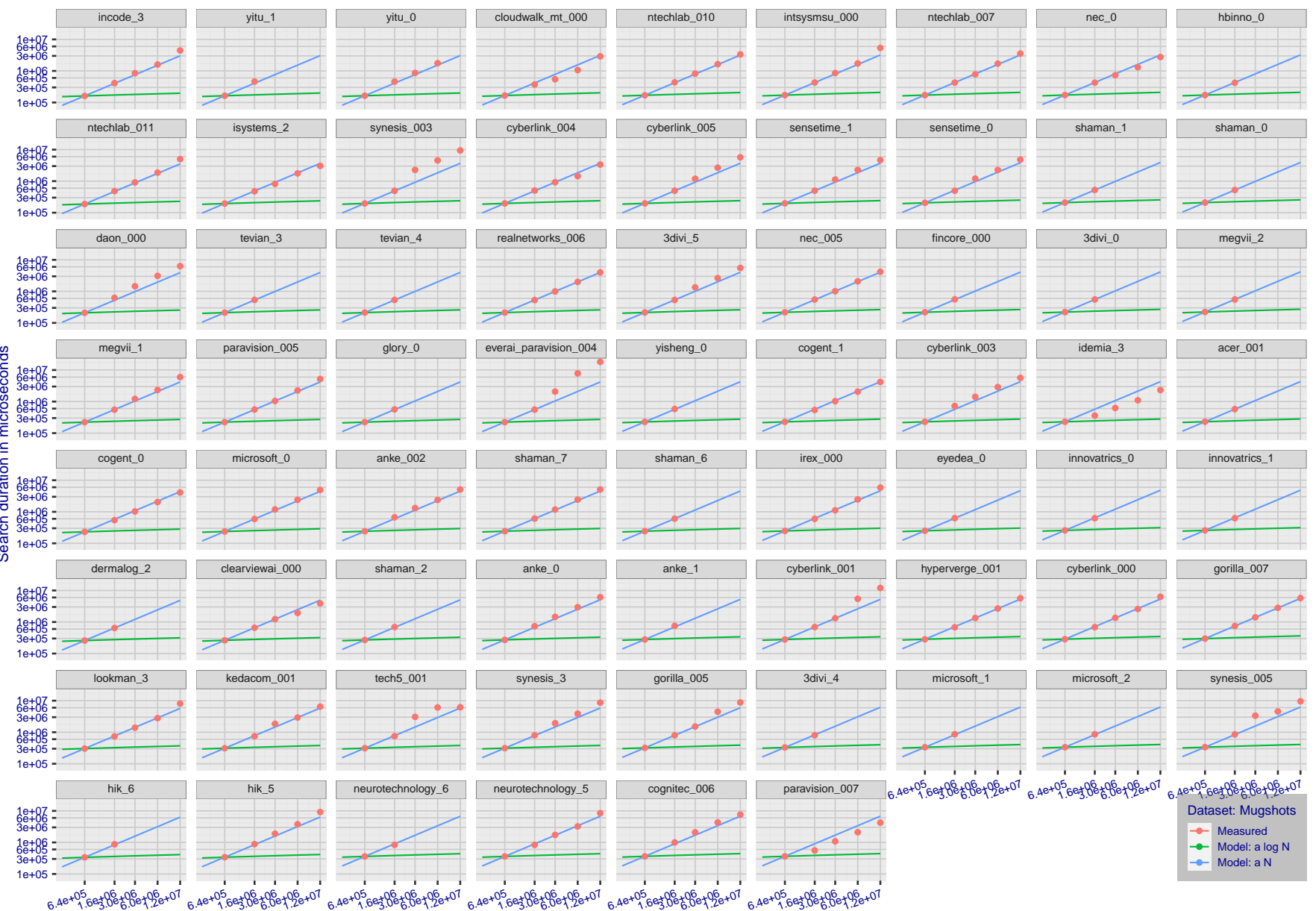
T = 0 → Investigation
T > 0 → Identification

Figure 136: [Mugshot Dataset] Search duration vs. enrolled population size. In red are the actual point durations measured on a single c. 2016 core. The blue shows linear growth from $N = 640\,000$. The green line shows logarithmic growth from that point to $N = 1\,600\,000$. Note the sublinear growth from algorithms from Camvi, Dermalog, EverAI, Innovatrics, and Visionlabs. The tiger_1 algorithm is also sublinear, but inaccurate and inoperable at $N \geq 3000000$. This capability sometimes comes at the additional expense of converting a linear gallery data structure into whatever fast-search data structure is used. Note that search times are sometimes dominated by the template generation times shown in Table 23.

2022/03/30
17:50:48FNIR(N, R, T) = False neg. identification rate
FPIR(N, T) = False pos. identification rateN = Num. enrolled subjects
R = Num. candidates examined

T = Threshold

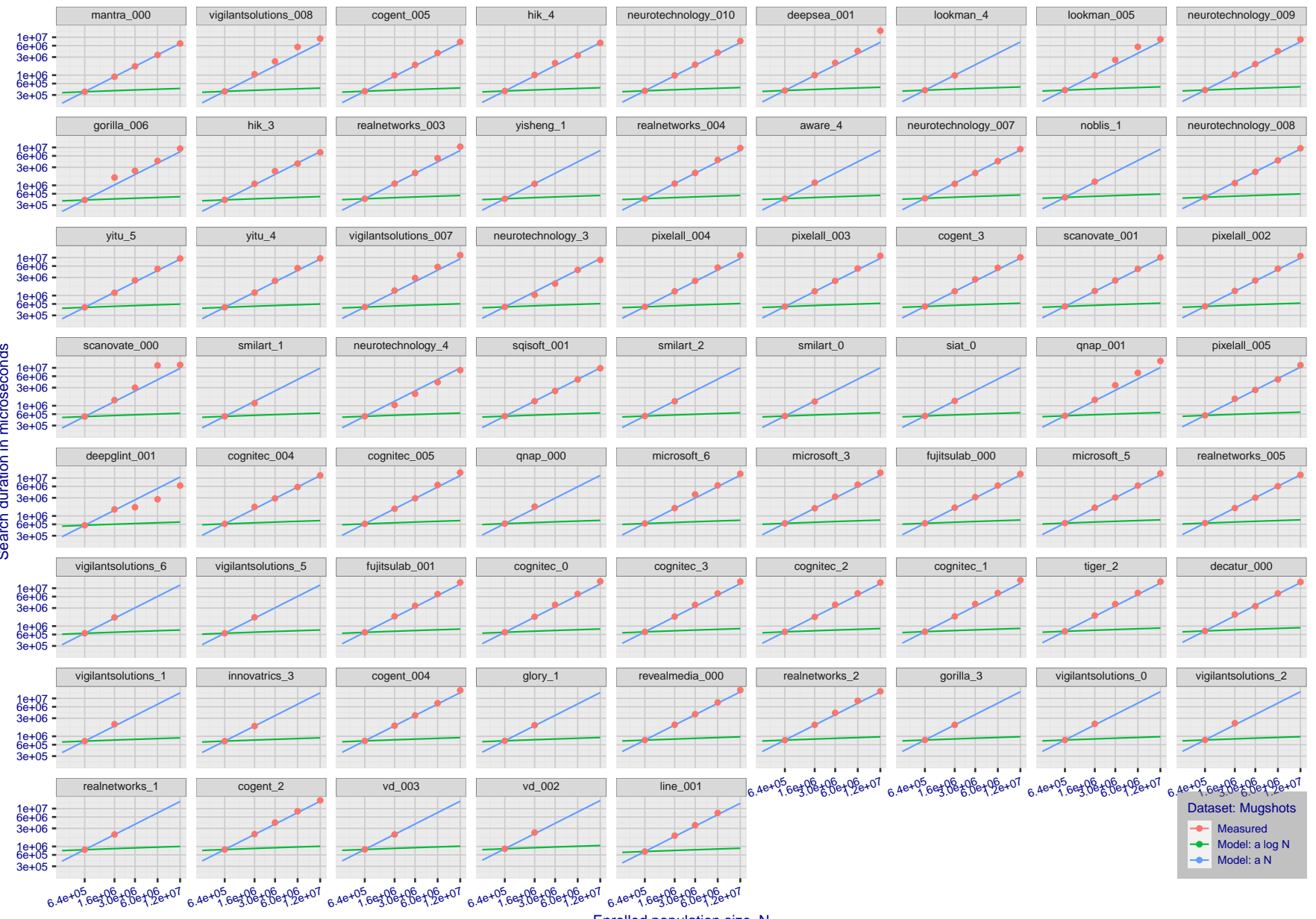
T = 0 → Investigation
T > 0 → Identification

Figure 137: [Mugshot Dataset] Search duration vs. enrolled population size. In red are the actual point durations measured on a single c. 2016 core. The blue shows linear growth from $N = 640\,000$. The green line shows logarithmic growth from that point to $N = 1\,600\,000$. Note the sublinear growth from algorithms from Camvi, Dermalog, EverAI, Innovatrics, and Visionlabs. The tiger_1 algorithm is also sublinear, but inaccurate and inoperable at $N \geq 3000000$. This capability sometimes comes at the additional expense of converting a linear gallery data structure into whatever fast-search data structure is used. Note that search times are sometimes dominated by the template generation times shown in Table 23.

2022/03/30
17:50:48FNIR(N, R, T) = False neg. identification rate
FPFR(N, T) = False pos. identification rateN = Num. enrolled subjects
R = Num. candidates examined

T = Threshold

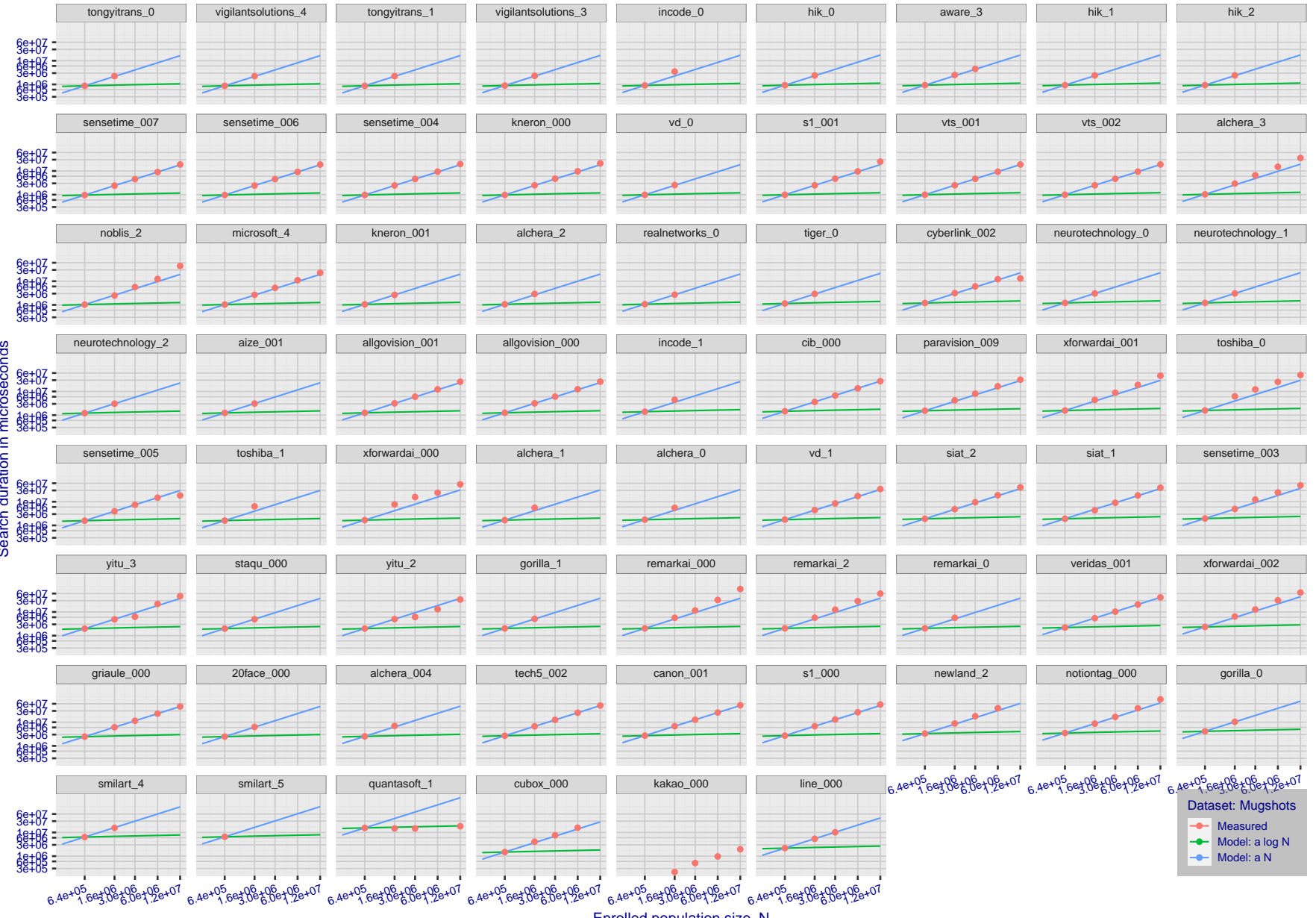
T = 0 → Investigation
T > 0 → Identification

Figure 138: [Mugshot Dataset] Search duration vs. enrolled population size. In red are the actual point durations measured on a single c. 2016 core. The blue shows linear growth from $N = 640\,000$. The green line shows logarithmic growth from that point to $N = 1\,600\,000$. Note the sublinear growth from algorithms from Camvi, Dermalog, EverAI, Innovatrics, and Visionlabs. The tiger_1 algorithm is also sublinear, but inaccurate and inoperable at $N \geq 3000000$. This capability sometimes comes at the additional expense of converting a linear gallery data structure into whatever fast-search data structure is used. Note that search times are sometimes dominated by the template generation times shown in Table 23.

Appendix G Gallery Insertion Timing

2022/03/30
17:50:48FNIR(N, R, T) = False neg. identification rate
FPIR(N, T) = False pos. identification rateN = Num. enrolled subjects
R = Num. candidates examined

T = Threshold

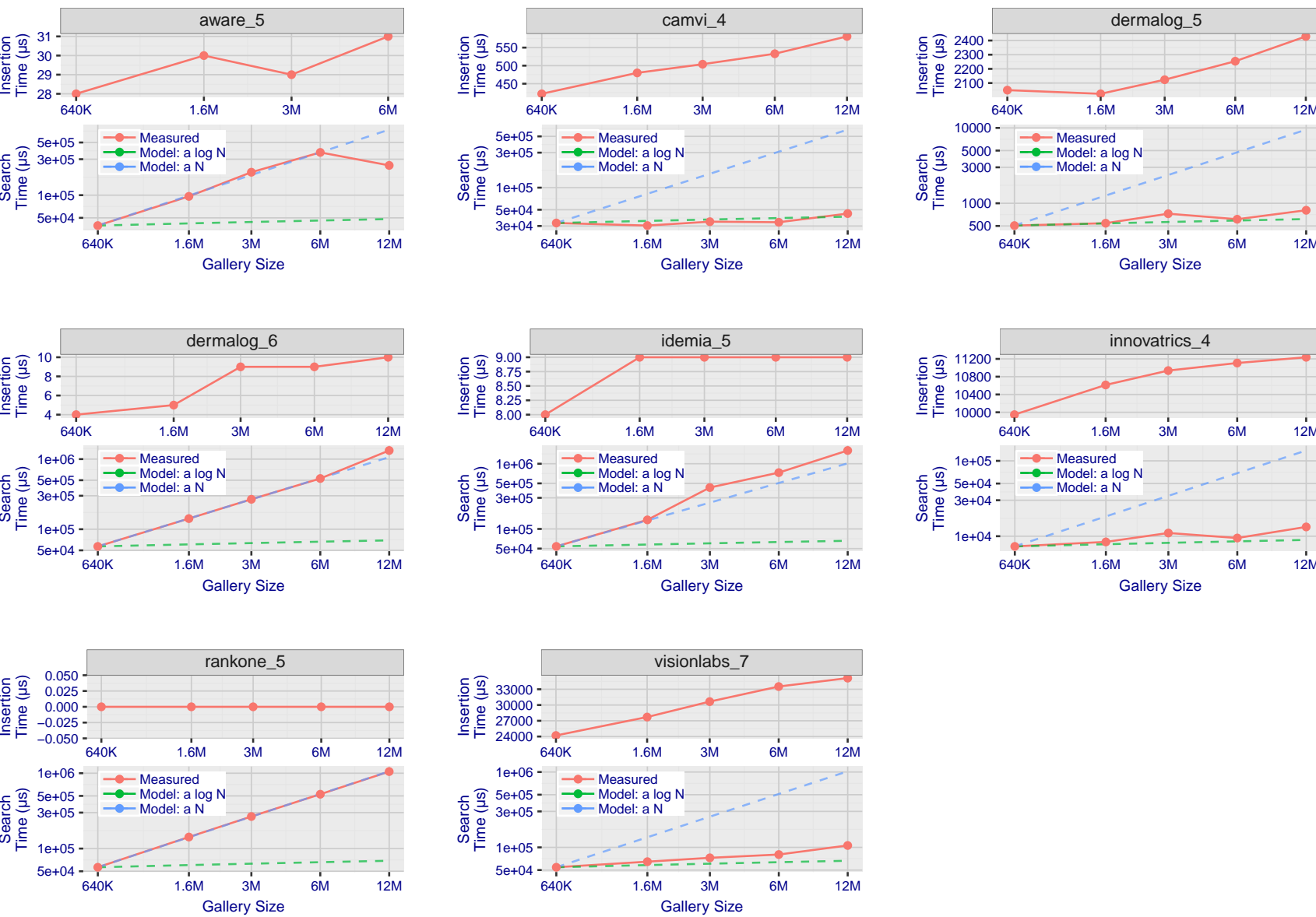
T = 0 → Investigation
T > 0 → Identification

Figure 139: [Mugshot Dataset] Gallery insertion duration vs. enrolled population size. This chart plots the time it takes to insert a single template into a finalized gallery, illustrated over increasing gallery sizes. For reference, search times on finalized galleries of corresponding sizes are plotted right underneath. Gallery insertion time plots were generated on algorithms that 1) successfully implemented gallery insertion with no errors and 2) that were run on galleries with N up to 12 000 000. Generally, only the more accurate algorithms were run on galleries with N up to 12 000 000.

2022/03/30
17:50:48FNIR(N, R, T) = False neg. identification rate
FPFR(N, T) = False pos. identification rateN = Num. enrolled subjects
R = Num. candidates examinedT = Threshold
T = 0 → Investigation

T > 0 → Identification

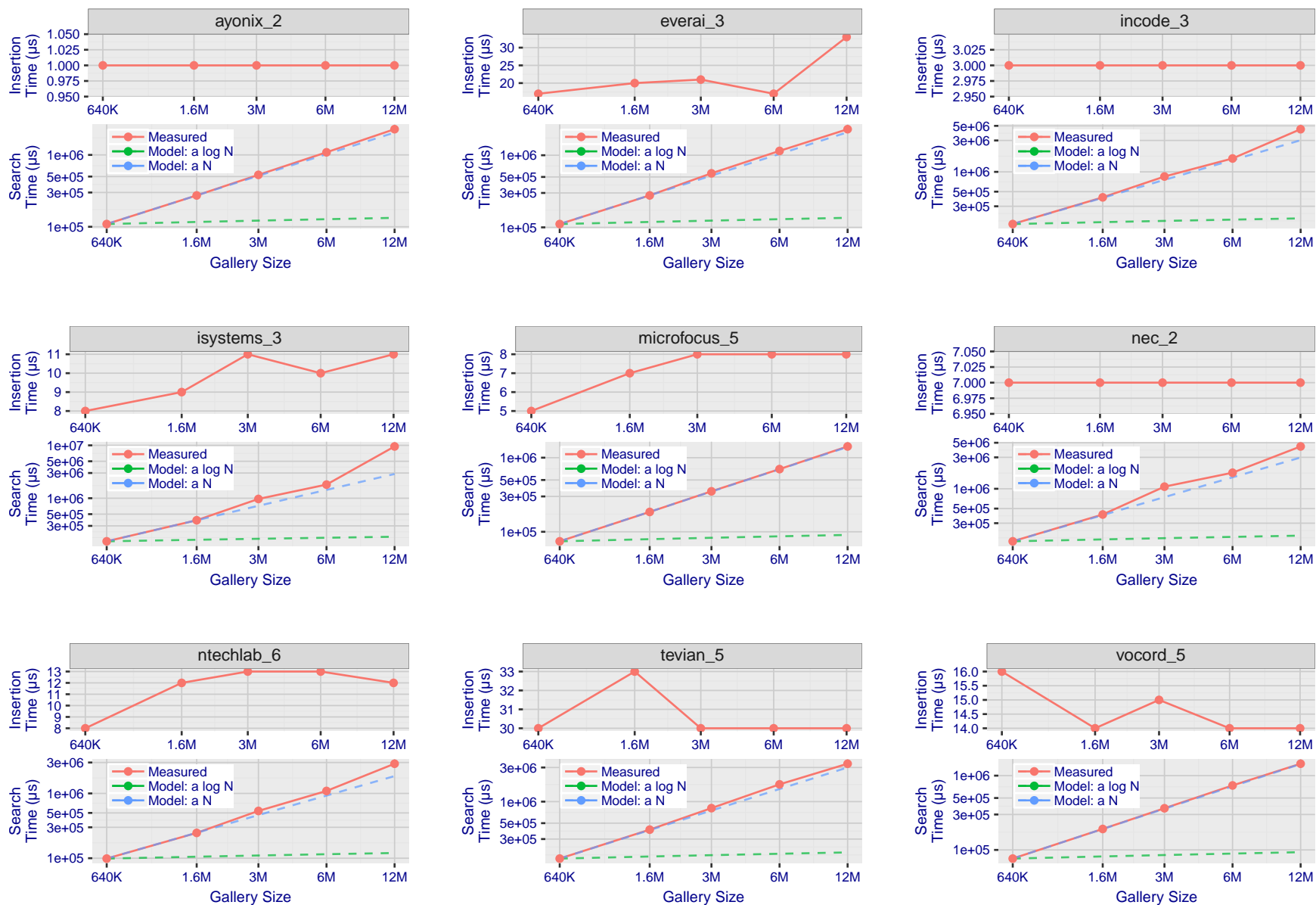


Figure 140: **[Mugshot Dataset] Gallery insertion duration vs. enrolled population size.** This chart plots the time it takes to insert a single template into a finalized gallery, illustrated over increasing gallery sizes. For reference, search times on finalized galleries of corresponding sizes are plotted right underneath. Gallery insertion time plots were generated on algorithms that 1) successfully implemented gallery insertion with no errors and 2) that were run on galleries with N up to 12 000 000. Generally, only the more accurate algorithms were run on galleries with N up to 12 000 000.

2022/03/30
17:50:48FNIR(N, R, T) = False neg. identification rate
FPTR(N, T) = False pos. identification rateN = Num. enrolled subjects
R = Num. candidates examinedT = Threshold
T = 0 → Investigation

T > 0 → Identification

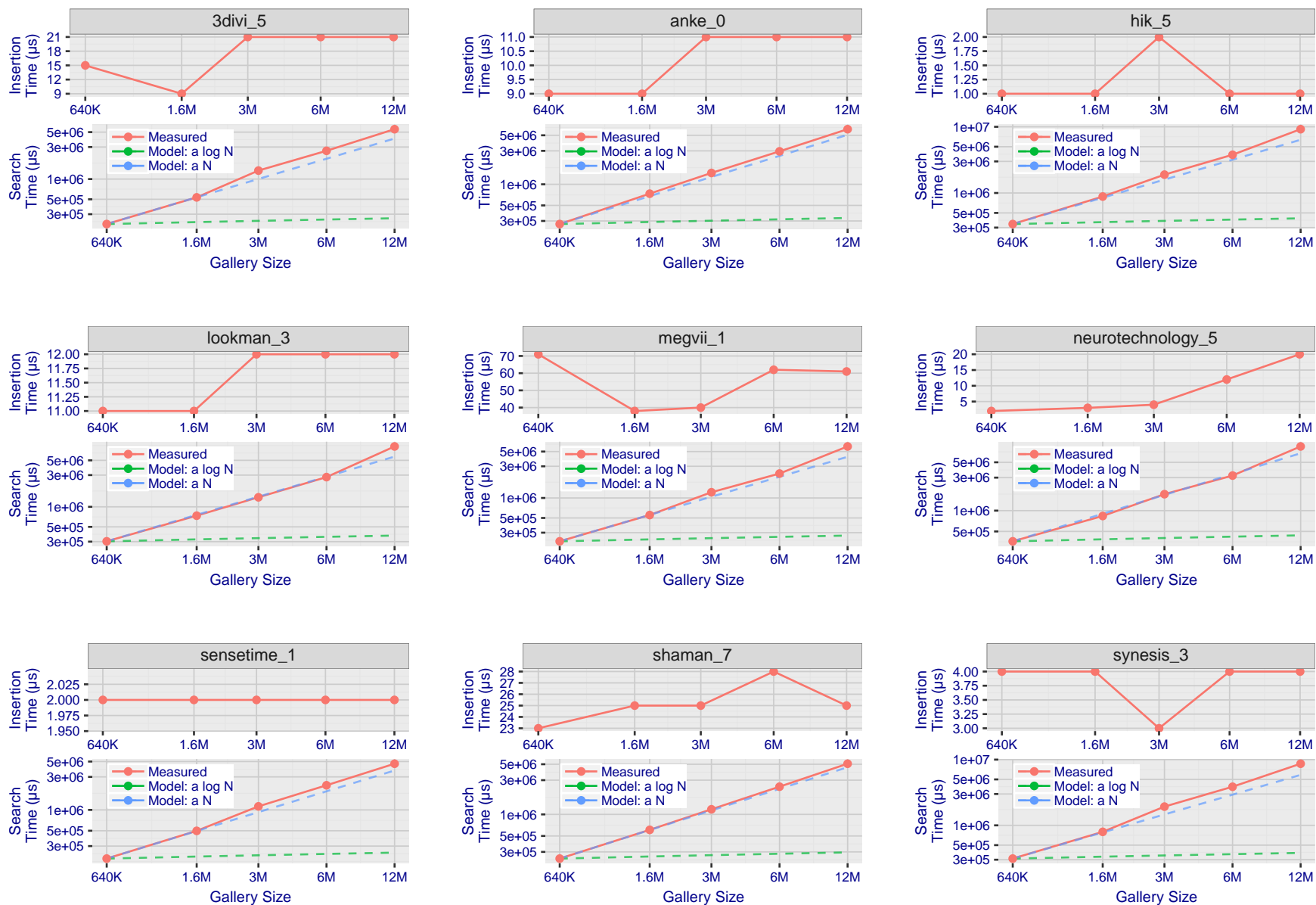


Figure 141: [Mugshot Dataset] Gallery insertion duration vs. enrolled population size. This chart plots the time it takes to insert a single template into a finalized gallery, illustrated over increasing gallery sizes. For reference, search times on finalized galleries of corresponding sizes are plotted right underneath. Gallery insertion time plots were generated on algorithms that 1) successfully implemented gallery insertion with no errors and 2) that were run on galleries with N up to 12 000 000. Generally, only the more accurate algorithms were run on galleries with N up to 12 000 000.

2022/03/30
17:50:48FNIR(N, R, T) = False neg. identification rate
FPTR(N, T) = False pos. identification rateN = Num. enrolled subjects
R = Num. candidates examinedT = Threshold
T = 0 → Investigation

T > 0 → Identification

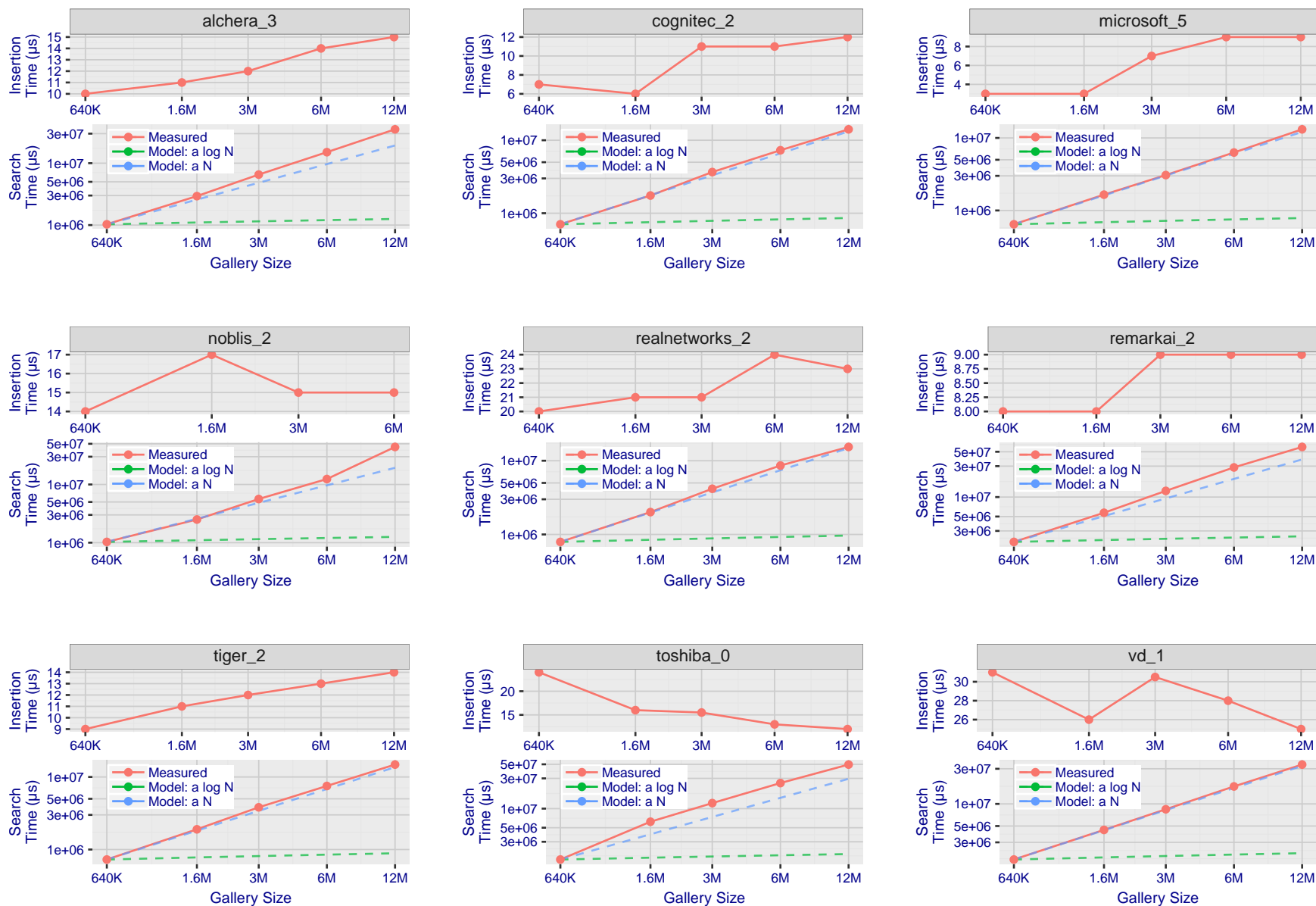


Figure 142: [Mugshot Dataset] Gallery insertion duration vs. enrolled population size. This chart plots the time it takes to insert a single template into a finalized gallery, illustrated over increasing gallery sizes. For reference, search times on finalized galleries of corresponding sizes are plotted right underneath. Gallery insertion time plots were generated on algorithms that 1) successfully implemented gallery insertion with no errors and 2) that were run on galleries with N up to 12 000 000. Generally, only the more accurate algorithms were run on galleries with N up to 12 000 000.

References

- [1] Artem Babenko and Victor Lempitsky. Efficient indexing of billion-scale datasets of deep descriptors. In *The IEEE Conference on Computer Vision and Pattern Recognition (CVPR)*, June 2016.
- [2] L. Best-Rowden and A. K. Jain. Longitudinal study of automatic face recognition. *IEEE Transactions on Pattern Analysis and Machine Intelligence*, 40(1):148–162, Jan 2018.
- [3] Blumstein, Cohen, Roth, and Visher, editors. *Random parameter stochastic models of criminal careers*. National Academy of Sciences Press, 1986.
- [4] Thomas P. Bonczar and Lauren E. Glaze. Probation and parole in the united statesm 2007, statistical tables. Technical report, Bureau of Justice Statistics, December 2008.
- [5] White D., Kemp R. I., Jenkins R., Matheson M, and Burton A. M. Passport officers' errors in face matching. *PLoS ONE*, 9(8), 2014. e103510. doi:10.1371/journal.pone.0103510.
- [6] P. Grother, G. W. Quinn, and P. J. Phillips. Evaluation of 2d still-image face recognition algorithms. NIST Interagency Report 7709, National Institute of Standards and Technology, 8 2010. <http://face.nist.gov/mbe> as MBE2010 FRVT2010.
- [7] P. J. Grother, R. J. Micheals, and P. J. Phillips. Performance metrics for the frvt 2002 evaluation. In *Proceedings of Audio and Video Based Person Authentication Conference (AVBPA)*, June 2003.
- [8] Patrick Grother and Mei Ngan. Interagency report 8009, performance of face identification algorithms. *Face Recognition Vendor Test (FRVT)*, May 2014.
- [9] Patrick Grother, George Quinn, and Mei Ngan. Face in video evaluation (five) face recognition of non-cooperative subjects. Interagency Report 8173, National Institute of Standards and Technology, March 2017. <https://doi.org/10.6028/NIST.IR.8173>.
- [10] Patrick Grother, George W. Quinn, and Mei Ngan. Face recognition vendor test - still face image and video concept, evaluation plan and api. Technical report, National Institute of Standards and Technology, 7 2013. http://biometrics.nist.gov/cs.links/face/frvt/frvt2012/NIST_FRVT2012.api_Aug15.pdf.
- [11] K. He, X. Zhang, S. Ren, and J. Sun. Deep residual learning for image recognition. In *2016 IEEE Conference on Computer Vision and Pattern Recognition (CVPR)*, pages 770–778, June 2016.
- [12] Gary B. Huang, Manu Ramesh, Tamara Berg, and Erik Learned-Miller. Labeled faces in the wild: A database for studying face recognition in unconstrained environments. Technical Report 07-49, University of Massachusetts, Amherst, October 2007.
- [13] Masato Ishii, Hitoshi Imaoka, and Atsushi Sato. Fast k-nearest neighbor search for face identification using bounds of residual score. In *2017 12th IEEE International Conference on Automatic Face & Gesture Recognition (FG 2017)*, pages 194–199, Los Alamitos, CA, USA, May 2017. IEEE Computer Society.
- [14] Jeff Johnson, Matthijs Douze, and Hervé Jégou. Billion-scale similarity search with gpus. *CoRR*, abs/1702.08734, 2017.

- [15] Ira Kemelmacher-Shlizerman, Steven M. Seitz, Daniel Miller, and Evan Brossard. The megaface benchmark: 1 million faces for recognition at scale. *CoRR*, abs/1512.00596, 2015.
- [16] Yury A. Malkov and D. A. Yashunin. Efficient and robust approximate nearest neighbor search using hierarchical navigable small world graphs. *CoRR*, abs/1603.09320, 2016.
- [17] Joyce A. Martin, Brady E. Hamilton, Michelle J.K. Osterman, Anne K. Driscoll, , and Patrick Drake. National vital statistics reports. Technical Report 8, Centers for Disease Control and Prevention, National Center for Health Statistics, National Vital Statistics System, Division of Vital Statistics, November 2018.
- [18] O. M. Parkhi, A. Vedaldi, and A. Zisserman. Deep face recognition. In *British Machine Vision Conference*, 2015.
- [19] P. Jonathon Phillips, Amy N. Yates, Ying Hu, Carina A. Hahn, Eilidh Noyes, Kelsey Jackson, Jacqueline G. Cava-zos, Géraldine Jeckeln, Rajeev Ranjan, Swami Sankaranarayanan, Jun-Cheng Chen, Carlos D. Castillo, Rama Chellappa, David White, and Alice J. O'Toole. Face recognition accuracy of forensic examiners, superrecognitioners, and face recognition algorithms. *Proceedings of the National Academy of Sciences*, 115(24):6171–6176, 2018.
- [20] Florian Schroff, Dmitry Kalenichenko, and James Philbin. Facenet: A unified embedding for face recognition and clustering. *CoRR*, abs/1503.03832, 2015.
- [21] Jeroen Smits and Christiaan Monden. Twinning across the developing world. *PLOS ONE*, 6(9):1–5, 09 2011.
- [22] Yaniv Taigman, Ming Yang, Marc'Aurelio Ranzato, and Lior Wolf. Deepface: Closing the gap to human-level performance in face verification. In *Proceedings of the 2014 IEEE Conference on Computer Vision and Pattern Recognition, CVPR '14*, pages 1701–1708, Washington, DC, USA, 2014. IEEE Computer Society.
- [23] A. Towler, R. I. Kemp, and D White. *Unfamiliar face matching systems in applied settings*. Nova Science, 2017.
- [24] Working Group 3. Ed. M. Werner. *ISO/IEC 19794-5 Information Technology - Biometric Data Interchange Formats - Part 5: Face image data*. JTC1 :: SC37, 2 edition, 2011. <http://webstore.ansi.org>.
- [25] David White, James D. Dunn, Alexandra C. Schmid, and Richard I. Kemp. Error rates in users of automatic face recognition software. *PLoS ONE*, 10:1–14, October 2015.
- [26] Bradford Wing and R. Michael McCabe. Special publication 500-271: American national standard for information systems data format for the interchange of fingerprint, facial, and other biometric information part 1. Technical report, NIST, September 2015. ANSI/NIST ITL 1-2015.
- [27] Andreas Wolf. Portrait quality - (reference facial images for mrtd). Technical report, ICAO, April 2018.
- [28] D. Yadav, N. Kohli, P. Pandey, R. Singh, M. Vatsa, and A. Noore. Effect of illicit drug abuse on face recognition. In *2016 IEEE Winter Conference on Applications of Computer Vision (WACV)*, pages 1–7, Los Alamitos, CA, USA, mar 2016. IEEE Computer Society.